Evaluating the response of mammalian cells to pH perturbations using a parallel microwell approach

Thesis submitted for the degree of

Doctor of Philosophy

by

Ana Catarina da Silva Damas Pinto

The Advanced Centre for Biochemical Engineering

Department of Biochemical Engineering

University College London

2015

Declaration

I, Ana Catarina da Silva Damas Pinto, confirm that all work presented in this thesis is my own work and that any sources used have been clearly and appropriated referenced.

Signature

To my family

Acknowledgment

I would like to thank my supervisors, Dr. Frank Baganz, and Prof. Mark Smales, for their time and support throughout my studies. I would also like to thank all the mammalian cell group members for the training and support, my family for all the care provided and FCT for the four years Ph.D. studentship (FRH/BD/67066/2009).

Abstract

Currently, the production of mAbs in mammalian cells plays a significant part in the biopharmaceutical industry. Consequently, the increased market has led to a need for increased production volumes and a drive to improve process efficiency. One of the key parameters that has a significant impact on the cell growth and metabolism, mAb productivity and quality is the pH. The understanding of the response of mammalian cells to pH perturbations is critical. Therefore, a scale-down model of the pH effects on an industrial GS-CHO cell line (CHO-CY01) growth and mAb (IgG4) production was developed. A scale translation criteria of matching mixing times ($< 5\ s$) and energy dissipation rates (10 $W\ m^{-3}$) was found to be more reliable to set the microwell plates (24-SRW MTPs) and shake flasks as a scale-down models of a 5L-STR bioreactor CHO-CY01 cell line bath and fed-batch cultures. A high-throughput online multi-parametric analysis method of mammalian cell cellular activity at 24-SRW MTP was developed, where the Presens 24-SRW MTPs were exclusively used for the online monitoring of the process parameter. Therefore, it was possible to evaluate the effects of different CO_2 and pH profiles created with CO_2/pH shifts on the CHO-CY01 cell line kinetics. A culture pH higher than 7.50 caused an excessive lactate production. While, culture pHs between pH 6.70 - 6.80 inhibited the cell growth and lactate production, pH 6.60 – 6.70 caused an increase in ammonium production and pH < 6.60 triggered cell apoptosis. Therefore, it became important to identify the lactate and ammonium inhibition kinetics. It was found that an initial lactate concentration of 4.08 $g\ L^{-1}$ and an initial ammonium concentration of 18.1 $mmol\ L^{-1}$ reduced to half the specific growth rate. Ultimately, the optimal pH for IgG4 production was at pH 6.85 ± 0.02, where the maximum specific antibody production rate (10.50 $mg\ 10^{-9}\ cells^{-1}\ day^{-1}$) with the minimal lactate production was reached.

Table of Contents

List of Figures 9
List of Tables 23
Abbreviations and Symbols 30
Chapter 1 Literature Review 34
1. Introduction 34
1.1. Monoclonal Antibodies 34
1.1.1. Antibody Structure and Function 34
1.1.2. Antibody Application and Market 36
1.1.3. Expression Systems for Antibody Production 39
1.1.4. Antibody Glycosylation 41
1.2. Antibody Production Process 43
1.2.1. Effects of Process Parameters 43
1.2.1.1. Temperature 44
1.2.1.2. pH 45
1.2.1.3. Carbon Dioxide 46
1.2.1.4. Osmolarity 50
1.2.1.5. Dissolved Oxygen 50
1.2.1.6. Glucose 51
1.2.1.7. Ammonia 52
1.2.1.8. Lactate 52
1.3. Bioreactor Systems for Small-Scale Production of mAbs 53
1.3.1. Stirred Tank Reactor 56
1.3.2. Shake Flask 58
1.3.3. Microtiter Plate 59
1.4. Engineering Parameters in Shaken Bioreactors 61
1.5. Aims and Objectives 65
Chapter 2 Materials and Methods 66
2.1. Cell Culture 66
2.1.1. Creation of Cell Bank and Revival of Cells from Liquid Nitrogen Storage 66
2.1.2. Shake Flask Cultures 66
2.1.3. Microwell Plate Cultures 67
2.1.4. Stirred Tank Bioreactor Cultures 69
2.1.5. Fed-Batch Strategy 69
2.1.6. Harvest Time 70
2.2. Analytical Techniques 70

2.2.1. Determination of Cell Concentration and Viability 70
2.2.2. Cell Size Analysis and Particle Size Distribution 70
2.2.3. Metabolites, Electrolytes, and IgG4 Concentration Quantification 72
2.2.4. Flow cytometry 73
2.2.4.1. Cell Cycle Analysis 73
2.2.4.2. Apoptosis Analysis 74
2.2.5. 2D-DIGE Proteomic Analysis 75
2.2.5.1 Identification of Protein Spots by Mass Spectrometry 77
2.2.6. Non-Invasive pH and Dissolved Oxygen Monitoring in 24-SRW MTPs 78
2.3. Calculated Kinetic Parameters 80
2.3.1. Volume Correction 80
2.3.2. Calculation of Inoculum Volume 81
2.3.3. Estimation of Specific Growth Rate and Doubling Time 81
2.3.4. Integral of Viable Cell Concentration 81
2.3.5. Specific Antibody Production Rate 82
2.3.6. Antibody Volumetric Productivity 82
2.3.7. Specific Glucose Consumption Rate 82
2.3.8. Specific Glutamate Consumption Rate 83
2.3.9. Specific Lactate Production Rate 83
2.3.10. Specific Ammonium Production Rate 83
2.3.11. Specific Sodium and Potassium Consumption Rates 84
2.3.12. Ratio of Lactate Production to Glucose Consumption 84
2.3.13. Observed Metabolic Yield Coefficients 85
2.3.14. Evaporation Rate in 24-SRW MTP 85
2.3.15. Ammonium, Lactate, and Osmolality Experiments 85
2.4. Engineering Characterisation of 24-SRW MTP 86
2.4.1. Description of Liquid-Phase Hydrodynamics 86
2.4.2. Prediction of Oxygen Mass Transfer Coefficients 86
2.4.3. Liquid-Phase Mixing Time Characterisation and Visualisation of Liquid Hydrodynamics by High-Speed Video Camera 86
2.5. Statistical Analysis 88
Chapter 3 High-Throughput Approach to CHO-CY01 Cell Culture Process Development 89
3.1. Introduction and Aims 89
3.2. Engineering Characterisation of 24-SRW MTP 90
3.2.1. Prediction of Liquid-Phase Hydrodynamics 90
3.2.2. Prediction of Oxygen Mass Transfer Coefficients 93

3.2.3. Liquid-Phase Mixing Time Characterisation 95
3.2.4. Impact of Different 24-SRW MTP Fill Volumes in CHO-CY01 Cell Culture 102
3.2.5. Impact of Different Shaking Speeds on CHO-CY01 Cell Growth and Productivity 109
3.3. Establishment of Microwell Batch Culture Conditions for CHO-CY01 Cell Line 116
3.3.1. Evaporation Rate Study in 24-SRW MTPs 116
3.3.2. Selection of a Sterile Closure 121
3.3.3. Evaluating the Effects of Different Microwell Plates for CHO-CY01 Cell Cultures 124
3.3.4. Impact of Different Methionine Sulfoximine Concentrations 129
3.4. Conclusion 133
Chapter 4 Inter-Scalability of the CHO-CY01 Cell Line Kinetics 134
4.1. Introduction and Aims 134
4.2. Mixing Time and Mean Energy Dissipation Rate as a Basis for Cell Culture Scale Translation 135
4.2.1. Apoptotic and Cell Cycle Population Balance in CHO-CY01 Cell Batch Culture 143
4.3. Effects of Ammonium, Lactate, and Osmolality on CHO-CY01 Cell Growth, Metabolism, and IgG4 Productivity 148
4.3.1. Effects of Lactate on CHO-CY01 Cell Line Kinetics 148
4.3.2. Effects of Ammonium on CHO-CY01 Cell Line Kinetics 159
4.3.3. Ammonium and Lactate Inhibition Kinetics on CHO-CY01 Cell Growth and IgG4 Productivity 168
4.3.4. Effects of Osmolality on CHO-CY01 Cell Line Kinetics 174
4.4. Establishment of a Fed-Batch Strategy for Productivity Optimisation 179
4.4.1. Development of a Suitable Fed-Batch Strategy at Small-Scale 179
4.4.2. Determination of the Correct Glucose Concentration in CHO-CY01 Cell Line Fed-Batch Culture 186
4.4.3. Inter Scalability of CHO-CY01 Cell Fed-Batch Cultures 193
4.5. Conclusion 201
Chapter 5 Effects of Carbon Dioxide on CHO-CY01 Cell Line Kinetics 204
5.1. Introduction and Aims 204
5.2. CHO-CY01 Cell Line Batch Cultures at Different Constant CO_2 Atmospheres 207
5.2.1 Determination of the Buffer Capacity of CHO-CY01 Cell Line Medium from Online pH Monitoring 228
5.3. CHO-CY01 Cell Line Fed-Batch Cultures at Different CO_2 Atmospheres 230
5.4. CO_2 Shifts in CHO-CY01 Cell Line Cultures 238

5.4.1. CO_2 Shifts in CHO-CY01 Cell Line Batch Cultures 238
5.4.2. CO_2 Shifts in CHO-CY01 Cell Line Fed-Batch Cultures 246
5.4.2.1. CO_2 Shifts in CHO-CY01 Cell Line Fed-Batch Cultures in Multiple Steps ... 246
5.4.2.2. CO_2 Shifts in CHO-CY01 Cell Line Fed-Batch Cultures in One Step at Different Cell Culture Times 253
5.5. Semi-empirical mathematical Modelling of the pH in CHO-CY01 Cell Line Cultures 261
5.6. Conclusion 266
Chapter 6 pH Impact on CHO-CY01 Cell Line Kinetics 270
6.1. Introduction and Aims 270
6.2. CHO-CY01 Cell Line Batch Cultures at Different pH values 272
6.3. CHO-CY01 Cell Line Fed-Batch Cultures at Different pH values 280
6.4. pH shifts in CHO-CY01 Cell Line Fed-Batch Cultures 286
6.5. Proteomic Analysis of CHO-CY01 Cell Line Varying Culture pH 296
6.5.1 2D-DIGE Proteomics 296
6.5.2 Protein Identification by Mass Spectrometry 304
6.6. Conclusion 306
Chapter 7 Final Conclusion and Future Work 310
7.1. Final Conclusion 310
7.2. Future Work 319
Chapter 8 References 320
Appendix A: Spearman´s Rank Correlation Coefficient 339
Appendix B: CASY Cell Counter Particle Size Distribution 359
Appendix C: Observed Metabolic Yield Coefficients 387
Appendix D: 5L-STR BIOSTAT Online Data 398
Appendix E: 24-SRW MTP Well-to-Well Reproducibility 410
Appendix F: Annotated 2D-DIGE Gels and Overlapped 2D-DIGE Gels 413
Appendix G: Protein Identification by Mass Spectrometry 416

List of Figures

Figure 1-1: Schematic representation of IgG showing the domain structure, intra- and interchain disulfide bonds, and glycosylation sites. H, heavy chain; L, light chain; V_H, variable-heavy domain; V_L, variable-light domain; C_H, constant-heavy domain; C_L, constant-light domain; Fc, constant region (fragment crystalline); Fab, fragment antigen binding. Image adapted from Burton 1987; Kunkel et al. 2000. 35
Figure 1-2: Values of the energy dissipation rate for various bioreactor environments and its effect on different cell lines. Reproduced from Heath et al. 2007. 41
Figure 1-3: Proteins (mAbs) that will be secreted from the cell enter the secretory pathway via the endoplasmic reticulum (ER) (ribosomes in the ER are depicted as blue dots). As proteins undergo folding and post-modifications within the ER, they are continually monitoring the quality-control systems. The newly modified proteins exit the ER in transport vesicles bound to the Golgi apparatus. Within the Golgi, glycosyltransferase enzymes mediate a vast network of glycosylation reactions (N- and O-glycosylation), resulting in a variety of glycan structures. The finished products are packed into vesicles at the trans-Golgi network (TGN), and from there are transported to the plasma membrane. Figure adapted from Dinnis et al. 2005 and Jacob et al. 2009 42
Figure 1-4: Typical antibody manufacturing process flowsheet with the various processing steps from the bioreactor train through purification. Figure adapted from Birch et al. 2006; Carson 2005 and Gronemeyer et al. 2014. TFF, tangential flow filtration; DFF, direct flow filtration. 44
Figure 1-5: Schematic of CO_2 and ion transfer between gas-liquid interface and cell membrane. Excess of CO_2 can act to inhibit respiration reactions, and may act as an acid poison by crossing membranes and changing intracellular compartment pH (pH_i). 49
Figure 1-6: Schematic diagram of a mammalian cell demonstrating how lactate and ammonia disturb the intracellular pH. Lactate and ammonia are produced inside the cell from glucose and glutamine. Unprotonated lactate (LAC^-) is transported along with a proton. Once outside the cell, the proton is released and the external pH decrease. The intracellular pH is in turn disturbed. Free ammonia escapes the cell quickly, and the charged species NH_4^+ enters the cell down its electrochemical gradient. Figure adapted from Wu et al., 1993. 53
Figure 1-7: Process information output versus experimental throughput capability trade-off for various cell cultivation devices at different scales. It is shown that as bioreactors scale increase, more process information is available due to improved monitoring and control systems. Figure adapted from Betts et al., 2006. 55
Figure 1-8: Commercialised scale-down cell culture systems: SimCell micro bioreactor array (Bareither et al., 2011) (A), Applikon Micro-Flask system (www.applikon-bio.com) (B), Applikon Micro-Matrix system (www.applikon-bio.com) (C), m2p Labs BioLectorTM (www.m2p-labs.com) (D), TPP TubeSpin® Bioreactor (www.tpp.ch) (E), Hexascreen multiple mini-bioreactor system (triplepoint.co.nz) (F), Pall micro24 (www.pall.com) (G), Applikon MiniBioreactor (www.applikon-bio.com) (H), TAP biosystems ambrTM system (www.tapbiosystems.com) (I) and Eppendorf DASbox® Mini Bioreactor (www.eppendorf.com) (J). 57

Figure 1-9: Diagram of individual microwell formats: 96-deep square well format (96-DSW) (A); 24-standard round well format (24-SRW) (B); 96-standard round well format (96-SRW) (C). V_W, total well volume; SA, static surface area available for gas - liquid mass transfer. Figure adapted from Lye et al. (2003). 60
Figure 1-10: Fluid motion and gas-liquid interfacial area available for oxygen transfer of a single-well from a 96-DSW (deep square well) MTP with increasing shaking frequency. Adapted from Micheletti et al., 2006b. 64
Figure 2-1: Schematic diagram of the 24-SRW MTP system components: 24-SRW MTP well dimensions (A), universal cover clamp with four positions where the 24-SRW MTP are placed (B); and schematics of a well closed with the ´system Duetz` lid with the representation of the gas exchange (C). Two ´system Duetz` lid configurations: CR1524 (rigid stainless steel plate, microfiber filter, ePTFE filter, and a soft silicone layer) and CR1524a (rigid stainless steel plate, microfiber filter, ePTFE filter, stainless steel foil, and a hard silicone layer) (D). 68
Figure 2-2: Representation of SDR SensorDish® Reader system components (A): software, splitter, SDR extension set, SDR SensorDish® readers (up to 10 SDR SensorDish® readers, can be used in parallel) and SensorDishes® in 24-well plate format (OxoDish®OD24 and HydroDish®HD24) (B); The SensorDish® can easily be correctly aligned on the SDR SensorDish® Reader due to a groove in the housing of the SDR (C); Measurement principle of the SDR SensorDish® Reader system (D). 79
Figure 2-3: Perspex mimic of a single well for a 24-SRW MTP used for the mixing time studies. 87
Figure 3-1: Fully developed fluid flow hydrodynamics of $850\ \mu L$ of water with $8.5\ \mu L$ of red food dye shaken with an orbital diameter of 25 mm at shaking speed of 100 rpm (below $Ncrit$) (a), 150 rpm (“out-of-phase”) (b), 220 rpm (“in-phase”) (c), and 300 rpm (“in-phase”) (d). 98
Figure 3-2: Fluid flow development of 1.0 mL of water with 10.0 μL of red food dye shaken with an orbital diameter of 25 mm at shaking speed of 300 rpm (“in-phase”). 99
Figure 3-3: Fluid flow development of 2.0 mL of water with 20.0 μL of red food dye shaken with an orbital diameter of 25 mm at shaking speed of 100 rpm (“out-of-phase”). 100
Figure 3-4: Viable cell concentration (A), cell viability (B), and IgG4 concentration (C) profiles for different 24-SRW MTP CHO-CY01 cell batch cultures with different fill volumes (0.50, 0.85, 1.00, 1.50, 2.00, and 2.50 mL) shaken at 220 rpm and, 5.00% (v/v) CO_2 (1 run (3-4 replicates) per fill volume). Error bars represent one standard deviation about the mean. 105
Figure 3-5: Lactate concentration (A), ammonium ion concentration (B), and osmolality (C) profiles for different 24-SRW MTP CHO-CY01 cell batch cultures with different fill volumes (0.50, 0.85, 1.00, 1.50, 2.00, and 2.50 mL) shaken at 220 rpm and, 5.00% (v/v) CO_2 (1 run (3-4 replicates) per fill volume). Error bars represent one standard deviation about the mean. 106
Figure 3-6: Glucose (A) and glutamate (B) concentration-time profiles for different 24-SRW MTP CHO-CY01 cell batch cultures with different fill volumes (0.50, 0.85, 1.00, 1.50, 2.00, and 2.50 mL) shaken at 220 rpm and, 5.00% (v/v) CO_2 (1 run (3-4 replicates) per fill volume). Error bars represent one standard deviation about the mean. 107
Figure 3-7: Viable cell concentration (A), cell viability (B), and IgG4 concentration (C) time profiles for 24-SRW MTP CHO-CY01 cell batch cultures at different shaking speeds (100, 150, 180, 220, 250, and

300 rpm) and 5.00% (v/v) CO_2 (1 run (3-4 replicates) per shaking speed). Error bars represent one standard deviation about the mean. 112
Figure 3-8: Lactate concentration (A), ammonium ion concentration (B), and osmolality (C) time profiles for 24-SRW MTP CHO-CY01 cell batch cultures at different shaking speeds (100, 150, 180, 220, 250, and 300 rpm) and 5.00% (v/v) CO_2 (1 run (3-4 replicates) per shaking speed). Error bars represent one standard deviation about the mean. 113
Figure 3-9: Glucose concentration (A), glutamate concentration (B), and pH (C) time profile for 24-SRW MTP CHO-CY01 cell batch cultures at different shaking speeds (100, 150, 180, 220, 250, 300, and 350 rpm) and 5.00% (v/v) CO_2 (1 run (3-4 replicates) per shaking speed). Error bars represent one standard deviation about the mean. 114
Figure 3-10: Evaporation rate for two different ´system Duetz´ lid configurations for 24-SRW-MTP (CR1524 and CR1524a). The study was performed with 0.85 mL of water shaken at 220 rpm in an orbital diameter of 25 mm at 5.00% (v/v) CO_2. 118
Figure 3-11: Classification of 24-SRW MTP wells by position. (A) ´Corner` wells; (B) ´Edge` wells; (C) ´Internal` wells. 119
Figure 3-12: Evaporation rates for a 24-SRW MTP and the three 24-SRW MTP well classifications. All microwell plates were sealed with a CR1524a ´system Duetz` lid. The study was performed with 0.85 mL of water shaken at 220 rpm in an orbital diameter of 25 mm at 5.00% (v/v) CO_2. 120
Figure 3-13: Viable cell concentration (A), viability (B), IgG4 concentration (C), lactate concentration (D), ammonium ion concentration (E), and osmolality (F) time profiles for 24-SRW MTP CHO-CY01 cell batch cultures sealed with CR1524 and CR1524a ´system Duetz` lids at 2.00% (v/v) CO_2 (1 run (3-4 replicates)). Error bars represent one standard deviation about the mean. 122
Figure 3-14: Viable cell concentration, viability, IgG4 concentration, lactate concentration, ammonium ion concentration, and osmolality time profiles of CHO-CY01 cell batch cultures in a standard 24-SRW MTP and HydroDish®HD24 at 2.00% (v/v) CO_2 (1 run (3-4 replicates)). Error bars represent one standard deviation about the mean. 125
Figure 3-15: Viable cell concentration, viability, IgG4 concentration, lactate concentration, ammonium ion concentration, and osmolality time profiles of CHO-CY01 cell batch cultures in a standard 24-SRW MTP and HydroDish®HD24 at 5.00% (v/v) CO_2 (1 run (3-4 replicates)). Error bars represent one standard deviation about the mean. 126
Figure 3-16: pH profile of CHO-CY01 cell batch cultures in a HydroDish®HD24 at 2.00% (A) and 5.00% (v/v) CO_2 (B) (1 run (24 replicates)). Error bars represent one standard deviation about the mean... 127
Figure 3-17: Viable cell concentration (A), cell viability (B), and IgG4 concentration (C) profiles of 24-SRW MTP CHO-CY01 cell batch cultures with different MSX concentrations (0, 25, 50, and 75 µM) at 5.00% (v/v) CO_2 (1 run (3-4 replicates)). Error bars represent one standard deviation about the mean. 130
Figure 3-18: Glucose concentration (A), glutamate concentration (B), and pH (C) time profile 24-SRW MTP CHO-CY01 cell batch cultures with different MSX concentrations (0, 25, 50, and 75 µM) at 5.00% (v/v) CO_2 (1 run (3-4 replicates)). Error bars represent one standard deviation about the mean. 131

Figure 4-1: Viable cell concentration (A), cell viability (B) and IgG4 concentration (C) profiles for CHO-CY01 cell batch culture at different bioreactor scales: 5L stirred tank (5L-STR) (1 replicate with historical data (p > 0.05)); 24-SRW MTP (3 runs (9-12 replicates)); shake flask with a total volume of 125 mL (SF 125 mL) (2 replicates); and shake flask with a total volume of 250 mL (SF 250 mL) (2 replicates). Standard culture operating conditions were used. Error bars represent one standard deviation about the mean. 139
Figure 4-2: Lactate concentration (A), ammonium ion concentration (B), and osmolality (C) profiles for CHO-CY01 cell batch culture at different bioreactor scales: 5L-STR (1 replicate with historical data); 24-SRW MTP (3 runs (9-12 replicates)); SF 125 mL (2 replicates); and SF 250 mL (2 replicates). Error bars represent one standard deviation about the mean. 140
Figure 4-3: Glucose (A) and glutamate (B) concentration profiles for CHO-CY01 cell batch culture at different bioreactor scales: 5L-STR (1 replicate with historical data); 24-SRW MTP (3 runs (9-12 replicates)); SF 125 mL (2 replicates); and SF 250 mL (2 replicates). Error bars represent one standard deviation about the mean. 141
Figure 4-4: Apoptotic (A) and cell cycle (B) population fractions, and viable cell diameter and IgG4 titer (C) of CHO-CY01 cell batch cultures in 5L-STR (1 replicate) and 24-SRW MTP (3 runs (9-12 replicates)). The error bars show the standard deviation about the mean. 147
Figure 4-5: Representation of a possible GS-CHO cell line lactate metabolism pathway. Highlighted is the lactate intracellular metabolic route in the cell. (A) During lactate production phase, cells produce lactate from glucose glycolysis. The cytosol lactate production causes a transient acidification of the cytosol. Cells use a monocarboxylic transporter that symports a proton to increase the internal pH; (B) With further lactate accumulation, there is lactate dehydrogenase inhibition that stops the cytosol production of the lactate. Lactate consumer (LC) cells use this lactate in the intracellular lactate shuttle to be fully oxidised via TCA cycle and ETC. Diagrams were adapted from Brooks et al., 1999; Gladden 2004 and Philp et al., 2005. 153
Figure 4-6: Schematic diagram indicating the pathways of glutamate metabolism in mammalian cells. Glutamate can be converted to α-ketoglutarate (α-KG) by the energy-producing enzyme glutamate dehydrogenase (GDH) or via one of the transaminase enzymes (primarily via aspartate aminotransferase (AspAT) but also by alanine aminotransferase (AlaAT). α-ketoglutarate formed from glutamate is metabolised via a partial TCA cycle to either malate or oxaloacetate (OAA) (malate-aspartate shuttle). For the complete oxidation of glutamate to occur malate (or OAA) must leave the TCA cycle, be converted to pyruvate by malic enzyme (ME) and then converted to acetyl-CoA by pyruvate dehydrogenase (PDH). The acetyl CoA formed by these pyruvate recycling reactions re-enters the TCA cycle and is subsequently oxidised for energy. Diagram adapted from Gladden 2004 and McKenna 2013. 154
Figure 4-7: Viable cell concentration (A), cell viability (B), and IgG4 concentration (C) profiles for CHO-CY01 cell batch culture at different initial lactate concentrations (0.0, 0.7, 1.9, 2.7, 3.6, and 4.7 $g\ L^{-1}$) (2 replicates per lactate concentration). Error bars represent one standard deviation about the mean. 155

Figure 4-8: Lactate concentration (A), ammonium ion concentration (B), and osmolality (C) profiles for CHO-CY01 cell batch culture at different initial lactate concentrations (0.0, 0.7, 1.9, 2.7, 3.6, and 4.7 $g\ L^{-1}$) (2 replicates per lactate concentration). Error bars represent one standard deviation about the mean. 156
Figure 4-9: Glucose (A) and glutamate (B) concentration profiles for CHO-CY01 cell batch culture at different initial lactate concentrations (0.0, 0.7, 1.9, 2.7, 3.6, and 4.7 $g\ L^{-1}$) (2 replicates per lactate concentration). Error bars represent one standard deviation about the mean. 157
Figure 4-10: Viable cell concentration (A), cell viability (B), and IgG4 concentration (C) profiles for CHO-CY01 cell batch culture at different initial ammonium concentrations (0.2, 4.8, 7.1, 9.7, and 11.2 $mmol\ L^{-1}$) (2 replicates per ammonium concentration). Error bars represent one standard deviation about the mean. 164
Figure 4-11: Lactate concentration (A), ammonium ion concentration (B), and osmolality (C) profiles for CHO-CY01 cell batch culture at different initial ammonium concentrations (0.2, 4.8, 7.1, 9.7, and 11.2 $mmol\ L^{-1}$) (2 replicates per ammonium concentration). Error bars represent one standard deviation about the mean. 165
Figure 4-12: Glucose concentration (A), glutamate concentration (B), and pH (C) profiles for CHO-CY01 cell batch culture at different initial ammonium concentrations (0.2, 4.8, 7.1, 9.7, and 11.2 $mmol\ L^{-1}$) (2 replicates per ammonium concentration). Error bars represent one standard deviation about the mean. The pH values were obtained by NOVA Bioprofile 400 analysis of cell cultures' supernatants at each time point. 166
Figure 4-13: Ammonium and lactate inhibition on CHO-CY01 cell culture kinetic parameters: specific growth rate (A, D); specific cell death rate (B, E); and IgG4 volumetric productivity (C, F). The solid line represents the best curve fitting model. 173
Figure 4-14: Viable cell concentration (A), cell viability (B), and IgG4 concentration (C) profiles for CHO-CY01 cell batch culture at different initial osmolalities (335.42, 310.04, 296.07, 285.92 and, 275.06 $mOsm\ kg^{-1}$) (1 replicate per osmolality). Error bars represent one standard deviation about the mean. 176
Figure 4-15: Lactate concentration (A), ammonium ion concentration (B), and osmolality (C) profiles for CHO-CY01 cell batch culture at different osmolalities (335.42, 310.04, 296.07, 285.92 and, 275.06 $mOsm\ kg^{-1}$) (1 replicate per osmolality). Error bars represent one standard deviation about the mean. 177
Figure 4-16: Definition of a typical pH perturbation amplitude, duration, frequency, and number. Image adapted from (Osman et al., 2002). 182
Figure 4-17: Viable cell concentration, viability, IgG4, lactate, ammonium, glucose and glutamate concentrations, and osmolality profiles for the first fed-batch strategy for CHO CHO-CY01 cell culture in 24-SRW MTP (1 run (3-4 replicates)) shaken under standard conditions (FB_Strategy 1). The arrow indicates when the feeding started. Error bars represent one standard deviation about the mean. .. 183
Figure 4-18: pH and temperature profiles for the first fed-batch strategy for CHO CHO-CY01 cell culture in 24-SRW MTP shaken under standard conditions. In the pH profile, three different peaks were

observed: sampling (A); diluted feed in bicarbonate solution feeding addition (42.5 µL) (B); and diluted feed in water feeding addition (42.5 µL) (C). 185
Figure 4-19: Glucose profiles for the four different fed-batch strategies tested for CHO-CY01 cell cultures in SF 125 mL (2 replicates) and SF 250 mL (2 replicates). The arrow indicates when the feeding started (FB Strategy 3 – blue; FB Strategy 2 and 5 – black; FB Strategy 4 – red). Error bars represent one standard deviation about the mean. 189
Figure 4-20: Viable cell concentration, viability, and IgG4 concentration profiles for the four fed-batch strategies for CHO-CY01 cell fed-batch cultures in SF 125 mL (2 replicates) (A) and SF 250 mL (2 replicates) (B). The arrow indicates when the feeding started (FB Strategy 3 – blue; FB Strategy 2 and 5 – black; FB Strategy 4 – red). Error bars represent one standard deviation about the mean. 190
Figure 4-21: Lactate concentration, ammonium ion concentration, and osmolality profiles for the four fed-batch strategies for CHO-CY01 cell fed-batch cultures in SF 125 mL (2 replicates) (A) and SF 250 mL (2 replicates) (B). The arrow indicates when the feeding started (FB Strategy 3 – blue; FB Strategy 2 and 5 – black; FB Strategy 4 – red). Error bars represent one standard deviation about the mean. 191
Figure 4-22: Viable cell concentration, viability, and IgG4 concentration profiles for CHO-CY01 cell line fed-batch strategy 4 (FB2) (A) and fed-batch strategy 5 (FB3) (B) cultures at different bioreactor scales: 5L-STR (1 replicate); 24-SRW MTP (1 run (3-4 replicates)); SF 125 mL (2 replicates); and SF 250 mL (2 replicates). The culture´s operating conditions were the standard. The arrow indicates when the feeding started (5L-STR – blue; 24-SRW MTP and SF 125 mL – black; SF 250 mL – red (solid line: FB2; dash line: FB3). Error bars represent one standard deviation about the mean. 197
Figure 4-23: Lactate concentration, ammonium ion concentration, and osmolality profiles for CHO-CY01 cell line fed-batch strategy 4 (FB2) (A) and fed-batch strategy 5 (FB3) (B) cultures at different bioreactor scales: 5L-STR (1 replicate); 24-SRW MTP (1 run (3-4 replicates)); SF 125 mL (2 replicates); and SF 250 mL (2 replicates). The arrow indicates when the feeding started (5L-STR – blue; 24-SRW MTP and SF 125 mL – black; SF 250 mL – red (solid line: FB2; dash line: FB3). Error bars represent one standard deviation about the mean. 198
Figure 4-24: Glutamate and glucose concentration profiles for CHO-CY01 cell line fed-batch strategy 4 (FB2) (A) and fed-batch strategy 5 (FB3) (B) cultures at different bioreactor scales: 5L-STR (1 replicate); 24-SRW MTP (1 run (3-4 replicates)); SF 125 mL (2 replicates); and SF 250 mL (2 replicates). The arrow indicates when the feeding started (5L-STR – blue; 24-SRW MTP and SF 125 mL – black; SF 250 mL – red (solid line: FB2; dash line: FB3). Error bars represent one standard deviation about the mean. 199
Figure 5-1: Diagram of mammalian cell pH homeostasis modulators (acid extruders and acid loaders) function. The acid extruders increase the pH_i while acid loaders decrease the pH_i of the cell. Steady-state pH_i depends on the balance between acid extruders (Na^+/H^+ exchanger, Na^+-dependent Cl^-/HCO_3^- antiporter, Na^+/HCO_3^- symporter, and H^+ pump) and acid loaders (Na^+-independent $Cl-/HCO_3^-$ antiporter and $Na+/HCO_3^-$ symporter). Adapted from Boron *(2004)*. 205
Figure 5-2: Viable cell concentration (1), viability (2) and IgG4 concentration (3) profiles for CHO-CY01 cell line batch cultures in 24-SRW-MTP below the standard CO_2 concentration (0.04%, 1.00%, 2.00%

and 5.00% (v/v) CO_2) (A) and above standard CO_2 concentration (5.00%, 10.00%, 15.00% and 20.00% (v/v) $CO2$) (B). Two CHO-CY01 cell line batch cultures runs (4-6 replicates) were done per CO_2 concentration, except for 0.04% and 10.00% (v/v) CO_2 (1 run (3-4 replicates)). Error bars represent one standard deviation about the mean. 215
Figure 5-3: Lactate concentration (4), ammonium ion concentration (5) and, osmolality (6) profiles for CHO-CY01 cell line batch cultures in 24-SRW-MTP below the standard CO_2 concentration (0.04%, 1.00%, 2.00% and 5.00% (v/v) CO_2) (A) and above standard CO_2 concentration (5.00%, 10.00%, 15.00% and 20.00% (v/v) CO_2) (B). Two CHO-CY01 cell line batch cultures runs (4-6 replicates) were done per $CO2$ concentration, except for 0.04% and 10.00% (v/v) CO_2 (1 run (3-4 replicates)). Error bars represent one standard deviation about the mean. 216
Figure 5-4: Glucose (7) and glutamate (8) concentrations profiles for CHO-CY01 cell line batch cultures in 24-SRW-MTP below the standard CO_2 concentration (0.04%, 1.00%, 2.00% and 5.00% (v/v) CO_2) (A) and above standard CO_2 concentration (5.00%, 10.00%, 15.00% and 20.00% (v/v) CO_2) (B). Two CHO-CY01 cell line batch cultures runs (4-6 replicates) were done per CO_2 concentration, except for 0.04% and 10.00% (v/v) CO_2 (1 run (3-4 replicates)) . Error bars represent one standard deviation about the mean. 217
Figure 5-5: Sodium (9) and potassium (10) concentrations profiles for CHO-CY01 cell line batch cultures in 24-SRW-MTP below the standard CO_2 concentration (0.04%, 1.00%, 2.00% and 5.00% (v/v) CO_2) (A) and above standard CO_2 concentration (5.00%, 10.00%, 15.00% and 20.00% (v/v) CO_2) (B). Two CHO-CY01 cell line batch cultures runs (4-6 replicates) were done per CO_2 concentration. Error bars represent one standard deviation about the mean 218
Figure 5-6: CHO-CY01 cell line batch culture pH profiles at 0.04% (A), 1.00% (B), 2.00% (C), 5.00% (D), 10.00% (E), 15.00% (F), and 20.00% (v/v) CO_2 (G). One CHO-CY01 cell line batch cultures run (24 replicates) was done per CO_2 concentration. Error bars represent one standard deviation about the mean. 219
Figure 5-7: Temperature profiles for CHO-CY01 cell line batch cultures at 0.04% (A), 1.00% (B), 2.00% (C), 5.00% (D), 10.00% (E), 15.00% (F), and 20.00% (v/v) CO_2 (G). One CHO-CY01 cell line batch cultures run (24 replicates) was done per CO_2 concentration. Error bars represent one standard deviation about the mean. 220
Figure 5-8: CHO-CY01 cell line batch culture dissolved oxygen, $pO2$ (% Air Saturation) 1.00% (B), 10.00% (E), and 15.00% (v/v) CO_2 (F). One CHO-CY01 cell line batch cultures run (24 replicates) was done per CO_2 concentration. Error bars represent one standard deviation about the mean. 221
Figure 5-9: Graphical representation of the CHO-CY01 cell line batch cultures at different CO_2 atmospheres kinetic parameters (Table 5-3) and observed trendlines. Dash line represent a no variation in the kinetic parameter; Blue line is the trendline for CO_2 atmospheres above 5% (v/v) CO_2; Red line is the trendline for CO_2 atmospheres above 10% (v/v) CO_2; Green line is the trendline for CO_2 atmospheres above 15% (v/v) CO_2. Error bars represent one standard deviation about the mean. 226
Figure 5-10: Apoptotic (A) and cell cycle (B) population fractions and, viable cell diameter and IgG4 titer (C) profiles for CHO-CY01 cell line batch cultures at different CO_2 concentrations (1.00%, 2.00%, 5.00%,

10.00%, 15.00% and 20.00% (v/v) CO_2) accordingly to cell growth phases (lag, exponential, stationary and decline or death phase). The error bars are the standard deviation about the mean. 227
Figure 5-11: Buffer capacity (β) determination of 1x CD-CHO cell culture medium by a similar method used by Jung et al. (2000). From pH online measurement it was possible to determine the pH variation (ΔpH) that a CO_2 shift from atmospheric level to 10.00% (v/v) CO_2 (ΔCO_2) caused and by using Equation 5.2, β was computed. 229
Figure 5-12: Viable cell concentration (A), cell viability (B), IgG4 concentration (C), lactate concentration (D), ammonium concentration (E) and osmolality (F) profiles for CHO-CY01 cell line fed-batch strategy 5 (FB3) cultures in 24-SRW-MTPs at 5.00% (1 run (3-4 replicates)), 10.00% (2 run (6-8 replicates)), and 15.00% (v/v) CO_2 (1 run). The arrow indicates when the feeding started (5.00%– blue; 10.00% – black; 15.00% – red). Error bars represent one standard deviation about the mean. 233
Figure 5-13: Glucose (A), glutamate (B), sodium (C) and potassium (D) concentrations profiles for CHO-CY01 cell line fed-batch strategy 5 (FB3) cultures in 24-SRW-MTPs at 5.00% (1 run (3-4 replicates)), 10.00% (2 run (6-8 replicates)), and 15.00% (v/v) CO_2 (1 run). The arrow indicates when the feeding started (5.00%– blue; 10.00% – black; 15.00% – red). Error bars represent one standard deviation about the mean. 234
Figure 5-14: pH (A) and temperature profiles (B) for CHO-CY01 cell line fed-batch strategy 5 (FB3) cultures in 24-SRW-MTPs at 5.00% (1) (1 runs (24 replicates), 10.00% (2) (2 run (48 replicates), and 15.00% (v/v) CO_2 (3) (1 run (24 replicates)). The arrow indicates when the feeding started (5.00%– blue; 10.00% – black; 15.00% – red). Error bars represent one standard deviation about the mean. 235
Figure 5-15: Decision tree used to control the CHO-CY01 cell line culture pH with exclusively manipulations of CO_2 level inside the CO_2 incubator. The online pH values were obtained from PreSens® software. 240
Figure 5-16: Viable cell concentration (A), cell viability (B), IgG4 concentration (C), lactate concentration (D), ammonium concentration (E) and osmolality (F) profiles for CHO-CY01 cell line batch culture at constant 5.00% (v/v) CO_2 (3 runs (9-12 replicates)) and the first CO_2 multiphasic CHO-CY01 cell line batch cultivation in 24-SRW-MTPs (pH shift 1) (1 run (3-4 replicates)). The dash lines indicate when the CO_2 shifts occurred. The error bars represent one standard deviation about the mean. 241
Figure 5-17: Glucose (A), glutamate (B), sodium (C) and potassium (D) concentrations profiles for CHO-CY01 cell line batch culture at constant 5.00% (v/v) CO_2 (3 runs (9-12 replicates)) and the first CO_2 multiphasic CHO-CY01 cell line batch cultivation in 24-SRW-MTPs (pH shift 1) (1 run (3-4 replicates)). The dash lines indicate when the CO_2 shifts occured. The error bars represent one standard deviation about the mean. 242
Figure 5-18: pH (A) and temperature profiles (B) with CO_2 level profile for the first CO_2 multiphasic CHO-CY01 cell line batch cultivation in 24-SRW-MTPs (pH shift 1). Error bars represent one standard deviation about the mean. 243
Figure 5-19: Apoptotic (A) and cell cycle (B) population fractions, and viable cell diameter and IgG4 titer (C) profiles for the first CO_2 multiphasic CHO-CY01 cell line batch cultivation in 24-SRW-MTPs (pH shift 1) accordingly to phases of cell growth (lag, exponential, stationary and decline or death phase). The error bars are the standard deviation about the mean. 244

Figure 5-20: Viable cell concentration (A), cell viability (B), IgG4 concentration (C), lactate concentration (D), ammonium concentration (E) and osmolality (F) profiles for CHO-CY01 cell line fed-batch strategy 5 (FB3) cultures in 24-SRW-MTPs (1 run (3-4 replicates)) with constant 5.00% (v/v) CO_2, CO_2 shift from 5.00% to 20.00% (v/v) $CO2$ on day 7 (1 step) and $CO2$ shift from 5.00% to 7.50% on day 2, 7.50% to 10.00% on day 7, 10.00% to 12.50% on day 8, and 12.50% to 15.0% (v/v) CO_2 on day 10 (4 steps). The horizontal long dash line and the horizontal dotted lines indicate when the 1 step and 4 steps CO_2 shifts occurred, respectively. The dash lines indicate when the CO_2 shifts occured The arrow indicates when the feeding started (5.00% and 1 step $CO2$ shift – blue; 4-steps CO_2 shift – black). Error bars represent one standard deviation about the mean. 249
Figure 5-21: Glucose (A), glutamate (B), sodium (C) and potassium (D) concentrations profiles for CHO-CY01 cell line fed-batch strategy 5 (FB3) cultures in 24-SRW-MTPs (1 run (3-4 replicates)) with constant 5.00% (v/v) CO_2, $CO2$ shift from 5.00% to 20.00% (v/v) CO_2 on day 7 (1 step) and $CO2$ shift from 5.00% to 7.50% on day 2, 7.50% to 10.00% on day 7, 10.00% to 12.50% on day 8, and 12.50% to 15.0% (v/v) CO_2 on day 10 (4 steps). The horizontal long dash line and the horizontal dotted lines indicate when the 1 step and 4 steps CO_2 shifts occurred, respectively. The arrow indicates when the feeding started (5.00% and 1 step CO_2 shift – blue; 4-steps CO_2 shift – black). Error bars represent one standard deviation about the mean. 250
Figure 5-22: pH (A) and temperature profiles (B) for CHO-CY01 cell line fed-batch strategy 5 (FB3) cultures in 24-SRW-MTPs (1 run (24 replicates)) with constant 5.00% (v/v) CO_2 (1), CO_2 shift from 5.00% to 7.50% on day 2, 7.50% to 10.00% on day 7, 10.00% to 12.50% on day 8, and 12.50% to 15.0% (v/v) $CO2$ on day 10 (4 steps) (2) and CO_2 shift from 5.00% to 20.00% (v/v) CO_2 on day 7 (1 step) (3). The arrow indicates when the feeding started (5.00% and 1 step CO_2 shift – blue; 4-steps CO_2 shift – black. Error bars represent one standard deviation about the mean. 251
Figure 5-23: Viable cell concentration (A), cell viability (B), IgG4 concentration (C), lactate concentration (D), ammonium concentration (E) and osmolality (F) profiles for CHO-CY01 cell line batch culture at constant 10.00% (v/v) CO_2 (2 runs (6-8 replicates)) and CO_2 shifts from 10.00% to 20.00% (v/v) CO_2 at day 3 (1 run (3-4 replicates)), 5 (2 runs) and 9 (1 run). The long dash lines indicate when the CO_2 shifts occurred. The arrow indicates when the feeding started (CO_2 shift at day 9 – blue; 10.00% (v/v) CO_2 and CO_2 shifts at day 5 – black; CO_2 shift at day 3 – red). The error bars represent one standard deviation about the mean. 256
Figure 5-24: Glucose (A), glutamate (B), sodium (C) and potassium (D) concentrations profiles for CHO-CY01 cell line fed-batch strategy 5 (FB3) cultures in 24-SRW-MTPs with constant 10.00% (v/v) CO_2 (2 runs (6-8 replicates)) and CO_2 shifts from 10.00% to 20.00% (v/v) CO_2 at day 3 (1 run (3-4 replicates)), 5 (2 runs) and 9 (1 run). The long dash lines indicate when the CO_2 shifts occurred. The arrow indicates when the feeding started (CO_2 shift at day 9 – blue; 10.00% (v/v) CO_2 and CO_2 shifts at day 5 – black; CO_2 shift at day 3 – red). The error bars represent one standard deviation about the mean. 257
Figure 5-25: pH (A) and temperature profiles (B) for CHO-CY01 cell line fed-batch strategy 5 (FB3) cultures in 24-SRW-MTPs (1 run (24 replicates)) with constant 10.00% (v/v) CO_2 (1) and CO_2 shifts from 10.00% (v/v) CO_2 to 20.00% (v/v) CO_2 at day 3 (2), day 5 (3) and day 9 (4). The arrow indicates when

the feeding started ($CO2$ shift at day 9 – blue; 10.00% (v/v) CO_2 and CO_2 shifts at day 5 – black; CO_2 shift at day 3 – red). The error bars represent one standard deviation about the mean. 258
Figure 5-26: CHO-CY01 cell line batch culture experimental (grey), model 1(solid line) and model 2 (dashed line) pH profiles at 1.00% (A), 2.00% (B), 5.00% (C), 10.00% (D), 15.00% (E) and 20.00% (v/v) CO_2 (F)..... 264
Figure 5-27: CHO-CY01 cell line fed-batch culture experimental (grey), model 1(solid line) and model 2 (dashed line) pH profiles at constant 5.00% (A), 10.00% (B), and 15.00% (v/v) CO_2 (C)..... 265
Figure 5-28: CHO-CY01 cell line fed-batch culture experimental (grey), model 1(solid line) and model 2 (dashed line) pH profiles for CO_2 shift from 10.00% (v/v) CO_2 to 20.00% (v/v) CO_2 on day 3 (A), 5 (B) and 9 (C). 265
Figure 6-1: Viable cell concentration (A), cell viability (B), IgG4 concentration (C), lactate concentration (D), ammonium concentration (E) and osmolality (F) profiles for 5L-STR CHO-CY01 cell line batch cultures at pH 6.80 (1 replicate), pH 7.10 (1 replicate with historical data ($p > 0.05$)) and pH 7.40 (1 replicate). Error bars represent one standard deviation about the mean. 275
Figure 6-2: Glucose (A), glutamate (B), sodium (C) and potassium (D) concentrations profiles for 5L-STR CHO-CY01 cell line batch cultures at pH 6.80 (1 replicate), pH 7.10 (1 replicate with historical data ($p > 0.05$)) and pH 7.40 (1 replicate). Error bars represent one standard deviation about the mean. 276
Figure 6-3: Apoptotic (A) and cell cycle (B) population fractions, and viable cell diameter and IgG4 titer (C) profiles for 5L-STR CHO-CY01 cell line batch cultures at different pHs (6.80, 7.10 and 7.40) accordingly to phases of cell growth (lag, exponential, stationary and decline or death phase). The error bars are the standard deviation about the mean. 277
Figure 6-4: Graphical representation of the 5L-STR CHO-CY01 cell line batch cultures at different pHs (6.80, 7.10 and 7.40) kinetic parameters (Table 6-1) and observed trendlines. Error bars represent one standard deviation about the mean..... 279
Figure 6-5: Viable cell concentration (A), cell viability (B), IgG4 concentration (C), lactate concentration (D), ammonium concentration (E) and osmolality (F) profiles for 5L-STR CHO-CY01 cell line fed-batch strategy 5 (FB3) cultures at pH 6.80, pH 7.10 and pH 7.80 (1 replicate per condition). The arrow indicates when the feeding started (pH 7.80 – blue; pH 7.10– black; pH 6.80 – red). Error bars represent one standard deviation about the mean..... 282
Figure 6-6: Glucose (A), glutamate (B), sodium (C) and potassium (D) concentrations profiles for 5L-STR CHO-CY01 cell line fed-batch strategy 5 (FB3) cultures at pH 6.80, pH 7.10 and pH 7.80 (1 replicate per condition). The arrow indicates when the feeding started (pH 7.80 – blue; pH 7.10– black; pH 6.80 – red). Error bars represent one standard deviation about the mean. 283
Figure 6-7: Graphical representation of the kinetic parameters determined for 5L-STR CHO-CY01 cell line fed-batch cultures at different pHs (6.80, 7.10 and 7.80) (Table 6-2) and observed trendlines. . 285
Figure 6-8: Viable cell concentration (A), cell viability (B), IgG4 concentration (C), lactate concentration (D), ammonium concentration (E) and osmolality (F) profiles for 5L-STR CHO-CY01 cell line fed-batch strategy 5 (FB3) cultures with constant pH 6.80 and pH 7.10, pH shift from pH 6.60 to pH 6.80 on day 2 (pH 6.60 – 6.80 Day 2), and pH shift from pH 7.60 to pH 7.10 on day 4 (pH 7.60 – 7.10 Day 4) (1 replicate per condition). The arrow indicates when the feeding started (pH 7.60 – 7.10 Day 4 – blue; pH

7.10– black; pH 6.80 – red; pH 6.60 – 6.80 Day 2– green). Error bars represent one standard deviation about the mean. 290
Figure 6-9: Glucose (A), glutamate (B), sodium (C) and potassium (D) concentrations profiles for Viable cell concentration (A), cell viability (B), IgG4 concentration (C), lactate concentration (D), ammonium concentration (E) and osmolality (F) profiles for 5L-STR CHO-CY01 cell line fed-batch strategy 5 (FB3) cultures with constant pH 6.80 and pH 7.10, pH shift from pH 6.60 to pH 6.80 on day 2 (pH 6.60 – 6.80 Day 2), and pH shift from pH 7.60 to pH 7.10 on day 4 (pH 7.60 – 7.10 Day 4) (1 replicate per condition). The arrow indicates when the feeding started (pH 7.60 – 7.10 Day 4 – blue; pH 7.10– black; pH 6.80 – red; pH 6.60 – 6.80 Day 2– green). Error bars represent one standard deviation about the mean. .. 291
Figure 6-10: Viable cell concentration (A), cell viability (B), IgG4 concentration (C), lactate concentration (D), ammonium concentration (E) and osmolality (F) profiles for 5L-STR CHO-CY01 cell line fed-batch strategy 5 (FB3) cultures with constant pH 6.80 and pH 7.10, pH shifts from pH 7.10 to pH 6.80 on day 5 (pH 7.10 – 6.80 Day 5) or 8 (pH 7.10 – 6.80 Day 8), and pH shift from pH 7.10 to pH 7.00 on day 4, then to pH 6.80 on day 5 (pH 7.10-7.00-6.80 Day 4/5) (1 replicate per condition). The arrow indicates when the feeding started (pH 7.10 and pH 7.10-7.00-6.80 Day 4/5– black; pH 7.10 – 6.80 Day 8 – blue; pH 7.10 – 6.80 Day 5– green; pH 6.80 - red). Error bars represent one standard deviation about the mean. 292
Figure 6-11: Glucose (A), glutamate (B), sodium (C) and potassium (D) concentrations profiles for 5L-STR CHO-CY01 cell line fed-batch strategy 5 (FB3) cultures with constant pH 6.80 and pH 7.10, pH shifts from pH 7.10 to pH 6.80 on day 5 (pH 7.10 – 6.80 Day 5) or 8 (pH 7.10 – 6.80 Day 8), and pH shift from pH 7.10 to pH 7.00 on day 4, then to pH 6.80 on day 5 (pH 7.10-7.00-6.80 Day 4/5) (1 replicate per condition). The arrow indicates when the feeding started (pH 7.10 and pH 7.10-7.00-6.80 Day 4/5– black; pH 7.10 – 6.80 Day 8 – blue; pH 7.10 – 6.80 Day 5– green; pH 6.80 - red). Error bars represent one standard deviation about the mean. 293
Figure 6-12: SDS-PAGE gel of the supernatant of CHO-CY01 cell line fed-batch culture at pH 7.10. Whole IgG4 antibody (~160 kDa), heavy Chain (~75 kDa), light Chain (~20 kDa) and impurities (~50 kDa). 298
Figure 6-13: Two-dimensional (2-D) fluorescence difference gel electrophoresis (DIGE) of the supernatants from 5L-STR CHO-CY01 cell line fed-batch cultures at different external pHs: pH 6.8 (day 6 (green (Cy3)) and day 8 (red (Cy5))) (A); pH 7.1 (day 4 (green (Cy3)) and day 6 (red (Cy5))) (B); pH shift from pH 7.1 to pH 6.8 on day 5 (day 4 (green (Cy3)) and day 6 (red (Cy5))) (C); and pH shift from pH 7.1 to pH 6.8 day 8 (day 7 (green (Cy3))) and day 9 (red (Cy5))) (D). 299
Figure 6-14: Quantitative analysis of protein content in the supernatants of 5L-STR CHO-CY01 cell line fed-batch cultures at different external pHs: pH 6.8 (day 6 and 8) (A); pH 7.1 (day 4 and 6) (B); pH shift from pH 7.1 to pH 6.8 on day 5 (day 4 and 6) (C); and pH shift from pH 7.1 to pH 6.8 on day 8 (day 7 and 9) (D). The spots indicate a protein difference ratio of 1.5. The protein spots that increased in intensity are represented in blue; the protein spots that did not change are in green; and the protein spots that decreased are in red. LC and HC labels represent light chain and heavy chain, respectively. 300

Figure 6-15: Histograms of spot frequency versus log volume ratio of the supernatants from 5L-STR CHO-CY01 cell line fed-batch cultures at different external pHs: pH 6.8 (day 6 and 8) (A); pH 7.1 (day 4 and 6) (B); pH shift from pH 7.1 to pH 6.8 on day 5 (day 4 and 6) (C); and pH shift from pH 7.1 to pH 6.8 on day 8 (day 7 and 9) (D). The differences between spot volumes were determined using 1.5-fold threshold mode. Blue Spots (increased spots), green spots (similar spots), red spots (decreased spots). 301
Figure 6-16: 2-D DIGE PAGE CHO-CY01 expression maps of 5L-STR CHO-CY01 cell line fed-batch cultures at different external pHs: pH 6.8 (day 6 and 8) (A); pH 7.1 (day 4 and 6) (B); pH shift from pH 7.1 to pH 6.8 on day 5 (day 4 and 6) (C); and pH shift from pH 7.1 to pH 6.8 on day 8 (day 7 and 9) (D). The spots indicate a protein difference ratio of 1.5 between sample points. LC and HC labels represent light chain and heavy chain, respectively. 302
Figure 6-17: 2-D DIGE PAGE CHO-CY01 expression map from 5L-STR CHO-CY01 cell line fed-batch culture with the pH shift from pH 7.10 to pH 6.80 on day 5. The annotated spots were selected for protein identification by mass spectrometry. 303
Figure B-1: CASY cell counter particle size distribution for 24-SRW MTP CHO-CY01 cell batch cultures with different fill volumes: 0.50 (A); 0.85 (B); 1.00 (C) and 1.50 mL (D). 359
Figure B-2: CASY cell counter particle size distribution for 24-SRW MTP CHO-CY01 cell batch cultures at different shaking speeds: 100 (A); 150 (B); 180 (C); 220 (D); 250 (E) and 300 rpm (F). 361
Figure B-3: CASY cell counter particle size distribution for standard CHO-CY01 cell batch culture at different bioreactor scales, 5L-STR (A); 24-SRW MTP (B); SF 125 mL (C) and SF 250 mL (D). 364
Figure B-4: CASY cell counter particle size distribution for CHO-CY01 cell line fed-batch strategy 4 (FB2) cultures at different bioreactor scales, 5L-STR (A); 24-SRW MTP (B); SF 125 mL (C) and SF 250 mL (D). 366
Figure B-5: CASY cell counter particle size distribution for CHO-CY01 cell line fed-batch strategy 5 (FB3) cultures at different bioreactor scales, 5L-STR (A); 24-SRW MTP (B); SF 125 mL (C) and SF 250 mL (D). 368
Figure B-6: CASY cell counter particle size distribution for CHO-CY01 cell line batch cultures in 24-SRW-MTP at different CO_2 (0.04% (A); 1.00% (B); 2.00% (C); 5.00% (D); 10.00% (E); 15.00% (F); and 20.00% (v/v) CO_2 (G)) 370
Figure B-7: CASY cell counter particle size distribution for CHO-CY01 cell line *f*ed batch strategy 5 (FB3) cultures in 24-SRW-MTPs at 5.00% (A), 10.00% (B), and 15.00% (v/v) CO_2 (C). 373
Figure B-8: CASY cell counter particle size distribution for CHO-CY01 cell line batch cultures in 24-SRW-MTPs at constant 5.00% (v/v) CO_2 (A) and the first CO_2 multiphasic culture (pH shift 1) (B). 375
Figure B-9: CASY cell counter particle size distribution for CHO-CY01 cell line fed batch strategy 5 (FB3) cultures in 24-SRW-MTPs with constant 5.00% (v/v) CO_2 (A), CO_2 shift from 5.00% to 20.00% (v/v) CO_2 on day 7 (1 step) (B) and CO_2 shift from 5.00% to 7.50% on day 2, then to 10.00% on day 7, then to 12.50% on day 8, and then to 15.0% (v/v) CO_2 on day 10 (4 steps) (C). 376
Figure B-10: CASY cell counter particle size distribution for CHO-CY01 cell line fed batch strategy 5 (FB3) cultures in 24-SRW-MTPs with constant 10.00% (v/v) CO_2 (A) and CO_2 shifts from 10.00% to 20.00% (v/v) CO_2 at day 3 (B), 5 (C) and 9 (D). 378

Figure B-11: CASY cell counter particle size distribution for 5L-STR CHO-CY01 cell line batch cultures at pH 6.80 (B), 7.10 (A) and 7.40 (C). 380
Figure B-12: CASY cell counter particle size distribution for 5L-STR CHO-CY01 cell line fed-batch strategy 5 (FB3) cultures at pH 6.80 (B), 7.10 (A) and 7.80 (C). 382
Figure B-13: CASY cell counter particle size distribution for 5L-STR CHO-CY01 cell line fed-batch strategy 5 (FB3) cultures with pH shift from pH 6.60 to 6.80 on day 2 (A), and pH shift from pH 7.60 to 7.10 on day 4 (B). 384
Figure B-14: CASY cell counter particle size distribution for 5L-STR CHO-CY01 cell line fed-batch strategy 5 (FB3) cultures with pH shifts from pH 7.10 to 6.80 on day 5 (A) or 8 (C), and pH shift from pH 7.10 to 7.00 on day 4, then to pH 6.80 on day 5 (B). 385
Figure D-1: CHO-CY01 cell line batch culture at pH 7.10 online process parameters, pH (A), pO_2 (% air saturation (% sat)) (B), volume of base added (C), temperature (D), and calculated CO_2 volume percentage (E). 398
Figure D-2: CHO-CY01 cell line batch culture at pH 6.80 online process parameters, pH (A), pO_2 (% air saturation (% sat)) (B), volume of base added (C), temperature (D), and calculated CO_2 volume percentage (E). 399
Figure D-3. CHO-CY01 cell line batch culture at pH 7.40 online process parameters, pH (A), pO_2 (% air saturation (% sat)) (B), volume of base added (C), temperature (D), and calculated CO_2 volume percentage (E). 400
Figure D-4: CHO-CY01 cell line fed-batch strategy 4 (FB2) culture at pH 7.10 online process parameters, pH (A), pO_2 (% air saturation (% sat)) (B), volume of base added (C), temperature (D), and calculated CO_2 volume percentage (E). 401
Figure D-5: CHO-CY01 cell line fed-batch strategy 5 (FB3) culture at pH 7.10 online process parameters, pH (A), pO_2 (% air saturation (% sat)) (B), volume of base added (C), temperature (D), and calculated CO_2 volume percentage (E). 402
Figure D-6: CHO-CY01 cell line fed-batch strategy 5 (FB3) culture at pH 6.80 online process parameters, pH (A), pO_2 (% air saturation (% sat)) (B), volume of base added (C), temperature (D), and calculated CO_2 volume percentage (E). 403
Figure D-7: CHO-CY01 cell line fed-batch strategy 5 (FB3) culture at pH 7.80 online process parameters, pH (A), pO_2 (% air saturation (% sat)) (B), volume of base added (C), temperature (D), and calculated CO_2 volume percentage (E). 404
Figure D-8: CHO-CY01 cell line fed-batch strategy 5 (FB3) culture with pH shift from pH 6.60 to pH 6.80 on day 2 online process parameters, pH (A), pO_2 (% air saturation (% sat)) (B), volume of base added (C), temperature (D), and calculated CO_2 volume percentage (E). 405
Figure D-9: CHO-CY01 cell line fed-batch strategy 5 (FB3) culture with pH shift from pH 7.60 to pH 7.10 on day 4 online process parameters, pH (A), pO_2 (% air saturation (% sat)) (B), volume of base added (C), temperature (D), and calculated CO_2 volume percentage (E). 406
Figure D-10: CHO-CY01 cell line fed-batch strategy 5 (FB3) culture with pH shift from pH 7.10 to pH 6.80 on day 5 online process parameters, pH (A), pO_2 (% air saturation (% sat)) (B), volume of base added (C), temperature (D), and calculated CO_2 volume percentage (E). 407

Figure D-11: CHO-CY01 cell line fed-batch strategy 5 (FB3) culture with pH shift from pH 7.10 to pH 7.00 on day 4, then to pH 6.80 on day 5 online process parameters, pH (A), pO_2 (% air saturation (% sat)) (B), volume of base added (C), temperature (D), and calculated CO_2 volume percentage (E). . 408
Figure D-12: CHO-CY01 cell line fed-batch strategy 5 (FB3) culture with pH shift from pH 7.10 to pH 6.80 at day 8 online process parameters, pH (A), pO_2 (% air saturation (% sat)) (B), volume of base added (C), temperature (D), and calculated CO_2 volume percentage (E). 409
Figure E-1: Normalisation of CHO-CY01 cell line fed-batch culture parameters at the harvest point (day 17), Viable cell concentration (VCC), viability (Viab), osmolality (Osm), pH, IgG4, glutamate (Glu), glucose (Gluc), lactate (Lact), ammonium (Amm), sodium (Na^+), and potassium (K^+) concentrations. The error bars are the standard deviation around the mean. 411
Figure E-2, z-scores of day 17 CHO-CY01 cell line fed-batch culture parameters, Viable cell concentration (VCC), viability, osmolality, pH, IgG4, glutamate, glucose, lactate and ammonium concentrations. For a 95% confidence level, the z-scores are -1.96 and 1.96 (straight solid lines)... 412
Figure F-1: Annotated 2-D DIGE PAGE CHO-CY01 expression maps of 5L-STR runs at different external pHs. pH 6.8 (A); pH 7.1 (B); day 5 pH shift from pH 7.1 to pH 6.8 (C); day 8 pH shift from pH 7.1 to pH 6.8 (D). The spots indicate a protein difference ratio of 1.5 between sample points. 413
Figure F-2: Image overlapping of the 2-D DIGE PAGE CHO-CY01 expression maps of 5L-STR CHO-CY01 cell line fed-batch cultures at different external pHs: pH 6.8 and pH 7.10 (A); pH 6.80 and pH shift from pH 7.1 to pH 6.8 on day 5 (B); pH 7.10 and pH shift from pH 7.1 to pH 6.8 on day 5 (C); pH shift from pH 7.1 to pH 6.8 on day 5 and pH shift from pH 7.1 to pH 6.8 on day 8 (D). The boxes are a visual indication of the overlapped spots. 414

List of Tables

Table 1-1: Characteristics and functional properties of human antibody isotypes (IgG1, IgG2, IgG3, IgG4, IgM, IgA1, IgA2, IgD, and IgE). Table adapted from Dijk et al. 2001. 36
Table 1-2: Examples of *in vivo* and *in-vitro* antibodies applications. Adapted from Roque et al., 2004. 37
Table 1-3: Monoclonal antibodies and related proteins on the market. Table adapted from Hale 2006; Rodrigues et al. 2009; Shukla et al. 2010 and FDA website. 38
Table 1-4: Summary of antibody expression systems. Table adapted from Chadd et al. 2001.Ch, chimeric; Hu, human; Hz, humanized; Mu, murine; S, secretory..... 39
Table 2-1: Specifications of the two CR1524 and CR1524a (Low-evaporation version of CR1524) ´System Duetz` lids[2]..... 68
Table 2-2: Chromatography method for IgG4 detection by Protein G HPLC 73
Table 2-3: Reagents and equipment used for 2D-DIGE proteomics analysis. 78
Table 2-4: Specifications and properties of HydroDish®HD24 and OXODish®OD24 plates[5]. 80
Table 2-5: Features of Phantom v7.1 high-speed camera 87
Table 3-1: 24-SRW MTP liquid-phase hydrodynamics. Critical shaken frequency (N_{crit}) Reynolds number (Re), Froude number (Fr), and Phase number (Ph) numbers for different fill volumes (V_L) and shaking speeds (N) in a 24-SRW MTP. All dimensionless numbers were calculated as described in Section 2.4.1. The value for surface tension used was 61 ($dyne\ cm^{-1}$) (Michaelis et al., 1995). Shaded in grey are the “in-phase” regions. 92
Table 3-2: Mean volumetric oxygen mass transfer coefficient (k_La) predicted for a 24-SRW MTP covered with ´system Duetz´ lids. Shaded in grey are the k_La values above 1 h^{-1}. 94
Table 3-3: 24-SRW MTP mixing times (t_m) in seconds at different shaking speed rates and fill volumes. 101
Table 3-4: Kinetic parameters determined for different 24-SRW MTP CHO-CY01 cell batch culture with different fill volumes (0.50, 0.85, 1.00 and, 1.50 mL) shaken at 220 rpm and, 5.00% (v/v) CO_2..... 108
Table 3-5: Kinetic parameters determined for different 24-SRW MTP CHO-CY01 cell batch cultures at different shaking speeds (100, 150, 180, 220, 250, and 300 rpm) at 5.00% (v/v) CO_2. The error represents one standard deviation about the mean. 115
Table 3-6: Kinetic parameters of 24-SRW MTP CHO-CY01 cell batch cultures sealed with CR1524 and CR1524a ´system Duetz` lids at 2.00% (v/v) CO_2. The error represents one standard deviation about the mean. 123
Table 3-7: Kinetic parameters of CHO-CY01 cell batch cultures in a standard 24-SRW MTP and HydroDish®HD24 at 2.00% CO_2 and 5.00% (v/v) CO_2. The error represents one standard deviation about the mean. 128
Table 3-8: Kinetic parameters of 24-SRW MTP CHO-CY01 cell batch cultures with different MSX concentrations (0, 25, 50, and 75 μM) at 5.00% (v/v) CO_2. The error represents one standard deviation about the mean. 132

Table 4-1: Comparison of scale translation criteria (mixing time, mean energy dissipation rate and $k_L a$) for CHO-CY01 cell line cultures in 24-SRW MTP, SF 125 mL, SF 250 mL and 5-L STR bioreactors at the experimental conditions used. 136
Table 4-2: Kinetic parameters determined for CHO-CY01 cell batch culture at different bioreactor scales: 5L-STR; 24-SRW MTP; SF 125 mL, and SF 250 mL. 142
Table 4-3: Kinetic parameters determined for CHO-CY01 cell batch culture at different initial lactate concentrations (0.0, 0.7, 1.9, 2.7, 3.6, and 4.7 $g\ L^{-1}$). 158
Table 4-4: Kinetic parameters determined for CHO-CY01 cell batch culture at different initial ammonium concentrations (0.2, 4.8, 7.1, 9.7, and 11.2 $mmol\ L^{-1}$). 167
Table 4-5: Ammonium and lactate inhibition kinetic parameters estimated by nonlinear curve fitting method. 172
Table 4-6: Kinetic parameters determined for CHO-CY01 cell batch culture at different initial osmolalities. 178
Table 4-7: Kinetic parameters determined for the first fed-batch strategy (FB_Strategy 1) for CHO CHO-CY01 cell culture in 24-SRW MTP shaken under the standard. 184
Table 4-8: Amplitude and duration of the three types of pH perturbations in the first fed-batch strategy for CHO CHO-CY01 cell culture in 24-SRW MTP shaken under standard conditions with the pH values before and after the pH perturbation. 185
Table 4-9: Kinetic parameters determined for the four fed-batch strategies for CHO-CY01 cell fed-batch cultures in SF 125 mL and SF 250 mL. 191
Table 4-10: Glucose and glutamate consumption rates during feeding for CHO-CY01 cell line fed-batch Strategy 4 (FB2) and fed-batch Strategy 5 (FB3) cultures at different bioreactor scales: 5L-STR; 24-SRW MTP; SF 125 mL and SF 250 mL. 200
Table 4-11: Kinetic parameters determined for CHO-CY01 cell line fed-batch Strategy 4 (FB2) (A) and fed-batch Strategy 5 (FB3) (B) cultures at different bioreactor scales: 5L-STR and; 24-SRW MTP. . 200
Table 5-1: Initial air composition inside the CO_2 incubator and the average and standard deviation values for the process parameters: pH, temperature and dissolved oxygen obtained during CHO-CYO1 cell line batch culture at different CO_2 levels. The initial dissolved CO_2, pCO_2 (mmHg) was computed by multiplying 7.2 to CO_2 (% (v/v)). 222
Table 5-2: Amplitude and duration of the sampling pH perturbation for CHO-CY01 cell line batch cultures in 24-SRW-MTP at different CO_2 concentrations (0.04%, 1.00%, 2.00%, 5.00%, 10.00%, 15.00% and 20.00% (v/v) CO_2). 223
Table 5-3: Kinetic parameters determined for CHO-CY01 cell line batch cultures in 24-SRW-MTP at different CO_2 concentrations (0.04%, 1.00%, 2.00%, 5.00%, 10.00%, 15.00% and, 20.00% (v/v) CO_2). 224
Table 5-4: Average and standard deviation values of process parameters: pH and temperature; glucose and glutamate consumption rates in fed-batch mode, and amplitude and duration of the first feeding pH perturbation for CHO-CY01 cell line fed-batch strategy 5 (FB3) cultures in 24-SRW-MTPs at 5.00%, 10.00%, and 15.00% (v/v) CO_2. The pH perturbations parameters were determined as described in the Section 4.4.1. 236

Table 5-5: Kinetic parameters determined for CHO-CY01 cell line fed-batch strategy 5 (FB3) cultures in 24-SRW-MTPs at 5.00%, 10.00%, and 15.00% (v/v) CO_2. 237
Table 5-6: Kinetic parameters determined for CHO-CY01 cell line batch culture at constant 5.00% (v/v) CO_2 and the first CO_2 multiphasic CHO-CY01 cell line batch cultivation in 24-SRW-MTPs (pH shift 1). 245
Table 5-7: Kinetic parameters determined for CHO-CY01 cell line fed-batch strategy 5 (FB3) cultures in 24-SRW-MTPs with constant 5.00% (v/v) CO_2, CO_2 shift from 5.00% to 20.00% (v/v) CO_2 on day 7 (1 step) and CO_2 shift from 5.00% to 7.50% (v/v) CO_2 on day 2, then to 10.00% on day 7, then to CO_2 on day 8, and then to 15.0% (v/v) CO_2 on day 10 (4 steps). 252
Table 5-8: Kinetic parameters determined for CHO-CY01 cell line fed-batch strategy 5 (FB3) cultures in 24-SRW-MTPs with constant 10.00% (v/v) CO_2 and CO_2 shifts from 10.00% to 20.00% (v/v) CO_2 at day 3, 5 and 9. 259
Table 5-9: Average and standard deviation values of process parameters: pH and temperature, and glucose and glutamate consumption rates on fed-batch mode for CHO-CY01 cell line fed-batch strategy 5 (FB3) cultures in 24-SRW-MTPs with different CO_2 shifts. 260
Table 6-1: Kinetic parameters determined for 5L-STR CHO-CY01 cell line batch cultures at different pH values (6.80, 7.10 and 7.40). 278
Table 6-2: Kinetic parameters determined for 5L-STR CHO-CY01 cell line fed-batch strategy 5 (FB3) cultures at pH 6.80, pH 7.10 and pH 7.80. 284
Table 6-3: Kinetic parameters determined for the 5L-STR CHO-CY01 cell line fed-batch cultures with pH shift from pH 6.60 to pH 6.80 on day 2, pH shift from pH 7.60 to pH 7.10 on day 4, pH shift pH 7.10 to pH 6.80 on day 5 or 8, and pH shift from pH 7.10 to pH 7.00 on day 4, then to pH 6.80 on day 5. 294
Table 6-4: Values for the process parameters (pH, $pO2$, temperature, CO_2, base), and daily glucose and glutamate consumption rates on fed-batch mode for all 5L-STR CHO-CY01 cell line cultures at different pHs. 295
Table 6-5: Quantitative analysis of two-dimensional (2-D) fluorescence difference gel electrophoresis (DIGE) of the supernatants from 5L-STR CHO-CY01 cell line fed-batch cultures at different external pHs: pH 6.8 (day 6 and 8); pH 7.1 (day 4 and 6); pH shift from pH 7.1 to pH 6.8 on day 5 (day 4 and 6); and pH shift from pH 7.1 to pH 6.8 on day 8 (day 7 and 9). The differences between spot volumes were determined using 1.5-fold threshold mode. 301
Table 6-6: Characterisation of the selected 2D-DIGE gel spots from day 4 and day 6 of 5L-STR pH shift from pH 7.1 to pH 6.8 on day 5. 303
Table 6-7: Hit number, protein name, organism, gene name, score, coverage (%), calculated mass, calculated pI, molecular function and biological process of the seven annotated protein spots chosen to be identified (www.uniprot.org/). In brackets is the volume ratio. 305
Table 7-1: Impact of different initial lactate concentrations on CHO-CY01 cell line kinetics. 314
Table 7-2: Impact of different ammonium concentrations on CHO-CY01 cell line kinetics. 314
Table 7-3: Impact of different pH values on CHO-CY01 cell line growth, metabolism and IgG4 productivity obtained from the CO_2 study in 24-SRW MTPs. 315

Table A-1: Spearman´s rank correlation coefficients (*r*) determined for 24-SRW MTP CHO-CY01 cell batch cultures with different fill volumes (0.50, 0.85, 1.00 and 1.50 mL).....340
Table A-2: Spearman´s rank correlation coefficients (*r*) determined for 24-SRW MTP CHO-CY01 cell batch cultures at different shaking speeds (100, 150, 180, 220, 250 and 300 rpm).....341
Table A-3: Spearman´s rank correlation coefficients (*r*) determined for 24-SRW MTP CHO-CY01 cell batch cultures sealed with CR1524 and CR1524a ´system Duetz` lids at 2.00% CO_2.....342
Table A-4: Spearman´s rank correlation coefficients (*r*) determined for CHO-CY01 cell batch in a standard 24-SRW MTP and in HydroDish®HD24 at 5.00% CO_2.....342
Table A-5: Spearman´s rank correlation coefficients (*r*) determined for CHO-CY01 cell batch in a standard 24-SRW MTP and in HydroDish®HD24 at 2.00% CO_2.....343
Table A-6: Spearman´s rank correlation coefficients (*r*) determined of 24-SRW MTP CHO-CY01 cell batch cultures with different MSX concentrations (0, 25, 50 and 75 µM).....343
Table A-7: Spearman´s rank correlation coefficients (*r*) determined for CHO-CY01 cell batch culture at different bioreactor scales, 5L-STR; 24-SRW MTP; SF 125 mL and SF 250 mL.....344
Table A-8: Spearman´s rank correlation coefficients (*r*) determined for CHO-CY01 cell batch culture at different initial lactate concentrations (0.0, 0.7, 1.9, 2.7, 3.6 and 4.7 $g\ L^{-1}$).....345
Table A-9: Spearman´s rank correlation coefficients (r) determined for CHO-CY01 cell batch culture at different initial ammonium concentrations (0.2, 4.8, 7.1, 9.7 and 11.2 $mmol\ L^{-1}$).....346
Table A-10: Spearman´s rank correlation coefficients (*r*) determined for CHO-CY01 cell batch culture at different initial sodium concentrations (95, 99, 103, 108 and 118 $mmol\ L^{-1}$).....347
Table A-11: Spearman´s rank correlation coefficients (*r*) determined for different CHO-CY01 cell fed-batch cultures in SF 125 mL and SF 250 mL.....348
Table A-12: Spearman´s rank correlation coefficients (*r*) determined for CHO-CY01 cell line fed-batch strategy 4 (FB2) and fed-batch strategy 5 (FB3) cultures at different bioreactor scales, 5L-STR; 24-SRW MTP; SF 125 mL and SF 250 mL.....349
Table A-13: Spearman´s rank correlation coefficients (*r*) determined for profiles for CHO-CY01 cell line batch cultures in 24-SRW-MTP at different CO_2 (0.04%; 1.00%; 2.00%; 10.00%; 15.00%; and 20.00% (v/v) CO_2).....350
Table A-14: Spearman´s rank correlation coefficients (r) determined for CHO-CY01 cell *line f*ed batch strategy 5 (FB3) cultures in 24-SRW-MTPs at 5.00%, 10.00%, and 15.00% (v/v) CO_2.....351
Table A-15: Spearman´s rank correlation coefficients (*r*) determined for CHO-CY01 cell line batch culture at constant 5.00% (v/v) CO_2 and the first CO_2 multiphasic CHO-CY01 cell line batch cultivation in 24-SRW-MTPs (pH shift 1).....352
Table A-16: Spearman´s rank correlation coefficients (*r*) determined for CHO-CY01 cell line fed batch strategy 5 (FB3) cultures in 24-SRW-MTPs with constant 5.00% (v/v) CO_2, CO_2 shift from 5.00% to 20.00% (v/v) CO_2 on day 7 (1 step) and CO_2 shift from 5.00% to 7.50% on day 2, then to 10.00% on day 7, then to 12.50% on day 8, and then to 15.0% (v/v) CO_2 on day 10 (4 steps).....353
Table A-17: Spearman´s rank correlation coefficients (r) determined CHO-CY01 cell line fed batch strategy 5 (FB3) cultures in 24-SRW-MTPs with constant 10.00% (v/v) CO_2 and CO_2 shifts from 10.00% to 20.00% (v/v) CO_2 at day 3, 5 and 9.....354

Table A-18: Spearman´s rank correlation coefficients (*r*) determined for 5L-STR CHO-CY01 cell line batch cultures at different pHs (pH 6.80, 7.10 and 7.40). 355
Table A-19: Spearman´s rank correlation coefficients (*r*) determined for 5L-STR CHO-CY01 cell line fed-batch strategy 5 (FB3) cultures at pH 6.80, 7.10 and 7.80. 356
Table A-20: Spearman´s rank correlation coefficients (*r*) determined for 5L-STR CHO-CY01 cell line fed-batch strategy 5 (FB3) cultures with pH shift from pH 6.60 to 6.80 on day 2, and pH shift from pH 7.60 to 7.10 on day 4. 357
Table A-21: Spearman´s rank correlation coefficients (r) determined for 5L-STR CHO-CY01 cell line fed-batch strategy 5 (FB3) cultures with pH shifts from pH 7.10 to 6.80 on day 5 or 8, and pH shift from pH 7.10 to 7.00 on day 4, then to pH 6.80 on day 5. 358
Table B-1: Viable cell number (VCN); cell diameter, viability, larger particles (> 40 µm), dead cells (7.6 – 12.8 µm), debris (< 7.6 µm) and total impurities in each stage of 24-SRW MTP CHO-CY01 cell batch cultures with different fill volumes (0.50, 0.85, 1.00 and 1.50 mL)..... 360
Table B-2: VCN; cell diameter, viability, larger particles, dead cells, debris and total impurities in each stage of 24-SRW MTP CHO-CY01 cell batch cultures in 24-SRW MTP at different shaking speeds (100, 150, 180, 220, 250 and 300 rpm). 363
Table B-3: VCN; cell diameter, viability, larger particles, dead cells, debris and total impurities for standard CHO-CY01 cell batch culture at different bioreactor scales, 5L-STR; 24-SRW MTP; SF 125 mL and SF 250 mL..... 365
Table B-4: VCN; cell diameter, viability, larger particles, dead cells, debris and total impurities for CHO-CY01 cell line fed-batch strategy 4 (FB2) cultures at different bioreactor scales, 5L-STR; 24-SRW MTP; SF 125 mL and SF 250 mL. 367
Table B-5: VCN; cell diameter, viability, larger particles, dead cells, debris and total impurities for CHO-CY01 cell line fed-batch strategy 5 (FB3) cultures at different bioreactor scales, 5L-STR; 24-SRW MTP; SF 125 mL and SF 250 mL. 369
Table B-6: VCN; cell diameter, viability, larger particles, dead cells, debris and total impurities for CHO-CY01 cell line batch cultures in 24-SRW-MTP at different $CO2$ (0.04%; 1.00%; 2.00%; 5.00%; 10.00%; 15.00%; and 20.00% (v/v) CO_2). 372
Table B-7: VCN, cell diameter, viability, larger particles, dead cells, debris and total impurities for CHO-CY01 cell line *f*ed batch strategy 5 (FB3) cultures in 24-SRW-MTPs at 5.00%, 10.00%, and 15.00% (v/v) CO_2. 374
Table B-8: VCN, cell diameter, viability, larger particles, dead cells, debris and total impurities for CHO-CY01 cell line batch cultures in 24-SRW-MTPs at constant 5.00% (v/v) CO_2 and pH shift 1. 375
Table B-9: VCN, cell diameter, viability, larger particles, dead cells (µm), debris and total impurities for CHO-CY01 cell line fed batch strategy 5 (FB3) cultures in 24-SRW-MTPs with constant 5.00% (v/v) CO_2, CO_2 shift from 5.00% to 20.00% (v/v) CO_2 on day 7 (1 step) and CO_2 shift from 5.00% to 7.50% on day 2, then to 10.00% on day 7, then to 12.50% on day 8, and then to 15.0% (v/v) CO_2 on day 10 (4 steps)..... 377

Table B-10: VCN, cell diameter, viability, larger particles, dead cells (µm), debris and total impurities for CHO-CY01 cell line fed batch strategy 5 (FB3) cultures in 24-SRW-MTPs with constant 10.00% (v/v) CO_2 and CO_2 shifts from 10.00% to 20.00% (v/v) CO_2 at day 3, 5 and 9. 379
Table B-11: VCN, cell diameter, viability, larger particles, dead cells (µm), debris and total impurities for 5L-STR CHO-CY01 cell line batch cultures at different pHs (pH 6.80, 7.10 and 7.40). 381
Table B-12: VCN, cell diameter, viability, larger particles, dead cells (µm), debris and total impurities for 5L-STR CHO-CY01 cell line fed-batch strategy 5 (FB3) cultures at pH 6.80, 7.10 and 7.80. 383
Table B-13: VCN, cell diameter, viability, larger particles, dead cells (µm), debris and total impurities for 5L-STR CHO-CY01 cell line fed-batch strategy 5 (FB3) cultures with pH shift from pH 6.60 to 6.80 on day 2, and pH shift from pH 7.60 to 7.10 on day 4. 384
Table B-14: VCN, cell diameter, viability, larger particles, dead cells (µm), debris and total impurities for 5L-STR CHO-CY01 cell line fed-batch strategy 5 (FB3) cultures with pH shifts from pH 7.10 to 6.80 on day 5 or 8, and pH shift from pH 7.10 to 7.00 on day 4, then to pH 6.80 on day 5. 386
Table C-1: $Y'_{P/S}$ for different 24-SRW MTP CHO-CY01 cell batch cultures fill volumes (0.50, 0.85, 1.00 and 1.50 mL). 387
Table C-2: $Y'_{P/S}$ for different 24-SRW MTP CHO-CY01 cell batch cultures at different shaking speeds (100, 150, 180, 220, 250 and 300 rpm) 387
Table C-3: $Y'_{P/S}$ for 24-SRW MTP CHO-CY01 cell batch cultures sealed with CR1524 and CR1524a ´system Duetz` lids at 2.00% (v/v) CO_2. 388
Table C-4: $Y'_{P/S}$ for CHO-CY01 cell batch in a standard 24-SRW MTP and in HydroDish®HD24 at 5.00% (v/v) CO_2. 388
Table C-5: $Y'_{P/S}$ for CHO-CY01 cell batch in a 24-SRW MTP and in HydroDish®HD24 at 2.00% (v/v) CO_2. 388
Table C-6: $Y'_{P/S}$ for 24-SRW MTP CHO-CY01 cell batch cultures with different MSX concentrations (0, 25, 50 and 75 µM). 389
Table C-7: $Y'_{P/S}$ for standard CHO-CY01 cell batch culture at different bioreactor scales, 5L-STR; 24-SRW MTP; SF 125 mL and SF 250 mL. 389
Table C-8: $Y'_{P/S}$ for CHO-CY01 cell batch culture at different initial lactate concentrations (0*.0*, *0.7*, *1.9*, *2.7*, *3.6 and 4.7* g L^{-1}). 390
Table C-9: $Y'_{P/S}$ for CHO-CY01 cell batch culture at different initial ammonium concentrations (0.2, 4.8, 7.1, 9.7 and 11.2 $mmol\ L^{-1}$). 391
Table C-10: $Y'_{P/S}$ for CHO-CY01 cell batch culture at different initial sodium concentrations (95, 99, 103, 108 and 118 $mmol\ L^{-1}$). 391
Table C-11: $Y'_{P/S}$ for CHO-CY01 cell line fed-batch strategy 4 (FB2) and fed-batch strategy 5 (FB3) cultures at different bioreactor scales, 5L-STR; 24-SRW MTP; SF 125 mL and SF 250 mL. 392
Table C-12: $Y'_{P/S}$ for CHO-CY01 cell line batch cultures in 24-SRW-MTP at different CO_2 (0.04%; 1.00%; 2.00%; 5.00%, 10.00%; 15.00%; and 20.00% (v/v) CO_2) 393
Table C-13: $Y'_{P/S}$ for CHO-CY01 cell *line f*ed batch strategy 5 (FB3) cultures in 24-SRW-MTPs at 5.00%, 10.00%, and 15.00% (v/v) CO_2 394

Table C-14: $Y'_{P/S}$ for CHO-CY01 cell line batch culture at constant 5.00% (v/v) CO_2 and the first CO_2 multiphasic CHO-CY01 cell line batch cultivation in 24-SRW-MTPs (pH shift 1). 394
Table C-15: $Y'_{P/S}$ for CHO-CY01 cell line fed batch strategy 5 (FB3) cultures in 24-SRW-MTPs with constant 5.00% (v/v) CO_2, CO_2 shift from 5.00% to 20.00% (v/v) CO_2 on day 7 (1 step) and CO_2 shift from 5.00% to 15.0% (v/v) CO_2 10 (4 steps). 395
Table C-16: $Y'_{P/S}$ for CHO-CY01 cell line fed batch strategy 5 (FB3) cultures in 24-SRW-MTPs with constant 10.00% (v/v) CO_2 and CO_2 shifts from 10.00% to 20.00% (v/v) CO_2 at day 3, 5 and 9. 395
Table C-17: $Y'_{P/S}$ for 5L-STR CHO-CY01 cell line batch cultures at different pHs (pH 6.80, 7.10 and 7.40). 396
Table C-18: $Y'_{P/S}$ for 5L-STR CHO-CY01 cell line fed-batch strategy 5 (FB3) cultures at pH 6.80, 7.10 and 7.80. 396
Table C-19: $Y'_{P/S}$ for 5L-STR CHO-CY01 cell line fed-batch strategy 5 (FB3) cultures with pH shift from pH 6.60 to 6.80 on day 2, pH shift from pH 7.60 to 7.10 on day 4, with pH shifts from pH 7.10 to 6.80 on day 5 or 8, and pH shift from pH 7.10 to 7.00 on day 4, then to pH 6.80 on day 5. 397
Table F-1: Annotation number of overlapped spots from Figure F-2 with volume ratio in brackets. The highlight spots indicate the spots chosen for protein identification. 415
Table G-1: Detailed description of the mass spectrometry conditions performed at each 2D-DIGE gel spot analysed. 416
Table G-2: Spot 344 protein ´hits` list with protein description (prot_desc), score, threshold (prot_thresh), mass, coverage (prot_cov) and pI. 417
Table G-3: Spot 344 protein identification short-list. 419
Table G-4: Spot 511 protein ´hits` list. 420
Table G-5: Spot 511 protein identification short-list. 422
Table G-6: Spot 581 protein ´hits` list. 423
Table G-7: Spot 581 protein identification short-list. 424
Table G-8: Spot 947 protein ´hits` list 425
Table G-9: Spot 947 protein identification short-list 426
Table G-10: Spot 1005 protein ´hits` list. 427
Table G-11: Spot 1005 protein identification short-list. 428
Table G-12: Spot 1282 protein ´hits` list. 429
Table G-13: Spot 1282 protein identification short-list. 430
Table G-14: Spot 1292 protein ´hits` list. 431
Table G-15: Spot 1282 protein identification short-list. 432

Abbreviations and Symbols

2D-DIGE	Two-dimensional Difference gel electrophoresis
2D-PAGE	Two-dimensional gel electrophoresis
Ab	Antibody
ADP	Adenosine diphosphate
a_i	Initial air-liquid specific surface area (m^{-1})
Amm	Ammonium concentration ($mmol\ L^{-1}$)
ATP	Adenosine triphosphate
BHK	Baby hamster kidney
Bo	Bond number
BP	Band pass
$cAmm$	Cumulative ammonium produced ($mmol\ L^{-1}$)
CDR	Complementary determining region
CER	Carbon dioxide evolution rate
CFD	Computational fluid dynamics
$CF_{V(t_i)}$	Volume-correction factor
$cGlu$	Cumulative glutamate consumed ($mmol\ L^{-1}$
$cGluc$	Cumulative glucose consumed ($g\ L^{-1}$)
Ch	Chimeric
C_H	Constant region of the heavy chain
CHO	Chinese hamster ovary
cK^+	Cumulative potassium consumed ($mmol\ L^{-1}$)
C_L	Constant-light domain
$cLact$	Cumulative lactate concentration ($g\ L^{-1}$)
cNa^+	cumulative sodium consumed ($mmol\ L^{-1}$)
CoGs	Process cost of goods
d_f	Maximum inner flask diameter (m)
D_{O_2}	Oxygen diffusion coefficient ($m^2 s^{-1}$)
DOT	Dissolved oxygen tension
d_s	Orbital diameter of the shaker platform (mm)
d_W	Microwell diameter (mm)
E. coli	*Escherichia coli*
ELISA	Enzyme-linked Immunosorbent Assay
ER	Endoplasmatic reticulum
Fab	Fab antigen-binding fragment
Fc	Constant region (fragment crystalline);
FDA	FDA Food and Drug Administration
Fv	Variable-region fragment
FFr	Froude number

g	Acceleration due to gravity ($m\ s^{-2}$)
Glu	Glutamate concentration ($mmol\ L^{-1}$)
Gluc	Glucose concentration ($g\ L^{-1}$)
GMP	GMP good manufacturing practice
GN	Gene Name
H, HC	Heavy chain
HCP	Host cell proteins
HT	High-throughput
hTSH	Human thyroid-stimulating hormone
Hu	Human
Hz	Humanized
IEF	Isoelectric focusing
IgG	Immunoglobulin of class G
$IgG4_{produced}\ (t$	Cumulative IgG4 concentration produced ($mg\ L^{-1}$)
IVCC	Integral viable cell concentration ($10^9\ cells\ day\ L^{-1}$)
$K_{a,CA}$	Acid dissociation of carbonic acid
K_{a2}	Second acid dissociation of carbonic acid
k_d	Maximum cell death rate absolute value (h^{-1})
$K_{Di,Amm}$	Half-maximum-rate concentration of ammonium for cell death rate ($mmol\ L^{-1}$)
$K_{Di,Glu}$	Half-maximum-rate concentration of glutamate for cell death rate ($mmol\ L^{-1}$)
$K_{Di,Gluc}$	Half-maximum-rate concentration of glucose for cell death rate ($g\ L^{-1}$)
$K_{Di,Lact}$	Half-maximum-rate concentration of lactate for cell death rate ($g\ L^{-1}$)
$K_{i,Amm}$	Half-maximum-rate concentration of ammonium for cell growth rate ($mmol\ L^{-1}$)
$K_{i,Glu}$	half-maximum-rate concentration of glutamate for cell growth rate ($mmol\ L^{-1}$)
$K_{i,Gluc}$	half-maximum-rate concentration of glucose for cell growth rate ($g\ L^{-1}$)
$K_{i,Lact}$	Half-maximum-rate concentration of lactate for cell growth rate ($g\ L^{-1}$)
$k_L a$	Oxygen mass transfer coefficients (h^{-1})
$K_{P,Amm}$	Half-maximum-rate concentration of ammonium for IgG4 production rate ($mmol\ L^{-1}$)
$K_{P,Glu}$	Half-maximum-rate concentration of glutamate for IgG4 production rate ($mmol\ L^{-1}$)
$K_{P,Gluc}$	Half-maximum-rate concentration of glucose for IgG4 production rate ($g\ L^{-1}$)
$K_{P,Lact}$	Half-maximum-rate concentration of lactate for IgG4 production rate ($g\ L^{-1}$)
K_S	Saturation constant for substrate
L, LC	Light chain
Lac^-	Unprotonated lactate
LC-MS/MS	Liquid chromatography–mass spectrometry
$Lact$	Lactate concentration ($g\ L^{-1}$)
$m_{24SRW-MTP}$	Mass of 24-SRW MTP (g)
mAb	Monoclonal antibody
MBRs	Miniaturised bioreactors

MS/MS	Tandem mass spectrometry
mPL-I	mouse placental latogen-I
MSX	L-Methionine sulfoximine
MTP	Microtiter or microwell plates
Mu	Murine
N	Shaking speed (rpm)
N_{crit}	Critical shaking frequency (rpm)
NS0	Mouse myeloma cell line
OS	Organism Name
OTR	Oxygen transfer rate
P	Product
pcd	pg antibody per cell per day
$P_0^{'}$	Modified power number
pCO_2	Dissolved CO_2 (% or mmHg)
pk_a	Acid dissociation constant at logarithmic scale
P/V	Energy dissipation rate ($W\ m^{-3}$)
PDI	Protein disulphide isomerase
PE	Protein existence
PFK	Phosphofructokinase
Ph	Phase number
PI	Propidium iodide
prot_acc	Protein account
prot_cover	Percentage of protein sequence covered by assigned peptide matches
prot_desc	FASTA title / description line
prot_hit_num	Protein hit number
prot_mass	Protein mass (Da)
prot_matches	Number of assigned peptide matches
prot_pi	Calculated pI value for the protein
prot_score	Protein score
prot_thresh	Protein score significance threshold (PMF only)
q_{Amm}	Specific ammonium production rate ($mmol\ 10^{-9}\ cells^{-1}day^{-1}$)
q_{Glu}	Specific glutamate consumption rate ($mmol\ 10^{-9}\ cells^{-1}day^{-1}$)
q_{Gluc}	Specific glucose consumption rate ($g\ 10^{-9}\ cells^{-1}day^{-1}$)
q_{K^+}	Specific potassium consumption rate ($mmol\ 10^{-9}\ cells^{-1}day^{-1}$)
q_{Lact}	Specific lactate production rate ($g\ 10^{-9}\ cells^{-1}day^{-1}$)
q_{mAb}	Specific IgG4 production rate ($mg\ 10^{-9}\ cells^{-1}day^{-1}$)
q_{Na^+}	Specific sodium consumption rate ($mmol\ 10^{-9}\ cells^{-1}day^{-1}$)
QbD	Quality by Design
R&D	Research and development

R^2	Regression coefficient
RIA	Radioimmunoassay
RQ	Respiratory quotient
Re	Reynold's number
RH	Relative humidity
S	Substrate
Sc	Scmidt number
scFv	Single chain Fv fragment
SDS-PAGE	Polyacrylamide gel electrophoresis
SF	Shake flask
SF 125 mL	Shake flask with a total volume of 125 mL
SF 250 mL	Shake flask with a total volume of 250 mL
SSE	Sum of squares error
SST	Total sum of squares
STR	Stirred tank bioreactor
SV	Sequence Version
$t_{1/2}$	Doubling time (h)
TCA	Tricarboxylic acid cycle
TGN	Trans-Golgi network
$V_{24SRW-MTP}$	Volume of 24-SRW MTP (mL)
V_H	Variable-heavy domain
V_L	Variable-light domain
V_L	Liquid fill volume (mL)
VP	Volumetric Productivity ($mg\ L^{-1}day^{-1}$)
VP_{max}	Maximum volumetric productivity ($mg\ L^{-1}day^{-1}$)
vvm	Volumetric flow rate per minute per unit volume of liquid
W	Wetting tension ($N\ m^{-1}$)
$(x_{fit})_i$	ith model fitted x value in a total of j observations
$(x_{meas})_i$	ith experimental x value
X_V	Viable cell concentration ($10^6 cells\ mL^{-1}$)
$Y'_{P/S}$	Yield coefficient product / substrate

Greek Letters

μ	Liquid viscosity ($Pa\ s^{-1}$); specific growth rate(h^{-1})
μ_{max}	Maximum specific growth (h^{-1})
ρ	Liquid density ($kg\ m^{-3}$)
σ	Surface tension ($dyne\ cm^{-1}$)
μ_d	Specific cell death rate absolute value (h^{-1})

Chapter 1 Literature Review

1. Introduction

Since the commercialisation of the first therapeutic monoclonal antibody (mAb) product in 1986, this class of biopharmaceutical products has grown significantly with an estimated worldwide sales of $125 billion by 2020 (Ecker et al., 2015). This is likely to be matched by increased global capacity for mammalian cell culture on the one hand and by technological progress on the other. Today, industrial mAb production levels often exceed 12 $g\ L^{-1}$ as the result of a steadily ongoing progress in mammalian cell culture technology, which is mainly due to improved high producer cell lines, optimised production media, and prolonged production processes at high cell densities (Frenzel et al., 2013). As concentrations increase, downstream processing will become a much more significant component of cost, and this will be a driver to develop more efficient processes, potentially using radically different approaches to those used now. It also seems likely that other expression technologies, especially those based on bacteria and/or fungi will become more dominant not just for fragments but potentially for whole antibodies as well. A final factor that will impact on process volumes and cost of goods is product potency. Some of the recent progress in improving effector functions by glycosylation engineering demonstrate the potential in this area (Birch et al. 2006).

1.1. Monoclonal Antibodies

1.1.1. Antibody Structure and Function

Antibodies (Ab) or immunoglobulins (Ig) are produced by plasma B-cells (B-lymphocytes) and occur naturally as part of the immune system of mammals by recognizing antigens in a “lock and key” fitting model. The structure of an antibody comprises two antigen-binding fragments (Fab’s) and a constant region (Fc), involved in effector functions and biodistribution of the antibody, linked via the flexible hinge region (Figure 1-1). These regions are part of two pairs of polypeptide chains, heavy and light chains, folded into compact globular domains. Each heavy and light chain has a similar structure with constant and variable regions. The main differences observed in the variable regions are located in three small hypervariable sequences, responsible for antigen binding, the so-called complementary determining regions (CDR), and corresponding to the N-terminal regions of the light and heavy chains (Fab portion) (Roque et al., 2004).

B-cells by themselves cannot grow outside an animal. For this reason, Kohler et al. (1975) developed a method to fuse B-cells of an immunised mouse with immortal

tumor cells derived from a mouse myeloma. The resulting 'hybridoma' is immortal and produces the same antibody as the original B-cell. For this discovery, they were awarded the 1984 Nobel prize for medicine. Although promising from the start, it has taken nearly two decades for the technology to reach a level at which monoclonal antibodies and their derivatives can be developed into safe and efficient therapeutics.

Currently, a full-length antibody of the IgG subclass, Fab fragments and single-chain variable fragments (scFv) are clinically used (Chadd et al. 2001). The most abundant antibody class found in human blood is IgG1, although B-cells may produce nine different types of antibody, also called isotypes (Table 1-1). These isotypes each have a set of unique properties. It is, therefore, crucial to select the correct isotype to achieve a desired therapeutic effect, and avoid side-effects. At present, IgG1 antibodies represent the therapeutic antibody type of choice because of their long biological half-life (>20 days) and their capacity to interact with the human immune system, however depending on the clinical application (Adams et al. 2005; Dijk et al. 2001; Roque et al. 2004).

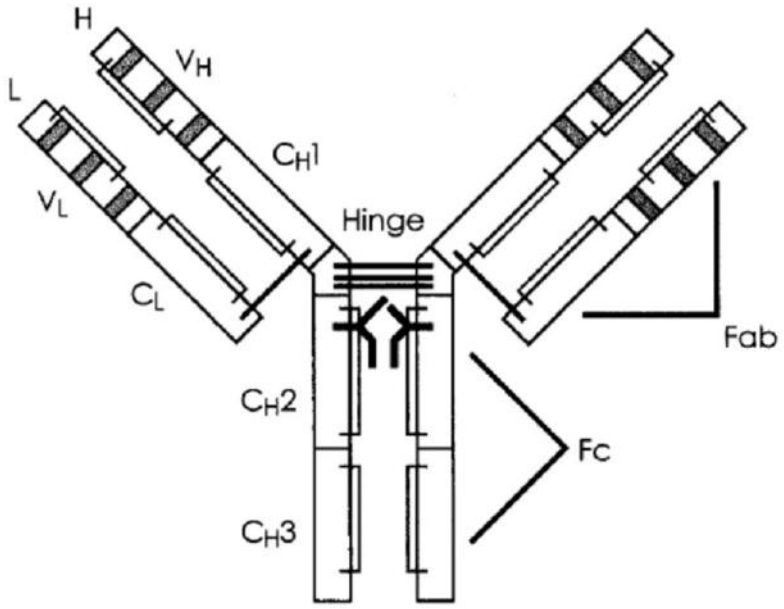

Figure 1-1: Schematic representation of IgG showing the domain structure, intra- and interchain disulfide bonds, and glycosylation sites. H, heavy chain; L, light chain; V_H, variable-heavy domain; V_L, variable-light domain; C_H, constant-heavy domain; C_L, constant-light domain; Fc, constant region (fragment crystalline); Fab, fragment antigen binding. Image adapted from Burton 1987; Kunkel et al. 2000.

Table 1-1: Characteristics and functional properties of human antibody isotypes (IgG1, IgG2, IgG3, IgG4, IgM, IgA1, IgA2, IgD, and IgE). Table adapted from Dijk et al. 2001.

	IgG1	IgG2	IgG3	IgG4	IgM	IgA1	IgA2	IgD	IgE
Molecular weight (kDa)	146	146	165	146	970	160	160	184	188
Adult serum level (mg/ml)	9	3	1	0.5	1.5	3	0.5	0.03	5×10^{-5}
Serum half-life (days)	21	20	7	21	10	6	6	3	2
Complement transfer	++	+	+++	+	+++	-	-	-	-
Placental transfer	+++	+	++	+/-	-	-	-	-	-
Mucosal transfer	+/-	+/-	+/-	+/-	+	+++	+++	-	-
Phagocyte binding	+++	++	+++	+/-	-	++	++	-	+
Binding to mast cells and basophils	-	-	-	-	-	+	+	-	+++

1.1.2. Antibody Application and Market

Antibodies bind to target molecules with high affinity and specificity. This high affinity and specificity of antibodies and engineered related molecules has been widely exploited in a plethora of applications, the emergence of therapeutic antibodies being particularly relevant (Table 1-2).

Monoclonal antibodies (mAbs) (homogenous isotype and antigen specificity) and related proteins have been shown to target a broad range of extracellular targets with high specificity successfully. This has led to their introduction to a variety of disease therapies, including several forms of cancer, multiple sclerosis and immunological disorders such as rheumatoid arthritis and psoriasis (Table 1-3) (Shukla et al., 2010).

By November 2014, there were forty-seven monoclonal antibody products approved by the FDA and on the market (Ecker et al. 2015) and approximately 200 antibodies and their derivatives are in clinical trials for the treatment of appropriate diseases. The total market for therapeutic monoclonal antibodies is a multibillion-dollar

opportunity, with cancer and arthritis the major therapeutic applications with estimated total markets of $15 billion and $25 billion in 2010, respectively (Roque et al., 2004; Scolnik, 2009).

Regarding sales, mAbs are the second largest class of biologics, closing in on the number one class, broadly defined as growth factors, which include the erythropoietins. Since 2001, mAb sales have increased at an average annual rate of 35%. Growth is fuelled by expansion into new indications, by often being the only available option in therapy areas with a largely unmet need, and growing (ageing) populations suffering from diseases targeted by mAbs. Over the period of 2008 - 2013, mAbs were forecast as a key growth segment in the prescription pharmaceutical market. This was driven by the expanding sales of existing products combined with new products, as pharmaceutical firms are continuing to invest actively in research and development (R&D) of therapeutic mAbs (Cohen et al. 2009; Scolnik 2009).

Table 1-2: Examples of *in vivo* and *in-vitro* antibodies applications. Adapted from Roque et al., 2004.

Immunoaffinity purification	
Analysis and diagnostic	
	ELISA and RIA
	Immunosensors
	Imaging
Therapeutics	
	Intrabodies/gene therapy
	Targeting/neutralizing
	Signaling/cross-linking
Catalytic antibodies and abzymes	
	Enzyme engineering
	therapeutics

Table 1-3: Monoclonal antibodies and related proteins on the market. Table adapted from Hale 2006; Rodrigues et al. 2009; Shukla et al. 2010 and FDA website.

Name	Target	Indication	Company	Year	Type
Monoclonal antibodies					
Orthoclone OKT3	CD3	Acute kidney transplant rejection	Ortho Biotech	1986	Murine
ReoPro	Platelet GP IIb/IIa	Prevention of blood clot	Centocor	1994	
Rituxan	CD20	Non-Hodgkin's Lymphoma	Genentech/ Biogen-Idec	1997	Chimeric
Zenapax	Il2Ra (CD25)	Acute kidney transplant rejection	Hoffman-LaRoche		Humanized
Simulect	Il2R	Prophylaxis of acute organ rejection	Novartis	1998	Chimeric
Remicade	TNFa	Rheumatoid arthritis	Centocor		
Mylotarg	CD33	Acute myelogenous lymphoma	Wyeth-Ayerst	2000	Humanized
Campath	CD52	B-cell chronic lymphocytic leukemia	Takeda	2001	
Zevalin	CD20	Non-Hodgkins Lymphoma	Biogen-Idec	2002	Murine
Bexxar	CD20	Non-Hodgkins Lymphoma	Corina/GSK	2003	
Xolair	IgE	Allergy	Genentech/Novartis		Humanized
Erbitux	EGFR/Her1	Colorectal cancer	Bristol-Myers Squibb/ImClone (Eli Lilly)	2004	
Avastin	VEGF	Colorectal cancer	Genentech		
Raptiva	CD11a	Psoriasis	Genentech/Xoma		
Vectibix	EGFR	Colorectal cancer	Amgen	2006	Human
Soliris	C5 complement	PNH – paroxysmal nocturnal hemoglobinuria	Alexion	2007	Humanized
Stelara	IL12 and IL23	Psoriasis	Centocor	2008	Human
Simponi	TNFa	Rheumatoid arthritis			
Ilaris	IL1b	Infalmmatory	Novartis	2009	
Stelara	IL-12/23	Autoimmune	Johnson & Johnson		
Arzerra	CD20	Cancer	Genmab		
Prolia	RANK ligand	Bone Loss	Amgen	2010	
ABThrax	*B. anthrasis*PA	Anti-infection	GSK	2012	
Benlysta	BLyS	Autoimmune	Human Genome Sciences	2011	
Adcetris	CD30	Hodgkin lymphoma	Seattle Genetics		Chimeric and drug-conjugate
Perjeta	Her2	Breast Cancer	Genentech/Roche	2012	Humanized
Kadcyla				2013	Humanized and drug-conjugate
Gazyva	CD20	Chronic lymphocytic leukemia (CLL)			Humanized and glycoengineered
Monoclonal antibody fragments					
Lucentis	VEGF-A	Age-related macular degeneration	Genentech	2006	Fab´
Cimzia	TNFα	Crohn's disease	UCB	2008	Pegylated Fab fragment
Fc fusion proteins					
Enbrel	TNFα	Rheumatoid arthritis, psoriasis, ankylosing spondylitis	Amgen	1998	Soluble TNFa receptor fused to IgG1 Fc
Amevive	CD 2	Psoriasis	Biogen-Idec	2003	LFA3 fused to IgG1 Fc
Orencia	CD80/86	Rheumatoid arthritis	Bristol-Myers Squibb	2005	CTLA4 fused to IgG1 Fc
Arcalyst	IL-1	CAPS – Cryopyrin-Associated Periodic Syndrome	Regeneron	2007	IL-1 receptor fused to Fc

1.1.3. Expression Systems for Antibody Production

Various expression systems can be used for the production of whole antibodies and antibody fragments. These include bacterial fermentation or mammalian cell culture and transgenic animals or plants. The expression system of choice is partially dependent upon the intended use of the antibody, as well as the antibody yield derived from each system. This yield affects the process cost of goods (CoG), which is comprised principally of two factors: the cost of the upstream process that generates the antibody, and the cost of the downstream process, that is, purification and final fill of the active pharmaceutical ingredient (Chadd et al. 2001). In Table 1-4 is highlighted the various expression systems used for the production of therapeutic or diagnostic antibodies.

Table 1-4: Summary of antibody expression systems. Table adapted from Chadd et al. 2001.Ch, chimeric; Hu, human; Hz, humanized; Mu, murine; S, secretory

System	Antibody form	Source	Use
Bioreactor			
Escherichia coli	Mu scFv	Cytosol, periplasm	Diagnostic, Therapeutic
Pichia pastoris	Mu scFv	Medium	
Drosophila melanogaster	Mu scFv	Medium	Diagnostic
Mammalian cell (CHO/NS0)	Ch IgG_1	Medium	
	Ch Fab		
	HZ IgG_1	Medium	Therapeutic
Hybridoma	Mu IgG_2	Medium	
	Mu IgM		
	Hu IgG_2	Medium	
Transgenic organism			
Animals			
Mouse	Ch IgG_1	Milk	
Goat	Ch IgG_1	Milk	Therapeutic
	Hu IgG_2		
Plants			
Tobacco	SIgA/G: Ch	Leaf	
Maize	Hz IgG	Seed	Therapeutic
Soy	Hz IgG	Pod, seed, stem, leaf	
Rice	Mu scFv	Seed	Diagnostic, Therapeutic
Wheat	Mu scFv	Seed	

Suspension-adapted mammalian cells have become the dominant system (60-70%) for the production of safe and effective therapeutic antibody molecules (chimeric, humanized, and phage display-derived human Ab's) due to their capacity for proper protein folding, secretion and post-translational modification (Chadd et al. 2001; Frenzel et al. 2013; Roque et al. 2004). Thus, the quality and efficacy of the antibody can be superior when expressed in mammalian cells compared to other systems, such as bacteria, plants, yeast and transgenic animals (Andersen et al. 2004; Dijk et al. 2001; Verma et al. 1998). Although there are differences in the glycosylation patterns, no clinical data suggest that these structural differences have any effect on antibody activity *in vivo* or the induction of antigenic responses (Kelley, 2009).

Mammalian cells have the advantage over transgenic plants and animals that protein can be produced approximately six months after the initial cloning. At present, the cost of production is very high in mammalian cells. Dove (2002) stated that the estimated production cost of a mammalian cell process is $150/g raw material, compared to $1-$2 from transgenic animals. Recombinant protein produced by mammalian cells has reached approximately grams per litre after a three-week culture, with a specific productivity of 90 pg $cell^{-1}$ day^{-1} (Merten, 2006; Wurm, 2004). With an increase in the number and demand for recombinant biopharmaceuticals, there is a requirement for greater biomanufacturing capacity (Butler, 2005). At a quantitative level, the mammalian-based production of mAb-based products is projected to reach 13.4 metric tonnes by 2016, almost double the 2010 value (Walsh, 2014).

The productivity of recombinant mammalian cell lines increased from initially 10 pg antibody per cell per day (pcd) in 1986 to about 90 pcd in 2004 (Frenzel et al., 2013). Today, the antibody production levels only rarely exceed 100 pcd because higher cellular productivity usually corresponds to lower maximum cell densities in the manufacturing process. Producer cell lines have also been genetically engineered regarding product homogeneity, improved metabolism, reduced apoptosis, and inducible cell cycle arrest (Butler 2005; Fussenegger et al. 1998) which allows prolonged production times for almost three weeks at high cell viability and cell densities.

Chinese hamster ovary (CHO) cells are the most current cells applied in the commercial production of biopharmaceuticals. This cell line isolated in the 1950s gave rise to a range of genetically different progeny, such as K1-, DukX B11-, DG44- cell lines and others which differ in protein product quality and achievable yield. Also, Per.C6 cells, mouse myeloma NS0 cells, baby hamster kidney (BHK) cells and the human embryonic kidney cell line HEK293 received regulatory approval for recombinant protein production (Wurm, 2004).

Although, mammalian cell systems have some potential disadvantages: they require complex media formulations, have low productivity, are slow growing and are relatively sensitive to changes in process conditions. In addition, one of the main concerns regarding mammalian cell culture is their susceptibility to “shear”, or, more correctly, hydrodynamic stress (Figure 1-2). It is now thought that sparging, rather than agitation, is responsible for cellular damage in bioreactors (Nienow et al., 1996). Therefore, mammalian cell culture is associated with high cost of goods during the manufacturing process, both at small and large scale (Birch et al. 2006). Figure 1-2 shows that energy dissipation rates that were found to lyse common mammalian cell-line are 2 - 4 order of magnitude greater than those experienced in typical stirred-tank reactors. Furthermore, these lethal values are comparable to those generated by a bursting bubble.

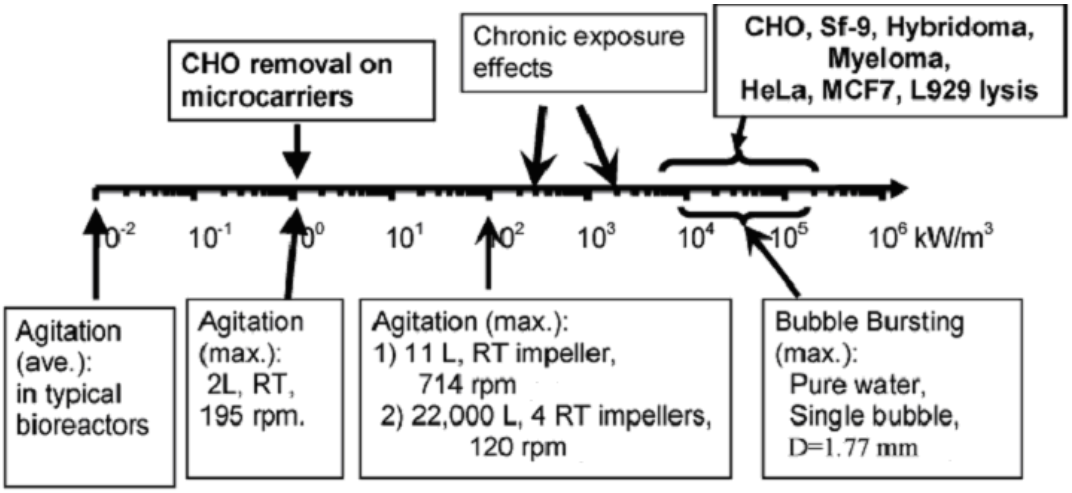

Figure 1-2: Values of the energy dissipation rate for various bioreactor environments and its effect on different cell lines. Reproduced from Heath et al. 2007.

1.1.4. Antibody Glycosylation

The most widely recognised form of post-translational modification is glycosylation that requires an extensive sequence of processing and trimming events in the endoplasmic reticulum (ER) and Golgi apparatus (Figure 1-3). Glycosylation has a major effect on the mAb biological properties (pharmacokinetics, bioactivity, secretion, *in vivo* clearance, solubility, receptor recognition, and antigenicity) (Butler, 2006; Storring, 1992). Hence, it is essential for quality by design (QbD) process to ensure that a consistent glycosylation profile is maintained between batches in the process of production (Li et al. 2006; Restelli et al. 2002). However, culture conditions,

such as temperature, pH (Quan et al., 2008), dissolved oxygen tension (DOT), carbon dioxide (CO_2), osmolarity (Jefferis, 2002), time of culture (Curling et al., 1990) as well as nutrient and metabolite concentrations (Clark et al., 2005; Jefferis, 2002; Quan et al., 2008), have been shown to affect glycosylation (Andersen et al. 2000; Goochee et al. 1990; Li et al. 2006). Therefore, it is of extreme importance to have a further understanding of the parameters that control protein glycosylation in bioreactors, and to monitor product quality during each step of the optimisation, to be able to ensure the quality and consistency needed for biopharmaceutical production (Butler, 2006).

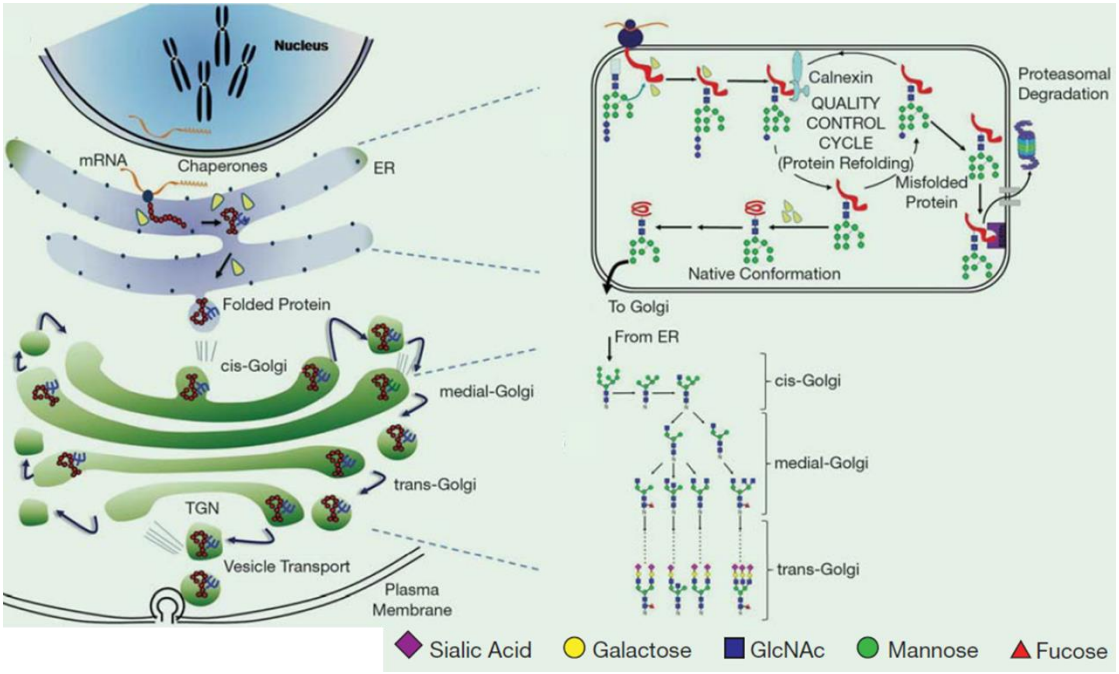

Figure 1-3: Proteins (mAbs) that will be secreted from the cell enter the secretory pathway via the endoplasmic reticulum (ER) (ribosomes in the ER are depicted as blue dots). As proteins undergo folding and post-modifications within the ER, they are continually monitoring the quality-control systems. The newly modified proteins exit the ER in transport vesicles bound to the Golgi apparatus. Within the Golgi, glycosyltransferase enzymes mediate a vast network of glycosylation reactions (N- and O-glycosylation), resulting in a variety of glycan structures. The finished products are packed into vesicles at the trans-Golgi network (TGN), and from there are transported to the plasma membrane. Figure adapted from Dinnis et al. 2005 and Jacob et al. 2009.

1.2. Antibody Production Process

Significant advances have been made over the years in the design of mAbs as therapeutics that have improved the therapeutic profiles of mAbs like bioavailability, optimised affinity, improved binding specificity, and human antibody sequences to reduce any immunogenic side effects. Further advances in protein engineering are improving the therapeutic profiles of mAbs. Several cases for which mAb therapeutics have been approved serve a large patient population and involve chronic therapy with high doses (greater than a gram per patient per year). This has led to the need for production processes that can be developed rapidly to produce consistently and reproducibly significant quantities of pharmaceutical-grade mAbs at moderate costs. Process platforms in both upstream cell culture and downstream purification have become widely established to meet this need in the industry.

Large-scale production of mAbs utilises mammalian production systems followed by cell removal and purification through sequential chromatographic and membrane filtration steps, to consistently reduce product- (e.g. protein variants) and non-product-related (e.g. host cell proteins (HCP)) impurities to acceptable levels (Figure 1-4). Two types of culture system are used for large-scale manufacture, fed-batch, and continuous perfusion culture. Fed-batch processes are by far the most common and are now operated at scales up to 2,0000 L working volume (Andersen et al. 2004; Birch et al. 2006; Kelley 2009; Shukla et al. 2010).

1.2.1. Effects of Process Parameters

Mammalian cell cultures performed in bioreactors allow the production of mAbs in large-scale quantities. However, this production can be further maximised using different strategies, such as nutrient optimisation, feeding, cell engineering, or manipulation of the cellular environment. Among these, the most common practice consists on the optimisation of bioreactor culture conditions, because it represents an economical and reliable way to ensure optimal productivity. For this, the culture parameters more relevant for cell growth and productivity need to be identified and their individual and interrelated effects better understood. Process parameters, such as temperature, pH, osmolarity, DOT, CO_2, and nutrient and metabolites concentration, have been shown to affect cell performance and are, therefore, generally seen as the most relevant for optimisation of production in mammalian cultures (Rodrigues et al., 2010).

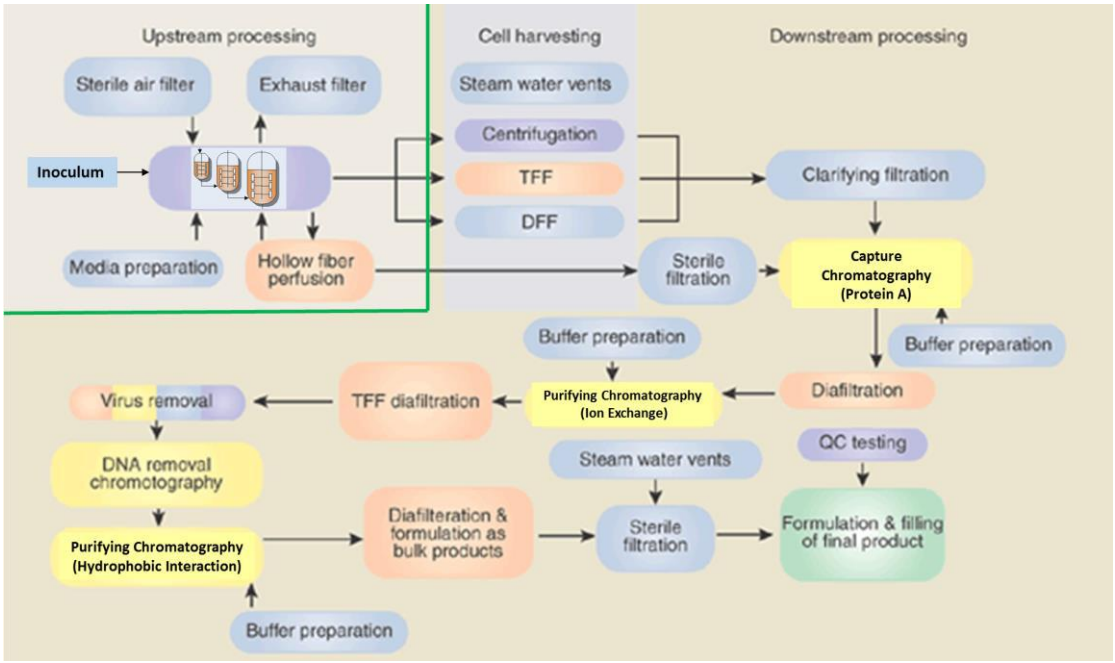

Figure 1-4: Typical antibody manufacturing process flowsheet with the various processing steps from the bioreactor train through purification. Figure adapted from Birch et al. 2006; Carson 2005 and Gronemeyer et al. 2014. TFF, tangential flow filtration; DFF, direct flow filtration.

1.2.1.1. Temperature

Temperature is one of the most critical and more studied variables in mammalian cell cultures (Andersen et al. 2000; Bloemkolk et al. 1992; Chuppa et al. 1997; Fogolín et al. 2004; Fox et al. 2004; Furukawa et al. 1998; Kaufmann et al. 1999; Moore et al. 1997; Rodriguez et al. 2005; Rössler et al. 1996; Sureshkumar et al. 1991; Yoon et al. 2003a, b, 2005). The influence of temperature on the specific growth rate of a microorganism shows an increasing tendency with an increase in temperature up to a certain value, which is microorganism specific and a rapid decrease is observed beyond this value (Karra et al., 2010). Although the ideal growth temperature for most mammalian cells is 37°C (the body temperature), it has been shown that this may not be the best temperature for recombinant protein/mAb production. Indeed, some studies (Bollati-Fogolín et al., 2005; Yoon et al., 2005) have demonstrated that a lower temperature (around 30-35°C) may have a positive outcome regarding mAb specific productivity while maintaining or improving product quality (Trummer et al. 2006b). However, the increase in specific productivity does not often results in improved volumetric productivity, because of the adverse effects that low temperatures have in the cell growth rate (Mohan et al., 2008). Therefore, the most advantageous

temperature strategy may be culturing cells at 37°C until a high cell density is reached and then shifting to lower temperatures to achieve higher product titers (Fox et al., 2004; Oguchi et al., 2006).

1.2.1.2. pH

The cell culture pH is considered to be one of the most critical parameters for mammalian cell culture, because of the severe effects its variation can cause to cells (Hanson et al., 2007; Osman et al., 2001). Indeed, even small variations in pH (0.1 pH units) can have an impact on cell growth, productivity, cell metabolism, and protein glycosylation. Furthermore, optimal pHs for specific growth rate and specific protein production may not be necessarily the same. For hybridoma cultures in bioreactors, pH should ideally be near 7.4 at the beginning of the culture and not fall below 7.0 during culture, (Borys et al. 1993; Jardon et al. 2003) although, values set between 6.5 and 7.8 are usually acceptable (Li et al., 2010). The highest values of pH are preferred for starting the culture because they favor cell growth (Li et al., 2006). However, they also increase the anaerobic cell metabolism that leads to the accumulation of metabolites (particularly lactate) (Rodrigues et al., 2009). For CHO cells expressing mPL-l (mouse placental latogen-I) cultures, it was found that maximal expression rates occurred when the pH was between 7.6 and 8.0, which coincided with the optimal pH for the other cellular processes (Borys et al., 1993). Few literature describes the impact of pH in the GS-CHO cell system. Sellick et al. (2009) describes in a tutorial the impact of pH on a GS-CHO cell line secreting IgG4 mAb, where the optimum pH was in the region of 7.0 to 7.2 with similar growth patterns and antibody titers. Also, the higher (pH 7.6) and lower (pH 6.8) values resulted in decreased growth rates and viable cell numbers as well as lower antibody titres. Therefore, their recommendation is to use pH 7.0.

Maintenance of pH stability in culture is affected by different factors, including buffer capacity and type bioreactor headspace, and glucose concentration (Griffiths, 2000). Mammalian cell culture medium is prepared with a buffer system to control pH variations, and it usually consists on the CO_2/bicarbonate system. This system requires the addition of CO_2 to the culture vessel headspace or the addition of bicarbonate base (Griffiths, 2000). Nevertheless, other buffer systems can be used to improve buffering and pH stability, such as the zwitterionic buffer (i.e., HEPES), that can be used alone or in combination with bicarbonate, or specialist media such as Leibovitz's L-15 (Rodrigues et al., 2010). Because the normal buffer system needs a certain level of CO_2 (5.00% (v/v) CO_2) to maintain a stable pH, it is important that the culture vessel has a large headspace or an open system with continuous flow of air (required in large

bioreactors). This will assure that CO_2 generated during cell growth adequately diffuses from the medium, without build-up and consequent decrease in pH. Nonetheless, the addition of base to the bioreactor is mandatory. In addition, glucose concentration in the medium also affects pH. Glucose is metabolised by cells at a greater rate than it is needed and results in the formation of toxic metabolites (pyruvic and lactic acids) that lower the pH to non-physiological levels. To avoid the fast build-up of metabolites and deterioration of the medium, glucose should be added in small concentrations (no more than 2 gL^{-1}) to the medium during culture. Other approach is to replace glucose by other carbon sources, such as galactose or fructose, which significantly reduces formation of lactic acid, but also results in slower cell growth (Rodrigues et al., 2010).

Extracellular pH affects many cellular functions and parameters, including intracellular pH, metabolism, glucose transport and the ATP/ADP ratio (Borys et al., 1993). Changes in intracellular pH can affect the activity of certain enzymes key to the metabolism. For example, it has been shown in animal cells that phosphofructokinase (PFK) is inhibited at pH 6.2, inhibiting glucose consumption and increasing glutamine consumption (Haggstrom, 2000). Although the dependence of cell activity on pH cannot be explained possibly by a simple model, it is found that a bell shaped curve gives an adequate fit for many microorganisms (Abu-Reesh et al. 1989).

Langheinrich et al. (1999) measured pH in different zones of an 8 m^3 reactor designed for mammalian cell culture, in which base was added to the liquid surface. They found pH gradients of up to one pH unit between the alkali addition zone and the bulk liquid. However. By changing the point of base addition to the well-mixed impeller region or utilising multiple addition points are simple strategies that can reduce pH gradients. Similarly, Ozturk (1996) observed localized cell lysis in mammalian cell cultures as a consequence of high pH in the point of base addition. McDowell et al. (2003) summarised other conditions that lead to pH gradients, such as culture aggregation, nutrient gradients, and the use of inhomogeneous bioreactors, such as packed beds or other systems with immobilised cells. However, pH gradients may be unavoidable in the case of high density or viscous cultures. Spatial pH gradients can lead to the accumulation of by-products or reduction of culture viability (Amanullah et al., 2001; Onyeaka et al., 2003). Moreover, pH gradients may expose proteins to conditions where they are chemically degraded, such as a high pH, which promotes deamidation, and reduction of biological activity (Zheng et al. 2006).

1.2.1.3. Carbon Dioxide

CO_2 is known to play an essential role in mammalian cell culture *in vitro* not only to maintain the culture pH at normally optimum range of 6.9 - 7.4 but also to regulate

many cellular activities (McLimas, 1972; Yoon et al., 2002). The control of pH in most mammalian cell culture processes uses the CO_2/bicarbonate ion (HCO_3^-) open buffer system present in the medium. Therefore, a change in atmospheric CO_2 can alter the pH of the medium. This can be represented by the following equation (DeZengotita et al., 2002):

$$CO_2(g) \Leftrightarrow CO_2(aq) \rightarrow H_2CO_3(aq) \overset{K_{a,CA}}{\Longleftrightarrow} HCO_3^-\ (aq) + \ H^+(aq) \overset{K_{a2}}{\Longleftrightarrow} CO_3^{2-}(aq) + 2H^+(aq)$$

Equation 1.1

Once dissolved in cell culture medium CO_2 gas reacts with water to form carbonic acid (H_2CO_3), which dissociates to form bicarbonate (HCO_3^-) and carbonate (CO_3^{2-}) ions. Since the mammalian cell culture pH is typically maintained between 6.6 and 7.6 the moles of carbonate CO_3^{2-} ions ($pk_{a2} = 10.25$) are less than 1% of the total moles of CO_2 and HCO_3^-. Also, because the equilibrium of CO_2 dissociation is far on the side of the anhydride (99.8%), concentrations of the carbonic acid (H_2CO_3) are very low (Blombach et al., 2015; Mostafa et al., 2003; Zhu et al., 2005). Therefore, Equation 1.1 can be simplified to:

$$CO_2(g) \Leftrightarrow CO_2(aq) \rightarrow H_2CO_3(aq) \overset{K_{a,CA}}{\Longleftrightarrow} HCO_3^-\ (aq) + \ H^+(aq)$$

Equation 1.2

where the $pK_{a,CA} = 6.37$ at 37°C (DeZengotita et al., 2002). At typical cultivation conditions (pH 7.0), 83.3% of the CO_2 species are present as HCO_3^- only 16.7% as CO_2 (Blombach et al., 2015). Inhibition by CO_2 is due in part to medium acidification if pH is not controlled. If pH is controlled by base addition, the equilibrium (Equation 1.2) will be driven farther to the right, such that an increase in dissolved CO_2 (pCO_2) will result in an increase in HCO_3^- concentration and, thus, an increase in osmolality (DeZengotita et al., 2002; Osman et al., 2002). Therefore, the physiological effect of pCO_2 may be a result of accumulation of the dissolved gas *per se*, of higher osmotic pressure, or both (Del Val et al., 2010; Lara et al., 2006;). Furthermore, the bicarbonate system is unique in that the acid component may be held at any desired steady state by maintaining a constant pressure of CO_2 in the atmosphere above the culture medium (MacKenzie et al., 1961). Most researchers usually use 4.0 – 10.0% CO_2 for most cell culture experiments. However, each medium has a recommended CO_2 tension and bicarbonate concentration to achieve the correct pH and osmolality. For example, the

CD CHO Medium requires a CO_2 tension of 8.0 – 10.0 %[1]. There is an optimal level of pCO_2 for cell culture, which vary from cell line to cell line (Mostafa et al., 2003).

There are three main sources of dissolved CO_2 in the culture, namely, CO_2 produced by cells during respiration (cellular metabolism), CO_2 added to culture to maintain pH early in the run, and CO_2 produced from sodium bicarbonate that is added as a buffer (Mostafa et al., 2003; Zhu et al., 2005) (Figure 1-5). CO_2 formation mirrors the final carbon oxidation steps of aerobic metabolism in microbial and mammalian cells. Anaplerotic reactions make use of this abundant CO_2/HCO_3^- levels for refuelling citric acid (TCA) cycle demands and for enabling oxaloacetate-derived products. At the same time, CO_2 is released manifold in metabolic reactions via decarboxylation activity. Besides, local CO_2/HCO_3^- levels might also act as metabolic inhibitors or transcriptional effectors triggering regulatory events inside the cells (Blombach et al., 2015). For mammalian cells, the respiratory quotient, RQ (mol CO_2 produced per mol O_2 consumed) ranges from about 0.6 to 1.2 (DeZengotita et al., 2002; Ozturk 1996), the amount of CO_2 generated increases at essential the same rate as oxygen is consumed. Multiple factors affect the balance of CO_2 in cell culture, including its production rate (CO_2 evolution rate (CER)), removal rate through the gas phase, bicarbonate addition for pH control, and the culture pH (Xie et al., 2003).

One of the recurring issues in industrial mammalian cell culture has been the accumulation of pCO_2 in large-scale bioreactors. The high levels of pCO_2 and associated high acidity plus increased osmolality associated with pH the control is considered to be one of the major scaling up difficulty in mammalian cell culture (Nienow, 2006). Therefore, reliable monitoring and control of dCO_2 are important for successful large-scale operation (Pattison et al., 2000). In small-scale reactors a significant portion of pCO_2 stripping occurs through surface aeration (Mostafa et al., 2003). In fact, it has been shown that high pCO_2 can have detrimental effects on cell growth, nutrient utilisation, productivity, and product quality (DeZengotita et al. 1998; Kimura et al. 1996; Schmelzer et al. 2002; Takuma et al. 2007). These detrimental effects must be carefully considered to achieve higher productivities and better product quality.

Several strategies can be employed to tackle the CO_2 accumulation at large scale with high cell density. A simple approach is to reduce the culture pH as long as the cell growth and protein synthesis and quality are not adversely affected. A low pH not only increases the driving force for CO_2 removal but also could potentially reduce

[1] CD CHO Medium Manual. www.thermofisher.com

lactate production significantly, which reduces the need for bicarbonate addition (DeZengotita et al., 1998; Miller et al., 1988; Ozturk et al., 1992). Another measure is to use a low concentration of sodium hydroxide (NaOH) for pH control instead of bicarbonate. The alkali addition needs to be carefully designed to avoid cell lysis due to local pH spikes due to poor mixing and (Nienow, 2006). However, there has been no need to cultivate recombinant mammalian cells under the very reduced level of CO_2 in the gas phase as CHO cells normally fail to grow in an incubator without CO_2 supply (Yoon et al., 2002). However, Oliveira et al. 2008 have reported an increase of 60% in the secretion yield of CHO-derived hTSH (human thyroid-stimulating hormone) by changing cell culture CO_2 conditions from 5% CO_2 to an air environment due to cell cycle arrest in the G1 phase.

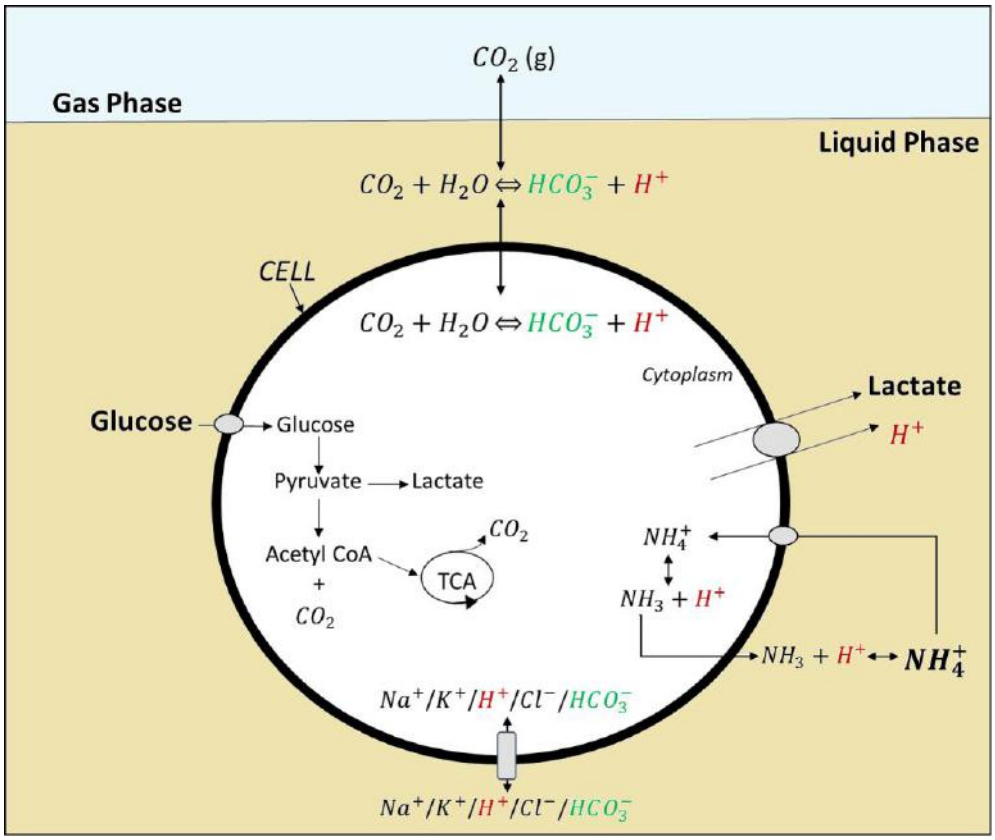

Figure 1-5: Schematic of CO_2 and ion transfer between gas-liquid interface and cell membrane. Excess of CO_2, can act to inhibit respiration reactions, and may act as an acid poison by crossing membranes and changing intracellular compartment pH (pH_i).

Techniques for real-time monitoring of cell proliferation and viability are crucial to the success of mammalian cell culture processes (Naciri et al., 2008). Advances in

optics and electronics have made optical sensors commercially available for the monitoring of such processes (Harms et al., 2002). The optical-chemical probes are non-interfering, non-destructive to cells, and the sensing is fast. Therefore the cell properties can be measured continuously during cell culture with no delay between measurement and results and with no sampling required (Naciri et al., 2008). A monitoring strategy based on direct measurements of the two major operational parameters, dissolved oxygen and pH, at microtiter plates will provide information on both the growth and cellular metabolism and may circumvent the problem with low throughput monitoring on this scale. Oxygen is necessary for cellular respiration and would decrease with increasing cell numbers, while the cell metabolism by-products, lactate and ammonium, will affect the pH (Hanson et al., 2007). For cells in the growth phase of batch culture, a steady but rapid lowering of pH and oxygen levels reflecting the increase in total viable cell numbers and cellular metabolism is expected. DOT and pH levels may also provide information about the onset of apoptosis, since both inhibition of oxygen utilisation and acidification has shown an association with cell death in culture (Perani et al., 1998; Simpson et al., 1997). The rate of cellular growth and metabolism of protein synthesis are strongly dependent on medium DOT and pH (Miller et al., 1988; Ozturk et al., 1990; Schmid et al., 1990).

1.2.1.4. Osmolarity

Osmolarity strongly influences mAb production, cell growth, and death rates, as well as the duration of exponential growth (Sandadi et al., 2005). Increases in osmolarity are observed due to additions of the base to control pH (KOH, NaOH, $NaHCO_2$, or Na_2CO_3) or glucose or medium concentrates to the culture (Bibila et al. 1994; Fenge et al. 2006; Sandadi et al., 2005). The resultant high levels of osmolarity cause decreased growth rates and cell concentrations. However, within a certain range (300–400 mOsm/kg) the osmolarity increase can be beneficial. Indeed, at this range, the negative consequences in cell growth can be compensated with increases on the specific mAb production rate, resulting in a higher final antibody concentration (Miller et al., 1988). For this reason, hyperosmolarity is sometimes described as one economical alternative to improve mAb production (DeZengotita et al., 2002; Kim et al., 2002).

1.2.1.5. Dissolved Oxygen

Mammalian cells require oxygen for the production of energy from organic carbon sources (Gódia et al. 2006). Therefore, oxygen available for cell use is an important parameter for mammalian cell culture. The amount of DOT in the medium is

dependent on a diversity of factors, such as cell growth rate, carbon source, and specific rate of consumption by the cells (Jorjani et al. 1999). Oxygen is essential and can affect in several ways cellular metabolism and physiology. DOT limitation affects the activity of enzymes in glycolysis, hexose monophosphate shunt, pentose phosphate pathway, TCA cycle, and glutamine metabolism (Haggstrom, 2000). In mammalian cell cultures, optimum DOT concentrations have been reported to be between 5 and 80% air saturation (Karra et al. 2010; Kunkel et al. 1998; Li et al. 2006; Palomares et al. 1996). Below such range, growth rate, and protein synthesis decrease and anaerobic metabolism increases, which lead to excessive lactate accumulation. Above such range, the excessively high DOT could cause oxidative damage (Hevehan et al. 1999; Li et al. 2010; Palomares et al. 1996). A DOT between 30 - 60% air saturation is accepted to be optimal for cell growth, although the sensitivity of cells to extreme DOT levels is known to vary. It has also been reported that protein synthesis is a function of DOT (Bibila et al., 1995). Also, scale-up represents a problem for guaranteeing correct levels of DOT in the culture, because the methods currently available for that purpose cannot assure high cell oxygenation without causing some cell damage (Griffiths, 2000).

1.2.1.6. Glucose

Glucose is one of the most critical nutrients for mammalian cells. It is utilised either through the pentose phosphate pathway to provide nucleotides for biosynthesis or through glycolysis to provide metabolic intermediates and energy. However, a significant portion of glucose carbon may end up in lactate. The portion of glucose entering the tricarboxylic acid cycle (TCA) is usually quite low (Fitzpatrick et al., 1993; Petch et al., 1994; Zielke et al., 1978; 1984). Hence, glucose is not only used for energy and biomass formation but also for product formation and other non-growth-associated functions, which are called maintenance functions. The main requirement for glucose appears to be for the supply of carbohydrate building blocks for anabolic metabolisms, such as nucleic acid or polysaccharide synthesis (Burton et al., 1981). High glucose levels (>2.5 gL^{-1}) can contribute to an early boost in culture expansion, but also can induce many cultures to shift to a metabolism known as the “Crabtree effect”. The high levels of glucose inhibit oxidative metabolism resulting in production of lactate and ammonia, which may cause premature cellular stress or apoptosis and/or product productivity inhibition (Lao et al., 1997) as well as affecting product’s glycosylation (Nyberg et al., 1999; Whitford, 2006). Some attempts have been made to avoid such outcome, which include reduction of ammonia formation by controlling glutamine concentration, modification of the energy metabolism by controlling glucose

concentration (e.g., by feeding less glucose to the culture but more periodically, in concentrations according to cell needs) (Europa et al., 2000; Lao et al.,1997; Zhou et al., 1997) or replacement of glucose by a slower utilised substrate such as galactose (Altamirano et al., 2001).

1.2.1.7. Ammonia

The cell growth is inhibited in the presence of ammonia because the whole cell machinery becomes affected. Ammonia alters enzyme activities, such as phosphofructokinase activity, primarily by the effect of cytoplasmatic acidification (McQueen et al., 1990a). When an ammonium ion enters the cell, it provokes cytoplasmatic acidification, a characteristic phenomenon of apoptosis (McQuenn et al., 1990). Cell growth inhibition by ammonia due to induction of apoptosis has been reported in a lymphoid cell line (Mirabet et al., 1997) and BHK cells (Cruz et a., 2000). In stirred cultures, the sensitivity to ammonia will be higher and can be attributed to the fact that agitation of the cultures may promote the uptake of the metabolite by the cells (Cruz et al., 2000). Total concentrations of ammonia and ammonium as low as 2-3 mM have been reported to reduce cell growth considerably, depending on the cell line and culture conditions (Schneider et al., 1996).

1.2.1.8. Lactate

In the presence of lactate in the culture medium, cell growth reduces with the increase in lactate concentration (Figure 1-6). However, to obtain a similar growth decrease to that of ammonia, the concentration of lactate had to be much higher (10-fold). This can be supported by the studies performed by Cruz et al. (2000) with BHK cells, where values obtained for Michaelis-Menton constant ($k_{1/2}$) of 22 mM for lactate and 1.1 mM for ammonia were observed. In their studies, the cell death was observed only at lactate concentrations higher than 38 mM. The reduction of cell growth by lactate was not the result of apoptosis, as in the case of ammonia, because the percentage of apoptotic nuclei did not change significantly in the presence of lactate, although the presence of lactate caused cytoplasmatic acidification, as shown by the in vivo NMR assays (Cruz et al., 2000). Nonetheless, lactate-induced cytoplasmatic acidification (pH decrease from 7.6 to 7.0 in presence of added 60 mM lactate) was much lower than that of ammonia (pH decrease from 7.6 to 6.6 in the presence of 10 mM added ammonia). Also, the inhibitory effect of lactate on cell growth was also partially due to osmolarity (Lao et al., 1997; Ozturk et al., 1992).

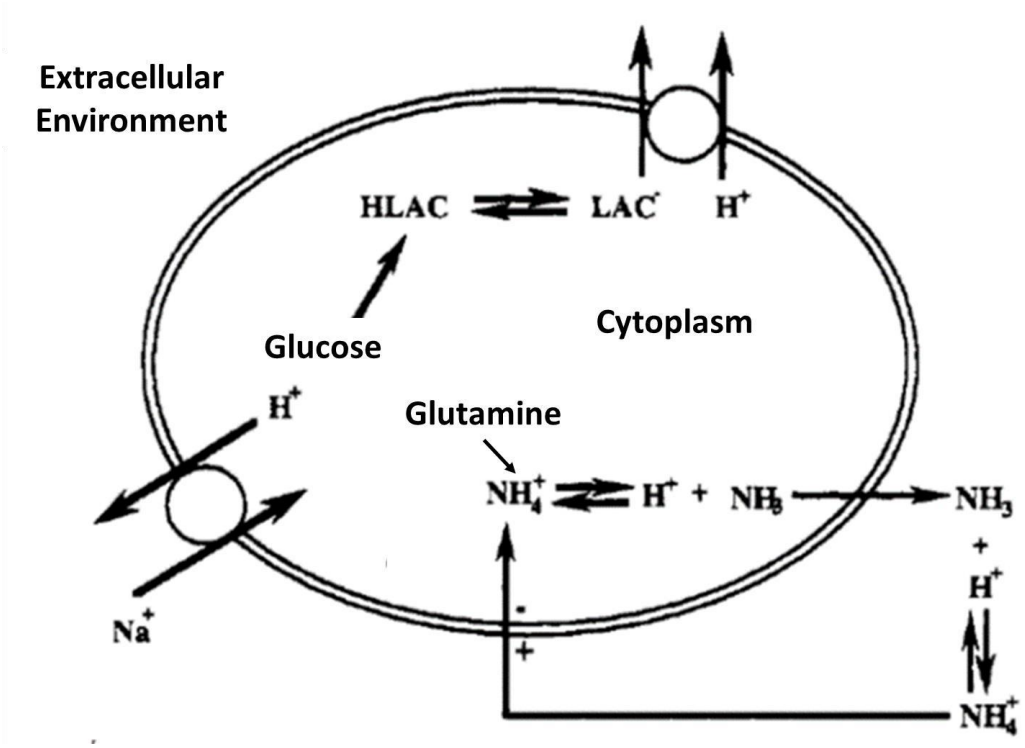

Figure 1-6: Schematic diagram of a mammalian cell demonstrating how lactate and ammonia disturb the intracellular pH. Lactate and ammonia are produced inside the cell from glucose and glutamine. Unprotonated lactate (LAC^-) is transported along with a proton. Once outside the cell, the proton is released and the external pH decrease. The intracellular pH is in turn disturbed. Free ammonia escapes the cell quickly, and the charged species NH_4^+ enters the cell down its electrochemical gradient. Figure adapted from Wu et al., 1993.

1.3. Bioreactor Systems for Small-Scale Production of mAbs

Process characterisation is important in the development of a pharmaceutical product because it is used to establish relationships between input and output parameters, define optimum process conditions, and establish acceptable operating ranges. More recently this has been done using risk-based approaches following the QbD paradigm (Tescione et al., 2015). Since performing a characterisation study at the manufacturing scale is not practically feasible due to the cost of operation and limited availability of large-scale bioreactors, scale-down models that represent the performance of manufacturing scale process are usually employed at the laboratory scale (Li et al., 2006). In turn, the scale-down model must approximate key performance attributes of the manufacturing data set, to ensure that the process characterisation data will be meaningful and representative of manufacturing performance (Rathore et al., 2005). Scale-down is a methodology that was originally

proposed by Oosterhuis (1984) for modelling and evaluating the effects of environmental gradients on culture performance. The goal when scaling-down is to create a small-scale or lab-scale system that mimics the performance of the large-scale (pilot or manufacturing) counterpart, when both the process parameters are varied within their operating ranges and also when a process parameter deviates outside its operating range. Before it can be used for lab studies, the scale-down model needs to be qualified and its equivalence to large-scale examined. Data from an inaccurate scale-down model could result in conclusions that may not apply to large-scale, resulting in an unsuccessful process-validation campaign or continued lot failures in a manufacturing campaign (Rathore et al., 2005).

The engineering principles that are used for scaling-up a bioreactor process can be applied to scaling-down a process. Development of a scale down model requires evaluating one or more scale-dependent parameters, holding these scaling criteria constant across scales, and performing experiments at bench scale to evaluate which of these scaling parameters is an appropriate scale down criterion for the process. For a stirred-tank bioreactor process, scaling criteria that are traditionally considered include specific energy dissipation rate (P/V) and volumetric mass transfer coefficient ($k_L a$). Other criteria that have been considered for scaling up or scaling down a process include mixing time and shear rate (or, impeller tip speed), but these are less commonly used because either the scaled values are not practical or, they are not the limiting parameter in the system. In order to select the appropriate scaling criteria, mass transfer and mixing characterisation data is required at all bioreactor scales (Amanullah et. al., 2004).

There is a keen interest in miniaturised bioreactors (MBRs) during the past decade (Kumar et al., 2004). Small-scale cultivation has the advantages of parallelisation, automatisation and cost reduction for medium constituents, especially for mammalian cell cultures. Of high importance in such small-scale studies is the transferability to manufacturing scale (Micheletti et al., 2006b) (Figure 1-7). However, the majority of small-scale culture systems usually have a simple design and a low level of instrumentation and control (Fenge et al., 2006). More recently, MBRs can be used in conjunction with automated robotic systems and other miniature process units to deliver a fully-integrated, high-throughput (HT) solution for cell cultivation process development.

Examples of MBRs for mammalian cells are shake flasks (SFs) (Bareither et al., 2011; Büchs et al., 2000a; b; Cowger et al., 1999; Liu et al., 2001; Maier et al., 2001; Mrotzek et al., 2001), roller bottles (Berson et al., 2008), spinner tubes (Fenge et al., 2006), stirred tank reactors (Bareither et al., 2011), test-tubes, T-flasks (Griffiths,

2000), microtiter plates (MTPs) (Duetz et al., 2000; 2001; Fenge et al., 2006; Girard et al., 2001; Hermann et al., 2003; John et al., 2001; Weiss et al., 2002; Wurm 2004), and microfluidics devices (Kostov et al., 2001; Micheletti et al., 2006b).

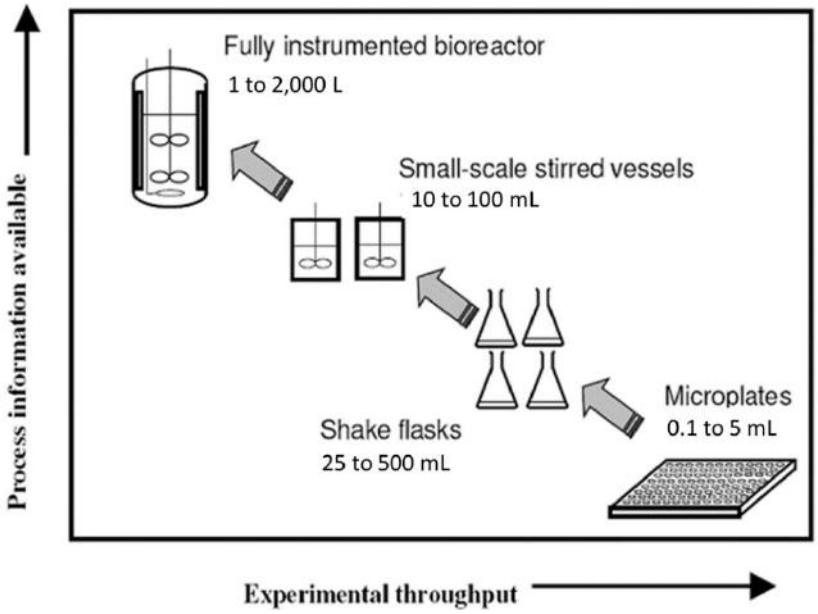

Figure 1-7: Process information output versus experimental throughput capability trade-off for various cell cultivation devices at different scales. It is shown that as bioreactors scale increase, more process information is available due to improved monitoring and control systems. Figure adapted from Betts et al., 2006.

Several scale-down cell culture systems have been commercialised based on these developments including the Bioprocessors SimCell microbioreactor array, Applikon Micro-Flask system, Applikon Micro-Matrix system, TPP TubeSpin® Bioreactor, Hexascreen multiple mini-bioreactor system, Pall micro24, m2p Labs BioLector™, Applikon MiniBioreactor, Eppendorf DASbox® Mini Bioreactor and TAP Biosystems ambr™ system (Figure 1-8). More recently, the ambr™ system has evoked significant interest in the biopharmaceutical industry as it comes closest to reproducing the performance of stirred tank bioreactors in a microscale system. This system has 24 - 48 single-use bioreactors controlled by an automated workstation. Each bioreactor has a 10–15 mL working volume, an internal impeller, and capability of gases being individually supplied and controlled to each vessel (Hsu et al., 2012; Lewis et al., 2010; Moses et al., 2012; Nienow et al., 2013).

The small-scale culture for mAb production at low concentrations (1–100 $\mu g/mL$) is enough to supply enough material for research and diagnostic purposes

(Nilsang et al., 2007). However, the market needs for therapeutic products require large-scale manufacturing capacity with demands on mAbs of 100–1,000 kg/year, which can only be achieved in large bioreactors and by efficient processes that produce several kg/day (Chu et al., 2001; Jain et al., 2008).

1.3.1. Stirred Tank Reactor

The engineering environment in stirred tank reactor (STR) has been extensively characterised. For a typical cell culture in an STR, the average energy dissipation rate is between 1 and 12 Wm^{-3} (Langheinrich et al., 1999; Nienow et al. 1996; Varley et al., 1999), typical values of $k_L a$ are between 1 and 10 h^{-1} (Fenge et al., 1993; Varley et al., 1999), while mixing times are generally less than 200 s. Given this understanding of the hyrodynamics and gas-liquid mass transfer, a variety of bases for scale-translation of suspension cell cultures have been successfully implemented including fluid turnover rate (Chisti, 1993); superficial gas velocity (Xie et al., 2003); vessel volumes per minute (vvm), impeller tip speed (Marks, 2003); energy dissipation rate (Li et al., 2006; Betts et al., 2006) and $k_L a$ (Lamping et al., 2003).

The advantages of using STRs include the ability to monitor and control parameters such as pH, DOT, foam height, nutrient concentration, and temperature. The disadvantages of using STRs as a scale-down tool for bioprocess development are the low throughput, the extensive requirements for raw material (> 1 L), the labour requirement for inoculation, sampling, harvesting and then cleaning (not applicable for disposable STRs); and the potential damage to mammalian cells caused by sparging. For these reasons, in recent years, the use of multiple miniature STRs for bioprocess development has received much interest (Bareither et al., 2011; Betts et al., 2006; Gill et al., 2008; Lamping et al., 2003; Vallejos et al., 2006) (Figure 1-8). These systems operate with a working volume comparable to that used in 24-deep well microtitre plates (5 – 10 mL). The attraction of this approach includes the ability to operate with higher oxygen transfer rates than surface aerated bioreactors; online measurement of dissolved oxygen, pH and optical density; and the ability to maintain geometric similarity with the production bioreactor (Ge et al., 2006; Lamping et al., 2003). However, the disadvantage of using miniature STRs is the lack of automation and low throughput compared to microwell plates and shake flasks.

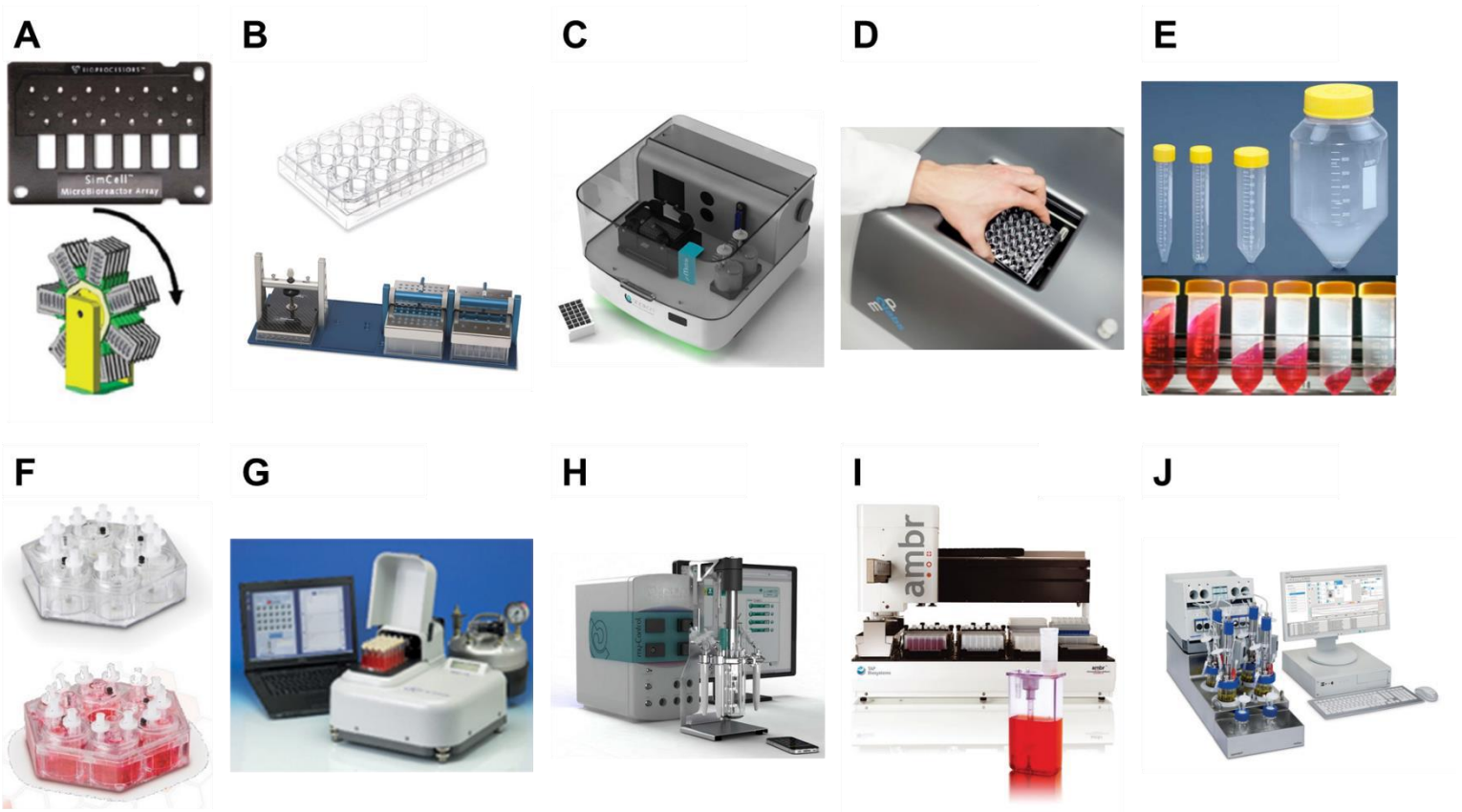

Figure 1-8: Commercialised scale-down cell culture systems: SimCell micro bioreactor array (Bareither et al., 2011) (A), Applikon Micro-Flask system (www.applikon-bio.com) (B), Applikon Micro-Matrix system (www.applikon-bio.com) (C), m2p Labs BioLectorTM (www.m2p-labs.com) (D), TPP TubeSpin® Bioreactor (www.tpp.ch) (E), Hexascreen multiple mini-bioreactor system (triplepoint.co.nz) (F), Pall micro24 (www.pall.com) (G), Applikon MiniBioreactor (www.applikon-bio.com) (H), TAP biosystems ambrTM system (www.tapbiosystems.com) (I) and Eppendorf DASbox® Mini Bioreactor (www.eppendorf.com) (J).

1.3.2. Shake Flask

Shake Flasks (SFs) are widely used in the biotechnology industry and academia for multi-parameter parallel screening experiments, culture optimisation or functional profiling of large number of mutants (Giaever et al., 2002), metabolic studies employing labeled substrates (Guilmanov et al., 2003), process development projects (Bareither et al., 2011; Betts et al., 2006; Büchs 2001; Fernandes et al., 2006; Freyer et al., 2004; Kumar et al., 2004; Marques et al., 2009; Suresh et al., 2009; Weuster-Botz et al., 2001) and, simply as bioreactors.

SFs are easy to operate, require small amounts of material (25 mL – 5 L) and cost very little (Büchs, 2001). SFs come in a variety of guises, can be made out of glass or plastic and some have baffles to aid aeration and mixing. They can be agitated using either orbital or linear shaking and housed in a temperature controlled cabinet. Factors that affect SF cultivations include vessel size, fill volume, construction material, geometry of baffles, shaking frequency and type of plug used to seal the vessel. Typical $k_L a$ values obtained in SFs are in the order of 150 h^{-1} up to 280 h^{-1} and thus in the range of medium stirred bioreactors (Kato et al., 1998; Wittmann et al., 2003). Under typical SF conditions for the growth of mammalian cells, CFD predicted $k_L a$ values of between 10 h^{-1} and 100 h^{-1} (Zhang et al., 2008). Only recently has there been the introduction of instrumented SFs, designed to measure and potentially control pH and DOT levels online (Sensolux from Sartorius Stedim biotech and SFR from PreSens) (Bareither et al., 2011; Tolosa et al., 2002; Wittmann et al., 2003). Other parameters that can now be measured online include oxygen transfer rate (OTR) and carbon dioxide evolution rate (CER) and from these the respiratory quotient (RQ) can be derived (Kumar et al., 2004).

A major limitation of SFs is their reliance on surface aeration, leading to reduced oxygen transfer relative to STRs, oxygen limitation, and pH excursion may occur without being observed. For sampling, it is necessary to take out the shake-flasks from the shaking devices, thus interrupting oxygen supply. Various researchers have modified the flask with baffles and steel springs and other enhancements to improve aeration (Büchs 2001; Henzler et al., 1991; Weuster-Botz et al., 2001). Oxygen and CO_2 ventilation were found limiting in SFs with cotton plugs. These limitations were successfully overcome by improved gas exchange using membranes to replace cotton plugs and even more by using box-shaped shake-flasks (Kato et al., 1998). Aerosol formation and excessively splashing during shaking can cause wetting and clogging of the sterility barriers (i.e. cotton plugs, silicone rubber foam), which significantly reduces oxygen transfer (Gupta et al., 2003; Lotter et al., 2004; Wittmann et al., 2003).

In general, the disadvantages of SFs with regards to bioprocess development are the lack of automation hence, considerable labour is required during large screening and

optimisation studies compared to alternative systems such as microwell plates, the large volumes of expensive raw materials required, the low throughputs and, they are most of the times non-instrumented, meaning shifts and deviations of important parameters like pH and DOT are not captured during a culture.

1.3.3. Microtiter Plate

The concept of microtiter plates (MTPs) (also called microwell plates) was first introduced in 1951 mainly for analytical purposes. MTPs have been used for decades in medical diagnostics and later by the pharmaceutical industry, in combinatorial chemistry and biotechnology. MTPs offer the possibility of providing a large number of parallel and miniaturised reactors with identical shape and fluid dynamics characteristics. MTP handling can be automated using robotics with modern pipetting, dispensing systems, centrifuges and, other analytical equipment. Thus, several thousands of samples may be handled in a short time (Harms et al., 2002; Lye et al., 2003). Such robots are currently available through commercial suppliers such as Tecan® and Perkin Elmer®. The use of MTPs have been shown to benefit the following applications: screening for secondary metabolites (Minas et al., 2000); screening for new drugs and antibiotics (Lueking et al., 1999); screening for new biocatalysts and enzymes (Doig et al., 2002; Duetz et al., 2001; Tsotsou et al., 2002); cultivation of clone libraries and clone selection (Connon et al., 2002); expression studies of different recombinant clones; media development and optimisation and strain development; small-scale cultivations for the cell cultures (Balcarcel et al., 2003; Deshpande et al., 2004; Duetz et al., 2000; Girard et al., 2001; John et al., 2003; Zimmermann et al., 2003); HT assay protocols (ELISA) (Ruitenberg et al., 1976; Severns et al., 1984).

Currently, various types of MTPs are available in the market, whereby standard well numbers in each plate varies from 6, 12, 24, 48, 96, 384 to 1536. The MTP wells can either be rectangular or cylindrical, with square geometries aiding mixing and oxygen transfer by mimicking the action of baffles (Figure 1-9). MTPs are usually fabricated from plastics such as polycarbonate or polypropylene. The typical culture volume used in the MTP well varies from 25 μL to 5 mL. Microtitre plates with pH and DOT integrated sensors were developed (Deshpande et al., 2004; Guarino et al., 2004; John et al., 2003; Kensy, et al., 2005a;b; Weiss et al., 2002) and are currently available on the market through companies such as PreSens and Applikon.

To date, microbial fermentation has been the unit operation most studied in MTPs (Doig et al., 2002; Duetz et al., 2000; Ferreira-Torres et al., 2005; Micheletti et al., 2006a,b). In general, good agreement is seen with biomass growth and product titers compared with commonly used laboratory formats. Work on the cultivation of yeast (Jansen et al., 2003), bacteria (Kensy, et al., 2005a), filamentous organisms (Elmahdi et al., 2003; Minas et al.,

2000), insect cells (Bahia et al., 2005) and immobilisation of enzymes (Brandt et al., 2006) in microwell format has also been reported. In contrast, little work has been focused on suspension-adapted mammalian cells.

Due to the increase in surface area caused by greater fluid dissipation up to the sides of each microwell and the increased driving force for oxygen caused by better mixing, OTR is proportional to shaking amplitude and frequency, therefore increasing these parameters can be beneficial (Duetz et al., 2000). In addition, Hermann et al. (2003) have reported OTR to be inversely proportional to fill volume, particularly at higher shaking frequencies. However, there is a point beyond which any increase in agitation results in spillage of process liquid (unless the well is capped – which has its problems, with reduced oxygen transfer into the well). Numerous studies on gas-liquid mass transfer in shaken microwell systems have been published. This is due to the predominance of studies on microbial fermentation (Doig et al., 2002; Duetz et al., 2000; 2001). In general, reduction in culture volume, an increase in shaking diameter, and increasing shaking speed all result in an increase in OTR (Duetz et al., 2000; 2001; Kensy, et al., 2005a;b).

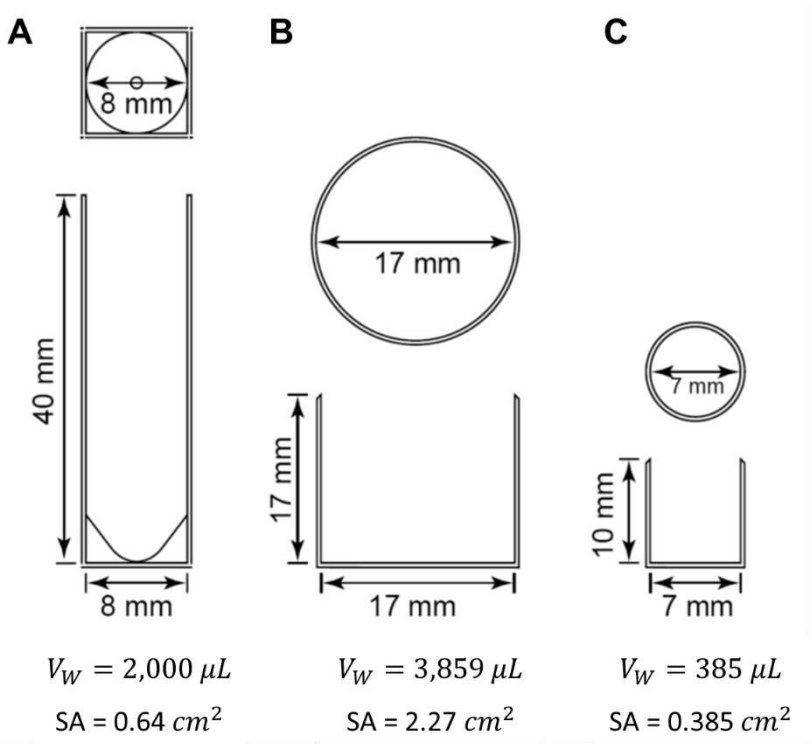

Figure 1-9: Diagram of individual microwell formats: 96-deep square well format (96-DSW) (A); 24-standard round well format (24-SRW) (B); 96-standard round well format (96-SRW) (C). V_W, total well volume; SA, static surface area available for gas - liquid mass transfer. Figure adapted from Lye et al. (2003).

Rapid and efficient mixing during liquid addition to individual wells underpins the reproducibility of all bioprocess studies (Micheletti et al., 2006b). Examples include pH control and nutrient additions during fed-batch cultures. Mixing can be achieved using pipette aspiration or magnetically-agitated stirrer bars; however, orbital shaking of the entire plate is by far the most common method (Betts et al., 2006). Liquid-phase mixing times in flat and round-bottomed 96-well plates, based on the dispersion of pH indicator dyes, were found to vary between 5 – 500 s (Weiss et al., 2002). These values were found to be a function of well geometry, shaking speed and the method of liquid addition.

Despite some progress, knowledge of the basic fluid mechanics in shaken microwells is still far from complete. For example, although the Reynolds number has been published for some microwell systems information on how it relates to laminar and turbulent flow regimes is still lacking. Understanding the engineering environment in microwell systems will ultimately underpin their use in bioprocess studies, ensuring the generation of reproducible, quantitative and scalable information (Ferreira-Torres et al., 2005).

The bottlenecks for the use of MTPs as MBRs are the risk of cross-contamination primarily caused by aerosol formation at high shaking rates and relatively poor aeration rates in many cases (Duetz et al., 2001); the lack of control in experimental parameters such as pH, DOT and OTR (Harms et al., 2002); limiting mixing at low shaking rates (Weiss et al., 2002); absence of off-line sampling of each well; stopping of the shaking device for sampling; high evaporation rate compared with other MBRs. The medium evaporation is a critical factor particularly for slowly growing organisms such as mammalian and insect cells (Bahia et al., 2005; Girard et al., 2001). However, this limitation can be overcome by using different types of membranes and suitable closures at the top of the plate (Duetz et al., 2000; 2001; Zimmermann et al., 2003). Careful selection of membranes or enclosure is required for a particular application to ensure sufficient oxygen permeability yet minimise the evaporation.

In spite of some of the inherent limitations of cell cultures in MTPs, progress has been made in the characterisation of mixing, mass transfer and instrumentation of these vessels, meaning that the unique advantages of these devices in terms of automation potential and intrinsic HT capability are leading to their growing use as early-stage MBRs and scale-down models.

1.4. Engineering Parameters in Shaken Bioreactors

It has been estimated that nearly 90% of all laboratory cell culture and fermentation experiments are performed in shaken bioreactors like the SFs and MTPs, yet only 2% of all relevant publications in the area have dealt with engineering aspects (Büchs, 2001). SFs have been characterised regarding power consumption by Büchs et al. (2000a; b), where

measurements were carried out with water for different shaking frequencies, flask sizes and fill volumes (Equation 1-3).

$$P_0^{'} = \frac{P}{\rho N^3 d_f^4 V_L^{1/3}} = C\ Re^{-0.2}$$

Equation 1-3

where $P_0^{'}$ is a modified power number, P is the energy dissipation rate, ρ is the liquid density, N is the shaking speed, V_L is the liquid fill volume, Re is the Reynolds number ($Re = \frac{\rho N d_f^2}{\mu}$), which was calculated using the maximum inner flask diameter d_f as the characteristic length scale, μ is the liquid viscosity and the constant C was found to be equal to 1.94 using least-squares non-linear fitting of experimental data points. The sated accuracy of the $P_0^{'}$ prediction is ± 30%.

From the power number variation with the Reynolds number, two flow conditions were identified: “in-phase” conditions in which the bulk of the liquid in the flask circulates in phase with the shaking table; “out-of-phase” conditions, in which only a minor fraction of the liquid is actually moving along the flask wall and the power consumption is greatly reduced. In order to systematically describe the two flow conditions, a new non-dimensional number, called the phase number (Ph), was introduced and can be expressed by equation 1-2, where “in-phase” operation is assumed to exist for $Ph > 1.26$ while “out-of-phase” conditions ($Ph < 1.26$) may exist when large flasks or high viscosity fluids are used (Micheletti et al., 2006a) (Equation 1-4).

$$Ph = \frac{d_s}{d_f}\left\{1 + 3log_{10}\left[\frac{\rho(2\pi N)d_f^2}{4\mu}\cdot\left(1 - \sqrt{1 - \frac{4}{\pi}\left(\frac{V_L^{1/3}}{d_f}\right)^2}\right)^2\right]\right\}$$

Equation 1-4

Where d_s is the shaker diameter and d_f is the maximum inner diameter of the SF.

Besides measurement of the torque on the drive shaft, other techniques, such as the temperature method (Kato et al., 2004; Raval et al., 2007) and CFD (Zhang et al., 2005; 2008), have been used to measure energy dissipations of up to 1 kWm^{-3} in shaken bioreactors. However, these studies have not published a simple correlation to accurately predict mean energy dissipation from known operating conditions. Besides quantification of mean energy

dissipation rate, a few studies have been published looking at local energy dissipation rates (Peter et al., 2006). Knowledge of spatial variation in energy dissipation can be important for bioprocesses that are limited by hydromechanical stress, such as animal cell culture (Chisti, 2001).

A relatively large number of studies have examined gas-liquid mass transfer in shaken systems. Hermann et al. (2003) measured OTR in a single well of a 96-well MTP using the sulphite oxidation method for a broad range of shaking frequencies (0–1000 rpm), shaking diameters and fill volumes. They observed that OTR increased exponentially, for shaking speeds higher than a critical value, called critical shaking frequency, N_{crit} (Equation 1-5). N_{crit} is the shaking speed above which the surface tension forces are overcome by the centrifugal force and a significant increase in the fluid motion and oxygen transfer is observed (increase in $k_L a$) (Figure 1-10). Studies on the well geometry also revealed that OTR values in wells with a square cross-section are approximately twice those measured in round wells for the same shaking frequency and fill volume. The latter observation may be explained by the baffling effect of the corners of the square well.

$$N_{crit} = \sqrt{\frac{\sigma d_w}{4\pi\rho V_L d_s}}$$

Equation 1-5

Where σ is the surface tension and d_w is the microwell diameter.

Gas-liquid mass transfer coefficients, $k_L a$, values for various round-well diameters MTPs have been reported by Doig et al. (2005), based on both dynamic gassing out measurements and on the growth kinetics of an obligate aerobe. The following correlation was proposed to enable prediction of $k_L a$ values:

$$k_L a = c_1 \frac{D_{O_2}}{d_w} a_i Re^{0.68} Sc^{0.36} Fr^x Bo^y$$

Equation 1-6

where c_1 is a coefficient that assumes different values for different geometries (0.55 for 24-well plate; 0.21 for 96-well plate and 0.11 for 384-well plate), D_{O_2} is the oxygen diffusion coefficient, a_i is the initial specific surface area, Re is the Reynolds number, Sc is the Scmidt number ($Sc = \frac{\mu}{\rho D_{O_2}}$), Fr is the Froude number ($Fr = \frac{d_s(2\pi N)^2}{2g}$), x is the coefficient that depends of the microplate geometry (0.86 for 24-well plates, 0.64 for 96-well plate and 0.51 for 384-

well plates), Bo is the Bond number ($Bo = \frac{\rho g d_w^2}{W}$), y is the second coefficient that depends on the microplate geometry (0.03 for 24-well plates, 0.15 for 96-well plates and 0.18 for 384-well plates), g is the acceleration of gravity and, W is the wetting tension. The stated accuracy of the $k_L a$ prediction is ± 30%.

Characterisation of the engineering environment in microwell systems will ultimately underpin their use in bioprocess studies, ensuring the generation of reproducible, quantitative and, above all, scalable bioprocess information.

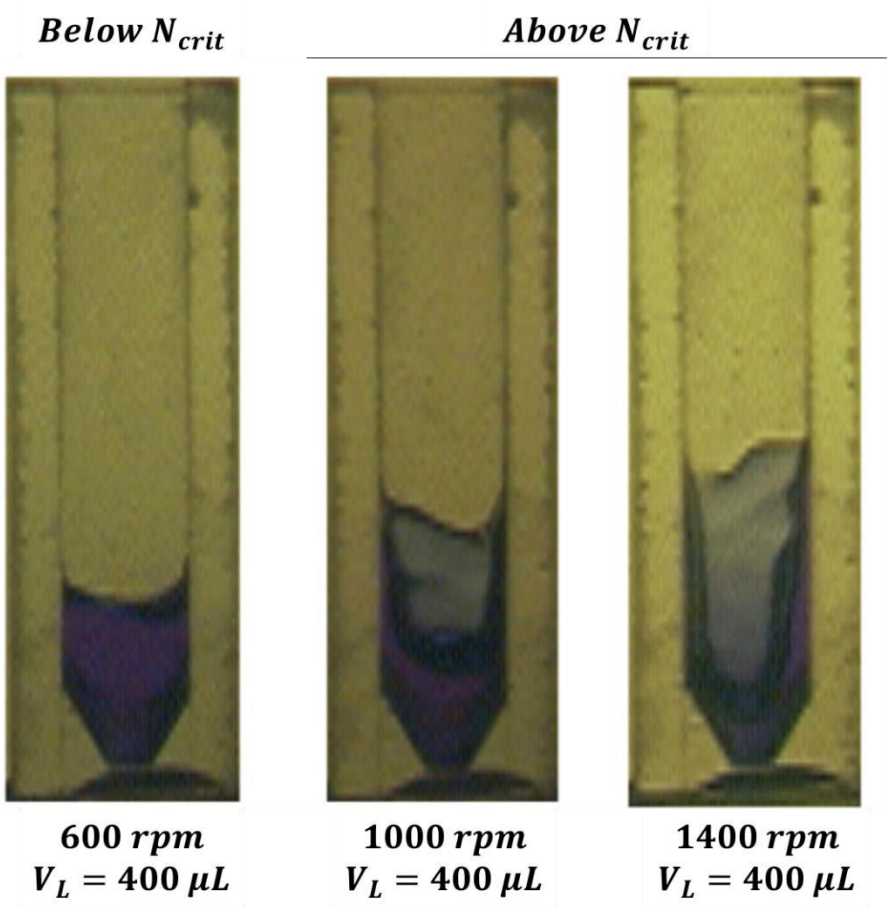

Figure 1-10: Fluid motion and gas-liquid interfacial area available for oxygen transfer of a single-well from a 96-DSW (deep square well) MTP with increasing shaking frequency. Adapted from Micheletti et al., 2006b.

1.5. Aims and Objectives

The primary goal of this study was to evaluate the response of mammalian cells to pH perturbations using a parallel microwell approach. To accomplish that purpose, a scale-down model to study the pH effect on growth and monoclonal (IgG4) production of an industrial GS-CHO cell line (CHO-CY01) was developed. The research methodology is divided into four parts: a high-throughput approach to CHO-CY01 cell culture process development (Chapter 3); inter-Scalability of the CHO-CY01 cell line kinetics (Chapter 4); effects of Carbon dioxide on CHO-CY01 cell line kinetics (Chapter 5); pH Impact on CHO-CY01 cell line kinetics (Chapter 6).

In Chapter 3 an engineering characterisation (mixing time, Reynolds, Froude, and Phase numbers and $k_L a$) of 24-SRW MTPs under conditions suitable for mammalian cell culture using the proven correlations was performed. To explore the potential of microwell cultures for batch and fed-batch cultivations of the CHO-CY01 cell line, several operating conditions (shaking speed, fill volume, sterile closure and, selective pressure) were tested. A suitable scale translation criteria for a 5-L STR scale-down model of batch and fed-batch CHO-CY01 cell cultures was developed in Chapter 4. Also, the scale-down model validation was performed with batch and fed-batch cultures at 24-SRW MTP and SFs (traditional models). Using the scale-down model of a 5L-STR, several fed-batch strategies were tested and validated for the purpose of improving IgG4 productivity. Inherent to all mammalian cell cultures is always the accumulation of waste by-products, like ammonia and lactate. Therefore, the identification of lactate and ammonium inhibitory concentrations and inhibition kinetics in CHO-CY01 cell culture was also done in Chapter 4. Having characterised the operating space, in Chapter 5 the analysis of pH perturbations in the system was performed, through the manipulation of CO_2 concentrations in headspace of the 24-SRW MTPs. With the development of a high-throughput online multi-parametric analysis method at the microwell scale it was possible to determine the effects of carbon dioxide on the CHO-CY01 cell line growth, cellular metabolism, and IgG4 production in order to find the optimum pH profile for high IgG4 production. Therefore, a series of CHO-CY01 cell line cultures at constant, biphasic and multiphasic CO_2 concentrations were carried out in Chapter 5. After this process development study, in Chapter 6 a series of batch and fed-batch cultures at different constant pH set-points and pH shifts were performed. Also, a proteomic analysis (2D-DIGE PAGE) of some CHO-CY01 cell line fed-batch cultures was done to better understand the CHO-CY01 cell metabolism.

Chapter 2 Materials and Methods

2.1. Cell Culture

An industrial GS-CHO cell line (Lonza Biologics, Slough, UK) producing IgG4 (supplied by MedImmune Ltd., Cambridge, UK) (CHO-CY01) was routinely sub-cultured by dilution at 3 to 4-day intervals using a viable cell seed density of $2.0 \times 10^5\ cells\ mL^{-1}$. The sub-cultures were performed in 250 mL SFs ($V_L = 50\ mL$) (Corning, New York, USA) polycarbonate Erlenmeyer flasks with vent caps (Sigma-Aldrich, Poole, Dorset, UK) at 37°C, 220 rpm ($d_s = 10\ mm$), and 5.00%(v/v) CO_2. The culture medium used was 1x CD-CHO (Invitrogen, Paisley, UK) supplemented with 25 μM L-Methionine sulfoximine (MSX). All cell operations requiring sterility were performed in a laminar flow cabinet (Walker Safety Cabinets, Derbyshire, UK). Transfer of liquid was performed using pre-sterilised pipettes of an appropriate volume.

2.1.1. Creation of Cell Bank and Revival of Cells from Liquid Nitrogen Storage

GS-CHO cells were cultured in 250 mL SFs for 48 hours, transferred into 50 mL centrifuge tubes, and centrifuged at 200 g for 5 minutes. The cells were resuspended at a density of $1.0 \times 10^7\ cells\ mL^{-1}$ in 1 mL of freezing medium and transferred into 1 mL sterile cryovials (Fisher Scientific, Loughborough, UK). These cryovials were loaded into a Nalgene Mr. Frosty freezing container (Sigma-Aldrich, Poole, Dorset, UK) and placed in a -80°C freezer. After 24 hours, the vials were transferred to CryoCanes and stored in a liquid nitrogen dewar.

GS-CHO cells were frozen in 50% (v/v) fresh growth medium and 50% (v/v) conditioned growth medium (day 2 to 4 cell conditioned media collected from GS-CHO cultures during the sub-culture procedure) and DMSO to a final concentration of 7.5% (v/v). DMSO was purchased from Sigma-Aldrich (Poole, Dorset, UK). The freezing medium was filter sterilised and chilled to 4°C before use.

The CryoCanes were removed from liquid nitrogen and rapidly thawed in a 37°C water bath to revive the GS-CHO cells from the liquid nitrogen storage. The contents of the cryovial were transferred into a 125 mL SF containing 27 mL of pre-warmed CD-CHO medium. This flask was incubated at 37°C, 220 rpm (d_s=10 mm), and 5.00% (v/v) CO_2 until new sub-passage of the cells.

2.1.2. Shake Flask Cultures

CHO-CY01 cells were routinely maintained in disposable SFs (Corning 125 or 250 mL polycarbonate Erlenmeyer flasks with vent caps; Sigma®) at working volumes between 50 mL and 100 mL, respectively. These were kept on an orbital shaker (CERTOMAT MO II, Sartorius)

inside a CO_2 incubator (MCO-19AIC, Panasonic Healthcare) at 37° C and 5.00% (v/v) CO_2. The orbital shaker was set to shake at 220 rpm with shaking diameter (d_s) of 25 mm. Cells were seeded at a density of $2.0 \times 10^5\ cells\ mL^{-1}$ and sub-cultivated every 3 - 4 days until the number of passages did not exceed 30.

2.1.3. Microwell Plate Cultures

Twenty-four-well ultra-low attachment standard round well microtiter plates (24-SRW MTPs) were used to minimise cell and protein attachment (Corning Life Sciences, New York, USA). Dimensions of a 24-SRW MTP individual well and schematics of the 24-SRW MTPs system used are represented in Figure 2-1 (A).

CHO-CY01 cells were seeded at the viable cell density of $2.0 \times 10^5\ cells\ mL^{-1}$ using diluted mid-exponential (72 h) culture. Microwell plates were sealed using the 'sandwich lid' system (Duetz et al., 2000) in conjunction with a metal clamp (´system Duetz`) to minimise evaporation over extended periods of culture (Figure 2-1(C)). The sandwich lids were sterilised by autoclaving and subsequently oven dried for 24 hours before use. After sterilisation, each well was filled with $0.85\ mL$ of inoculum using a matrix multichannel electronic pipette (15 – 1,250 μL) (Thermo Scientific, Paisley, UK). The ´system Duetz` lids were carefully placed on top of the 24-SRW MTP, i.e. the 5 positioning pins were placed in the spaces between the wells. The maximum number of 24-SRW MTPs with ´system Duetz` lids that can be stacked is 4 (Figure 2-1 (B)). The stacked microwell plates were screwed down using the clamp system to the extent that the stainless steel of the sandwich covers (Figure 2-1 (C)) touched the (polystyrene) top of the 24-SRW MTPs. Two different configurations of the ´system Duetz` lids were tested. One included a stainless steel foil in combination with a hard silicone layer (CR1524a), and the other included a soft silicone layer with no stainless steel foil (CR1524) (Figure 2-1 (D)). With the first configuration, the exchange of the headspace air is further reduced compared with the second configuration, which ultimately corresponds to a further reduction in the evaporation rate (Table 2-1). CHO-CY01 cell cultures were shaken at 220 rpm in an orbital shaker platform (KS 260 control, IKA®/ CERTOMAT MO II, Sartorius) (d_s= 25 mm) inside a CO_2incubator (MCO-19AIC, Panasonic Healthcare/MCO-18AC, Sanyo) at 37° C. The CO_2 atmosphere used ranged from 0% to 20% (v/v). Evaporation rate of the cell culture was monitored throughout the culture period by weighing the microwell plates before and after sampling or feeding. The sacrificial well sampling method was used for sampling 3 or 4 (after 7 days) wells daily per time point as required (3 to 4 replicates) (Micheletti et al., 2006b).

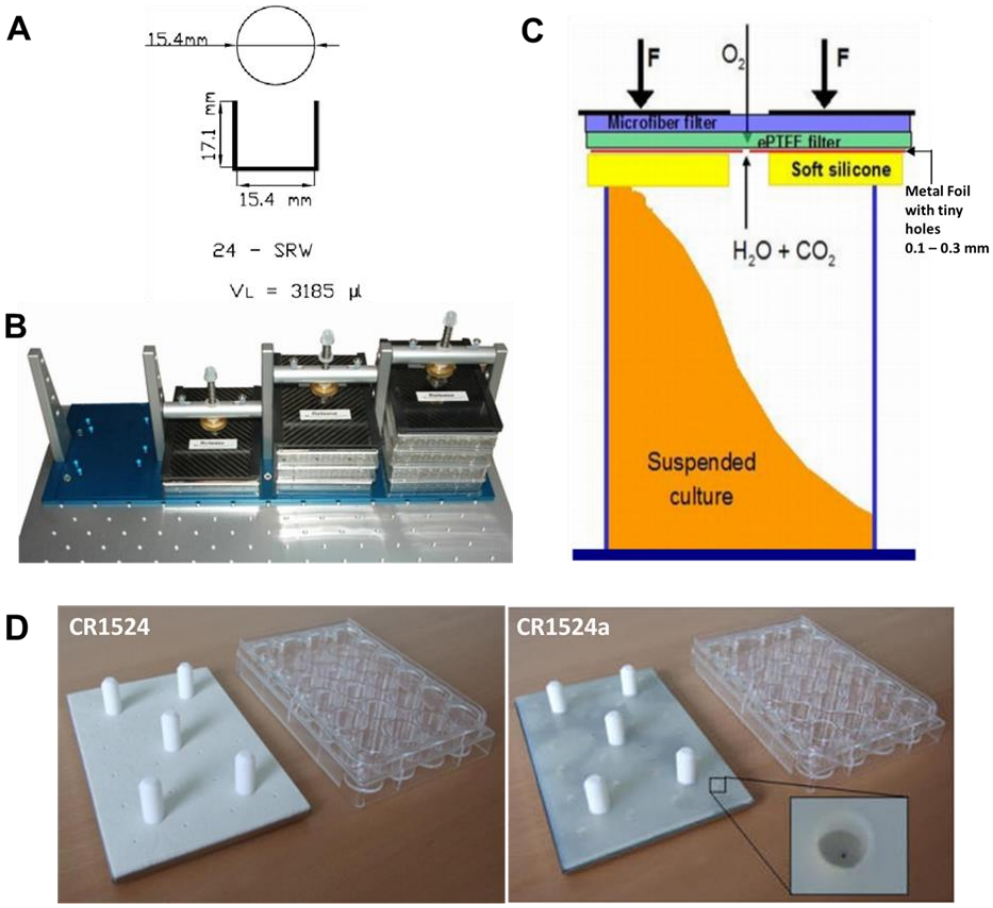

Figure 2-1: Schematic diagram of the 24-SRW MTP system components: 24-SRW MTP well dimensions (A), universal cover clamp with four positions where the 24-SRW MTP are placed (B); and schematics of a well closed with the ´system Duetz` lid with the representation of the gas exchange (C). Two ´system Duetz` lid configurations: CR1524 (rigid stainless steel plate, microfiber filter, ePTFE filter, and a soft silicone layer) and CR1524a (rigid stainless steel plate, microfiber filter, ePTFE filter, stainless steel foil, and a hard silicone layer) (D)[2].

Table 2-1: Specifications of the two CR1524 and CR1524a (Low-evaporation version of CR1524) ´System Duetz` lids[2].

	CR1524	**CR1524a**
Culture volumes	0.5-1 mL	0.5-1 mL
Hole size in silicone layer	1 x 3 mm	3 x 3 mm
Hole diameter in stainless steel foil	NA	0.2 mm
Exchange of headspace air	1.1 $mL/minute$	0.25 $mL/minute$
Evaporation rate (30ºC, 50% humidity)	30 $\mu L/well/day$	6 $\mu L/well/day$

[2] www.enzyscreen.com

2.1.4. Stirred Tank Bioreactor Cultures

STR experiments were performed using a 5-L BIOSTAT B-DCU (B. Braun Biotech, Sartorius, Surrey, UK) with 3.5 L working volume (diameter of the vessel, 160 mm). The vessel was unbaffled and stirred by a single, down-pumping (blade angle 45º), three-bladed segment impeller rotating at 260 rpm. Supervisory and data acquisition were managed by an MFCS/Win 2.0 system. The temperature was controlled at 37.0 ± 0.1ºC using an electrical heating blanket. The DOT was maintained at 30 ± 1% saturation by sparging a mixture of air, oxygen, CO_2, and nitrogen at a flow rate of 100 $mL\ min^{-1}$ using a horseshoe sparger. pH was controlled by sparging of carbon dioxide and/or by the addition of a sodium carbonate buffer ($100\ mM\ Na_2CO_3; 100mM\ NaHCO_3$ (Sigma-Aldrich).). The vessel containing 2.0 L of Milli-Q water was sterilised on a fluid cycle at 121ºC for 20 minutes. Before inoculation, the water was aseptically removed. Cells were seeded at a viable cell density of $2.0 \times 10^5\ cells\ mL^{-1}$ using diluted mid-exponential (72 h) culture. The 1x CD-CHO medium (Life Technologies) was supplemented with a 1% (w/v) solution of antifoam C emulsion (Sigma-Aldrich).

2.1.5. Fed-Batch Strategy

Two different *bolus* feeding strategies were applied. CHO-CY01 cell cultures were *bolus* fed when glucose concentration reached levels below $2.00\ g\ L^{-1}$ or $3.00\ g\ L^{-1}$. The feed used for STR cultures was 10 times concentrated CD-CHO medium (Life Technologies) with glucose (Sigma-Aldrich) added to a glucose concentration of $150.00\ g\ L^{-1}$. The fed-batch cultures in 24-SRW MTPs and SFs used a 3.5 – 10 times dilution of STR feed to accommodate accurately measured feeding volumes. All feed stocks prepared were tested for contaminations 48 hours before use, and the concentrations of metabolites were determined. The volume to feed CHO-CY01 cell cultures was determined by Equation 2.1.

$$V_{Feed}(t_i) = \frac{[Gluc]_{FB} - [Gluc\ (t_i)]}{[Gluc]_{Feed}} \cdot 1000$$

Equation 2.1

where $V_{Feed}(t_i)$ is the volume of feed added at the sample time, t_i (mL); $[Gluc]_{FB}$ is the fed-batch glucose concentration ($2.00\ g\ L^{-1}$ or $3.00\ g\ L^{-1}$); $[Gluc\ (t_i)]$ is the glucose concentration at the sample time, t_i (gL^{-1}); and $[Gluc]_{Feed}$ is the glucose concentration in the feed (gL^{-1}).

The feed used contained, apart from glucose, glutamate, and ammonium. These metabolite additions were acknowledged in the calculations by Equation 2.2.

$$[Glu(t_{i+1})] = [Glu\ (t_i)] + \frac{V_{Feed}(t_i) \times [Glu]_{Feed}}{V\ (t_i)}$$

Equation 2.2

where $[Glu(t_{i+1})]$ is the glutamate (Glu) concentration after feeding ($mmol\ L^{-1}$); $[Glu\ (t_i)]$ is the glutamate concentration at the sample time, t_i ($mmol\ L^{-1}$); $V_{Feed}(t_i)$ is the volume of feed added at the sample time, t_i (mL) (Equation 2.2); $[Glu]_{Feed}$ is the glutamate concentration in the feed; and $V\ (t_i)$ is the measured volume at each sample time point, t_i (mL) (Equation 2.6 and Equation 2.7). The ammonium concentration after feeding was calculated similarly.

2.1.6. Harvest Time

In today´s mammalian cell cultures, higher concentrations of cells and longer fermentation times result in greater product yields. These bioreactor conditions reduce cell viability, and increase the amount of cell debris, colloids, and other solid impurities in the cell broth, which complicate the separation process downstream (Yavorsky et al., 2003). All CHO-CY01 cell line batch cultures in this work were harvested when all cells were dead, to understand the cell culture profile and to observe the impurities profiles. The CHO-CY01 cell line fed-batch cultures were harvested considering the downstream process. Therefore, a set of criteria was imposed. The cell culture was harvested when the cell viability fell below 50% (Iammarino et al., 2007) and/or glucose concentration was null.

2.2. Analytical Techniques

2.2.1. Determination of Cell Concentration and Viability

Cell concentration and viability were measured daily by the trypan blue dye exclusion method using a Vi-Cell XR automated viability analyser (Beckman Coulter). The samples were diluted with Dulbecco's PBS (Sigma-Aldrich) as necessary. Within the Vi-Cell, the cell suspension was mixed with trypan blue solution, before being loaded onto a haemocytometer slide for image capture. Viable cells actively export the trypan blue dye from the cytoplasm, while dead cells are unable to do this and can thus be distinguished visually by their blue appearance. The Vi-Cell captures images of the cells using a digital camera, and subsequently analyses these to determine the viable and dead cell numbers, percentage viability and mean diameter. All analyses were performed in triplicate (where sample volume permitted).

2.2.2. Cell Size Analysis and Particle Size Distribution

The average cell diameter and particle size distribution were determined using a CASY cell counter analyser (Roche Innovatis, Germany). The CASY cell counter analyser was used

with a 150 µm orifice and set to measure up to 40 µm with a five times repeat measurement, from which an average was reported. $10.0 - 100.0\ \mu L$ of the sample were diluted in $10.0\ mL$ of CASY®ton buffer (Roche Innovatis, Germany) and then analysed. The CASY cell counter analyser combines the resistance measurement principle (particle measurement technique) with a modern method of signal evaluation (pulse area analysis).

Measurement is performed by suspending the cells in CASY®ton (an electrolyte) and aspirating one by one through a precision measuring pore at a constant flow speed. During the measurement process, a pulsed low voltage field with 1 MHz is applied to the measuring pore via two platinum electrodes. The electrolyte-filled measuring pore represents a defined electrical resistance. During their passage through the measuring pore, the cells displace a quantity of electrolyte corresponding to their volume. Since intact cells can be considered isolators, an increased level of resistance is achieved over the measuring pore. This resistance is a dimension for the volume of the cells. By contrast, dead cells whose membrane no longer acts as an electrical barrier, are recorded by the size of their cell nucleus. Since the cells are scanned at such high frequency, a precise result and a high resolution can be produced. These results from each cell are cumulated and assigned in a calibrated multichannel analyser with over 500,000 channels. So, for the CASY technology, as the cell flow cytometry, it can present data of each cell as a cell size distribution graph, which has two variables, the change in cell volume and cell viability (Roche Innovatis AG, 2002).

The CASY cell counter analyser data (number of counts per particle diameter) was normalised, standardised, and corrected to the dilution factor of 200, using Equation 2.3.

$$CASY\ Count_{Corrected} = \frac{CASY\ Count\ \cdot (Dilution\ Factor/200)}{\max(CASY\ Count) \cdot \sum CASY\ Count}$$

Equation 2.3

where $CASY\ Count_{Corrected}$ is the number of particles present at the particular diameter normalised, standardised, and corrected to one dilution factor; $CASY\ Count$ is the number of particles present at the particular diameter measured; $Dilution\ Factor$ is the ratio of CASY®ton buffer volume ($10.0\ mL$) and sample volume ($10.0 - 100.0\ \mu L$); $\max(CASY\ Count)$ is the maximum number of particles in the sample; and $\sum CASY\ Count$ is the total sum of the number of particles in the sample.

With the CASY cell counter analyser, the sample´s particle size distribution can be divided into three regions: Debris (< 7.6 µm); Dead cells (cell nucleus) (7.6 – 12.8 µm), and Larger particles (> 40 µm) (Roche Innovatis AG, 2002). With the number of particles in each of these regions, parameters including the percentages of debris, dead cells, larger particles

and, total impurities (larger particles, dead cells and, debris) were calculated. The mean diameter obtained from CASY was considered as the cell diameter.

2.2.3. Metabolites, Electrolytes, and IgG4 Concentration Quantification

The sample was spun for 10 minutes in a microcentrifuge 5430R (Eppendorf, Stevenage, UK) at maximum speed (17,500 rpm). The supernatant was used for the quantification of metabolites, electrolytes, and IgG4, and the rest of the volume was stored at -20 ºC.

Metabolites (glutamine, glutamate, glucose, lactate and, ammonium), electrolytes (sodium and, potassium), pH, and osmolality concentration for culture supernatant were monitored daily using NOVA Bioprofile® 400 (Nova Biomedical, Deeside, UK). Osmolalities were calculated using Equation 2.4, where Osm is the sample´s osmolality; $[Na^+]$ is sodium concentration; $[K^+]$ is potassium concentration; $[NH_4^+]$ is ammonium concentration; $[Gluc]$ is glucose concentration; $[Lact]$ is lactate concentration; and C is a constant. C was determined by the difference in NOVA value and calculated (without volume correction) value ($\approx 61\ mOsm\ kg^{-1}$).

$$Osm = 1.86\ ([Na^+] + [K^+] + [NH_4^+]) + \frac{[Gluc]}{0.18} + \frac{[Lact]}{0.096} + C$$

Equation 2.4

All metabolite, electrolyte, and pH measurements were performed in triplicate when sample volume allowed. Milli-Q water was used for sample dilution if this was necessary to bring the metabolite and/or electrolyte concentrations into the appropriate range for analysis. For all diluted samples, the osmolality was recalculated using Equation 2.4. Variations of NOVA Bioprofile® 400 sensors recalibration over time and/or batch to batch differences in reagent pack composition were neglected.

The IgG4 concentration in the sample supernatant was determined using 1 mL HiTrap Protein G HPLC (column from GE Healthcare, HPLC Agilent 1200 series using Agilent ChemStation) and the method is shown in Table 2-1 (Loading buffer: 20 mM sodium phosphate buffer pH 7.00 ($10\ mM\ NaH_2PO_4$/ $10\ mM\ Na_2HPO_4 \cdot H_2O$) (Buffer A) and elution buffer: 20 mM glycine buffer pH 2.80 (Buffer B). A 96-well ($1.0\ mL$) plate with a sealing mat was used to reduce the evaporation rate during the automated sampling. If dilution was necessary due to low sample volumes, the sample was diluted with Buffer A. In order to convert the IgG4 absorbance peak at 280 nm into IgG4 concentration, a calibration curve was run in parallel. The calibration curve was built with standards of different dilutions (0%, 5%,

10%, 20%, 40%, 60%, 80%, and 100%) of pure IgG4 ($1.82\ g\ L^{-1}$ or $3.74\ g\ L^{-1}$). Considering the sample IgG4 concentration, the calibration curve was truncated up to the maximum IgG4 peak maximum of the samples. In the HPLC runs, where the standards were not present, it was considered an area under the curve of 2,100 absorbance units to correspond to $1.00\ g\ L^{-1}$. All HPLC measurements were done in triplicate, when sample volume permitted.

Table 2-2: Chromatography method for IgG4 detection by Protein G HPLC

Time (minutes)	% Buffer A	% Buffer B	Flow rate ($mL\ min^{-1}$)
0.00	100	0	1
4.00	100	0	2
4.01	0	100	2
11.50	0	100	2
11.51	100	0	2
14.00	100	0	2

2.2.4. Flow cytometry

Flow cytometry is a general method for rapidly analysing large numbers of cells individually using light scattering, fluorescence, and absorbance measurements on stained and unstained cells. The power of this approach lies both in the broad range of cellular parameters that can be determined (cell cycle, size distribution, and intracellular components) and in the ability to acquire information about how these parameters are distributed in the cell population. This segregated data, representing different subpopulations, can provide more information and understanding, which ultimately will contribute to a more efficient bioprocess optimisation (Rieseberg et al., 2001).

2.2.4.1. Cell Cycle Analysis

The cell cycle can be subdivided into four phases: the G1-phase with protein synthesis, the S-phase with DNA replication, the G2-phase from the end of the replication to the eventual cell division, and finally the M-phase with mitosis. Cells can also enter arrest phase, called G0, from the G1-phase. Cells at different stages of the cell cycle can also be distinguished by their DNA content. Cell cycle distribution was determined by flow cytometer using a fluorescent nucleic acid dye, propidium iodide (PI), which binds to DNA by intercalating between the base pairs often after enzymatic removal of RNA (Sitton et al., 2008). Mammalian cells in G1 are diploid (containing two copies of each chromosome), so their DNA content is referred to as 2n

(n designates the haploid DNA content of the genome). During S phase, replication increases the DNA content of the cell from 2n to 4n, so that cells in S have DNA contents ranging from 2n to 4n. DNA content then remains at 4n for cells in G2 and M, decreasing to 2n after cytokinesis (Alberts et al., 2008). Thereby, subpopulations of cells in G1, S, and G2/M phases are identified based on the distribution of relative DNA content per cell (Dutton et al., 2006).

5L-STR or 24-SRW MTP CHO-CY01 cell culture samples containing $2.0 - 5.0 \times 10^6\ mL^{-1}$ viable cell concentration were transferred to Eppendorf tubes and centrifuged at 100 × g, 4°C for 5 min using the 5415D or 5415R centrifuges (Eppendorf, Stevenage, UK). The supernatant was removed and pellet washed in 1 mL of cold PBS, and the centrifugation step was repeated using the same conditions. The supernatant was removed, and the pellet was re-suspended in 1 mL ice cold 70% (v/v) ethanol (Sigma-Aldrich). This was added dropwise whilst vortexing the pellet to prevent cell aggregation. The cells were then allowed to fix in the ethanol for 45 ± 15 minutes at 4°C. Samples were then either analysed immediately or stored at -20°C prior to analysis. The fixed sample was centrifuged at 1,500 × g, 20°C for 5 min, the supernatant was removed, and the pellet was washed in 1 mL PBS before being centrifuged at 800 × g, 20°C for 5 min. The supernatant was then removed and the pellet was re-suspended in 150 μL of 100 mg/mL ribonuclease A solution (Sigma-Aldrich). This sample was incubated at room temperature for 5 min before adding 1.5 mL of 50 mg/mL PI solution (Sigma-Aldrich). Samples were mixed well and incubated at room temperature for a further 5 to 10 minutes prior to analysis. Samples were analysed using a Beckman Coulter Epics XL-MCL flow cytometer, collecting 50,000 events per sample or for 300 seconds. Stained samples were excited using 488 nm wavelength light and the 675 ± 25 nm bandpass filter (FL4) used for emission collection. A flow check (Flow-Check Fluorospheres, Beckman Coulter) to verify optical alignment and fluidics was carried out before every experiment. The histogram data file generated using Expo 32 software (Beckman Coulter) was converted to an FCS file format using the WinMDI program (The Scripps Research Institute, La Jolla, CA, USA) before analysing cell cycle distribution using the Cylchred program (Cardiff University, Cardiff, UK, Freeware).

2.2.4.2. Apoptosis Analysis

Apoptosis analysis of CHO-CY01 cell culture was performed using a flow cytometer (Beckman Coulter Epics XL-MCL) and an Annexin V-FITC/7AAD kit (PM3546 -Beckman Coulter). Annexin V is a member of the annexin family of intracellular proteins that bind to phosphatidylserine (PS) in a calcium-dependent manner. In viable cells, PS is located in the inner leaflet of the plasma membrane. In the early phase of apoptosis, the integrity of the cell membrane is maintained, but the cells lose the asymmetry of their membrane phospholipids.

The PS in apoptotic cells translocates to the external leaflet of the plasma membrane and becomes exposed at the cell surface and forms one of the specific signals for the recognition and removal of apoptotic cells by macrophages. Fluorochrome-prelabeled Annexin V (Annexin-FITC) can then be used to target and identify apoptotic cells (Van Engeland et al., 1998). Through flow cytometry, the difference in fluorescence intensity of annexin-V-PS complexes between apoptotic and non-apoptotic cells can be detected and measured (Arden et al., 2004; Rieseberg et al., 2001; Van Engeland et al., 1998). However, this technique is not entirely specific for the detection of apoptotic cells, because annexin V can also bind to the PS on the inside of the damaged cell membranes of necrotic cells (Van Cruchten et al., 2002). Distinguishing apoptotic from oncotic cells is possible by performing a double staining technique with Annexin V and 7-amino-actinomycin D (7-AAD), as the latter does not penetrate cells with an intact cell membrane (Van Cruchten et al., 2002). Early apoptotic cells will exclude 7-AAD while late stage apoptotic cells will stain positively, due to the passage of these dyes into the nucleus where they bind to DNA. Therefore, the Annexin V-FITC/7ADD kit is an apoptosis detection kit can distinguished cells as living cells, early or late apoptotic cells, and no viable cells in a fast, simple, and sensitive way (Rieseberg et al., 2001; Van Engeland et al., 1998).

Apoptosis analysis was done with CHO-CY01 cells grown in 5L-STR or 24-SRW MTP. Cells were prepared following the manufacture's protocol. CHO-CY01 cell culture supernatant was centrifuged (Eppendorf 5415, Cambridge, UK) for 5 min at 500 × g at 20°C. The supernatant was discarded, and the cell suspension was washed with ice-cold phosphate-buffered saline (PBS) and centrifuged (5 min, 500 × g at 20°C). The supernatant was discarded, and the cell pellet was re-suspended in 1X binding buffer to a concentration of $5.0 - 10.0 \times 10^6\ cells\ mL^{-1}$ and stored on ice. 10 μL of annexin V-FITC solution and 20 μL of 7-ADD viability dye were added to 100 μL of prepared cell suspension and mixed gently. The tubes were stored in the dark and incubated on ice for 15 minutes. 400 µL of ice-cold 1X binding buffer was added to the stained sample and analysed by flow cytometry within 30 minutes of staining. The stained samples were excited using a 488 nm wavelength, 525 nm band-pass filter (FL1) used for emission collection of annexin V-FITC and 675 nm band-pass filter (FL4) used for collection of 7-ADD. Samples were collected for 300 seconds or 10,000 events. A flow check (Flow-Check Fluorospheres, Beckman Coulter) to verify optical alignment and fluidics was carried out before every experiment.

2.2.5. 2D-DIGE Proteomic Analysis

Two-dimensional difference gel electrophoresis (2D-DIGE) is an advanced version of classical two-dimensional gel electrophoresis (2D-PAGE). 2D-DIGE is a powerful tool for separating complex protein mixtures by charge (isoelectric focusing (IEF)) and size

(polyacrylamide gel electrophoresis (SDS-PAGE)), scanning and analysing the resulting second dimension SDS-PAGE gel images for protein differences. IEF separates proteins according to their isoelectric point (pI), and SDS-PAGE separates according to their molecular weight (MW). The major advantages of 2D-DIGE technology are the use of an internal standard that virtually eliminates experimental gel-to-gel variation, thereby accuracy and reproducibility are improved, the increased throughput significantly reduces analysis time and cost and, detection of true differences in protein expression with extremely high statistical confidence (Lilley et al., 2004). Combining new fluorescence technology, sample multiplexing, and image analysis, 2D-DIGE is a fully integrated system offering significant benefits over classical second dimension SDS-PAGE.

The ability to analyse a sample effectively by 2-D electrophoresis is often limited by the presence of non-protein impurities in the sample. Excess salts and buffers from sample preparation can render the solution too conductive for effective first dimension IEF. Charged detergents, lipids, phenolics, and nucleic acids can also interfere both with first dimension IEF separation and visualisation of the 2-D result. Protein precipitation is therefore often employed to separate selectively proteins in the sample from contaminating substances. Protein precipitation is also used to concentrate proteins from samples that are too dilute for effective 2-D analysis[3].

5L-STR CHO-CY01 cell culture supernatant samples were precipitated using the ammonium acetate method. Five volumes of 0.1 M ammonium acetate in 100% methanol were added to the sample and left overnight to precipitate at -20ºC. The mixture was centrifuged for 10 min at 13,000 x g, and the supernatant was discarded. The pellet was washed twice with 80% ammonium acetate and centrifuged for 2 min at 13,000 x g. The pellet was lysed using CHAPS/Thiourea buffer vortexed and sonicated until fully soluble. pH was checked to be 8.5. Total protein concentration was quantified using Quick Start™ Bradford. 50 ug of the sample was taken for labelling with $250\ pmol$ of dye (Chromis 550 (Cy3) and Chromis 645 (Cy5) ($250\ pmol/\mu L$). All samples to be labelled were normalised to the same volume. The labelling reaction proceeded for 30 min at room temperature, protected from light. Each gel then had $50\ \mu g$ of the sample labelled with Cy3 and $50\ \mu g$ of comparing sample labelled with Cy5. After 30 minutes of incubation with dye, $10\ mM$ lysine was added to quench the reaction. That process was continued for 10 minutes at room temperature.

The appearance of streaks that distort 2-D electrophoresis maps and the nonspecific oxidation of proteins that generate extra spots are common issues that lead to poorly resolved protein patterns and reduce reproducibility between electrophoresis runs. The DeStreak

[3] www.gelifesciences.com

Rehydration solution method was used before IEF to prevent streaking and to eliminate nonspecific oxidation by maintaining protein thiol groups in a single oxidation state[3].

The samples were combined and loaded on 13 cm, 3-10NL Immobiline Dry Strip Gel (pH range 3-10) (IPG strips) for the first dimension focusing using a Protean® i12 IEF Cell unit from Bio-Rad. Parameters used: 50 V for 10 hours, 500 V for 1 hour, 1,000 V for 1 hour, and 8,000 V until 48,000 Vhrs was achieved. After the first dimension, IPG strips were equilibrated for 15 minutes in equilibration buffer-reducing and equilibration buffer-alkylation. For size separation, IPG strips were loaded on 12% SDS-polyacrylamide gels and run for the second dimension on vertical system Hoefer SE 600 Ruby from Amersham. Gels were scanned using a Typhoon 9400 laser scanner and analysed using DIA (Differential Analysis) DeCyder 5.02 version software. In the DeCyder DIA program, the volumes of detected spots are compensated for the background level, and the ratio of changes was calculated for all spots. A normal distribution was fitted to the frequency histogram generated for spot frequency against log volume ratio. The list of materials and equipment used for the 2D-DIGE work is in Table 2-3. This experimental work was kindly done by the Cambridge Centre for Proteomics, University of Cambridge, UK[3].

2.2.5.1 Identification of Protein Spots by Mass Spectrometry

The Cambridge Centre for Proteomics[4].performed the identification of protein spots by mass spectrometry. The protein spots were detected using the silver stain PlusOne protocol (Amersham Bioscience). Spot excision and protein digestion were essentially carried out as previously reported (Smales et al., 2004; Tait et al., 2012). Individual protein samples that were to be compared were reduced, alkylated, and digested. Each digest was then labelled with isobaric amine reactive tags. The samples were then pooled and separated according to charge by strong cation exchange chromatography or hydrophobicity by high pH reverse-phase chromatography. Fractions were collected, lyophilised, resuspended, and desalted before being individually analysed by LC-MS/MS. The resulting MS/MS spectra were then searched against the relevant database using the Mascot search engine. Simultaneously, each reporter was quantified (peak areas) using the in-house iSPY software. Finally, the protein IDs and peak areas were merged to create an output file containing both data sets.

[4] proteomics.bio.cam.ac.uk

Table 2-3: Reagents and equipment used for 2D-DIGE proteomics analysis.

CHAPS/Thiourea buffer	6.0 M Urea; 2 M Thiourea; 4% CHAPS; 5.0 mM Mg Acetate; 10.0 mM Tris pH 8.5 (GE Healthcare Life Sciences)
Protein Estimation Assay	Quick Start™ Bradford Kit 1(Bio-Rad)
2x Sample Buffer	8.0 M Urea; 4%CHAPS; 2%DTT; 2% IPG buffer 3-10NL (add DTT and IPG just before use) (GE Healthcare Life Sciences)
DeStreak Rehydration Solution	7.0 M Urea; 2.0 M Thiourea; 4% CHAPS; 0.002% Bromophenol Blue (GE Healthcare Life Sciences)
Chromis DGE Minimal Labelling Kit	Chromis 645 equivalent to Cy5; Chromis 550 equivalent to Cy3 Dye (GE Healthcare Life Sciences)
Equilibration buffer-reducing	6.0 M Urea; 75 mM Tris pH 8.8; 30% Glycerol; 2% SDS; 1% DTT (add fresh just before use) (GE Healthcare Life Sciences)
Equilibration buffer-alkylation:	6.0 M Urea; 75 mM Tris pH 8.8; 30% Glycerol; 2% SDS; 2.5% iodoacetamide (add fresh just before use) (GE Healthcare Life Sciences)
Sealing agarose	0.5% Agarose; 0.002% Bromophenol blue dissolved in SDS running buffer (GE Healthcare Life Sciences)
SDS Running Buffer	10 x TGS (Tris/Glycine/SDS) (Bio-Rad)
Immobiline DryStrip 3-10NL	IPG strip (GE Healthcare Life Sciences)
Protean i12 IEF Cell	IEF apparatus (Bio-Rad)
Hoefer SE 600 Ruby system	Electrophoresis unit (Amersham Biosciences)
Typhoon 9400 Variable Model Imager	Gel Scanner. Parameters for scan: Cy3 image -532 nm laser and 580 nm band pass (BP) 30 emission filter. Cy5 image 633 nm laser and 670 nm BP 30 emission filter (Amersham Biosciences)

2.2.6. Non-Invasive pH and Dissolved Oxygen Monitoring in 24-SRW MTPs

Non-invasive measurements of pH and DOT of CHO-CY01 cell cultures were made using the SDR SensorDish® Reader system from Presens Precision Sensing (Regensburg, Germany). The SDR SensorDish® Reader is a small 24-channel reader for the non-invasive detection of oxygen and pH in multidishes (Sensor Dishes®). These contain a sensor spot at the bottom of each well, and the non-invasive read is through the transparent bottom. SensorDishes® for oxygen (OxoDish®), and pH (HydroDish®) used were in the 24-well format (OxoDish®OD24 and HydroDish®HD24) (Figure 2-2 and Table 2-4). The sensor spot contains a luminescent dye. It is excited by LED light generated by the SensorDish® Reader placed below the multidish, and its luminescence lifetime is detected non-invasively through the transparent bottom. The luminescence lifetime of the dye depends on the oxygen partial

pressure (OxoDish®) and the pH of the sample (HydroDish®), respectively. It is converted to oxygen and pH values by the software without plate calibration by the user. The software was set to take readings every 3 or 10 min interval to avoid sensor bleaching. A continuous visual display of current and past pH and/or DO data readings was possible. All SensorDishes® were covered with CR1524a ´system Duetz` lids (Figure 2-1 D) to secure well-to-well reproducibility, i.e. to standardise homogeneous evaporation and oxygen ingress. Simultaneously, the SDR SensorDish® system (Figure 2-2) was incorporated in the Universal cover clamp for 24-SRW MTP (**Figure 2-1** B).

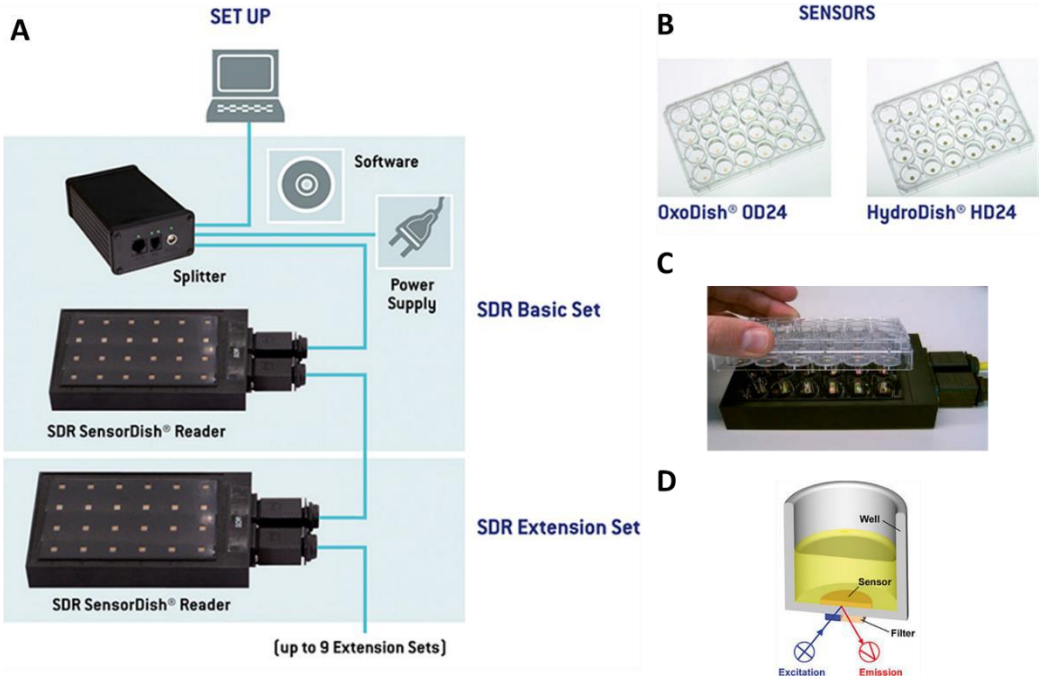

Figure 2-2: Representation of SDR SensorDish® Reader system components (A): software, splitter, SDR extension set, SDR SensorDish® readers (up to 10 SDR SensorDish® readers, can be used in parallel) and SensorDishes® in 24-well plate format (OxoDish®OD24 and HydroDish®HD24) (B); The SensorDish® can easily be correctly aligned on the SDR SensorDish® Reader due to a groove in the housing of the SDR (C); Measurement principle of the SDR SensorDish® Reader system (D)[5].

[5] www.presens.de

Table 2-4: Specifications and properties of HydroDish®HD24 and OXODish®OD24 plates[5].

	pH - HydroDish®HD24	DOT - OXODish®OD24
Measurement range	6.0 - 8.5	0.0 – 50.0% O_2
Resolution	± 0.05 pH at pH= 7.0	± 0.4% O_2 at 20.9% O_2
Precision	± 0.2 pH at pH= 7.0 (Sensor batch calibration); ± 0.1 pH at pH= 7.0 (Sensor spot calibration)	± 1% O_2 at 20.9% O_2
Drift	< 0.1 pH within one week	< ± 0.2% O_2 within one week
	(sampling interval 10 min)	
Measurement temperature range	15 - 45°C	
Response time (t_{90})	< 30 s	
Compatibility	Aqueous solutions, ethanol, methanol (max. 10% v/v), pH 2-10	
Cross-sensitivity	Reduced to ionic strength (salinity); high concentration of small fluorescent molecule in the visible range can interfere	
Calibration	Pre-calibrated	

2.3. Calculated Kinetic Parameters

2.3.1. Volume Correction

All CHO-CY01 volume dependable cell culture data (viable cell number, metabolites and electrolytes concentrations, osmolality, and IgG4 concentration) were volume-corrected ($CF_{V(t_i)}$) using the ratio between the measured volume at each sample time point ($V\ (t_i)$) and the initial volume ($V\ (t_{initial})$) (Equation 2.5).

$$CF_{V(t_i)} = \frac{V\ (t_i)}{V\ (t_{initial})}$$

Equation 2.5

At 24-SRW MTP cell culture scale, the volume changes with the culture time ($t_{initial} \leq t_i \leq t_{final}$) through evaporation losses and feed addition. By weighting the 24-SRW MTP before ($m_{24SRW-MTP_{Before\ Sampling}}$) and after sampling ($m_{24SRW-MTP_{After\ Sampling}}$) and dividing it by the number of wells sampled ($Nr\ Wells\ sampled$), the volume of the 24-SRW MTP well at each sampling time ($V_{24SRW-MTP}(t_i)$) was determined (Equation 2.6).

$$V_{24SRW-MTP}(t_i) = \left(\frac{m_{24SRW-MTP_{Before\ Sampling}} - m_{24SRW-MTP_{After\ Sampling}}}{Nr\ Wells\ sampled}\right)$$

Equation 2.6

At SF and 5L-STR cell culture scale, the evaporation losses are neglected; however, when applicable, the volume variation ($V_{STR,\ SF}$) with sampling (V_{Sample}), base addition (V_{Base}),

antifoam addition ($V_{Antifoam}$), and feeding (V_{Feed}) were considered throughout the culture time ($t_{initial} \leq t_i \leq t_{final}$) (Equation 2.7).

$$V_{STR,SF}(t_i) = V_{STR,SF}(t_{i-1}) - V_{Sample}(t_i) + V_{Antifoam}(t_i) + V_{Base}(t_i) + V_{Feed}(t_{i-1}),$$

Equation 2.7

The density of the 1x CD-CHO media and base was considered as $1000\ kg\ m^{-3}$, the antifoam was $1200\ kg\ m^{-3}$, and feed was $1100\ kg\ m^{-3}$ (experimentally measured).

2.3.2. Calculation of Inoculum Volume

To inoculate (seed) cultures at a pre-determined cell density, it is necessary to calculate the volume of the existing culture that should be added to fresh media (V_{Seed}) (mL). This is dependent on a number of variables including cell density of stock/seed culture ($Inoculum\ Density$) ($10^6 cells\ mL^{-1}$), volume of new culture ($V_{New\ Culture}$) (mL), and desired inoculation density ($Inoculation\ Density_{New\ Culture}$ ($0.2 \times 10^6\ cells\ mL^{-1}$)). The volume of inoculum to add can be calculated using Equation 2.8.

$$V_{Seed} = \frac{V_{New\ Culture} \times Inoculation\ Density_{New\ Culture}}{Inoculum\ Density}$$

Equation 2.8

2.3.3. Estimation of Specific Growth Rate and Doubling Time

The growth rate was estimated by plotting the natural logarithm of viable cell concentration measured during the exponential phase against time. The gradient of the resultant straight line ($R^2 > 0.7$) was taken as the maximum specific growth rate (μ) (h^{-1}). With the value of μ, the doubling time ($t_{1/2}$) (h), which is the period of time required for a quantity to double in size, can be determined using Equation 2.9.

$$t_{1/2} = \frac{ln2}{\mu}$$

Equation 2.9

2.3.4. Integral of Viable Cell Concentration

Integral of viable cell concentration (IVCC) is a measure of the overall number of viable cells present in the cell culture over a defined time period. IVCC for each discrete time interval was obtained using the trapezoidal rule. For each cell culture experiment performed, the mean

of the viable cell density (X_V) ($10^6 cells\, mL^{-1}$) between each sampling point ($t_{i+1} - t_i$) was taken and multiplied by the number of hours between sampling (to give units of $10^6\ cells\ h\ mL^{-1}$). The values for every time point were then summed to yield a cumulative figure, which was divided by 24 to have units of $10^6\ cells\ day\ mL^{-1}$, which is equivalent to ($10^9\ cells\ day\ L^{-1}$). (Equation 2.10).

$$IVCC = \int_{t_{initial}}^{t_{final}} X_V dt = \sum_{t_i=t_{initial}}^{t_{final}} \frac{X_V(t_i) + X_V(t_{i+1})}{2} \cdot (t_{i+1} - t_i)$$

Equation 2.10

2.3.5. Specific Antibody Production Rate

The specific antibody (IgG4) production rate, q_{mAb} ($mg\ 10^{-9}\ cells^{-1} day^{-1}$), was determined from the linear slope of the plot of cumulative IgG4 concentration produced ($IgG4_{produced}\ (t)$) ($mg\ L^{-1}$) (Equation 2.11) versus the time integral of IVCC ($10^9\ cells\ day\ L^{-1}$) (Equation 2.10) for each CHO-CY01 cell culture (Suberbie, 2013).

$$IgG4_{produced}\ (t) = \sum_{t_{initial}}^{t_{final}} IgG4\ (t_i) - IgG4\ (t_{i-1})$$

Equation 2.11

where $IgG4(t_i)$ is the antibody concentration at time t_i ($mg\ L^{-1}$).

2.3.6. Antibody Volumetric Productivity

Antibody volumetric productivity (VP) ($mg\ L^{-1} day^{-1}$) was determined by plotting antibody concentration against time. The gradient of the resultant straight line ($R^2 > 0.7$) was taken as the antibody VP.

2.3.7. Specific Glucose Consumption Rate

The specific glucose ($Gluc$) consumption rate, q_{Gluc} ($g\ 10^{-9}\ cells^{-1} day^{-1}$), was determined from the linear slope of the plot of cumulative glucose consumed ($cGluc$) ($g\ L^{-1}$) (Equation 2.12) versus the time integral of IVCC (Equation 2.10) for each CHO-CY01 cell culture (Yuk et al., 2011).

$$cGluc = \sum_{t_i=t_{initial}}^{t_{final}} Gluc\ (t_{i-1}) - Gluc\ (t_i) + Gluc_{Feed}(t_i)$$

Equation 2.12

where $Gluc\ (t_i)$ is the glucose concentration at time t_i ($g\ L^{-1}$) and $Gluc_{Feed}(t_i)$ is the glucose concentration added during fed-batch mode ($g\ L^{-1}$).

2.3.8. Specific Glutamate Consumption Rate

The specific glutamate (Glu) consumption rate, q_{Glu} ($mmol\ 10^{-9}\ cells^{-1}day^{-1}$), was determined from the linear slope of the plot of cumulative glutamate consumed ($cGlu$) ($mmol\ L^{-1}$) (Equation 2.13) versus the time integral of IVCC (Equation 2.10) for each CHO-CY01 cell culture.

$$cGlu = \sum_{t_i=t_{initial}}^{t_{final}} Glu\ (t_{i-1}) - Glu\ (t_i) + Glu_{Feed}(t_i)$$

Equation 2.13

where $Glu\ (t_i)$ is the glucose concentration at time t_i ($mmol\ L^{-1}$) and $Glu_{Feed}(t_i)$ is the glucose concentration added during fed-batch mode ($mmol\ L^{-1}$).

2.3.9. Specific Lactate Production Rate

Lactate ($Lact$) is produced and consumed by CHO-CY01 cells. Therefore, the specific lactate production rate, q_{Lact} ($g\ 10^{-9}\ cells^{-1}day^{-1}$), was determined from the linear slope of the plot of cumulative lactate concentration ($cLact$) ($g\ L^{-1}$) (Equation 2.14) versus the time integral of IVCC (Equation 2.10) for each CHO-CY01 cell culture.

$$cLact = \sum_{t_i=t_{initial}}^{t_{final}} Lact\ (t_i)$$

Equation 2.14

where $Lact\ (t_i)$ is the lactate concentration at time t_i ($g\ L^{-1}$).

2.3.10. Specific Ammonium Production Rate

The specific ammonium (Amm) production rate, q_{Amm} ($mmol\ 10^{-9}\ cells^{-1}day^{-1}$), was determined from the linear slope of the plot of cumulative ammonium produced ($cAmm$)

($mmol\ L^{-1}$) (Equation 2.15) versus the time integral of IVCC (Equation 2.10) for each CHO-CY01 cell culture.

$$cAmm = \sum_{t_{initial}}^{t_{final}} Amm\ (t_i) - Amm\ (t_{i-1}) + Amm_{Feed}(t_i)$$

Equation 2.15

where $Amm\ (t_i)$ is the ammonium concentration at time t_i ($mmol\ L^{-1}$) and $Amm_{Feed}(t_i)$ is the ammonium concentration added during fed-batch mode ($mmol\ L^{-1}$).

2.3.11. Specific Sodium and Potassium Consumption Rates

The specific sodium (Na^+) and potassium (K^+) consumption rates, q_{Na^+} ($mmol\ 10^{-9}\ cells^{-1}day^{-1}$) and q_{K^+} ($mmol\ 10^{-9}\ cells^{-1}day^{-1}$), were determined from the linear slope of the plot of cumulative sodium (cNa^+) and potassium (cK^+) consumed ($mmol\ L^{-1}$) (Equation 2.16) versus the time integral of IVCC (Equation 2.10) for each CHO-CY01 cell batch culture, respectively. When q_{Na^+} and q_{K^+} assume negative values, it means that the cells are producing sodium and/or potassium.

$$\begin{vmatrix} cNa^+ \\ cK^+ \end{vmatrix} = \sum_{t_i=t_{initial}}^{t_{final}} \begin{vmatrix} Na^+(t_{i-1}) \\ K^+(t_{i-1}) \end{vmatrix} - \begin{vmatrix} Na^+(t_i) \\ K^+(t_i) \end{vmatrix}$$

Equation 2.16

where $Na^+(t_i)$ is the sodium concentration at time t_i ($mmol\ L^{-1}$) and $K^+(t_i)$ is the potassium concentration at time t_i ($mmol\ L^{-1}$).

2.3.12. Ratio of Lactate Production to Glucose Consumption

The ratio of lactate production to glucose consumption (g/g) was determined from the quotient of the maximal lactate concentration produced with the cumulative glucose consumption (Equation 2.17).

$$Lactate\ produced/Glucose\ Consumed = \frac{Lact_{max}(t_{max}) - Lact(t_{initial})}{cGluc(t_{max})}$$

Equation 2.17

where $Lact_{max}(t_{max})$ is the highest lactate concentration (gL^{-1}), $Lact(t_{initial})$ is the initial lactate concentration (gL^{-1}) and, $cGluc(t_{max})$ is the cumulative glucose consumed when the maximal lactate concentration was reached (gL^{-1}) calculated by Equation 2.12.

2.3.13. Observed Metabolic Yield Coefficients

Assuming a linear relationship between the amount of product (P) produced and substrate (S) consumed, during the exponential phase, the observed metabolic yield coefficient ($Y'_{P/S}$) was determined by plotting the product concentration against the substrate concentration for each CHO-CY01 cell batch culture. The gradient of the resultant straight line ($R^2 > 0.7$) was taken as the $Y'_{P/S}$. It was considered as the product the viable cell, IgG4, lactate, and ammonium concentrations and as the substrate glucose, glutamate, lactate and ammonium concentrations.

2.3.14. Evaporation Rate in 24-SRW MTP

The evaporation rate of a well in 24-SRW MTP was determined throughout the CHO-CY01 cell culture using Equation 2.18.

$$Evaporation\ Rate\ (\%) = \frac{V_{t_{initial}} - (V_{24SRW-MTP}(t_i) - \sum_{t_{initial}}^{t_{final}} V_{Feed}\ (t_{i-1}))}{V_{t_{initial}}} \times 100$$

Equation 2.18

where $V_{t_{initial}}$ is the well initial volume ($0.85\ mL$); $V_{24SRW-MTP}(t_i)$ is the total well volume of the 24-SRW MTP at each sampling time and was determined previously with Equation 2.6 ($mL\ well^{-1}$); and $V_{Feed}\ (t_{i-1})$ is the volume of the feed per well at the previous sampling point ($mL\ well^{-1}$).

The 24-SRW MTP evaporation rate per day was determined by Equation 2.19:

$$Evaporation\ Rate\ (\mu L\ day^{-1}) = \frac{V_{t_{initial}} - (V_{24SRW-MTP}(t_i) - \sum_{t_{initial}}^{t_{final}} V_{Feed}\ (t_{i-1}))}{t_i} \times 1000$$

Equation 2.19

2.3.15. Ammonium, Lactate, and Osmolality Experiments

The ammonium, lactate, and osmolality inhibition tests were performed in SFs with total volume of 125 mL. In the experiments with ammonium, the CHO-CY01 cell line was cultured with different initial concentrations of ammonium chloride (Sigma-Aldrich) (4.8, 7.1, 9.7, and 11.2 $mmol\ L^{-1}$). For the lactate inhibition test, cells were inoculated with different concentrations of sodium lactate (Sodium DL-lactate solution (60% w/w), Sigma-Aldrich) (0.7, 1.9, 2.7, 3.6, and 4.7 $g\ L^{-1}$). In the osmolality test, the cell cultures were diluted with a solution of sodium chloride (Sigma-Aldrich) (108, 103, 99, and 95 $mmol\ L^{-1}$).

2.4. Engineering Characterisation of 24-SRW MTP

2.4.1. Description of Liquid-Phase Hydrodynamics

Predictions of the liquid-phase hydrodynamics in shaken 24-SRW MTPs were made using Reynold's number (Re) (Equation 2.20), Froude number (Fr) (Equation 2.21), Phase number (Ph) (Equation 1-2), and the critical shaking frequency (N_{crit}) (Equation 1-3).

$$Re = \frac{\rho N d_W^2}{\mu}$$

Equation 2.20

$$Fr = \frac{(2\pi N)^2 d_s}{2g}$$

Equation 2.21

where ρ is the liquid density, μ is the liquid viscosity, N is the shaking speed, d_W is the characteristic length that was taken as the 24 SRW-MTP diameter ($15.4\ mm$), and g is the acceleration due to gravity ($9.81\ m\ s^{-2}$). Liquid properties were assumed to be those of water at 37°C. The orbital diameter of the shaker platform (d_s) was $25.0\ mm$.

2.4.2. Prediction of Oxygen Mass Transfer Coefficients

Oxygen mass transfer coefficients, $k_L a$, in 24-SRW MTP were predicted using Equation 1.4. As mentioned previously (Section 2.1.3), all 24-SRW MTPs were sealed using the 'system Duetz´ lids to maintain sterility and reduce evaporation, but these lids cause gas exchange resistance. Ultimately, this causes a reduction in the $k_L a$. A reduction of 2.25 times in the $k_L a$ of a well covered with a Breathe-Easy® sealing membrane compared with the uncovered well was been reported (Barrett et al., 2010). The following physical properties were used in Equation 1.4: orbital shaking diameter (d_s) of $25.0\ mm$, 24-SRW MTP diameter (d_W) of $15.4\ mm$, oxygen diffusion coefficient (D_{O_2}) of $2.69 \times 10^{-9}\ m^2 s^{-1}$ (Micheletti et al., 2006a), initial air-liquid specific surface area (a_i) of $249.9\ m^{-1}$ (Doig et al., 2005), and wetting tension (W) of $0.0012\ N\ m^{-1}$ (Doig et al., 2005). Liquid properties were assumed to be those of water at 37°C.

2.4.3. Liquid-Phase Mixing Time Characterisation and Visualisation of Liquid Hydrodynamics by High-Speed Video Camera

All 24-SRW-MTP mixing studies and liquid hydrodynamics visualisation were conducted in a Perspex mimic of a single well from a 24-SRW MTP (Figure 2-3). This was fabricated at the University College London (UCL) workshop. The mimic was designed with square faces to avoid distortion of video images; also, it was mounted on a larger Perspex

block to improve stability while shaking. All liquid additions to the wells were made using a $10.0\ \mu L$ pipette tip held directly over the center of the well using an expanded polystyrene cap. All experiments were conducted on an orbital shaker platform (CERTOMAT MO II, Sartorius) with a shaking diameter (d_s) of $25.0\ mm$. Images of the liquid hydrodynamics and mixing kinetics in 24-SRW MTP were captured using a Phatom v7.1 high-speed camera from Vision Research, New Jersey, USA (Table 2-5).

Figure 2-3: Perspex mimic of a single well for a 24-SRW MTP used for the mixing time studies.

Table 2-5: Features of Phantom v7.1 high-speed camera

Resolution	800 x 600
Frame Rate (fps)	2000
Exposure (µs)	470
Extreme Dynamic Range (EDR)	280

To visualise the mixing of a small liquid addition into a well liquid content, 1% (v/v) inert red food dye (Dr. Oetker, Leeds, UK) was injected into water to enhance the contrast at the gas–liquid interface. This dye has been shown not to alter the physical properties of the fluid significantly (Nealon et al., 2006). Each flow visualisation experiment was performed in triplicate. Video images were captured at 2,000 frames/s, and individual frames could be extracted from the software.

Iodine decolourisation (Iodine clock) using sodium thiosulphate ($Na_2S_2O_3$) was used to quantify liquid-phase mixing times (Bujalski et al., 1999). Upon the addition of thiosulphate, iodine solution changes from a dark-orange colour to completely colourless. The chemical reaction is shown below:

$$I_2 + Na_2S_2O_3 \longrightarrow 2NaI + NaS_4O_6$$

The addition was performed dropwise before turning on the shaker, resulting in the formation of a thin liquid layer of thiosulphate at the base of the vessel. The duration of this colour transition was defined as the mixing time. 1% (v/v) additions of 1.8 M sodium thiosulphate were made to 5 mM iodine solution using the apparatus described above. Both reagents were purchased from Sigma-Aldrich (Poole, Dorset, UK). The progression of the decolourisation was monitored using a stop-watch and the Phantom v7.1 high-speed camera. To estimate mixing times using the video footage, the number of frames between addition and complete decolourisation were divided by the frame speed. All mixing time measurements were made in triplicate. For 24-SRW MTP, both the flow visualisation and mixing time quantification experiment were performed over the range of shaking speeds of 0 to 300 rpm with 850 μL, 1.0 and, 2.0 mL of fill volume.

2.5. Statistical Analysis

In all experimental measurements and calculated parameters, error propagation theory was considered. A 95% confidence interval was used. When a variable was measured more than once and in CHO-CY01 cell culture repeats, an average and the standard deviation of the variables were determined. The regression coefficient R^2 was considered to measure the quality of the fit to the model. An R^2 greater than 0.7 was considered to be a good fit. To understand the relationship between the different cell culture variables, Spearman's rank correlation coefficient was computed with the Excel 2013 Analysis ToolPak ´add-in` module. The Spearman's rank correlation coefficient is a nonparametric measure of statistical dependence between two variables. The sign of the Spearman´s correlation coefficient indicates the direction of the association, where the perfect coefficients (strong correlation) are 1 or -1. To check whether two CHO-CY01 cell culture runs are statistically equal or different, Student´s t-test was performed and a *p*-value was obtained. Student´s t-test was performed with the Excel 2013 Analysis ToolPak add-in, assuming the null hypothesis and different variances.

Chapter 3 High-Throughput Approach to CHO-CY01 Cell Culture Process Development

3.1. Introduction and Aims

Until recently, there was a relatively limited understanding of the engineering environment of shaken microwell plate. This limited their use in the optimisation of cell culture processes and delayed their implementation as a rational scale-up strategy for STRs (Barrett et al., 2010). Nonetheless, some studies including University College London (UCL) work (Barrett et al., 2010; Doig et al., 2005; Silk 2014; Zhang et al., 2008) and several publications from Jochen Büchs´group at RWTH Aachen have enhanced our understanding of these small-scale systems and have made it possible to take full advantage of their HT properties. Previous work has demonstrated the utility of shaken 24-SRW MTPs for the suspension of a hybridoma cell line (Barrett et al., 2010) and CHO-S cell line (Silk, 2014). These UCL studies were underpinned by engineering characterisation studies that examined the oxygen transfer, energy dissipation, and mixing characteristics in different microwell systems.

The aims of this chapter are to conduct an engineering characterisation of 24-SRW MTPs under conditions suitable for mammalian cell culture using the proven correlations, to explore the potential of microwell cultures for batch and fed-batch cultivations of the CHO-CY01 cell line, and to examine the influence of microwell culture conditions on cell growth kinetics.

The specific objectives of this chapter are:

- To use appropriate methods to estimate the mixing time and adequate correlations to predict dimensionless numbers such as Reynolds, Froude, and Phase numbers, as well as the oxygen mass transfer coefficient for 24-SRW microwell plates;
- To determine the ideal operating conditions (shaking speed, fill volume, sterile closure and, selective pressure) for the CHO-CY01 cell line in 24-SRW MTP regarding productivity optimisation;
- To select an appropriate sterile closure for 24-SRW MTP to reduce the impact of evaporation over the extended fed-batch cultivation period.

3.2. Engineering Characterisation of 24-SRW MTP

3.2.1. Prediction of Liquid-Phase Hydrodynamics

Considering a liquid-phase hydrodynamics perspective, the choice of appropriate operating parameters for orbital mixing at microwell scale, especially the shaking speed (mixing frequency) and the shaker amplitude (d_s), depends on fill volume (V_L); well geometry, surface tension of fluid and construction material; fluid density and kinematic viscosity and, surface tension.

The most important requirement for an efficient mixing process is the formation of a macroscopic flow. The high surface area-to-volume ratio of these systems increases the surface tension, significantly increasing the motion resistance. For this reason, it is necessary to generate high centrifugal acceleration to achieve an intensive macroscopic flow. That may cause an adverse impact on the cells through shear stress and high energy dissipation (Hu et al., 2011).

In this work, the liquid-phase hydrodynamic operating window to successfully grow CHO-CY01 cells in 24-SW MTP only included a range of fill volumes and shaking speeds; all other parameters are kept constant.

In Section 2.4, Reynolds (Re), Froude (Fr), and Phase (Ph) dimensionless numbers and critical shaken frequency (N_{crit}) were introduced as parameters used to characterise liquid-phase hydrodynamics of shaken microwells. Re is defined as the ratio of inertial forces to viscous forces, and may be defined for shaken systems using Equation 2.19. Fr is defined by Equation 2.20 as the ratio of radial to axial forces for shaken systems (Büchs et al., 2000a). Ph is defined by Equation 1-2, and marks the boundary between “in-phase” (Ph >1.26, Fr > 0.4 (Büchs et al., 2000b)) and “out-of-phase” operating conditions. During “in-phase” conditions, the whole of the liquid moves with the rotation of the shaker platform. Operation under “out-of-phase” conditions is characterised by a significant proportion of the liquid not following the motion of the shaker. As a direct result, both the oxygen transfer rate and mixing intensity are reduced (Büchs et al., 2000a). N_{crit} is defined as the shaking speed at which the centrifugal force exceeds the surface tension, and it is determined with Equation 1-4.

Table 3-1 presents the calculated *Re*, *Fr*, and *Ph* numbers for a range of different 24-SRW MTP fill volumes and shaking speeds used in this work as well as the critical shaking frequency for various 24-SRW MTP fill volumes. Reynolds and Froude numbers vary with the shaking speed while Phase number varies with fill volume and shaking speed. To date, there have been no studies linking *Re* to flow regimes in shaken microwell plates (Micheletti et al., 2006a). Consequently, while the values are determined and presented in Table 3-1, it is not possible to conclude whether the flow is turbulent or not.

When the operating conditions of CHO-CY01 cell cultures in 24-SRW MTP are said to be “in-phase”, i.e. the Phase number higher than 1.26 and the Froude number greater than 0.4 (Barrett et al., 2010), the liquid inside each of the 24 wells rotates with the movement of the shaker. However, if those operating conditions become “out-of-phase”, there is an uncontrolled swashing of the liquid on the bottom of the well. Consequently, the specific power consumption is reduced, mixing is poor, and the gas-liquid mass transfer is compromised. The probability of the culture to become “out-of-phase” increases with lower shaking diameters, low fill volumes, and especially with the viscosity of the cell culture. The CHO-CY01 cell culture in 24-SRW MTP was shaken at a shaking speed higher than the critical shaken frequency to induce fluid motion in the well and to improve the gas-liquid mass transfer, which is key for cell growth. Therefore, these factors need to be considered when deciding which liquid-phase hydrodynamic conditions a CHO-CY01 cell line should run in 24-SRW MTP.

For the standard CHO-CY01 cell culture conditions used in this work ($N = 220\,rpm$ and $V_L = 0.85\,mL$), the liquid inside each of the 24 wells in the microwell is “in-phase” and is being orbitally shaken at speeds higher than the critical shaking frequency determined (113 rpm). The liquid inside a 24-SRW MTP well would become “out-of-phase” when the shaking speed was below 180 rpm for all fill volumes. Even considering the fill volume lost due to evaporation, the liquid-phase is “in-phase”.

Multiple CHO-CY01 cell culture operating conditions were tested to understand the impact of different liquid-phase hydrodynamics on mammalian cell growth and antibody productivity (Section 3.2.4 and 3.2.5). In Section 3.2.4, various fill volumes were tested against a constant shaking speed (220 rpm); the liquid-phase hydrodynamics are “in-phase”, and the shaking speed is higher than the critical one for all fill volumes. In Section 3.2.5, different shaking speeds were tested with a constant fill volume (0.85 mL). In this case, the liquid-phase hydrodynamics are not all “in-phase”, and the shaking speed is not always sufficient to move the liquid.

Table 3-1: 24-SRW MTP liquid-phase hydrodynamics. Critical shaken frequency (N_{crit}) Reynolds number (Re), Froude number (Fr), and Phase number (Ph) numbers for different fill volumes (V_L) and shaking speeds (N) in a 24-SRW MTP. All dimensionless numbers were calculated as described in Section 2.4.1. The value for surface tension used was 61 ($dyne\ cm^{-1}$) (Michaelis et al., 1995). Shaded in grey are the "in-phase" regions.

		$N\ (rpm)$						
		100	**150**	**180**	**220**	**300**	**350**	
	Re	600.6	900.9	1081.1	1321.3	1801.8	2102.1	
	Fr	0.14	0.31	0.45	0.68	1.26	1.71	N_{crit}
	$V_L\ (mL)$							(rpm)
Ph	**0.20**	6.22	7.08	7.46	7.89	8.54	8.87	233
	0.50	9.01	9.87	10.25	10.68	11.33	11.66	147
	0.60	9.59	10.44	10.83	11.25	11.91	12.24	134
	0.85	10.73	11.59	11.97	12.40	13.05	13.38	113
	1.00	11.29	12.14	12.53	12.95	13.61	13.93	104
	1.50	12.79	13.64	14.03	14.45	15.11	15.44	85
	2.00	14.06	14.92	15.30	15.73	16.38	16.71	74
	2.50	15.65	16.51	16.89	17.32	17.97	18.30	66

3.2.2. Prediction of Oxygen Mass Transfer Coefficients

One of the key challenges for shaken microwell systems is to provide adequate quantities of oxygen for the cells to grow. Results obtained under such conditions are likely to be misleading, particularly for scale-up purposes (Doig et al., 2005; Büchs et al., 2001). Some methodologies have been applied to the measurement of oxygen mass transfer in microwells and subsequent calculation of oxygen mass transfer coefficient ($k_L a$) values. These include the monitoring of the growth rate of an obligate aerobe (Duetz et al., 2000), the measurement of sodium sulphite oxidation (Hermann et al., 2003), and the standard dynamic gassing-out method (Doig et al., 2005). Experimental data for some round-well geometries shaken at a range of speeds and orbital diameters were correlated by Doig et al. 2005 to enable the prediction of $k_L a$ values. These predicted $k_L a$ values were found to agree with experimentally determined values within $\pm$ 30% over a wide range of conditions (Equation 1.4). In the majority of the microwell literature, the range of operating conditions over which oxygen transfer was studied involved the cultivation of micro-organisms rather than mammalian cells. The minimum shaking speed used in the development of Equation 1.4 was 200 rpm and this was experimentally corroborated by Silk 2014 for shaking speeds below 200 rpm. Knowing this, it was possible to estimate $k_L a$ values with Equation 1.4 for all the possible 24-SRW MTP culture conditions tested in this work. Due to the fact that all CHO-CY01 cell cultures in 24-SRW MTP used the ´system Duetz ` lids to prevent further evaporation and to maintain sterility throughout the cell culture, $k_L a$ values were corrected to include this oxygen uptake reduction. Due to the lack of data for this configuration, it was used the oxygen uptake reduction of he Breathe-Easy® sealing membrane (2.25) (Section 2.4.2).

The predicted values of $k_L a$ for 24-SRW MTPs are summarised in Table 3-2. $k_L a$ values greater than 1 h^{-1} are generally considered sufficient to support the oxygen demand of $10^6 - 10^7\ cells\ ml^{-1}$ (Barrett et al., 2010), while $10^8\ cells\ mL^{-1}$ require a $k_L a$ value between $5 - 55\ h^{-1}$ (Zeng et al., 2005). From Table 3-2, it can be observed that $k_L a$ values for the 24-SRW MTPs increase with the shaking speed and decrease with fill volume, as expected. However, when selecting the ideal CHO-CY01 cell growth conditions in terms of $k_L a$, two important aspects need to conjugated with that decision. One is that mammalian cells are generally sensitive to shear, so that high shaking speeds will translate into cell necrosis or induced apoptosis (Senger et al., 2003). The other is that mammalian cells have low oxygen uptake requirements and present oxidative stress in the presence of high oxygen concentration (Baez et al., 2014). The impacts on CHO-CY01 cell growth and IgG4 productivity with different $k_L a$ values were studied in Sections 3.2.4 and 3.2.5. In general, even considering the correlation error of $\pm$30%, the predicted values of $k_L a$ suggest that the 24-SRW MTP system can support at least $10^6\ cells\ mL^{-1}$.

Table 3-2: Mean volumetric oxygen mass transfer coefficient ($k_L a$) predicted for a 24-SRW MTP covered with ´system Duetz´ lids. Shaded in grey are the $k_L a$ values above 1 h^{-1}.

$\boldsymbol{k_L a\ (h^{-1})}$	$\boldsymbol{N\ (rpm)}$					
$\boldsymbol{V_L\ (mL)}$	**100**	**150**	**180**	**220**	**300**	**350**
0.20	1.70	4.49	6.96	11.26	23.71	34.33
0.50	0.68	1.80	2.78	4.51	9.49	13.73
0.60	0.57	1.50	2.32	3.75	7.90	11.44
0.85	0.40	1.06	1.64	2.65	5.58	8.08
1.00	0.34	0.90	1.39	2.25	4.74	6.87
1.50	0.23	0.60	0.93	1.50	3.16	4.58
2.00	0.17	0.45	0.70	1.13	2.37	3.43
2.50	0.03	0.14	0.30	0.69	2.47	4.67

3.2.3. Liquid-Phase Mixing Time Characterisation

A detailed understanding of the hydrodynamic environment in shaken microwells is essential to strengthen future developments in the automation of microwell plates for industrial cell culture processes and to expand their use as scale-up tools (Elmahdi et al., 2003). Poor mixing will lead to heterogeneities inside the cell culture that most certainly affect cell growth, productivity, and product quality (Lara et al., 2006). Clearly, this would impact the validity of small-scale process characterisation and the success of scale-up work. The use of the high-speed camera and the the addition of a red food dye (Section 2.4.3) allowed the visualisation of the fluid flow and the determination of mixing times in shaken 24-SRW MTPs. The liquid-phase hydrodynamics at different shaking speeds and fill volumes can be observed in Figure 3-1 - Figure 3-3.

In Figure 3-1, the liquid-phase surface distortion of $850\ \mu L$ of water shaken can be observed with an orbital diameter of $25\ mm$ at shaking speeds of 100, 150, 220, and 300 rpm. From Table 3-1, it is predicted 113 rpm as the minimum shaking speed at which there is liquid motion at this fill volume. Therefore, at 100 rpm, as expected, there is no liquid motion, the concave water meniscus can be observed inside the microwell. At 150 rpm, the N_{crit} is exceeded and the liquid-phase hydrodynamic is “out-of-phase”. The liquid moves along with the shaker, which provokes a small liquid surface deformation. This deformation accentuates with shaking speed i.e., the liquid creates a larger angle with the base of the microwell. Liquid surface deformation improves the gas-liquid mass transfer by increasing the aeration surface, and subsequently the $k_L a$ value increases and enables a better mixing by creating “turbulence eddies”. At 220 rpm, the maximum deformation angle is reached such that the deformation now extends to the microwell base. At 300 rpm, the liquid-phase hydrodynamic is “in-phase” with the maximum deformation angle, but the liquid distribution is extreme, i.e. the liquid distribution inside the microwell reaches more than 50% of the height of the microwell, increasing the risk of cross-contamination and liquid losses.

Two distinct mixing patterns were observed following the addition of a small liquid aliquot of red food dye to the shaken 24-SRW MTPs (Figure 3-2 and Figure 3-3). Figure 3-2 shows the mixing pattern representative of “in-phase” liquid-phase hydrodynamics and Figure 3-3 represents the “out-of-phase” operating conditions in shaken 24-SRW MTPs. Initially, in both cases, the dye flowed to the bottom of the well as it is denser than water. Dispersion along the bottom surface followed. In the “in-phase” operating conditions, there is an axial-flow pattern conjugated with the centrifugal force motion. The dye dispersed in the microwell bottom ascends the liquid bulk along the microwell wall. In “out-of-phase” operating conditions, a significant portion of the liquid, especially in the bottom-half of the microwell, does not follow

the motion of the shaker. The dye sinks to the bottom of the microwell and remains there. The dye mixing in the bulk liquid occurs by diffusion.

From all images collected, it was apparent that heterogeneities will exist in the 24-SRW MTPs. The duration of those heterogeneities is the mixing time of that particular operating condition. The presence of heterogeneities represents a significant problem if the liquid additions are toxic to the cells at high concentrations. For example, if a base with higher density than the cell culture is added, initially a zone of high pH would exist at the bottom of the well. However, any adverse effects caused by the liquid additions would depend on the frequency and duration of such perturbations (Osman et al., 2001, 2002). The impact of multiple pH perturbations by the addition of liquid at high pH (feed) in CHO-CY01 growth and productivity will be studied in Section 4.4.

A minimum level of mixing is required simply to ensure the complete suspension of cells in the medium and homogeneous conditions to allow optimal growth, avoiding potentially harmful nutrient, pH, dissolved oxygen, and CO_2 gradients (Lara et al., 2006). The "iodine clock reaction" method (Bujalski et al., 1999), as described in Section 2.4.3, was used to quantify the mixing times in 24-SRW MTP. This method utilises the decolourisation of a dark-orange iodine solution using a colourless sodium thiosulphate solution. Mixing time is defined by the complete decolourisation of iodine. This method was chosen because the end-point is very distinct, and the hydrodynamics associated with mixing can also be visualised, unlike many pH-based methods (Langheinrich et al., 1999). The hydrodynamics of the decolourisation of iodine, in 24-SRW MTP, is visually similar to the patterns observed with the injection of a small liquid aliquot (Barrett et al., 2010). The experimentally determined mixing times for 24-SRW MTP are summarised in Table 3-3.

It can be seen in Table 3-3 that the greatest range of mixing times (t_m) is observed for the shaken 24-SRW MTP. The measured mixing times decreased with increasing shaking speed (Re) and decreasing fill volume V_L, as expected. With no shaking, the mixing times varied from $3651 \pm 668\ s$ ($V_L = 0.85\ mL$) to $13 \times 10^4 \pm 398\ s$ ($V_L = 2.00\ mL$). When $Re = 1801.76$, the mixing time estimated for $0.85\ mL$ and $1.00\ mL$ are very similar. However for $2.00\ mL$, the contents of the microwell rapidly splashed out, and the mixing time measurements were impossible to perform. For orbital shaking diameters of 25 mm, shaking speed lower than 150 rpm resulted in mixing times in excess of those found in the SF and 5-L STR, which was less than 100 seconds (Barrett et al., 2010). Therefore, it is important to highlight that, in order to obtain mixing times in 24-SRW MTP that are comparable to those in SFs and STRs, shaking speeds in excess of 150 rpm and fill volume lower than $2.00\ mL$ are required. It can also be observed that the mixing times have a quick drop when Re is 1,321.29 and present an approximate plateau for Re below 600.59.

In summary, the shaking speed of 220 rpm has been chosen to be the standard shaking speed. In this 24-SRW MTP operating condition: the maximum deformation angle is reached with liquid distribution below microwell mid-height, the mixing times are comparable to those of SFs and STRs, the liquid-phase hydrodynamics are “in-phase” and; the $k_L a$ is larger than 1 h^{-1}.

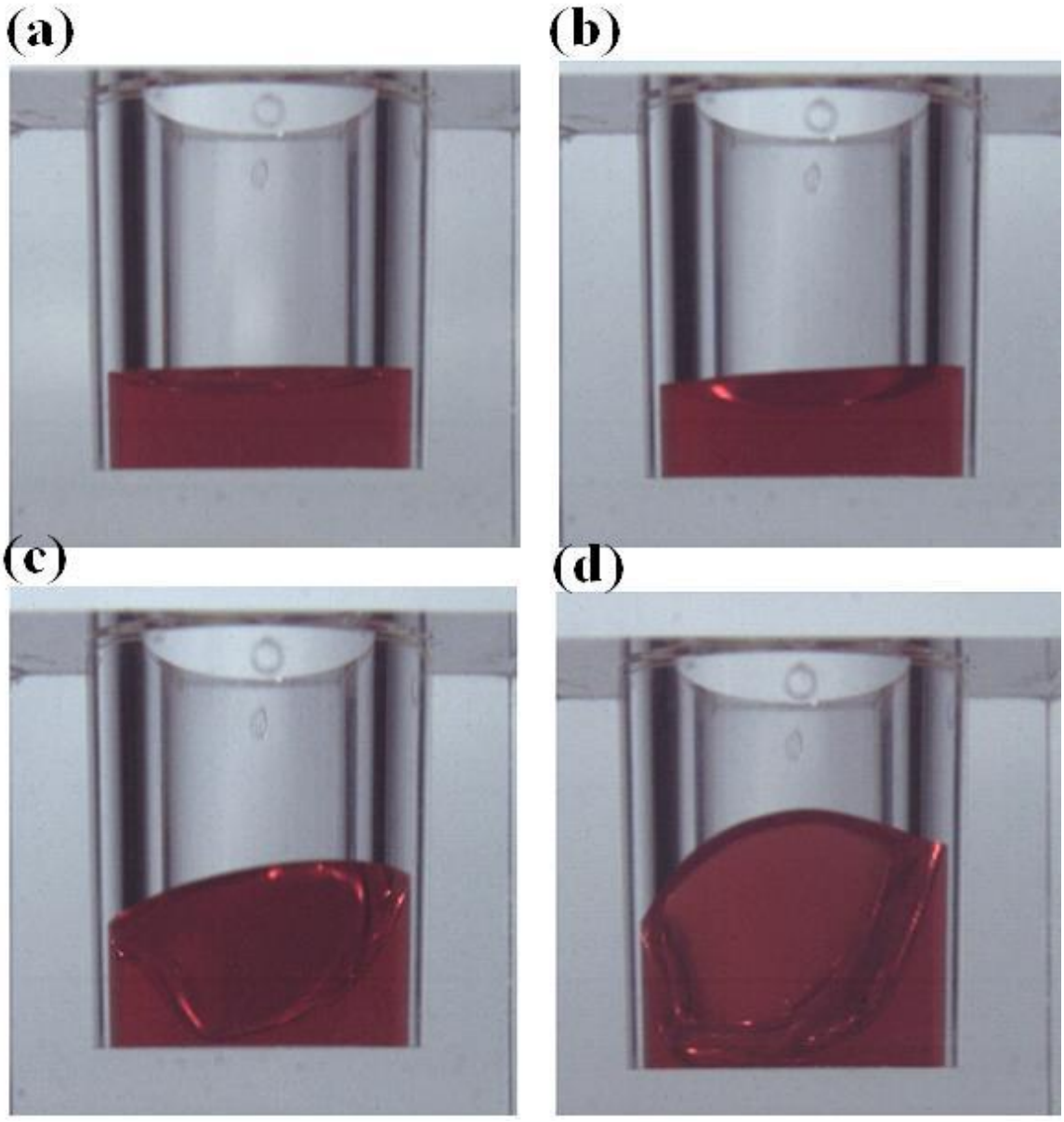

Figure 3-1: Fully developed fluid flow hydrodynamics of $850\ \mu L$ of water with $8.5\ \mu L$ of red food dye shaken with an orbital diameter of 25 mm at shaking speed of 100 rpm (below N_{crit}) (a), 150 rpm (“out-of-phase”) (b), 220 rpm (“in-phase”) (c), and 300 pm (“in-phase”) (d).

$t = Injection$

$t = 0.1s\ after\ Injection$

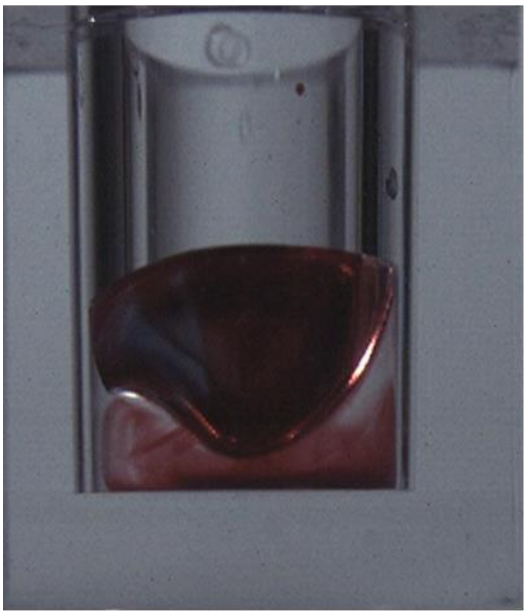

$t = 0.8\ s\ after\ Injection$

$t = 1.7\ s\ after\ Injection$

Figure 3-2: Fluid flow development of 1.0 mL of water with 10.0 μL of red food dye shaken with an orbital diameter of 25 mm at shaking speed of 300 rpm (“in-phase”).

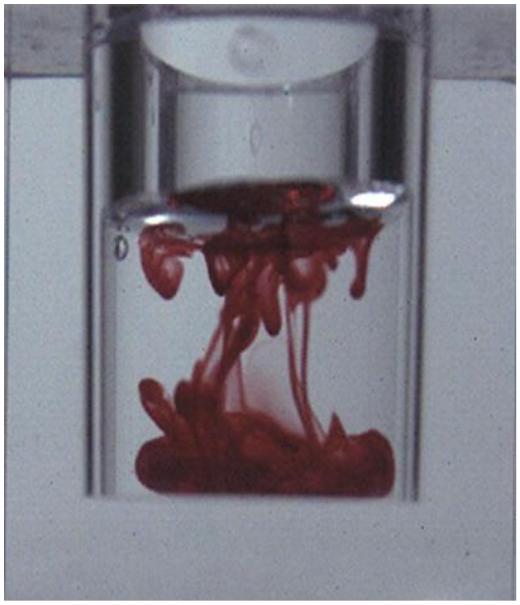

$t = Injection$

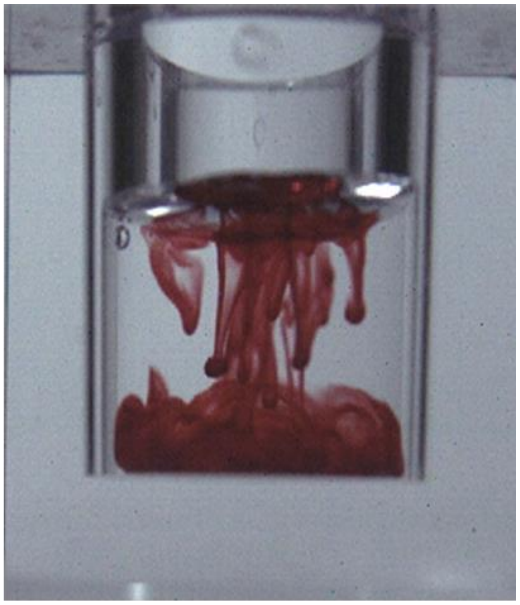

$t = 10\ s\ after\ Injection$

$t = 5\ 000\ s\ after\ Injection$

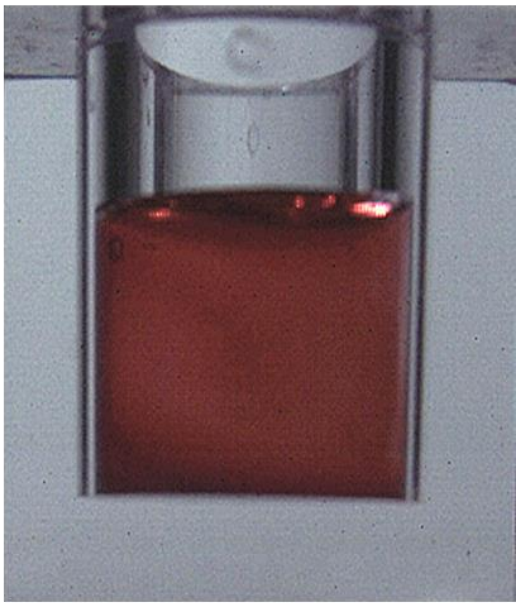

$t = 11\ 002\ s\ after\ Injection$

Figure 3-3: Fluid flow development of 2.0 mL of water with 20.0 μL of red food dye shaken with an orbital diameter of 25 mm at shaking speed of 100 rpm (“out-of-phase”).

Table 3-3: 24-SRW MTP mixing times (t_m) in seconds at different shaking speed rates and fill volumes.

$\boldsymbol{t_m\ (s)}$	$\boldsymbol{N\ (rpm)}$				
$\boldsymbol{V_L\ (mL)}$	**0**	**100**	**150**	**220**	**300**
$\boldsymbol{Re}$	0	600.59	900.88	1321.29	1801.76
0.85	3651 ± 348	2131 ± 205	986 ± 52	4.7 ± 0.7	2.40 ± 0.1
1.00	4500 ± 281	2977 ± 259	1501 ± 150	75 ± 34	1.70 ± 0.1
2.00	$13 \times 10^4 \pm 398$	$11 \times 10^4 \pm 506$	7251 ± 412	954 ± 146	-

3.2.4. Impact of Different 24-SRW MTP Fill Volumes in CHO-CY01 Cell Culture

A variety of different microwell fill volumes (0.50, 0.85, 1.00, 1.50, 2.00, and 2.50 mL) for CHO-CY01 cell culture were tested at standard shaking speed (220 rpm). The CR1524a 'system Duetz' lid was used to cover the 24-SRW MTPs, since it is the best lid for long cell culture runs as stated by the manufacture. However, different ´system Duetz´ lids were also tested (Section 3.3).

In this way, the impact of different mixing times and $k_L a$ values were analysed for CHO-CY01 cell cultures in 24-SRW MTPs at the same Reynolds numbers and "in-phase" condition. As the fill volume increases, the mixing time increases (Table 3-3), the $k_L a$ decreases (Table 3-2), and the risk of contamination increases (Figure 3-2). For both microbial systems (*Pseudomonas putida*) (Hermann et al., 2003) and mammalian cells (VPM 8 hybridoma) (Barrett et al., 2010) grown in microwell plates, it has been shown that the liquid fill volume has a significant impact on both $k_L a$ and cell growth rate. Therefore, it is important, before performing any environmental perturbation to the system, to establish the best fill volume in 24-SRW MTP with respect to inter-scalability.

The CHO-CY01 culture kinetics are shown in Figure 3-4, Figure 3-5, and Figure 3-6. In Table 3-4 and Table C-1, the calculated kinetic parameters are represented. To understand the relationship between the different cell culture parameters with fill volumes, the Spearman's rank correlation coefficients were calculated and the strong dependencies are shown in Table A-1.

It was found that for 2.00 mL and 2.50 mL liquid fill volumes, shaking at 220 rpm was not sufficient to sustain cell growth, as expected. At these fill volumes, the liquid-phase when shaken rises above the mid-height of the microwell. Consequently, the cell culture medium touches the silicone layer of the ´system Duetz´ lid, resulting in cross-contamination and contamination of the cell culture (day 8 (2.00 mL) and day 5 (2.50 mL)). None of the kinetic parameters were determined for these cultures due to their inability to grow cells, as previously explained (Figure 3-4 and Figure 3-5).

Although the $k_L a$ value (4.51 h^{-1}) supports cell culture growth, at 0.50 mL it was found that the liquid-phase hydrodynamic is too vigorous. CHO-CY01 cells grew no more than $0.49 \times 10^6\ cells\ mL^{-1}$ (Figure 3-4), and the IgG4 productivity was very low ($31.70\ mg\ 10^{-9}\ cells\ day^{-1}$) (Table 3-4).

At the fill volume of 1.50 mL, it was found that the *lag* phase is more prolonged in relation to the other fill volumes. The cell viability profile goes below 50% in the beginning, and then after four days recovers to high cell viabilities (90%). This suggests that with the help of the evaporation rate, the fill volume decreases to a volume suitable for mammalian cells.

Therefore, the appropriate range to grow the CHO-CY01 cell line is between 0.50 and 1.50 mL.

From CASY data (Figure B-1: and Table B-1:), a pattern in particle size distribution can be observed for CHO-CY01 cell culture. It can be categorised into the following four stages:

- **Adaptation period**: At the beginning of the cell culture, cells are adjusting to the new cell culture vessel. High debris (>10%) and high cell viabilities (~90%) characterise this phase. It usually lasts 3 – 4 days
- **Exponential period**: The cells are growing and there is a viable cell population domain (>50%). It is characterised by the decrease of debris and by the increase in the dead cells population, larger particles (> 40 μm), cell size, and cell numbers
- **Beginning of decline period**: In this phase, the cell size reaches the maximum, as do the cell numbers. It is characterised by the increase in debris and larger particles and the decrease in dead cells (cell nucleus)
- **Decline period**: In this stage of cell culture, there is no cell growth. It is characterised by the increase in debris and dead cells (cell nucleus) and, a decrease in viable cells and larger particles. There is a shift to smaller (< 12.8 μm) particles

These CASY periods are in agreement with the cell profiles observed for all fill volumes.

Glucose is one of the essential substrates for mammalian cell culture. It is from glucose metabolism that cells receive energy and building blocks to grow and eventually create the products of interest (monoclonal antibodies). Glucose is firstly metabolised into pyruvate during glycolysis and then enters the TCA cycle (glucose oxidation). However, the "Warburg effect" exists (Mulukutla et al., 2010), in which at low oxygen tension mammalian cells switch from the oxidation of glucose to anaerobic glycolysis, producing lactate. The CHO-CY01 cell line is a GS cell line (no glutamine synthetase) and therefore, glutamine-free media are used. Glutamate, a non-essential amino acid, has been reported as a substitute for the multiple cellular actions of glutamine, and it is associated with lower ammonia production. Glutamate enters the cellular membrane by the glutamate-aspartate exchange carrier. The enzyme complex known as glutamate dehydrogenase (GDH) partially oxidises the glutamate in alpha-ketoglutarate, which is a TCA cycle intermediate. Further glutamate oxidation in the TCA cycle generates ammonia (McDermott et al., 1993). Apart from 0.50 mL, glucose and glutamate are totally depleted at different rates (Table 3-4) by the end of the CHO-CY01 cell batch culture with different fill volumes, which is expected (Figure 3-6).

Lactate and ammonium ions are considered as waste products that can affect the growth rate and monoclonal antibody production. Lactate is the result of the incomplete oxidation of glucose by the glycolytic pathway. The toxic action of lactate is probably due to the effect on the pH and osmolality. The ammonium ion is formed by amino acid metabolism, and its toxicity is reported to be higher than that of lactate. The ammonium toxicity affects intracellular pH, protein excretion, secretion, and glycosylation, and reduces metabolic efficiency (Schneider et al., 1996). Therefore, it is beneficial for an industrial process to minimise the concentration of those waste products. From the metabolites' profiles (Figure 3-5 and Table 3-4), the CHO-CY01 cell line is a lactate producer (LP) and consumer (LC) cell line and, depending on the fill volume, an ammonium consumer cell line, as well (Figure 3-5). This means that the lactate metabolic shift made the CHO-CY01 cell line a CHO cell line with efficient energy metabolism (Zagari et al., 2013). Also, this metabolic shift leads to process performance improvements in cell growth, productivity, process robustness, and scalability (Luo et al., 2012). For the ammonium ion, the CHO cells produce it during the exponential phase, but then two different pathways are available:

- Cells stop producing ammonium ion until the lactate concentration is zero and then production resumes, probably to readjust the intracellular pH (1.00 mL).
- Cells start consuming the ammonium ion around the same time the lactate is being consumed. When there is no more lactate, the ammonium ion concentration increases and reaches a plateau towards the end of the culture (0.85 mL).

It can be said that CHO-CY01 cell line cultures in 24-SRW MTP with 0.85 and 1.00 mL are statistically similar in terms of cell number, antibody generated, and metabolite profile (t-test $p > 0.05$). However, what makes the distinction is that at 0.85 mL the mixing time is comparable to the one found on a larger scale (Barrett et al., 2010). For that reason and also to reduce the costs of media, the fill volume of 24-SRW MTP was chosen to be 0.85 mL.

By looking at the Spearman´s rank correlation table (Table A-1), for the CHO-CY01 cell cultures with fill volume of 0.85 mL, it was noticed that the viable cell number had a strong and very strong positive correlation with IgG4 and ammonium concentrations and, a negative correlation with glucose and glutamate concentrations, as expected. Also, the IgG4 concentration have a strong and very strong correlation with ammonium concentration and a negative correlation with glucose and glutamate concentrations. Therefore, CHO-CY01 cells at this operating conditions (0.85 mL, 220 rpm, $d_s = 25\,mm$ and, 5.00% (v/v) CO_2) produce IgG4 and increase numbers with the consumption of substrates such as glucose and glutamate. As the cell numbers increase there is an ammonium accumulation along with the increase of IgG4 concentration. These correlations between cell growth, metabolites and IgG4 concentration were set as reference.

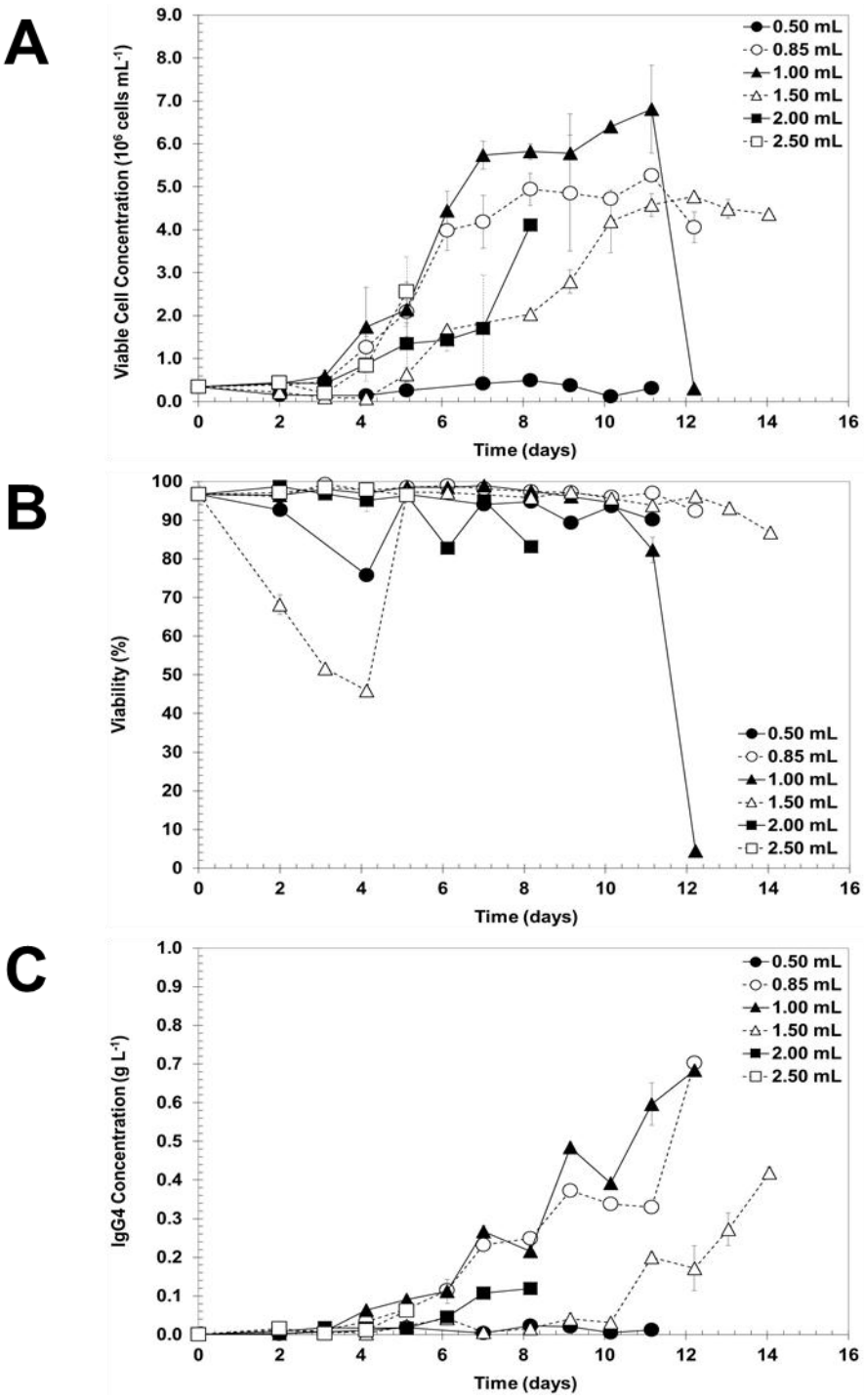

Figure 3-4: Viable cell concentration (A), cell viability (B), and IgG4 concentration (C) profiles for different 24-SRW MTP CHO-CY01 cell batch cultures with different fill volumes (0.50, 0.85, 1.00, 1.50, 2.00, and 2.50 mL) shaken at 220 rpm and, 5.00% (v/v) CO_2 (1 run (3-4 replicates) per fill volume). Error bars represent one standard deviation about the mean.

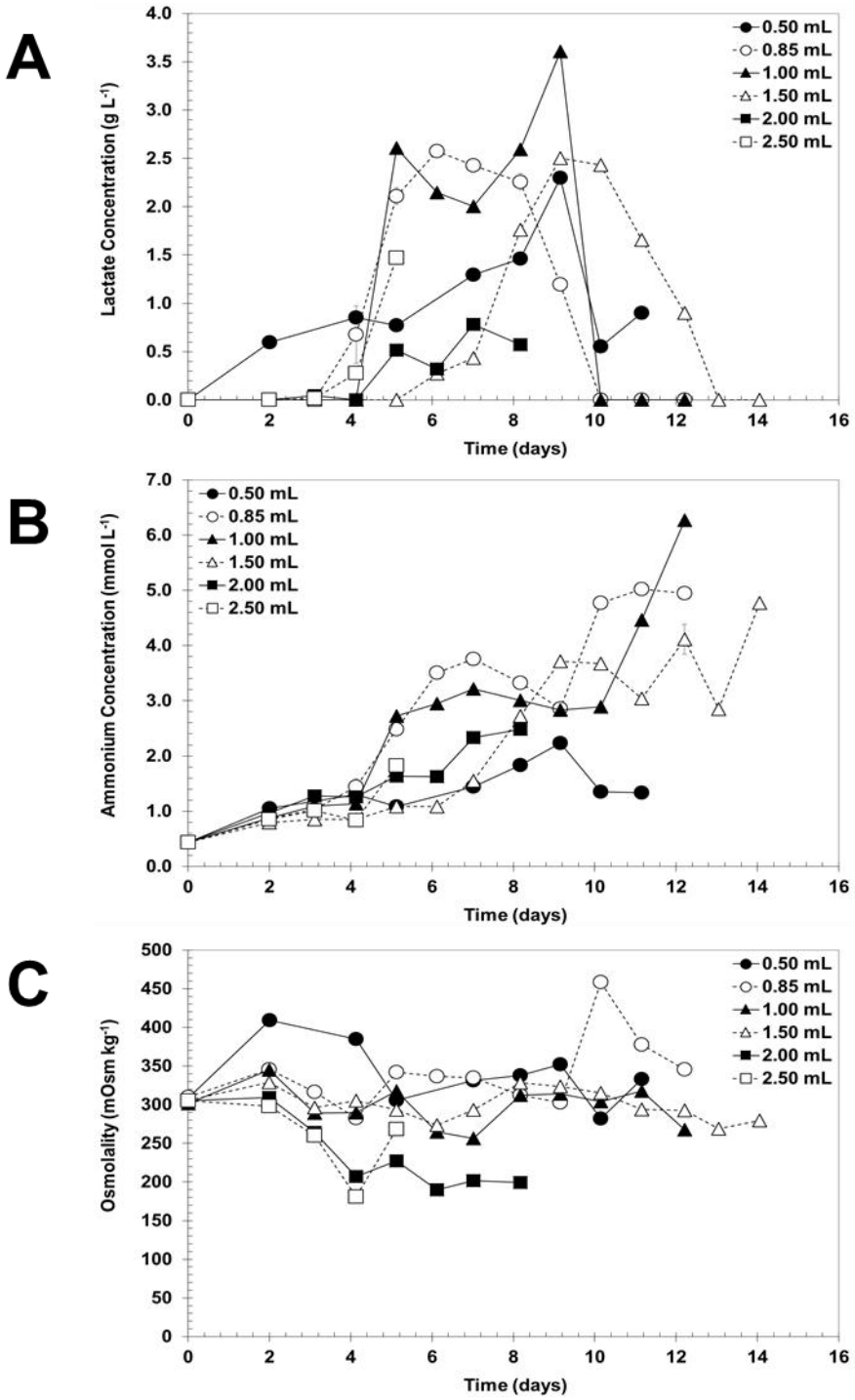

Figure 3-5: Lactate concentration (A), ammonium ion concentration (B), and osmolality (C) profiles for different 24-SRW MTP CHO-CY01 cell batch cultures with different fill volumes (0.50, 0.85, 1.00, 1.50, 2.00, and 2.50 mL) shaken at 220 rpm and, 5.00% (v/v) CO_2 (1 run (3-4 replicates) per fill volume). Error bars represent one standard deviation about the mean.

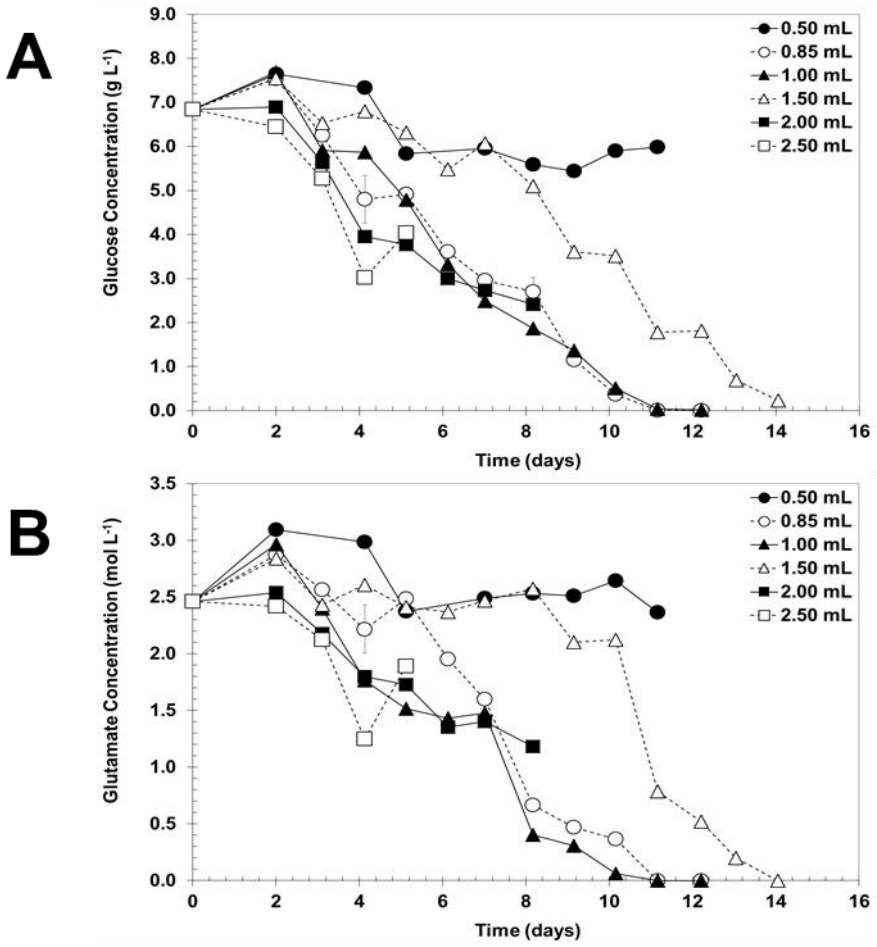

Figure 3-6: Glucose (A) and glutamate (B) concentration-time profiles for different 24-SRW MTP CHO-CY01 cell batch cultures with different fill volumes (0.50, 0.85, 1.00, 1.50, 2.00, and 2.50 mL) shaken at 220 rpm and, 5.00% (v/v) CO_2 (1 run (3-4 replicates) per fill volume). Error bars represent one standard deviation about the mean.

Table 3-4: Kinetic parameters determined for different 24-SRW MTP CHO-CY01 cell batch culture with different fill volumes (0.50, 0.85, 1.00 and, 1.50 mL) shaken at 220 rpm and, 5.00% (v/v) CO_2.

$V_L\ (mL)$	**0.50**	**0.85**	**1.00**	**1.50**
Volumetric productivity (VP) $(mg\ L^{-1}day^{-1})$	1.6	30.6	41.3	14.5
Integral of viable cell concentration (IVCC) $(10^9\ cells\ day\ L^{-1})$	3.06	35.21	41.09	27.75
Specific growth rate (μ) (h^{-1})	0.006	0.014	0.016	0.010
Doubling time ($t_{1/2}$) (h)	115.5	49.9	44.7	73.0
Specific IgG4 production rate $(q_{mAb})(mg\ 10^{-9}\ cells^{-1}\ day^{-1})$	5.74	16.04	15.89	12.02
Specific glucose consumption rate (q_{Gluc}) $(g\ 10^{-9}\ cells^{-1}\ day^{-1})$	-0.75	-0.27	-0.23	-0.31
Specific glutamate consumption rate (q_{Glu}) $(mmol\ 10^{-9}\ cells^{-1}\ day^{-1})$	-0.24	-0.10	-0.09	-0.11
Specific sodium consumption rate (q_{Na^+}) $(mmol\ 10^{-9}\ cells^{-1}\ day^{-1})$	-17.54	0.76	-0.47	-0.53
Specific potassium consumption rate (q_{K^+}) $(mmol\ 10^{-9}\ cells^{-1}\ day^{-1})$	-0.722	0.031	-0.064	-0.099
Specific lactate production rate (q_{Lact}) $(g\ 10^{-9}\ cells^{-1}\ day^{-1})$	2.63	0.42	0.39	0.46
Specific ammonium production rate (q_{Amm}) $(mmol\ 10^{-9}\ cells^{-1}\ day^{-1})$	0.49	0.16	0.12	0.17
Lactate produced / Glucose consumed (g/g)	1.04	0.66	0.57	0.64
Evaporation Rate $(\mu L\ day^{-1})$	26.0 ± 4.9	38.8 ± 7.3	29.4±14.3	22.8 ± 7.5

3.2.5. Impact of Different Shaking Speeds on CHO-CY01 Cell Growth and Productivity

The shaking speed (N) is a parameter in any cell culture with strong influence on engineering parameters such as mixing times, $k_L a$ values and Phase number. To understand the effect of shaking speed on CHO-CY01 cell growth and IgG4 production, 24-SRW MTP were inoculated and shaken at speeds ranging from 100 to 350 rpm. At this shaking speed range, the liquid-phase hydrodynamics are not all "in-phase", and the shaking speed is not always sufficient to move the liquid. The CR1524a 'system Duetz' lid was used to cover the 24-SRW MTPs, since it is the best lid for long cell culture runs as stated by the manufacture. However, different ´system Duetz´ lids were also tested (Section 3.3). The cell culture kinetics can be visualised in Figure 3-7, Figure 3-8 and Figure 3-9. In Table 3-5 and Table C-2, the kinetic parameters determined are represented. All CASY information, particle size distribution with time, and population distribution are included in Figure B-2: and Table B-2:. The correlations between the parameters of the CHO-CY01 cell batch cultures are shown in Table A-2.

From the 24-SRW MTP engineering characterisation study, at 100 rpm the liquid-phase is "out-of-phase", below critical shaking speed, and the $k_L a$ value is incapable of supporting more than $10^6\ cells\ mL^{-1}$. At 150 rpm, the liquid-phase is still "out-of-phase" but above the critical shaking speed, and with $k_L a$ values capable of supporting the growth of more than $10^6\ cells\ mL^{-1}$. For the remaining shaking speeds, the liquid-phase is "in-phase", above the critical speed, and with $k_L a$ values capable of $10^6 - 10^7\ cells\ mL^{-1}$. In terms of mixing time, above 220 rpm there is the possibility to compare microwell with SF and STR CHO-CY01 cell cultures. Below 220 rpm, the mixing time is in the range of minutes, and heterogeneities in the liquid-phase are present. To maintain reproducibility, those shaking speeds were not considered in the research presented in this thesis. Apart from 100 rpm, where the evaporation rate was unexpectedly the highest, the evaporation rate increased with the shaking speed (Table 3-5). This observation was in agreement with the literature (Girard et al., 2001).

At 350 rpm, the agitation of the liquid-phase was too vigorous to the CHO-CY01 cell culture, as after four days all of the initial cells were dead. For this operating condition, no kinetic parameter was determined. At the other extreme of 100 rpm, cells managed to grow very slowly ($t_{1/2} = 41.51\ h$) and were able to generate very low titer of IgG4 (Figure 3-7). Therefore, 100 rpm is not the most suitable shaking speed to grow the CHO-CY01 cell line for productivity optimisation reasons. At 150 rpm, the "out-of-phase" phenomenon has prolonged the *lag* phase and slowed the cell growth rate (Figure 3-7 and, Table 3-5). The shaking speed range at which the CHO-CY01 cell line grows was found to be from 180 to 300 rpm. These are shaking speeds considerably higher than the shaking speeds tested for another CHO cell

line (CHO-S) (Silk, 2014). This indicates that the CHO-CY01 cell line is a shear-resistant cell line, which is beneficial for large-scale production. In this range, with the increase of shaking speed, the μ diminished, extending the cell culture time.

The lactate profile for the CHO-CY01 cell line in 24-SRW MTP with 0.85 mL fill volume did not change with shaking speed for shaking speeds higher than 180 rpm. Lactate production (LP) continued until the mid-point of the exponential phase (day 4 – 5); then, it shifts to consumption (LC). The lactate shift usually occurred when glucose concentration was $3.0 - 4.0\ g\ L^{-1}$ and glutamate was $2.5 - 3.5\ mol\ L^{-1}$. These was an important association made when designing the fed-batch strategy (Chapter 4). Independently of the shaking speed, it was observed that the CHO-CY01 cells stopped ammonium production and began to degrade it slowly at the same time they shifted to LC. When CHO-CY01 cells entered the decline phase, a new ammonium formation period began, followed by a plateau at the maximal ammonium concentration until the end of cell culture run (no glucose and no lactate present). To avoid further ammonium accumulation and cell impurities caused by cell breakage, CHO-CY01 cell culture should be stopped when glucose levels reach values near zero.

The pH profile of the CHO-CY01 cell line at different shaking speeds reflects the metabolite shifts. When cells are producing lactate and ammonium, the external pH changes. The lactate lower the pH and the ammonium increases the external pH. The pH range is similar for all suitable shaking speeds (7.5 ± 0.3). In Chapter 5, a study of the effect of different external pH values was conducted at 24-SRW MTP scale.

The osmolality of the CHO-CY01 cell batch culture at different shaking speeds had a slight increase ($370\ mOsm\ kg^{-1}$) until the mid-exponential point and then decreased to create a plateau around $325\ mOsm\ kg^{-1}$. It has been reported that osmolality values higher than $290\ mOsm\ kg^{-1}$ have improved antibody secretion rate (Lee et al., 2009). On the other hand, osmolality values higher than $400\ mOsm\ kg^{-1}$ are known to decrease cell density (Miller et al., 1988; Zhu et al., 2005). At 5.00% (v/v) CO_2, the CHO-CY01 cell line was cultured at a hyperosmotic condition, which may resulted in higher production rates.

At 180 rpm and 220 rpm, CHO-CY01 cell growth and IgG4 productivity are similar (p > 0.05), but higher lactate and ammonium concentrations were observed in the CHO-CY01 cell batch culture at 180 rpm. For shaking speeds higher than 220 rpm, there was an impact on the cell growth and metabolism with longer *lag* phase, decreased cell numbers, and increases in the specific IgG4, lactate, and ammonium production rates. At 300 rpm, the highest q_{mAb} was reached. At this shaking speed, CHO-CY01 cells were unusually large compared with the other operating conditions (Figure B-2: and Table B-2:). At the same time, the percentage of debris and dead cells throughout the culture were high. This elevated degree of cell breakage is likely behind the IgG4 concentration increase instead of a plateau

towards the end of the culture. IgG4 and IgG4 fragments present inside the cells were detected by protein G HPLC, creating the illusion of higher productivity. Further investigation is needed to corroborate this hypothesis.

Since using a microwell approach for productivity optimisation is the goal, the reference shaking speed was chosen to be 220 rpm. At this shaking speed, there is a low concentration of waste products, high cell density and productivity, low level of cell breakage, and a liquid-phase hydrodynamic similar to that of larger cell culture vessels.

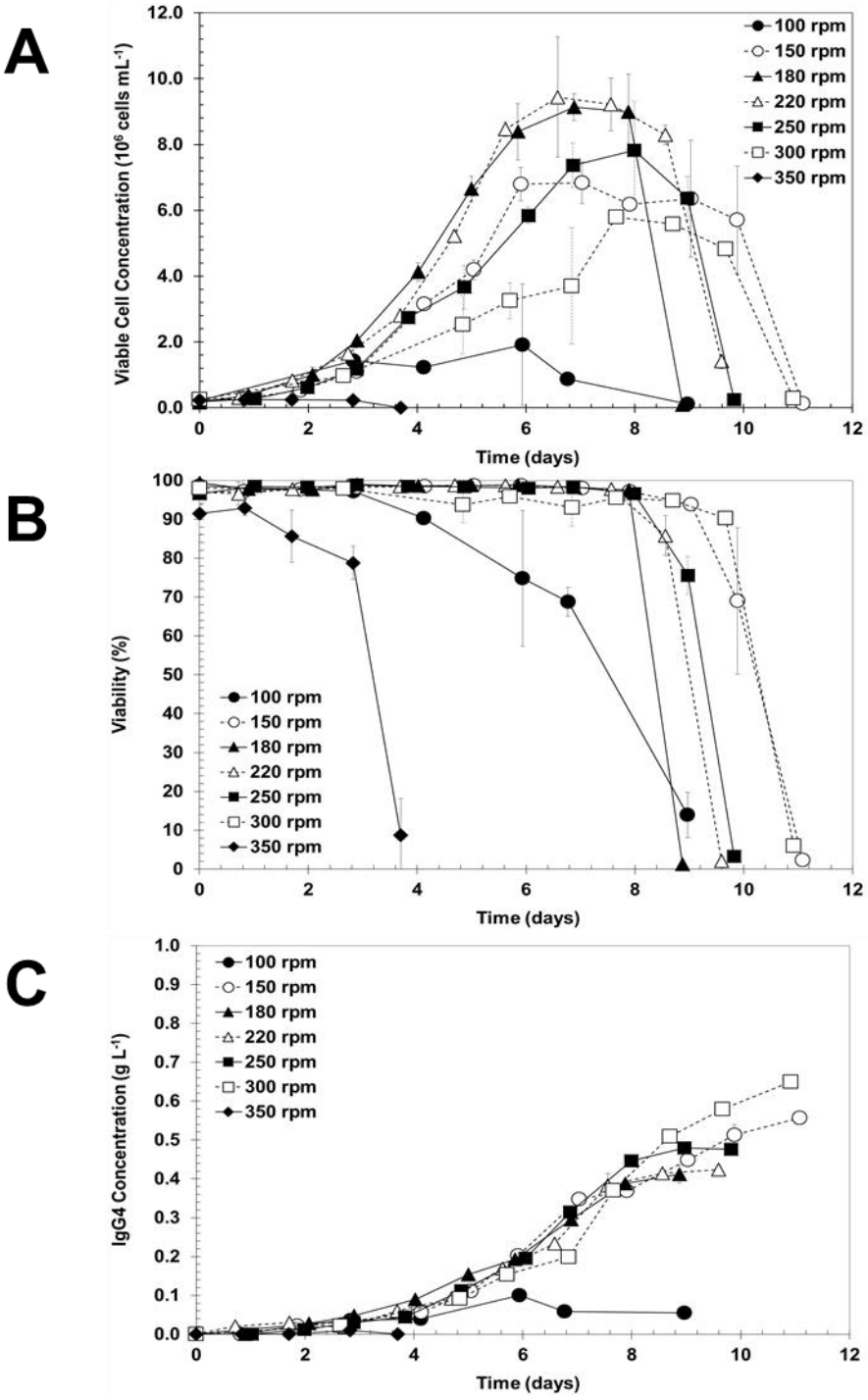

Figure 3-7: Viable cell concentration (A), cell viability (B), and IgG4 concentration (C) time profiles for 24-SRW MTP CHO-CY01 cell batch cultures at different shaking speeds (100, 150, 180, 220, 250, and 300 rpm) and 5.00% (v/v) CO_2 (1 run (3-4 replicates) per shaking speed). Error bars represent one standard deviation about the mean.

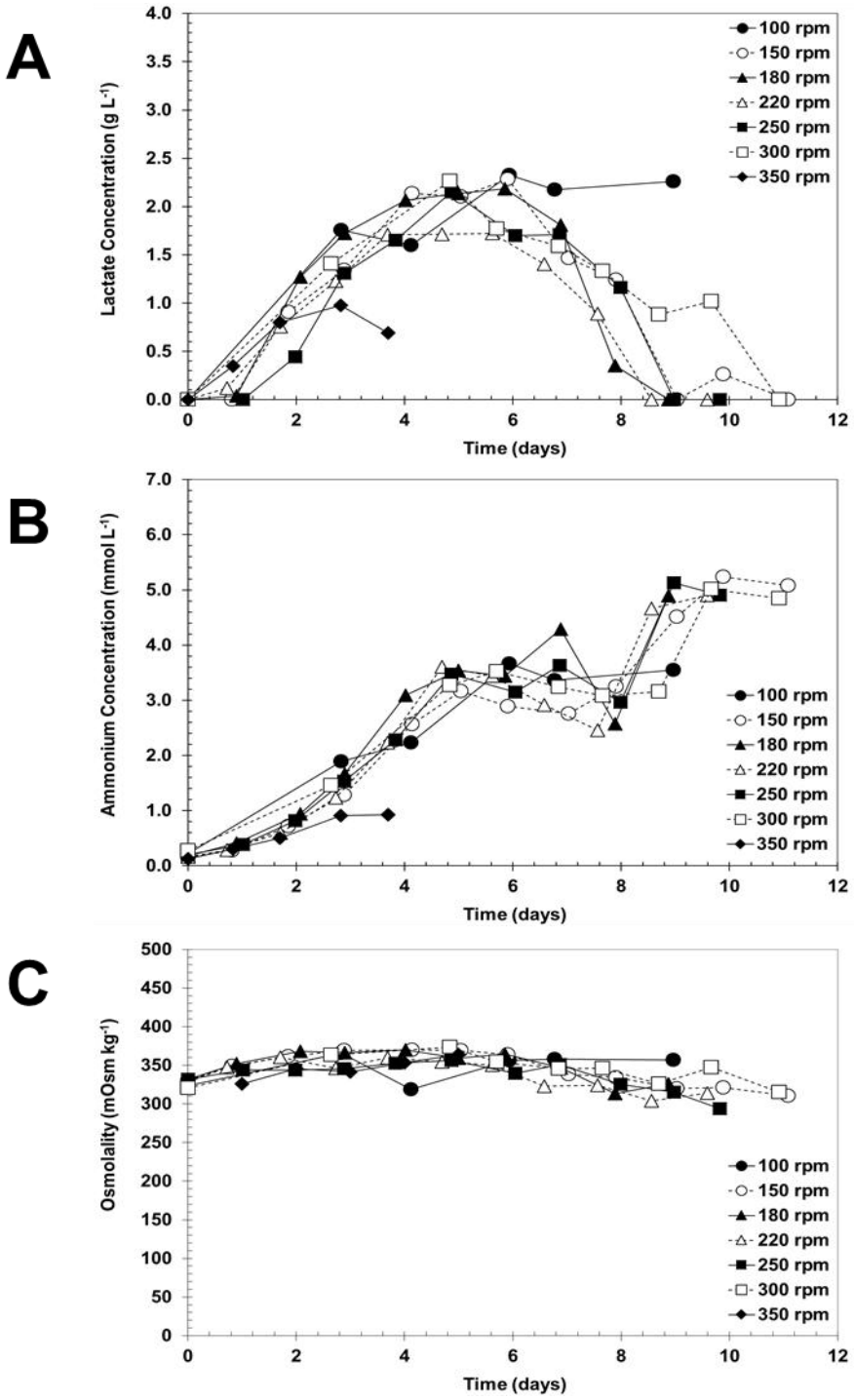

Figure 3-8: Lactate concentration (A), ammonium ion concentration (B), and osmolality (C) time profiles for 24-SRW MTP CHO-CY01 cell batch cultures at different shaking speeds (100, 150, 180, 220, 250, and 300 rpm) and 5.00% (v/v) CO_2 (1 run (3-4 replicates) per shaking speed). Error bars represent one standard deviation about the mean.

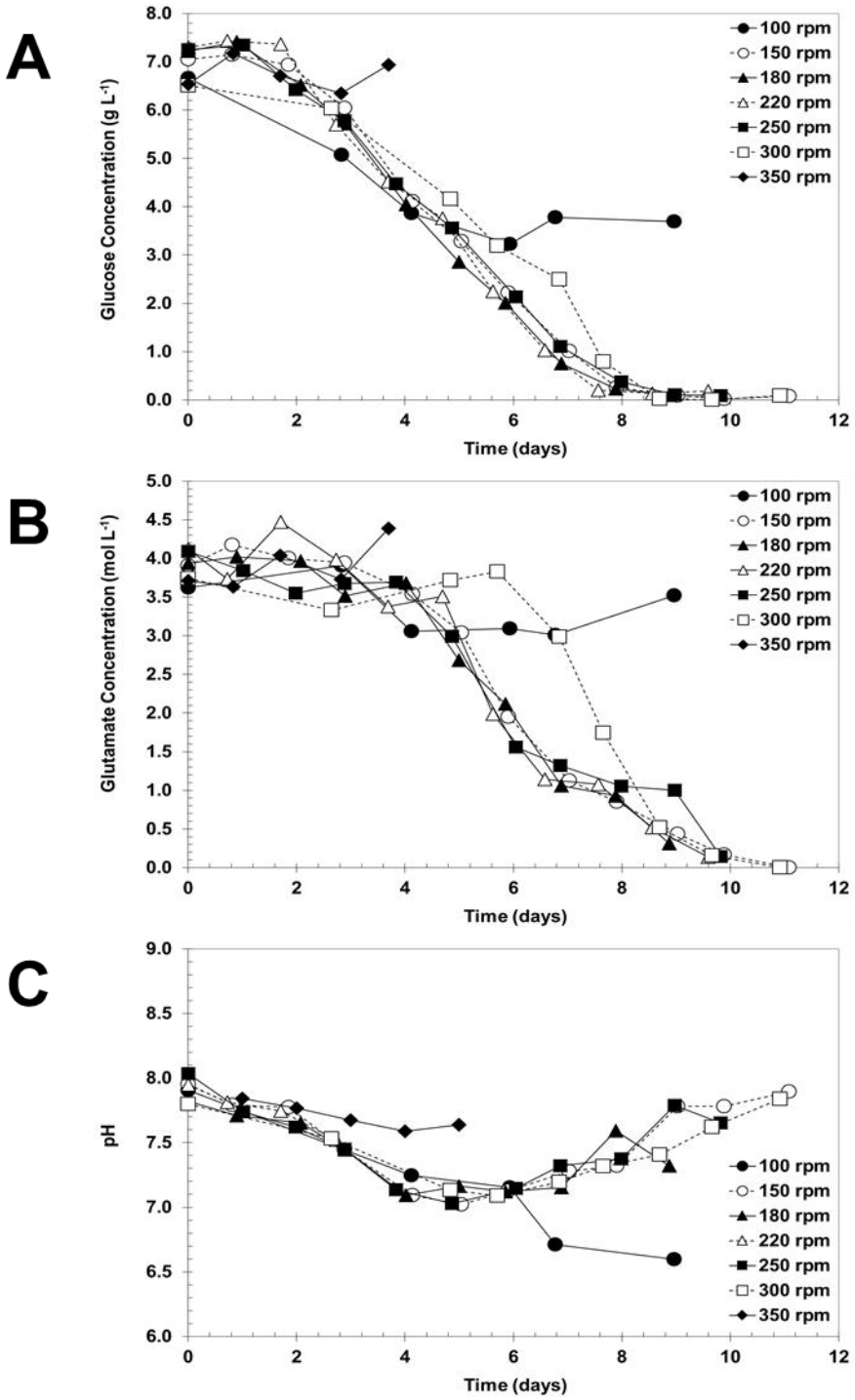

Figure 3-9: Glucose concentration (A), glutamate concentration (B), and pH (C) time profile for 24-SRW MTP CHO-CY01 cell batch cultures at different shaking speeds (100, 150, 180, 220, 250, 300, and 350 rpm) and 5.00% (v/v) CO_2 (1 run (3-4 replicates) per shaking speed). Error bars represent one standard deviation about the mean.

Table 3-5: Kinetic parameters determined for different 24-SRW MTP CHO-CY01 cell batch cultures at different shaking speeds (100, 150, 180, 220, 250, and 300 rpm) at 5.00% (v/v) CO_2. The error represents one standard deviation about the mean.

$\boldsymbol{N\ (rpm)}$	**100**	**150**	**180**	**220**	**250**	**300**
VP ($mg\ L^{-1}day^{-1}$)	9.4	45.2	40.4	40.0	44.4	49.7
IVCC ($10^9\ cells\ day\ L^{-1}$)	9.13	41.3	40.06	46.07	35.98	29.96
$\mu\ (h^{-1})$	0.017	0.025	0.029	0.025	0.024	0.017
$t_{1/2}\ (h)$	41.5	27.73	23.7	28.2	28.5	39.8
$q_{mAb}\ (mg\ 10^{-9}\ cells^{-1}\ day^{-1})$	8.84	14.05	10.86	10.17	14.90	21.76
$q_{Gluc}\ (g\ 10^{-9}\ cells^{-1}\ day^{-1})$	-0.41	-0.22	-0.22	-0.20	-0.25	-0.30
$q_{Glu}\ (mmol\ 10^{-9}\ cells^{-1}\ day^{-1})$	-0.09	-0.12	-0.10	-0.09	-0.11	-0.14
$q_{Na^+}\ (mmol\ 10^{-9}\ cells^{-1}\ day^{-1})$	1.24	0.35	0.43	0.26	0.23	0.16
$q_{K^+}\ (mmol\ 10^{-9}\ cells^{-1}\ day^{-1})$	-0.061	-0.026	-0.046	-0.019	-0.022	-0.040
$q_{Lact}\ (g\ 10^{-9}\ cells^{-1}\ day^{-1})$	0.98	0.36	0.36	0.27	0.35	0.41
$q_{Amm}\ (mmol\ 10^{-9}\ cells^{-1}\ day^{-1})$	0.42	0.13	0.12	0.11	0.15	0.17
Lactate produced / Glucose consumed (g/g)	0.68	0.46	0.40	0.33	0.57	0.73
Evaporation rate ($\mu L\ day^{-1}$)	30.8 ± 9.9	20.2 ± 18.6	22.3 ± 5.3	24.0 ± 4.9	24.4 ± 6.5	29.1 ± 5.9

3.3. Establishment of Microwell Batch Culture Conditions for CHO-CY01 Cell Line

3.3.1. Evaporation Rate Study in 24-SRW MTPs

The Achilles heel of microwell systems is water loss due to evaporation and cross-contamination due to spill-over. Microplates can be sealed with commercially available covers to avoid these drawbacks. There are two strategies to consider when reducing the evaporation rate in microwell plates. The first strategy is to increase the relative humidity (RH) in the shaken CO_2 incubator used for cultures, thus decreasing the driving force for water diffusion from the microwell headspace. The RH is usually controlled by fill Milli-Q water into the tray in the bottom of the inside of the CO_2 incubator. The downside of this approach is that it is a potential source of contamination. The second strategy is to increase the mass transfer resistance of the sterile closure used to seal the plates (Zimmermann et al., 2003). In this work, the latter startegy was used and two ´system Duetz´ lids, CR1524 and CR1524a, (Figure 2-1 D and, Table 2-1) were tested (Section 3.3.2.).

An adequate sampling strategy was necessary and so, developed to create a robust and reproducible CHO-CY01 cell culture model in 24-SRW MTPs. One of the goals was to keep the evaporation rate to a minimum and similar across the microwell plate. Positional effects have been noted in the literature; for example, the observation that the rate of evaporation from wells at the edges of the plate exceeds that of those located in the centre (Girard et al., 2001). Therefore, an evaporation rate evaluation in 24-SRW MTPs was conducted. Firstly, the evaporation rate across the microwell plate of two different ´system Duetz´ lids configurations (CR1524 and CR1524a) was calculated. Secondly, a positional evaporation rate study was conducted.

All 24-SRW MTPs evaporation studies were performed at the optimised operating conditions found in the previous section (Section 3.2.). They were shaken at 220 rpm with an orbital shaking diameter of 25 mm and 0.85 mL of fill volume at 5.00% (v/v) CO_2 and 37°C. For economic reasons and because the density of water is similar to the CD-CHO medium, the 24-SRW MTPs were filled with water instead. The 24-SRW MTPs were weighed every day to determine the difference in volume, which would correspond to differential evaporation rates across the plate or wells. This evaporation study was conducted over an extended period of days to quantify the water loss during CHO-CY01 cell fed-batch cultures.

In Figure 3-10, the evaporation rate is represented for 24-SRW MTP with CR1524 and CR1524a ´system Duetz` lids shaken at 220 rpm and 37°C with atmospheric humidity (65%)[6]. From the manufacturer´s evaporation rate data (Table 2-1), it was known that the CR1524a lid has an improvement (5 times) over the CR1524 lid in relation to water loss. Nevertheless,

[6] Average value for relative humidity in London in July 2014. Source: www.weatheronline.co.uk

there was the need to determine it for the chosen operating. For the CR1524 ´system Duetz` lid, there was an evaporation rate of $54\ \mu L\ well^{-1}day^{-1}$, and for the CR1524a lid, it was $15\ \mu L\ well^{-1}day^{-1}$, with a 3.6-fold difference. It was noticed that these values were higher and less separated than what the manufacture has stated. It was then suggested as a good practice to weigh the 24-SRW MTPs before and after sampling to determine the exact well volume instead of assuming the manufacturer's evaporation rate or the one determined in this work.

The CR1524 ´system Duetz` lid was considered an unsuitable sealing cover due to its inability to maintain the same liquid-phase hydrodynamics for the duration of a cell culture. After seven days, half of the contents had been lost. The effects on the CHO-CY01 cell batch culture at this high evaporation rate are analysed in the following section (Section 3.3.2.). With CR1524a lid, there was a well content loss of no more than 34%, maintaining the same liquid-phase environment during a mammalian cell culture.

The use of microwell systems is based on the assumption that each well provides an identical environment, especially when a sacrificial method of sampling is being used. Even minor differences in temperature, number of times that the CO_2 incubator door is opened, number of times that the sealing covers are open during sampling, and the type of sealing cover used, will have an effect on the cell culture performance and the risk of contamination. These factors have a particular interest and impact on long fed-batch cell cultures.

Positional variability in the microwell systems has been reported (Girard et al., 2001). Therefore, to assess the reproducibility across the microwell plate, the 24-SRW MTP was divided into three different areas: ´corner` wells; ´edge` wells, and ´internal` wells (Figure 3-11). Evaporation studies in microwell plates divided into these three sections were performed. From Figure 3-12, it can be observed that the major contributor for the water lost are the ´corner` wells, whereas the ´edge` and ´internal` wells presented similar low values of evaporation. With regards to well-to-well reproducibility, the sacrificial sampling strategy, adopted to maintain the same liquid-phase hydrodynamics and minimise the evaporation of the well´s contents and its osmotic effects, was to sample firstly the ´corner` wells followed by the ´edge` wells and ´internal` wells.

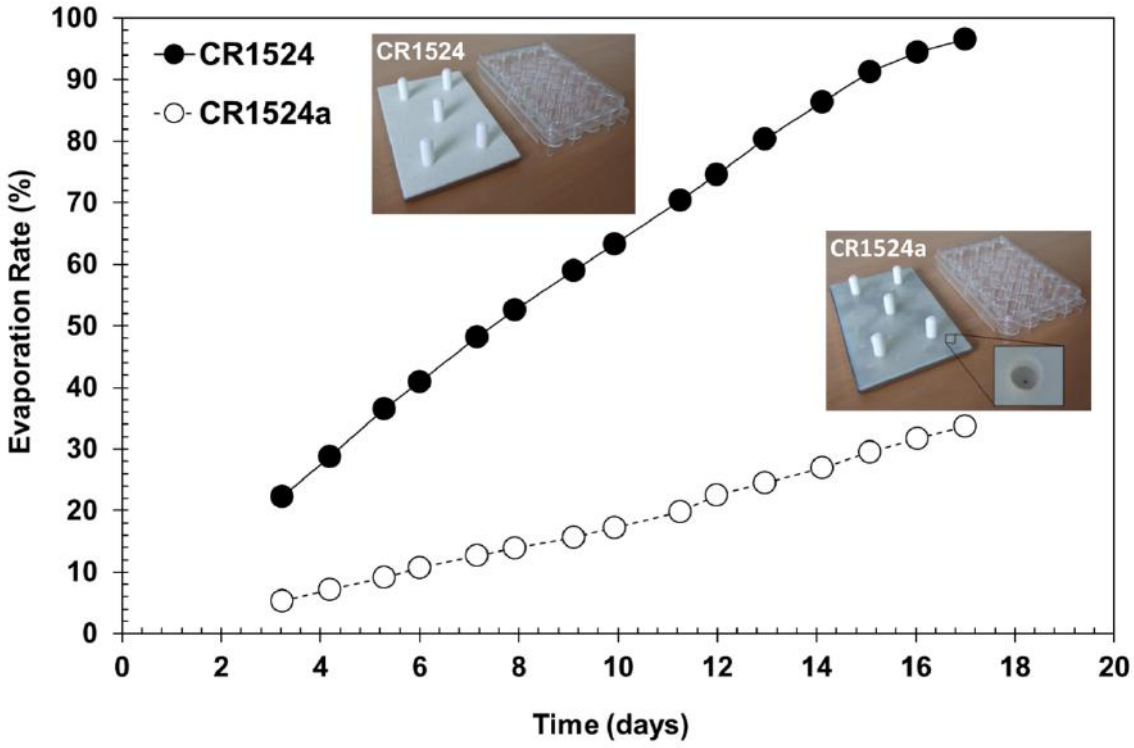

Figure 3-10: Evaporation rate for two different ´system Duetz´ lid configurations for 24-SRW-MTP (CR1524 and CR1524a). The study was performed with 0.85 mL of water shaken at 220 rpm in an orbital diameter of 25 mm at 5.00% (v/v) CO_2.

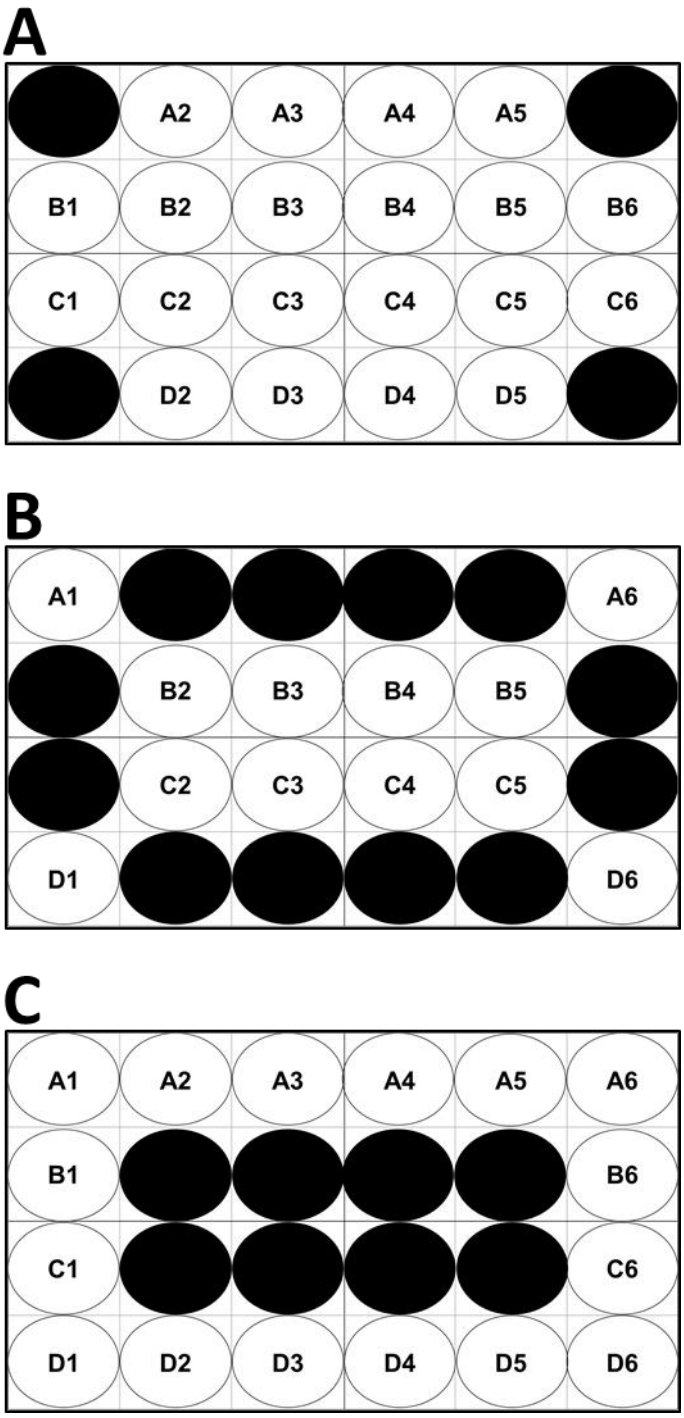

Figure 3-11: Classification of 24-SRW MTP wells by position. (A) ´Corner` wells; (B) ´Edge` wells; (C) ´Internal` wells.

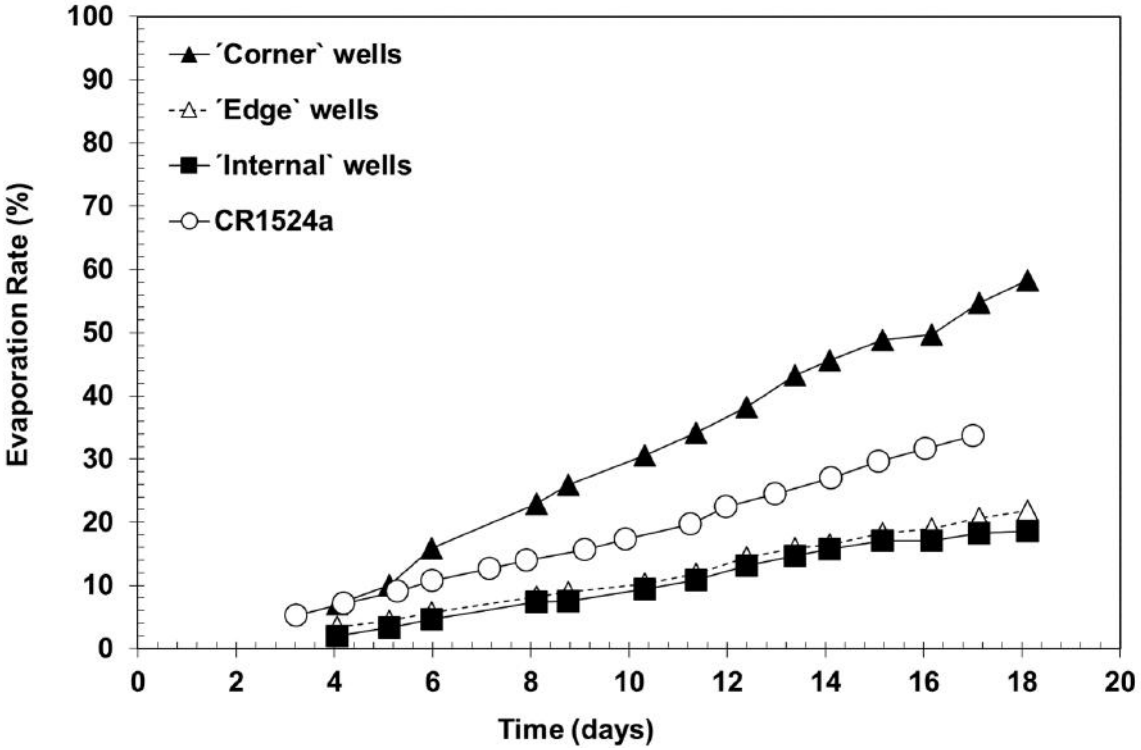

Figure 3-12: Evaporation rates for a 24-SRW MTP and the three 24-SRW MTP well classifications. All microwell plates were sealed with a CR1524a ´system Duetz` lid. The study was performed with 0.85 mL of water shaken at 220 rpm in an orbital diameter of 25 mm at 5.00% (v/v) CO_2.

3.3.2. Selection of a Sterile Closure

A cover system for microwell plates during orbital shaking should meet the following requirements: (i) the cover should prevent direct well-to-well spilling of cell suspension by small splashes or aerosols, (ii) the cover should prevent airborne contaminants from entering the wells, (iii) the cover should prevent excessive evaporation of water from the culture (no more than 5% volume loss per day), (iv) the cover should allow a sufficient degree of replacement of the headspace air (venting) to maintain an oxygen level in the headspace of more than 75% of air saturation (Duetz et al., 2001). The above criteria are met when applying the CR1524 and CR1524a ´system Duetz´ sandwich lids.

CHO-CY01 cell batch culture in 24-SRW MTP with CR1524 and CR1524a ´system Duetz´ lids were cultured at 2.00% (v/v) CO_2 and 37ºC to test the previous section outcome. In Figure 3-13 and Figure 3-14, CHO-CY01 cell kinetics are visualised, and in Table 3-6 and Table C-3 the kinetic parameters are calculated. The statistical correlation test is presented in Table A-3.

For CHO-CY01 cell batch culture sealed with the CR1524 ´system Duetz` lid, a higher evaporation rate (2.9-fold) and waste products accumulation, a lower antibody productivity (39%) and cell growth were observed when compared with CHO-CY01 cell culture sealed with the CR1524a ´system Duetz` lid. The correlation obtained with cell culture parameters were more realistic for the cell culture using the CR1524a lid (Table A-3). For instance, in CHO-CY01 cell batch culture with CR1524, there was only one strong correlation: between viable cell numbers and ammonium, while with CR1524a viable cell numbers had four strong and very strong correlations (glucose, glutamate, IgG4 and, osmolality). Therefore, the CR1524a ´system Duetz´ lid was selected as the standard 24-SRW MTP sealing cover.

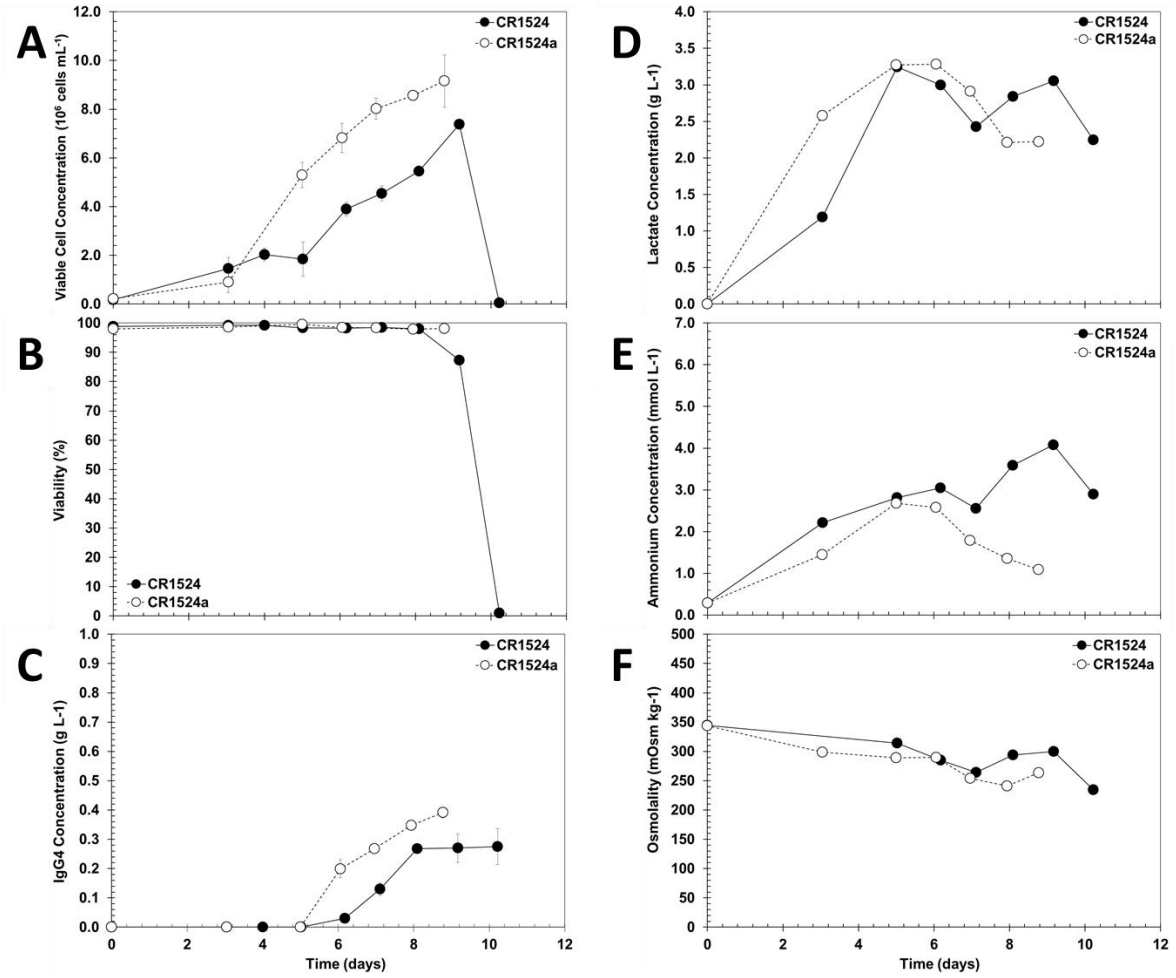

Figure 3-13: Viable cell concentration (A), viability (B), IgG4 concentration (C), lactate concentration (D), ammonium ion concentration (E), and osmolality (F) time profiles for 24-SRW MTP CHO-CY01 cell batch cultures sealed with CR1524 and CR1524a ´system Duetz` lids at 2.00% (v/v) CO_2 (1 run (3-4 replicates)). Error bars represent one standard deviation about the mean.

Table 3-6: Kinetic parameters of 24-SRW MTP CHO-CY01 cell batch cultures sealed with CR1524 and CR1524a ´system Duetz` lids at 2.00% (v/v) CO_2. The error represents one standard deviation about the mean.

´System Duetz` Lid	**CR1524**	**CR1524a**
VP ($mg\ L^{-1}day^{-1}$)	21.8	35.7
IVCC ($10^9\ cells\ day\ L^{-1}$)	29.14	36.37
$\mu\ (h^{-1})$	0.019	0.021
$t_{1/2}\ (h)$	36.5	33.8
$q_{mAb}\ (mg\ 10^{-9}\ cells^{-1}day^{-1}\ )$	10.11	11.43
$q_{Gluc}\ (g\ 10^{-9}\ cells^{-1}\ day^{-1})$	-0.31	-0.22
$q_{Glu}\ (mmol\ 10^{-9}\ cells^{-1}day^{-1})$	-0.09	-0.06
$q_{Na^+}\ (mmol\ 10^{-9}\ cells^{-1}\ day^{-1})$	-1.81	-1.62
$q_{K^+}\ (mmol\ 10^{-9}\ cells^{-1}\ day^{-1})$	-0.04	-0.02
$q_{Lact}\ (g\ 10^{-9}\ cells^{-1}day^{-1})$	0.76	0.50
$q_{Amm}\ (mmol\ 10^{-9}\ cells^{-1}day^{-1})$	0.15	0.05
Lactate produced / Glucose consumed (g/g)	1.07	0.98
Evaporation rate ($\mu L\ day^{-1}$)	43.18 ± 10.85	15.23 ± 8.52

3.3.3. Evaluating the Effects of Different Microwell Plates for CHO-CY01 Cell Cultures

Non-invasive measurements of pH and DOT of CHO-CY01 cell cultures were made using the SDR SensorDish® Reader system (Section 2.2.7). For the development of a robust and reproducible sampling method, it was mandatory to determine whether the sensor and the measurement method (LED light) were affecting the CHO-CY01 cell culture in contrast with a standard 24-SRW polystyrene microwell plate. The majority of mammalian cell culture media use a CO_2/bicarbonate buffer system and it is usually kept at 2.00% or 5.00%(v/v) CO_2 to maintain the medium at physiological pH (Yoon et al., 2002). It is assumed that cell behaviour in the HydroDish®HD24 is equivalent to that found in an OxoDish®OD24 plate.

A standard 24-SRW MTP and HydroDish®HD24 were inoculated with the CHO-CY01 cell line at 5.00% (v/v) CO_2 and 2.00% (v/v) CO_2, and 37ºC. The CHO-CY01 cell batch culture kinetics is visualised in Figure 3-14 (2.00% (v/v) CO_2) and Figure 3-15 (5.00% (v/v) CO_2). HydroDish®HD24 online pH and temperature profiles are presented in Figure 3-16 (2.00% and 5.00% (v/v) CO_2). The determined kinetic parameters are listed in Table 3-7. Table C-4 (5.00% (v/v) CO_2), and Table C-5 (2.00% (v/v) CO_2). The statistical comparison between the two different types of microwell plates was performed through a t-test assuming unequal variances.

It was observed that both 2.00% and 5.00% (v/v) CO_2 CHO-CY01 cell batch cultures in a standard 24-SRW MTP and in a HydroDish®HD24 plate are statistically equivalent (p > 0.05) for all of the cell culture parameters. Usually, the cells in the standard 24-SRW MTPs have a tendency to multiply slightly more (15.8%) in contrast with the higher rate at which cells in HydroDish®HD24 plates produce lactate and ammonium, which it may be attributed to batch-to-batch variability.

Accordingly, a new sampling strategy was established for 24-SRW MTPS cell cultures with online parameters measured. The standard 24-SRW MTPs were used for sacrificial sampling, and the HydroDish®HD24 or OxoDish®OD24 plates were exclusively used for online pH, DO, and temperature readings.

From Figure 3-16, it can be seen how sensitive the pH and temperature measurements were. The pH peaks simultaneously tandem with a temperature drop representing the opening of the CO_2incubator during sampling. The higher the CO_2concentration inside the incubator, the higher the pH peaks were. Another point observed was the impact that CO_2 concentration had on the bicarbonate buffered medium's pH and on the cell kinetics and productivity. The latter point will be developed in depth in Chapter 5. The pH value and range at 2.00% (v/v) CO_2 (7.32 ± 0.29) was higher than at 5.00% (v/v) CO_2 (7.13 ± 0.14).

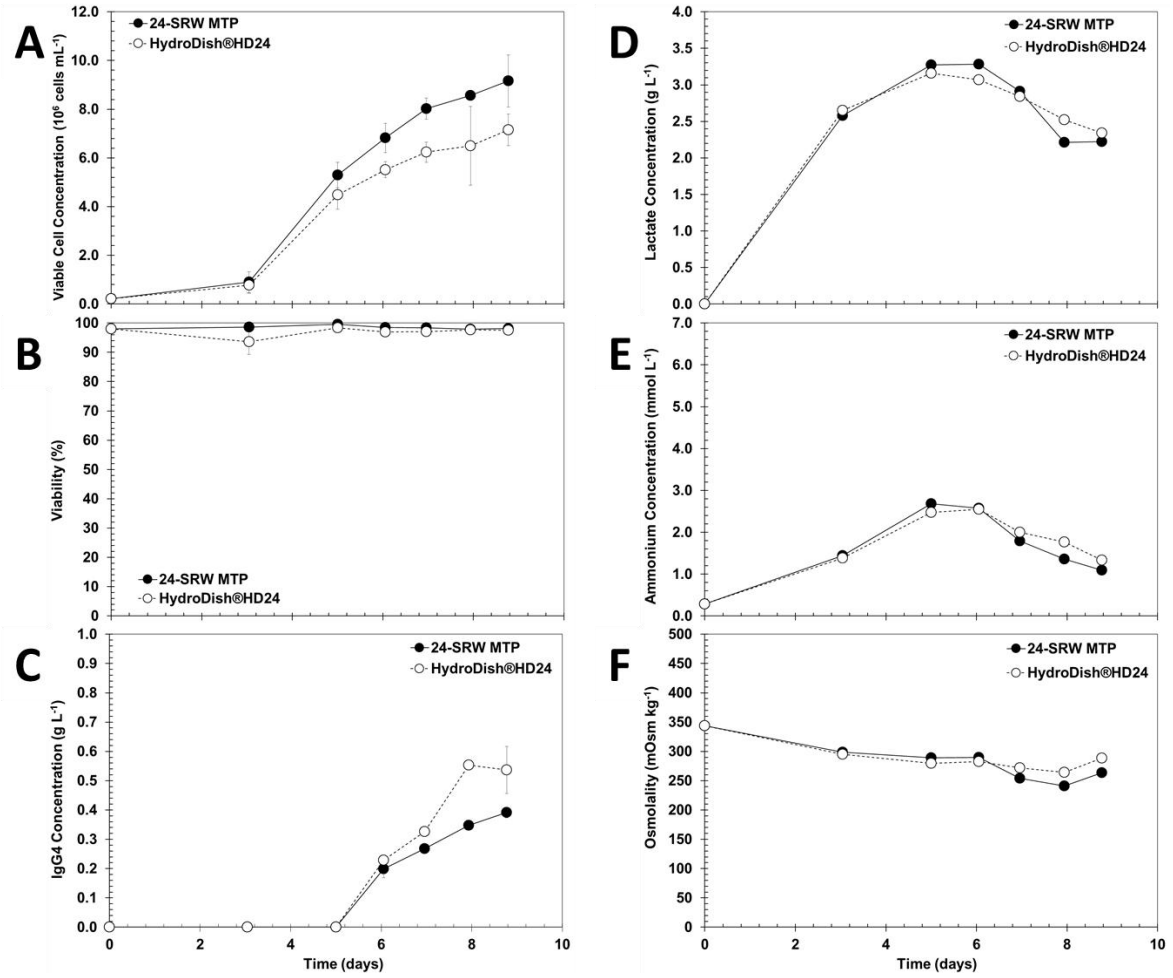

Figure 3-14: Viable cell concentration, viability, IgG4 concentration, lactate concentration, ammonium ion concentration, and osmolality time profiles of CHO-CY01 cell batch cultures in a standard 24-SRW MTP and HydroDish®HD24 at 2.00% (v/v) CO_2 (1 run (3-4 replicates)). Error bars represent one standard deviation about the mean.

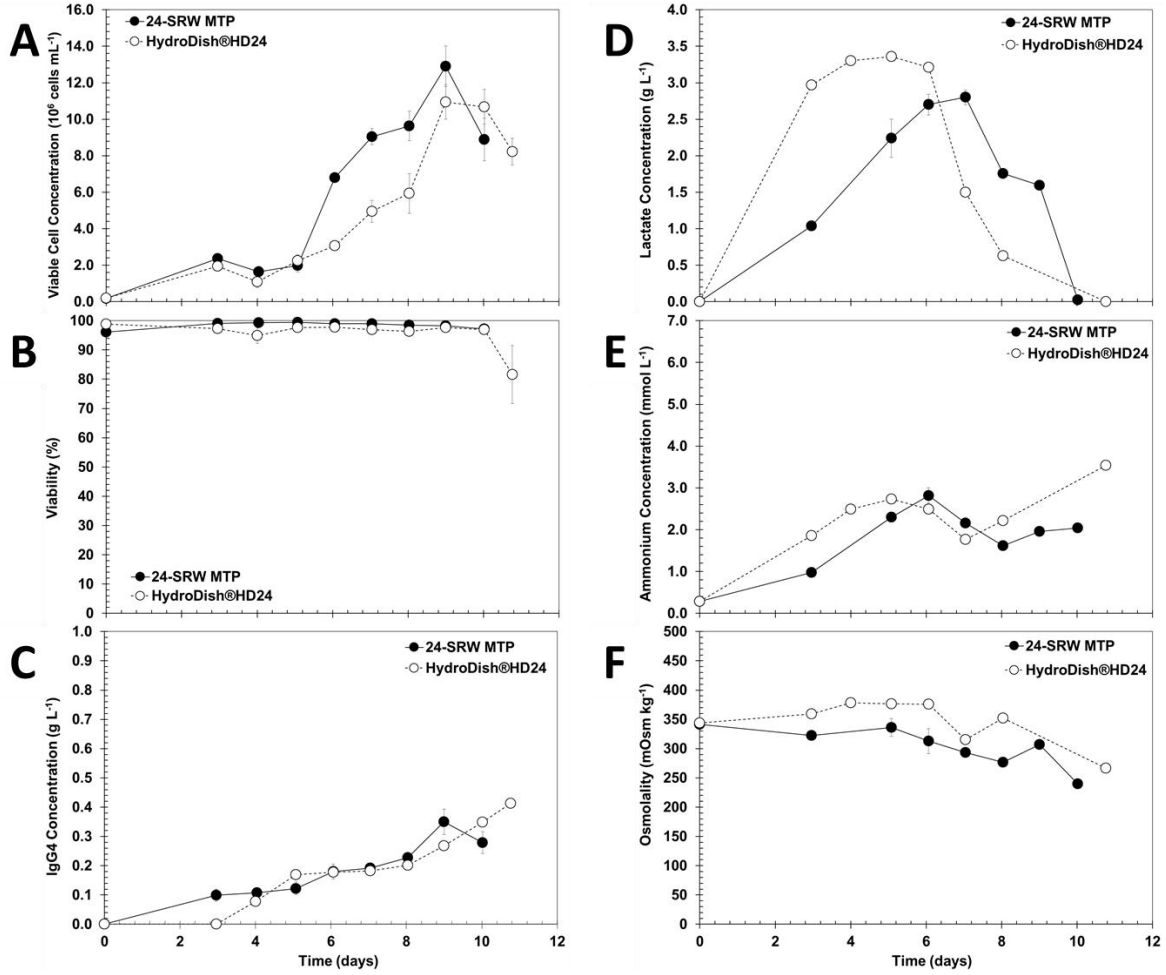

Figure 3-15: Viable cell concentration, viability, IgG4 concentration, lactate concentration, ammonium ion concentration, and osmolality time profiles of CHO-CY01 cell batch cultures in a standard 24-SRW MTP and HydroDish®HD24 at 5.00% (v/v) CO_2 (1 run (3-4 replicates)). Error bars represent one standard deviation about the mean.

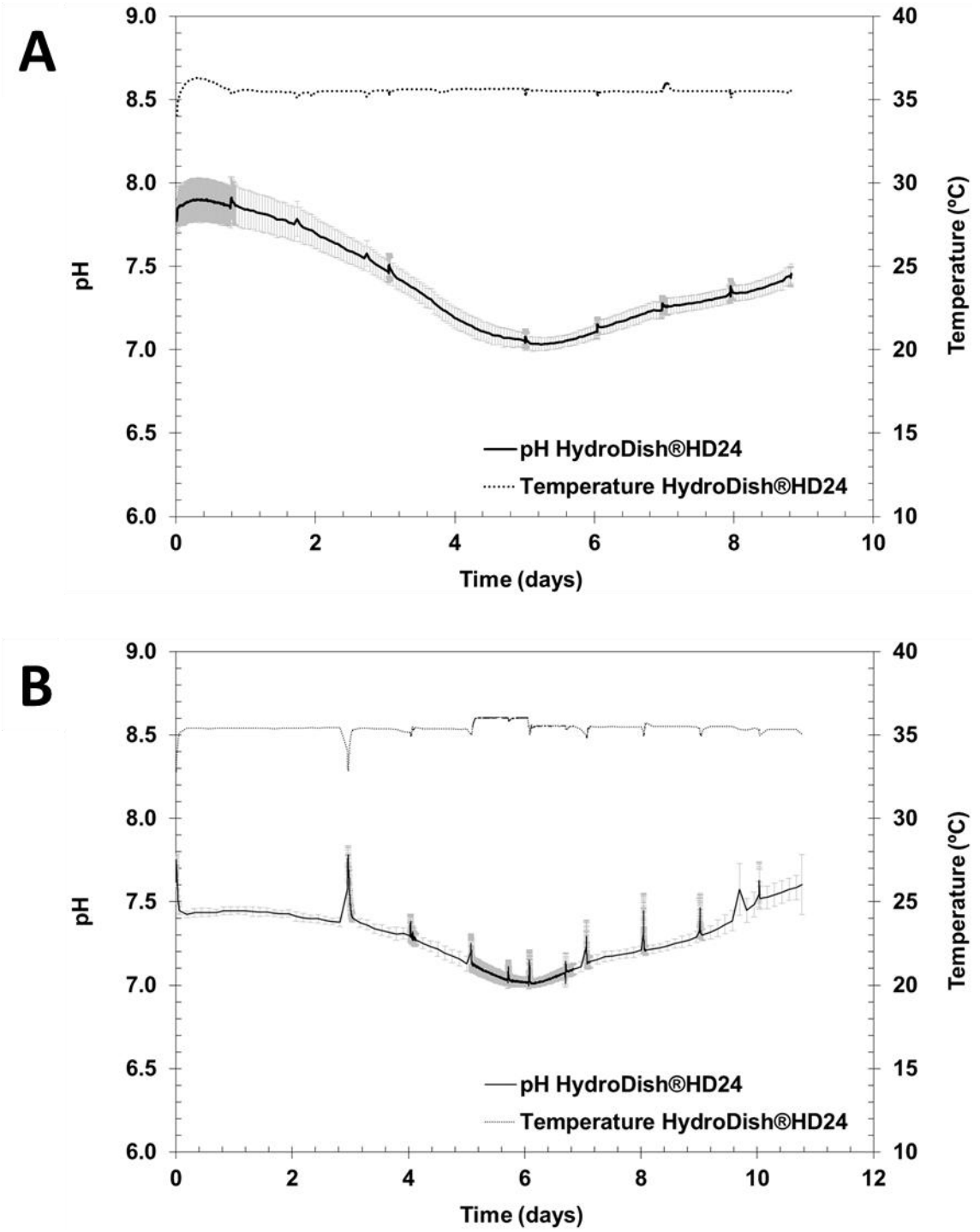

Figure 3-16: pH profile of CHO-CY01 cell batch cultures in a HydroDish®HD24 at 2.00% (A) and 5.00% (v/v) CO_2 (B) (1 run (24 replicates)). Error bars represent one standard deviation about the mean.

Table 3-7: Kinetic parameters of CHO-CY01 cell batch cultures in a standard 24-SRW MTP and HydroDish®HD24 at 2.00% CO_2 and 5.00% (v/v) CO_2. The error represents one standard deviation about the mean.

	2.00% (v/v) CO_2		**5.00% (v/v) CO_2**	
	24-SRW MTP	**HydroDish®HD24**	**24-SRW MTP**	**HydroDish®HD24**
VP ($mg\ L^{-1}day^{-1}$)	35.7	49.2	30.2	31.1
IVCC ($10^9 cells\ day\ L^{-1}$)	36.37	29.17	51.15	44.72
$\mu\ (h^{-1})$	0.021	0.019	0.022	0.019
$t_{1/2}\ (h)$	33.8	36.3	31.1	36.1
$q_{mAb}\ (mg\ 10^{-9}\ cells^{-1}\ day^{-1})$	11.43	19.60	7.49	9.99
$q_{Gluc}\ (g\ 10^{-9}\ cells^{-1} day^{-1})$	-0.22	-0.27	-0.18	-0.23
$q_{Glu}\ (mmol\ 10^{-9}\ cells^{-1}\ day^{-1})$	-0.08	-0.09	-0.08	-0.08
$q_{Na^+}\ (mmol\ 10^{-9}\ cells^{-1}\ day^{-1})$	-1.62	-1.69	-0.68	-0.17
$q_{K^+}\ (mmol\ 10^{-9}\ cells^{-1}\ day^{-1})$	-0.07	-0.04	-0.038	-0.004
$q_{Lact}\ (g\ 10^{-9}\ cells^{-1}\ day^{-1})$	0.50	0.62	0.35	0.50
$q_{Amm}\ (mmol\ 10^{-9}\ cells^{-1}\ day^{-1})$	0.050	0.073	0.051	0.084
Lactate produced / Glucose consumed (g/g)	0.98	0.99	0.54	0.86
Evaporation rate ($\mu L\ day^{-1}$)	15.2 ± 8.5	19.6 ± 4.6	20.7 ± 3.4	18.3 ± 4.5

3.3.4. Impact of Different Methionine Sulfoximine Concentrations

The CHO-CY01 cell line has the glutamine synthetase (GS) expression system from Lonza. GS is a dominant selectable marker that can be used with CHO cells that contain an active endogenous GS gene. The latter, however, requires the GS enzyme inhibitor methionine sulfoximine (MSX) (selective pressure). Approximately 20 – 25 μM of MSX is usually sufficient to suppress endogenous GS activity to ensure that any transfectants that emerge on deficient glutamine medium possess the target genes of interest. Because GS-derived cell lines require no external glutamine supplementation, very low accumulation of toxic ammonia is observed in these systems (Agrawal et al., 2012; Brown et al., 1992). MSX is typically applied during stable pool generation and is continued at the same concentration throughout the cloning process. A previous study indicates that increasing the concentration of MSX can result in gene amplification and increased productivity (Jun et al., 2006). However, the effect of different MSX concentrations and consequent selective pressures on cell growth and productivity have not yet been studied. It is regarded as a good cell culture practice to add 25 μM of MSX at the beginning of the cell culture in 24-SRW MTPs and SFs, but not to pilot-plant scale bioreactors due to economic reasons.

Various MSX concentrations (0, 25, 50, and 75 μM) were added at the beginning of 24-SRW MTPs CHO-CY01 cell batch culture at optimal operating conditions, 5.00% (v/v) CO_2 and 37°C to understand the impact of different selective pressures in CHO-CY01 cell line culture. The CHO-CY01 cell culture kinetics are represented in Figure 3-17 and Figure 3-18. The calculated cell culture parameters are presented in Table 3-8 and Table C-6.

It was observed that different selective pressures had an impact on CHO-CY01 cell growth and productivity. The higher the MSX concentration in the cell culture medium, the slower the cell growth was and, consequently, fewer cells were generated during longer culture times (Table 3-8). Therefore, MSX has a toxic effect in mammalian cell cultures.

At 75 μM MSX, the cell batch culture duration was too long at this stage of the bioprocess development, and the cell numbers and IgG4 concentration prior to purification were reduced, accompanied by the highest by-product formation and the least substrate consumption. Therefore, this MSX concentration was excluded. At 25 μM MSX, the CHO-CY01 cells produced the highest IgG4 concentration in the shortest time (34.6 $g\ L^{-1}day^{-1}$) with identical cell numbers compared with the no selective marker condition. Between the conditions with 25 μM MSX and without MSX, the latter presented higher with lower final antibody concentration (25%) (Table C-6). However, due to the high cost of MSX, the STR CHO-CY01 cell cultures were all performed without MSX.

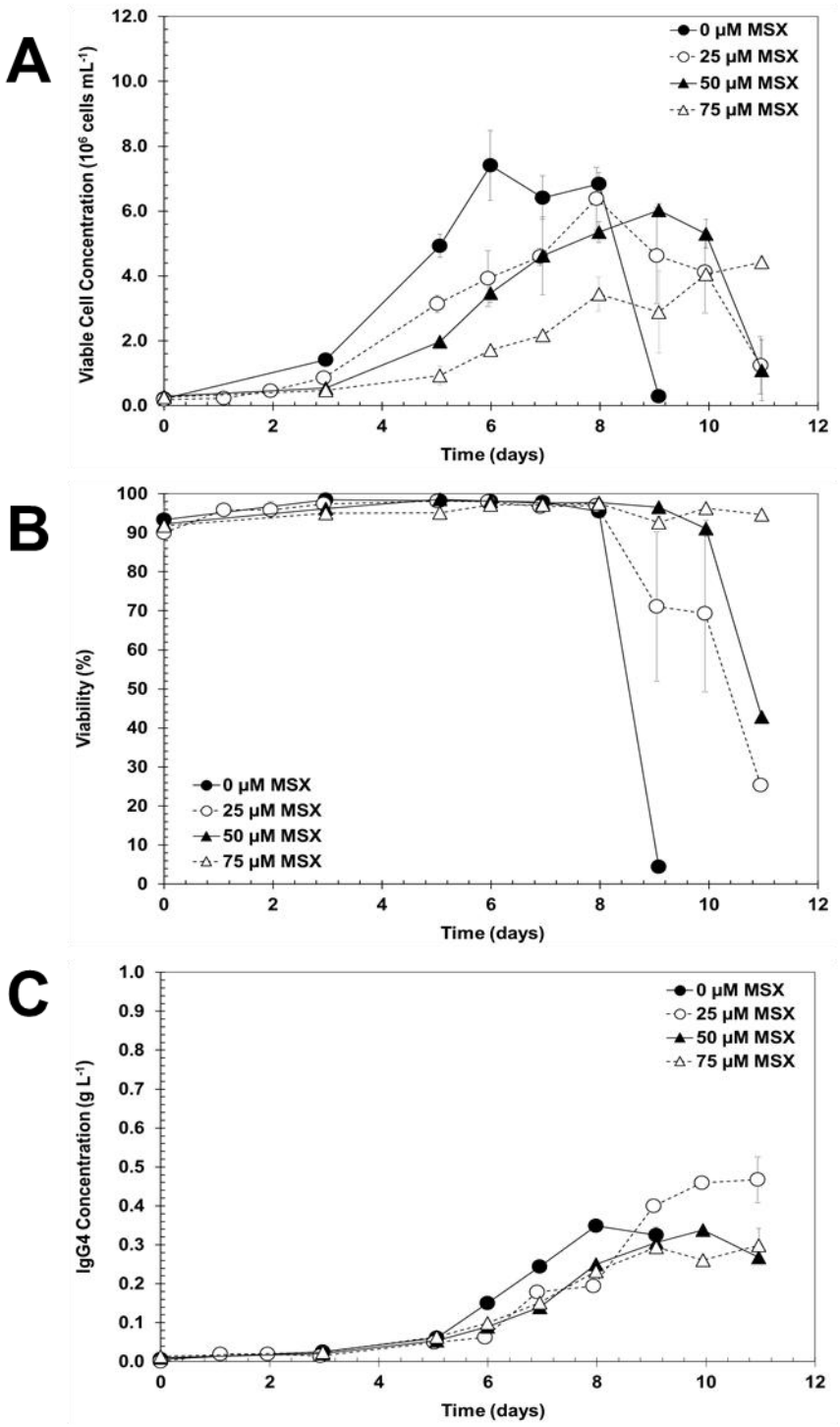

Figure 3-17: Viable cell concentration (A), cell viability (B), and IgG4 concentration (C) profiles of 24-SRW MTP CHO-CY01 cell batch cultures with different MSX concentrations (0, 25, 50, and 75 µM) at 5.00% (v/v) CO_2 (1 run (3-4 replicates)). Error bars represent one standard deviation about the mean.

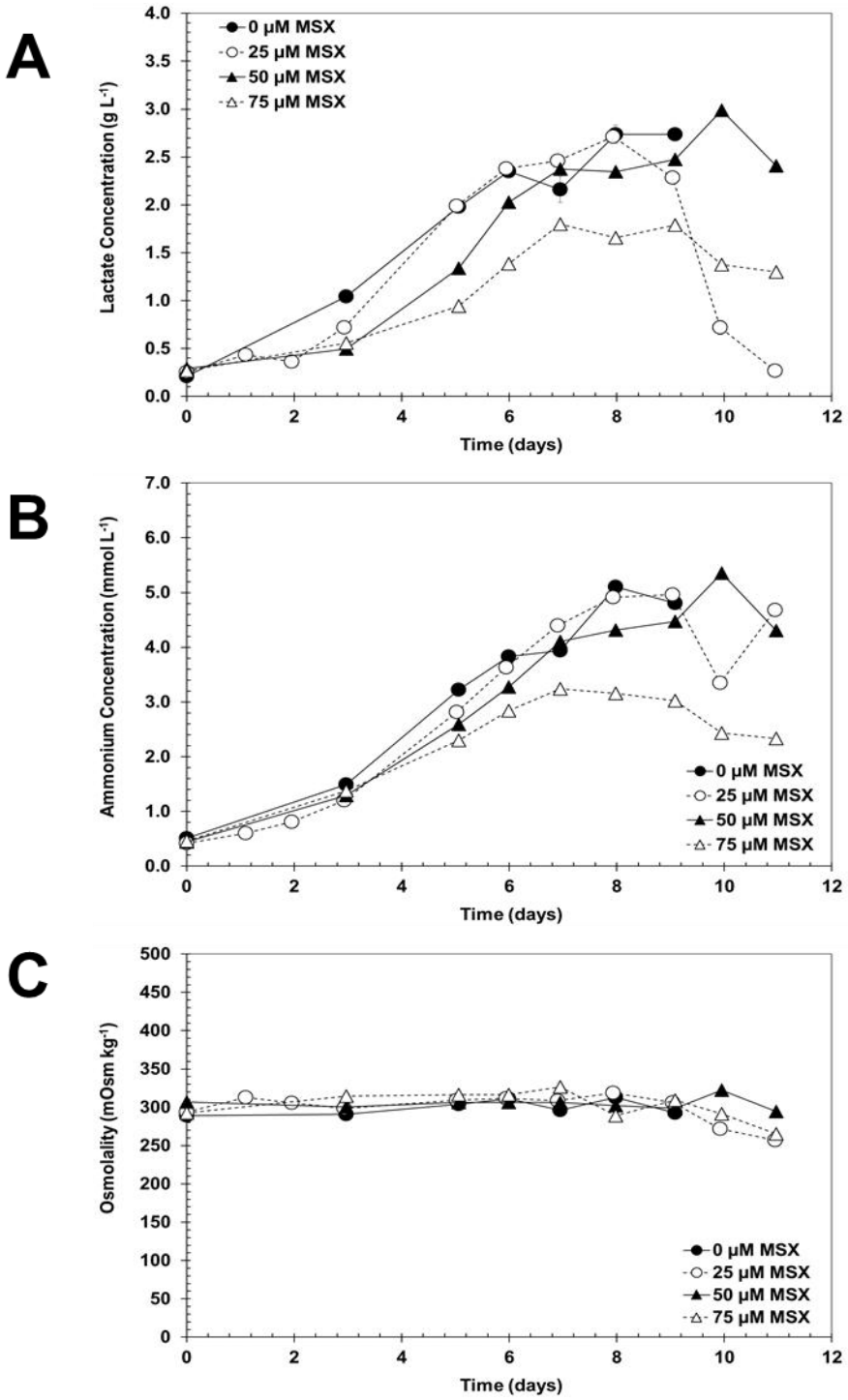

Figure 3-18: Glucose concentration (A), glutamate concentration (B), and pH (C) time profile 24-SRW MTP CHO-CY01 cell batch cultures with different MSX concentrations (0, 25, 50, and 75 µM) at 5.00% (v/v) CO_2 (1 run (3-4 replicates)). Error bars represent one standard deviation about the mean.

Table 3-8: Kinetic parameters of 24-SRW MTP CHO-CY01 cell batch cultures with different MSX concentrations (0, 25, 50, and 75 μM) at 5.00% (v/v) CO_2. The error represents one standard deviation about the mean.

MSX Concentration (μM)	**0**	**25**	**50**	**75**
VP ($mg\ L^{-1} day^{-1}$)	32.9	34.6	26.7	25.2
IVCC ($10^9\ cells\ day\ L^{-1}$)	32.15	31.04	29.86	19.37
$\mu\ (h^{-1})$	0.026	0.020	0.016	0.013
$t_{1/2}\ (h)$	27.2	34.3	43.3	55.0
$q_{mAb}\ (mg\ 10^{-9}\ cells^{-1}\ day^{-1})$	10.66	14.83	11.60	20.48
$q_{Gluc}\ (g\ 10^{-9}\ cells^{-1}\ day^{-1})$	-0.21	-0.25	-0.22	-0.34
$q_{Glu}\ (mmol\ 10^{-9}\ cells^{-1}\ day^{-1})$	-0.07	-0.08	-0.08	-0.11
$q_{Na^+}\ (mmol\ 10^{-9}\ cells^{-1}\ day^{-1})$	0.23	0.16	-0.14	-0.34
$q_{K^{-1}}\ (mmol\ 10^{-9}\ cells^{-1}\ day^{-1})$	-0.007	-0.019	-0.007	-0.034
$q_{Lact}\ (g\ 10^{-9}\ cells^{-1}\ day^{-1})$	0.38	0.52	0.54	0.63
$q_{Amm}\ (mmol\ 10^{-9}\ cells^{-1}\ day^{-1})$	0.161	0.169	0.185	0.172
Lactate produced / Glucose consumed (g/g)	0.49	0.52	0.54	0.77
Evaporation rate ($\mu L\ day^{-1}$)	18.7 ± 9.9	18.9 ± 6.9	23.2 ± 8.6	29.1 ± 11.4

3.4. Conclusion

Through engineering characterisation of 24-SRW MTP by established correlations and measurement of mixing times with subsequent evaluation of different liquid-phase hydrodynamics in CHO-CY01 cell culture, it was possible to establish the ideal operating conditions for the CHO-CY01 cell line. Under these operating conditions, the CHO-CY01 cell culture in 24-SRW MTP is considered to represent the CHO-CY01 cell culture on a larger scale with associated economic and HT advantages. The 24-SRW MTP ideal operating conditions are a shaking speed of 220 rpm with an orbital diameter of 25 mm, with a fill volume of 0.85 mL. In this condition, the liquid-phase is "in-phase", $k_L a$ value is $2.65\ h^{-1}$, and the mixing time is $4.7 \pm 0.7\ s$.

There was the need to establish the CHO-CY01 cell batch culture conditions and to develop an adequate sampling strategy. This is because the water loss due to evaporation is one of the disadvantages of microwell systems, as is the lack of process control. Two different sterile closures were tested, and Presens technology (SDR® system) was used to obtain online readings of process parameters such as pH, dissolved oxygen, and temperature. With the ´system Duetz` lid CR1524a, which has a silicone layer and a metal foil layer with tiny holes for air exchange, the evaporation rate was no more than 34% of the total volume after seventeen days. It was considered adequate for both the CHO-CY01 cell batch and the fed-batch cultures. The online measurement of process parameters did not affect the CHO-CY01 cell performance, nor the IgG4 production. Therefore, a 24-SRW MTP sampling strategy was employed for a semi-process controlled system. The standard 24-SRW MTPs were used for the sacrificial sampling method to determine the viable cell concentration, viability, and metabolite and electrolyte concentrations. The Presens 24-SRW MTPs (HydroDish®HD24 and OxoDish®OD24 plates); were exclusively used for the online process parameter measurement. With regards to well-to-well reproducibility, the 24-SRW MTP sacrificial sampling strategy adopted to maintain the same liquid-phase hydrodynamics and minimise the evaporation of the well´s contents and its osmotic effects was to sample firstly the ´corner` wells followed by the ´edge` wells and ´internal` wells. Finally, it was required to establish a standard MSX concentration for this GS-CHO cell line. The selective pressure that yielded the highest productivity was at 25 µM of MSX. However, for exclusively economic reasons, this selective marker was only added to CHO-CY01 cell line cultures in SFs and 24-SRW MTPs.

Chapter 4 Inter-Scalability of the CHO-CY01 Cell Line Kinetics

4.1. Introduction and Aims

The objective of process characterisation is to demonstrate the robustness of a manufacturing process by understanding the relationship between the main operating parameters and final cell culture performance for culture growth and productivity. Since performing such characterisation study at the manufacturing scale (20 m^3) is not practically feasible due to cost of operation and limited availability of large-scale bioreactors, scale-down models that represent the performance of manufacturing scale are usually employed at the laboratory scale for process optimisation (Doig et al., 2006; Li et al., 2006). Stainless steel tanks have traditionally been used at laboratory and pilot scales for process development and production of research grade, toxicology, and Phase 1 clinical materials. Li et al. (2006) have developed a scale scale-down model of the 2000-L commercial scale CHO cell manufacturing process using a 2-L bioreactor. The performance parameters including cell growth, viability, product titer, and product glycosylation isoform were comparable between the two scales. During development of a scale-down model, it is important to demonstrate equivalency of the key performance parameters between the bench and commercial scales. Ideally, cell culture performances at the commercial scale should be used as a baseline to guide scale-down model development. If the full-scale data is not available, pilot-scale performances can be used to provide preliminary information. Under these circumstances, process characterisation has to proceed at risk, and the models should be re-evaluated once the commercial scale data becomes available (Li et al., 2006).

With mammalian cell cultures, there is the concern of waste by-products, such as lactate and ammonium accumulation, due to their inhibitory effects on cell growth and productivity. Excessive lactate build-up can result in increased medium osmolality or, in the absence of pH control, decrease the culture pH. Ammonia can permeate the cell wall and partition into cellular compartments, disrupting the local pH (McQueen et al., 1990b).

Much of the published literature has focussed on the use of nutrient feeding to increase cell density or to increase the specific productivity. Basic batch suspension processes have become increasingly less frequent because nutrient feeding schemes can reduce the waste accumulation and nutrient fluctuations, which allows higher cell densities and productivities to be achieved (Chu et al., 2001).

The aim of this chapter is to find a scale translation criterion suitable to develop an (ultra) scale-down model for batch and fed-batch CHO-CY01 cell cultures. Specific objectives of this chapter are:

- To define an appropriate engineering basis for scale translation to create a scale-down model at 24-SRW MTP that represents the large-scale (5-L STR) CHO-CY01 cell cultures
- To perform cultivation of the CHO-CY01 cell line under suitable engineering scale translation criteria (matched mixing time and mean energy dissipation rate) in 24 SRW MTP, SF, and STR bioreactors, simultaneously.
- To identify lactate and ammonium inhibitory concentrations and kinetics in CHO-CY01 cell batch culture
- To develop a fed-batch strategy for all CHO-CY01 cell culture scales for productivity optimisation

4.2. Mixing Time and Mean Energy Dissipation Rate as a Basis for Cell Culture Scale Translation

Reproduction of cell culture performance between small-scale shaken bioreactors and currently established stirred-tank bioreactor scale-down models of production-scale vessels requires the identification of a suitable basis for scale translation (Li et al., 2006). This must apply across different scales, for different mechanisms of energy input, i.e. shaken or stirred, and for different mechanisms of oxygen transfer, i.e. surface aeration or a dispersed gas phase. Fundamental to culture performance is the engineering of a homogeneous and well-controlled environment (Varley et al., 1999) to which the entire population of cells is exposed. A variety of bases has been used as scale translation between lab-scale STR and manufacturing scale. The most common bases are matched $k_L a$, matched mean energy dissipation per unit volume, and matched mixing time (Li et al., 2006; Yang et al., 2007) (Table 4-1). For scale translation between small-scale vessels and different geometries, no such basis for scale translation has yet been fully established. The principle of matched mean energy dissipation was used by Barrett et al. 2010 to achieve a relatively close match across shaken MTPs, SFs and, STRs for hybridoma cells. The matched mixing time criterion was chosen by Silk (2014) as a suitable scale translation between different small-scale bioreactor geometries. By combining two strategies: matched mean energy dissipation energy and mixing times, it would be expected to obtain an even closer very close agreement between scales.

Table 4-1: Comparison of scale translation criteria (mixing time, mean energy dissipation rate and $k_L a$) for CHO-CY01 cell line cultures in 24-SRW MTP, SF 125 mL, SF 250 mL and 5-L STR bioreactors at the experimental conditions used.

	24-SRW MTP	**SF 125 mL**	**SF 250 mL**	**5L-STR**
	$N = 220\ rpm$	$N = 220\ rpm$	$N = 220\ rpm$	$N = 260\ rpm$
	$V_L = 850\ \mu L$	$V_L = 50\ mL$	$V_L = 100\ mL$	$V_L = 3.5\ L$
	$d_s = 25\ mm$	$d_s = 25\ mm$	$d_s = 25\ mm$	45º pitch blade
Mixing Time (s)	4.7 ± 0.7	5.0 ± 0.6 [b]	1.8 [c]	6.0 ± 0.6 [b]
Mean Energy Dissipation Rate ($W\ m^{-3}$)	10 [a]	~10 [d]	~10 [d]	14 [a]
$k_L a$ (h^{-1}h^{-1})	> 20	> 10 [b]	> 10 [b]	4.1 [b]

[a] (Barrett et al., 2010); [b] (Silk, 2014); [c] (Tan, Eberhard, & Büchs, 2011); [d] (Büchs et al., 2000b)

This work involves the attempt to combine two scale translation criteria, mean energy dissipation rate and mixing times. Combining the 24-SRW MTP mixing times ($4.7 \pm 0.7\ s$) determined in this work with the mean energy dissipation rate (P/V) determined by the studies by Barrett et al. (2010) related to CFD at the operating conditions of that mixing time (10 $W\ m^{-3}$), it was possible to determine the STR and SFs operating conditions at which the mixing time and P/V were similar (Barrett et al., 2010; Silk 2014; Tan et al., 2011). This new scale translation criterion was tested by inoculating CHO-CY01 cells in 24-STR MTPs, two different sizes of SFs (125 and 250 mL), and 5L-STR at operating conditions with mixing time of approximately 5 s and mean energy dissipation rate of 10 $W\ m^{-3}$ .The operating conditions for the SFs and 5L-STR are stated in Section 2.1; for 24-SRW MTPs, the operating conditions were those found in the previous chapter and are stated as standard. Three replicates of CHO-CY01 cell batch culture in 24-STW MTP, two replicates at each SF size were performed and one replicate with historic data in 5-L STR. By performing replicates, the batch-to-batch variability, different cell passage number and variation in the initial metabolite concentration and inoculum concentration, were considered. With the use of replicates, there was a better measurement of parameter variation and improved precision; thus, the hypothesis test was more accurate. Cell growth kinetics, antibody production, metabolism, and particle size distribution were compared between the different bioreactor scales. A statistical t-test of two samples assuming unequal variances with 95% of confidence was performed for the following parameters: viable cell number, IgG4 concentration, glutamate concentration, glucose

concentration, lactate concentration, and ammonium concentration. The reference sample was the CHO-CY01 cell batch culture in 5L-STR.

The CHO-CY01 cell batch culture kinetics can be visualised in Figure 4-1, Figure 4-2 and Figure 4-3. The calculated kinetic parameters are presented in Table 3-4 and Table C-7. The particle size distributions for CHO-CY01 cell batch culture at different bioreactor scales were segmented into four periods: adaptation, exponential, beginning of the decline, and decline period (Section 3.2.4). In Figure B-3:, the histograms of the particle distribution are presented. The calculated portion of impurities (debris, dead cells, and larger particles) as well as viable cell number, viability, and cell diameter are listed in Table B-3 for all bioreactor scales.

Regarding viable cell numbers, all CHO-CY01 cell batch cultures were equivalent in the growth phases, as can be observed in Figure 4-1. The growth rate of all the bioreactor scale was equal ($0.023 \pm 0.002\ h^{-1}$). However, in 5L-STR, there were slightly more cells ($48.29\ 10^9\ cells\ day\ L^{-1}$) compared with the other bioreactors ($35.26 \pm 7.12\ 10^9\ cells\ day\ L^{-1}$), but statically similar. The reason for that may be associated with the pH (7.14 ± 0.04), temperature (37.00 ± 0.01℃), and dissolved oxygen tension (DOT) ($30.0 \pm 0.01\ \%\ Air\ sat.$) control in the 5L-STR. With the 24-SRW MTP cell culture system, it was possible (Section 2.2.7) to monitor the pH and temperature of the cell cultures. The pH range observed for the standard 24-SRW MTP cell batch culture was 7.27 ± 0.17, and the temperature range was 36.92 ± 0.19 ℃. With SF cell cultures, it was not possible to control or monitor any process parameter. However, it was assumed that the temperature and DOT ranges in the SFs were similar to the ones at 24-SRW MTP. For the latter bioreactors, it was considered that inside a CO_2 incubator at 5.00% (v/v) CO_2, the dissolved oxygen was $95.04\ \%\ Air\ sat$ (Table 5-1), assuming a negligible oxygen transfer resistance from the ´system Duetz´ lid or SF lids.

For all bioreactors, the IgG4 concentration-time profile was the same. There was an intense production until around day 7 (end of exponential phase) followed by a slow production rate that created a plateau towards the end of the culture. In the SF system, CHO-CY01 cell batch cultures produced more and quicker IgG4, but with a high variability associated.

In terms of the waste by-products lactate and ammonium, the time profiles for all bioreactor scales were identical. Lactate production and consumption occurred during the exponential phase followed by full exhaustion. Ammonium was produced simultaneously with lactate, started to be consumed at the same time, was soon followed by a slow consumption until none of the carbon sources (glutamate, glucose, and lactate) were present, after which the ammonium concentration exploded. CHO-CY01 cells in 24-SRW MTPs produced more ammonium, which immediately increased the osmolality, compared with the other contenders. Therefore, a harvest criterion was established. The cell culture was stopped when the carbon

sources reached levels near zero, to avoid the accumulation of ammonium in the medium and to prevent product quality damages (Andersen et al., 1995).

It was observed that any cell growth and metabolite parameter variation from the reference, 5L-STR CHO-CY01 cell culture, was due to different initial metabolite and inoculum concentrations, the lack of pH, temperature, and dissolved oxygen control, still statistically all bioreactors are equivalent ($p > 0.05$).

Assessing the particle size distribution across the cell culture time for all bioreactor scales, there was the adaptation period during the first three days characterised by high cell viability and debris, followed by the exponential period from days 3 to 8 characterised by high cell viability, increased viable cell numbers, and size, considerable decrease of debris, and increase of dead cell (DNA) and larger particle (>40 μm) portions. Subsequently, the beginning of the decline period came with a rise of debris and larger particles and with the decrease of dead cell (cell nucleus) fraction. By the end of the cell culture, there was the decline period described by the decrease of cell numbers and the shift to smaller particles. At these two late periods, the impurities composed more than half of the cell culture content. Even at the particle size distribution level, it can be said that there was no difference between the bioreactor scales.

From the Spearman´s rank correlation coefficients calculated for all bioreactor types between the cell growth, metabolite, and process parameters, it was observed that the very strong correlations were maintained or, if not, became strong (Table A-7). Apart from the 5L-STR CHO-CY01 cell culture, all of the others were run at a constant CO_2 concentration as a pH control attempt. From this CO_2 concentration variation at the pilot plant scale (Figure D-1), it was possible to realise the very strong correlation between CO_2 (% (v/v)) and IgG4, glutamate, and glucose concentrations. The variation of CO_2 concentration at 24-SRW MTP scale was extensively investigated, and the results are presented in Chapter 5.

Through the combination of two scale translation criteria, mixing time and mean energy dissipation rate, a scale-down model of 5L-STR CHO-CY01 cell line batch culture was achieved in the 24-SRW MTP.

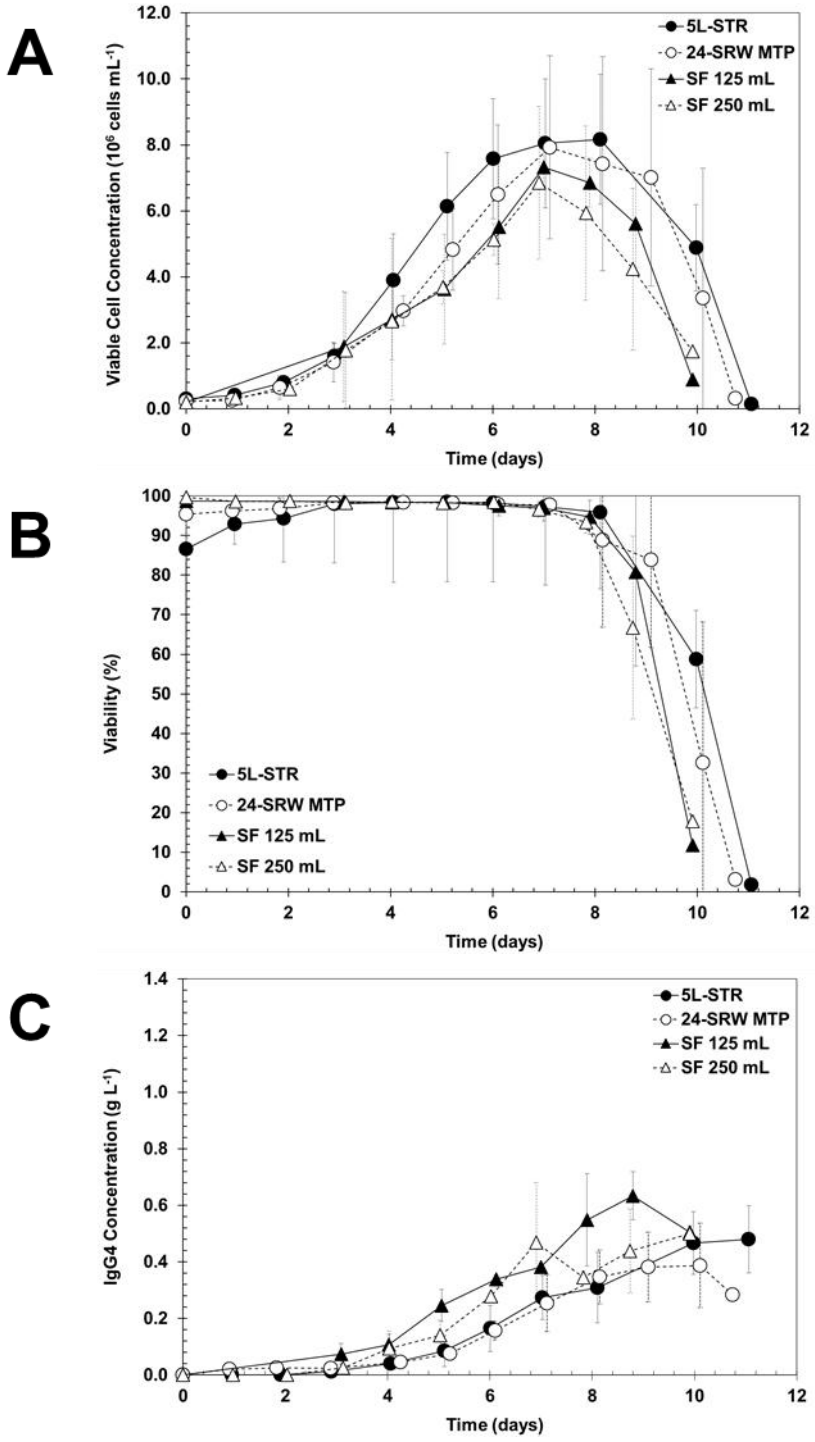

Figure 4-1: Viable cell concentration (A), cell viability (B) and IgG4 concentration (C) profiles for CHO-CY01 cell batch culture at different bioreactor scales: 5L stirred tank (5L-STR) (1 replicate with historical data ($p > 0.05$)); 24-SRW MTP (3 runs (9-12 replicates)); shake flask with a total volume of 125 mL (SF 125 mL) (2 replicates); and shake flask with a total volume of 250 mL (SF 250 mL) (2 replicates). Standard culture operating conditions were used. Error bars represent one standard deviation about the mean.

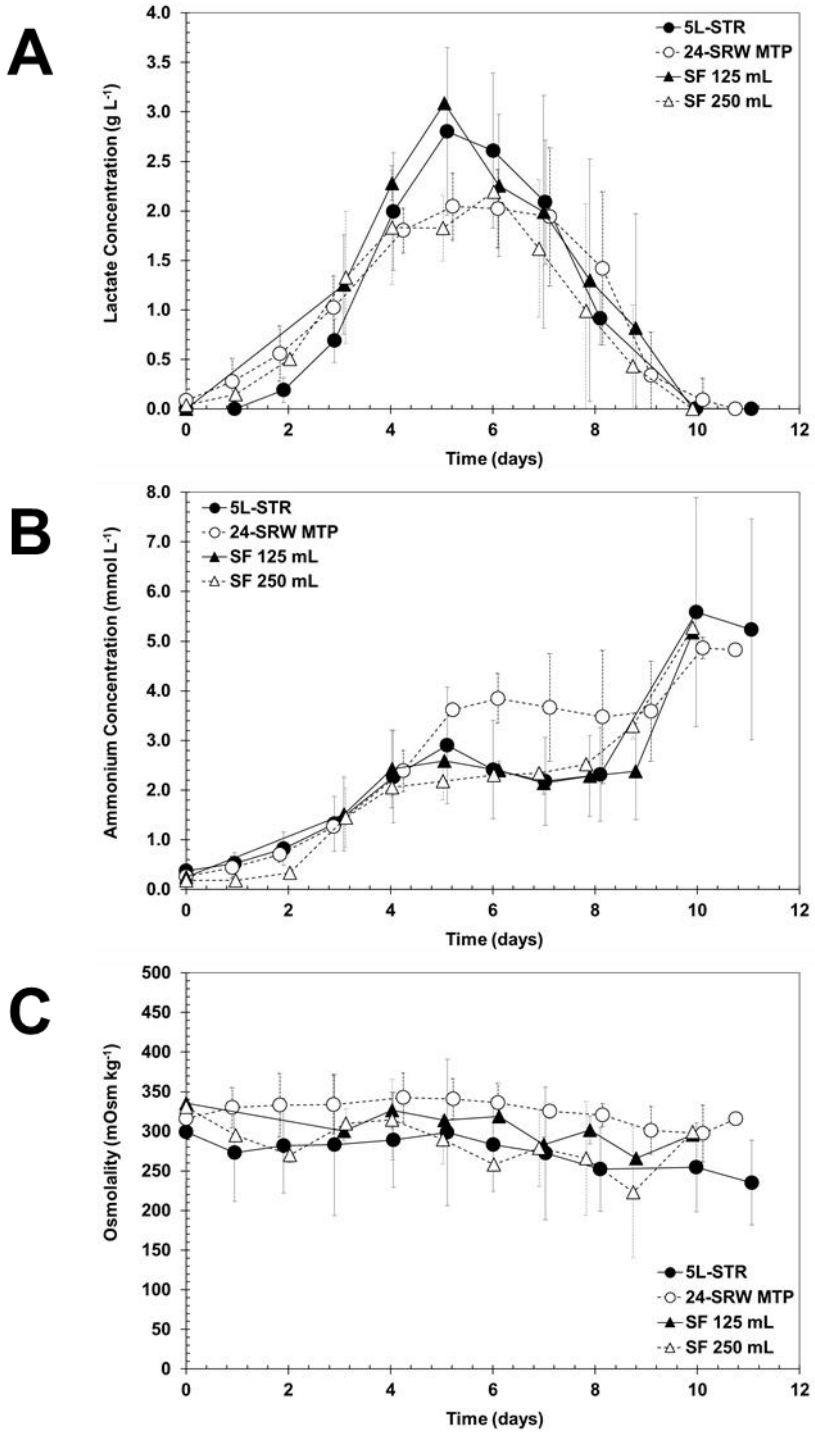

Figure 4-2: Lactate concentration (A), ammonium ion concentration (B), and osmolality (C) profiles for CHO-CY01 cell batch culture at different bioreactor scales: 5L-STR (1 replicate with historical data); 24-SRW MTP (3 runs (9-12 replicates)); SF 125 mL (2 replicates); and SF 250 mL (2 replicates). Error bars represent one standard deviation about the mean.

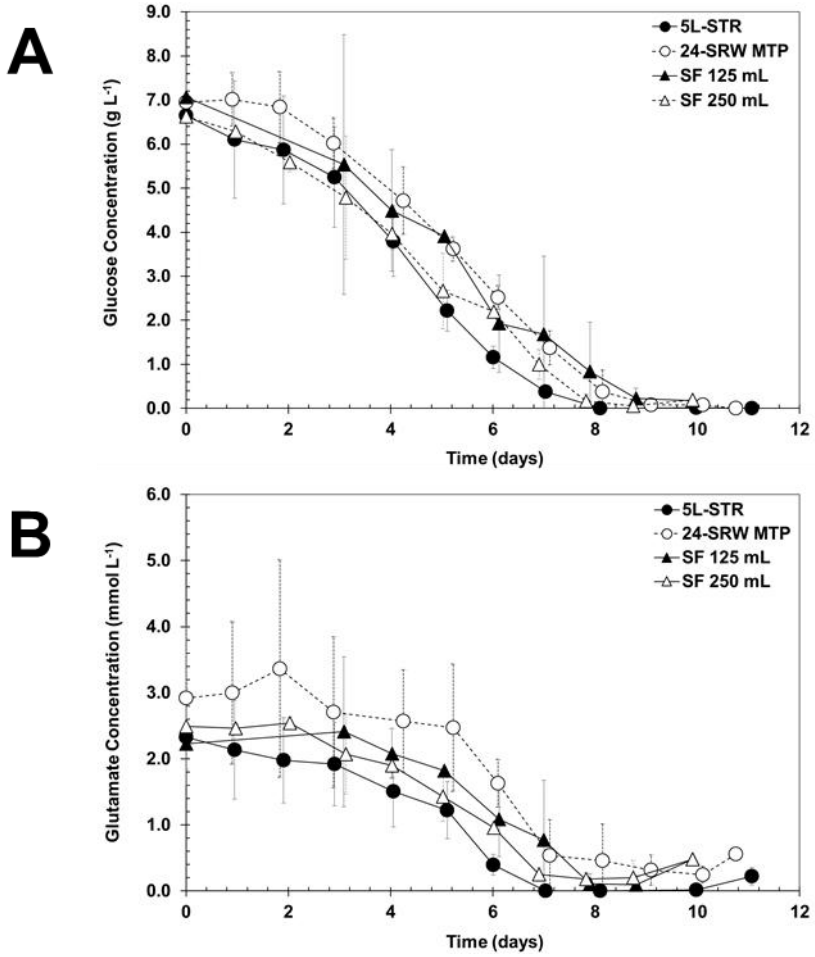

Figure 4-3: Glucose (A) and glutamate (B) concentration profiles for CHO-CY01 cell batch culture at different bioreactor scales: 5L-STR (1 replicate with historical data); 24-SRW MTP (3 runs (9-12 replicates)); SF 125 mL (2 replicates); and SF 250 mL (2 replicates). Error bars represent one standard deviation about the mean.

Table 4-2: Kinetic parameters determined for CHO-CY01 cell batch culture at different bioreactor scales: 5L-STR; 24-SRW MTP; SF 125 mL, and SF 250 mL.

	5L-STR	**24-SRW MTP**	**SF 125 mL**	**SF 250 mL**
VP ($mg\ L^{-1}day^{-1}$)	37.3 ± 3.3	33.9 ± 4.8	58.0 ± 2.8	46.7 ± 3.7
IVCC ($10^9\ cells\ day\ L^{-1}$)	48.39 ± 9.1	41.43 ± 7.23	33.65 ± 5.80	30.91 ± 6.72
$\mu\ (h^{-1})$	0.024 ± 0.002	0.023 ± 0.002	0.023 ± 0.002	0.023 ± 0.002
$t_{1/2}\ (h)$	29.1 ± 2.3	30.3 ± 2.7	29.7 ± 2.3	30.0 ± 2.3
$q_{mAb}\ (mg\ 10^{-9}\ cells^{-1}\ day^{-1})$	9.96 ± 2.16	10.58 ± 3.01	20.06 ± 3.02	5.89 ± 10.17
$q_{Gluc}\ (g\ 10^{-9}\ cells^{-1}\ day^{-1})$	-0.17 ± 0.03	-0.21 ± 0.03	-0.25 ± 0.05	-0.27 ± 0.05
$q_{Glu}\ (mmol\ 10^{-9}\ cells^{-1}\ day^{-1})$	-0.06 ± 0.02	-0.08 ± 0.02	-0.09 ± 0.04	-0.10 ± 0.04
$q_{Na^+}\ (mmol\ 10^{-9}\ cells^{-1}\ day^{-1})$	-0.29	0.29 ± 0.11	-0.73 ± 0.66	-0.50 ± 0.67
$q_{K^+}\ (mmol\ 10^{-9}\ cells^{-1}\ day^{-1})$	-0.06	-0.01 ± 0.01	-0.03 ± 0.01	-0.06 ± 0.05
$q_{Lact}\ (g\ 10^{-9}\ cells^{-1}\ day^{-1})$	0.29 ± 0.11	0.35 ± 0.12	0.48 ± 0.18	0.41 ± 0.17
$q_{Amm}\ (mmol\ 10^{-9}\ cells^{-1}\ day^{-1})$	0.100 ± 0.016	0.126 ± 0.029	0.103 ± 0.014	0.127 ± 0.013
Lactate produced / Glucose consumed (g/g)	0.65 ± 0.15	0.52 ± 0.13	0.72 ± 0.11	0.58 ± 0.16
Evaporation rate ($\mu L\ day^{-1}$)		19 ± 9		

4.2.1. Apoptotic and Cell Cycle Population Balance in CHO-CY01 Cell Batch Culture

A major problem faced in mammalian cell bioreactor cultures is cell death, which decreases overall productivity. Cell death in bioreactors has various causes, including mechanical agitation, nutrient depletion, by-product waste accumulation, hypoxia, and viral infections (Arden et al., 2004). Cell death occurs in two general forms: necrosis and programmed cell death (apoptosis and autophagy) (Hwang et al., 2008). Necrosis results from immediate and extreme conditions that physically damage cells, causing them to swell (oncosis) and rupture, and releasing their cellular contents into the surrounding environment (Arden et al., 2004; Van Cruchten et al., 2002). Apoptosis, however, is a regulated physiological response resulting from a non-lethal stimulus (for example, withdrawal of growth factors or DNA damage) that activates a cellular cascade of events culminating in cell death (Arden et al., 2004). Apoptosis is well-characterised by cell shrinkage, chromatin condensation, production of membrane-bound apoptotic bodies, and nucleosomal DNA fragmentation in the cell (Al-Rubeai et al., 1998; Arden et al., 2004; Bursch et al., 2008; Hwang et al., 2008; Van Engeland et al., 1998). Programmed cell death is the genetically controlled destruction of cells. Whereas apoptosis is an outcome of the caspase-dependent cascade, Autophagy is a normal caspase-independent degradation process that constitutes a cell's survival strategy in response to metabolic challenges such as glucose or amino acid deprivation, or starvation in general (Van Engeland et al., 1998). Mammalian cells respond to nutrient deprivation by downregulating the energy-consuming processes such as proliferation and protein synthesis, and in turn, by stimulating catabolic processes (nutrient recycling) such as autophagy (Bursch et al., 2008). Notably, the death of CHO cells triggered by glucose deprivation may result in autophagic as well as apoptotic pathways (Hwang et al., 2008). For hybridoma cells during decline phase, where there is a deprivation of glucose and amino acids, apoptosis is attributed to the prevailing mode of cell death (Al-Rubeai et al., 1998; Franek, 1995). Thus, apoptosis may be viewed as an expression of population cell vitality, similarly to mitosis (Franek, 1995).

In the commercial production process of mammalian cell cultures, one of the most important parameters is the specific productivity of each cell. If a particular subpopulation of cells within the process is more productive than another, processes can be designed, and control strategies can be developed to favour such subpopulation. This subpopulation synchronous culture can be treated as a single cell. One obvious difference between cells in a population is the cell cycle stage of each cell (Lloyd et al., 2000). Protein production is dependent on the cell cycle stage of the cells (Kumar et al., 2007; Lloyd et al., 2000). Cells arrested at the end of G1-phase of the cell cycle are metabolically more active and larger in size than non-arrested cells. For these reasons, the G1-phase of the cell cycle is considered the ideal time for increased production of recombinant proteins, and a G1 arrest has been

used to enhance the productivity in some commercially relevant cell lines such as hybridomas and CHO (Kumar et al., 2007). However, some studies have reported the S-phase as the optimal production phase (Lloyd et al., 2000). The relationship between cell cycle stage and productivity may not be universal for all mammalian cells (Lloyd et al., 2000). Therefore, determining this relationship for the CHO-CY01 cell line is necessary for developing an optimised process through automated nutritional control strategies, chemical approaches, or online control strategies for cell arrest.

The molecular mechanisms that regulate the cell cycle and apoptosis are inextricably linked. This is illustrated by the c-myc and p53 proteins, which play an essential role in mediating both cellular proliferation and apoptosis (Al-Rubeai et al., 1998; Van Cruchten et al., 2002).

Cell cycle and apoptotic analysis were performed in CHO-CY01 cells in 5L-STR and 24-SRW MTP in batch mode following the procedures described in Section 2.2.4 and Section 2.2.5, respectively. The results of these cell population studies were coupled with the cell diameter and IgG4 titer throughout the cell culture and are visualised in Figure 4-4. These tests were not performed with CHO-CY01 cell batch cultures in SFs. It was assumed that cell behaviour in the shaken culture bioreactors is similar to cell culture kinetics (Section 4.2). We note that the goal of this work is to demonstrate the 24-SRW MTP as the scale-down model of the 5L-STR.

In 5L-STR, CHO-CY01 cells are faced with an extra stress that otherwise will not be encountered at shaken 24-SRW-MTP, which are air bubbles and an impeller rotating at 260 rpm (Hu et al., 2011). Therefore, it was expected that the cell death in 5L-STR may not be exclusively due to programmed cell death. At the 5L-STR, the fraction of viable cells in the population heterogeneity was dominant up to the decline phase. In parallel, the no viable cells fraction was insignificant until the decline phase, when their fraction rose to 36%. In the 24-SRW MTP, the viable cells were predominant during all phases of cell culture, and the no viable cells fraction maintained 10% participation. The 5L-STR produced a higher degree of cell disintegration that 24-SRW MTP. This was an observation already achieved through the particle size distribution analysis (Figure B-3: and Table B-3). It indicates that the degree of cell destruction was different between the two bioreactors, which have not established the type of cell death. In the two bioreactor configurations, during the *lag* phase, it can be inferred that the minimal cell death was due to apoptosis, as the late apoptotic fraction increased to up to 20% of the population. As soon as the cells started the exponential phase, the late apoptosis fraction had a reduction in the population participation. This trend continued through the stationary phase. In the 5L-STR, the late apoptosis fraction continued to decrease (1.4%/day), where 24-SRW MTP maintained the 5.0% participation. Regarding the early apoptotic cells, 5L-STR had a constant 2.5% presence although, in the 24-SRW MTP, it had double the

participation. Therefore, it is clear that the cell death in 24-SRW MTP was due to apoptosis. In the 5L-STR, the cell death was a combined effect of necrosis (decline phase) and apoptosis until the stationary phase, where glucose and glutamate deprivation and ammonium accumulation started. Since the cell culture kinetics are equivalent between the two bioreactors, the type of cell death is exclusively attributed to the bioreactor hydrodynamic environment.

In 5L-STR, the passive release of antibody from necrotic and dying cells during the death phase of batch culture led to a substantial increase in antibody concentration in the medium(Al-Rubeai et al., 1990). In contrast, in the 24-SRW MTP, the IgG4 concentration decreased during the late decline phase as a result of programmed cell death.

The CHO-CY01 cell dynamics began with cells in G1-phase (49.7%), which is consistent with G1 arrest associated with the lag phase, in response to the step change in the associated environment. In the 24-SRW MTP, it was not possible to obtain cell cycle population dynamics during the first three days of cell culture due to volume restrictions. At 5-L STR, during the *lag* phase, S-phase subpopulation increased up to 48.2%, with G1-phase and G2/M decreasing. During the exponential phase, cells re-entered the G1-phase, which is consistent with the probabilistic model proposed by Smith et al. (1973), in which random re-entry of G1 cells into the cycling fraction is coupled with a portion of the population not arrested in G1, thereby preventing complete synchrony of the population. For all bioreactor scales, the proportion in S phase decreases through the balanced growth, as the proportion in G1-phase increased, presumably as cells arrest in G1 in response to diminishing nutrient pools. Until the decline phase, the CHO-CY01 cell line batch culture presented a curious cell cycle profile, since the probability of a cell being in G1 or S-phase is around 50%. Once the cells reach the decline phase, there was a characteristic step flip between S-phase and G1-phase. Cells in G1-phase increased to 63%, and S-phase decreased to 22%. This cell G1-phase accumulation and S-phase depletion were previously observed by Leelavatcharamas et al. (1999) for CHO cells. In 24-SRW MTP CHO-CY01 cell batch culture, a relationship between apoptotic and cell cycle populations can be made. The G1-phase fraction accumulation with an increase in early and late apoptotic cells during the decline phase may suggest that CHO-CY01 cells enter apoptosis from the G1 stage. The G2/M subpopulation remained constant at less than 10% of the population distribution in the two bioreactor formats. Therefore, the CHO-CY01 cell line exhibited asynchronous growth. On cell cycle population, CHO-CY01 cell population dynamics strongly agree among bioreactor scales, which further validates 24-SRW MTP as a scale-down model of the 5-L STR scale.

In all cases, there was no suggestion that product formation was limited to any specific cell cycle phase, as there was IgG4 production in all cell cycle phases. It seems that the regulation of synthesis and secretion of IgG4 is time-dependent, and the productivity increased

when cells are arrested and maintained in G1/S phases with decreasing cell viabilities and increasing cell diameters (stationary phase). Therefore, a fed-batch strategy that prolongs the stationary phase of a CHO-CY01 cell line is beneficial to increase the IgG4-specific productivity of the CHO cells, as it can be regarded as a nutritional approach for G1/S-phase cell arrest.

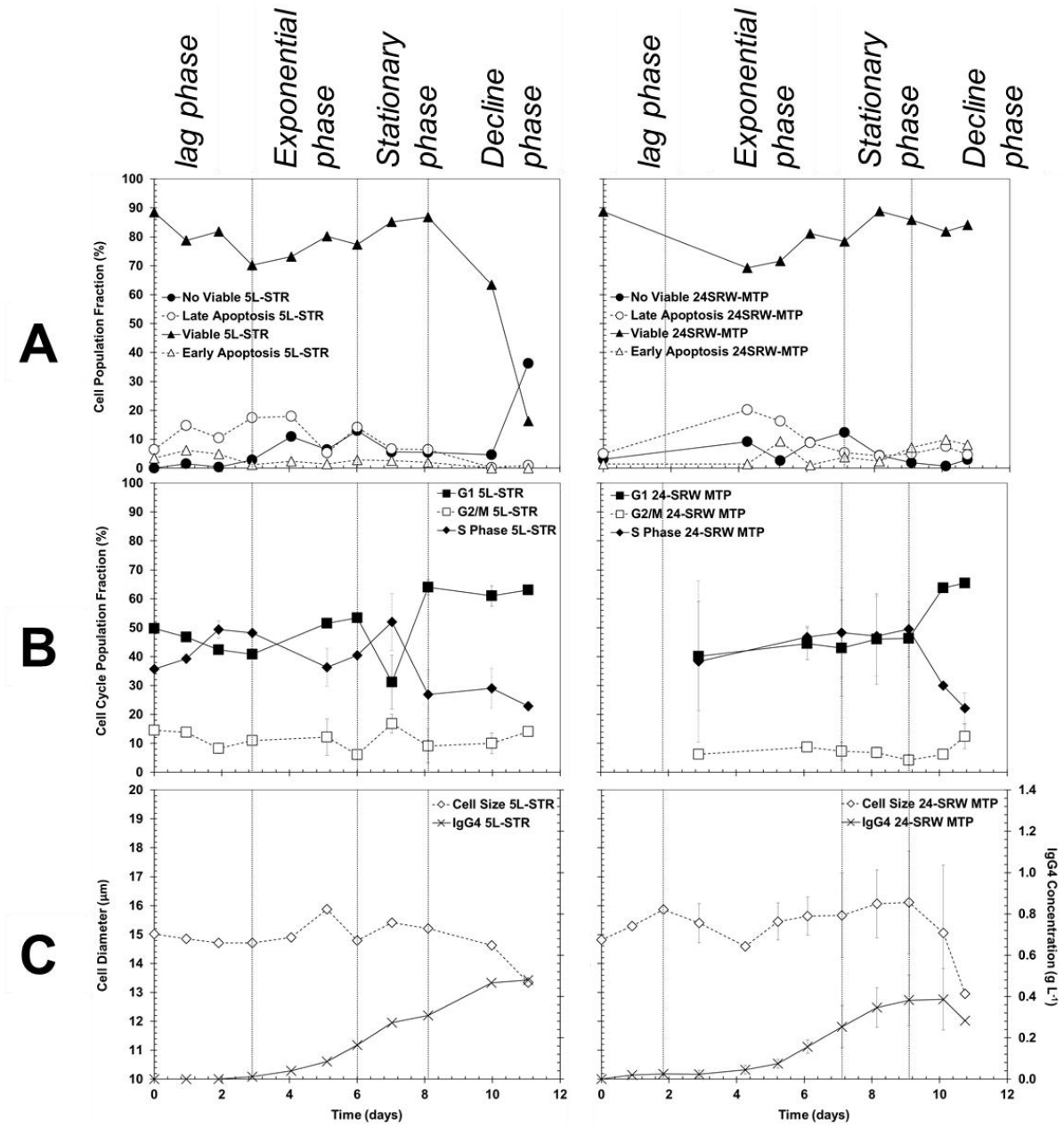

Figure 4-4: Apoptotic (A) and cell cycle (B) population fractions, and viable cell diameter and IgG4 titer (C) of CHO-CY01 cell batch cultures in 5L-STR (1 replicate) and 24-SRW MTP (3 runs (9-12 replicates)). The error bars show the standard deviation about the mean.

4.3. Effects of Ammonium, Lactate, and Osmolality on CHO-CY01 Cell Growth, Metabolism, and IgG4 Productivity

The influence of culture parameters such as ammonium/ammonia, lactate, and osmolality on mammalian cell cultures has been extensively reported in the literature (Lee et al., 2009; Schneider et al., 1996; Tsao et al., 2005). The toxic effects of ammonia and lactate on mammalian cell cultures and product glycosylation are widely described for various cell lines, mainly hybridoma cells (Lao et al., 1997). The tolerance levels towards these two metabolic waste products seem to be cell line-specific and vary widely (Hassell et al., 1991). In fed-batch processes, with higher glucose available there is a more significant concern about the accumulation of these waste by-products. The accumulating effect of these two by-products has an impact on the osmolality of the cell culture medium. Osmolality is one of the most important physical factors in mammalian cell cultures. Osmolality has been shown to affect both cell growth and protein production (Bi et al., 2005; DeZengotita et al., 1998; Kimura et al., 1997; Kurano et al., 1990a; Zhu et al., 2005). The impact of osmolality on cell growth is cell-type specific, with CHO cells exhibiting less growth inhibition than hybridoma cells exposed to similar medium osmolality (Lee et al., 2009). However, less information is available on the influence of ammonium, lactate, and osmolality on the growth and productivity of a GS-CHO cell line. In this work, comprehensive and detailed kinetic studies on the effects of ammonium, lactate, and osmolality were performed for the characterisation and optimisation of CHO-CY01 cell cultures.

In the previous section, it was found that the CHO-CY01 cell line, in batch mode, had similar cell growth, metabolism, and productivity for 24-SRW MTPs, SFs and, 5L-STR. Therefore, a scale-down model of the batch culture of the CHO-CY01 cell line at pilot-plant scale was established with the 24-SRW MTPs and SF. With this premise, a study was conducted in SFs (total volume of 125 mL) on the effects of different initial ammonium, lactate, and sodium chloride concentrations on CHO-CY01 cell growth, metabolism, and productivity. Moreover, it can be noted that the findings on this scale could be translated to the other scales.

4.3.1. Effects of Lactate on CHO-CY01 Cell Line Kinetics

Glucose is the main carbon source and an important energy source in standard mammalian cell medium formulations. Entry of glucose into the glycolytic pathway leads to the formation of pyruvate as the end product. The pyruvate can either be shuttled into the TCA cycle or be converted into lactate. Due to the high flux of glucose to pyruvate and the inefficient coupling between glycolysis and TCA cycle, lactate accumulation tends to occur. Lactate build-up, in turn, leads to the acidification of the culture environment (Tsao et al., 2005). In addition, lactate itself has been reported to be toxic to mammalian cells even under controlled

pH (Glacken et al., 1986; Hassell et al., 1991; Lao et al., 1997; Ozturk et al., 1992). The accumulation of lactate is a critical limiting factor in the cell culture process, and strategies to minimise it are sought-after.

The metabolic model of Mulukutla et al. (2012) of the recombinant mouse myeloma cell line (NS0) has shown that lactate consumption occurs when the glycolytic flux is low under the conditions of low glucose and at moderately high lactate. Also, high lactate consumption was observed when pH is low. Their results demonstrate that lactate inhibition may lead to glycolytic flux reduction and lactate consumption at high glucose concentrations, but only when lactate concentration is high. Zhou et al. (2011) have demonstrated that simultaneous knockdown of lactate dehydrogenase (LDH) and pyruvate dehydrogenase kinases (PDHK) was effective in CHO cells in reducing lactate levels and increasing antibody titers without noticeable impact on cell growth and product quality.

It has repeatedly been observed, in this work, that lactate concentration decreases at low glucose concentrations. The working hypothesis is that the lactate produced by the consumption of glucose can be converted back to pyruvate and then proceeds to enter the TCA cycle (Tsao et al., 2005). Therefore, glucose and lactate are both considered as fuel sources in CHO cells' oxidative phosphorylation. With this type of metabolism presented by CHO-CY01 cells in batch mode, this indicates that the accumulation of lactate is limited to a maximum. However, the lactate cell metabolism was observed to assume a different profile in a large-scale fed-batch mode with pH control (Section 4.4).

In order to investigate the inhibitory effects of lactate on the CHO-CY01 cell line in batch mode, six different initial lactate concentrations (0.0, 0.7, 1.9, 2.7, 3.6, and 4.7 $g\ L^{-1}$) were tested in duplicate. The choice behind the values for the initial lactate concentration resides on the maximum lactate concentration obtained in batch (3.0 $g\ L^{-1}$) (Section 4.2) and fed-batch (4.0 - 7.0 $g\ L^{-1}$) (Section 4.4) cell cultures and the range values studied in the literature (2.0 – 4.0 $g\ L^{-1}$) (Ozturk et al., 1992). The CHO-CY01 cell culture growth and metabolism in the presence of various initial lactate concentration is presented in Figure 4-7 and Figure 4-8. The kinetic calculated parameters are shown in Table 4-3 and Table C-8. Through the statistical determination of the correlation between the culture parameters (Table A-8), it was possible to observe the metabolic shift between parameters.

As shown in Figure 4-7, initial lactate concentration had an adverse effect on cell growth but not on the initial cell viabilities (> 90%). Regarding viable cell numbers, the data can be visually clustered into three initial lactate ranges: ($\leq$ 1.9; 1.9 – 3.6; and $\geq$ 3.6 $g\ L^{-1}$. At low lactate concentrations ($\leq$ 1.9 $g\ L^{-1}$), CHO-CY01 cells grew at similar μ ($0.02\ h^{-1}$) compared with standard conditions (0.0 $g\ L^{-1}$). The same was observed for IgG4 production and cell metabolism (glucose and glutamate). At lactate concentrations from 1.9 $g\ L^{-1}$ to 3.6

$g\ L^{-1}$, the inhibitory effect of lactate started to be observed with a reduction of the μ, VP, and metabolism. For initial lactate concentration higher than 1.9 $g\ L^{-1}$, the cells were not able to metabolically produce lactate any longer as a glucose by-product. The lactate concentration is so high that the CHO-CY01 cells convert the lactate into pyruvate and then proceed to enter the TCA cycle (working hypothesis). Therefore, a more efficient use of the carbon sources was expected. However, the final IgG4 concentration and maximum viable cell concentration reached were lower than in standard conditions; this indicates the toxic effect of lactate in the cell culture. That effect can be caused by different phenomena: the direct chemical action of the lactate, a decrease in external pH, or an increase in medium osmolality. Observing the osmolality profile in Figure 4-8 for this lactate concentration range, osmolality has decreased with time, and the variation between conditions was around 10%, which eliminates the osmolality effect on the lactate inhibition. An association between lactate and ammonium concentration was observed. The higher the lactate concentration in the medium, the lower was the ammonium accumulation. This may indicate a perturbation of the intracellular pH and electrochemical gradients. For initial lactate concentrations higher than 3.6 $g\ L^{-1}$, the CHO-CY01 cell growth was severely compromised as well as IgG4 production, which decreased by 30% compared with no lactate run. For lactate concentrations higher than 4.7 $g\ L^{-1}$, the cells managed to survive for a week with almost no growth. At this concentration, the osmolality with the conjugation of the lactate toxic effect were responsible from this outcome.

The understanding of lactate in mammalian cells has changed over the past decades. For a long time, lactate was only considered as a waste product from the anaerobic metabolism of glucose (Warburg effect). Currently, lactate in mammalian cell metabolism is regarded as a metabolite with dual action. Since the introduction of an intracellular lactate shuttle hypothesis proposed by Professor George Brooks and further reported as evidence of the existence of mitochondrial lactate carriers (Brooks et al., 1999; Luo et al., 2012), it became possible to explain why there are lactate consumer cells. From a thorough literature review, the lactate metabolic shift could be related to the oxidative metabolic capacity of cells (Zagari et al., 2013).

Early in the culture, cells engage heavily in cytosolic energy production via the consumption of glucose during glycolysis, especially during the rapid exponential growth phase. At this stage, cells are lactate producers (LP), and lactate accumulation occurs (Figure 4-5 A). Consequently, this decreases the cytosol pH, which is neutralised when cells symport the lactate with a proton to the cell culture medium (Poole et al., 1993). At this low lactate concentration, the steady-state internal pH is not affected (Wu et al., 1993). With the progression of the cell culture, mammalian cells can be divided into two categories: lactate consumers (LC) or lactate producers (LP). The primary finding of Luo et al. (2012) was that

LP cells exhibited a less efficient energy metabolism, with glucose primarily being converted into pyruvate, sorbitol, lactate, and other glycolytic intermediates. This decrease in energy efficiency may be due to an inability of pyruvate and acetyl-CoA to progress into the TCA cycle. The lack of progression into the TCA cycle or overflow metabolism in the LP phenotype results in the inadequate supply of ATP for the cells. As a consequence, the glycolysis pathway remains the primary source of ATP.

A negative aspect of the excessive lactate accumulation by the cells (lactic acidosis) is the acidification of the cytosol. The low internal pH significantly decreases the overall glycolytic flux and inhibits the activity of all glycolytic enzymes, which ceases lactate formation (Roos et al., 1981; Xie et al., 2014). For an LP cell, this represents imminent cell death. However, for an LC cell, this lactate is used as fuel (Figure 4-5 B). With lactic acidosis, the high lactate level inhibits lactate dehydrogenase (LDH), which ceases the lactate production. Also, the higher proton level on the medium side than on the cytosol side facilitates the lactate transport into cells by the monocarboxylic transporter (MCT1) (Poole et al., 1993), because MCT1 is a symporter for lactate and protons (Xie et al., 2014). In a cascade of lactate transport to inside the mitochondrial matrix by the mitochondrial monocarboxylic transporter (mMCT) and by the presence of mitochondrial lactate dehydrogenase (mLDH), the lactate is oxidised to pyruvate, and pyruvate is oxidised via the tricarboxylic acid (TCA) cycle and electron transport chain (ETC) (Figure 4-5) (Brooks et al., 1999; Gladden 2004; Wu et al., 1993). Xie et al., (2014) have reported the transition from the Warburg effect to non-glycolytic phenotype by lactic acidosis as an advantage that cancer cells, especially in solid tumours, have to use more economically glucose that is limiting. The drawback of this non-glycolytic lactate switch is the accumulation of NADH. Increased efficiency of the malate-aspartate shuffle to transport NADH across the mitochondrial membrane would be one of the cell responses. Therefore, an increase in the aspartate demand could be met by diverting more glutamate flux towards the aspartate aminotransferase (AspAT) pathway (malate-aspartate shuttle) (McKenna, 2013) from alanine aminotransferase (AlaAT), glutamate dehydrogenase (GDH) pathways and glutamine synthetase (GS) (Figure 4-6). Thus, a decrease in the ammonia production rate is expected (Lao et al., 1997).

In summary, this was the first lactate inhibition study with a CHO cell line with the glutamine synthetase expression system. Lactate has a negative effect on cell growth as the μ decreases and switches the metabolic pathways inside the cells. Three lactate concentration tolerance ranges were observed in the CHO-CY01 cell line: 0-1.9 7 $g\ L^{-1}$, 1.9 - 3.6 $g\ L^{-1}$, and > 3.6 $g\ L^{-1}$. In the first range, lacate has an impact only on the cell growth, as the lacate and ammonium profiles were similar. In the middle range, the metabolism shift occurred with further growth inhibition. At lactate concentrations higher than 1.9 $g\ L^{-1}$, the cells became strictly lacate consumers. It was hypothetised that at this high lacate concentrations, the

lactate dehydrogenase was inhibited as the glucose consumption rate decreased, and that the cells were utilising the lactate as a fuel through intracellular lactate shuttle. This metabolic "switch" is presumed to be driven by a decreased dependence on glycolysis and an enhanced engagement in oxidative pathways for energy production. As a consequence, the ammonium production rate decreased. Due to the diminished energy production from lower glycolytic rate with the diversion of more energy into maintenance of ion gradients to counter the effects of the hypertonic environment, growth was inhibited by this higher concentrations of lactate. For extremely high lactate concentrations (> 3.6 $g\ L^{-1}$), cell growth is almost negligible, and not only the direct toxic effect of the lactate on the cells but also the osmolality increase were responsible. Several publications have emphasised the role of the osmolality in lactate inhibition as the major contributor (Cruz et al., 2000; Hassell et al., 1991; Lao et al., 1997; Ozturk et al., 1992). However, in this work, the osmolality effect at high lactate concentration was not observed, as the profiles were similar.

When cells are so challenged by living in a harsh environment (lactic acidosis) where they struggle to grow, the production of such glycosylated proteins as IgG4, which are extremely demanding of the metabolic machinery, is most likely compromised. The decrease in the VP, which is the rate of IgG4 production, with the lactate concentration has proven the inhibitory effect of lactate in mAb production.

The desirable phenotype, considering both cell growth and productivity, is characterised by limited lactate synthesis during the initial growth phase, ideally no more than 2.7 $g\ L^{-1}$, followed by lactate consumption. The undesirable phenotype is characterised by a high level of lactate production and accumulation throughout the entire process.

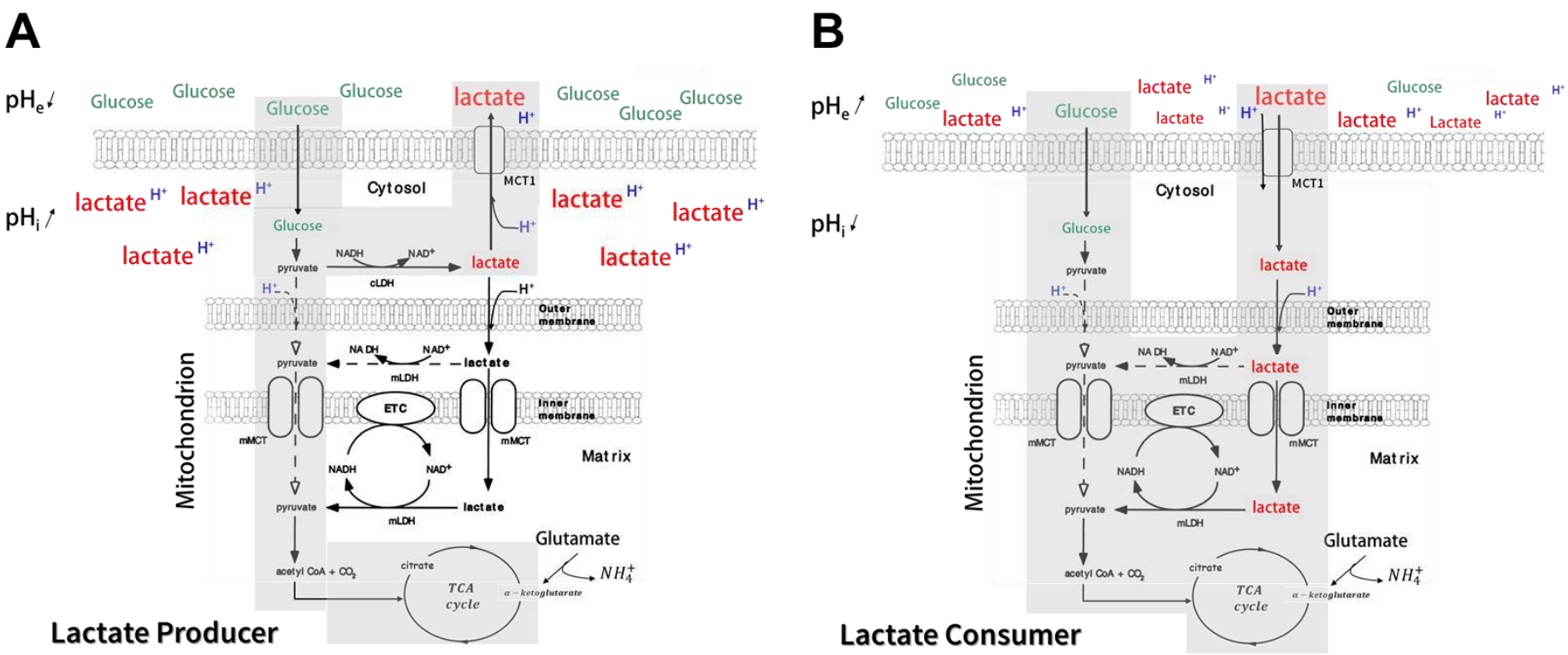

Figure 4-5: Representation of a possible GS-CHO cell line lactate metabolism pathway. Highlighted is the lactate intracellular metabolic route in the cell. (A) During lactate production phase, cells produce lactate from glucose glycolysis. The cytosol lactate production causes a transient acidification of the cytosol. Cells use a monocarboxylic transporter that symports a proton to increase the internal pH; (B) With further lactate accumulation, there is lactate dehydrogenase inhibition that stops the cytosol production of the lactate. Lactate consumer (LC) cells use this lactate in the intracellular lactate shuttle to be fully oxidised via TCA cycle and ETC. Diagrams were adapted from Brooks et al., 1999; Gladden 2004 and Philp et al., 2005.

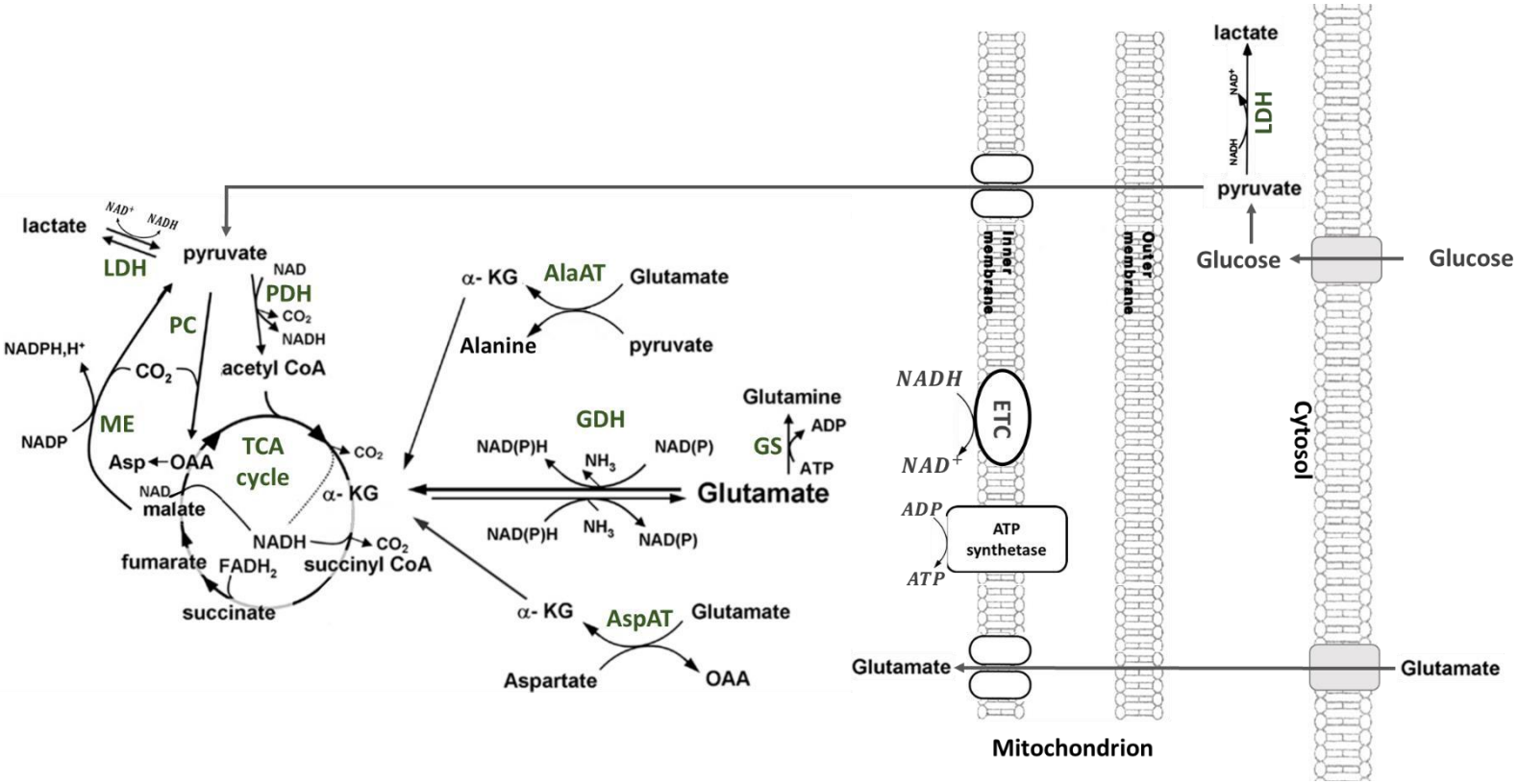

Figure 4-6: Schematic diagram indicating the pathways of glutamate metabolism in mammalian cells. Glutamate can be converted to α-ketoglutarate (α-KG) by the energy-producing enzyme glutamate dehydrogenase (GDH) or via one of the transaminase enzymes (primarily via aspartate aminotransferase (AspAT) but also by alanine aminotransferase (AlaAT). α-ketoglutarate formed from glutamate is metabolised via a partial TCA cycle to either malate or oxaloacetate (OAA) (malate-aspartate shuttle). For the complete oxidation of glutamate to occur malate (or OAA) must leave the TCA cycle, be converted to pyruvate by malic enzyme (ME) and then converted to acetyl-CoA by pyruvate dehydrogenase (PDH). The acetyl CoA formed by these pyruvate recycling reactions re-enters the TCA cycle and is subsequently oxidised for energy. Diagram adapted from Gladden 2004 and McKenna 2013.

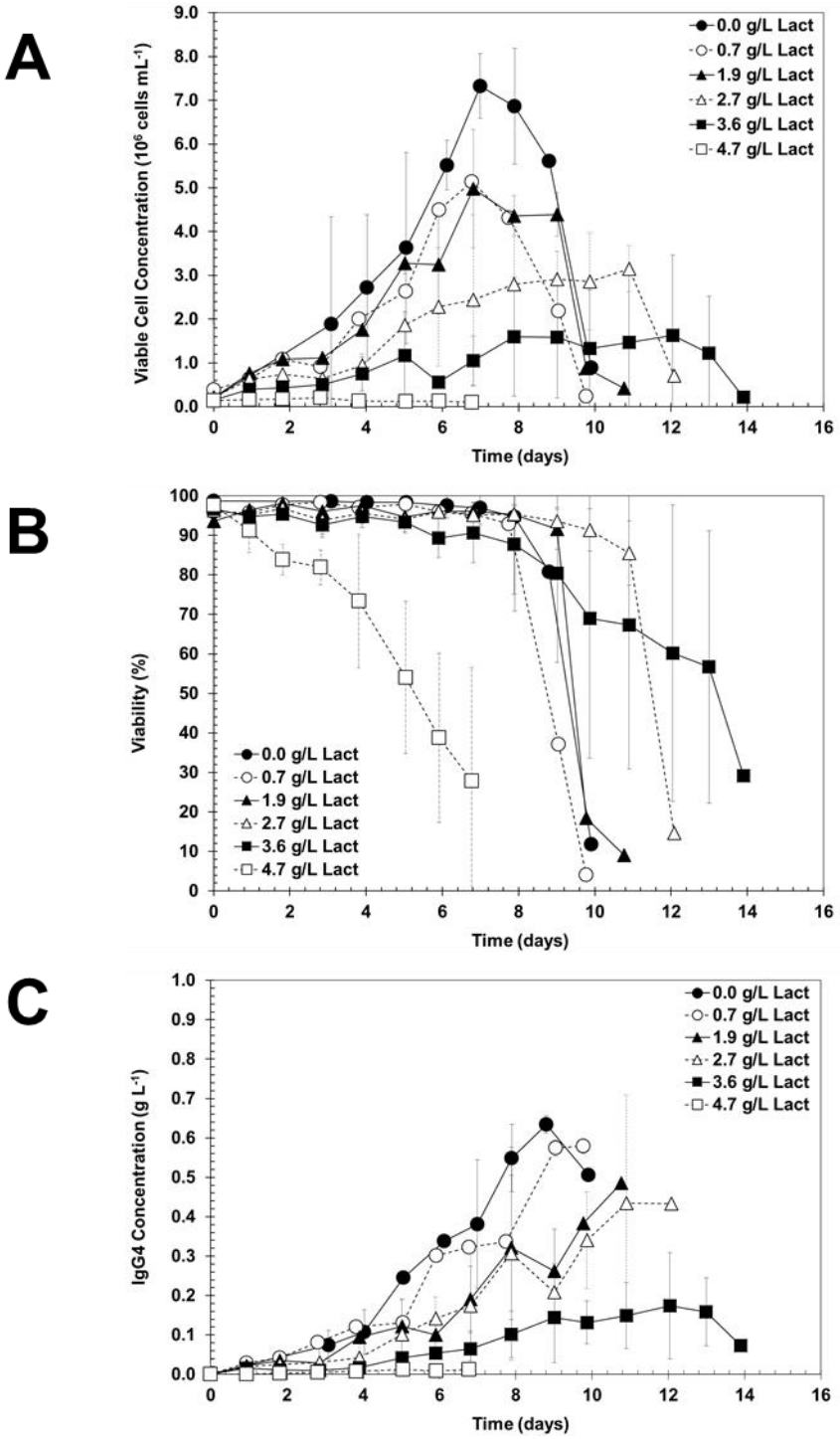

Figure 4-7: Viable cell concentration (A), cell viability (B), and IgG4 concentration (C) profiles for CHO-CY01 cell batch culture at different initial lactate concentrations (0.0, 0.7, 1.9, 2.7, 3.6, and 4.7 $g\ L^{-1}$) (2 replicates per lactate concentration). Error bars represent one standard deviation about the mean.

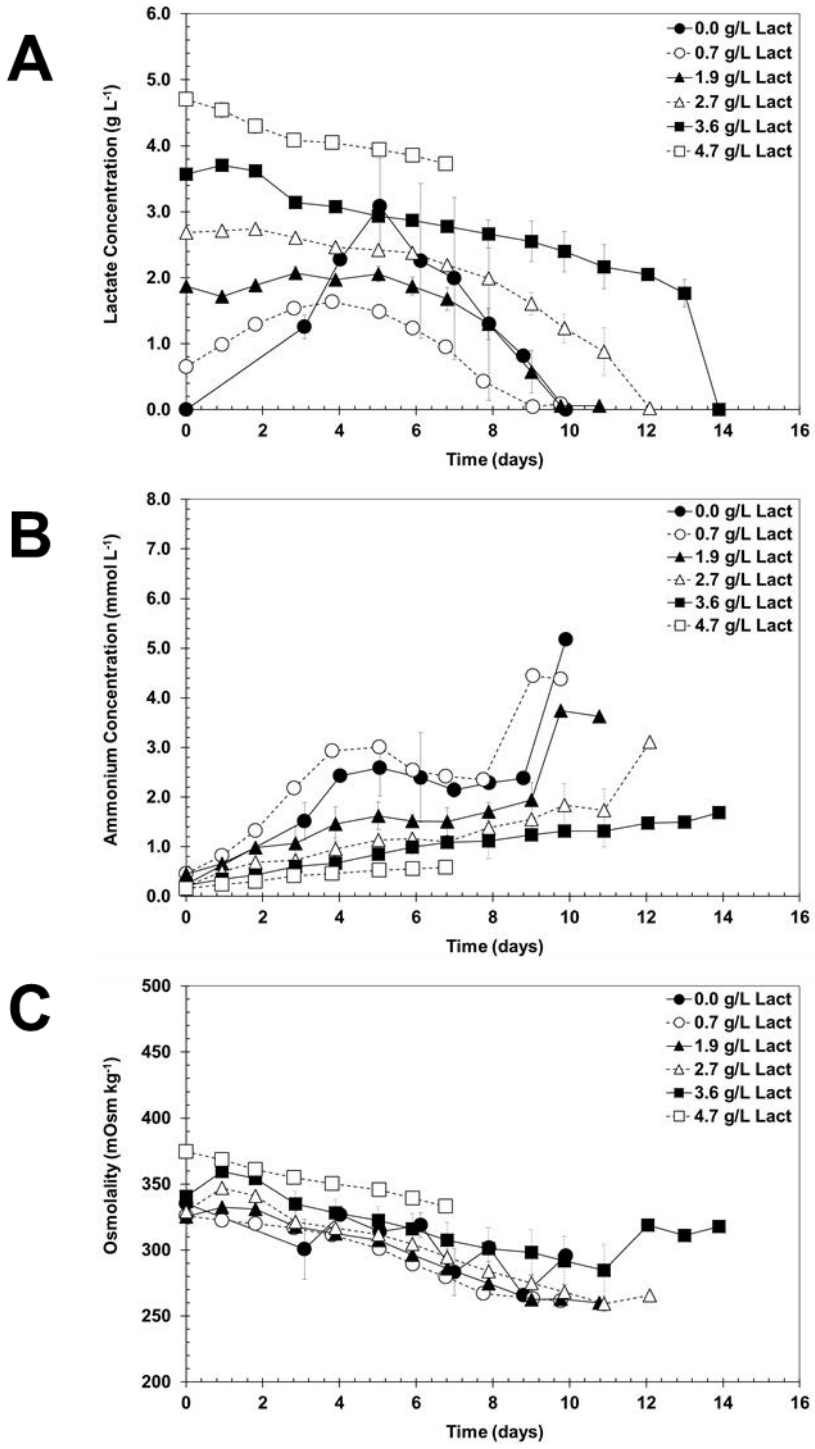

Figure 4-8: Lactate concentration (A), ammonium ion concentration (B), and osmolality (C) profiles for CHO-CY01 cell batch culture at different initial lactate concentrations (0.0, 0.7, 1.9, 2.7, 3.6, and 4.7 $g\,L^{-1}$) (2 replicates per lactate concentration). Error bars represent one standard deviation about the mean.

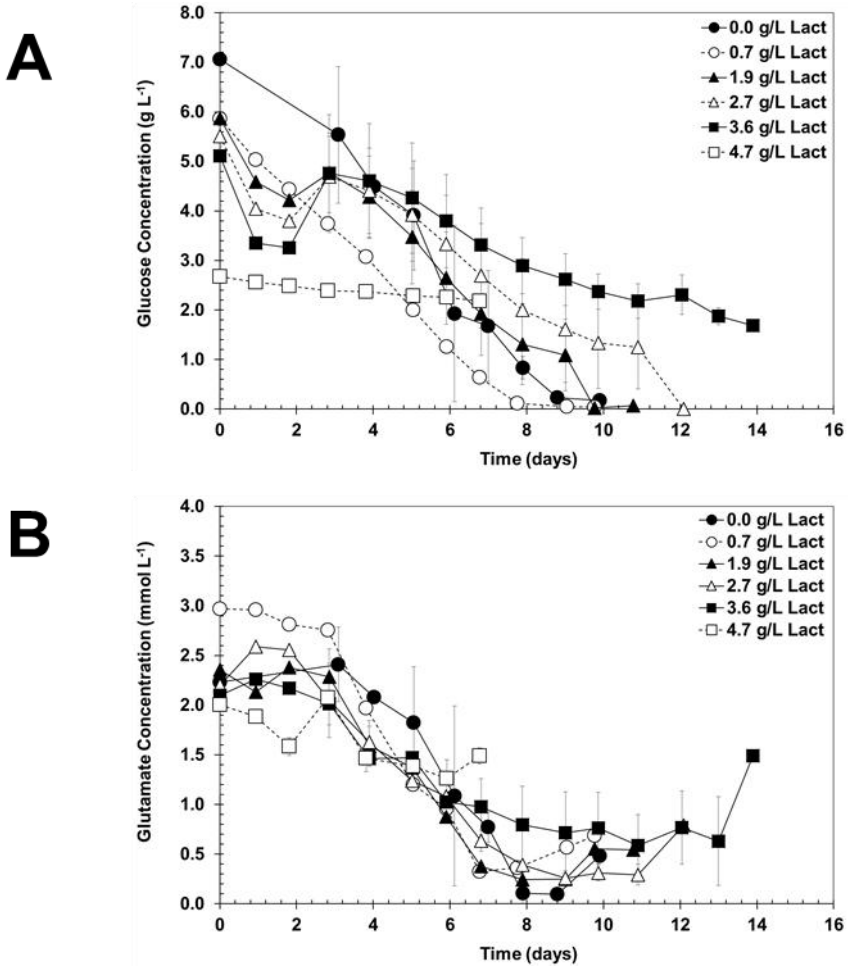

Figure 4-9: Glucose (A) and glutamate (B) concentration profiles for CHO-CY01 cell batch culture at different initial lactate concentrations (0.0, 0.7, 1.9, 2.7, 3.6, and 4.7 $g\,L^{-1}$) (2 replicates per lactate concentration). Error bars represent one standard deviation about the mean.

Table 4-3: Kinetic parameters determined for CHO-CY01 cell batch culture at different initial lactate concentrations (0.0, 0.7, 1.9, 2.7, 3.6, and 4.7 $g\ L^{-1}$).

Lactate Concentration $(g\ L^{-1})$	**0.0**	**0.7**	**1.9**	**2.7**	**3.6**	**4.7**
VP $(mg\ L^{-1}day^{-1})$	58.0 ± 2.8	51.0	31.3 ± 10.7	30.7 ± 12.3	19.0 ± 12.5	1.7 ± 0.7
IVCC $(10^9 cells\ day\ L^{-1})$	33.65 ± 5.80	23.46	24.81 ± 4.43	21.03 ± 6.46	13.70 ± 7.58	1.10 ± 0.43
$\mu\ (h^{-1})$	0.023 ± 0.002	0.016	0.021 ± 0.003	0.015 ± 0.001	0.012 ± 0.005	0.008 ± 0.004
$t_{1/2}\ (h)$	29.7 ± 2.3	42.7	32.9 ± 4.1	45.3 ± 2.7	63.3 ± 28.7	97.3 ± 44.0
$q_{mAb}\ (mg\ 10^{-9}\ cells^{-1}\ day^{-1})$	20.06 ± 3.02	23.90	14.09 ± 2.89	14.08 ± 12.18	9.86 ± 8.60	6.80 ± 6.33
$q_{Gluc}\ (g\ 10^{-9}\ cells^{-1}\ day^{-1})$	-0.25 ± 0.05	-0.30	-0.23 ± 0.02	-0.25 ± 0.05	-0.21 ± 0.05	-0.13 ± 0.32
$q_{Glu}\ (mmol\ 10^{-9}\ cells^{-1}\ day^{-1})$	-0.09 ± 0.04	-0.12	-0.10 ± 0.02	-0.12 ± 0.01	-0.13 ± 0.02	-0.41 ± 0.22
$q_{Na^+}\ (mmol\ 10^{-9}\ cells^{-1}\ day^{-1})$	-0.73 ± 0.66	-0.76	-0.52 ± 0.15	-1.21 ± 0.44	-2.57 ± 1.38	-14.67 ± 5.14
$q_{K^+}(mmol\ 10^{-9}\ cells^{-1}\ day^{-1})$	-0.03 ± 0.01	-0.09	0.07 ± 0.02	-0.12 ± 0.03	-0.13 ± 0.04	-0.51 ± 0.15
$q_{Lact}\ (g\ 10^{-9}\ cells^{-1}\ day^{-1})$	0.48 ± 0.18	0.52	0.69 ± 0.09	0.09 ± 0.01*	0.16 ± 0.02*	1.04 ± 0.42*
$q_{Amm})\ (mmol\ 10^{-9}\ cells^{-1}\ day^{-1})$	0.103 ± 0.014	0.169	0.094 ± 0.009	0.104 ± 0.004	0.144 ± 0.088	0.455 ± 0.056
Lactate produced / Glucose consumed (g/g)	0.81 ± 0.19	0.42	0.14 ± 0.10	0.00 ± 0.00	0.00 ± 0.00	0.00 ± 0.00

* Stricly consumed

4.3.2. Effects of Ammonium on CHO-CY01 Cell Line Kinetics

It is widely known that one of the most important inhibitory substances accumulating in the mammalian cell cultures is ammonia/ammonium. Several different effects of elevated concentrations of ammonia in mammalian cell cultures have been reported. These include the decrease of cell growth (Doyle et al., 1990; Kurano et al., 1990b; McQueen et al., 1990a; 1990b; 1991), productivity (Hansen et al., 1994), and specific alterations of protein glycosylation (Andersen et al., 1995; Borys et al., 1994). Ammonia has been reported to induce apoptosis (Borys et al., 1994; Cruz et al., 2000). The ammonium ion (0-10 mM) may adversely affect glycosylation in mammalian cell cultures by decreasing the sialic acid and galactose contents, varying the site of occupancy and increasing the glycosylation branching (Altamirano et al., 2013; Andersen et al., 1995) (Figure 1-3). The toxic effect of ammonia is often one order of magnitude higher than that of lactate for a variety of cell lines (Cruz et al., 2000). The mechanisms underlying such toxicity are very complex and are not entirely understood. Ammonium accumulation disturbs the electrochemical cell gradient and induces cytoplasm acidification, thus increasing energy consumption to maintain pH homeostasis through Na^+/K^+ ATPase and $Na^+K^+2Cl^-$ cotransporters (Martinelle et al., 1998). The cells under ammonia stress have access to extra energy mainly from the incomplete oxidation of glucose to lactate through the glycolytic pathway, the increase in lactate production, and the decrease in oxygen consumption, with increasing ammonia concentration confirming this (Cruz et al., 2000).

The impact of ammonia on hybridoma cell lines has been extensively studied. Very few ammonia inhibition studies have been conducted in the CHO cell line, and the existing ones were performed on cell lines in media with glutamine. Of particular importance is whether the ammonia concentration normally accumulated in culture causes growth inhibition and thus may affect final cell yields in a GS-CHO cell line. In this work, such evaluation was conducted by inoculating the CHO-CY01 cell line in SFs with total volume of 125 mL with five different ammonium concentrations (0.2, 4.8, 7.1, 9.7, and 11.2 $mmol\,L^{-1}$). The choice of the ammonium chloride concentrations considered the standard values found in the literature (0-10 mM), and the values for ammonium ion were selected from values observed during batch ($< 6.0\ mmol\,L^{-1}$) (Section 4.2) and fed-batch ($< 8.0\ mmol\,L^{-1}$) (Section 4.4) cell cultures. It is important to notice that the cell medium (CD-CHO) where CHO-CY01 cells were cultured already had a small ammonium concentration (0.2 mM) in its composition. Therefore, the null ammonium condition could not be tested. The CHO-CY01 cell culture kinetics can be visualised in Figure 4-10, Figure 4-11 and Figure 4-12. The kinetic parameters determined are presented in Table 4-4 and Table C-9. Through the determination of the correlation factor between the different culture parameters (Table A-9), it was possible to observe the metabolic shifts occurring and cluster the conditions accordingly.

The primary strategy to reduce the accumulation of ammonia focusses on the substitution of glutamine for glutamate. The advantages of this substitution are that glutamate has a higher chemical stability than glutamine (i.e., no ammonia formation due to the chemical degradation of glutamate), is less ammoniagenic, as it has only one amine group and, glutamine can be directly synthesised from glutamate through glutamine synthetase (GS). This glutamate is then converted into α-ketoglutarate (Figure 4-6). This replacement proved to be a good strategy for CHO cells, resulting in cell growth improvement and a considerable reduction in the accumulated ammonium (Altamirano et al., 2013; McDermott et al., 1993;). In a GS-CHO cell line that has several copies of the glutamine synthetase gene, the ammonia accumulation is expected to be lower thus allowing extended fed-batch culture. However, ammonia accumulation can occur depending on what is fed to the cells (Altamirano et al., 2004).

The CHO-CY01 cell growth was negatively affected by the initial ammonium concentration. As in the lactate inhibition study, the impact of the initial ammonium concentrations on cell growth, metabolism, and productivity can be segmented into three different ranges: 0.2- 4.8; 4.8 – 9.7; and > 9.7 $mmol\ L^{-1}$. In terms of cell growth, it was noticed that with increasing ammonium concentration, a stationary phase uncharacteristic of a mammalian cell batch appeared. During this stationary phase, the cell growth rate equalled the cell death rate, and the majority of the IgG4 was formed. When the cell death rate became dominant, the IgG4 production stopped, and a plateau around the maximum IgG4 concentration reached was obtained in the cell culture.

At low ammonium concentrations (0.2 - 4.8 $mmol\ L^{-1}$), CHO-CY01 cell growth was not affected, but the q_{mAb} diminished by 23%. In terms of cell metabolism, the glucose consumption rate slowed down slightly, the glutamate consumption rate had a significant reduction, and the accumulative lactate production decreased by 63%. In the middle range of initial ammonium concentration (4.8 – 9.7 $mmol\ L^{-1}$), there was a longer *lag* phase, and the total number of cells produced declined by 37% at higher ammonium concentration. However, the IgG4 secretion was not changed as the VP, and the accumulative IgG4 production rate did not vary considerably. For high initial ammonium concentrations (> 9.7 $mmol\ L^{-1}$), CHO-CY01 cell growth was considerably negatively altered, and the same happened to productivity.

In an aqueous solution, ammonia and ammonium are linked in a pH-dependent equilibrium (pKa of 9.24 at 37ºC). At the physiological pH of 7.1 - 7.5, only about 1% of the total concentration of ammonia and ammonium is present as NH_3, with the rest being NH_4^+. NH_3 (unprotonated ammonia) is a small, uncharged, lipophilic molecule that readily diffuses across cellular membranes. The diffusion will follow the gradient of the chemical potential of NH_3, which can be approximated by the gradient of the partial pressure of the NH_3. The small percentage of NH_3 present in the extra- and intracellular aqueous phases will diffuse across

the membranes, thus rapidly equilibrating any transmembrane gradient of NH_3. As protonation occurs extremely quickly, the pH equilibrium will be reconstituted immediately. In a compartment with low pH, the partial pressure of NH_3 is lower, leading to a constant flow of NH_3 across the membrane into this compartment, until equilibrium is attained, i.e., the pH rises. In this way, ammonia can seriously disturb the functioning of the organelles with low internal pH, such as lysosomes and Golgi apparatus (protein glycosylation). Andersen et al. (1995) hypothesised through a mathematical model that an ammonia-induced increase in *trans*-Golgi pH was responsible for the decrease in sialylation, which decreases circulatory half-life and loss of *in vivo* activity of granilocyte colony-stimulating factor (G-CSF) produced by CHO cells. On the other hand, diffusion of the protonated form, NH_4^+, across cellular membranes is extremely slow. Values for the diffusion rate range from four to five orders of magnitude below those for NH_3. However, NH_4^+ can be transported actively across the cell membrane by specific transport proteins such as Na^+K^+*-ATPase*, by facilitated diffusion by means of the $Na^+K^+2Cl^-$ cotransporter, and possibly by the Na^+/H^+ exchanger to maintain the sodium and potassium gradients. In this way, NH_4^+ is in competition with K^+, which perturbs the transmembrane transport of the K^+. Martinelle et al. (1998) have proposed that the combination of NH_3 diffusion and NH_4^+ transport across membranes leads to futile cycles and an increase in the maintenance energy to maintain the new steady-state pH.

Ammonia is produced, in the form of NH_4^+, inside the mitochondria by the action of glutamate dehydrogenase, with the equilibrium between the NH_3 and NH_4^+ being immediately established according to the pH of the matrix. The inner mitochondrial membrane is extremely impermeable to ions; however, NH_3 readily passes from the mitochondrial matrix into the cytoplasm. This NH_3 outflow from the mitochondria leads to a decrease of the pH in the matrix, since a proton is left behind. NH_3 can diffuse out of the cytoplasm into the environment; however, it can be transported back as NH_4^+ by the carrier proteins (Figure 1-6). The net result of ammonium production is an acidification of the mitochondrial matrix and cytoplasm, and an alkalinisation of the cellular organelles and cellular environment. However, externally added ammonium will transiently increase the pH of the cytoplasm due to rapid diffusion of NH_3 into the cell. This alkalinisation is followed by an acidification due to the transport of NH_4^+ by carrier proteins. Diffusion of NH_3 into the mitochondria and other organelles leads to an increase of the pH inside these compartments. The result is an alkalinisation of the cellular environment and of the interior of the organelles, mitochondria included, and an acidification of the cytoplasm. Thus, it is very important to realise that the physiological consequences of adding ammonia extracellularly to the medium are very different than those resulting from ammonia produced intracellularly. The first provokes an increase of the pH of the mitochondrial matrix, while the second will decrease this pH. This has to be taken into account when the ammonia

sensitivity of a cell line is determined by the common practice of adding different amounts of ammonia to the medium (McQueen et al., 1990a; 1990b; Schneider et al., 1996). For this reason, the inhibitory effect upon cell growth is believed to be due to NH_3, and not the NH_4^+, in the culture (Doyle et al., 1990).

The ammonium (NH_4^+) profile itself during the CHO-CY01 cell culture has changed with increasing ammonium levels. For initial ammonium concentrations higher than 4.8 mM, during the lag phase there was no ammonium production or consumption. Once the cells had entered the exponential phase, they started to form small amounts of ammonium. By the mid-point of the exponential phase, an uptake of ammonium occurred. Towards the end of the cell culture (glucose and lactate deprivation), when cell viability had reached values below 80%, an ammonium concentration peak was observed, as mention before. This phenomenon may be due to cell breakage and subsequent exposure of the mitochondrial ammonium matrix instead of net ammonium production by the cells or an alternative option is the cell attempt to adjust the intracellular pH, once there is no more lactate.

The Henri-Michaelis-Menten constant for NH_4^+, a substrate of glutamate dehydrogenase (GDH), is 0.5 to 3.2 mM (Cruz et al., 2000). Therefore, the accumulation of ammonium ions higher than 3.2 mM changes the GDH reaction equilibrium towards glutamate formation (Figure 4-6). The glutamate thus produced can subsequently be converted into alanine or aspartate. This consists of a detoxification process of the cell against ammonia accumulation (Glacken, 1988a). This equilibrium shift causes the depletion of α-ketoglutarate, a TCA cycle intermediate, and the oxidation of NADH. The ammonia detoxification then has an effect on the electron transport chain (ETC) as it consumes the NADH needed for ATP production by the cell. Therefore, the cell energy metabolism is constrained, and this may explain the cell growth inhibition by ammonium. The CHO-CY01 cell line presented such a detoxification process, as there was ammonium uptake by the cells, and the net glutamate consumption rate and μ decreased with increasing ammonium concentration.

The cells may undergo a less efficient pathway to obtain energy, which is the glycolic pathway with lactate formation (2 ATP) to compensate for the ETC suppression during ammonium detoxification. That translated into an increase in the lactate production rate, but because the cytoplasm is already more acidified than usual by the rise in ammonium concentration, LDH is already inhibited compared with standard cell conditions. The cytosol acidification is accentuated by the lactate formation that inhibits, even more, LDH, forcing the cells towards the intracellular lactate shuttle and lactate uptake to its exhaustion. The higher the ammonium concentration, the lower the lactate uptake by the cells was. This can be a possible explanation for the decreasing accumulative lactate production with increasing initial ammonium concentration.

The initial osmolality decreased with the increase of ammonium concentration due to the dilution factor of adding the ammonium chloride solution. However, that dilution was not considered relevant to perform a correction by adding sodium chloride to the cell culture medium. Due to the relatively small ammonia concentrations used, osmolality effects were considered to be negligible; thus, an osmolality assay was not performed. The osmolality profile was similar to all of the initial ammonium concentrations tested. There was an increase in osmolality during lactate production and a subsequent decrease once lactate started to be consumed by the cells (Equation 2.4).

For initial ammonium concentration higher than 4.8 mM, the pH profile had not changed with the ammonium concentration. However, these pH readings were not online cell cultures, but an offline measurement of the cell culture´s supernatants. Consequently, it was possible to approximately visualise the pH variation in the cell culture. Initial pH was high (7.5), but as cells formed lactate, the pH decreased to a minimum (6.8), and as soon as the lactate started to be consumed, the pH increased (7.0-7.5), as expected.

Two possible mechanisms can justify CHO-CY01 cell growth inhibition. The first mechanism is that uptake of the weak base NH_3 into intracellular organelles such as lysosomes, mitochondria, and Golgi apparatus causes alkalinisation, as Doyle et al. (1990) have proposed. The second mechanism is that uptake of the weak acid NH_4^+ into the cytoplasm causes acidification; this was proposed by Martinelle et al. (1998). McQueen et al. (1990a) correlated these two mechanisms with external pH. The second mechanism of growth inhibition by NH_4^+ was important at all external pH values, while the first mechanism contributing to growth inhibition by NH_3 was only important at higher pH values. This explained why the cells with increasing added ammonium concentration had longer *lag* phases and lower viable cell numbers. Thus, if the pH were deliberately lowered during cell culture, the ammonia (NH_3) concentration could be minimised, this cell growth inhibitory mechanism could be eliminated, and product quality could be maintained. This type of strategy was tested, and the effects on cell growth and especially productivity were evaluated. These results are presented in Chapters 5 and 6.

In summary, with increasing ammonium concentration, the CHO-CY01 cell line's specific growth rate, glutamate consumption rate, VP and, ammonium production rate decreased, the lactate production rate increased, and the glucose consumption rate remained approximately constant (± 10%).

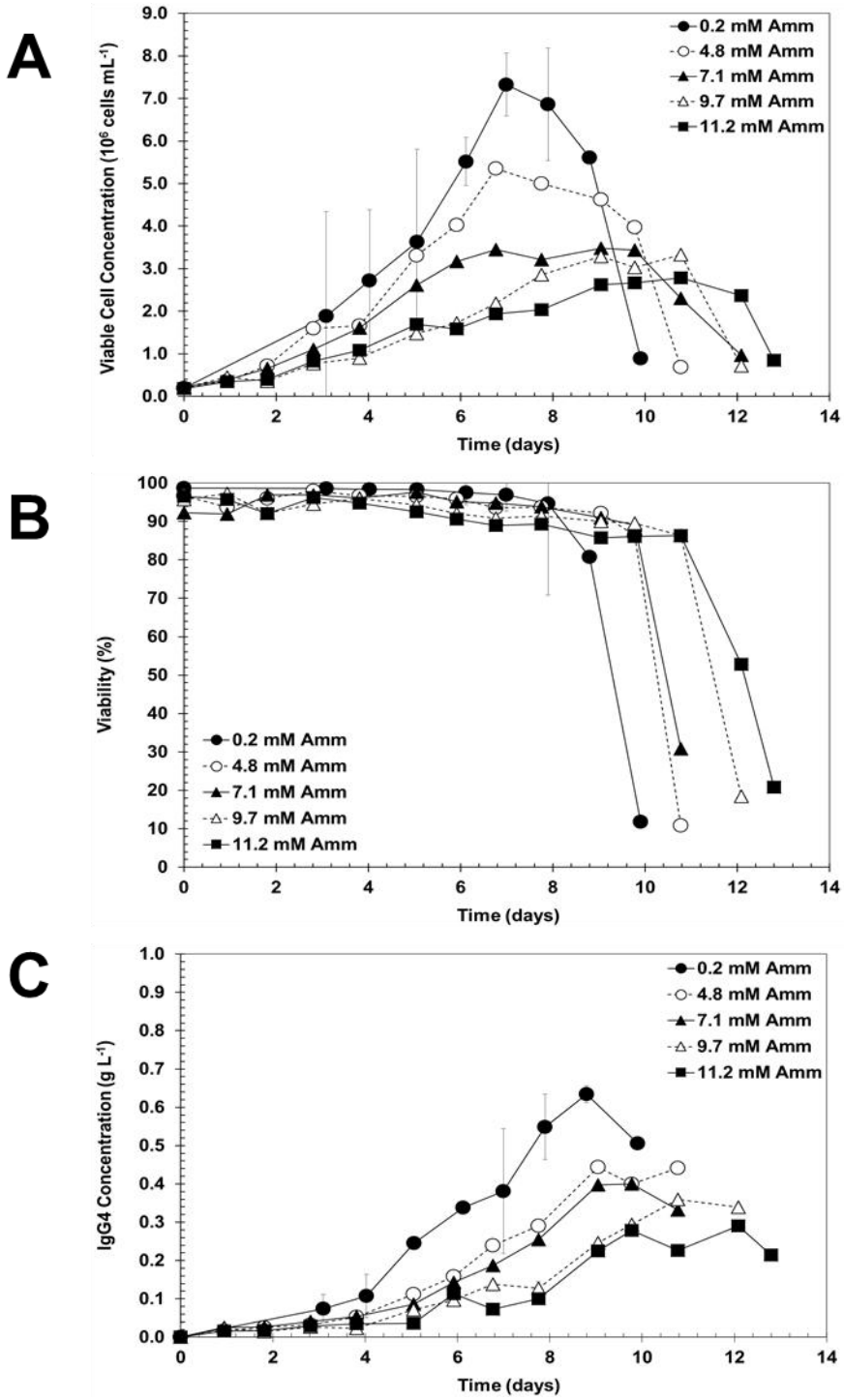

Figure 4-10: Viable cell concentration (A), cell viability (B), and IgG4 concentration (C) profiles for CHO-CY01 cell batch culture at different initial ammonium concentrations (0.2, 4.8, 7.1, 9.7, and 11.2 $mmol\ L^{-1}$) (2 replicates per ammonium concentration). Error bars represent one standard deviation about the mean.

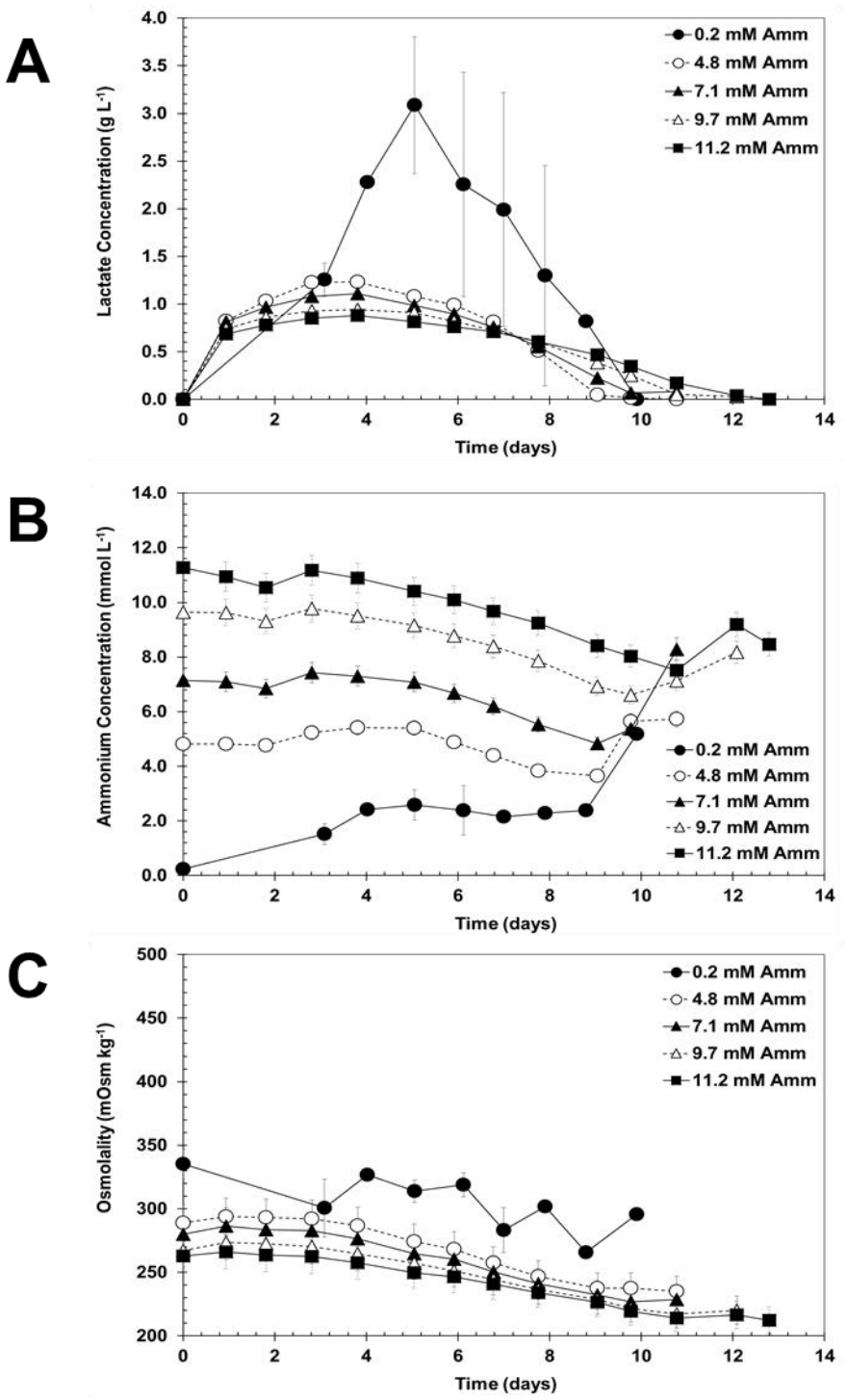

Figure 4-11: Lactate concentration (A), ammonium ion concentration (B), and osmolality (C) profiles for CHO-CY01 cell batch culture at different initial ammonium concentrations (0.2, 4.8, 7.1, 9.7, and 11.2 $mmol\ L^{-1}$) (2 replicates per ammonium concentration). Error bars represent one standard deviation about the mean.

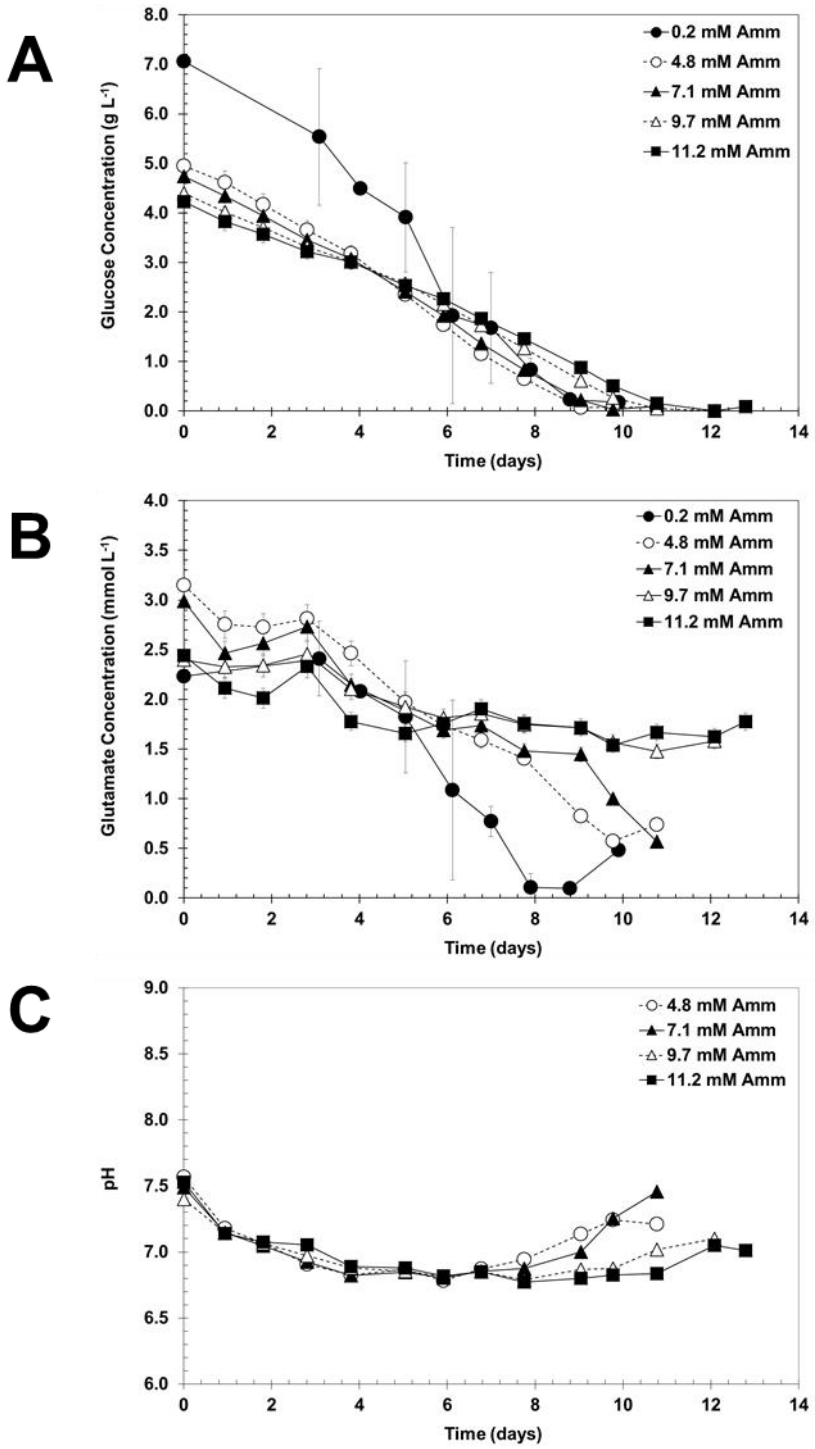

Figure 4-12: Glucose concentration (A), glutamate concentration (B), and pH (C) profiles for CHO-CY01 cell batch culture at different initial ammonium concentrations (0.2, 4.8, 7.1, 9.7, and 11.2 $mmol\ L^{-1}$) (2 replicates per ammonium concentration). Error bars represent one standard deviation about the mean. The pH values were obtained by NOVA Bioprofile 400 analysis of cell cultures' supernatants at each time point

Table 4-4: Kinetic parameters determined for CHO-CY01 cell batch culture at different initial ammonium concentrations (0.2, 4.8, 7.1, 9.7, and 11.2 $mmol\ L^{-1}$).

Ammonium Concentration ($mmol\ L^{-1}$)	**0.2**	**4.8**	**7.1**	**9.7**	**11.2**
VP ($mg\ L^{-1}day^{-1}$)	58.0 ± 2.8	37.9	32.0	25.6	19.9
IVCC ($10^9 cells\ day\ L^{-1}$)	33.65 ± 5.80	30.55	26.03	21.17	20.93
$\mu\ (h^{-1})$	0.023 ± 0.002	0.023	0.019	0.014	0.015
$t_{1/2}\ (h)$	29.7 ± 2.3	30.6	36.7	48.7	47.5
$q_{mAb}\ (mg\ 10^{-9}\ cells^{-1}\ day^{-1})$	20.06 ± 3.02	15.44	16.40	17.94	14.19
$q_{Gluc}\ (g\ 10^{-9}\ cells^{-1}\ day^{-1})$	-0.25 ± 0.04	-0.19	-0.22	-0.25	-0.23
$q_{Glu}\ (mmol\ 10^{-9}\ cells^{-1}\ day^{-1})$	-0.086 ± 0.044	-0.077	-0.076	-0.006	0.002
$q_{Na^+}\ (mmol\ 10^{-9}\ cells^{-1}\ day^{-1})$	-0.73 ± 0.66	-0.02	-0.57	-0.57	-0.60
$q_{K^+}\ (mmol\ 10^{-9}\ cells^{-1}\ day^{-1})$	-0.028 ± 0.006	-0.004	-0.075	-0.097	-0.087
$q_{Lact}\ (g\ 10^{-9}\ cells^{-1}\ day^{-1})$	0.48 ± 0.18	0.33	0.38	0.47	0.45
$q_{Amm}\ (mmol\ 10^{-9}\ cells^{-1}\ day^{-1})$	0.103 ± 0.014	0.002	0.004	0.140*	0.175*
Lactate produced / Glucose consumed (g/g)	0.72 ± 0.11	1.32	0.89	0.97	1.09

*Consumption

4.3.3. Ammonium and Lactate Inhibition Kinetics on CHO-CY01 Cell Growth and IgG4 Productivity

In the previous sections, it was shown that the toxic effect of ammonium on the CHO-CY01 cell line was higher than that of lactate, i.e. the cell growth, metabolism, and productivity was inhibited first by ammonia and then by ammonium and lactate. Mathematical models of cell growth and product formation kinetics are useful to quantify and to predict the effects of changes in environmental conditions (Gadgil, 2014). They have been used extensively to simulate cell metabolism, growth, and protein expression in animal cells (Bree et al., 1988; Gadgil 2014; Glacken et al., 1988b; Goudar et al., 2005; Miller et al., 1988; O'Callaghan et al., 2008; Omasa et al., 1992; Pörtner et al., 1996; Sidoli et al., 2004; Xing et al., 2010; Zeng 1996). An accurate and representative quantitative description of mammalian cell culture dynamics can then be used to predict culture behaviour, which, in turn, can serve as a basis for alternative production methods. Such simulations are essential for designing, controlling, and optimising production (Glacken et al., 1988b). Though the mechanisms of inhibition by lactate and ammonium are not entirely clear, at a minimum, it can be considered that ammonium and lactate have no direct influence on cell affinity to a growth-limiting substrate (e.g. glucose and glutamate) (Kurano et al., 1990b).

In this work, the lactate and ammonium inhibition of cell growth and IgG4 productivity were mathematically described by a non-competitive type inhibition model similar to the kinetic expressions described in a number of other publications (Gadgil 2014; Glacken et al., 1988b; Omasa et al., 1992; Pörtner et al., 1996; Xing et al., 2009; Zeng 1996). It was assumed that the glucose and glutamate inhibition in the cell growth, death, and mAb productivity ($f_{inhibition}(Gluc, Glu,\ K_{i,Gluc}, K_{i,Glu}, K_{Di,Gluc}, K_{Di,Glu}, K_{P,Gluc}, K_{P,Glu}\ )$) were the same in all experiments and so, they were neglected. The Monod-type kinetic expressions used to describe the lactate and ammonium inhibition effects on cell growth and productivity are presented in Equation 4.1, Equation 4.2 and Equation 4.3. In these equations, μ is the specific growth rate (h^{-1}), μ_{max} is the maximum specific growth rate (h^{-1}), $K_{i,Amm}$ is the half-maximum-rate concentration of ammonium for cell growth rate ($mmol\ L^{-1}$), Amm is the ammonium concentration ($mmol\ L^{-1}$), $K_{i,Glu}$ is half-maximum-rate concentration of glutamate for cell growth rate ($mmol\ L^{-1}$), Glu is the glutamate concentration ($mmol\ L^{-1}$), $K_{i,Gluc}$ is half-maximum-rate concentration of glucose for cell growth rate ($g\ L^{-1}$), $Gluc$ is the glucose concentration ($g\ L^{-1}$), $K_{i,Lact}$ is the half-maximum-rate concentration of lactate for cell growth rate ($g\ L^{-1}$), $Lact$ is the lactate concentration ($g\ L^{-1}$), $|\mu_d|$ is the specific cell death rate absolute value (h^{-1}), $|k_d|$ is the maximum cell death rate absolute value (h^{-1}), $K_{Di,Amm}$ is the half-maximum-rate concentration of ammonium for cell death rate ($mmol\ L^{-1}$), $K_{Di,Glu}$ is the half-maximum-rate concentration of glutamate for cell death rate ($mmol\ L^{-1}$), $K_{Di,Gluc}$ is the

half-maximum-rate concentration of glucose for cell death rate ($g\ L^{-1}$), $K_{Di,Lact}$ is the half-maximum-rate concentration of lactate for cell death rate ($g\ L^{-1}$), VP is the volumetric productivity ($mg\ L^{-1}\ day^{-1}$), VP_{max} is the maximum VP ($mg\ L^{-1}\ day^{-1}$), $K_{P,Amm}$ is the half-maximum-rate concentration of ammonium for IgG4 production rate ($mmol\ L^{-1}$), $K_{P,Glu}$ is the half-maximum-rate concentration of glutamate for IgG4 production rate ($mmol\ L^{-1}$), $K_{P,Gluc}$ is the half-maximum-rate concentration of glucose for IgG4 production rate ($g\ L^{-1}$) and, $K_{P,Lact}$ is the half-maximum-rate concentration of lactate for IgG4 production rate ($g\ L^{-1}$).

$$\mu = \mu_{max} \cdot f_{inhibition}\left(Gluc, Glu, Amm, Lact, K_{i,Gluc}, K_{i,Glu}, K_{i,Amm}, K_{i,Lact}\right) = \\ = \mu_{max} \frac{K_{i,Amm}}{K_{i,Amm} + Amm} \cdot \frac{K_{i,Lact}}{K_{i,Lact} + Lact}$$

Equation 4.1

$$|\mu_d| = |k_d| \cdot f_{inhibition}\left(Gluc, Glu, Amm, Lact, K_{Di,Gluc}, K_{Di,Glu}, K_{Di,Amm}, K_{Di,Lact}\right) = \\ = |k_d| \frac{K_{Di,Amm}}{K_{Di,Amm} + Amm} \cdot \frac{K_{Di,Lact}}{K_{Di,Lact} + Lact}$$

Equation 4.2

$$VP = VP_{max} \cdot f_{inhibition}\left(Gluc, Glu, Amm, Lact, K_{P,Gluc}, K_{P,Glu}, K_{P,Amm}, K_{P,Lact}\right) \\ = Prod_{mAb}^{max} \frac{K_{P,Amm}}{K_{P,Amm} + Amm} \cdot \frac{K_{P,Lact}}{K_{P,Lact} + Lact}$$

Equation 4.3

Equation 4.1 is exclusively related to the exponential phase while Equation 4.2 is related to the decline phase. Equation 4.3 covers the entire cell culture. For determining the parameters above, lactate concentrations in the ammonium experiment were independent of the ammonium concentrations and constant when μ, μ_d and q_{mAb} were determined and, vice versa. These latter are to be considered good approximations by observing Figure 4-7B and Figure 4-10A. In this way, the Equation 4.1 can be transformed as follows:

In the ammonium experiment:

$$\mu = Constant \frac{K_{i,Amm}}{K_{i,Amm} + Amm}$$

Equation 4.4

In the lactate experiment:

$$\mu = Constant \frac{K_{i,Lact}}{K_{i,Lact} + Lact}$$

Equation 4.5

Equation 4.2 and Equation 4.3 were transformed in the same way. Nonlinear curve fitting yields a much more reliable estimation than a reciprocal plot followed by linear regression (Kurano et al., 1990b). The parameters were estimated by minimising the sum of squared error (SSE) between the experimental and model fit data (Goudar et al., 2005):

$$SSE = \sum_{i=1}^{j} \left\{ (x_{meas})_i - \left(x_{fit}\right)_i \right\}^2$$

Equation 4.6

where $(x_{meas})_i$ is the ith experimental x value and $\left(x_{fit}\right)_i$ is the ith model fitted x value in a total of j observations. The algorithm used for nonlinear parameter estimation was the generalised reduced gradient method. For all parameters, a random pattern of residuals ($(x_{meas})_i - \left(x_{fit}\right)_i$) supported a linear model. Therefore, R squared (R^2) was used to measure the goodness of the fit. R^2 was determined to measure the quality of the fit as follows:

$$R^2 = 1 - \frac{SSE}{SST}$$

Equation 4.7

where SST is the total sum of squares calculated with Equation 4.8, where $\overline{(x_{meas})_\iota}$ is the average of the the ith experimental x value in a total of j observations.

$$SST = \sum_{i=1}^{j} \left\{ (x_{meas})_i - \overline{(x_{meas})_\iota} \right\}^2$$

Equation 4.8

In Figure 4-13 are represented the ammonium and lactate effects on the CHO-CY01 cell culture kinetic parameters such as growth rate, cell death, and IgG4 productivity. Also, the proposed mathematical model for ammonium and lactate inhibition represented by Equation 4.1, Equation 4.2 and Equation 4.3 with the estimated parameters are presented in Table 4-5. These estimated parameters can be then incorporated into a mathematical description of the CHO-CY01 cell culture. For a CHO cell line (with glutamine in the medium), the reported value range for $K_{i,Amm}$ is between 1.0 and 20.0 mM, and for $K_{i,Lact}$, it is between 0.7 – 12.5 $g\ L^{-1}$ (Bree et al., 1988; Miller et al., 1988; Xing et al., 2008). The estimated values $K_{i,Amm}$ and $K_{i,Lact}$ in this work are within these ranges. To understand the differences of ammonium and lactate inhibition between a GS and non-GS CHO cell line, the values estimated by the generalised reduced gradient method were compared with the estimation of Xing et al., (2010) via the Markov chain Monte Carlo method (MCM) sampling procedure ($K_{i,Amm}$ 6.51 mM and $K_{i,Lact}$ 3.8 $g\ L^{-1}$). The half-maximum-rate concentration of ammonium for cell growth rate

estimated for the GS-CHO cell line had a 2.8-fold increase when the same parameter for lactate was just 7% higher. Therefore, as expected, the GS system made the CHO cells more ammonium-resistant, mainly because of the elimination of glutamine from the cell culture medium, and did not alter the glucose glycolytic pathway. However, to obtain a similar growth decrease to that of ammonium, the concentration of lactate had to be much higher in both CHO cell line types.

Since the specific cell death rate in an absolute value decreased with the increasing value of ammonium and lactate, this is the opposite of what has been reported in the literature (Xing et al., 2010). Therefore, the kinetic expression for cell death in Equation 4.2 is a new way to describe the ammonium and lactate inhibition of a GS-CHO cell line. Monoclonal antibodies are considered in the majority of the cell culture mathematical model as a growth-associated product, and their specific production rate is the product of the μ with the observed yield of product formed per cell. However, considering the impact of the lactate and ammonium on the VP, an inhibition model for IgG4 formation in CHO-CY01 cell culture was created.

Table 4-5: Ammonium and lactate inhibition kinetic parameters estimated by nonlinear curve fitting method.

	Lactate Experiment		**Ammonium Experiment**	
	Value	R^2	Value	R^2
$\mu_{max}(h^{-1})$	0.025	0.97	0.025	0.71
$K_{i,Amm}(mM)$	-	-	18.10	0.71
$K_{i,Lact}(g\ L^{-1})$	4.08	0.97	-	-
$\lvert k_d \rvert(h^{-1})$	0.027	0.71	0.022	0.97
$K_{Di,Amm}(mM)$	-	-	9.66	0.97
$K_{Di,Lact}\ (g\ L^{-1})$	2.23	0.71	-	-
$VP_{max}(mg\ L^{-1}\ day^{-1})$	61.5	0.96	60.2	0.99
$K_{P,Amm}\ (mM)$	-	-	7.17	0.99
$K_{P,Lact}(g\ L^{-1})$	1.74	0.96	-	-

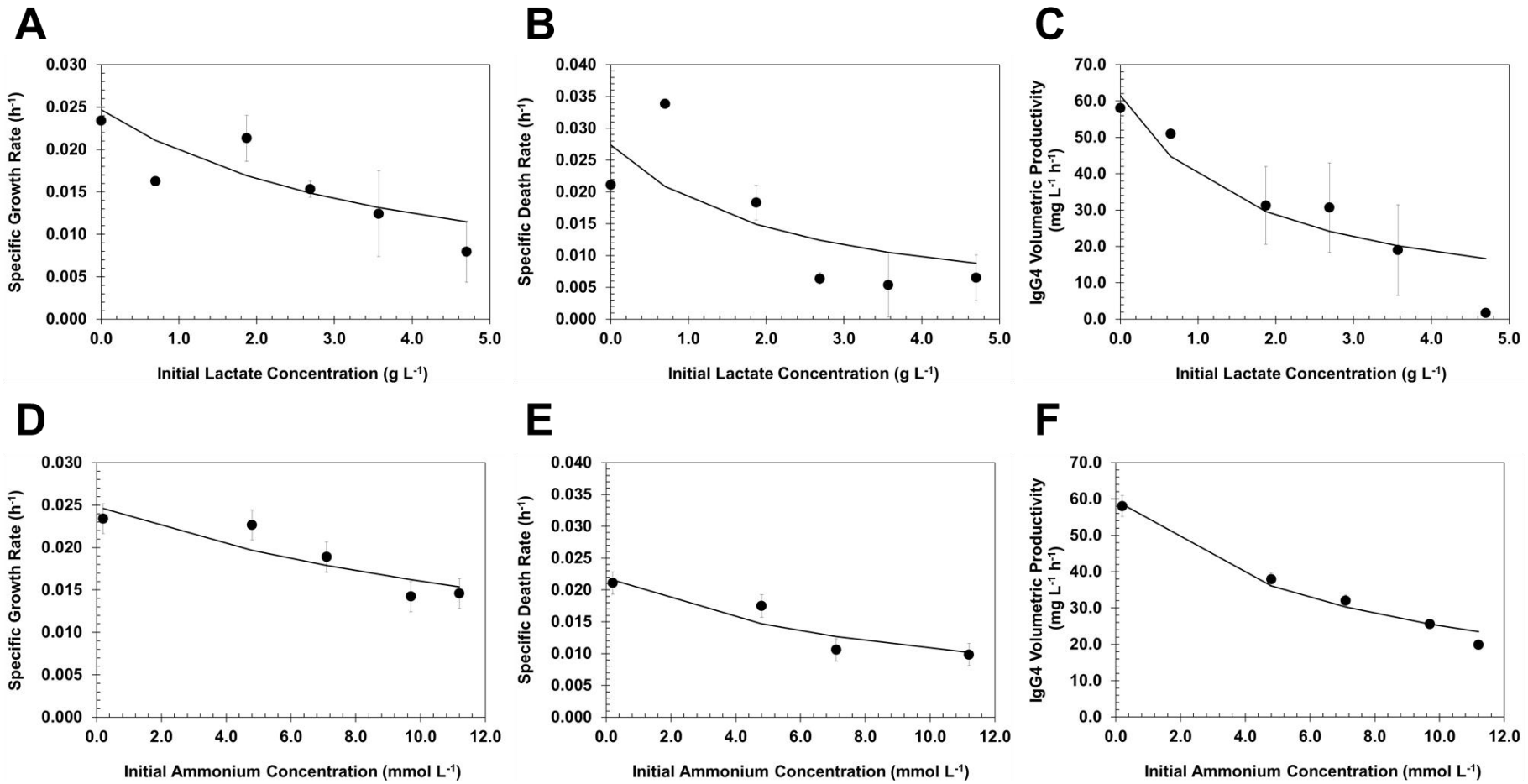

Figure 4-13: Ammonium and lactate inhibition on CHO-CY01 cell culture kinetic parameters: specific growth rate (A, D); specific cell death rate (B, E); and IgG4 volumetric productivity (C, F). The solid line represents the best curve fitting model.

4.3.4. Effects of Osmolality on CHO-CY01 Cell Line Kinetics

Different possibilities exist for approaching a redistribution of mammalian cell metabolism to obtain more efficient cell behaviour in culture. This entails obtaining a culture profile without the severe deregulation of glucose metabolism, leading to limiting conditions in the culture (lactate or ammonium accumulation, media depletion or imbalance, high osmolality) and an inefficient use of medium components. Avoiding or, at least, diminishing this situation should allow increased cell growth and, most probably, higher product concentrations and productivities (Gódia et al., 2006). Mammalian cell culture medium is buffered using the bicarbonate buffer system, and the culture pH is affected by CO_2 and lactate formation. If the base addition is used to compensate for the acid formation, a concurrent increasing osmolality is observed. It has been shown that the culture pH, CO_2, and an increased osmolality may affect productivity and glycosylation (Dezengotita et al., 1998; Gray et al., 1996; Kimura et al., 1996; 1997). Most cell culture media are designed to have an osmolality in the range of 260 – 330 $mOsm\ kg^{-1}$, which is known to be acceptable for most cells (Ozturk et al., 1991a). The impact of osmolality on cell growth is cell-type specific, with CHO cells exhibiting less growth inhibition than hybridoma cells exposed to similar medium osmolality (DeZengotita et al., 1998; Kimura et al., 1997; Kurano et al., 1990a; Ozturk et al., 1991a). Zhu et al. (2005) has observed for CHO cell culture at controlled pCO_2 no change in viable cell density and product titer when elevating osmolality from 316 to 450 $mOsm\ kg^{-1}$. However, further increase of osmolality to 460-500 $mOsm\ kg^{-1}$ caused a decrease of viable cell density (5%) and viability (8%), but no change in the final titer. They have found that it is the combined effect from high pCO_2 and elevated osmolality that caused more stress on the cells. Osmolality compensation by decreasing the concentration of NaCl in the basal medium has been found to partially mitigate the inhibitory effect of elevated pCO_2 on cell growth and protein production by CHO cells (161 $mmol\ L^{-1}$) (DeZengotita et al., 1998; Kimura et al., 1997; Zanghi et al., 1999).

Evaluation of different initial osmolalities through various initial sodium chloride concentrations (118, 108, 103, 99, 95 $mmol\ L^{-1}$) was performed in the CHO-CY01 cell culture. These sodium chloride concentrations match the following initial osmolalities: 335.42, 310.04, 296.07, 285.92 and, 275.06 $mOsm\ kg^{-1}$. The cell culture kinetics can be visualised in Figure 4-14 and Figure 4-15. The culture parameters determined are presented in Table 4-6 and Table C-10. Spearman´s rank correlation coefficients were also computed for all of the different conditions and are presented in Table A-10. It was observed that the lactate concentration relationship with the other cell culture parameters became stronger with the decrease of sodium in the cell culture medium. Ammonium concentration had the same fate, but only in relation with the IgG4, glutamate, and glucose concentrations (Table A-10).

The sodium concentration in the cell culture medium directly affects the osmolality of the medium. The lower the initial sodium chloride concentration, the lower was the initial osmolality. Observing the cell culture growth curve, decreasing initial sodium concentration decreased the μ and IVCC of the CHO-CY01 cell line, but it did not alter the cell viability. Glucose and glutamate consumption rates did not change with the initial sodium chloride concentration. The same can be said about the ammonium profile. However, lactate accumulation decreased with decreasing initial osmolality mainly because of lower cell numbers obtained at lower initial sodium chloride concentrations. Over the range of 95 to 103 mM of sodium chloride, which corresponds to an initial osmolality of 275.06 to 296.07 $mOsm\ kg^{-1}$, the CHO-CY01 cell line growth, metabolism, and antibody productivity did not show any variation. Therefore, CHO-CY01 cells are less sensitive to changes in osmolality than to changes in pH caused by lactate and ammonium accumulation in the cell culture medium.

In summary, a possible osmolality compensation by decreasing the basal sodium chloride (through dilution) concentration, appeared to be harmful to CHO-CY01 cells. The availability of sodium and chloride ions, key components of cellular transport, diminished, which contributed to an arrest of the cell metabolism (glucose, glutamate, lactate and ammonium specific rates almost constant at sub-basal sodium chloride concentration).

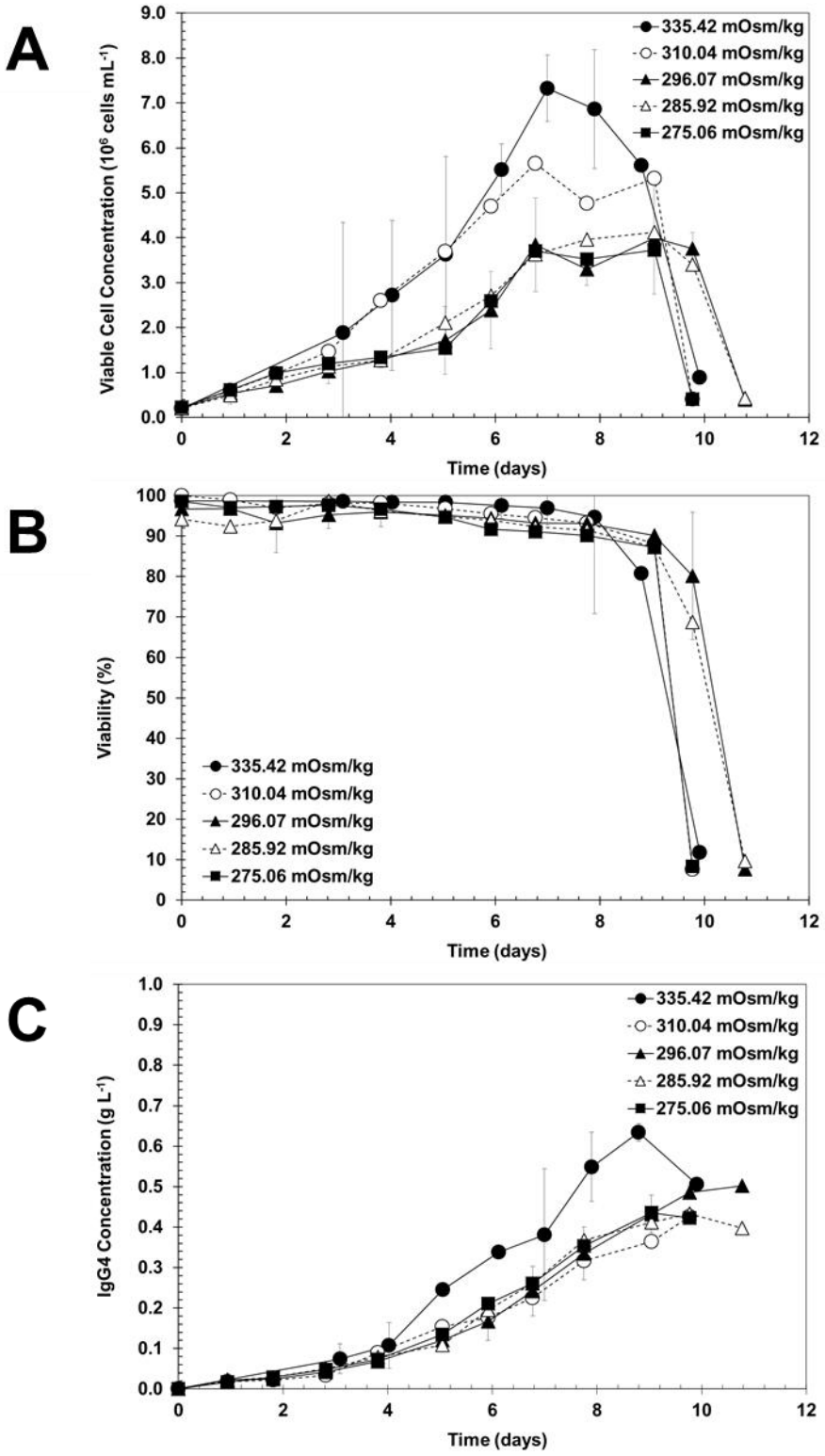

Figure 4-14: Viable cell concentration (A), cell viability (B), and IgG4 concentration (C) profiles for CHO-CY01 cell batch culture at different initial osmolalities (335.42, 310.04, 296.07, 285.92 and, 275.06 $mOsm\,kg^{-1}$) (1 replicate per osmolality). Error bars represent one standard deviation about the mean.

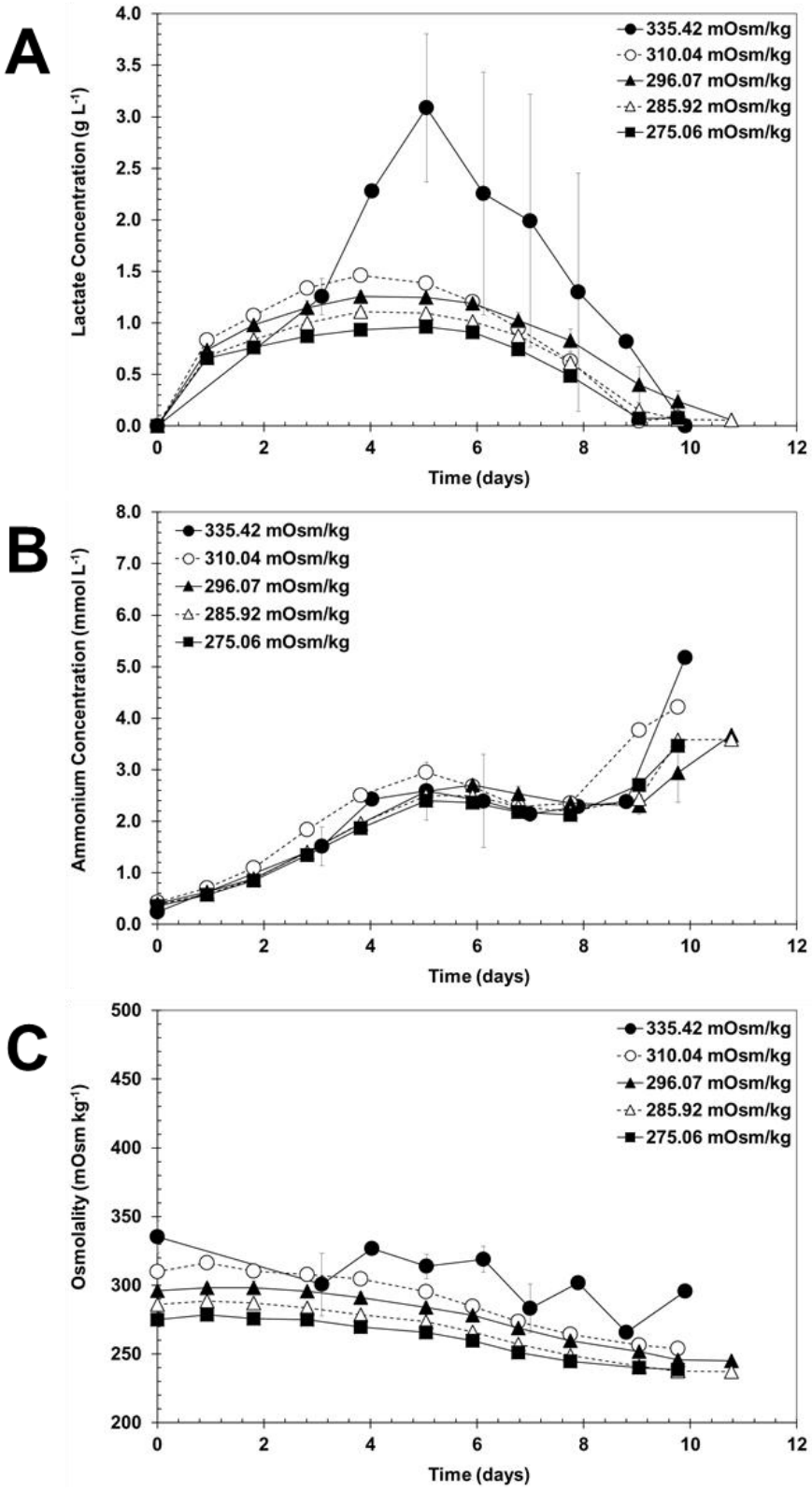

Figure 4-15: Lactate concentration (A), ammonium ion concentration (B), and osmolality (C) profiles for CHO-CY01 cell batch culture at different osmolalities (335.42, 310.04, 296.07, 285.92 and, 275.06 $mOsm\,kg^{-1}$) (1 replicate per osmolality). Error bars represent one standard deviation about the mean.

Table 4-6: Kinetic parameters determined for CHO-CY01 cell batch culture at different initial osmolalities.

Osmolality ($mOsm\ kg^{-1}$)	**275.06**	**285.9**	**296.07**	**310.04**	**335.42**
VP ($mg\ L^{-1}day^{-1}$)	40.5	39.2	41.0 ± 4.1	37.1	58.0 ± 2.8
IVCC ($10^9 cells\ day L^{-1}$)	19.46	23.61	21.68 ± 4.41	30.00	33.65 ± 5.80
$\mu\ (h^{-1})$	0.018	0.018	0.018 ± 0.003	0.022	0.023 ± 0.002
$t_{1/2}\ (h)$	38.7	38.5	39.0 ± 7.2	31.0	29.7 ± 2.3
$q_{mAb}\ (mg\ 10^{-9}\ cells^{-1}\ day^{-1})$	24.24	20.68	24.43 ± 2.63	14.13	20.06 ± 3.02
$q_{Gluc}\ (g\ 10^{-9}\ cells^{-1}\ day^{-1})$	-0.26	-0.24	-0.28 ± 0.05	-0.22	-0.25 ± 0.04
$q_{Glu}\ (mmol\ 10^{-9}\ cells^{-1}\ day^{-1})$	-0.12	-0.11	-0.14 ± 0.02	-0.11	-0.09 ± 0.04
$q_{Na^+}\ (mmol\ 10^{-9}\ cells^{-1}\ day^{-1})$	-0.54	-0.70	-0.79 ± 0.15	-0.57	-0.73 ± 0.66
$q_{K^+}\ (mmol\ 10^{-9}\ cells^{-1}\ day^{-1})$	-0.08	-0.08	-0.11 ± 0.04	-0.08	-0.03 ± 0.01
$q_{Lact}\ (g\ 10^{-9}\ cells^{-1}\ day^{-1})$	0.43	0.41	0.56 ± 0.18	0.38	0.48 ± 0.18
$q_{Amm}\ (mmol\ 10^{-9}\ cells^{-1}\ day^{-1})$	0.17	0.15	0.15 ± 0.01	0.13	0.10 ± 0.01
Lactate produced / Glucose consumed (g/g)	0.52	0.53	0.79 ± 0.25	0.78	0.72 ± 0.11

4.4. Establishment of a Fed-Batch Strategy for Productivity Optimisation

In Section 4.2, the inter scalability was shown between 24 SRW MTP, SF, and 5L-STR in CHO-CY01 cell batch cultures. Since the majority of the industrial cell culture processes are operated in fed-batch or perfusion modes (Chu et al., 2001), it would clearly be of great benefit to have a small-scale model of such culture conditions.

Fed-batch culture can substantially increase the final antibody concentration and culture VP, as compared with batch culture, while retaining the relative simplicity and reliability of batch cell culture. However, the higher titers of fed-batch cultures must be weighted against the extra labour and equipment, and possible contamination, associated with nutrient additions (Bibila et al., 1995; Hu et al., 1997). While the most common approach to develop a feed medium is to concentrate the basal medium, sophisticated optimisation of feed composition and feeding strategy requires consideration of nutrient consumption, by-product accumulation, and the balance between promoting growth versus VP. Several strategies can be followed to minimise by-product accumulation in fed-batch cell cultures. Maintaining low glucose and glutamine concentrations through frequent or continuous feeding can minimise lactate and ammonia accumulation, significantly improving culture performance (Bibila et al., 1995; Li et al., 2010;). For GS-CHO cell lines, the ammonia build-up is far reduced by the elimination of glutamine from the medium (Bibila et al., 1995). Step-wise bolus addition of the feed solution to the production bioreactor is most widely used in industry due to its simplicity and scalability (Li et al., 2010). In general, medium development is labour-intensive and time-consuming. A combination of HT cell culture scale-down systems with statistical design of experiment (DoE) approaches is commonly applied to reduce development time (Li et al., 2010).

In this work, a discrete closed-loop feeding strategy was employed. CHO-CY01 cell culture was fed by the on-line and off-line measurements of cell performance. The goal was to improve the process productivity and minimise the lactate and ammonia build-up, which ultimately improve the CHO-CY01 process performance robustness. This was accomplished by daily feeding with concentrated CD-CHO medium supplemented with glucose (Section 2.1.5). Different fed-batch strategies were tested in small-scale (24-SRW MTPs and SFs) first, and then the best candidates were assessed for productivity and inter scalability in the 5L-STR.

4.4.1. Development of a Suitable Fed-Batch Strategy at Small-Scale

Fed-batch operation at the small-scale, particularly in the microscale, presents challenges in accurate liquid handling and implementation of continuous feeding (Silk et al., 2009). At the microscale, the liquid evaporation from wells becomes more significant over extended culture periods and may lead to increases in culture osmolality. The extended culture

time also makes the maintenance of sterility more difficult. In addition to liquid evaporation, the need for repeated manual intervention for feed addition in the absence of appropriate microwell automation also increases the risk of contamination (Lye et al., 2003). Silk et al. (2009) have developed two feeding strategies for a GS-CHO cell line with the goal of reducing the evaporation rate. One of the feeding strategies involved the addition of bolus feeds of a concentrated basal medium (2% (v/v)) immediately followed by a shot of bicarbonate solution (0.25% (v/v)) for pH control at constant volumes. A second feeding strategy employing diluted feed (4% (v/v)) and bicarbonate solution (2.5% (v/v)) was used to minimise evaporation. Feeding started at day 4 and continued for five consecutive days. Methods to further reduce evaporation rates, in the microwells would be advantageous in removing the need for the use of diluted feeds. The use of thicker or less permeable sealing films, however, would likely result in a reduction in gas–liquid mass transfer rates (Zimmermann et al., 2003).

The first attempt to find an adequate feeding strategy for productivity optimisation was an adaptation of the fed-batch method of Silk et al. (2009). The CHO-CY01 cell line was inoculated in 24-SRW MTP at standard operational conditions (V_L=0.85 mL, 220 rpm and d_s= 25 mm), and when glucose levels went below 2.0 $g\ L^{-1}$, a 5 % (v/v) diluted concentrated feed (see Section 2.1.5 for details) in bicarbonate solution (75 $mM\ Na_2CO_3$ and 50 $mM\ NaHCO_3$) (pH = 10.5) or water was added every day (FB_Strategy 1). By diluting the feed with the bicarbonate solution, the pH control strategy of Silk et al. (2009) was replicated, and at the same time, the number of manual interventions was reduced. The cell culture pH was monitored online through *Presens* Technology (Section 2.2.7). The pH of the concentrated feed (pH = 7.68), diluted feed in water (pH = 8.23), and diluted feed in bicarbonate solution (pH = 9.66) were measured. Therefore, it was expected when feeding the cell culture that pH peaks would be present on the pH profile. The amplitude and duration of such peaks are dependent on the cell culture medium buffer capacity and feed. The first fed-batch strategy for CHO-CY01 cell culture kinetics can be visualised in Figure 4-17, and Table 4-7presents the calculated kinetic parameters. The pH profile for this cell culture is presented in Figure 4-18.

In the carbon source metabolites' profiles (glucose and glutamate), there are three different consumption scopes. During the *lag* phase, there is no glucose or glutamate consumption. In the exponential phase, there was a linear consumption, and when the fed-batch mode initiated, the feeding characteristic peaks emerged. As the feeding was done at constant volume, an accumulation of glucose and glutamate was observed. The excessive amount of glucose may have triggered the Warburg effect on the cells (Lactate produced / Glucose consumed ≈ 1) (Table 4-7). This excessive lactate accumulation added its inhibitory effects to an already osmolality increased cell culture medium from feeding.

With the feeding addition of the diluted feed in the bicarbonate solution, there was an immediate effect on the cell growth as it anticipated the decline phase. The viability dropped

10% in less than 24 hours, and the viable cell numbers started to decrease. To understand which was the responsible agent, the following feeds were performed with diluted feed in water, and a CHO-CY01 cell batch culture with bicarbonate solution addition on day 8 was performed. Clearly, the bicarbonate solution was responsible for initiating the cell death. When the bicarbonate solution was added at day 8 of CHO-CY01 cell batch culture, it caused immediate (less than 24 hours) cell death (data not shown). Therefore, the extra nutrients and other constituents present in the feed helped the CHO-CY01 cells to survive the stress caused by this shot of base. However, the IgG4 productivity was impaired, as the VP and the specific production rate are comparable to the batch cell culture (Table 4-1). Additionally, the osmolality reached values that were intolerable for cell survival and antibody production. The 24-SRW MTP evaporation rate was similar to the batch mode ($19 \pm 9\ \mu L\ day^{-1}$) (Table 4-7). Therefore, it has been proved once again that the CR1524a ´Duetz system` lid is the correct closure system for batch or fed-batch CHO-CY01 cell cultures.

In this first attempt at employing fed-batch mode with the CHO-CY01 cell line, a lesson was learned. This GS-CHO cell line does not need to have such harsh pH control correction. The feed used is alkaline, so when adding bicarbonate, the feed became, even more, alkaline. Therefore, feeding the CHO-CY01 cell line is considered as a pH perturbation to the cell culture pH.

From the online monitoring of the pH and temperatures of the 24-SRW MTP CHO-CY01 cell line culture, three types of pH perturbations (peaks) were identified (Figure 4-18): sampling (pH peak A), feeding addition of diluted feed in bicarbonate solution (pH peak B), and feeding addition.(pH peak C).

Osman et al. (2002) have described the pH perturbations with four main characteristics: amplitude, duration, frequency, and number (Figure 4-16). The amplitude, duration, and the pH values before and after the pH perturbation for the three types of pH perturbations are presented in Table 4-8. The frequency of any pH perturbation was approximately one day, and the number of pH perturbations to the cell culture is equal to the number of culture days.

Temperature is associated with these pH peaks, as the signal of the optical sensor depends on temperature. When the CO_2 incubator door is open for sampling or feeding, the temperature decreases and at the same time, CO_2 diffuses out of the incubator. As the pH of the buffer for cell cultivation is regulated by the CO_2 atmosphere in the incubator, this leads to a higher pH within the sample. The pH perturbation that sampling creates cannot be eliminated, but can be minimised with shorter times of the incubator door opened. The amplitude of these perturbations is within the measurement precision error. For those reasons, sampling pH perturbation is considered to have a negligible effect on CHO-CY01 cell cultures.

When feeding CHO-CY01 cells with a diluted bicarbonate solution or water, these pH perturbations have an effect on the cells. The best feed will be the one with the smaller pH perturbation amplitude and duration, as well as lower pH before feeding is restored. Regarding this and cell kinetics, the ideal fed-batch method for small-scale CHO-CY01 cell line cultures is feeding additions of the water-diluted concentrated basal medium. Another point to note is that the daily constant volume feed strategy is not suitable: it does not promote metabolic efficiency in the CHO-CY01 cells, leading to glucose accumulation, and is expensive in view of scale up.

As a result, a new fed-batch methodology for small-scale systems, i.e. 24-SRW MTP and SFs, was developed in this work. The strategy is to customise the amount of feed to the requirements of the cells with the goal of productivity optimisation. In the next section, the correct amount of glucose to achieve higher IgG4 productivity and to lower the accumulation of waste by-products will be determined.

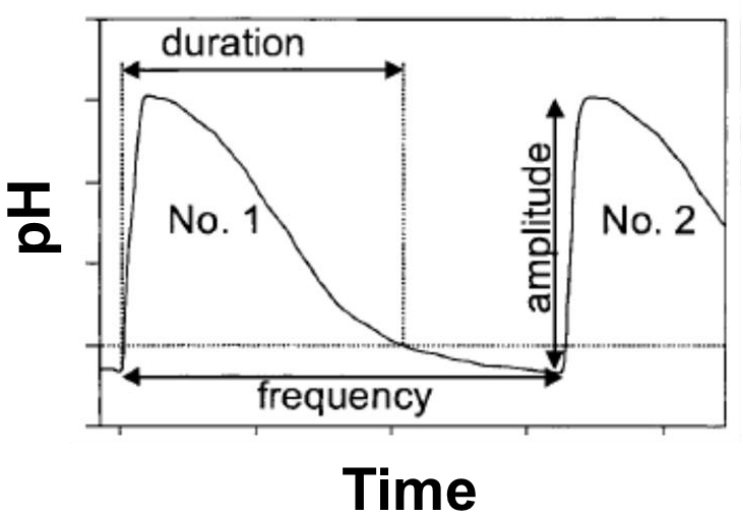

Figure 4-16: Definition of a typical pH perturbation amplitude, duration, frequency, and number. Image adapted from (Osman et al., 2002).

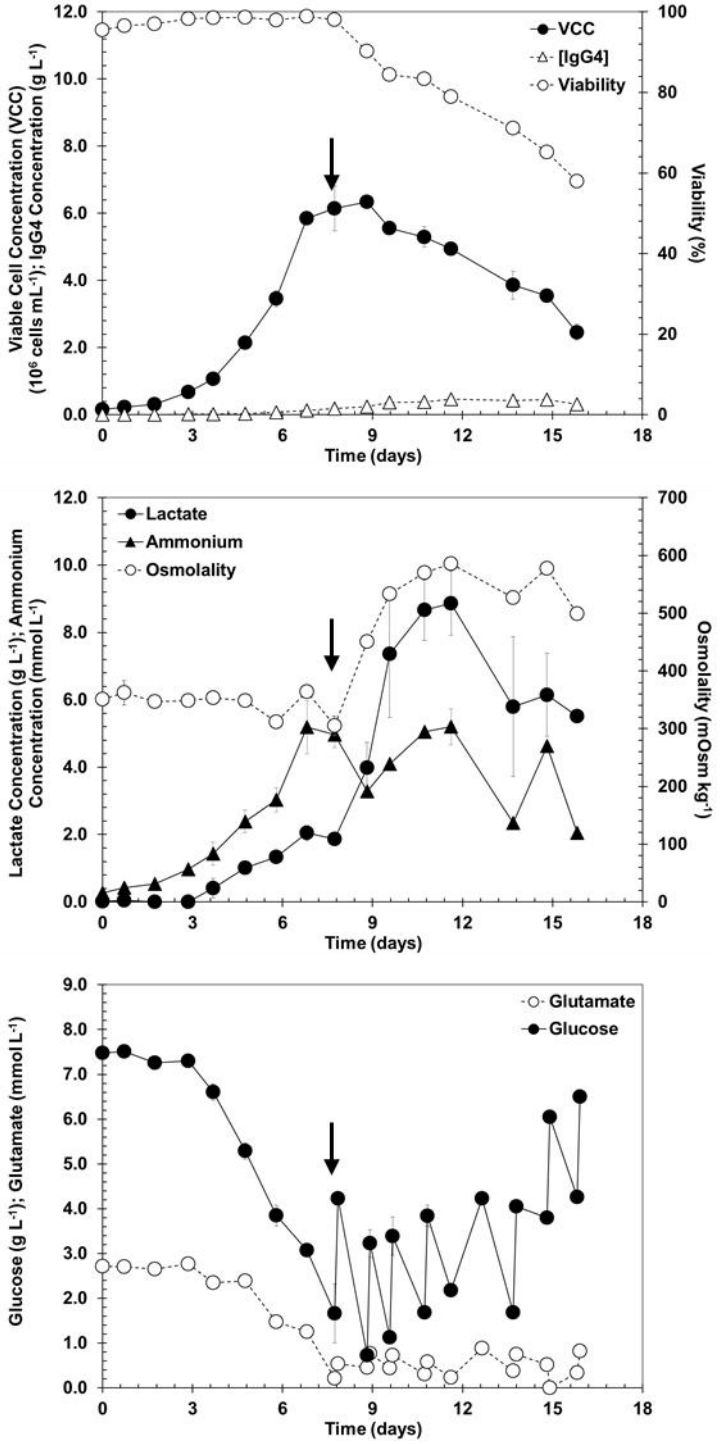

Figure 4-17: Viable cell concentration, viability, IgG4, lactate, ammonium, glucose and glutamate concentrations, and osmolality profiles for the first fed-batch strategy for CHO CHO-CY01 cell culture in 24-SRW MTP (1 run (3-4 replicates)) shaken under standard conditions (FB_Strategy 1). The arrow indicates when the feeding started. Error bars represent one standard deviation about the mean.

Table 4-7: Kinetic parameters determined for the first fed-batch strategy (FB_Strategy 1) for CHO CHO-CY01 cell culture in 24-SRW MTP shaken under the standard.

	FB_Strategy 1
VP ($mg\ L^{-1}day^{-1}$)	28.0
IVCC ($10^9\ cells\ day\ L^{-1}$)	54.94
$\mu\ (h^{-1})$	0.023
$t_{1/2}\ (h)$	30.7
$q_{mAb}\ (mg\ 10^{-9}\ cells^{-1}\ day^{-1})$	8.88
$q_{Gluc}\ (g\ 10^{-9}\ cells^{-1}\ day^{-1})$	-0.42
$q_{Glu}\ (mmol\ 10^{-9}\ cells^{-1}\ day^{-1})$	-0.10
$q_{Lact}\ (g\ 10^{-9}\ cells^{-1}\ day^{-1})$	0.85
$q_{Amm}\ (mmol\ 10^{-9}\ cells^{-1}\ day^{-1})$	0.09
Lactate produced / Glucose consumed (g/g)	0.53
Evaporation rate ($\mu L\ day^{-1}$)	18.24 ±1.19

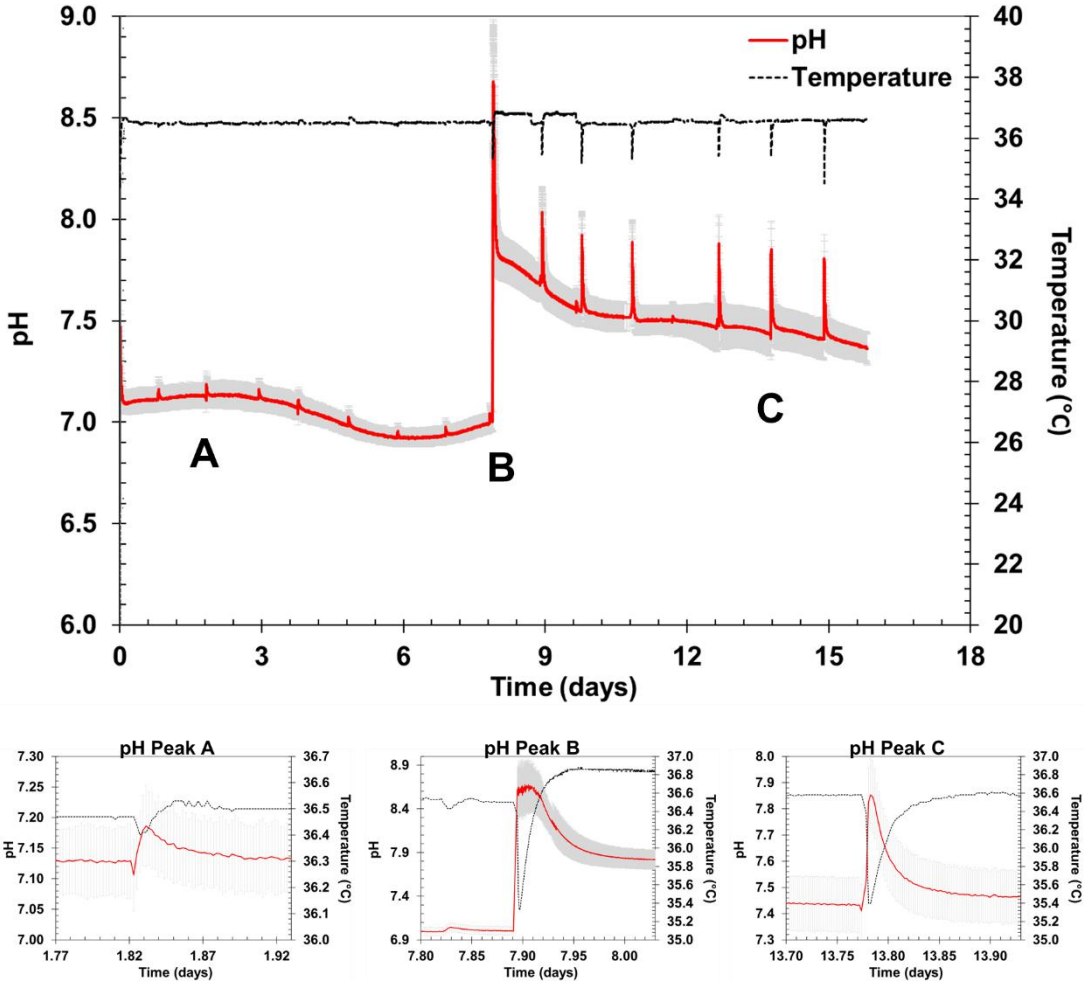

Figure 4-18: pH and temperature profiles for the first fed-batch strategy for CHO CHO-CY01 cell culture in 24-SRW MTP shaken under standard conditions. In the pH profile, three different peaks were observed: sampling (A); diluted feed in bicarbonate solution feeding addition (42.5 µL) (B); and diluted feed in water feeding addition (42.5 µL) (C).

Table 4-8: Amplitude and duration of the three types of pH perturbations in the first fed-batch strategy for CHO CHO-CY01 cell culture in 24-SRW MTP shaken under standard conditions with the pH values before and after the pH perturbation.

	Amplitude	Duration (hours)	pH Before Perturbation	pH After Perturbation
pH peak A	0.08	1.8	7.11	7.13
pH peak B	1.65	3.3	7.00	7.82
pH peak C	0.44	2.6	7.41	7.47

4.4.2. Determination of the Correct Glucose Concentration in CHO-CY01 Cell Line Fed-Batch Culture

The objective of a fed-batch mode in mammalian cell culture is to keep the cell numbers at the maximum viable cell number for as long as possible. At this stationary phase, cells are triggered to use glucose and other nutrients for antibody production and so, the focus is not on cell division. However, if too much glucose is given, cells will divert the glucose to produce lactate (Warburg effect), becoming less metabolically efficient. Concurrently, if too much glutamate is added, there is a higher ammonium accumulation (GDH pathway). However, since the glucose concentration is eight times greater than the glutamate concentration in the feed used, the focus for developing a fed-batch suitable for productivity optimisation in CHO-CY01 cell culture will be on the glucose concentration. It is important to highlight that this is a very simplistic approach, since the amino acids, vitamins, trace elements, inorganic salts, lipids, and growth factors are also present in the feed, as well (Birch et al., 2006).

Four different fed-batch strategies that manipulated the glucose concentration inside the CHO-CY01 cell culture medium were tested. Figure 4-19 presents the glucose profiles. There were two main lines of thought in these fed-batch strategies. The first was to give a high concentration of glucose while the viable cell number increased, followed by a lower glucose concentration (Strategies 2 and 3). The second was to maintain glucose concentration after feeding around a maximum concentration (Strategies 4 and 5). The details of each fed-batch strategy are provided below:

- Fed-Batch Strategy 2: Once the cells reached glucose levels below 2.00 $g\ L^{-1}$, feed was added. Glucose concentration was topped up in the first feeds to 5.00 $g\ L^{-1}$. Once the viable cell number started to decline (day 10), glucose top-up was reduced to 3 $g\ L^{-1}$.
- Fed-Batch Strategy 3: Once the cells reached glucose levels below 3.00 $g\ L^{-1}$, feed was added. Glucose concentration was topped up in the first feeds to 6.00 $g\ L^{-1}$. Once the viable cell number started to decline (day 9), glucose top-up was reduced to 4.00 $g\ L^{-1}$.
- Fed-Batch Strategy 4: Once the cells reached glucose levels below 2.00 $g\ L^{-1}$, feed was added. Glucose concentration was always topped up to 2.00 $g\ L^{-1}$.
- Fed-Batch Strategy 5: Once the cells reached glucose levels below 3.00 $g\ L^{-1}$, feed was added. Glucose concentration was always topped up to 3.00 $g\ L^{-1}$.

The difference between fed-batch Strategies 2 and 3 is that glucose concentration in the cell culture medium with fed-batch Strategy 3 was $1.00\ g\ L^{-1}$ higher than in fed-batch Strategy 2. The same difference was established between fed-batch Strategies 4 and 5.

In Figure 4-20 and Figure 4-21 are shown the kinetics for the four fed-batch strategies for CHO-CY01 cell fed-batch cultures in SF 125 mL and SF 250 mL. The calculated kinetic parameters are presented in Table 4-8. This fed-batch strategy test was performed in SFs, as they are the traditional cell culture vessel for such studies and are easier to operate than 24-SRW MTP, although they are associated with higher medium costs. Most importantly, from Section 4.2 it is known that CHO-CY01 cell batch cultures in 24-SRW MTP, SF 125 mL, SF 250 mL, and 5L-STR are equivalent at the operating conditions used. The CHO-CY01 cell fed-batch cultures in these four bioreactor scales were verified, as well, and the results are presented in Section 4.4.3. It was established for all scales the harvest criteria of 70 % of cell viability.

For the scope of this work, the ´best` fed-batch strategy will be the one that combines the following factors:

- Balance between promoting growth versus VP
- Low lactate accumulation (less than $K_{i,Lact}$)
- Low ammonium accumulation (less than $K_{i,Amm}$)

The first observation made is that the CHO-CY01 cell fed-batch cultures in SF 125 mL are equivalent to SF 250 mL cultures. The minor differences observed in the cell culture parameters were most likely due to batch-to-batch variability. CHO-CY01 cells during fed-batch Strategies 2 and 3 had a longer exponential phase driven by the excessive glucose concentration present, and the maximum of viable cell counts reached was lower than in Strategies 3 and 4. The feeding in Strategies 2 and 3 caused an immediate cell viability drop. This latter fact suggests a glucose inhibition of the CHO-CY01 cell growth. Also, Kurano et al. (1990b) have shown non-competitive inhibition kinetics for glucose in the CHO cell line with a half-maximum-rate concentration of glucose for cell growth rate of $5.03 \pm 1.54\ g\ L^{-1}$. In relation to IgG4 production, the fed-batch strategies have changed the IgG4 production profiles in the CHO-CY01 cell line. In all of the fed-batch strategies, the final IgG4 concentrations were almost double the one in batch mode (0.5 $g\ L^{-1}$). In the strategies with constant glucose, the IgG4 production had a linear relationship with the culture time. However, in Strategies 2 and 3, the cells produced almost 60% of the final IgG4 concentration around the end of the exponential phase, with the remaining IgG4 produced during the stationary phase. Therefore, in Strategies 2 and 3, the cells were quicker (high VP) than in Strategies 4 and 5. On the other hand, the longer the IgG4 remains in the cell culture environment, the higher is the risk of

affecting the product quality (Del Val et al., 2010). Lactate accumulation and ammonium accumulation in any fed-batch strategy did not reach inhibitory concentrations. In Strategies 2 and 3, the accumulations of waste by-products were equal to each other, but were higher than in Strategies 4 and 5. The higher volume of feed added to the CHO-CY01 cell culture in Strategies 2 and 3 produced severe changes in the medium osmolality, which caused osmotic stress in the cells. Another point to raise is the volume of feed required for the four different fed-batch strategies. For Strategies 2 and 3, the total volume of feed added was more than half of the initial bioreactor volume, and for Strategies 4 and 5, it was only 30%. It is also important to keep the added feed volume low to prevent a change in the hydrodynamic environment in the cell culture, dilution of nutrients, bioreactor overflow, and excessive material costs.

In Strategy 3, there was an increase in the VP (~11%) and IVCC (~17%) in comparison with Strategy 2. This indicates that the increase in IgG4 production was exclusively due to a higher number of viable cells, not because the cells are more efficient at metabolising the glucose. In contrast, in Strategy 5, the VP increased 24%, and IVCC increased 4% compared with Strategy 4, which implies that establishing a constant glucose top-up threshold of 3 $g\ L^{-1}$ made the CHO-CY01 cells more metabolically efficient.

Subsequently, it was found that the maximisation of IgG4 production by CHO-CY01 cells was with the fed-batch strategies with the constant glucose concentration top-up of 2.00 $g\ L^{-1}$ (FB2) or 3.00 $g\ L^{-1}$ (FB3) . Those fed-batch strategies were the ones chosen to proceed for the inter scalability of CHO-CY01 cell fed-batch cultures test (next section).

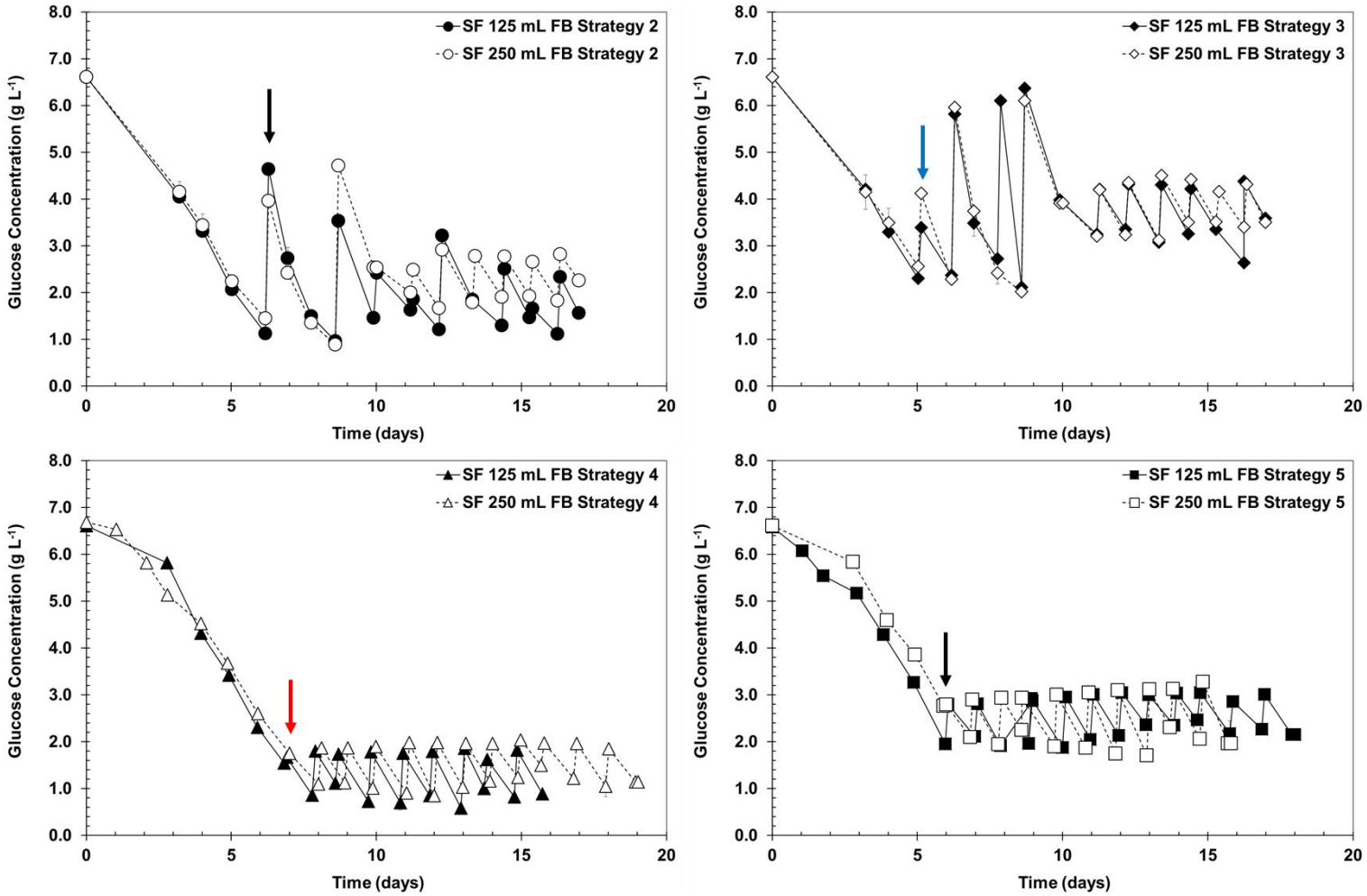

Figure 4-19: Glucose profiles for the four different fed-batch strategies tested for CHO-CY01 cell cultures in SF 125 mL (2 replicates) and SF 250 mL (2 replicates). The arrow indicates when the feeding started (FB Strategy 3 – blue; FB Strategy 2 and 5 – black; FB Strategy 4 – red). Error bars represent one standard deviation about the mean.

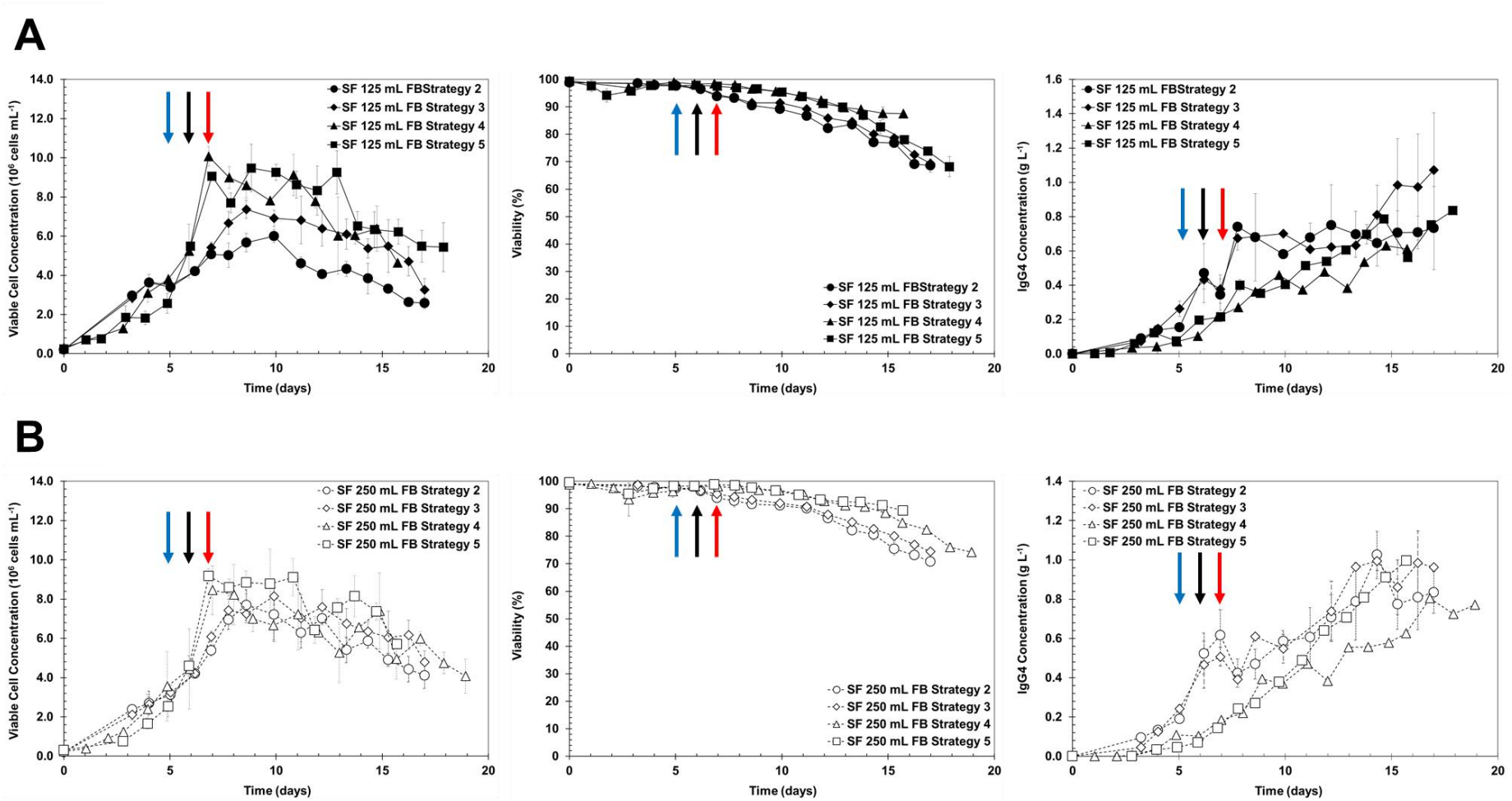

Figure 4-20: Viable cell concentration, viability, and IgG4 concentration profiles for the four fed-batch strategies for CHO-CY01 cell fed-batch cultures in SF 125 mL (2 replicates) (A) and SF 250 mL (2 replicates) (B). The arrow indicates when the feeding started (FB Strategy 3 – blue; FB Strategy 2 and 5 – black; FB Strategy 4 – red). Error bars represent one standard deviation about the mean.

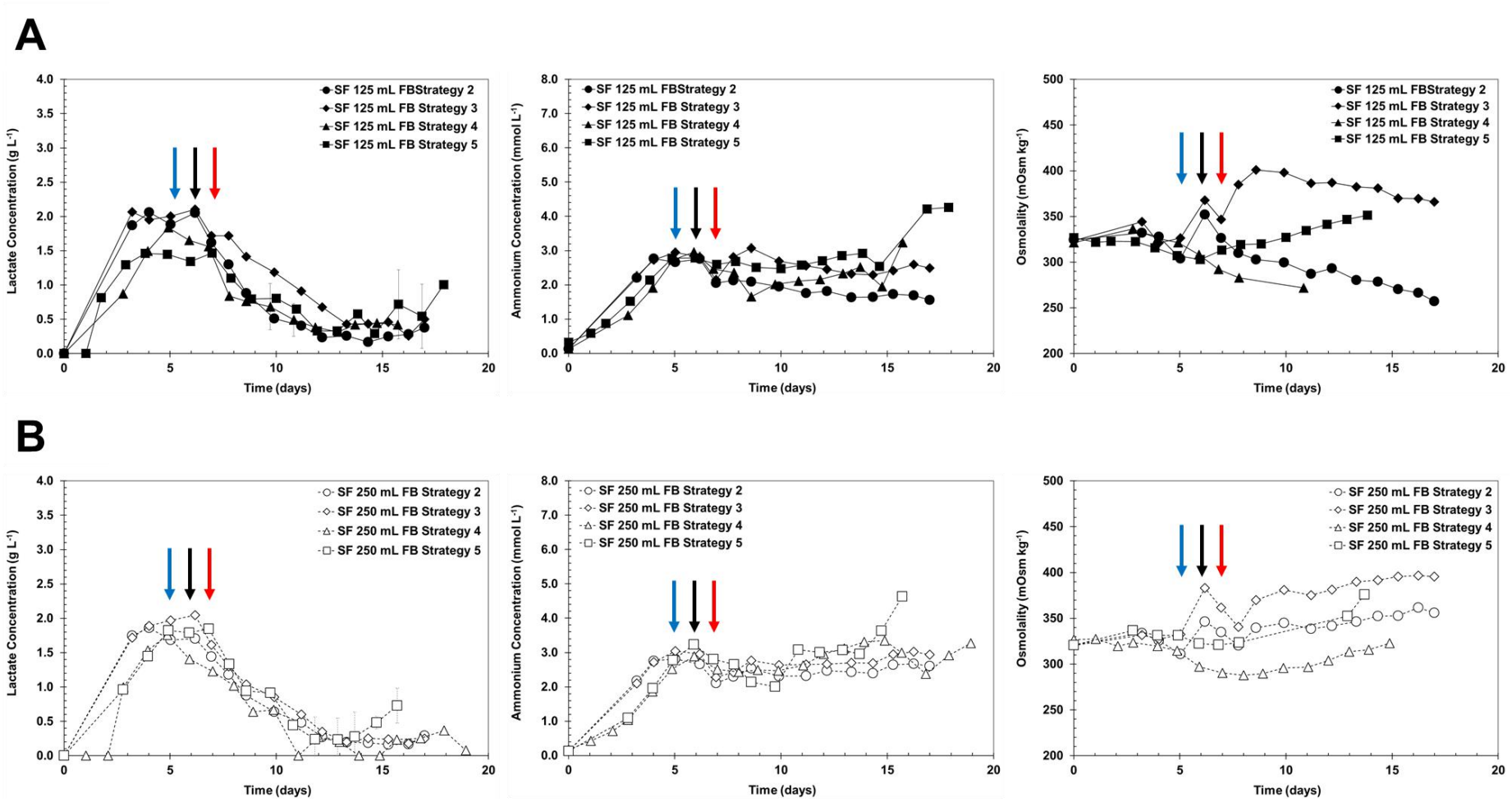

Figure 4-21: Lactate concentration, ammonium ion concentration, and osmolality profiles for the four fed-batch strategies for CHO-CY01 cell fed-batch cultures in SF 125 mL (2 replicates) (A) and SF 250 mL (2 replicates) (B). The arrow indicates when the feeding started (FB Strategy 3 – blue; FB Strategy 2 and 5 – black; FB Strategy 4 – red). Error bars represent one standard deviation about the mean.

Table 4-9: Kinetic parameters determined for the four fed-batch strategies for CHO-CY01 cell fed-batch cultures in SF 125 mL and SF 250 mL.

	FB Strategy 2		***FB Strategy 3***		***FB Strategy 4 (FB2)***		***FB Strategy 5 (FB3)***	
	SF 125 mL	**SF 250 mL**	**SF 125 mL**	**SF 250 mL**	**SF 125 mL**	**SF 250 mL**	**SF 125 mL**	**SF 250 mL**
VP ($mg\ L^{-1}day^{-1}$)	52.0	56.4	59.3	61.4	37.1	39.4	44.4	50.1
IVCC ($10^9\ cells\ day\ L^{-1}$)	63.59	78.77	80.69	86.14	87.08	93.67	101.87	86.04
$\mu\ (h^{-1})$	0.018	0.020	0.021	0.019	0.022	0.022	0.022	0.019
$t_{1/2}\ (h)$	37.7	34.1	33.6	36.3	32.2	31.1	31.5	36.1
$q_{mAb}\ (mg\ 10^{-9}\ cells^{-1}\ day^{-1})$	14.01	12.87	13.24	13.26	7.38	8.61	8.46	10.98
$q_{Gluc}\ (g\ 10^{-9}\ cells^{-1}\ day^{-1})$	-0.26	-0.23	-0.31	-0.25	-0.17	-0.18	-0.16	-0.19
$q_{Glu}\ (mmol\ 10^{-9}\ cells^{-1}\ day^{-1})$	-0.08	-0.05	-0.06	-0.05	-0.05	-0.04	-0.04	-0.05
$q_{Lact}\ (g\ 10^{-9}\ cells^{-1}\ day^{-1})$	0.27	0.20	0.27	0.21	0.17	0.15	0.17	0.19
$q_{Amm}\ (mmol\ 10^{-9}\ cells^{-1}\ day^{-1})$	0.037	0.042	0.042	0.044	0.036	0.041	0.039	0.051
Lactate produced / Glucose consumed (g/g)	0.63	0.59	0.24	0.21	0.58	0.58	0.24	0.35
$\mu_d\ (h^{-1})$	-0.0046	-0.0031	-0.0032	-0.0025	-0.0030	-0.0020	-0.0021	-0.0017
Feed volume (% of reactor working volume)	58	54	97	70	29	34	37	36

4.4.3. Inter Scalability of CHO-CY01 Cell Fed-Batch Cultures

In the previous section, the preliminary conclusion was reached that, in SFs, the fed-batch strategies at constant glucose concentration (2.00 or 3.00 $g\ L^{-1}$) were more beneficial to the cells for producing more IgG4. In this section, these two fed-batch strategies were applied to CHO-CY01 cell line cultures in 24-SRW MTP and 5L-STR. In this way, the inter scalability of two fed-batch strategies were tested, which is important for building the scale-down model of the CHO-CY01 cell line culture in 5L-STR.

In Figure 4-22 to Figure 4-24, the CHO-CY01 cell line fed-batch culture kinetics for fed-batch Strategies 4 and 5 can be visualised for all of the bioreactor scales. In Table 4-9, Table 4-10, Table 4-11 and Table C-11 are presented the determined kinetic parameters for all of these CHO-CY01 cell cultures. A particle size distribution comparison between scales was also performed and can be visualised in Figure B-4 and Table B-4 for fed-batch Strategy 4 (FB2), and in Figure B-5 and Table B-5 for fed-batch Strategy 5 (FB3). The correlation coefficients were also determined and are presented in Table A-12. For the 5L-STR, the online process parameters, such as pH, dissolved oxygen, temperature, volume of base added, and computed CO_2 volume percentage are presented in Figure D-4: for fed-batch Strategy 4 (FB2) and Figure D-5: for fed-batch Strategy 5 (FB3).

In all bioreactor scales, the CHO-CY01 cells have an initial *la*g phase, followed by the exponential phase for around six days, and an approximately three-day stationary phase with a slow decrease in the viable cell numbers at its end. This same division in the cell growth was observed in the particle size distributions for both fed-batch strategies. The four stages defined for CHO-CY01 cell batch cultures continued to be found (Section 3.2.4): adaptation period, exponential period, beginning of decline period, and decline period. However, a new stage was considered to describe the stationary phase, called the stationary period. In this stage, the viable cell numbers reach the maximum, cell diameter increases, debris is maintained below 10%, the concentration of larger particles (>40 µm) almost doubles, and it marks the beginning of the dead cells' population decline.

Regarding the fed-batch strategies, when the glucose level was topped-up to 3.00 $g\ L^{-1}$ (FB3), the maximum viable cell concentration was 5% higher than for the fed-batch strategy with glucose top-up levels of 2.00 $g\ L^{-1}$ (FB2), but with a 32% increase in the IgG4 peak concentration ($1.00 \pm 0.13\ g\ L^{-1}$). Moreover, the stationary phase was more prolonged for the fed-batch Strategy 5. In Section 4.2.1, it was shown with the cell cycle analysis that CHO-CY01 cells in the stationary phase produced the highest amounts of IgG4. CHO-CY01 cells in the 5L-STR presented a slightly lower cell viability due to the extra cell damage components that exist in a STR, impeller, and air bubbles. In the shaken bioreactors (24-SRW MTP and SFs), the cell viability decay along the cell culture time was very similar. The fed-

batch strategy does not have a direct impact on this parameter. Regarding inter scalability, 24-SRW MTP, 125 mL SF, and 250 mL SF are considered as good scale-down models of CHO-CY01 cell fed-batch culture (FB2 & FB3) cell growth and IgG4 production with less variation regarding fed-batch Strategy 5 (FB3) (6% variation). In terms of carbon source utilisation, as expected the CHO-CY01 cells were fed earlier in the fed-batch Strategy 5 (FB3). Once the feeding started, CHO-CY01 cells exhibited different glucose and glutamate consumption rates during feeding for the various fed-batch strategies (Table 4-10). Cells in 5L-STR consumed glucose and glutamate almost twice as fast compared with the shaken cultures. Therefore, in terms of inter scalability, 24-SRW MTP, 125 mL SF, and 250 mL SF under-estimate this parameter. Nonetheless, CHO-CY01 cells showed a higher glucose and glutamate consumption rate during feeding with a higher glucose top-up threshold established in the fed-batch strategy (FB3/FB2 (Glucose) = $1.34 \pm 0.39\ g\ L^{-1}\ day^{-1}$), regardless of the scale.

The CHO-CY01 cell line IgG4 productivity differed with the fed-batch strategies. The fed-batch Strategy 5 (FB3) improved 35% of the q_{mAb} across all of the scales. Moreover, when compared with CHO-CY01 cell batch culture values for q_{mAb} in 5L-STR, for instance, there was a 39% increase with FB2 and 59% with FB3 (Table 4-1). The CHO-CY01 cells in the FB2 generated more IgG4 for 24-SRW MTP and SF cultures than for 5L-STR. The 5L STR CHO-CY01 cell cultures were controlled by pH (7.1), temperature (37.0°C), and dissolved oxygen (30.0% air saturation), while the other bioreactors were only controlled by temperature (37.0°C). For 5L-STR, the pH control is accomplished by manipulating the amount of CO_2 and base added to the system. A profound effect on cell growth and productivity, when there is elevated CO_2 accumulation with high osmolality derived from base additions, has been reported (Zhu et al., 2005). Furthermore, the feeding process is itself a pH perturbation to the pH system (pH peaks in Figure D-4: and Figure D-5:) (Section 4.4.1). Therefore, it seems that the 5L-STR pH controller caused a sub-production of IgG4, accumulation of lactate and ammonium, and elevated osmolality (Figure 4-23). This divergent CHO-CY01 cell behaviour was more pronounced for FB2, where the CHO-CY01 cells were exclusively lactate producers. However, they overestimated by 20% the IgG4 production for CHO-CY01 cell cultures with fed-batch Strategy 4 (FB2), while with fed-batch Strategy 5 (FB3) the peak IgG4 concentration is accurately estimated.

For FB2, CHO-CY01 cells were daily faced with near glucose depletion followed by a shot of 2.00 $g\ L^{-1}$ of glucose, while for FB3, there was always a residual glucose concentration of 1.00 $g\ L^{-1}$. This type of metabolic stress may have prompted the cells towards the apoptotic pathway and cell death. This can be visualised by the appearance of ´dead cell` populations towards the end of the CHO-CY01 cell culture (days 13-19) in the particle size distribution

(Figure B-4). Those ´dead cells` population were most likely apoptotic bodies, since CHO cells in fed-batch mode inside a 5L-STR have been reported to be due to apoptosis (Suberbie, 2013).

It is in the profiles of the waste by-products that the difference of bioreactor operating scales is shown. For 5L-STR, CHO-CY01 cells in the fed-batch Strategy 4 (FB2) were no longer lactate consumers, which led to an excessive lactate accumulation beyond the $K_{i,Lact}$.value. The reason for this highly glycolytic glucose flux resides with the cells' management of continuous base addition (Figure D-4:). The occasional high glutamate concentration in the basal medium reinforced with feed addition, in the FB2 CHO-CY01 cell line culture, pushed the cells to produce more ammonium through the GDH pathway, yet this was not true for values higher than 3.2 mM, where the GDH pathway favours glutamate production. The accumulation of these waste by-products may cause the IgG4 productivity inhibition at this scale. At FB3, CHO-CY01 cells showed a reduced lactate accumulation around the $K_{i,Lact}$ value, but the cells were not consuming the lactate at the same rate as the shaken bioreactors. CHO-CY01 cells in the 24-SRW MTP, SF 125 mL, and SF 250 mL achieved the ideal lactate profile in both fed-batch strategies. This is characterised by limited lactate synthesis during the initial growth phase, of no more than 2.7 $g\ L^{-1}$, followed by lactate consumption. The ammonium profile in FB3 CHO-CY01 cell line cultures was similar among all scales, due to the same initial glutamate concentration. During the exponential phase, cells are producing ammonium as soon as the feeding begins there is the utilisation of ammonium for the initiation of the various nitrogen metabolic pathways. During the stationary phase, the ammonium production and consumption is in equilibrium. Once the viable cell concentration started to decrease and cell viability fell below 80%, there was an increase in ammonium concentration due to cell breakage. Therefore, for FB3 the harvest criteria can be set to be 80% cell viability in order to avoid further ammonium accumulation.

The excessive waste by-products plus the base addition with elevated CO_2 (< 10% (v/v)) at the 5L-STR scale resulted in a raised osmolality with CHO-CY01 cell fed-batch cultures time. For 24-SRW and SFs, the CHO-CY01 cell culture medium osmolality was maintained at a constant value with any fed-batch cell culture. The osmolality in the 24-SRW MTP CHO-CY01 cell fed-batch cultures (FB2 & FB3) was marginally higher than in the SF because of a higher evaporation rate.

24-SRW MTP, 125 mL SF, and 250 mL SF are not useful scale-down models for CHO-CY01 cell fed-batch cultures' (FB2 & FB3) lactate and osmolality profiles. However, for FB3, they manage to describe accurately the CHO-CY01 cell line ammonium profile.

Once more, at the 5L-STR scale, a very strong correlation was found between the CO_2 level and CHO-CY01 cell growth, IgG4 productivity, and cell metabolism. Additionally, the

connection between base addition and lactate accumulation (r = 0.70) was established for the FB2 cell culture, which corroborates the highly glycolytic flux hypothesis (Table A-12).

Subsequently, when the CHO-CY01 cell line was grown in different bioreactor scales, all with similar mixing times and energy dissipation rates, it was found that CHO-CY01 cells prefer the fed-batch strategy with constant glucose concentration topped-up to 3.00 $g\ L^{-1}$ (FB3) in order to maximise the IgG4 formation. Also, 24-SRW MTP, 125 mL SF, and 250 mL SF CHO-CY01 cell fed-batch cultures (FB2 & FB3) are statistically equivalent ($p > 0.05$) for all cell culture parameters. However, 24-SRW MTP, 125 mL SF, and 250 mL SF were found to be a good scale-down model of 5L-STR CHO-CY01 cell fed-batch cultures in terms of cell growth and IgG4 productivity, but they cannot replicate the waste by-products profiles, as they are not pH-controlled systems.

.

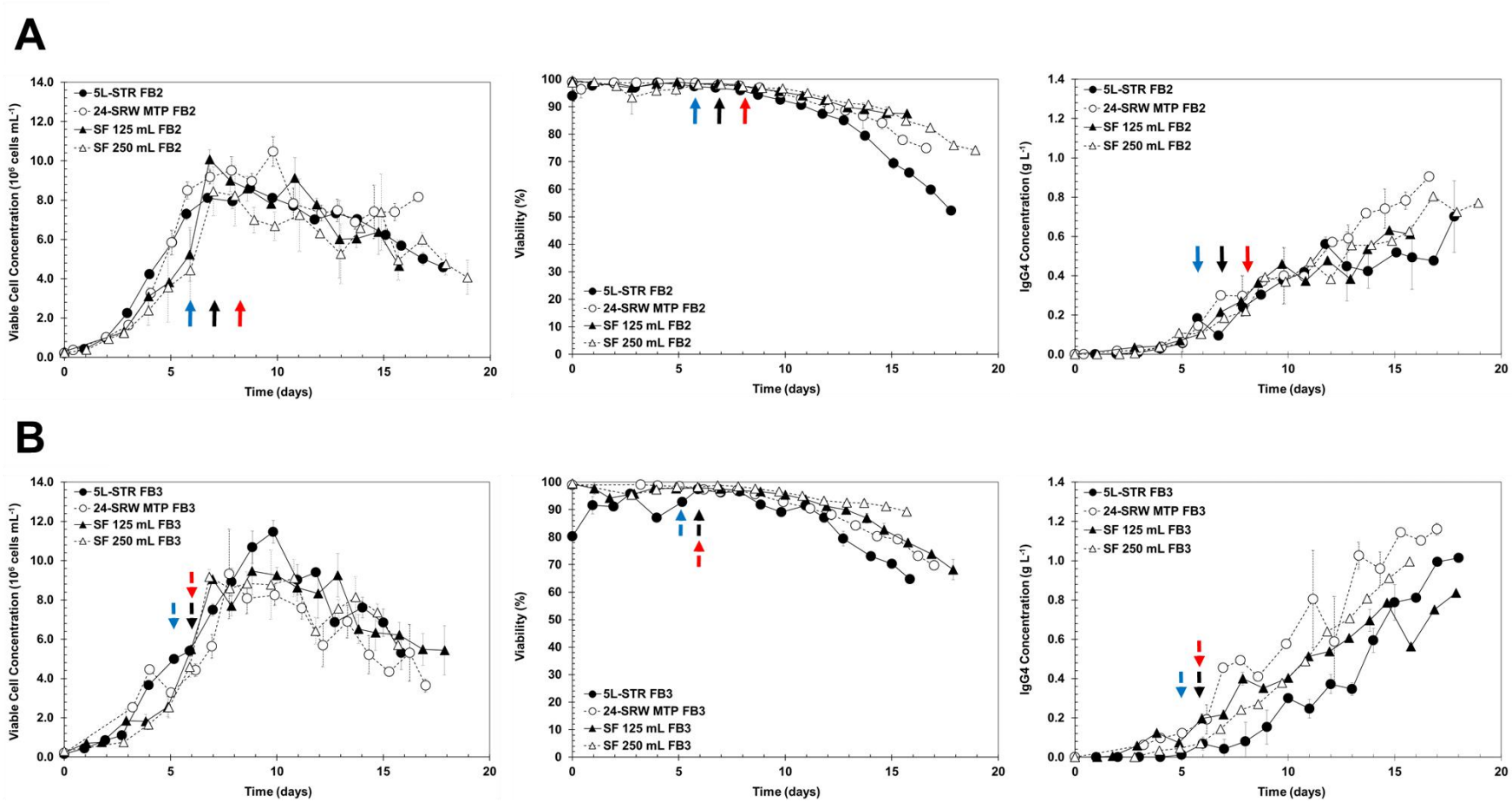

Figure 4-22: Viable cell concentration, viability, and IgG4 concentration profiles for CHO-CY01 cell line fed-batch strategy 4 (FB2) (A) and fed-batch strategy 5 (FB3) (B) cultures at different bioreactor scales: 5L-STR (1 replicate); 24-SRW MTP (1 run (3-4 replicates)); SF 125 mL (2 replicates); and SF 250 mL (2 replicates). The culture´s operating conditions were the standard. The arrow indicates when the feeding started (5L-STR – blue; 24-SRW MTP and SF 125 mL – black; SF 250 mL – red (solid line: FB2; dash line: FB3). Error bars represent one standard deviation about the mean.

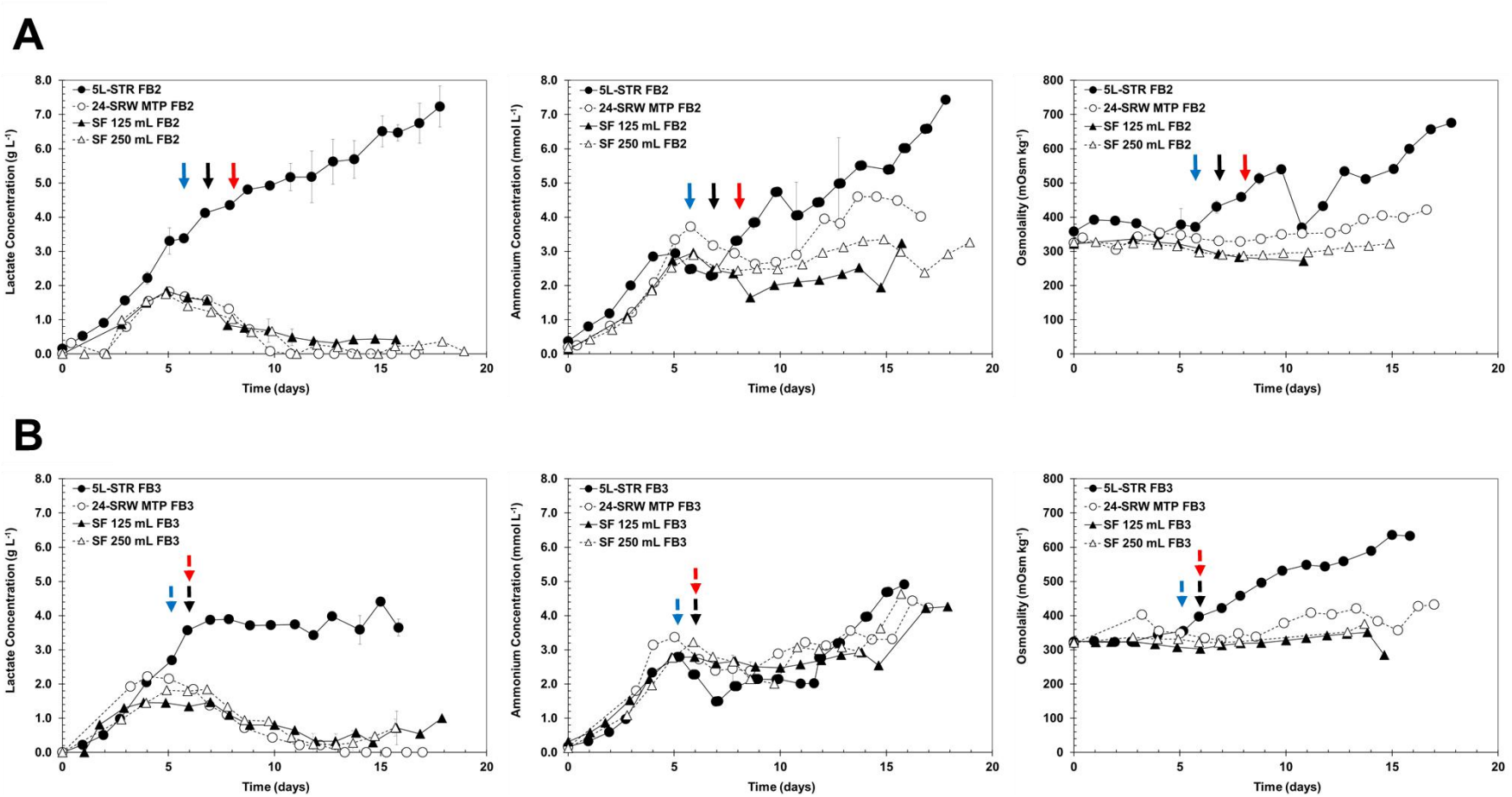

Figure 4-23: Lactate concentration, ammonium ion concentration, and osmolality profiles for CHO-CY01 cell line fed-batch strategy 4 (FB2) (A) and fed-batch strategy 5 (FB3) (B) cultures at different bioreactor scales: 5L-STR (1 replicate); 24-SRW MTP (1 run (3-4 replicates)); SF 125 mL (2 replicates); and SF 250 mL (2 replicates). The arrow indicates when the feeding started (5L-STR – blue; 24-SRW MTP and SF 125 mL – black; SF 250 mL – red (solid line: FB2; dash line: FB3). Error bars represent one standard deviation about the mean.

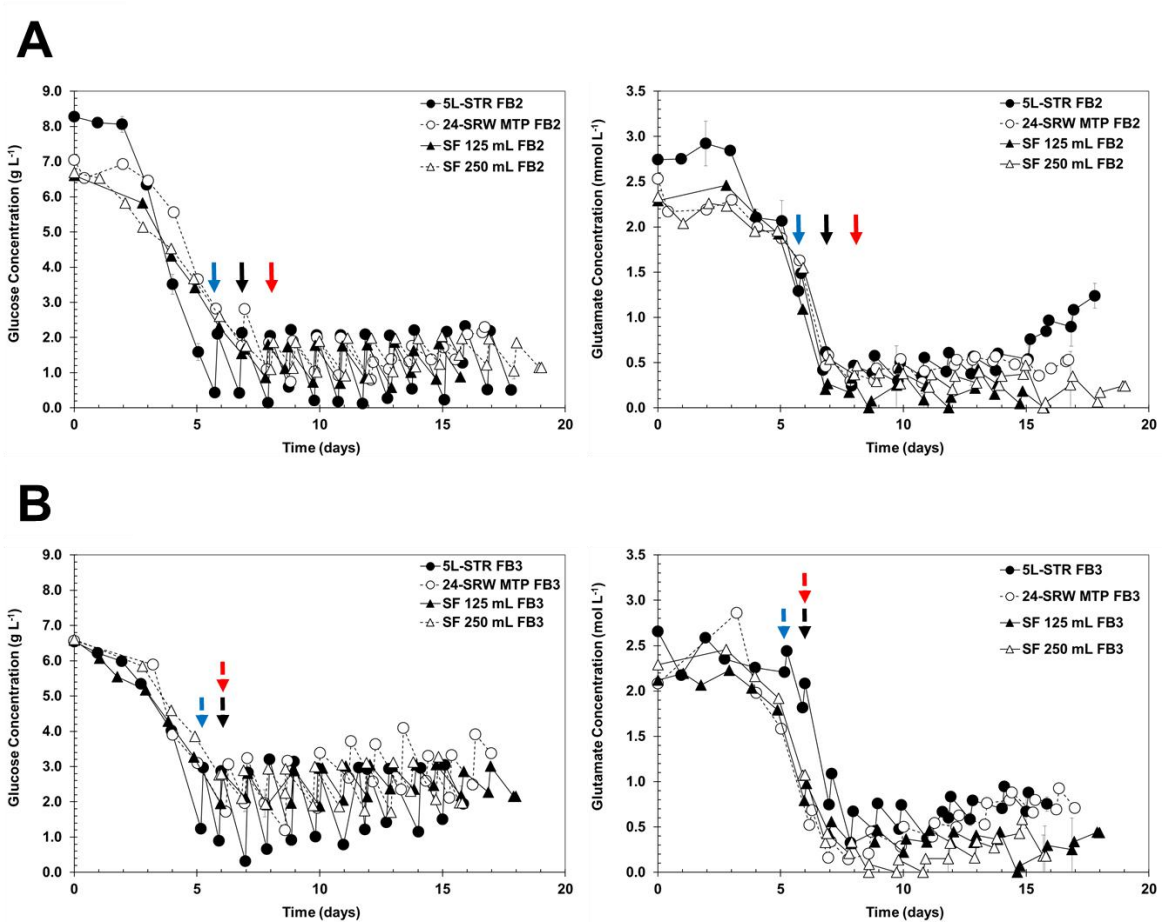

Figure 4-24: Glutamate and glucose concentration profiles for CHO-CY01 cell line fed-batch strategy 4 (FB2) (A) and fed-batch strategy 5 (FB3) (B) cultures at different bioreactor scales: 5L-STR (1 replicate); 24-SRW MTP (1 run (3-4 replicates)); SF 125 mL (2 replicates); and SF 250 mL (2 replicates). The arrow indicates when the feeding started (5L-STR – blue; 24-SRW MTP and SF 125 mL – black; SF 250 mL – red (solid line: FB2; dash line: FB3). Error bars represent one standard deviation about the mean.

Table 4-10: Glucose and glutamate consumption rates during feeding for CHO-CY01 cell line fed-batch Strategy 4 (FB2) and fed-batch Strategy 5 (FB3) cultures at different bioreactor scales: 5L-STR; 24-SRW MTP; SF 125 mL and SF 250 mL.

		Glucose Consumption Rate ($g\ L^{-1}day^{-1}$)	**Glutamate Consumption Rate ($mmol\ L^{-1}day^{-1}$)**
FB2	**5L-STR**	1.73 ± 0.36	0.19 ± 0.03
	24-SRW MTP	0.67 ± 0.35	0.08 ± 0.04
	SF 125 mL	0.85 ± 0.34	0.14 ± 0.05
	SF 250 mL	0.76 ± 0.29	0.10 ± 0.04
FB3	**5L-STR**	1.97 ± 0.36	0.27 ± 0.05
	24-SRW MTP	1.23 ± 0.30	0.17 ± 0.05
	SF 125 mL	0.81 ± 0.16	0.12 ± 0.03
	SF 250 mL	1.10 ± 0.25	0.14 ± 0.03

Table 4-11: Kinetic parameters determined for CHO-CY01 cell line fed-batch Strategy 4 (FB2) (A) and fed-batch Strategy 5 (FB3) (B) cultures at different bioreactor scales: 5L-STR and; 24-SRW MTP.

	FB Strategy 4		***FB Strategy 5***	
	24-SRW MTP	**5L-STR**	**24-SRW MTP**	**5L-STR**
VP ($mg\ L^{-1}day^{-1}$)	44.8	33.7	64.7	50.0
IVCC ($10^9\ cells\ day\ L^{-1}$)	105.12	101.15	85.93	96.90
$\mu\ (h^{-1})$	0.026	0.027	0.022	0.023
$t_{1/2}\ (h)$	27.1	26.0	30.9	29.9
$q_{mAb}\ (mg\ 10^{-9}\ cells^{-1}\ day^{-1})$	8.12	6.28	13.71	9.50
$q_{Gluc}\ (g\ 10^{-9}\ cells^{-1}\ day^{-1})$	-0.15	-0.31	-0.21	-0.32
$q_{Glu}\ (mmol\ 10^{-9}\ cells^{-1}\ day^{-1})$	-0.04	-0.05	-0.04	-0.06
$q_{Lact}\ (g\ 10^{-9}\ cells^{-1}\ day^{-1})$	0.13	0.70	0.19	0.49
$q_{Amm}\ (mmol\ 10^{-9}\ cells^{-1}\ day^{-1})$	0.05	0.07	0.05	0.05
Lactate produced / Glucose consumed (g/g)	0.54	0.25	0.84	0.16
$\mu_d\ (h^{-1})$	-0.001	-0.002	-0.004	-0.005
Feed volume (% of reactor volume)	63.3	13.7	109.4	14.9
Evaporation rate ($\mu L\ day^{-1}$)	9.4 ± 8.3	-	21.5 ± 5.1	-

4.5. Conclusion

In this chapter, it was found that the combination of two common scale translation parameters, mixing time ($< 5\ s$) and energy dissipation rate (P/V = 10 $W\ m^{-3}$), were most suitable of defining the operating conditions at which 24-SRW MTP and SF with total volume of 125 mL (SF 125 mL) and 250 mL (SF 250 mL) should be running in order to be a useful scale-down model of the CHO-CY01 cell line culture at the 5L-STR. It was noted that CHO-CY01 cell batch cultures in 24-SRW MTP, 125 mL SF, and 250 mL SF accurately describe the cell growth, IgG4 productivity, and cell metabolism encountered at a larger scale. However, in fed-batch cultures, the waste by-products, lactate and ammonium, and osmolality are under-estimated by these small-scale bioreactors. The reason for this is the lack of pH control; therefore, no base addition or variable CO_2 concentration was done on these systems. Also, for 5L-STR CHO-CY01 cell cultures (batch or fed-batch), the level of cell damage and subsequent contamination of the harvest point with high concentration of debris was greater. The reason for this is related to the impeller and air bubble cell damage.

In order to understand whether the CHO-CY01 cells' death had the same origin (necrosis or programmed cell death) across the bioreactor scales, an apoptotic population analysis of the cell in the 24-SRW MTP and 5L-STR was performed. It is apparent that the cell death in 24-SRW MTP was due to apoptosis while the lab-scale bioreactor showed a combined effect of necrosis (decline phase) and apoptosis until the stationary phase, when glucose and glutamate deprivation and ammonium accumulation started.

In the commercial production process of mammalian cell cultures, one of the most important parameters is the specific productivity of each cell. If a particular subpopulation of cells within the process is more productive than another, processes can be designed, and control strategies can be developed to favour such a subpopulation. One obvious difference between cells in a population is the cell cycle stage of each cell (Lloyd et al., 2000). For 5L-STR and 24-SRW MTP, the CHO-CY01 cell line exhibited asynchronous growth. On the cell cycle population, the CHO-CY01 cell population dynamics strongly agree among bioreactor scales. In all cases, there was no suggestion that product formation was limited to any specific cell cycle phase. It appears that the regulation of synthesis and secretion of IgG4 is time-dependent and that the productivity is increased when cells are arrested and maintained in G1/S phases with decreasing cell viabilities and increasing cell diameters (stationary phase).

The influence of culture parameters such as ammonium/ammonia, lactate, and osmolality on mammalian cell cultures has been extensively reported in the literature (Lee et al., 2009; Schneider et al., 1996; Tsao et al., 2005). However, less information is available on their influence on the cell growth and mAb productivity of a GS-CHO cell line. Therefore, comprehensive and detailed kinetic studies on the effects of ammonium, lactate, and

osmolality were performed for the characterisation and optimisation of CHO-CY01 cell cultures.

Initial lactate concentration had an adverse effect on cell growth, but not on cell viability. Three initial lactate concentration ranges were found to have a different impact on CHO-CY01 cell line culture. At low lactate concentrations, with values lower than 1.9 $g\ L^{-1}$, the specific growth rate, IgG4 production, and cell metabolism had not changed. For moderate initial lactate concentrations of 1.9 – 3.6 $g\ L^{-1}$, the inhibitory effect of lactate started to be observed with the reduction of the specific cell growth rate, mAb productivity, and metabolism. For initial lactate concentration higher than 3.6 $g\ L^{-1}$, the cell growth was severely compromised. At lactate concentrations higher than 1.9 $g\ L^{-1}$, the cells became strictly lactate consumers. It was hypothetised that at high lactate concentrations, the lactate dehydrogenase (LDH) was inhibited as the glucose consumption rate decreased, and the cells were utilising the lactate as a fuel through intracellular lactate shuttle. This metabolic "switch" is presumed to be driven by a decreased dependence on glycolysis and an enhanced engagement in oxidative pathways for energy production (Brooks et al., 1999; Luo et al., 2012; DeZengotita et al., 1998).

The CHO-CY01 cell growth was negatively affected by the initial ammonium concentration. As with the lactate inhibition study, the initial ammonium concentration's impact on cell growth, metabolism, and productivity can be segmented into three different ranges: 0.2- 4.8 mM; 4.8 – 9.7 mM; and ≥ 9.7 mM. At low ammonium concentrations (≤ 4.8 mM), CHO-CY01 cell growth was not affected, but the IgG4 production diminished by 16%. In the middle range of initial ammonium concentration (4.8 – 9.7 mM), there was a longer *lag* phase, and the total number of cells produced declined by 78%, with no impact on IgG4 production. For high initial ammonium concentrations (≥ 9.7 mM), CHO-CY01 cell growth and mAb productivity were negatively altered. Two possible mechanisms can explain Ammonia/ammonium CHO-CY01 cell growth inhibition: The first mechanism involves the uptake of the weak base NH_3 into intracellular organelles such as lysosomes, mitochondria, and Golgi apparatus, causing alkalinisation, as Doyle et al. (1990) have proposed. The second mechanism involves the uptake of the weak acid NH_4^+ into the cytoplasm, causing acidification, as proposed by Martinelle et al. (1998). These two mechanisms are correlated with the external pH of the medium. The second mechanism of growth inhibition by NH_4^+ is important at all CHO-CY01 cell culture medium pH values, while the growth inhibition by NH_3 is only important at higher pH values (*lag* phase).

It was proven that the toxic effect of ammonium on the CHO-CY01 cell line was higher than that of lactate, i.e. the cell growth, metabolism, and productivity were inhibited first by ammonia and then by ammonium and lactate.

Mathematical models of cell growth and product formation kinetics are useful to quantify and to predict the effect of changes in environmental conditions (Gadgil, 2014). In this work, the lactate and ammonium inhibition of cell growth and IgG4 productivity were mathematically described by a non-competitive type of inhibition model similar to the kinetic model. Half-maximum-rate concentrations of lactate and ammonium for cell growth, cell death, and mAb productivity were determined by a non-linear curve fitting method. An initial lactate concentration of 4.08 $g\ L^{-1}$ and an initial ammonium concentration of 18.1 $mmol\ L^{-1}$ reduced the specific cell growth rate to half its previous values. The CHO-CY01 cell death rate increased to double its initial value, with 2.23 $g\ L^{-1}$ of lactate or 9.66 $mmol\ L^{-1}$ of ammonium. The IgG4 production rate was found to be more sensitive to lactate and ammonium. At just 1.74 $g\ L^{-1}$ of the initial lactate concentration or at 7.17 $mmol\ L^{-1}$ of the ammonium concentration, the VP was reduced to half (~30 $mg\ L^{-1}\ day^{-1}$).

CHO-CY01 cells are less sensitive to changes in osmolality than to changes in pHi caused by lactate and ammonium accumulation in the cell culture medium. In the range of initial osmolality of 275.06 to 296.07 $mOsm\ kg^{-1}$, no change was observed in the CHO-CY01 cell line cultures.

Fed-batch culture can substantially increase the final antibody concentration and culture VP, as compared with batch culture, while retaining the relative simplicity and reliability of batch cell culture. As a result, a new fed-batch methodology for small-scale systems, i.e. 24-SRW MTPs, and SFs, was developed in this work. This was accomplished by daily feeding (variable volumes) with water-diluted concentrated CD-CHO medium supplemented with glucose. Different fed-batch strategies were tested in small-scale (24-SRW MTPs and SFs) first, and then the best candidates were assessed for productivity and inter scalability in the 5L-STR. At small-scale, it was found that to maximise IgG4 production CHO-CY01 cells need to be fed at constant glucose concentration top-up of 2.00 $g\ L^{-1}$ (FB2) or 3.00 $g\ L^{-1}$ (FB3). Subsequently, when the CHO-CY01 cell line was grown at different bioreactor scales, all with similar mixing times and energy dissipation rates, it was found that CHO-CY01 cell performance at both fed-batch strategies (FB2 and FB3) were statistically equivalent ($p > 0.05$) for all cell culture parameters, except for lactate (FB2 and FB3) and ammonium (FB2) profiles. Therefore, it was established that the best fed-batch strategy for CHO-CY01 cells was the constant top-up at a glucose concentration of 3.00 $g\ L^{-1}$ (FB3).

In conclusion, 24-SRW MTPs and SFs at appropriate operating conditions are equivalent to a fully controlled and larger bioreactor, such as the 5L-STR. This finding represents the potential for considerable economic savings and the ability to characterise the CHO-CY01 cell culture more easily and quickly with HT resources (24-RW MTP).

Chapter 5 Effects of Carbon Dioxide on CHO-CY01 Cell Line Kinetics

5.1. Introduction and Aims

Since the commercialisation of the first therapeutic monoclonal antibody product in 1986, this class of biopharmaceutical products has grown significantly. At the current approval rate (four products per year), combined worldwide sales will be near $125 billion by 2020 (Ecker et al., 2015). This increased market has led to a need for increased production volumes and a drive to improve process efficiency (Osman et al., 2002). Culture pH, temperature, dissolved oxygen and CO_2 levels, and nutrient concentrations have a significant impact on cell growth, metabolism, and product synthesis. As the scale of the culture vessel increases, it becomes increasingly more challenging to ensure rapid mixing to reach homogeneity after the addition of a concentrated base solution for pH control. The same is true to ensure sufficient oxygenation and CO_2 removal, while the surface-to-volume ratio decreases with scale, and to ensure similar exposure of cells to mechanical shear as in a small-scale (Xie et al., 2003).

Several approaches to enhance the productivity of CHO-derived recombinant proteins have been currently reported in the literature. Improvement of the bioprocess has been observed in response to cell-culture strategies involving culture temperature (Bollati-Fogolín et al., 2005; Fox et al., 2004; Shi et al., 2005; Schatz et al., 2003;), culture temperature and medium pH (Kim et al., 2007; Oguchi et al., 2006; Yoon et al., 2005; 2006a; b), DOT level (Trummer et al., 2006a), medium pH (Zhu et al., 2005), pCO_2 (Yoon et al., 2002), or medium additives (Chen et al., 2005; Rodriguez et al., 2005; Sung et al., 2004; Yun et al., 2005). The effects of these factors have been found to be cell line- and protein-specific (Oliveira et al., 2008).

CO_2 is a weak acid that freely diffuses across cell membranes so rapidly that pCO_2 inside cells is only rarely different from that outside (Thomas, 1995). Once inside, CO_2 re-establishes equilibrium with H^+ and HCO_3^- so that pH_i initially decreases in response to an increase in pCO_2. However, the decrease in pH_i is counteracted by ion transport systems. To reduce acidity, protons are directly transported out of the cell or HCO_3^- is brought into the cell to neutralize H^+ in the cytosol. Since HCO_3^- is in contrast to CO_2 not permeable, mammalian cells are equipped with about 13 genes encoding different types of bicarbonate transporters allowing the intercellular exchange of the former species (Blombach et al., 2015). Some of the transporters involved in this pH_i regulation in cultured mammalian cells, called modulators of pH homeostasis are: Na^+/H^+ exchanger, Na^+-dependent and -independent Cl^-/HCO_3^- antiporter, Na^+/HCO_3^- symporter, and H^+ translocating ATPases (proton pumps) (Figure 5-1)

(Boron, 2004; DeZengotita et al., 2002; Christi et al., 2003). In addition to a role in pH homeostasis, these modulators play roles in regulating cell volume and osmolality, the transcellular absorption of Na^+, acid/base equivalents, and water and possibly cell proliferation (McDowell et al., 2003). Depending on the cell type and conditions, the steady-state pH_i may be less than, the same as, or greater than pH_i prior to the increase in pCO_2 (DeZengotita et al., 1998). DeZengotita et al. 2002 have proven that that elevated pCO_2 decreases the pH_i in hybridoma cells by 0.1 ± 0.2 pH units. In contrast, hybridoma pH_i did not decrease further with increasing pCO_2 above 140 mmHg.

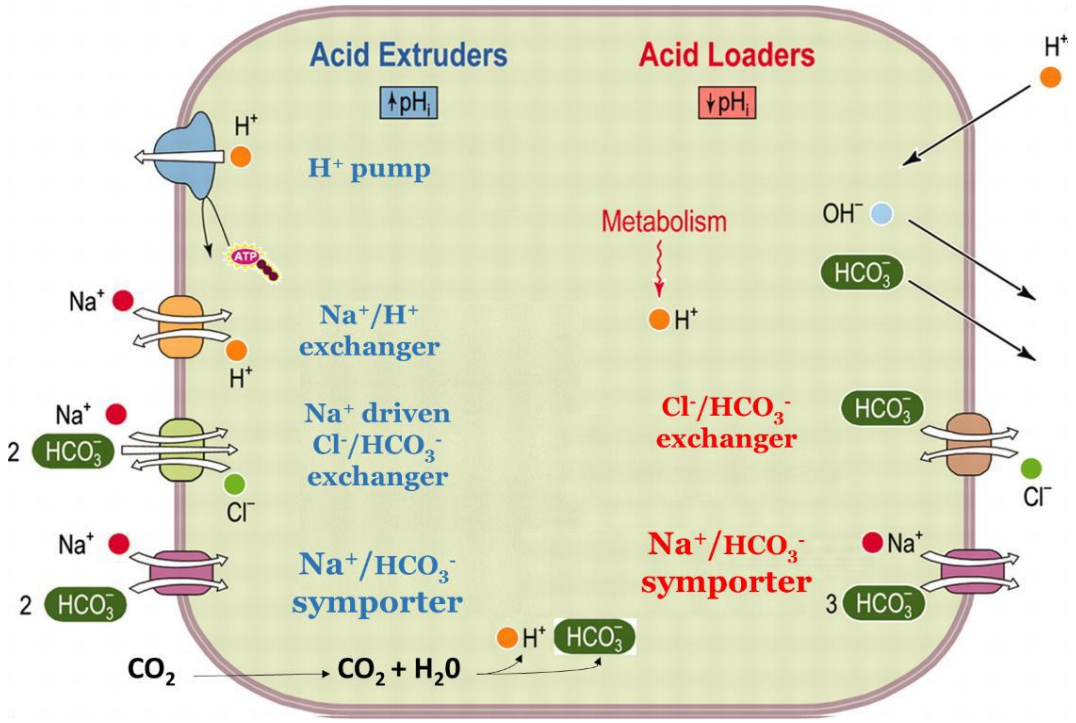

Figure 5-1: Diagram of mammalian cell pH homeostasis modulators (acid extruders and acid loaders) function. The acid extruders increase the pH_i while acid loaders decrease the pH_i of the cell. Steady-state pH_i depends on the balance between acid extruders (Na^+/H^+ exchanger, Na^+-dependent Cl^-/HCO_3^- antiporter, Na^+/HCO_3^- symporter, and H^+ pump) and acid loaders (Na^+-independent Cl^-/HCO_3^- antiporter and Na^+/HCO_3^- symporter). Adapted from Boron *(2004)*.

Detrimental effects of pCO_2 on cell culture have been reported on cell growth, productivity and product quality of hybridoma, NS0, CHO, BHK and insect cells (Blombach et al., 2015; Cheng et al., 2012; Dezengotita et al., 1998; 2002; Kimura et al., 1996;1997; Mostafa et al., 2003; Ozturk et al., 1991b; Takuma et al., 2007; Yoon et al., 2002; Zanghi et al., 1999).

Enhanced levels of pCO_2 in mammalian cell cultures also affect the quality of recombinant glycoproteins by altering the glycosylation pattern of the recombinant protein, such as the percentage of N-glycolyneuraminic or sialylation (Yoon et al., 2002; Zanghi et al., 1999). High pCO_2 (>165 mmHg (36 mmHg (physiological CO_2 level) is equivelant to 5.0% CO_2 level in the gas phase) caused a decreased in CHO cells growth rate but depending on the product secreted some studies have reported a decrease in specific productivity, others claim no change (Mostafa et al., 2003). Also, it led to decreased glucose, lactate and glutamine specific metabolite rates (DeZengotita et al., 1998). One possible mechanism through which CO_2 may affect cell growth and metabolism is by changes in the intracellular pH (pH_i), which affects different aspects of cell growth, metabolism, and protein production such as enzyme activity, transport mechanisms, induction of proliferation, and demand for maintenance energy (Blombach et al., 2015; DeZengotita et al., 1998; Mostafa et al., 2003). For example, phosphofructokinase, which is a rate-limiting enzyme in the glycolytic pathway, is inhibited by low intracellular pH (McQueen et al., 1990a). Therefore, it can be argued that high pCO_2 inhibits in a dose-dependent manner the glycolysis. These detrimental effects of elevated pCO_2 should be overcome if one would like to obtain higher productivity and better quality of the product from the mammalian cell culture. Especially, in the production of recombinant glycoprotein biopharmaceuticals, it is essential to obtain well and consistently glycosylated protein products to ensure their biological activity and stability.

In this work, the use of disposable non-invasive online optical detection probes from PreSens Precision Sensing (Regensburg, Germany) for monitoring of pH and oxygen concentration in cell cultures at different CO_2 concentrations (0.3 to 144.0 mmHg) were used. The aim in this chapter is to understand the effects of CO_2 in the CHO-CY01 cell line growth, cellular metabolism, and IgG4 production to find the optimum pH profile for IgG4 optimisation purposes. All CHO-CY01 cell line cultures in this chapter were performed in 24-SRW MTP scale coupled with PreSens Precision Sensing (Regensburg, Germany) technology (OxoDish®OD24 and HydroDish®HD24) (Section 2.2.7) to have process parameters online readings. The specific objectives of this chapter are:

- Develop a high-throughput online multi-parametric analysis method of mammalian cell cellular activity.
- Perform a series of CHO-CY01 cell line batch cultures at different CO_2 atmospheres (0.04% (v/v) CO_2 - 20.00% (v/v) CO_2)
- Perform CHO-CY01 cell line fed-batch cultures at the CO_2 levels where the highest IgG4 productivities were obtained at CHO-CY01 cell line batch cultures

- Execute several CO_2 biphasic and multiphasic shifts in CHO-CY01 cell line batch and fed-batch cultures.
- Develop a semi-empirical mathematical models to describe the external pH profile of CHO-CY01 cell line cultures.

5.2. CHO-CY01 Cell Line Batch Cultures at Different Constant CO_2 Atmospheres

Mammalian cells have various levels of CO_2, pH and osmolality sensitivities as described above. With PreSens Precision Sensing (Regensburg, Germany) technology (OxoDish®OD24 and HydroDish®HD24) process parameters such as pH, temperature and dissolved oxygen were online monitored during the CHO-CY01 cell line batch cultures at different constant CO_2 concentrations (0.04%, 1.00%, 2.00%, 5.00%, 10.00%, 15.00% CO_2 and 20.00 % (v/v) CO_2). Replicates were performed for most of CO_2 concentrations. The CO_2 concentration of reference was 5.00% (v/v) CO_2, which was the standard CO_2 concentration used before (Chapter 3 and 4). The different CO_2 concentrations tested were divided into below and above the reference CO_2 concentration to facilitate the comparison. At Section 3.3.3 it was proved that the CHO-CY01 cell line batch cultures in a standard 24-SRW MTP and in HydroDish®HD24 plate were statistical equivalent for all the cell culture parameters ($p > 0.05$). So, 24-SRW MTPs and HydroDish®HD24 plates were inoculated with CHO-CY01 cells in parallel for each CO_2 concentrations. In this way, the HydroDish®HD24 plates were never sampled and all the CHO-CY01 cell line kinetic parameters analysis were done with 24-SRW MTP samples.

A comprehensive analysis of the cell behaviour was done to understand the CO_2 effects on this CHO cell line model. The cell growth, metabolism and IgG4 production rates (Figure 5-2, Figure 5-3 and Figure 5-4), apoptosis and cell cycle analysis (Figure 5-10), particle size distribution (Figure B-6 and Table B-6), process parameters profiles (external pH (Figure 5-6)), temperature profile (Figure 5-7), dissolved oxygen (Figure 5-8)), ions (Na^+ and K^+) concentration variation profiles (Figure 5-5), parameters correlations (Table A-13) and kinetic parameters (Table 5-3; Figure 5-9 and, Table C-12) were compared among the different CHO-CY01 cell line batch cultures. In Figure 5-9 the kinetic parameters for CHO-CY01 cell line batch at different CO_2 concentrations were plotted against CO_2 concentrations and trendlines were generated. In the Table 5-1 is represented the initial air composition inside the CO_2 incubator as well as the experimental pH, temperature and dissolved oxygen ranges for each CO_2 concentration. It was noticed that inside the CO_2 incubator, when CO_2 concentration increases the other air components, such as oxygen and nitrogen fractions diminished. For instance, the dissolved oxygen (pO_2) range at 15.00% (v/v) CO_2 run was $81.05 \pm 3.41\%$ (Air

Sat.). This value was 2.7 fold higher than the dissolved oxygen value applied at the larger scale (5L-STR), 30% (Air Sat.). Therefore, it can be claimed that even though the CO_2 incubators had no oxygen control, there was no oxygen limitation to the cells. Generally, pO_2 range between 30.0% (air saturation) and 60.0% (air saturation) is accepted to be optimal, although the sensitivity of cells to extreme pO_2 levels is known to vary. At high oxygen concentration oxidative damage is observed and at low oxygen concentration there is excessive lactate synthesis (Feng et al., 2010). Mammalian cells have an optimal dissolved oxygen range suitable for cell proliferation. Kurano et al. (1990a) have shown for CHO cells that pO_2 values between 50-100% (air saturation), the specific growth rate, glucose consumption rate, lactate production and yield coefficients values did not change significantly. Therefore, it was assumed that the effects of this 2.7 fold increase in pO_2 at 24-SRW MTP scale was negligible e in comparison with CO_2 effects.

At atmospheric CO_2 concentration (0.04% (v/v) CO_2) CHO-CY01 cells were unable to exponentially grow at this condition. However, the few cells present (maximum viable cell number $2.0 \times 10^5 cells\ mL^{-1}$) excessively, produced lactate ($14.12\ g\ 10^{-9}\ cells\ day^{-1}$) from a reduced glucose consumption as it can be seen from the small slope on glucose concentration profile (Figure 5-4). This type of cell behaviour is a cellular survivor mechanism against the high pH ($pH = 8.5 \pm 0.4$) during the first two days of culture (Figure 5-6). During those first two days of culture, the glucose was exclusively used to produce high amounts of lactate (3.5 $g\ L^{-1}$), as consequence the cell number decreased as well as the cell viability. With this lactate accumulation the cell culture medium pH started to sharply dropping to physiological levels at day 7. With the pH decrease, the cells managed to stabilise their internal pH to a more acceptable range, which led to an increase in viable cell numbers and cell viability. At the same time, the lactate production stopped. As observed before (Section 4.3.1), when cells produce high concentrations of lactate, the ammonium production rate is negatively affected. At atmospheric CO_2, the maximum ammonium concentration reached was the smallest (2.92 $mmol\ L^{-1}$). Nevertheless, the elevated osmolality resultant of the high lactate accumulation (370.0 $mOsm\ kg^{-1}$) was another factor to contribute to CHO-CY01 cell death.

A buffer solution is a solution that can maintain a nearly constant pH when diluted or when small amounts of strong acids or bases are added (Kohn et al., 1998). For mammalian cell culture, all cell culture media need to be buffered to smother the pH variation caused cellular metabolism by-products, especially lactate. The cell culture medium used in this work (1x CD-CHO (Section 2.1)) is a CO_2/bicarbonate buffered with around 29 $mmol\ L^{-1}$ of sodium bicarbonate ($NaHCO_3$). The pH of a CO_2/bicarbonate buffer solution can be described by the Henderson-Hasselbalch equation, where $[CO_2]$ is the total CO_2 concentration and $[HCO_3^-]$ is the total bicarbonate concentration (Kohn et al., 1998):

$$pH = 6.37 + log_{10}\frac{[HCO_3^-]}{[CO_2]}$$

Equation 5.1

At atmospheric conditions, there is almost no buffer conjugated acid (0.0156 $mmol\ L^{-1}$ CO_2[7]) dissolved in the medium. So, from Equation 5.1 and Figure 5-6, it is understandable that the cell culture medium used is basic ($pH = 8.5 \pm 0.4$). From the inability of CHO-CY01-cells to grow at such initial pH, it can be claimed that CHO-CY01 cell line cultures at the culture conditions used during this work, demands a carbon dioxide concentration higher than 0.04% (v/v) CO_2 to grow and produce monoclonal antibody.

At 1.00% (v/v) CO_2 condition, the initial pH is lower than the one found at 0.04%. With increasing CO_2 concentrations, the initial CHO-CY01 cell culture medium pH decreased. At the higher CO_2 concentration (20% (v/v) CO_2), the initial pH reaches the minimum of $pH = 6.93 \pm 0.05$. At the same time, pH variation throughout the CHO-CY01 cell culture diminished with increasing CO_2 level. From 10.00% (v/v) CO_2 concentration onwards, it can be claimed that the cell culture broth behaved as a buffer solution (Figure 5-6). Therefore, it was possible to determine the CHO-CY01 cell culture medium buffer capacity (Section 5.2.1). In Table 5-2 is presented the amplitude, duration and initial and final pH for the sampling pH perturbation for all CO_2 concentrations. It is important to notice that the sampling pH perturbation took around 1.5 ± 0.5 hours and only for CO_2 concentrations higher than 10.00% (v/v) CO_2 the pH value was restored (pH before perturbation is equal to pH after pH perturbation). However, the amplitude of the pH perturbation was lower than the pH error and so, these sampling pH perturbations were considered negligible.

It is important to record from Chapter 4, that when mammalian cells produce lactate, acidification of the environment occurs, and the opposite occurs when mammalian cells produce ammonium (NH_4^+). It may seems counterproductive but if one looks at the maximum lactate concentration obtain (~4.0$g\ L^{-1}$) against the maximum ammonium concentration (10 mM = 0.18$g\ L^{-1}$), it is clear that lactate is the dominant acid/base specie.

CO_2 concentrations higher that atmospheric had an impact on CHO-CY01 cell line growth, metabolism and IgG4 productivity. To facilitate the comparison and analysis, the CHO-CY01 cell line batch cultures were divided into below and above standard CO_2 concentration (5.00% (v/v) CO_2).

[7] The Dalton´s and Henry´s laws with a Henry´s constant of 39.0 $mmol\ atm^{-1}L^{-1}$ for CO_2 at 37°C were applied to covert CO_2 volume percentage to molar concentration.

Below standard CO_2 concentration (1.00% (v/v) CO_2, 2.00% (v/v) CO_2 and 5.00% (v/v) CO_2), CHO-CY01 cell line batch culture duration decreased, i.e., higher cell death rate with increasing CO_2 level (Figure 5-2 A1 and Table 5-3). This phenomenon was caused by the increase of glucose and glutamate consumption by the CHO-CY01 cells from 1.00% to 5.00% (v/v) CO_2 (Figure 5-4), which lead to a quicker carbon source deprivation. The CHO-CY01 cell batch cultures at 1.00% and 2.00% (v/v) CO_2 were statistically considered equivalent (p > 0.05). This fact can be explained by similar pH profiles (~7.4 ± 0.7). In the beginning of CHO-CY01 cell line batch culture the pH is higher than 7.50, which firstly drops as a result of lactate production (until day 5) and then increases as the lactate is consumed with simultaneous increase of ammonium concentration from cell lysis towards the end. The same level of similarity was observed on the Spearman´s rank correlation with the same number of very strong correlation between all cell culture parameters (Table A-13). From 2.00% to 5.00% (v/v) CO_2, the q_{mAb}, VP, and $q_{NH_4^+}$ were similar. The differentiator was the increase in the specific cell growth, with the decrease of the q_{Gluc} and q_{Lact}, which puts 5.00% (v/v) CO_2 as a good candidate for the optimum CO_2 concentration. The lower lactate concentration at 5.00% (v/v) CO_2 culture can be intercorrelated with lower culture pH, as it has been already proved from 0.04% (v/v) CO_2 condition, that the survival mechanism used by CHO-CY01 cells against high environmental pH was to increase lactate production. At this range of CO_2 concentrations, the pH variation during culture was too high, almost one pH unit, to be considered as an optimal CO_2 range for CHO-CY01 cell line batch cultures.

Above standard CO_2 concentration (10.00%, 15.00% and 20.00% (v/v) CO_2), pH variation in the CHO-CY01 cell batch culture were at most 0.24 pH units. For this reason, it can be said that the CHO-CY01 cell line batch culture pH was controlled at 7.12 ± 0.24 for 10.00%; 7.05 ± 0.12 for 15.00%; and 7.02 ± 0.10 for 20.00% (v/v) CO_2. Therefore, a new method for an easy and simple pH control at 24-SRW MTP was found for CHO-CY01 cell line batch culture in the 1xCD-CHO medium. CHO-CY01 cell line batch culture at 5.00% (v/v) CO_2 and 10.00% (v/v) CO_2 can be considered similar for cell growth, IgG4 productivity and cell metabolism (p > 0.05). With the increase of CO_2 concentration, the *lag* phase duration increased and with that the duration of the CHO-CY01 cell batch culture up to three extra days. Also, with increasing CO_2 level, the specific growth rate and overall viable cell concentration (IVCC) decreased (Figure 5-9) which cascaded a lower glucose and glutamate consumption due to fewer number of cells or due to CO_2 glycolysis inhibition (DeZengotita et al., 2002). However, due to low IVCC, the specific glucose and glutamate consumption rate had a marginal increase (Figure 5-9). Simultaneously, the maximum lactate concentration decreased, but the duration of the maximum lactate plateau was longer compared with the below the standard CO_2 concentration cultures. It has been already proved in Chapter 3 and

hypothesised the cellular metabolic mechanisms involved in Chapter4 for the fact that CHO-CY01 cell line is a lactate consumer, and so more energetically efficient. This lactate shift was consistently observed when glucose concentration was 3.00 – 4.00 $g\ L^{-1}$ and glutamate was below 2.5 $mmol\ L^{-1}$. So, as CHO-CY01 cell line batch cultures at pH below 7.12 ± 0.24 took more time to consume the glucose and glutamate, the cells had to endure lactate concentrations around 1.5 $g\ L^{-1}$ for longer, which is around 63% lower than the half-maximum-rate concentration of lactate for cell growth rate ($K_{i,Lact} = 4.08 g\ L^{-1}$) (Section 4.3.3). With regards to ammonium concentration profiles, it can be claimed that they were similar, except during the decline period. In this CO_2 concentration range, the specific lactate and ammonium production rate increased with the CO_2 concentration, due to diminishing IVCC. The maximum ammonium concentration obtained was 45% lower than the half-maximum-rate concentration of ammonium for cell growth rate ($K_{i,Amm} = 18.1\ mmol\ L^{-1}$) (Section 4.3.3). The osmolality of the CHO-CY01 cell line batch for any CO_2 concentration was within the normal range (300 – 350 $mOsm\ kg^{-1}$). All these facts lead to the conclusion that CO_2 concentrations higher than 10.00 % (v/v) CO_2 have a toxic effect on cell growth and an CO_2 inhibitory effect on glycolysis.

The CHO-CY01 cell line batch cultures at CO_2 concentration higher than 10.00% (v/v) CO_2 showed a different IgG4 concentration profile compared with lower CO_2 concentrations. A similar maximum IgG4 concentration (0.40 ± 0.11 $g\ L^{-1}$) was reached in all the CHO-CY01 cell line batch cultures. After reaching the maximum IgG4 concentration, cells presented three different behaviours: the IgG4 concentration stayed constant for cell cultures at CO_2 levels higher than 10.00% (v/v) CO_2, decreased for cultures at CO_2 concentrations between 2.00% and 5.00% (v/v) CO_2 and increased at 1.00% (v/v) CO_2. Nevertheless, the cell growth inhibition at CO_2 > 10.00% (v/v) CO_2, CHO-CY01 cells were able to produce the same specific IgG4 production rate (q_{mAb}) between 5.00% and 15.00% (v/v) CO_2 and an 1.81 fold increase at 20.00% (v/v) CO_2. This resulted in q_{mAb} of $19.83 \pm 0.88\ mg\ 10^{-9}\ cells^{-1} day^{-1}$ for this latter CO_2 condition. Therefore, CHO-CYO1 cells utilised the glucose more for IgG4 production than for cell division or lactate production.

Since the CO_2 concentration directly affected the HCO_3^-/H^+ transport inside the cell and ammonium ions transport involves $Na^+K^+2Cl^-$ cotransporters and Na^+/H^+-exchangers (Martinelle et al., 1998) (Figure 5-1), a variation on sodium (Na^+) and potassium (K^+) concentrations with CO_2 was expected. CHO-CY01 cells consumed K^+ at different rates accordingly to the CO_2 concentration (Figure 5-9). For CO_2 levels above 5.00% (v/v) CO_2, there was an increase in q_{K^+} with increasing CO_2 concentration. The ammonium active transport by the cells utilises one K^+ and a Na^+ futile cycle. As the cells produce more NH_4^+ and the intracellular acidification occurs, the cells use the pH homeostasis modulators, $Na^+K^+2Cl^-$ cotransporters and Na^+/H^+-exchangers, which are acid extruders to regulate the internal pH.

Therefore, for CHO-CY01 cell cultures at CO_2 concentrations higher than 5.00% (v/v) CO_2 an increase in the K^+ consumption alongside with the production increase of NH_4^+ was expected. In the case of Na^+, this cation is mainly use a pH homeostasis modulator by the cells. Since the CO_2 concentration, directly affect the intracellular and extracellular H^+ concentrations (Figure 1-5), the Na^+ cellular utilisation indicates which pH homeostasis the cell is in at a particular CO_2 concentration. CHO-CY01 cells at CO_2 concentration below 10% (v/v) CO_2 are excreting Na^+ (acid loaders), thus a negative q_{Na^+}. While above that CO_2 concentration, they consumed Na^+ (acid extruders). The meaning of such behaviour is explained by the excessive decrease in the internal pH by the high CO_2 concentrations (> 10.00% (v/v) CO_2), which have led the cells to consume Na^+, to remove H^+ from the intracellular environment. All this cellular effort at those CO_2 concentrations may have caused the cell growth inhibition observed. Nevertheless, the q_{Na^+} relation with CO_2 concentration was to be found linear (Figure 5-9).

As mention before (Section 4.2.1), a major problem faced by mammalian cell bioreactor cultures is cell death, which decreases overall productivity (Hwang et al., 2008). Therefore, it was key to understand the effect of different CO_2 concentrations on cell death origins. At the same time, the population heterogeneity in terms of the cell cycle may change with CO_2 concentration, which will affect mAb productivity (Kumar et al., 2007; Lloyd et al., 2000). Therefore, an apoptotic and cell cycle analysis of CHO-CY01 cell cultures was performed at different CO_2 concentrations (1.00%, 2.00%, 5.00%, 10.00%, 15.00% and 20.00% (v/v) CO_2).

In Figure 5-10, it is observed for any CO_2 concentration that during the stationary phase, there was an increase in the ´late apoptotic`cell population, followed by a decrease in the ´viable` cell population and, cell size coupled with an increase in the ´non viable` population. This is indicative that the CHO-CY01 cell death at 24-SRW MTP is due to apoptosis independently of the CO_2 concentration.

From Figure 5-2, it can be observed that IgG4 was a growth associated product. However, the impact of CO_2 on the cell cell stage of the cell is unknown. For all CO_2 concentrations, CHO-CY01 cell line batch cultures exhibited an asynchronous growth. During the log phase, 40-50% of CHO-CY01 cells were arrested at G1-phase, another 40-50% were in S-phase and the extent in G2/M phase. At 20.00% (v/v) CO_2, there was no stationary phase, where the IgG4 peak production occured at the other CO_2 concentrations cultures. Nevertheless, CHO-CY01 cell line batch cultures at the CO_2 range tested produced the same maximum IgG4 concentration. This has led to the conclusion, that CHO-CY01 cell line batch cultures should be stopped before the cells enter the decline phase (low cell viability with decrease in cell size and cell numbers), e.g. at stationary phase for cell cultures at CO_2 lower than 20.00% (v/v) or at exponential phase for cultures at CO_2 higher than 20.00%. During the

stationary phase, it is where the cell cycle population distribution differences were noticed. There were three cell behaviours: for CO_2 levels below 10.00%, there was an maintenance on the G1 and S - phases distributions with no cell size variation; at 10.00% (v/v) CO_2 there was a decrease in G1-phase, an increase in S-phase and cell size coupled with a ´viable` cell population drop and a ´non viable` cell population increment; At 15.00% (v/v) CO_2, there was a decrease in G1-phase with increase in S-phase linked with a drop in the ´viable` cell population and a significant increase in the ´non viable`cell population, but with cell size maintance. Therefore, there was no suggestion that IgG4 production was limited to any specific cell cycle phase. It seems that the regulation of synthesis and secretion of IgG4 is time-dependent, and the productivity increased when cells are arrested and maintained in a 40-50% G1/S-phases distribution with decreasing cell viabilities and increasing cell diameters (> 15 μm).

For the 20.00% (v/v) CO_2 condition, it is suspected that the low cell culture pH (7.02 ±0.10) caused an osmotic stress to CHO-CY01 cells and altered the water homeostasis in the cell (Ho, 2006). In this condition, the IgG4 production is correlated with the large cell diameter. Other characteristic difference was CHO-CY01 cells entered the decline phase with the majority of the cells in S phase, instead of G1 phase as in the other cases. A possible explanation for this phenomena is the presence of cell aggregates (particle size bigger than 20 μm) population peak at the decline phase of 20.00% (v/v) CO_2 condition. These clusters are formed around decaying and dead cells, and it was found that DNA released from these cells mediate the cell-cell adhesion (Renner et al., 1993). Therefore, this DNA was wrongly classified as CHO-CY01 cells in S phase.

The dissolved oxygen (pO_2) profiles obtained for the three different CO_2 concentrations, 1.00%, 10.00% and 15.00% (v/v) CO_2, indirectly indicated the different cell growth stages and directly the CHO-CY01 cell oxygen requirements (Figure 5-8). At 1.00% (v/v) CO_2, the dissolved oxygen never drops the 95% (air saturation) mark. No characteristic pO_2 drop was observed during the exponential phase (day 2 to 8 (Table C-12)), an oxygen uptake by the cells was observed from day 5 to day 8 ($Y'_{X/O_2} = -1.01$ ($10^{-9}\ cells\ L^{-1}/\%\ Air\ Sat$) (Table 5-3)), where the viable cell concentration was around $4.0 \times 10^6\ cells\ mL^{-1}$. An increase in the pO_2 value at around day 8 coincided with the beginning of cell decline and so, as the viable cell numbers decline, less oxygen is required for the cellular metabolism. At 10.00% and 15.00% (v/v) CO_2, the pO_2 profile can be divided into four stages with different pO_2 profiles: At the first stage, there was an increase of pO_2 as the result of the solubility equilibrium of the oxygen in the gas phase to the cell culture medium until day 2.5. Since the CO_2 has a higher solubility than the oxygen, it was expected a longer time for the system to reach the true oxygen saturation equilibrium. The ratio of those times (2.2/0.05 days) was approximately equal to the

ratio of solubilities in water at 37°C (1.2/0.031[8]). This is a further indication that the hydrodynamic environment at 24-SRW MTP (Section 3.2), did not limit the gas transfer. However, the initial observed pO_2 after saturation was lower than the theoretically calculated (Table 5-1 and Figure 5-8), which points out the gas transfer resistance from the CR1524a ´System Duetz` lid (Section 2.1.3). The difference of these $pO_2$ values were considered as a gas transfer resistance constant and for CR1524a ´System Duetz` lid the value obtained was 3.25 ± 0.70% O_2; The second stage coincides with a CHO-CY01 cell line exponential cell growth period, with a drop of pO_2 percentage. At this stage, the observed yield coefficient for oxygen (Y'_{X/O_2}) was determined (Table 5-3). It was observed that CHO-CY01 cells consumed more oxygen at 10.00% (v/v) CO_2 than at 15.00% (v/v) CO_2 which agrees with the higher cell density and IgG4 concentration present at 10.00% (v/v) CO_2 at the exponential phase (day 2 to 7 (Table C-12)). Since the minimum pO_2 level was 75% (air saturation), it can be claimed that up to 15.00% (v/v) CO_2 (17.81% O_2 (Table 5-1), there was no oxygen limitation; At the third stage, it was observed a pCO_2 level approximately constant, which coincide to the stationary phase in the cell growth curve; In the four stage, the pO_2 have a rise, as the viable cell number decline, the amount of oxygen need for the cells diminish and so, pO_2 tend to saturation level.

Regarding particle size distribution (Figure B-6 and Table B-6), the four particle size distributions (adaptation, exponential, beginning of decline and decline periods) were observed at all the different CO_2 concentrations CHO-CY01 cell cultures. At 0.04% (v/v) CO_2 since there was no cell growth, the particle size distribution translated the cell decline. However, for CO_2 concentration higher than the atmospheric one, it can be stated that the particle distribution, although with the small variation, did not change with CO_2 concentration. The only remarks to make is at 20.00% (v/v) CO_2 CHO-CY01 cell size was considerably bigger than the remaining CO_2 culture conditions, with more 2.0 μm in average on the viable cell diameter and the lack of debris at the decline phase.

Assuming an optimisation view on productivity and also to facilitate the downstream process, CO_2 concentrations higher than 10.00% (v/v) CO_2 which is equivalent to saying CHO-CY01 cell line cultures with pH between 7.02 ± 0.10 and 7.12 ± 0.24 were cell culture conditions preferable for IgG4 optimisation productivity.While CO_2 concentrations lower than 10% (v/v) CO_2, pH between 7.12 ± 0.24 and 7.51 ± 0.81, favour the cell production.

[8] http://www.engineeringtoolbox.com/gases-solubility-water-d_1148.html

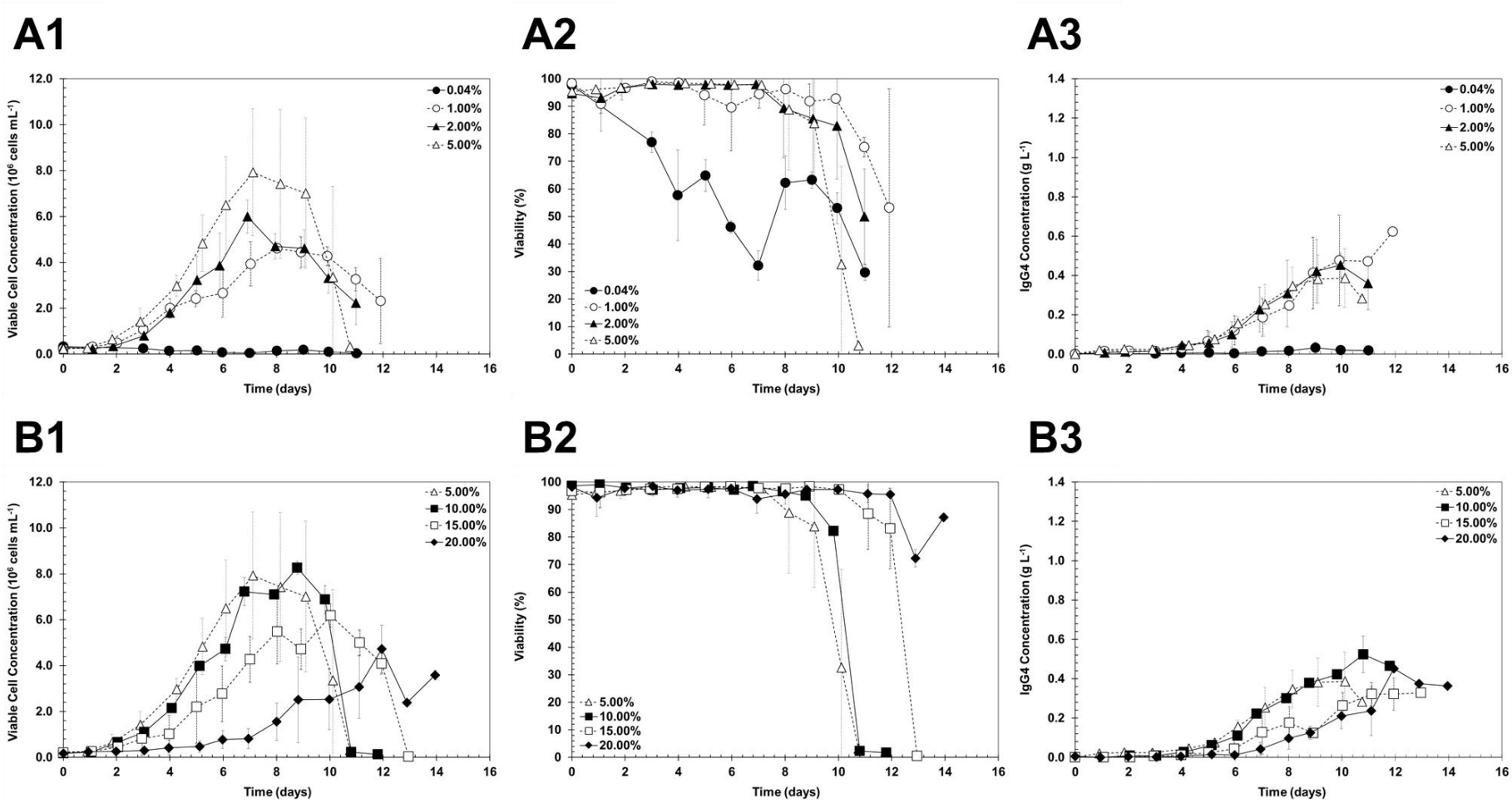

Figure 5-2: Viable cell concentration (1), viability (2) and IgG4 concentration (3) profiles for CHO-CY01 cell line batch cultures in 24-SRW-MTP below the standard CO_2 concentration (0.04%, 1.00%, 2.00% and 5.00% (v/v) CO_2) (A) and above standard CO_2 concentration (5.00%, 10.00%, 15.00% and 20.00% (v/v) CO_2) (B). Two CHO-CY01 cell line batch cultures runs (4-6 replicates) were done per CO_2 concentration, except for 0.04% and 10.00% (v/v) CO_2 (1 run (3-4 replicates)). Error bars represent one standard deviation about the mean.

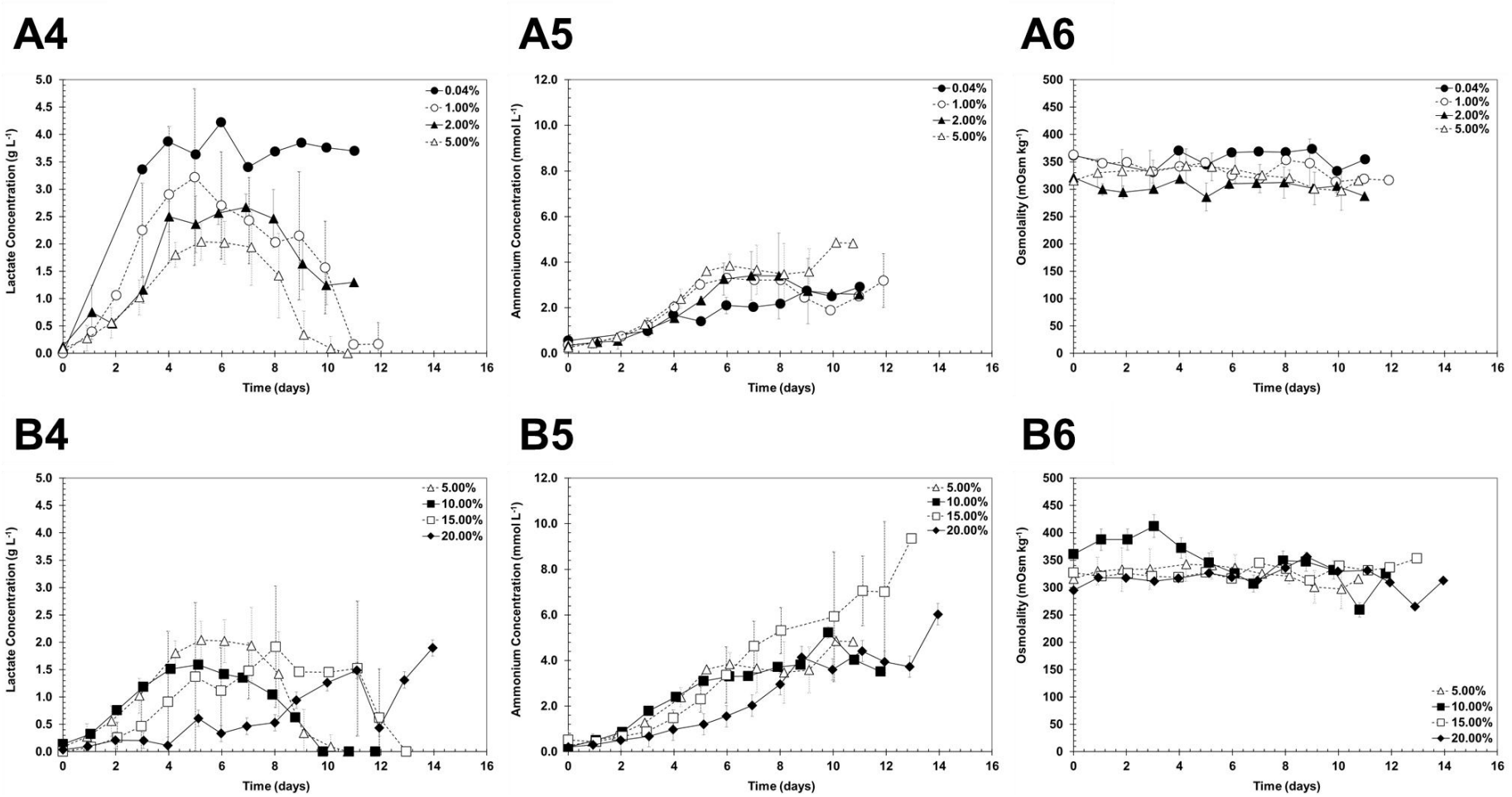

Figure 5-3: Lactate concentration (4), ammonium ion concentration (5) and, osmolality (6) profiles for CHO-CY01 cell line batch cultures in 24-SRW-MTP below the standard CO_2 concentration (0.04%, 1.00%, 2.00% and 5.00% (v/v) CO_2) (A) and above standard CO_2 concentration (5.00%, 10.00%, 15.00% and 20.00% (v/v) CO_2) (B). Two CHO-CY01 cell line batch cultures runs (4-6 replicates) were done per CO_2 concentration, except for 0.04% and 10.00% (v/v) CO_2 (1 run (3-4 replicates)). Error bars represent one standard deviation about the mean.

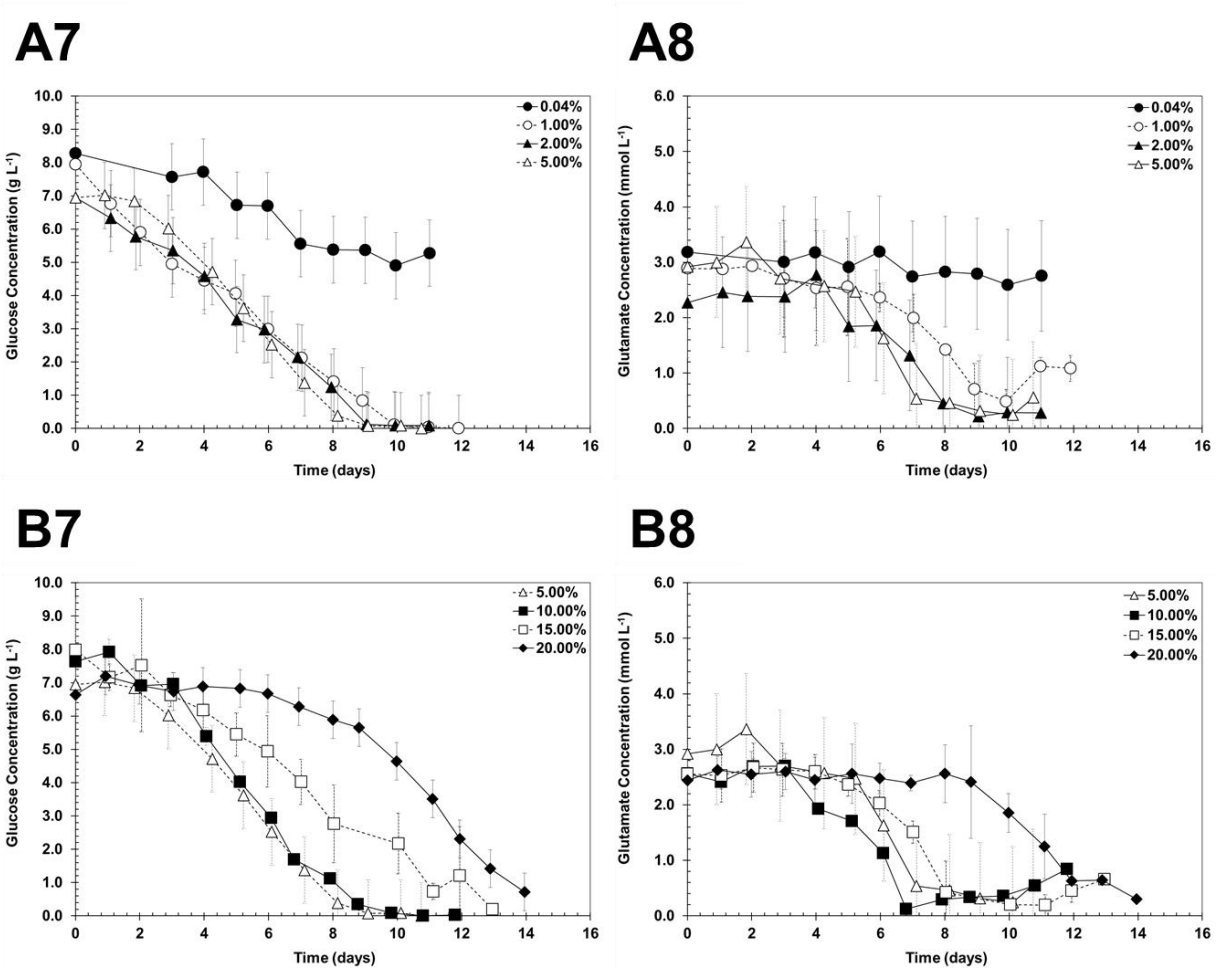

Figure 5-4: Glucose (7) and glutamate (8) concentrations profiles for CHO-CY01 cell line batch cultures in 24-SRW-MTP below the standard CO_2 concentration (0.04%, 1.00%, 2.00% and 5.00% (v/v) CO_2) (A) and above standard CO_2 concentration (5.00%, 10.00%, 15.00% and 20.00% (v/v) CO_2) (B). Two CHO-CY01 cell line batch cultures runs (4-6 replicates) were done per CO_2 concentration, except for 0.04% and 10.00% (v/v) CO_2 (1 run (3-4 replicates)) . Error bars represent one standard deviation about the mean.

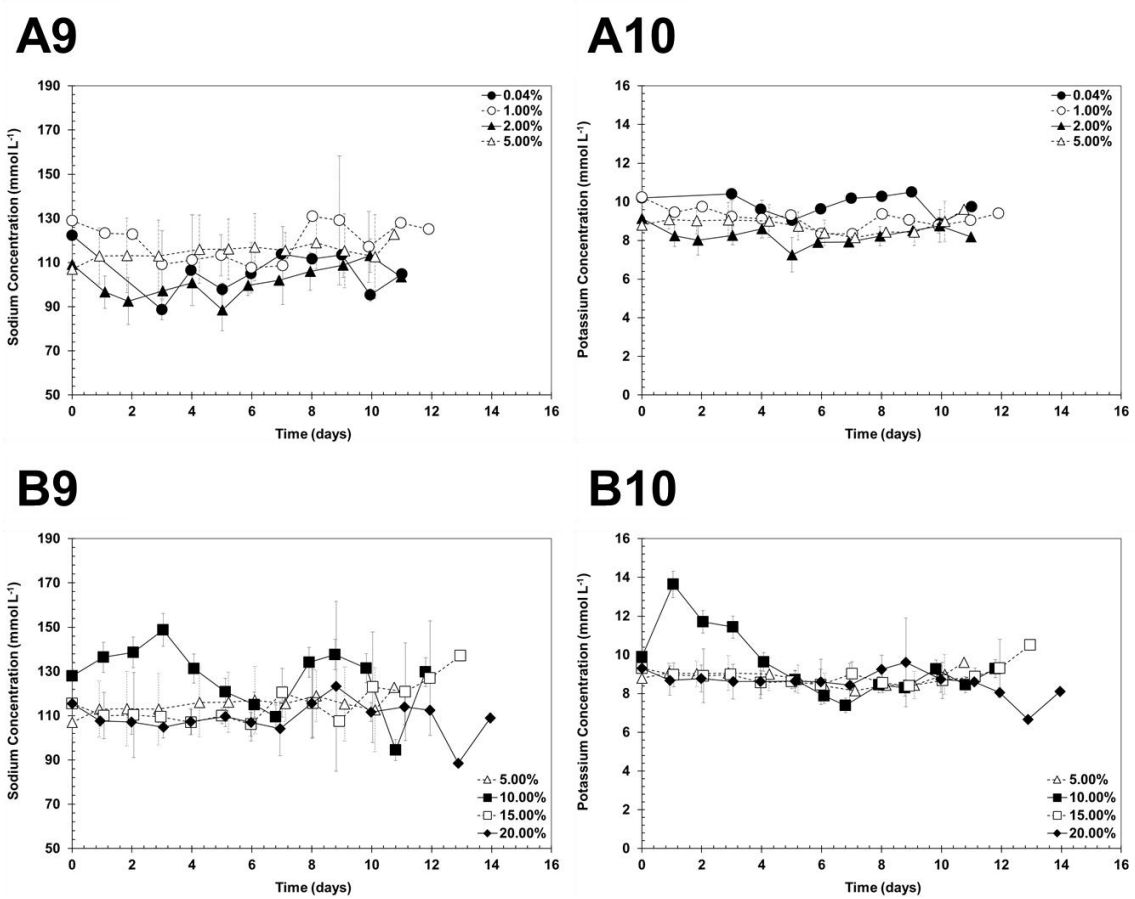

Figure 5-5: Sodium (9) and potassium (10) concentrations profiles for CHO-CY01 cell line batch cultures in 24-SRW-MTP below the standard CO_2 concentration (0.04%, 1.00%, 2.00% and 5.00% (v/v) CO_2) (A) and above standard CO_2 concentration (5.00%, 10.00%, 15.00% and 20.00% (v/v) CO_2) (B). Two CHO-CY01 cell line batch cultures runs (4-6 replicates) were done per CO_2 concentration. Error bars represent one standard deviation about the mean

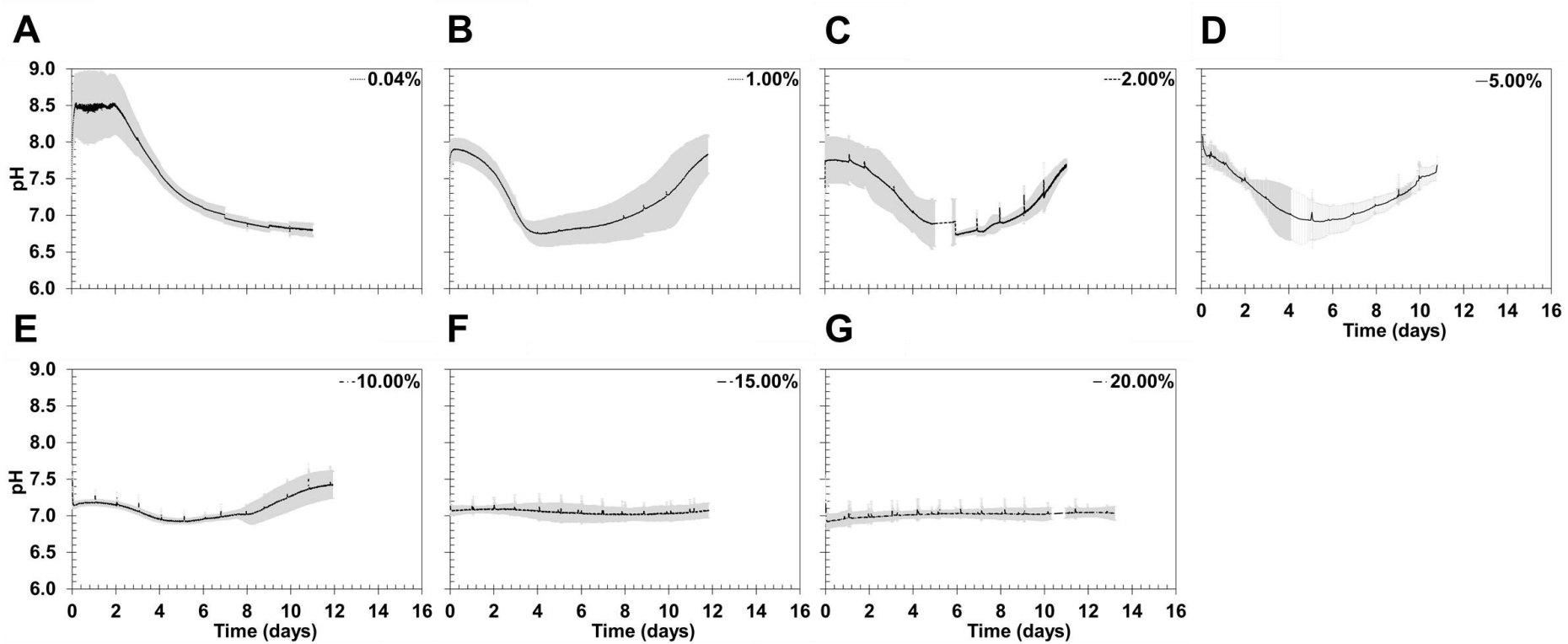

Figure 5-6: CHO-CY01 cell line batch culture pH profiles at 0.04% (A), 1.00% (B), 2.00% (C), 5.00% (D), 10.00% (E), 15.00% (F), and 20.00% (v/v) CO_2 (G). One CHO-CY01 cell line batch cultures run (24 replicates) was done per CO_2 concentration. Error bars represent one standard deviation about the mean.

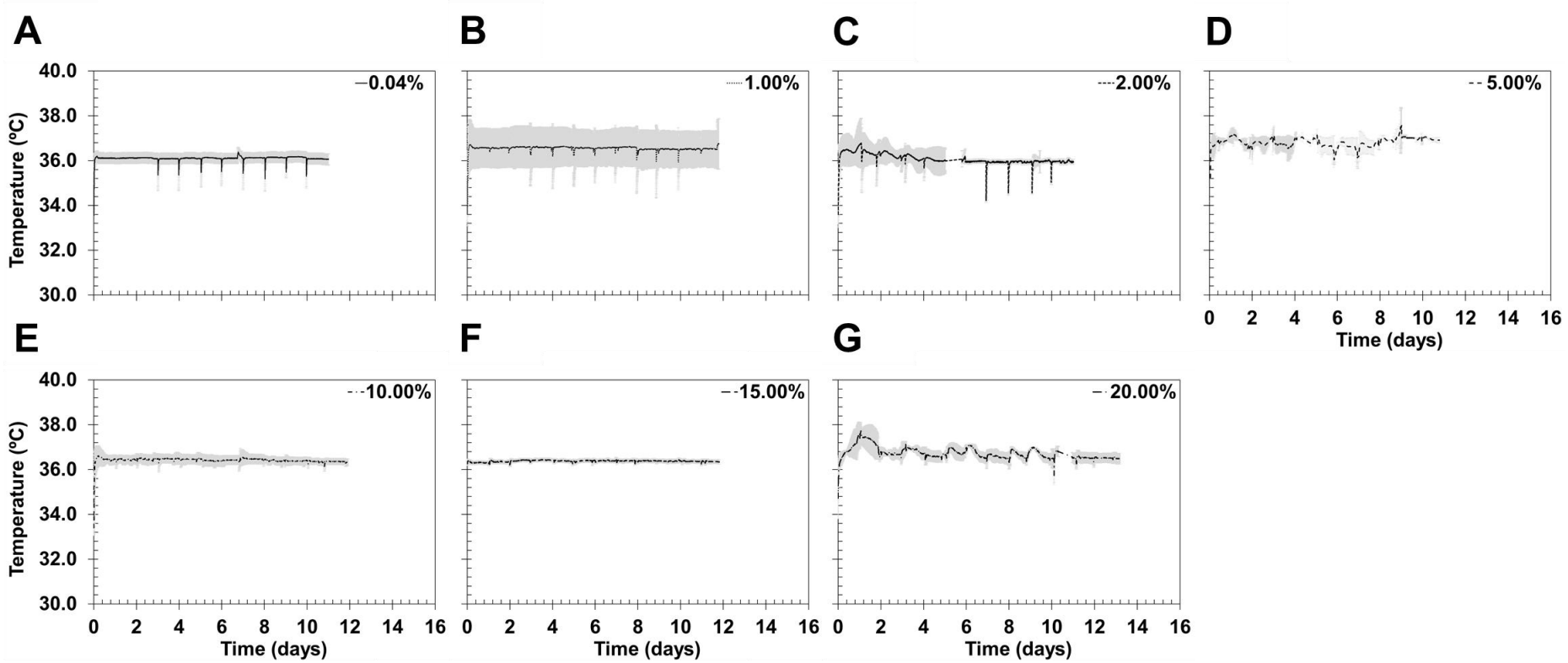

Figure 5-7: Temperature profiles for CHO-CY01 cell line batch cultures at 0.04% (A), 1.00% (B), 2.00% (C), 5.00% (D), 10.00% (E), 15.00% (F), and 20.00% (v/v) CO_2 (G). One CHO-CY01 cell line batch cultures run (24 replicates) was done per CO_2 concentration. Error bars represent one standard deviation about the mean.

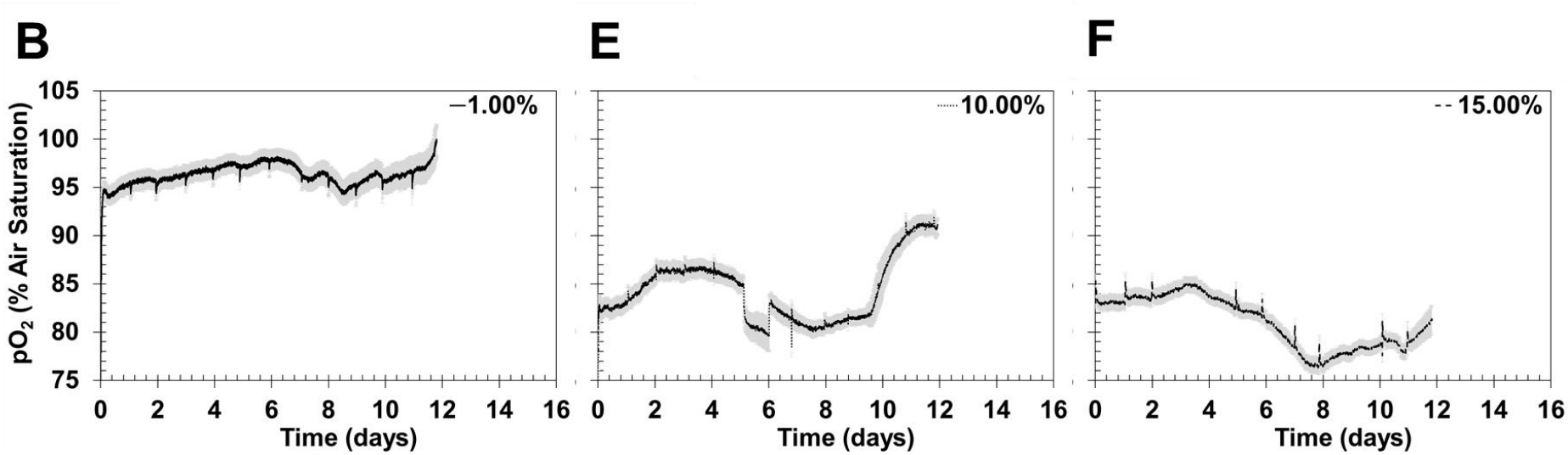

Figure 5-8: CHO-CY01 cell line batch culture dissolved oxygen, pO_2 (% Air Saturation) 1.00% (B), 10.00% (E), and 15.00% (v/v) CO_2 (F). One CHO-CY01 cell line batch cultures run (24 replicates) was done per CO_2 concentration. Error bars represent one standard deviation about the mean.

Table 5-1: Initial air composition inside the CO_2 incubator and the average and standard deviation values for the process parameters: pH, temperature and dissolved oxygen obtained during CHO-CYO1 cell line batch culture at different CO_2 levels. The initial dissolved CO_2 pCO_2 (mmHg) was computed by multiplying 7.2 to CO_2 (% (v/v)).

Initial Air Composition							
CO_2 (% (v/v))	**Dissolved CO_2 pCO_2 (mmHg)**	**Nitrogen, N_2 (%)**	**Oxygen, O_2 (%)**	**Dissolved Oxygen, pO_2 (% Air Saturation)**	**pH**	**Temperature (°C)**	**Dissolved Oxygen, pO_2 (% Air Saturation)**
0.04	0.3	78.08	20.95	100.00	7.51 ± 0.81	36.1 ± 0.4	
1.00	7.2	77.33	20.74	99.04	7.33 ± 0.67	36.5 ± 0.9	97.09 ± 3.12
2.00	14.4	76.55	20.54	98.04	7.42 ± 0.61	36.2 ± 0.8	
5.00	36.0	74.21	19.91	95.04	7.27 ± 0.36	36.9 ± 0.4	
10.00	72.0	70.30	18.86	90.04	7.12 ± 0.24	36.4 ± 0.6	84.16 ± 4.23
15.00	108.0	66.40	17.81	85.03	7.05 ± 0.12	36.4 ± 0.1	81.05 ± 3.41
20.00	144.0	62.49	16.76	80.03	7.02 ± 0.10	36.7 ± 0.5	

Table 5-2: Amplitude and duration of the sampling pH perturbation for CHO-CY01 cell line batch cultures in 24-SRW-MTP at different CO_2 concentrations (0.04%, 1.00%, 2.00%, 5.00%, 10.00%, 15.00% and 20.00% (v/v) CO_2).

CO_2 (% (v/v))	Amplitude	Duration (hours)	pH before pH perturbation	pH after pH perturbation
0.04	0.00	0.00	0.00	0.00
1.00	0.08	1.49	7.07	7.10
2.00	0.26	1.02	7.02	7.05
5.00	0.05	1.57	7.24	7.26
10.00	0.09	1.15	6.93	6.93
15.00	0.04	1.70	7.02	7.02
20.00	0.06	2.35	7.02	7.02

Table 5-3: Kinetic parameters determined for CHO-CY01 cell line batch cultures in 24-SRW-MTP at different CO_2 concentrations (0.04%, 1.00%, 2.00%, 5.00%, 10.00%, 15.00% and, 20.00% (v/v) CO_2).

CO_2 (% (v/v))	**0.04**	**1.00**	**2.00**	**5.00**
VP ($mg\ L^{-1}day^{-1}$)	2.1	40.7 ± 7.2	35.6 ± 2.8	33.93 ± 4.81
IVCC ($10^9\ cells\ day\ L^{-1}$)	1.84	30.48 ± 0.22	30.51 ± 1.00	41.43 ± 7.23
$\mu\ (h^{-1})$		0.017 ± 0.001	0.018 ± 0.002	0.023 ± 0.002
$t_{1/2}\ (h)$		41.7 ± 3.2	39.1 ± 7.81	30.34 ± 2.69
$q_{mAb}\ (mg\ 10^{-9}\ cells^{-1}\ day^{-1})$	10.50	19.64 ± 3.96	15.27 ± 1.67	10.58 ± 3.01
$q_{Gluc}\ (g\ 10^{-9}\ cells^{-1}\ day^{-1})$	-1.61	-0.33 ± 0.06	-0.27 ± 0.04	-0.21 ± 0.03
$q_{Glu}\ (mmol\ 10^{-9}\ cells^{-1}\ day^{-1})$	-0.23	-0.08 ± 0.01	-0.08 ± 0.01	-0.08 ± 0.02
$q_{Na^+}\ (mmol\ 10^{-9}\ cells^{-1}\ day^{-1})$	-10.86	0.44 ± 0.32	0.47 ± 0.32	0.29 ± 0.11
$q_{K^+}\ (mmol\ 10^{-9}\ cells^{-1}\ day^{-1})$	-0.28	-0.07 ± 0.05	-0.05 ± 0.03	-0.01 ± 0.01
$q_{Lact}\ (g\ 10^{-9}\ cells^{-1}\ day^{-1})$	14.12	0.83 ± 0.16	0.66 ± 0.09	0.35 ± 0.12
$q_{Amm}\ (mmol\ 10^{-9}\ cells^{-1}\ day^{-1})$	1.11	0.11 ± 0.01	0.11 ± 0.01	0.13 ± 0.03
Lactate produced / Glucose consumed (g/g)	2.67	0.81 ± 0.15	0.56 ± 0.06	0.52 ± 0.13
$\mu_d\ (h^{-1})$	-0.006	-0.007 ± 7.2	-0.007 ± 0.004	-0.024 ± 0.016
Evaporation rate ($\mu L\ day^{-1}$)	11 ± 2	11 ± 8	24 ± 18	19 ± 9
Observed yield coefficient for oxygen (Y'_{X/O_2}) ($10^9\ cells\ L^{-1}/\%\ Air\ Sat$)		-1.01		

Table 5-3 (Continued)

CO_2 (% (v/v))	10.00	15.00	20.00
VP ($mg\ L^{-1}day^{-1}$)	37.4	24.1 ± 4.8	18.9 ± 7.6
IVCC ($10^9\ cells\ day\ L^{-1}$)	41.07	34.08 ± 4.93	18.47 ± 8.07
$\mu\ (h^{-1})$	0.021	0.017 ± 0.001	0.011 ± 0.001
$t_{1/2}\ (h)$	32.7	40.2 ± 1.6	63.3 ± 2.6
$q_{mAb}\ (mg\ 10^{-9}\ cells^{-1}\ day^{-1})$	12.13	10.91 ± 2.50	19.83 ± 0.88
$q_{Gluc}\ (g\ 10^{-9}\ cells^{-1}\ day^{-1})$	-0.22	-0.24 ± 0.05	-0.30 ± 0.04
$q_{Glu}\ (mmol\ 10^{-9}\ cells^{-1}\ day^{-1})$	-0.06	-0.08 ± 0.01	-0.10 ± 0.00
$q_{Na^+}\ (mmol\ 10^{-9}\ cells^{-1}\ day^{-1})$	-0.18	-0.35 ± 0.04	-0.72 ± 0.43
$q_{K^+}\ (mmol\ 10^{-9}\ cells^{-1}\ day^{-1})$	-0.04	-0.03 ± 0.01	-0.08 ± 0.01
$q_{Lact}\ (g\ 10^{-9}\ cells^{-1}\ day^{-1})$	0.29	0.41 ± 0.22	0.55 ± 0.23
$q_{Amm}\ (mmol\ 10^{-9}\ cells^{-1}\ day^{-1})$	0.12	0.23 ± 0.03	0.35 ± 0.13
Lactate produced / Glucose consumed (g/g)	0.40	0.37 ± 0.12	0.34 ± 0.08
$\mu_d\ (h^{-1})$	-0.065	-0.050 ± 0.041	-0.003 ± 0.003
Evaporation rate ($\mu L\ day^{-1}$)	19 ± 3	33 ± 20	21 ± 2
Observed yield coefficient for oxygen (Y'_{X/O_2}) ($10^9\ cells\ L^{-1}/\%\ Air\ Sat$)	-1.24	-0.63	

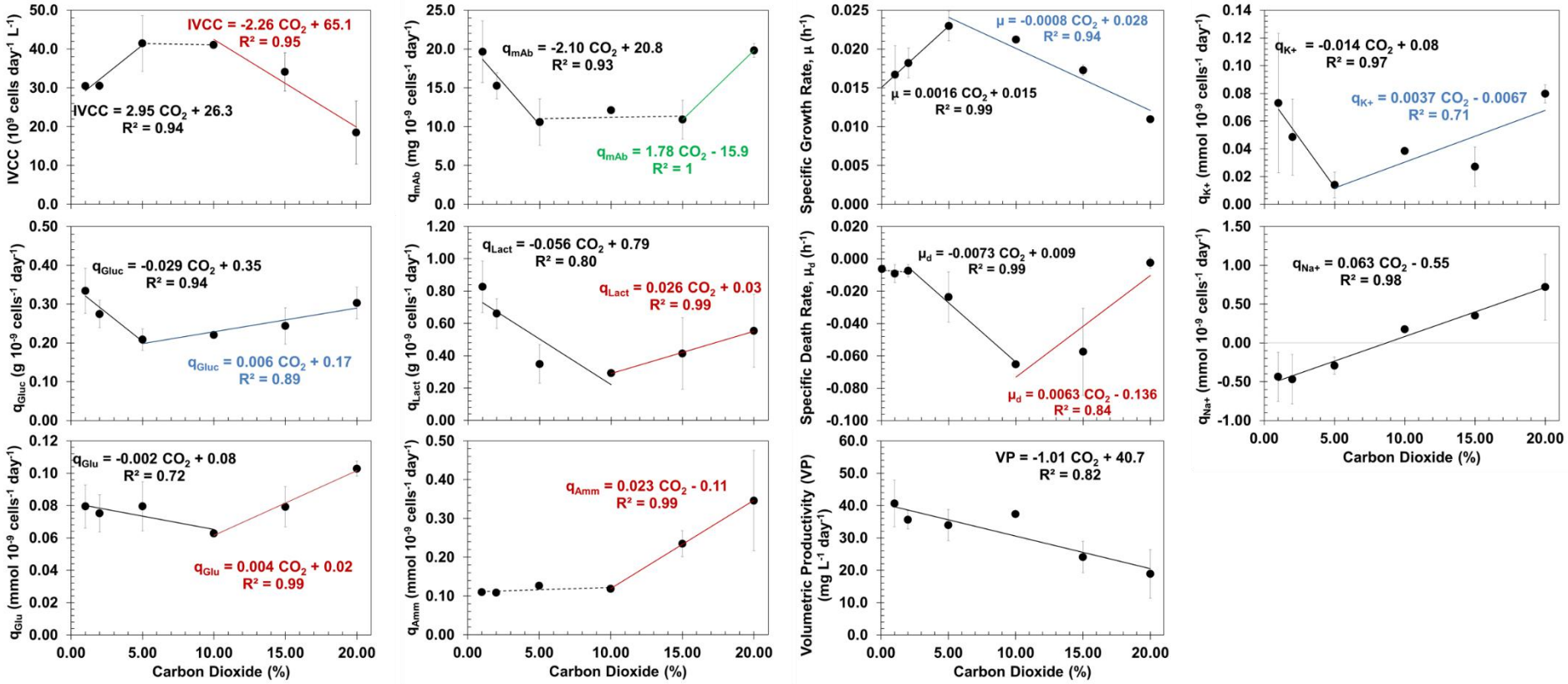

Figure 5-9: Graphical representation of the CHO-CY01 cell line batch cultures at different CO_2 atmospheres kinetic parameters (Table 5-3) and observed trendlines. Dash line represent a no variation in the kinetic parameter; Blue line is the trendline for CO_2 atmospheres above 5% (v/v) CO_2; Red line is the trendline for CO_2 atmospheres above 10% (v/v) CO_2; Green line is the trendline for CO_2 atmospheres above 15% (v/v) CO_2. Error bars represent one standard deviation about the mean.

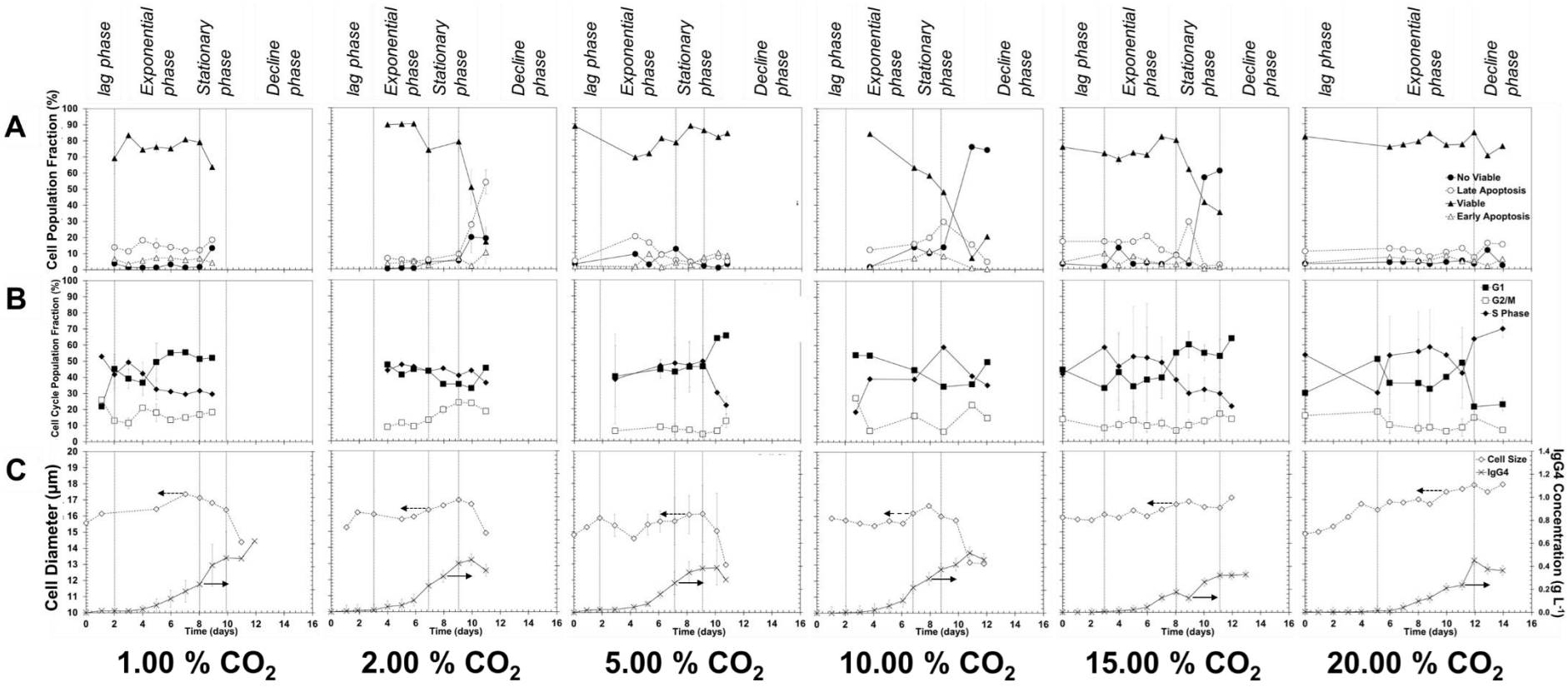

Figure 5-10: Apoptotic (A) and cell cycle (B) population fractions and, viable cell diameter and IgG4 titer (C) profiles for CHO-CY01 cell line batch cultures at different CO_2 concentrations (1.00%, 2.00%, 5.00%, 10.00%, 15.00% and 20.00% (v/v) CO_2) accordingly to cell growth phases (lag, exponential, stationary and decline or death phase). The error bars are the standard deviation about the mean.

5.2.1 Determination of the Buffer Capacity of CHO-CY01 Cell Line Medium from Online pH Monitoring

With the increase of CO_2 concentration inside the CO_2 incubator, the direct result is the initial acidification of the cell culture. The level of acidification depends on the buffer capacity of the cell culture medium, which is interconnected by definition (the amount of strong acid or base that a buffer can neutralise) with the amount of CO_2 (acid) injected inside the CO_2 incubator. The buffer capacity of the 1xCD-CHO medium can be determined from the online pH readings (Figure 5-6). In the beginning of any cell culture, there is a CO_2 shift from atmospheric CO_2 to a predetermined incubator CO_2. When sampling the CHO-CY01 cell line cultures, there is again a CO_2 shift but as no pCO_2 reading is available, one can not know how much CO_2 level drops when the incubator door is open. So, using the initial CO_2 shift and a similar method to determine the buffer capacity (β) used by Jung et al. (2000). The cell culture medium buffer capacity (β) ($mmol\ L^{-1}$ per 1 pH unit or % (v/v) per 1 pH unit) was calculated by dividing the initial difference of CO_2 added, $\Delta CO_{2_{initial}}$ ($mmol\ L^{-1}$), by the net decrease in the cell culture pH, $-\Delta pH$:

$$\beta = \frac{\Delta CO_{2_{initial}}}{-\Delta pH}$$

Equation 5.2

Below 5.00 % (v/v) CO_2, the initial CO_2 amount added is not enough to cause any initial pH drop. For CO_2 levels higher than 5.00 % (v/v) CO_2, there is an initial pH drop (Figure 5-6). However, at 5% CO_2 the pH profile is still not yet of a buffer solution (pH = 7.27 ± 0.36). Accurate determination of cell culture medium buffer capacity was only possible when a ´constant` pH profile was reached from 10.00% (v/v) CO_2 onwards, which agrees with the 8.00 – 10.00% (v/v) CO_2 concentration recommendation from the cell culture medium manufacture. The 10.00% (v/v) CO_2 cell culture was used to determined the initial buffer capacity of CHO-CY01 cell line culture medium. As a one off, the pH readings time intervals were set for 15 seconds during the first 1.5 hour of the culture instead of the usual 3-10 minutes, in order to increase the pH reading accuracy (Figure 5-11).

There is a particular aspect of all pH profiles at any CO_2 concentration cell culture, which is the unrealistic increase on pH in the beginning of the cell culture (Figure 5-6 and Figure *5-11*). It is related with the slight temperature drop of cell culture medium when setting-up the 24-SRW MTPs and the fact that PreSens software uses the user-defined temperature constant to convert the signal of the optical sensor. So, when the HydroDish®HD24 plates were put inside the CO_2 incubator, they were at a temperature lower than 37°C, and therefore a lower pH reading. As the temperature inside the HydroDish®HD24 plates increased, the pH increased as well. Once the temperature equilibrium is reached after 6.5 minutes, the cell

culture medium pH reading given by the PreSens software is the real one (pH = 7.60 ± 0.08). The equilibrium kinetics for temperature is much quicker than the CO_2 solubility equilibrium kinetics, so it can be considered that after 6.5 minutes there was no CO_2 equilibrium.

The CO_2 solubility and subsequent acid-base equilibrium with the bicarbonate present in the CHO-CY01 cell line culture medium took around one hour to be reached (Figure *5-11*) and the buffer capacity of the initial CHO-CY01 cell line medium culture was 7.76 ± 0.32 $mmol\ L^{-1}\ CO_2$ per 1 pH unit or 23.29 ± 0.32% (v/v) CO_2 per 1 pH unit. Thus, to lower the CHO-CY01 cell line culture medium pH by one unit, it is necessary to inject 7.76 ± 0.32 $mmol\ L^{-1}\ CO_2$ or 23.29 ± 0.32 % (v/v) inside the CO_2 incubator. At 20.00% (v/v) CO_2 condition, it can be seen that CO_2 level was not enough to reduce one pH unit as the cell culture pH was 7.02 ± 0.10, which corroborates the determined β value.

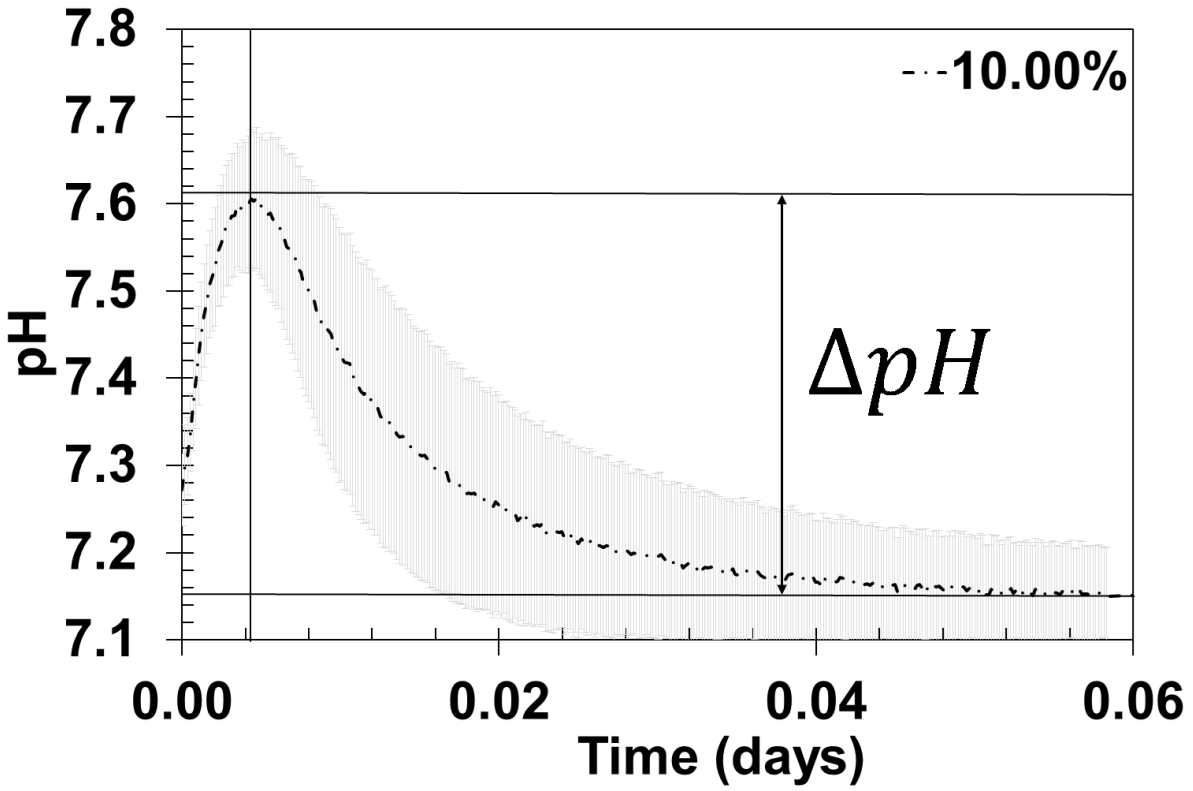

Figure 5-11: Buffer capacity (β) determination of 1x CD-CHO cell culture medium by a similar method used by Jung et al. (2000). From pH online measurement it was possible to determine the pH variation (ΔpH) that a CO_2 shift from atmospheric level to 10.00% (v/v) CO_2 (ΔCO_2) caused and by using Equation 5.2, β was computed.

5.3. CHO-CY01 Cell Line Fed-Batch Cultures at Different CO_2 Atmospheres

From the evaluation of the effects of different CO_2 concentrations in CHO-CY01 cell line batch cultures done in the previous section, it was found that CO_2 concentrations that showed a bigger impact on CHO-CY01 cell line growth, metabolism and IgG4 production were from 10.00% to 20.00% (v/v) CO_2, being 5.00% (v/v) CO_2 still considered as reference. Since the majority of CHO cells production systems are done in either fed-batch mode or perfusion, in this section the impact of CO_2 concentrations higher than 10.00% (v/v) CO_2 in CHO-CY01 cell line fed-batch strategy 5 (FB3) cultures (Section 4.4.2) were evaluated. The 20.00% (v/v) CO_2 CHO-CY01 cell line fed-batch condition was not performed, as the glucose concentration only reached values below 3.00 $g\ L^{-1}$ at day 12 (Figure *5-4*), which implied a fed-batch culture of more than 20 days.In Figure 5-12 and Figure 5-13, the CHO-CY01 cell line fed-batch strategy 5 (FB3) culture kinetics can be visualised for 5.00% (reference), 10.00% and 15.00% (v/v) CO_2. The determined kinetic parameters are in the Table 5-5, Table 5-9 and the observed yields are in the Table C-13. In Figure 5-14 are presented the pH and temperature profiles of these CO_2 concentrations. The average and standard deviation of the cell culture pH and temperature, as well as the first feed pH perturbation with the glucose and glutamate consumption rate during feeding are presented in the Table 5-4. The particle size distribution can be visualised in the Figure B-7 and the values for the different cell culture parameters (viable cell number, cell diameter, viability, larger particles, dead cells, debris and total impurities) per period are presented in the Table B-7. The correlations coefficients were also determined and are presented in Table A-12.

Previously, it was found that all CHO-CY01 cell line batch culture parameters at 5.00% and 10.00% (v/v) CO_2 were equivalent and CHO-CY01 cell line growth was inhibited at 15.00% (v/v) CO_2 with subsequent lowering of glucose, glutamate and lactate metabolic rates. CHO-CY01 cell line fed-batch cultures where glucose was top-up to 3.00 $g\ L^{-1}$ (strategy 5 (FB3)), showed that CO_2 concentrations had an impact on CHO-CY01 cell growth, productivity and metabolism. The harvest criteria chosen was to stop the CHO-CY01 cell line fed-batch cultures when cell viability dropped below 70%, to reduce the amount of total impurities (Table B-7) to around 66.0%. Observing Figure *5-12* A, the viable cell concentration profiles at different CO_2 concentrations were equivalent after day 8. This similarity was correlated with the same pH range (pH~7.0) that CHO-CY01 cells showed at that time point for all CO_2 concentrations. Before day 8, the viable cell numbers variation between CO_2 concentrations can be explained by the different initial pH profiles. At 5.00% (v/v) CO_2, the CHO-CY01 cell culture had a pH > 7.5 in the beginning of the cell culture (day 0 to 2), which triggered the cell survival mechanism to control the internal pH with readily lactate production and excessive glucose consumption. Once the optimal pH was obtained at around day 3 (pH = 6.80), CHO-CY01 cells initiated

exponential phase until day 8, when the maximum viable cell concentration ($8.08 \pm 0.41 \times 10^6\ cells\ mL^{-1}$) was reached. For 10.00% and 15.00% (v/v) CO_2, as the initial pH was lower 7.5 the lactate production started later and never attained the 5.00% (v/v) CO_2 levels. The higher μ observed at 15.00% (v/v) CO_2 can be explained through the pH. At 15.00% (v/v) CO_2 cells had an initial pH of 7.2 compared with 7.5 at 10.00% (v/v) CO_2, this 0.3 pH units difference, lead to higher viable cell numbers and consequently higher glucose and glutamate consumption by the cells and unfortunately higher lactate and ammonium accumulation compared with 10.00% (v/v) CO_2. However, for any CO_2 concentration, the lactate and ammonium accumulation levels were comparable to batch accumulative values (Figure 5-3). The CHO-CY01 cell line glucose consumption rate at the different CO_2 concentrations dictated then the feeding profile. CHO-CY01 cells at 5.00% (v/v) CO_2 required more feeding than 10.00% and 15.00% (v/v) CO_2 (Table 5-4). As feeding is a pH perturbation to the system and because the cell culture pH at 10.00% (v/v) CO_2 and 15.00% (v/v) CO_2 was lower than the cell culture pH at 5.00% (v/v) CO_2 when feeding started (Figure 5-14) the amplitude of these pH perturbations were bigger but culture pH was restored in almost half the time because CHO-CY01 cell culture at 5.00% (v/v) CO_2 is not yet a well buffered medium (Section 5.2). As a direct result of feeding, the cell culture osmolality increased (Figure *5-12* (F)). Although the osmolality range found for any CO_2 concentration (320 – 420 $mOsm\ kg^{-1}$) was higher than the observed at batch mode, it was not considerable inhibitory. Another consequence of feeding was the addiction of Na^+ and K^+ to an already Na^+ and K^+ enriched cell culture. Nonetheless, it was observed from day 11 to 15 a reduction of both cations, followed by an increase for all of the CO_2 concentrations. This trend may be connected with the fact that all CHO-CY01 cell line fed-batch from day 11 to 15 had the same ammonium ion (NH_4^+) concentration. It seems that CHO-CY01 cells were trying to counterbalance the cytoplasmic acidification caused by the high concentration of NH_4^+ by the H^+ extrusion (Figure 5-1). After day 16, CHO-CY01 cells were in cell decline and the increase in cation concentration may be due to the cell lysis.

In terms of IgG4 productivity, at 15.00% (v/v) CO_2 CHO-CY01 cells produce the same maximum IgG4 concentration of 5.00% (v/v) CO_2 but quicker compared with all other CO_2 concentrations cell cultures (66.4 $mg\ L^{-1}day^{-1}$). Nonetheless, it presented the lowest q_{mAb} due to higher viable cell density. At 5.00% and 10.00% (v/v) CO_2 CHO-CY01 cells stopped the IgG4 production at the maximum 1.14 ± 0.03 $g\ L^{-1}$ on day 15 and 1.29 ± 0.24 $g\ L^{-1}$ on day 17, respectively. For a CHO-CY01 cell line fed-batch culture with a pH range of 6.98 ± 0.28 (10.00% (v/v) CO_2), there was a 225% increase in IgG4 production compared with IgG4 concentration obtained in batch mode (0.40 ± 0.11$g\ L^{-1}$). Again, no difference in the particle size distribution was verified with different CO_2 concentrations (Figure B-7 and Table B-7). One important aspect to mention, even with the 70% cell viability harvest criteria, was the

appearance of a dead cells population peak at the particle size decline period (day 16 - 5.00%; day 17 - 10.00% and 15.00% (v/v) CO_2) may be correlated with the IgG4 production stagnation observed and it is definitely an preannouncement of cell death.

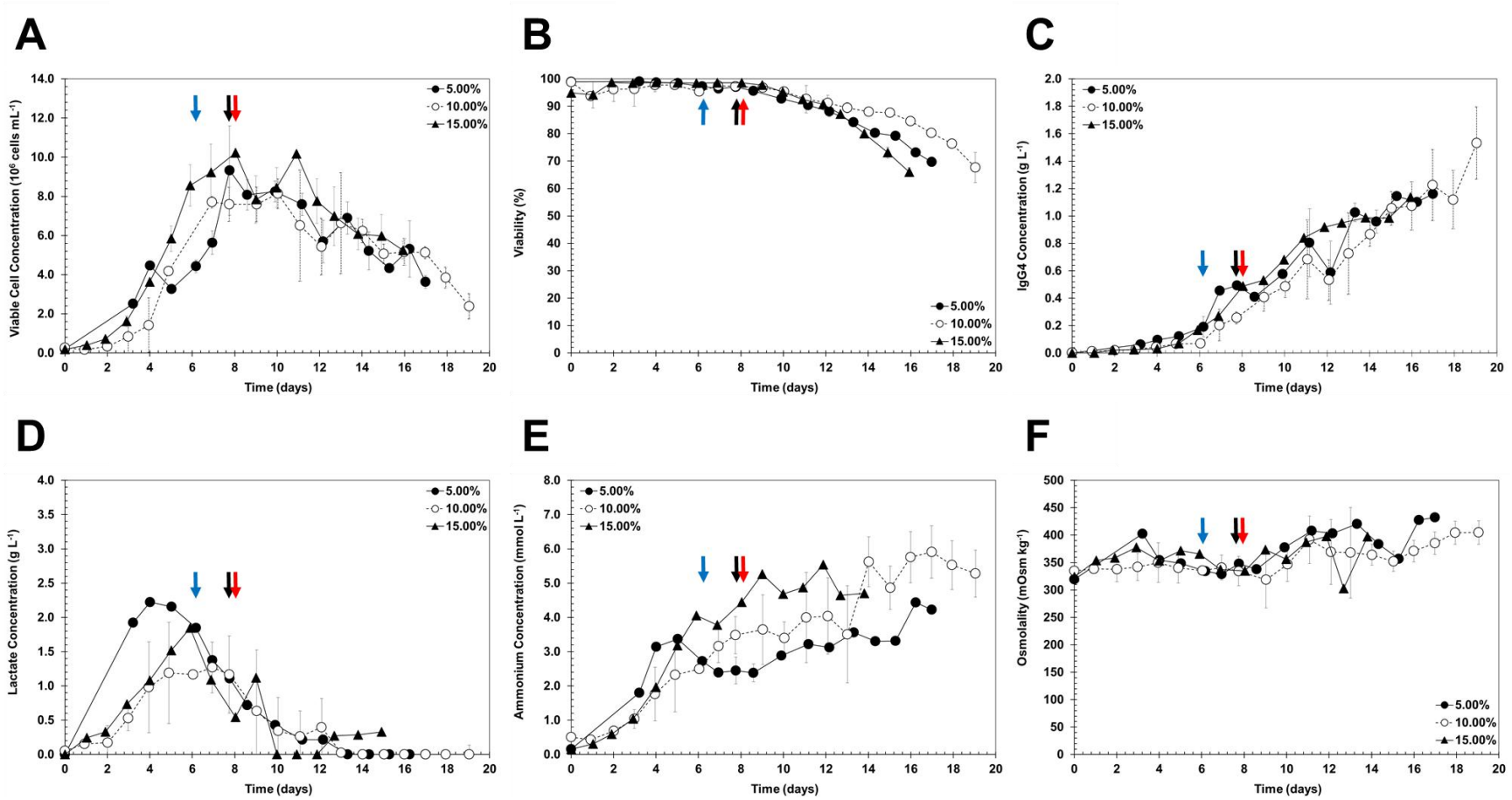

Figure 5-12: Viable cell concentration (A), cell viability (B), IgG4 concentration (C), lactate concentration (D), ammonium concentration (E) and osmolality (F) profiles for CHO-CY01 cell line fed-batch strategy 5 (FB3) cultures in 24-SRW-MTPs at 5.00% (1 run (3-4 replicates)), 10.00% (2 run (6-8 replicates)), and 15.00% (v/v) CO_2 (1 run). The arrow indicates when the feeding started (5.00%– blue; 10.00% – black; 15.00% – red). Error bars represent one standard deviation about the mean.

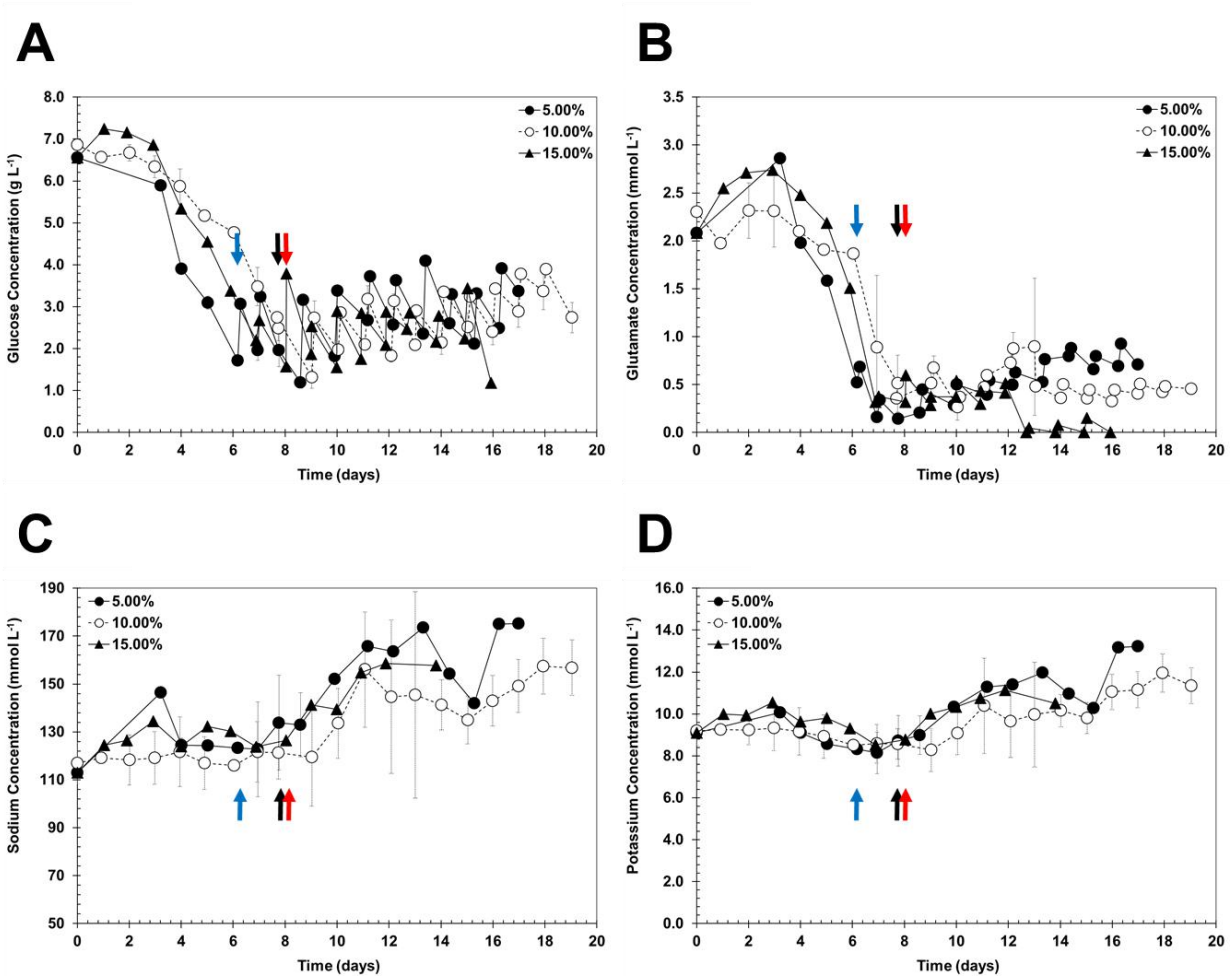

Figure 5-13: Glucose (A), glutamate (B), sodium (C) and potassium (D) concentrations profiles for CHO-CY01 cell line fed-batch strategy 5 (FB3) cultures in 24-SRW-MTPs at 5.00% (1 run (3-4 replicates)), 10.00% (2 run (6-8 replicates)), and 15.00% (v/v) CO_2 (1 run). The arrow indicates when the feeding started (5.00%– blue; 10.00% – black; 15.00% – red). Error bars represent one standard deviation about the mean.

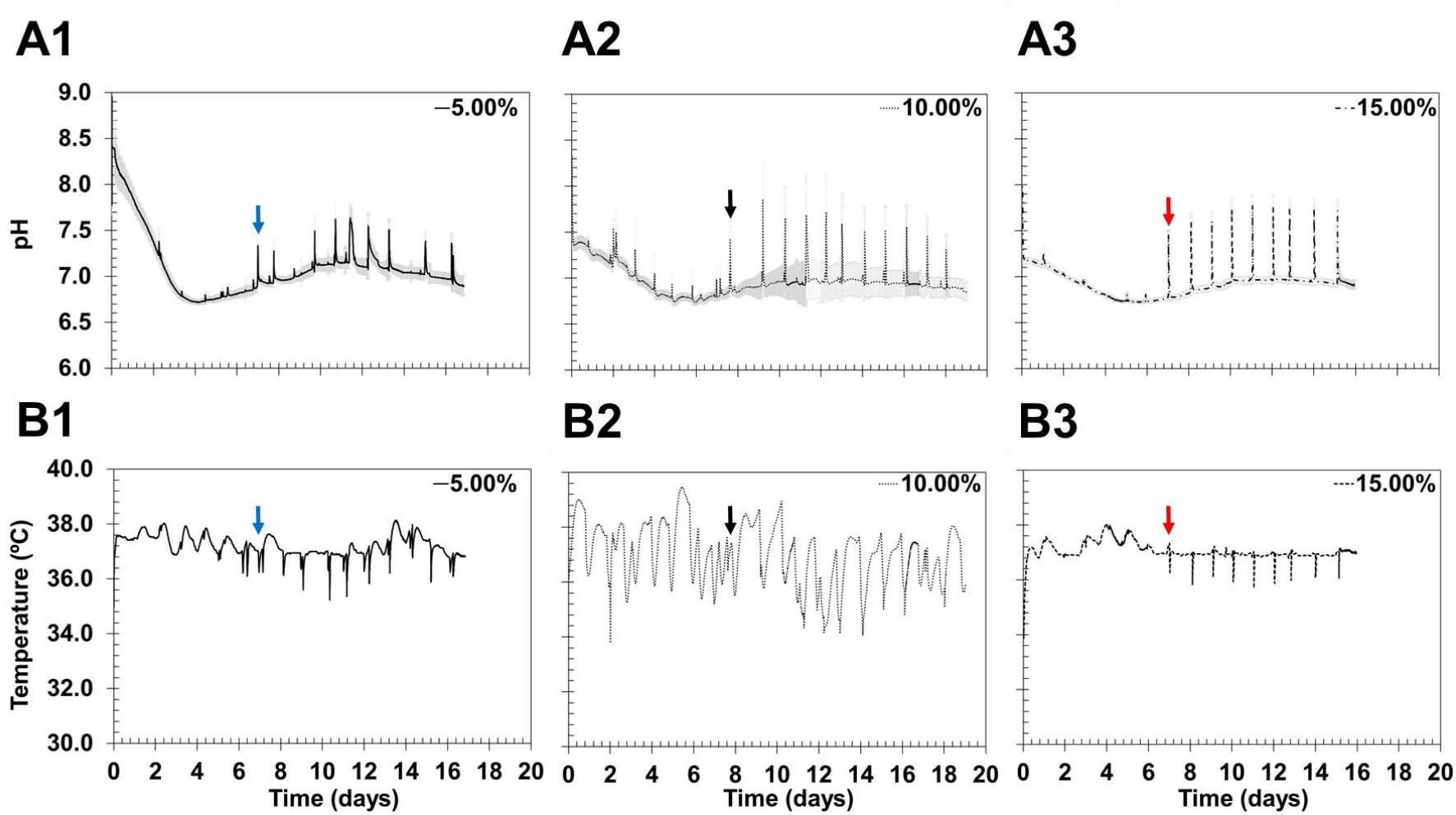

Figure 5-14: pH (A) and temperature profiles (B) for CHO-CY01 cell line fed-batch strategy 5 (FB3) cultures in 24-SRW-MTPs at 5.00% (1) (1 runs (24 replicates), 10.00% (2) (2 run (48 replicates), and 15.00% (v/v) CO_2 (3) (1 run (24 replicates)). The arrow indicates when the feeding started (5.00%– blue; 10.00% – black; 15.00% – red). Error bars represent one standard deviation about the mean.

Table 5-4: Average and standard deviation values of process parameters: pH and temperature; glucose and glutamate consumption rates in fed-batch mode, and amplitude and duration of the first feeding pH perturbation for CHO-CY01 cell line fed-batch strategy 5 (FB3) cultures in 24-SRW-MTPs at 5.00%, 10.00%, and 15.00% (v/v) CO_2. The pH perturbations parameters were determined as described in the Section 4.4.1.

CO_2 (% (v/v))	pH	Temperature (°C)	Daily Glucose Consumption rate ($g\ L^{-1}day^{-1}$)	Daily Glutamate consumption rate ($mmol\ L^{-1}day^{-1}$)	1st Feed pH perturbation			
					Amplitude	Duration (hours)	pH before pH perturbation	pH after pH perturbation
5.00	7.08 ± 0.36	37.2 ± 0.5	1.33 ± 0.39	0.18 ± 0.06	0.37	6.0	6.97	6.95
10.00	6.98 ± 0.28	36.9 ± 1.1	0.92 ± 0.34	0.04 ± 0.17	0.56	3.3	6.86	6.86
15.00	6.88 ± 0.21	37.2 ± 0.4	0.97 ± 0.57	0.12 ± 0.07	0.67	3.4	6.77	6.78

Table 5-5: Kinetic parameters determined for CHO-CY01 cell line fed-batch strategy 5 (FB3) cultures in 24-SRW-MTPs at 5.00%, 10.00%, and 15.00% (v/v) CO_2.

CO_2 (% (v/v))	**5.00**	**10.00**	**15.00**
VP ($mg\ L^{-1}day^{-1}$)	64.7	53.3 ± 15.3	66.4
IVCC ($10^9\ cells\ day\ L^{-1}$)	85.93	69.88 ± 29.75	95.61
$\mu\ (h^{-1})$	0.022	0.017 ± 0.006	0.029
$t_{1/2}\ (h)$	30.9	44.1 ± 18.2	24.3
$q_{mAb}\ (mg\ 10^{-9}\ cells^{-1}\ day^{-1})$	13.71	17.28 ± 4.81	12.16
$q_{Gluc}\ (g\ 10^{-9}\ cells^{-1}\ day^{-1})$	-0.21	-0.23 ± 0.09	-0.17
$q_{Glu}\ (mmol\ 10^{-9}\ cells^{-1}\ day^{-1})$	-0.04	-0.05 ± 0.02	-0.05
$q_{Lact}\ (g\ 10^{-9}\ cells^{-1}\ day^{-1})$	0.19	0.19 ± 0.15	0.12
$q_{Amm}\ (mmol\ 10^{-9}\ cells^{-1}\ day^{-1})$	0.05	0.09 ± 0.04	0.08
Lactate produced / Glucose consumed (g/g)	0.84	0.49 ± 0.26	0.48
$\mu_d\ (h^{-1})$	-0.0035	-0.011 ± 0.007	-0.005
Feed volume (% of reactor volume)	109.4	88.1	33.3
Evaporation rate ($\mu L\ day^{-1}$)	21.5 ± 5.1	9.3 ± 2.6	10.0 ± 6.6

5.4. CO_2 Shifts in CHO-CY01 Cell Line Cultures

Once known the effects that a constant CO_2 concentration has on CHO-CY01 cell line cultures growth, metabolism, IgG4 productivity and most importantly on cell culture pH. CO_2 concentration inside the CO_2 incubator can be manipulated in order to obtain any desirable pH profile for IgG4 productivity optimisation. At a first perspective, CO_2 concentration was changed multiple times from a high CO_2 concentration to lower CO_2 concentration in a step-by-step method in a CHO-CY01 cell line batch culture (Section 5.4.1). In order to have a more realistic view, CO_2 shifts were performed in CHO-CY01 cell line fed-batch cultures in multiples steps (Section 5.4.2.1) and then a one-step shift at different cell culture times (Section 5.4.2.2). The goal was to design a CHO-CY01 cell line fed-batch culture where the manipulation of CO_2 levels would lead initially to a high cell growth rate (5.00% or 10.00% (v/v) CO_2), followed by high IgG4 production rate (15.00% or 20.00% (v/v) CO_2). So, the viable cell numbers were firstly maximised and then those CHO-CY01 cells were put in conditions where IgG4 production rate was optimal.

5.4.1. CO_2 Shifts in CHO-CY01 Cell Line Batch Cultures

In this section, the first attempt at a pH control through exclusively CO_2 manipulation in 24-SRW MTP was performed (pH shift 1). As no mathematical treatment occurred, the decision for a step-by-step shifting of CO_2 concentrations was intuitively done using a simple decision tree (Figure 5-15). Since the highest IgG4 concentration obtained in fed-batch mode had a cell culture around pH 7.00, the pH set point value considered was 7.00. In Figure 5-18 the CO_2 level profile with pH and temperature profiles can be observed. The CHO-CY01 cell line pH shift 1 culture kinetics are presented in Figure 5-16 and Figure 5-17, the determined kinetic parameters are in Table 5-6 and Table C-14. An apoptotic and cell cycle analysis was also performed and the apoptotic population and cell cycle fraction are represented in Figure 5-19.The particle size distribution histograms are presented in Figure B-8 and the diverse population fraction are in Table B-8. The cell culture parameter correlation coefficient table is presented in Table A-15.

In this first attempt, the pH range obtained was 6.86 ± 0.20, which includes the set point. Starting the CHO-CY01 cell line batch culture at 8.00% (v/v) CO_2 and slowly decrease the CO_2 concentration to 6.00% (v/v) CO_2 until day 3 was effective enough to put the cell culture pH at around physiological pH (pH 7.00) (Figure 5-18 A). After day 3, the cell culture pH had a pH drop of 0.3 units due to lactate production from the cells (Figure 5-16 D). Following the decision tree, the CO_2 level was lowered at 3.50% (v/v) CO_2. At this CO_2 concentration, the pH cell culture increased but proved defective against the increasing lactate concentration. So, at day 4 a new CO_2 shift from 3.50% to 2.00% (v/v) CO_2 was made. This CO_2 shift was able to

increase the pH to 6.8, which stopped the lactate production and initiated the stationary phase in batch culture. Therefore, it seems that CHO-CY01 cells at cell culture pH between 6.70 and 6.80 have a null net lactate production rate and specific growth rate. At day 5 the lowest pH was reached (pH=6.60 ± 0.04), so there was a CO_2 shift from 2.00% to 1.00% (v/v) CO_2, which was able to push the pH around 6.70 and so it maintained CHO-CY01 cells in stationary phase with no more lactate production. Since the pH set point was not reached, the final CO_2 shift from 1.00% to 0.04% (v/v) CO_2 was made at day 7. At day 7, CHO-CY01 cells had no more glucose and glutamate, which triggered the cell decline period. After day 7, the pH of the cell culture increased and met the set point value as a result of cell lysis NH_4^+ release.

CHO-CY01 cell line batch cultures at constant 5.00% (v/v) CO_2 and at the pH shift 1 condition presented the same glucose consumption rate ($0.8 g\ L^{-1} day^{-1}$) and maximum IgG4 concentration ($0.34 \pm 0.17 g\ L^{-1}$). However, at pH shift 1 the total number of viable CHO-CY01 cells was about 55% lower than at 5.00% (v/v) CO_2 concentration. This meant that CHO-CY01 cells at pH shift 1 condition had an increase of 123.8% in the specific glucose consumption of ($0.47\ g\ 10^{-9}\ cells^{-1}\ day^{-1}$ (Table 5-6)) for a 24.4% increment in the q_{mAb}. Besides, CHO-CY01 cells in pH shift 1 condition were not lactate consumers, which lead to a 35.5% increase in the cumulative lactate concentration. In terms of the specific Na^+ and K^+ consumption rates, the CHO-CY01 cells at pH shift 1 increased the consumption of K^+ resulting from the increase in the $q_{NH_4^+}$. The cells started to consume the Na^+ instead of excreting it as in the 5.00% CO_2 culture. This is likely a result of the low intracellular pH caused by the CO_2 shifts.

From the apoptotic analysis, it was observed that cell death in pH shift 1 condition was triggered on day 5 (pH = 6.60 ± 0.04) by apoptotic cells as the decline of viable cells fraction was concurrent with the increase in early and late apoptotic cell fractions (Figure 5-19). In terms of cell cycle profile was equivalent to the one for 5.00% (v/v) CO_2 (Figure 5-10). From Figure 5-19 C, it is clearly visible the relationship between cell diameter and IgG4 concentration. At pH shift 1 conditions, the diameter of CHO-CY01 cells at the peak of IgG4 production was almost 2 μm bigger than compared with the diameters found at the reference condition.

Several significant and useful facts were learned from this rudimentary pH control experience: CHO-CY01 cell line culture medium pH between 6.70 and 6.80 caused a cell growth and lactate arrest. It also increased the cell size, which promoted IgG4 production. However, lactate consumer advantageous phenotype was lost by the CHO-CY01 cells. Cell culture medium pH below 6.60 was associated with promoting apoptotic pathway. Therefore, for IgG4 optimisation purposes, CHO-CY01 cells should be run at a constant pH range of 6.70 to 6.80.

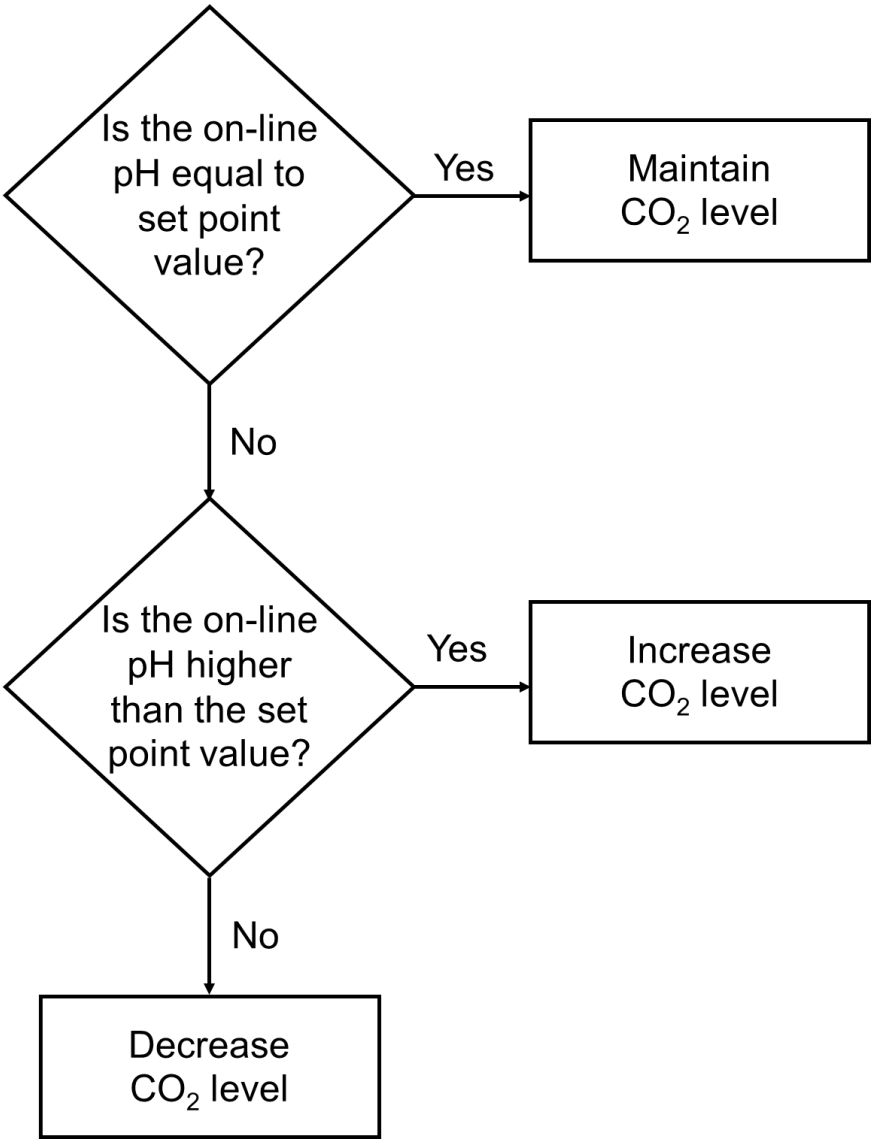

Figure 5-15: Decision tree used to control the CHO-CY01 cell line culture pH with exclusively manipulations of CO_2 level inside the CO_2 incubator. The online pH values were obtained from PreSens® software.

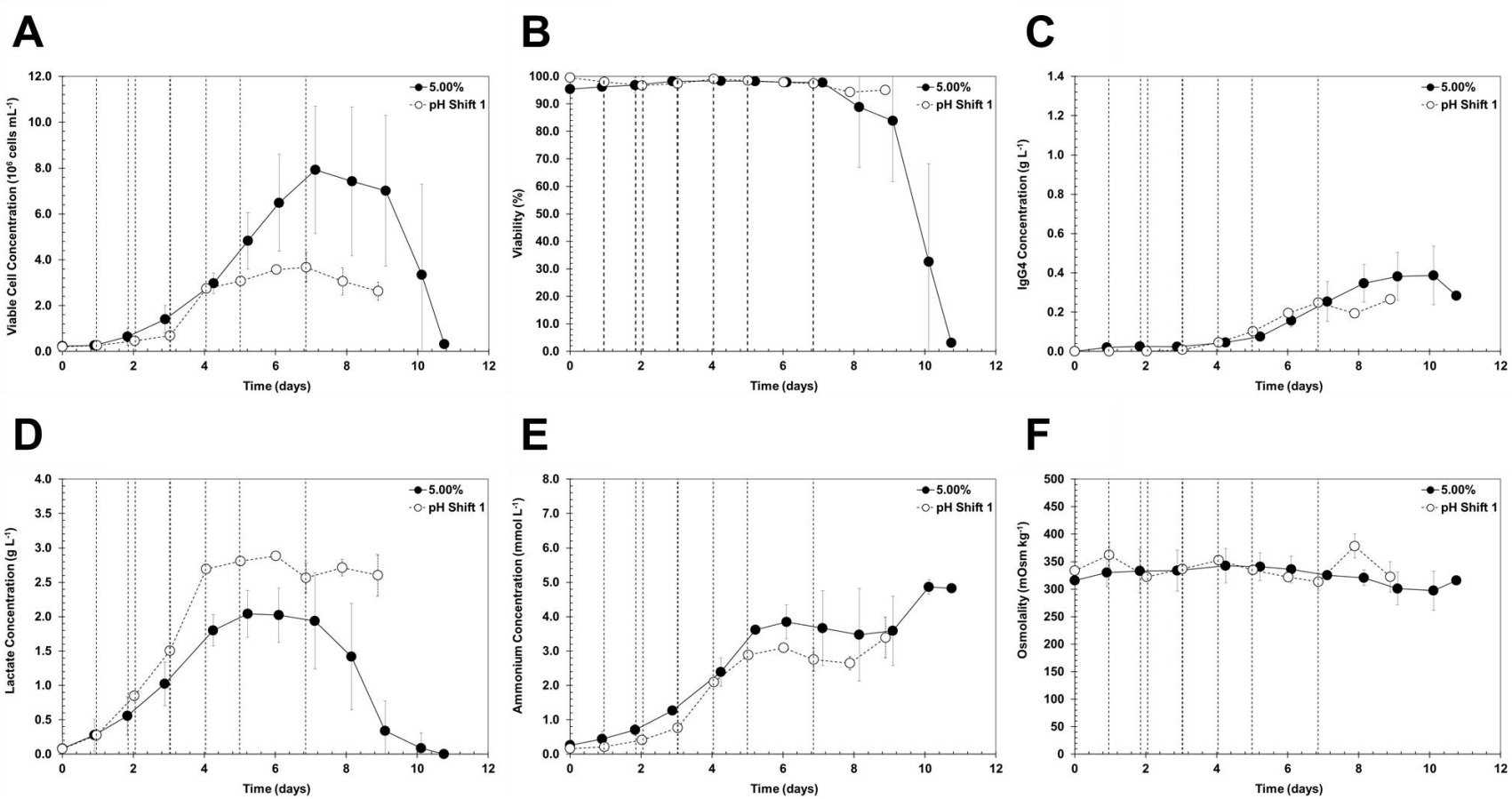

Figure 5-16: Viable cell concentration (A), cell viability (B), IgG4 concentration (C), lactate concentration (D), ammonium concentration (E) and osmolality (F) profiles for CHO-CY01 cell line batch culture at constant 5.00% (v/v) CO_2 (3 runs (9-12 replicates)) and the first CO_2 multiphasic CHO-CY01 cell line batch cultivation in 24-SRW-MTPs (pH shift 1) (1 run (3-4 replicates)). The dash lines indicate when the CO_2 shifts occurred. The error bars represent one standard deviation about the mean.

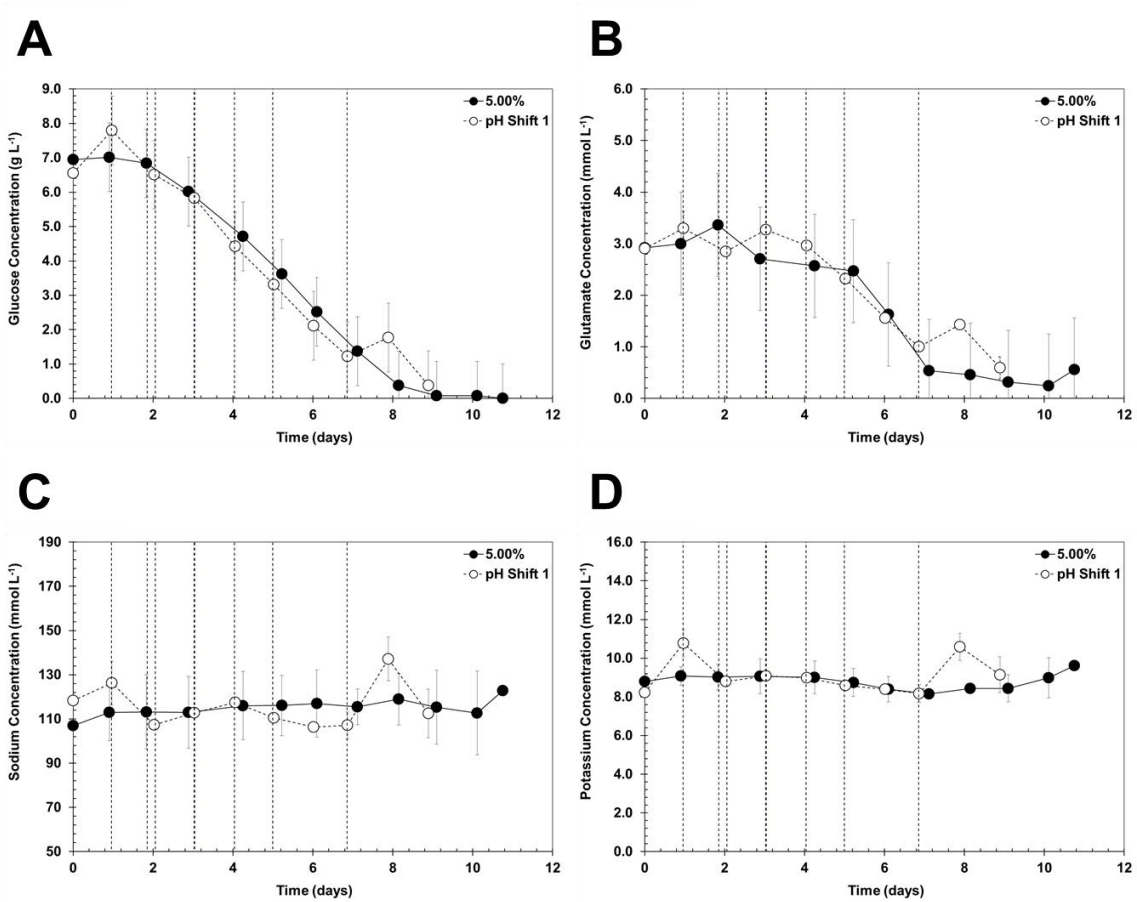

Figure 5-17: Glucose (A), glutamate (B), sodium (C) and potassium (D) concentrations profiles for CHO-CY01 cell line batch culture at constant 5.00% (v/v) CO_2 (3 runs (9-12 replicates)) and the first CO_2 multiphasic CHO-CY01 cell line batch cultivation in 24-SRW-MTPs (pH shift 1) (1 run (3-4 replicates)). The dash lines indicate when the CO_2 shifts occured. The error bars represent one standard deviation about the mean.

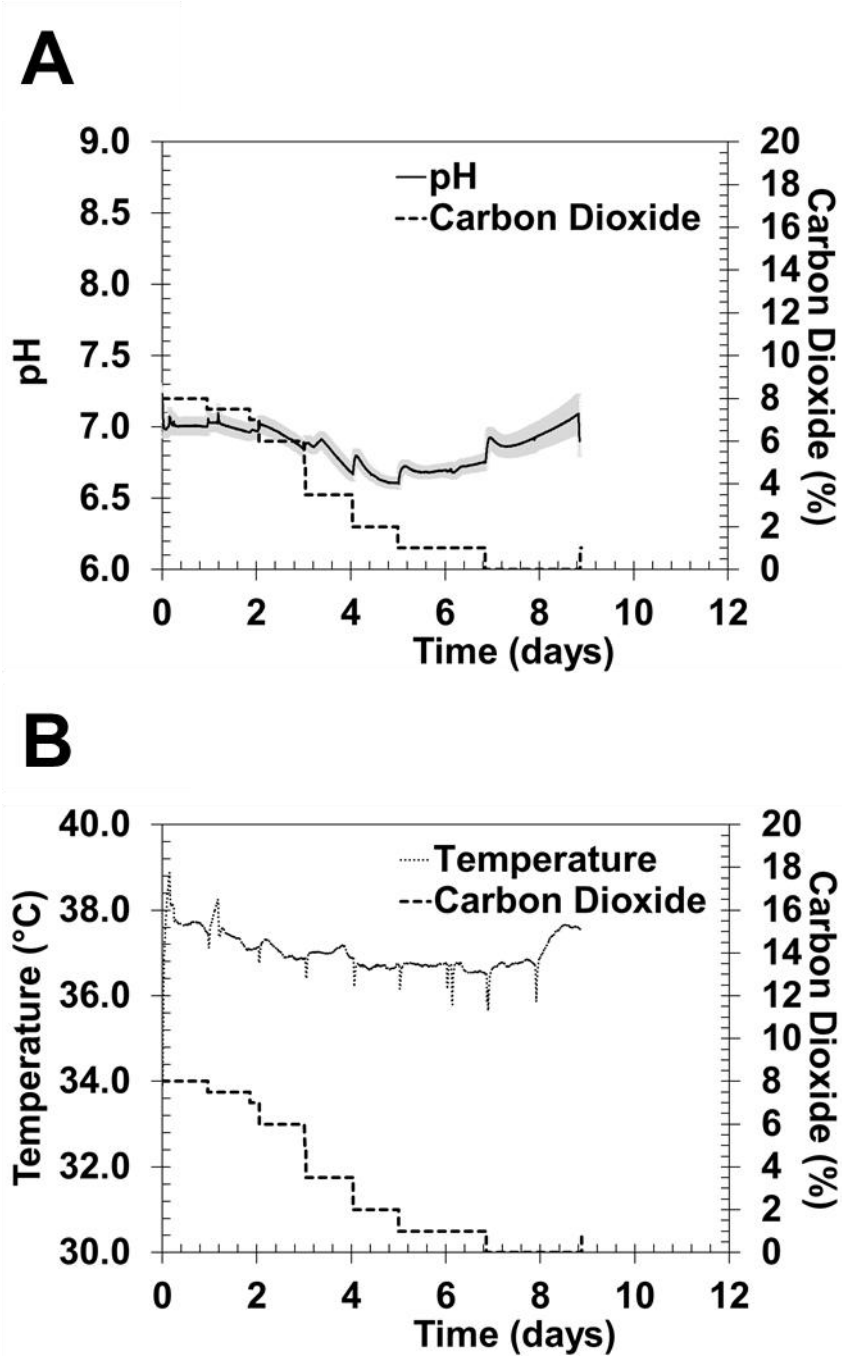

Figure 5-18: pH (A) and temperature profiles (B) with CO_2 level profile for the first CO_2 multiphasic CHO-CY01 cell line batch cultivation in 24-SRW-MTPs (pH shift 1). Error bars represent one standard deviation about the mean.

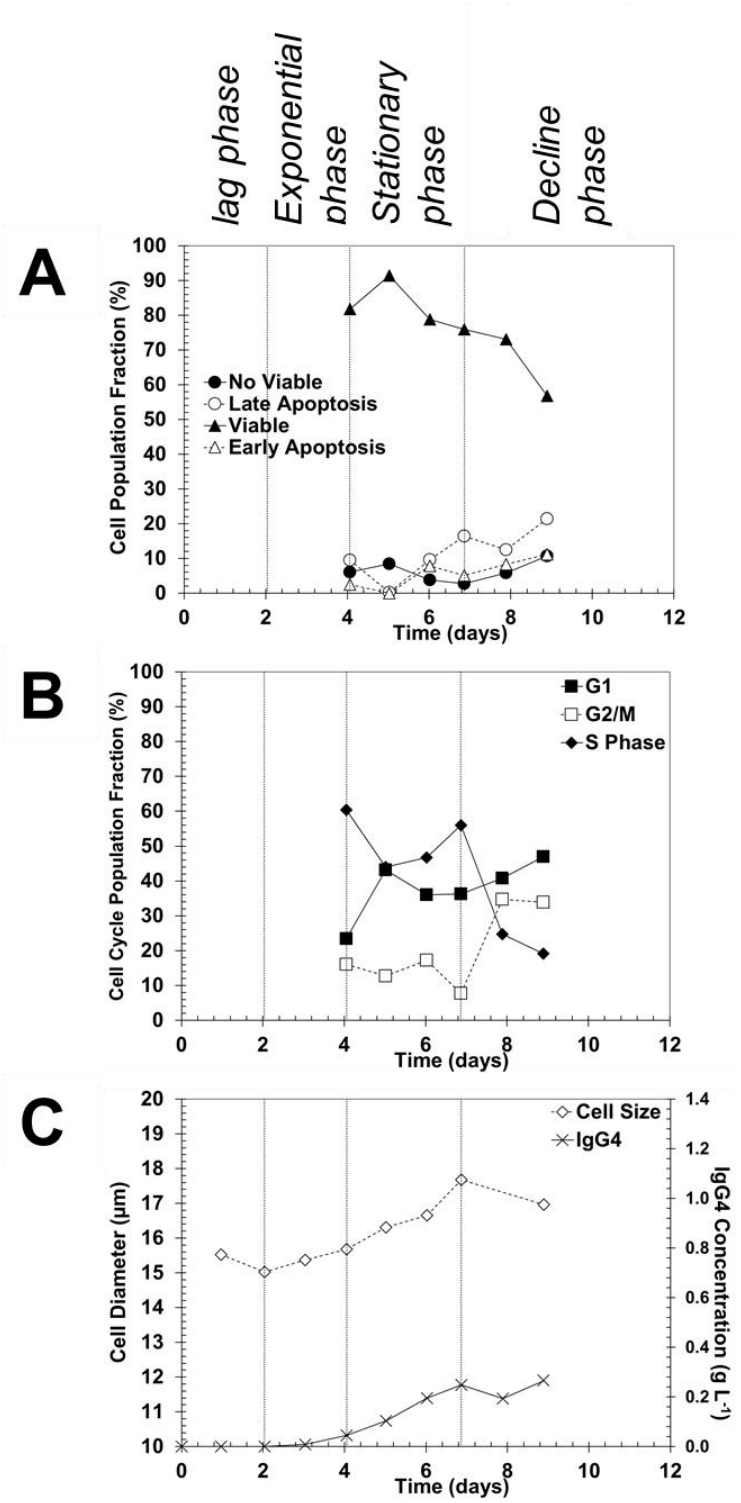

Figure 5-19: Apoptotic (A) and cell cycle (B) population fractions, and viable cell diameter and IgG4 titer (C) profiles for the first CO_2 multiphasic CHO-CY01 cell line batch cultivation in 24-SRW-MTPs (pH shift 1) accordingly to phases of cell growth (lag, exponential, stationary and decline or death phase). The error bars are the standard deviation about the mean.

Table 5-6: Kinetic parameters determined for CHO-CY01 cell line batch culture at constant 5.00% (v/v) CO_2 and the first CO_2 multiphasic CHO-CY01 cell line batch cultivation in 24-SRW-MTPs (pH shift 1).

	5.00 % (v/v) CO_2	**pH Shift 1**
VP ($mg\ L^{-1} day^{-1}$)	34.33 ± 5.8	26.7
IVCC ($10^9\ cells\ day\ L^{-1}$)	41.24 ± 8.84	18.46
$\mu\ (h^{-1})$	0.02 ± 0.002	0.022
$t_{1/2}\ (h)$	30.46 ± 3.3	31.9
$q_{mAb}\ (mg\ 10^{-9}\ cells^{-1}\ day^{-1})$	10.58 ± 3.01	15.70
$q_{Gluc}\ (g\ 10^{-9}\ cells^{-1}\ day^{-1})$	-0.21 ± 0.03	-0.47
$q_{Glu}\ (mmol\ 10^{-9}\ cells^{-1}\ day^{-1})$	-0.08 ± 0.02	-0.15
$q_{Na^+}\ (mmol\ 10^{-9}\ cells^{-1}\ day^{-1})$	0.29 ± 0.11	-0.14
$q_{K^+}\ (mmol\ 10^{-9}\ cells^{-1}\ day^{-1})$	-0.014 ± 0.009	-0.126
$q_{Lact}\ (g\ 10^{-9}\ cells^{-1}\ day^{-1})$	0.35 ± 0.12	1.09
$q_{Amm}\ (mmol\ 10^{-9}\ cells^{-1}\ day^{-1})$	0.126 ± 0.029	0.208
Lactate produced / Glucose consumed (g/g)	0.52 ± 0.13	0.49
$\mu_d\ (h^{-1})$	-0.03 ± 0.011	-0.007
Evaporation rate ($\mu L\ day^{-1}$)	19 ± 9	19 ± 6

5.4.2. CO_2 Shifts in CHO-CY01 Cell Line Fed-Batch Cultures

CHO-CY01 cell line with fed-batch strategy 5 (FB3) have shown to produce 1.29 ± 0.24 $g\ L^{-1}$ of IgG4 at constant 10.00% (v/v) CO_2, which represented a pH range of 6.98 ± 0.28 (Section 5.3). Therefore, in order to further maximise IgG4 productivity, CO_2 shifts were performed in CHO-CY01 cell line fed-batch cultures. CO_2 biphasic (Section 5.4.2.2) and multiphasic (Section 5.4.2.1) CHO-CY01 cell line cultures were performed. The goal was to design a CHO-CY01 cell line fed-batch culture where the manipulation of CO_2 levels would lead initially to a high cell growth rate (5.00% or 10.00% (v/v) CO_2), followed by high IgG4 production rate (15.00% or 20.00% (v/v) CO_2). At the same time, further understanding of CO_2 impact on CHO-CY01 cell line culture pH was also established. From that, it was possible to recognise pH ranges where CHO-CY01 cell line growth, metabolism and IgG4 production were different. With this knowledge, a bridge between 24-SRW MTP and 5L-STR CHO-CY01 cell line performance could be formed for IgG4 productivity optimisation.

5.4.2.1. CO_2 Shifts in CHO-CY01 Cell Line Fed-Batch Cultures in Multiple Steps

In this section, a CO_2 multiphasic and biphasic CHO-CY01 cell line fed-batch cultures were performed and compared with the reference fed-batch culture: 5.00% (v/v) CO_2 (1.14 ± 0.03 $g\ L^{-1}$ IgG4). For a first analysis and to keep the consistency, both CHO-CY01 cell line fed-batch cultures with CO_2 shifts started at the CO_2 concentration of reference (5.00% (v/v) CO_2). Knowing the pH profile of CHO-CY01 cell line fed-batch at constant 5.00% (v/v) CO_2 (Figure 5-14), it was possible a pH manipulation though changing the CO_2 level at different cell culture time points, e. g. changing the cell culture pH at different time points.

Since the pH range for a CHO-CY01 cell line fed-batch culture at constant 5.00% (v/v) CO_2 was 7.08 ± 0.36 and the maximum IgG4 productivity was obtain at pH 6.98 ± 0.28, the decision tree for pH control with exclusively CO_2 level manipulation (Figure 5-15) was applied. Therefore, the CO_2 shifts performed were from 5.00% (v/v) CO_2 to a higher CO_2 level, the contrary of what was done in Section 5.4.1. In this case, the maximum CO_2 shift amplitude available was the CO_2 shift from 5.00% to 20.00% (v/v) CO_2. Two different strategies were used to perform this increase in CO_2 concentration. The first strategy was to do a step-by-step increase of CO_2 level (2.50% (v/v) CO_2 per step) from the beginning of exponential phase (day 3) with a total of four steps. The second strategy was a one step CO_2 shift when CHO-CY01 cell line fed-batch culture at constant 5.00% (v/v) CO_2 reached the maximum viable cell concentration (day 7).

CHO-CY01 cell line fed-batch culture kinetics can be visualised in Figure 5-20 and Figure 5-21, and the determined parameters are shown in Table 5-7, and Table C-15. pH and temperature profiles for the CHO-CY01 cell line fed-batch culture at the reference CO_2

concentration, CO_2 shift in 1 step and CO_2 shift in 4 steps are presented in Figure 5-22. The pH and temperature ranges throughout the cell culture and the glucose and glutamate consumption rate are in Table 5-9. A study on the effect of CO_2 shifts on the CHO-CY01 cell line fed-batch culture particle size distribution was performed, and the particle size histograms are presented in Figure B-9, and the particle fraction distribution is presented in Table B-9. Spearman´s correlation coefficients were also determined, and the table of relationships between cell culture parameters are in Table A-16.

The decision for when the CO_2 shifts occurred at the CHO-CY01 cell line fed-batch culture with CO_2 shifts in 4 steps, relied on the same principle used for the pH control in the section 5.4.1. The first CO_2 shift was performed in the beginning at the exponential phase (day 3) in order to accelerate the drop in the initial pH (pH > 8.00) and to minimise the maximum lactate concentration. Indeed, with this first CO_2 shift, the pH of the CHO-CY01 cell line fed-batch culture reached a pH value around 6.80 and a lactate concentration of 1.9 ± 0.1 $g\ L^{-1}$, which was lower than the values observed at the reference condition. The Na^+ and K^+ concentrations after this first CO_2 shift, decreased until day 5 (end of exponential phase) (Figure 5-21). This fact reflected the cytoplasmic acidification caused by an increase in CO_2 concentration. Since 7.50% (v/v) CO_2 was able to maintain the cell culture pH constant until day 6, and the lactate concentration stagnated around 1.9 ± 0.1 $g\ L^{-1}$, there was no need for a CO_2 shift. During this period (day 3 to 6), CHO-CY01 cells were in exponential phase but once again the net lactate production rate was almost null at pH 6.70 - 6.80. The other CO_2 shifts were done when the glucose level went below 3.00 $g\ L^{-1}$, e.g. when the fed-batch mode started. It was decided to do the CO_2 shifts before feeding to possibly cancel the pH perturbation caused by the feed. However, this plan caused the exact opposite, i.e. by increasing the CO_2 level, the cell culture pH decreased, which incremented the amplitude of the feed´s pH perturbation. The CO_2 shift from 7.50% to 10.00% (v/v) CO_2 at day 7, lowered the pH to values below 6.70, which triggered a boost in ammonium production rate, and so increased the cell culture osmolality. The CO_2 shift from 10.00% to 12.50% (v/v) CO_2 at day 8, continued to lowered the pH to values around 6.60 (during 2.4 hours), which caused the immediate cell death due to apoptosis (Section 5.4.1). From day 5 to 8 (pH 6.78 ± 0.06), CHO-CY01 cells presented a second exponential phase at a μ of 0.05 h^{-1} with no lactate accumulation. The IgG4 concentration was maintained at 0.27 ± 0.03 $g\ L^{-1}$ during this period. From the particle size distribution (Figure B-9), it was observed in the particle size stationary phase (day 6 to 8), CHO-CY01 cells were larger than the other CO_2 shifts conditions and had a larger cell aggregates peak population (cell diameter > 20 μm). This was a clear indication that CHO-CY01 cells were under osmotic stress. The final CO_2 shift from 12.50% to 15.00% (v/v) CO_2 at day 10, sealed the CHO-CY01 cell faith by lowering the pH to around 6.50. The

high glucose consumption rate during the fed-batch (1.70 ± 0.98 $g\ L^{-1}day^{-1}$ (Table 5-9) was a reflection of the cellular struggle to keep the pH homeostasis.

The CHO-CY01 cell line fed-batch culture with one step CO_2 shift from 5.00% to 20.00% (v/v) CO_2, had a catastrophic effect on CHO-CY01 cell line growth. This extreme CO_2 shift caused a pH decrease to values below 6.70 (Figure 5-22 (A3)), which again triggered an increment in ammonium production rate (Figure 5-20 E). That day feed was able to beneficially increase the pH to around 6.80 for almost a day. However, by keeping the CO_2 level at 20.00% (v/v) CO_2, the CHO-CY01 cell culture pH dropped to values below 6.60, at day 8, which initiated the cell decline phase. Since CHO-CY01 cells were dying one day after the CO_2 shift, the glucose consumption rate decreased after shift (Table 5-9). Also, this CO_2 shift changed the lactate profile of the cells (Figure 5-20 D). Before the CO_2 shift, CHO-CY01 cells were consuming both glucose and lactate as carbon source for cellular metabolism. One day after the CO_2 shift, cells were again producing lactate from glucose. Therefore, IgG4 production stopped at 0.29 ± 0.02 $g\ L^{-1}$, a value much lower than the one obtained in a CHO-CY01 cell line batch culture (0.40 ± 0.11 $g\ L^{-1}$).

These CO_2 shifts have not fulfilled the aim of increasing CHO-CY01 cell line IgG4 productivity, but from them it was found that CHO-CY01 cells were unable to grow and produce IgG4 at cell culture pH below 6.70. Therefore, in the quest of finding the optimal pH profile from these CHO-CY01 cell line fed-batch cultures, it was found the minimum of such pH range. Also, CO_2 shifts of 15.00% (v/v) CO_2 difference were found to be too brutal for the cells and 5.00% (v/v) CO_2 was considered as an inadequate reference CO_2 concentration.

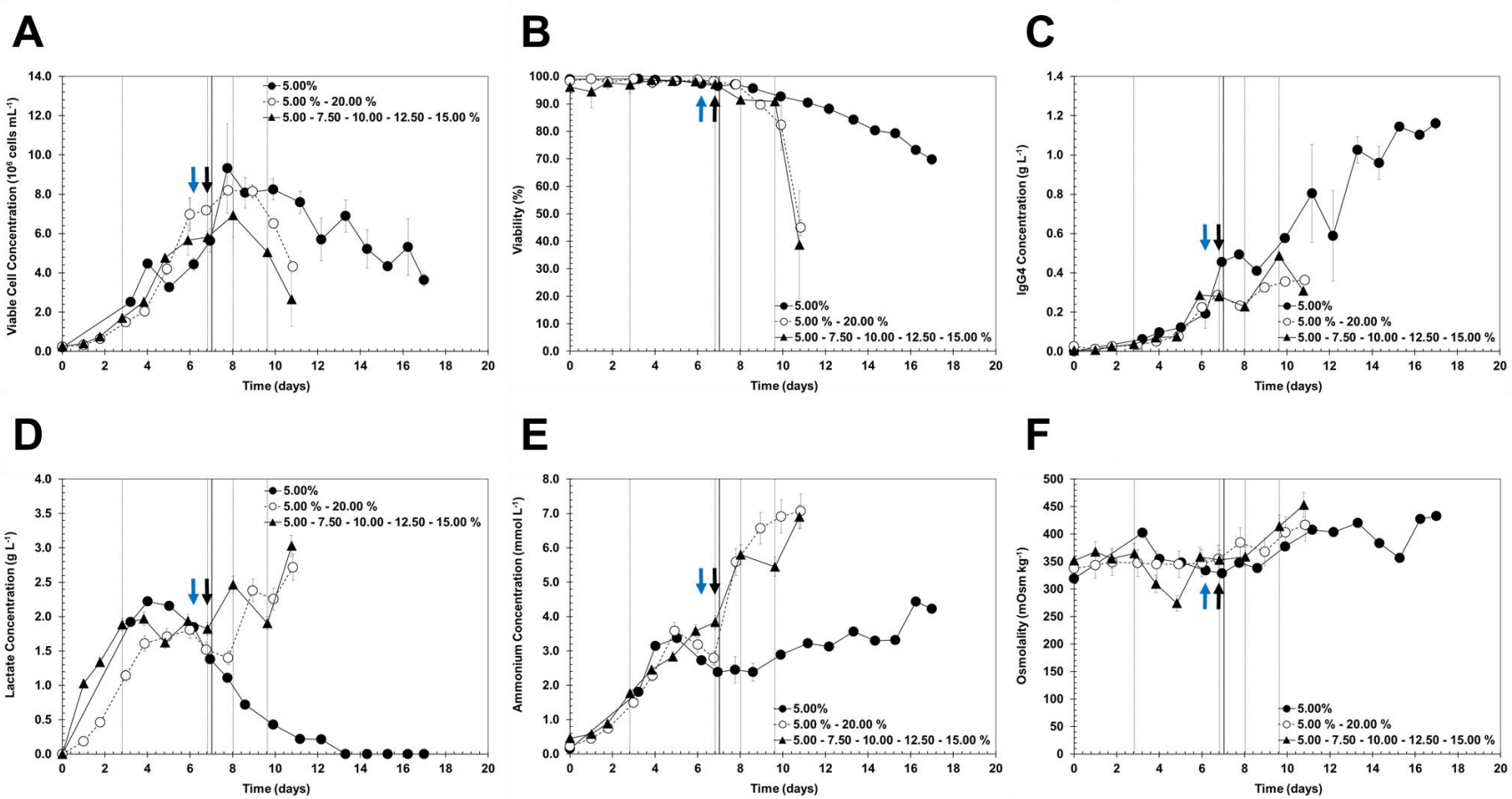

Figure 5-20: Viable cell concentration (A), cell viability (B), IgG4 concentration (C), lactate concentration (D), ammonium concentration (E) and osmolality (F) profiles for CHO-CY01 cell line fed-batch strategy 5 (FB3) cultures in 24-SRW-MTPs (1 run (3-4 replicates)) with constant 5.00% (v/v) CO_2, CO_2 shift from 5.00% to 20.00% (v/v) CO_2 on day 7 (1 step) and CO_2 shift from 5.00% to 7.50% on day 2, 7.50% to 10.00% on day 7, 10.00% to 12.50% on day 8, and 12.50% to 15.0% (v/v) CO_2 on day 10 (4 steps). The horizontal long dash line and the horizontal dotted lines indicate when the 1 step and 4 steps CO_2 shifts occurred, respectively. The dash lines indicate when the CO_2 shifts occured The arrow indicates when the feeding started (5.00% and 1 step CO_2 shift – blue; 4-steps CO_2 shift – black). Error bars represent one standard deviation about the mean.

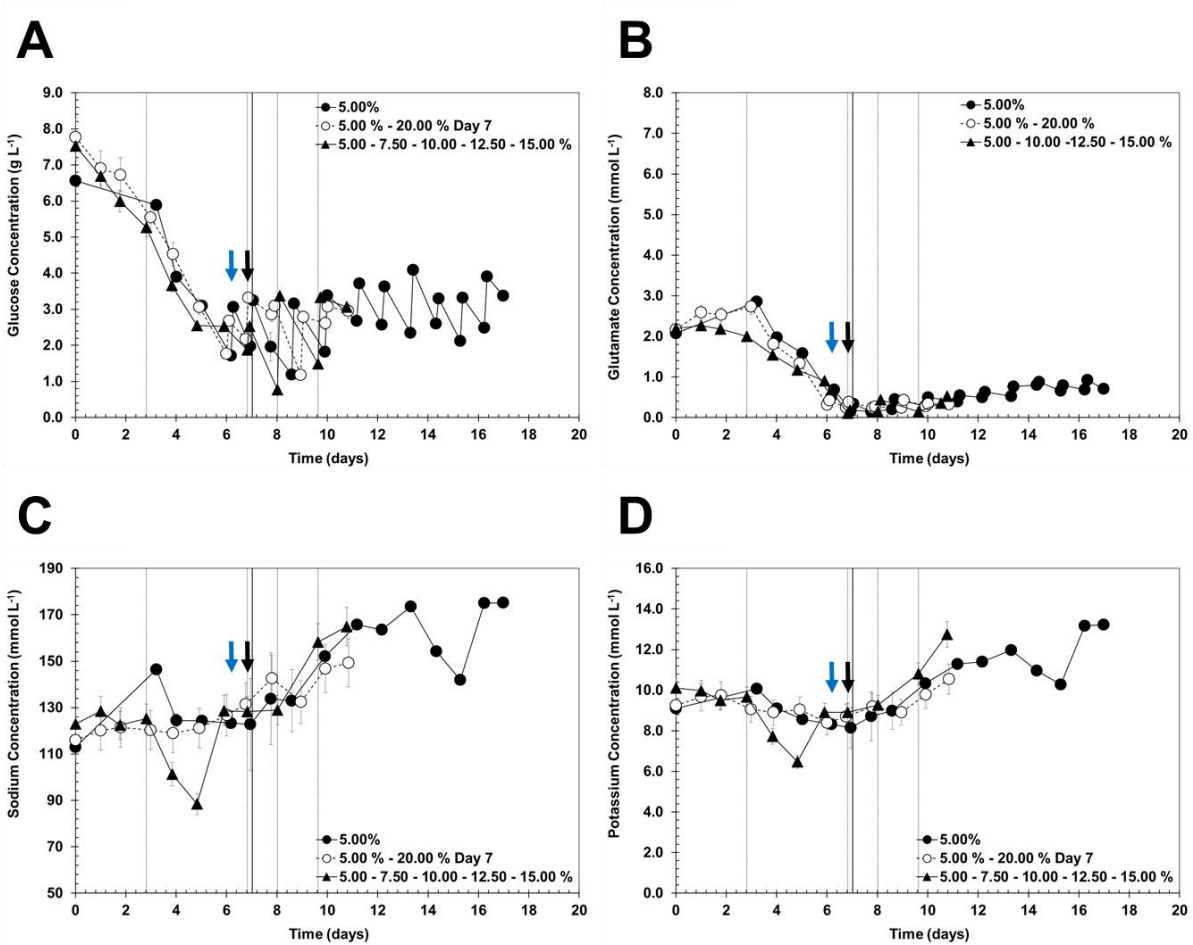

Figure 5-21: Glucose (A), glutamate (B), sodium (C) and potassium (D) concentrations profiles for CHO-CY01 cell line fed-batch strategy 5 (FB3) cultures in 24-SRW-MTPs (1 run (3-4 replicates)) with constant 5.00% (v/v) CO_2, CO_2 shift from 5.00% to 20.00% (v/v) CO_2 on day 7 (1 step) and CO_2 shift from 5.00% to 7.50% on day 2, 7.50% to 10.00% on day 7, 10.00% to 12.50% on day 8, and 12.50% to 15.0% (v/v) CO_2 on day 10 (4 steps). The horizontal long dash line and the horizontal dotted lines indicate when the 1 step and 4 steps CO_2 shifts occurred, respectively. The arrow indicates when the feeding started (5.00% and 1 step CO_2 shift – blue; 4-steps CO_2 shift – black). Error bars represent one standard deviation about the mean.

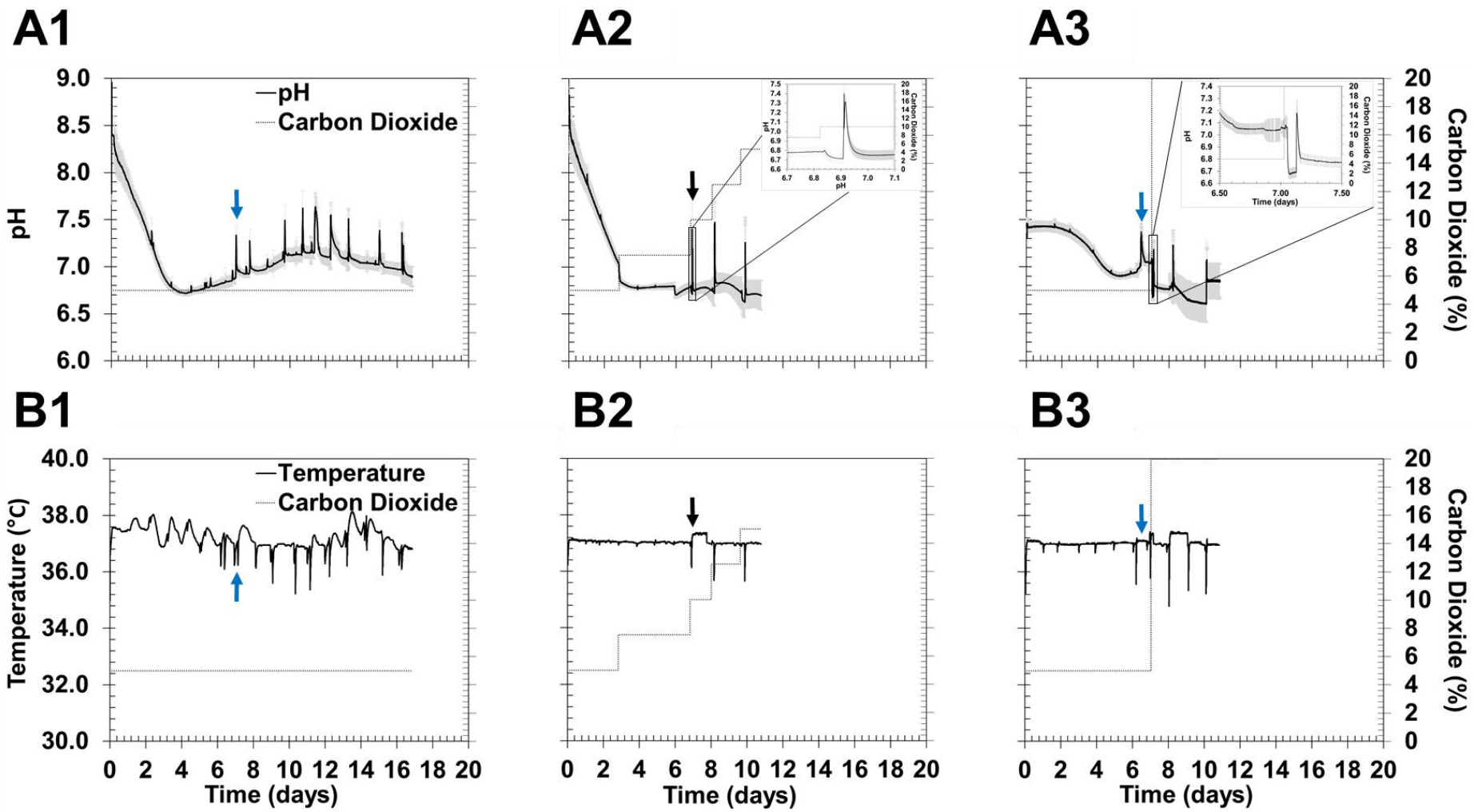

Figure 5-22: pH (A) and temperature profiles (B) for CHO-CY01 cell line fed-batch strategy 5 (FB3) cultures in 24-SRW-MTPs (1 run (24 replicates)) with constant 5.00% (v/v) CO_2 (1), CO_2 shift from 5.00% to 7.50% on day 2, 7.50% to 10.00% on day 7, 10.00% to 12.50% on day 8, and 12.50% to 15.0% (v/v) CO_2 on day 10 (4 steps) (2) and CO_2 shift from 5.00% to 20.00% (v/v) CO_2 on day 7 (1 step) (3). The arrow indicates when the feeding started (5.00% and 1 step CO_2 shift – blue; 4-steps CO_2 shift – black. Error bars represent one standard deviation about the mean.

Table 5-7: Kinetic parameters determined for CHO-CY01 cell line fed-batch strategy 5 (FB3) cultures in 24-SRW-MTPs with constant 5.00% (v/v) CO_2, CO_2 shift from 5.00% to 20.00% (v/v) CO_2 on day 7 (1 step) and CO_2 shift from 5.00% to 7.50% (v/v) CO_2 on day 2, then to 10.00% on day 7, then to CO_2 on day 8, and then to 15.0% (v/v) CO_2 on day 10 (4 steps).

CO_2 (% (v/v))	**5.00**	**5.00 - 20.00 (day 7)**	**5.00 -7.50 -- 10.00 – 12.50 - - 15.00 (day 2, 7, 8, 10)**
VP ($mg\ L^{-1} day^{-1}$)	64.7	33.0	35.2
IVCC ($10^9\ cells\ day\ L^{-1}$)	85.93	47.61	40.33
μ (h^{-1})	0.022	0.023	0.025
$t_{1/2}$ (h)	30.9	30.1	29.4
q_{mAb} ($mg\ 10^{-9}\ cells^{-1}\ day^{-1}$)	13.71	8.20	10.70
q_{Gluc} ($g\ 10^{-9}\ cells^{-1}\ day^{-1}$)	-0.21	-0.25	-0.31
q_{Glu} ($mmol\ 10^{-9}\ cells^{-1}\ day^{-1}$)	-0.04	-0.08	-0.08
q_{Lact} ($g\ 10^{-9}\ cells^{-1}\ day^{-1}$)	0.19	0.37	0.51
q_{Amm} ($mmol\ 10^{-9}\ cells^{-1}\ day^{-1}$)	0.05	0.166	0.169
Lactate produced / glucose consumed (g/g)	0.84	0.30	0.32
μ_d (h^{-1})	-0.0035	-0.014	-0.014
Evaporation rate ($\mu L\ day^{-1}$)	109.4	18.8 ± 7.2	18.1 ± 2.8
Feed volume (% of reactor volume)	21.5 ± 5.1	11.2	13.1

5.4.2.2. CO_2 Shifts in CHO-CY01 Cell Line Fed-Batch Cultures in One Step at Different Cell Culture Times

In this section, CO_2 shifts were done in CHO-CY01 cell line fed-batch cultures at 10.00% (v/v) CO_2. It has been proven before (section 5.2) that at CO_2 concentration higher than 10.00% (v/v) CO_2, the CHO-CY01 cell line cultures behaved as a buffer solutions (Table 5-1 and Figure 5-6). Also, the buffer capacity of CHO-CY01 cell line medium at this CO_2 concentration is known (23.29 ± 0.32% (v/v) CO_2 per 1 pH unit (section 5.2.1)). Besides, it was at 10.00% (v/v) CO_2 concentration that the highest IgG4 concentration was obtained in fed-batch mode. Therefore, CO_2 shifts from 10.00% to 20.00% (v/v) CO_2 were tested at several cell culture time points. In this way, the maximum CO_2 perturbation to this system was tested. The beginning of the exponential phase (day 3), mid-exponential point (day 5) and mid-stationary phase where the viable cell concentration was at maximum (day 9) were chosen. The goal was to understand the CO_2 effects at different phases of cell growth.

The CHO-CY01 cell kinetics can be visualised in Figure 5-23 and Figure 5-24, the calculated kinetic parameters are in Table 5-8, Table 5-9 and Table C-16. The pH and temperature profiles are in Figure 5-25. The particle size distribution study is presented in Figure B-10 and Table B-10. The spearman´s rank correlation coefficients tables are shown in Table A-17.

For the CO_2 shift from 10.00% to 20.00% (v/v) CO_2 at day 3, i.e. beginning of the exponential phase, the increase in the CO_2 level caused cell growth inhibition with no impact on cell viability. Glucose consumption rate diminished (Table 5-8 and Table 5-9), which lead to a maximum lactate plateau concentration around 1.15 ± 0.11$g\ L^{-1}$ for longer time (7 days) (6.60< pH< 6.80) . It is important to note that this maximum lactate concentration was similar to the maximum lactate concentration at constant 10.00% (v/v) CO_2 condition (1.27 ± 0.37$g\ L^{-1}$). Also, at this CO_2 shift condition CHO-CY01 cells were lactate consumers when cell culture pH was higher than pH 6.80 (day 10 onwards). There was not observed any effect on IgG4 production even with the cell diameter increased (Table B-10). Specific ammonium production rate increased 61% in comparison with the constant 10.00% (v/v) CO_2 culture. However, the maximum ammonium concentration was always below toxic levels (18.1 $mmol\ L^{-1}$ (Section 4.3.3). Once again this excessive ammonium production can be related with cell culture pH. When the CO_2 shift occurred the pH went below 6.70 for almost four days. In terms of overall pH profile, this CO_2 shift slightly lowered the cell culture pH to 6.82 ± 0.24. The advantage of such early CO_2 shift resides on feed volume reduction by 5.6 fold and a 1.8 fold decline in IVCC.

For the CO_2 shift from 10.00% to 20.00% (v/v) CO_2 at day 5, i.e. mid-exponential point, the 10.00% (v/v) increase in CO_2 level had an inhibitory effect on the CHO-CY01 cells but in a

less extent compared with the CO_2 shift at day 3. Again, the cell viability was unaffected. Up to day 16, the IgG4 production rate at constant 10.00% (v/v) CO_2 and CO_2 shifts at day 3 and 5 were equivalent. However, from day 16 to 18 the IgG4 concentration at CHO-CY01 cell line fed-batch culture with CO_2 shift at day 5 decreased 45%. After day 16, IgG4 concentration returned to the previous maximum concentration (1.14 ± 0.04 $g\ L^{-1}$). When the CO_2 shift occurred at day 5, the CHO-CY01 cell line fed-batch culture pH dropped below pH 6.60, which has been found to cause cell death trough apoptosis (section 5.4.1). Although, no apoptotic analysis was done in this cell culture condition, it can be observed from the particle size distribution (Figure B-10 and Table B-10) that CHO-CY01 cell diameter after CO_2 shift was slightly smaller than the cell diameter of CHO-CY01 cells at constant 10.00% (v/v) CO_2. The dead cells (cell diameter between 7.6 and 12.8 μm) population fraction increased as well. This is a strong indication of the cell death by apoptosis, as the CHO-CY01 cell shrinked and the number of apoptotic bodies increased. A possible explanation for the IgG4 concentration profile is that from day 16 to 18, there was an increase of CHO-CY01 cells in either early or late apoptosis, which transferred to no viable/necrosis cells on day 18 (cell viability below 70%). So, the IgG4 concentration decrease was due to fewer producing cells and the subsequent increase was due to cell leaking. However, for a more complete understanding of the real reasons, an apoptotic analysis would be needed. For the same reasons as the CO_2 shift at day 3 condition, CHO-CY01 cells had to endure for longer a high lactate concentration (1.2 -1.7 gL^{-1}) and cells were lactate consumer when pH was around pH 6.80. The CO_2 shift at day 5, also triggered ammonium production as the pH culture around the CO_2 shift went below pH 6.70. The fact that IgG4 was lost in this CO_2 shift culture at cell viabilities higher than 71.5%, raised concerns on choosing this pH profile for IgG4 productivity optimisation purposes.

For the CO_2 shift from 10.00% to 20.00% (v/v) CO_2 at day 9, i.e. mid-stationary phase, there was no impact on cell growth. This CO_2 shift caused a pH drop of 0.14 pH units, which started the decline phase and shortened the cell cultures by four days. This led to an increase of 10% in the VP. Apart from ammonium production increase all the other kinetic parameters were equivalent to those found at constant 10.00% (v/v) CO_2 CHO-CY01 cell line fed-batch culture. The glucose and glutamate consumption rate decrease after CO_2 shift as CHO-CY01 cells were dying. The advantage of doing a CO_2 shift in a mid-stationary phase was to reach the same high IgG4 concentration (1.19 ± 0.05 $g\ L^{-1}$) as the constant CO_2 counterpart with a shorter cell culture.

The general increase in osmolality, Na^+ and K^+ concentrations after day 9 for all CO_2 shifts CHO-CY01 cell line fed-batch cultures was exclusively due to feeding (Figure 5-23 (F) and Figure 5-24 (C, D)). 10.00% (v/v) CO_2 concentration proved to be an adequate buffer

solution. At this CO_2 concentration, the cell culture pH oscillations due to by-waste product accumulation were cushioned by the high buffer capacity of the cell culture medium and so the pH was kept at 6.92 ± 0.48. (Table 5-9). Also, the characteristic increase in ammonium production immediately after the CO_2 shift for all CHO-CY01 cell line fed-batch cultures with CO_2 shifts, was related with the decrease of cell culture pH below 6.70 which stopped for cell culture pH higher than 6.80. This is the way that CHO-CY01 have to balance the internal pH homeostasis. The CO_2 shift for a higher CO_2 level caused the acidification of the external cell medium, therefore the instant internal pH of the cells was higher than the external one. CHO-CY01 cells in order to find a new internal steady-state pH produced ammonium from glutamate. This is why the glutamate consumption rate before feeding increased as early the CO_2 shift occurred (-0.23 $mmol\ L^{-1}day^{-1}$ CO_2 shift day 3; -0.21 $mmol\ L^{-1}day^{-1}$ CO_2 shift day 5; -0.14 $mmol\ L^{-1}day^{-1}$ CO_2 shift day 9; and -0.20 $mmol\ L^{-1}day^{-1}$ at 10.00% (v/v) CO_2).

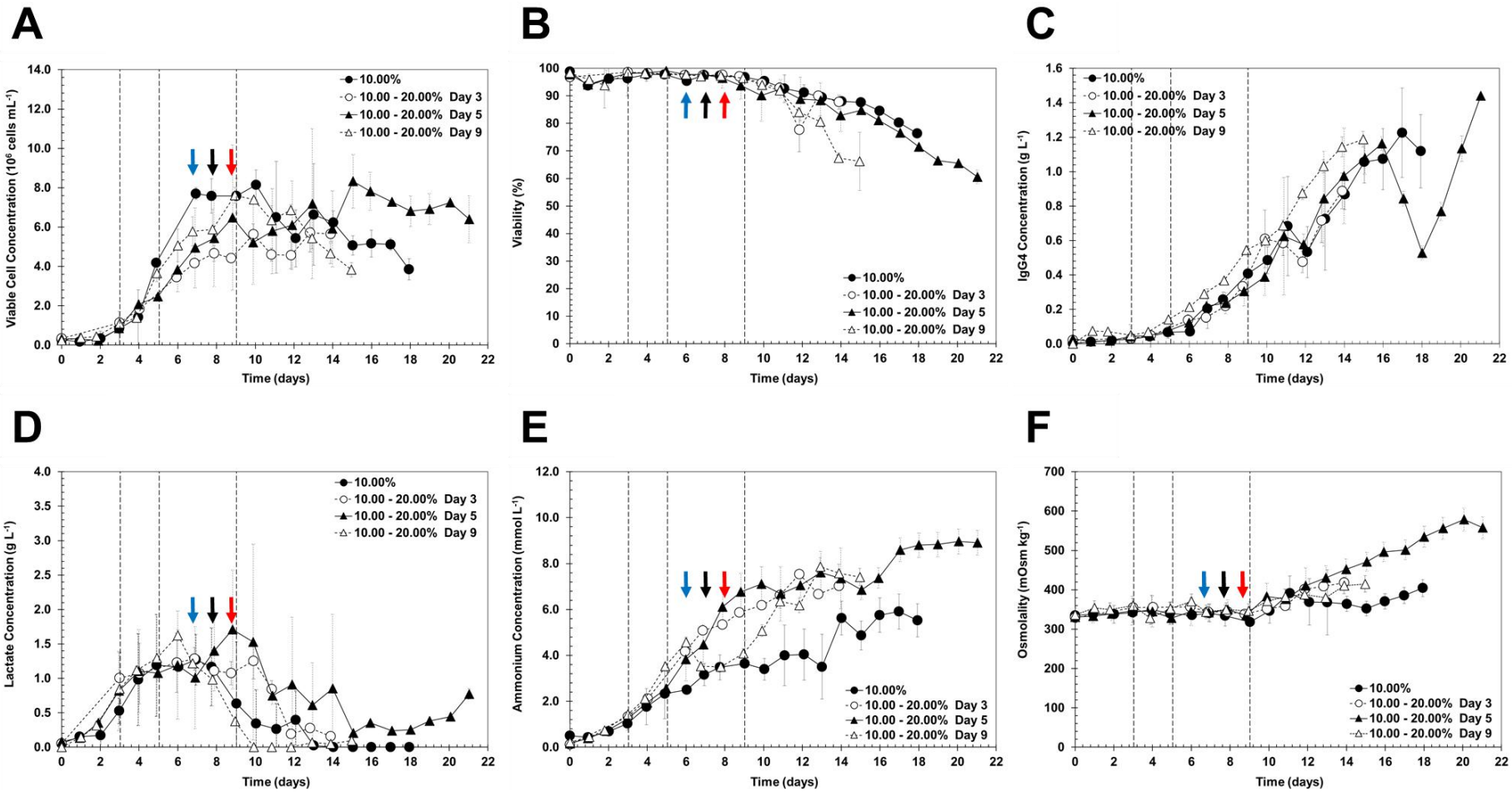

Figure 5-23: Viable cell concentration (A), cell viability (B), IgG4 concentration (C), lactate concentration (D), ammonium concentration (E) and osmolality (F) profiles for CHO-CY01 cell line batch culture at constant 10.00% (v/v) CO_2 (2 runs (6-8 replicates)) and CO_2 shifts from 10.00% to 20.00% (v/v) CO_2 at day 3 (1 run (3-4 replicates)), 5 (2 runs) and 9 (1 run). The long dash lines indicate when the CO_2 shifts occurred. The arrow indicates when the feeding started (CO_2 shift at day 9 – blue; 10.00% (v/v) CO_2 and CO_2 shifts at day 5 – black; CO_2 shift at day 3 – red). The error bars represent one standard deviation about the mean.

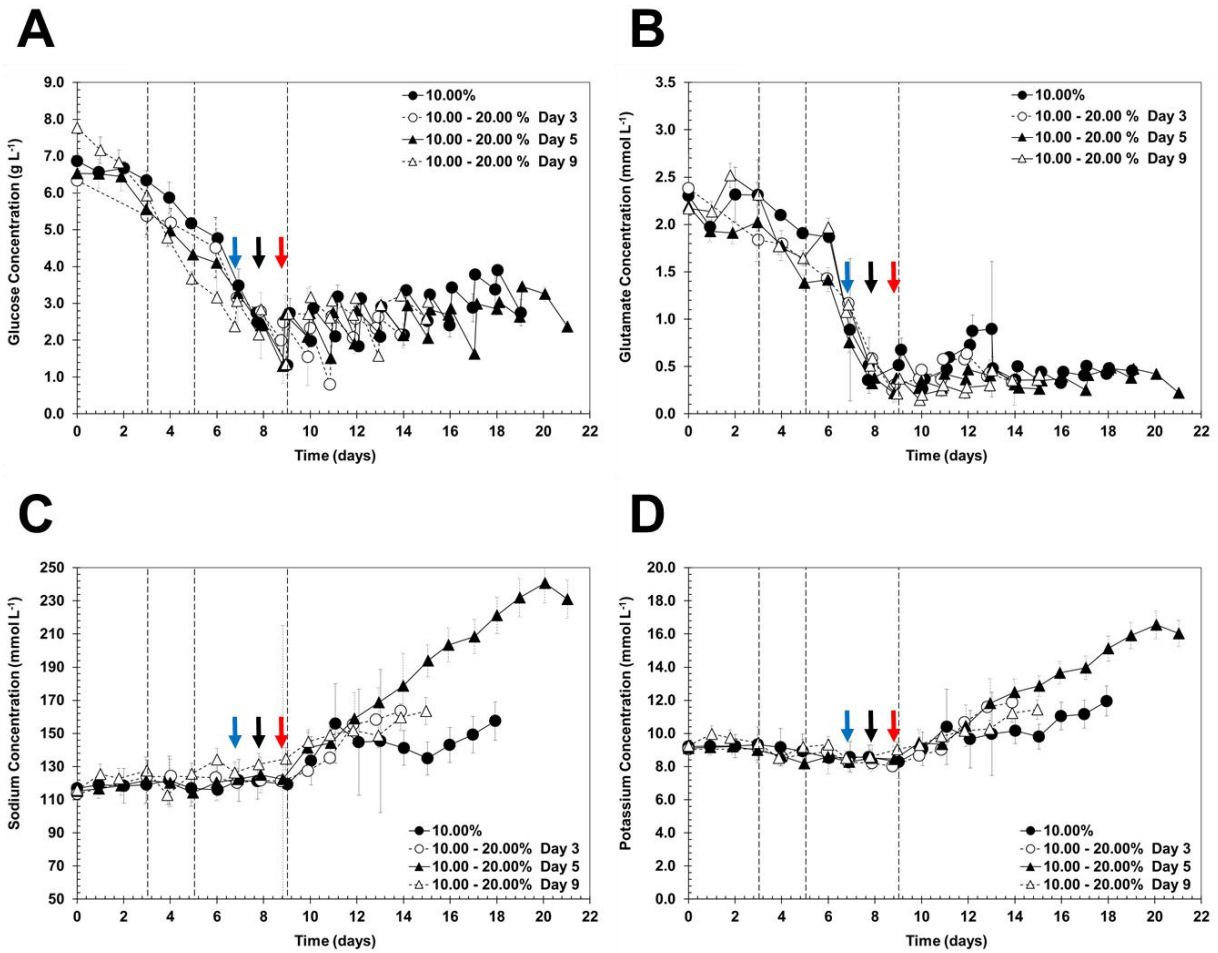

Figure 5-24: Glucose (A), glutamate (B), sodium (C) and potassium (D) concentrations profiles for CHO-CY01 cell line fed-batch strategy 5 (FB3) cultures in 24-SRW-MTPs with constant 10.00% (v/v) CO_2 (2 runs (6-8 replicates)) and CO_2 shifts from 10.00% to 20.00% (v/v) CO_2 at day 3 (1 run (3-4 replicates)), 5 (2 runs) and 9 (1 run). The long dash lines indicate when the CO_2 shifts occurred. The arrow indicates when the feeding started (CO_2 shift at day 9 – blue; 10.00% (v/v) CO_2 and CO_2 shifts at day 5 – black; CO_2 shift at day 3 – red). The error bars represent one standard deviation about the mean.

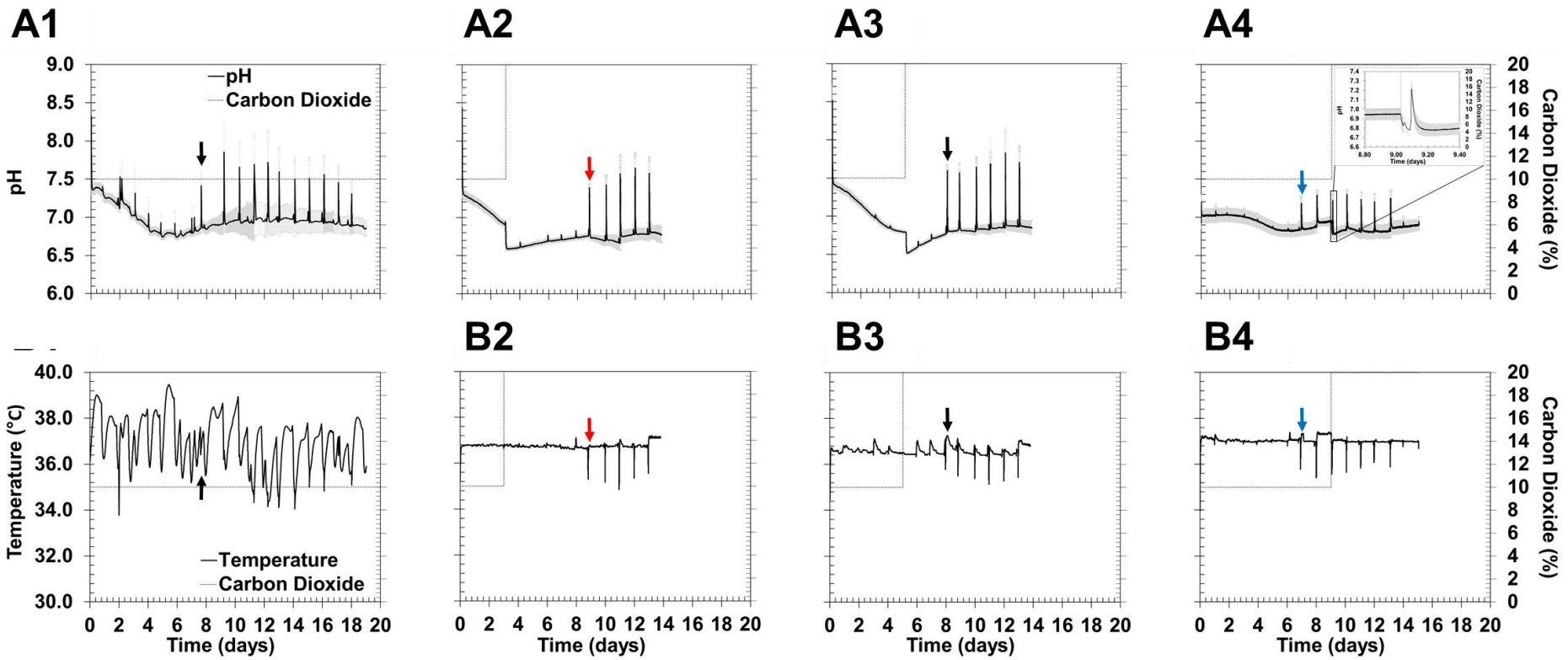

Figure 5-25: pH (A) and temperature profiles (B) for CHO-CY01 cell line fed-batch strategy 5 (FB3) cultures in 24-SRW-MTPs (1 run (24 replicates)) with constant 10.00% (v/v) CO_2 (1) and CO_2 shifts from 10.00% (v/v) CO_2 to 20.00% (v/v) CO_2 at day 3 (2), day 5 (3) and day 9 (4). The arrow indicates when the feeding started (CO_2 shift at day 9 – blue; 10.00% (v/v) CO_2 and CO_2 shifts at day 5 – black; CO_2 shift at day 3 – red). The error bars represent one standard deviation about the mean.

Table 5-8: Kinetic parameters determined for CHO-CY01 cell line fed-batch strategy 5 (FB3) cultures in 24-SRW-MTPs with constant 10.00% (v/v) CO_2 and CO_2 shifts from 10.00% to 20.00% (v/v) CO_2 at day 3, 5 and 9.

CO_2 (% (v/v))	**10.00**	**10.00 - 20.00**		
		Day 3	**Day 5**	**Day 9**
VP ($mg\ L^{-1}day^{-1}$)	53.3 ± 15.3	48.3	51.7 ± 3.5	68.4
IVCC ($10^9\ cells\ day\ L^{-1}$)	69.88 ± 29.75	47.03	88.60 ± 37.71	64.21
$\mu\ (h^{-1})$	0.017 ± 0.006	0.015	0.016 ± 0.001	0.021
$t_{1/2}\ (h)$	44.1 ± 18.2	45.0	42.7 ± 3.0	33.3
$q_{mAb}\ (mg\ 10^{-9}\ cells^{-1}\ day^{-1})$	17.28 ± 4.81	16.79	13.13 ± 2.53	18.47
$q_{Gluc}\ (g\ 10^{-9}\ cells^{-1}\ day^{-1})$	-0.23 ± 0.09	-0.21	-0.18 ± 0.05	-0.21
$q_{Glu}\ (mmol\ 10^{-9}\ cells^{-1}\ day^{-1})$	-0.05 ± 0.02	-0.07	-0.05 ± 0.02	-0.05
$q_{Lact}\ (g\ 10^{-9}\ cells^{-1}\ day^{-1})$	0.19 ± 0.15	0.25	0.23 ± 0.14	0.17
$q_{Amm}\ (mmol\ 10^{-9}\ cells^{-1}\ day^{-1})$	0.090 ± 0.039	0.197	0.140 ± 0.063	0.133
Lactate produced / glucose consumed (g/g)	0.49 ± 0.26	0.39	0.24 ± 0.09	0.35
$\mu_d\ (h^{-1})$	-0.011 ± 0.007	0.000	-0.002 ± 0.003	-0.008
Feed volume (% of reactor volume)	88.1	15.7	28.8 ± 14.2	15.3
Evaporation rate ($\mu L\ day^{-1}$)	9.3 ± 2.6	17.8 ± 1.8	11.0 ± 2.4	26.4 ± 10.0

Table 5-9: Average and standard deviation values of process parameters: pH and temperature, and glucose and glutamate consumption rates on fed-batch mode for CHO-CY01 cell line fed-batch strategy 5 (FB3) cultures in 24-SRW-MTPs with different CO_2. shifts.

CO_2 (% (v/v))	pH	Temperature (°C)	Daily Glucose Consumption rate ($g\ L^{-1}day^{-1}$)	Daily Glutamate consumption rate ($mmol\ L^{-1}day^{-1}$)
5.00	7.08 ± 0.36	37.22 ± 0.50	1.33 ± 0.39	0.18 ± 0.06
10.00	6.98 ± 0.28	36.91 ± 1.05	0.92 ± 0.34	0.04 ± 0.17
15.00	6.88 ± 0.21	37.22 ± 0.39	0.97 ± 0.57	0.12 ± 0.07
5.00 - 20.00 (day 7)	6.92 ± 0.37	37.13 ± 0.32	0.86 ± 0.63	0.10 ± 0.07
Before shift			1.03 ± 0.16	0.12 ± 0.02
After shift			0.76 ± 0.74	0.09 ± 0.09
5.00 - 7.50 - 10.00 - 12.50 - 15.00 (day 2, 7, 8, 10)	7.17 ± 0.43	37.11 0.17	1.70 ± 0.98	0.20 ± 0.11
10.00 - 20.00 (day 3)	6.82 ± 0.24	36.96 ± 0.32	0.79 ± 0.62	0.09 ± 0.07
10.00 - 20.00 (day 5)	6.91 ± 0.25	36.75 ± 0.31	0.76 ± 0.45	0.08 ± 0.06
10.00 - 20.00 (day 9)	6.92 ± 0.15	37.12 ± 0.26	0.72 ± 0.43	0.08 ± 0.05
Before shift			0.92 ± 0.40	0.11 ± 0.05
After shift			0.60 ± 0.45	0.07 ± 0.05

5.5. Semi-empirical mathematical Modelling of the pH in CHO-CY01 Cell Line Cultures

Cellular metabolism is complex, and a number of acids and bases are produced and consumed during the cell culture process. Therefore, it becomes necessary to make some assumptions and approximations in order to estimate the pH.

CHO-CY01 cell line culture is a CO_2/bicarbonate buffered system, therefore the Henderson-Hasselbalch equation (Equation 5.1) is able to calculate the cell culture pH. However, CHO-CY01 cells produce lactate and ammonium, which play a counter role in the acid-base equilibrium of a non pH controlled cell culture. Two simplified models of the pH in a mammalian cell culture were developed (Equation 5.3 and Equation 5.5). These were validated with experimentally obtained pH profiles (Figure 5-26, Figure 5-27 and Figure 5-28) The starting point was the semi-empirical mathematical model proposed by Gramer et al., (2007) and the Gadgil (2014) to simule the changing in the culture pH. It was assumed equilibrium between bicarbonate and gaseous CO_2 (which is maintained constant in the incubator, mass transfer of CO_2 between gas and liquid phase is assumed to be not limiting). It was considered an initial bicarbonate concentration in the medium of 29 $mmol\ L^{-1}$ and it was assumed to be constant during the cell culture duration. Since this mathematical modelling exercise is a non-linear model, no regression coefficient can be determined. Therefore, the goodness of the model was evaluated by visual comparison with the experimentally obtained pH profiles.

In the pH model 1, it was considered that for every mole of lactate produced, one mole of bicarbonate is utilised. Therefore, the Henderson-Hasselbalch equation for model 1 was:

$$pH = 6.37 + log_{10}\frac{[HCO_3^-] - [Lact]}{[CO_2]}$$

Equation 5.3

where $[HCO_3^-]$ is the bicarbonate concentration (mM), $[Lact]$ is the lactate concentration in the medium (mM) and $[CO_2]$ is the dissolved CO_2 concentration determined with Equation 5.4 (mM).

The CO_2 is soluble in water and at the equilibrium the amount of dissolved CO_2 ($[CO_2\ (aq)]$) is proportional to the amount of CO_2 in the gas phase (pCO_2) as provided by Henry's Law, with a solubility in water (s) of $0.39\ mM/\%$ (Gramer et al., 2007).

$$[CO_2\ (aq)] = s \cdot pCO_2$$

Equation 5.4

In the pH model 2, it was accounted the effect of alkalization of the cell medium by ammonium ions produced by the cells as well as the acidification effect of lactate production. So, for every mole of ammonium ion produced, one mole of bicarbonate was generated and at the same time for every mole lactate produced, one mole of bicarbonate is used. It may seem these opposite pH effects would cancel each other. However, it is important to notice that lactate production rate in CHO-CY01 cell line cultures is, at least, five times higher than ammonium production. Also, the dissociation constant for lactate is bigger than ammonium one. Therefore, the Henderson-Hasselbalch equation for model 2 was:

$$pH = 6.37 + log_{10}\frac{[HCO_3^-] - [Lact] + [NH_4^+]}{[CO_2]}$$

Equation 5.5

where $[NH_4^+]$ is the ammonium ion concentration in the medium (mM).

Both models were tested for CHO-CY01 cell line batch (Figure 5-26), fed-batch cultures at constant CO_2 concentrations (Figure 5-27) and CO_2 shifts from 10.00% *to 20*.00% (v/v) CO_2 on day 3, 5 and 9 (Figure 5-28). For CHO-CY01 cell batch cultures below 5.00% (v/v) CO_2 the pH model1 can not describe the culture pH, for those CO_2 concentrations the cell culture is not a buffer solution, as mention before (section 5.2). The reason behind the break in the pH model line was the lactate concentration exceeded the initial bicarbonate concentration. However, the pH model 2 can estimate the CHO-CY01 cell line batch culture pH at CO_2 concentrations higher than at 2.00% (v/v) CO_2. For CHO-CY01 cell line batch cultures with more than 10.00% (v/v) CO_2, both models tend to underestimate the culture pH. The reason for that may be the bicarbonate concentration did not stayed constant during the cell culture, but it increased with time resulting from the high CO_2 level. The level of underestimation was slightly mitigated by pH model 2. It can be claimed that both models can correctly estimate CHO-CY01 cell line batch cultures between 5.00% (v/v) CO_2 and 10.00% (v/v) CO_2. For CHO-CY01 cell line batch cultures, pH model 2 managed to estimate the culture pH between 2.00% and 15.00% (v/v) CO_2, and so it was chosen as the best pH model.

For CHO-CY01 cell line fed-batch cultures at constant CO_2 concentrations both models overestimated the culture pH. Again, the bicarbonate concentration in the medium did not stayed constant with addition of feed, it seems that it started to decrease around day 4. The level of overestimation decreased with increasing CO_2 concentration. Nevertheless, the culture pH changing trends throughout the cell culture were predicted by both pH models. At fed-batch mode, it was the pH model 1 that described marginally better the culture pH. For CHO-

CY01 cell line fed-batch culture with CO_2 shift from 10.00% to 20.00% (v/v) CO_2 on day 3, 5 and 9, both pH model were able to estimate correctly the culture pH.

The assumption of constant bicarbonate concentration during CHO-CY01 cell cultures has proved to introduce an error in the estimation of culture pH. Also, it was assumed the same bicarbonate concentration for all cell cultures, which did not account for the batch-to-batch variability of the initial cell culture medium. With the bicarbonate concentration profile during CHO-CY01 cell line cultures, this pH estimation would improve. Nevertheless, it can be said that a modified Henderson-Hasselbalch equation was able to simulate the pH changes in CHO-CY01 cell line cultures.

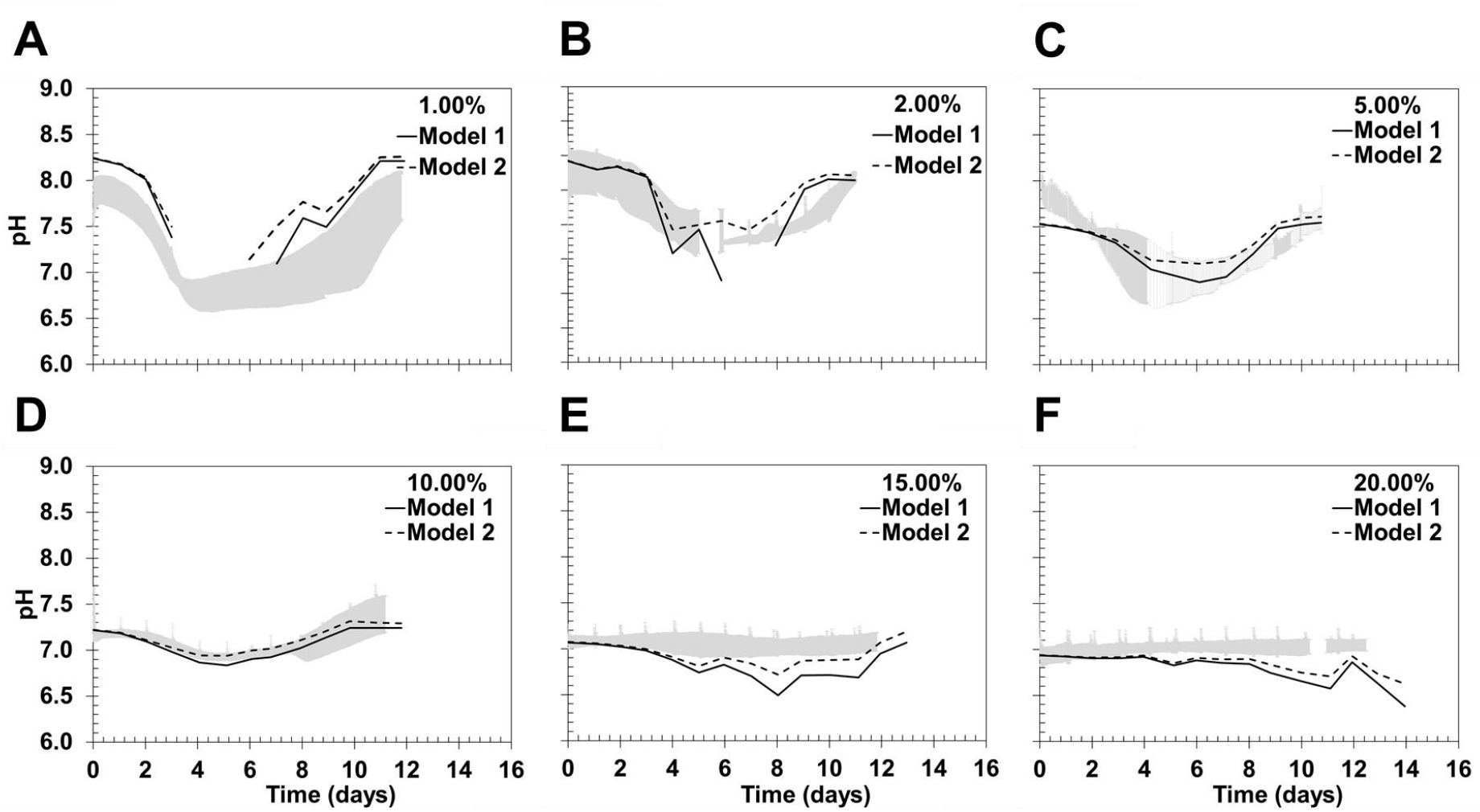

Figure 5-26: CHO-CY01 cell line batch culture experimental (grey), model 1(solid line) and model 2 (dashed line) pH profiles at 1.00% (A), 2.00% (B), 5.00% (C), 10.00% (D), 15.00% (E) and 20.00% (v/v) CO_2 (F).

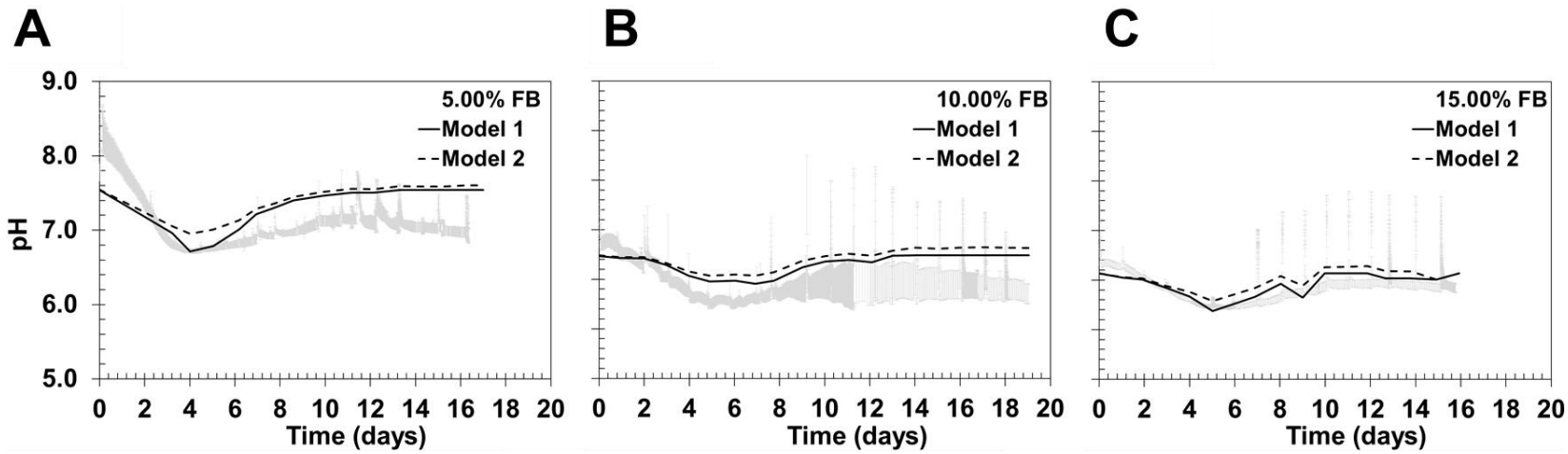

Figure 5-27: CHO-CY01 cell line fed-batch culture experimental (grey), model 1(solid line) and model 2 (dashed line) pH profiles at constant 5.00% (A), 10.00% (B), and 15.00% (v/v) CO_2 (C).

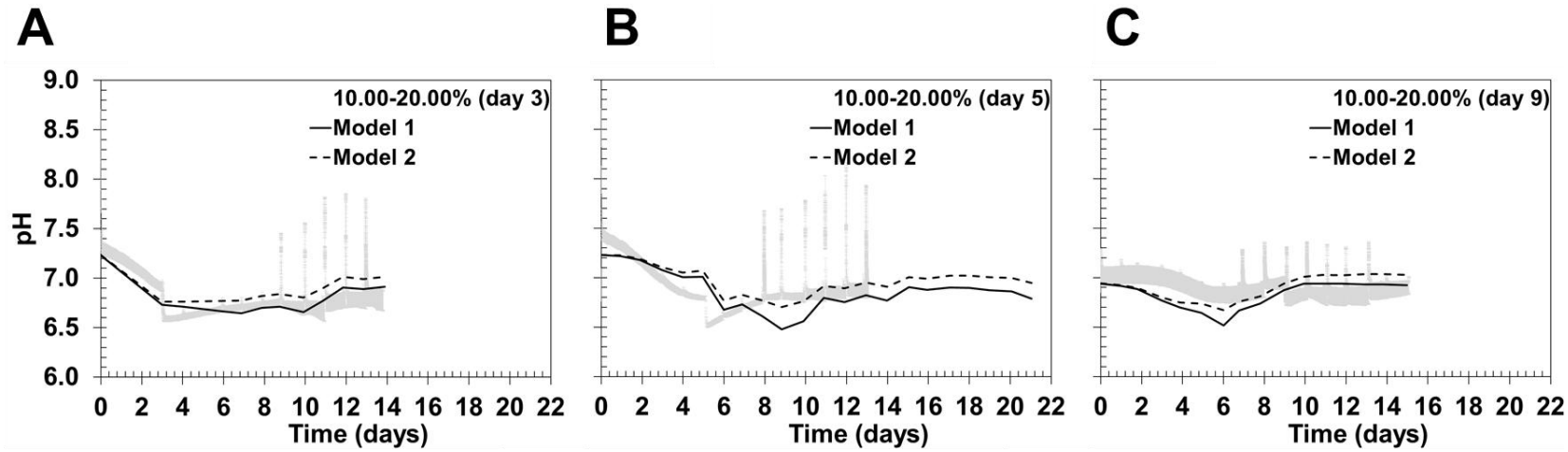

Figure 5-28: CHO-CY01 cell line fed-batch culture experimental (grey), model 1(solid line) and model 2 (dashed line) pH profiles for CO_2 shift from 10.00% (v/v) CO_2 to 20.00% (v/v) CO_2 on day 3 (A), 5 (B) and 9 (C).

5.6. Conclusion

A reliable high-throughput online monitoring technique contributes to the success of bioproduction processes. The integrated high throughput continuous monitoring of pH and DOT by optical sensors can be considered as being reliable and feasible. The rapid response of optical sensors to altering pH and oxygen levels, together with further kinetic data, will allow rapid and accurate identification of the state of bioreactions (Naciri et al., 2008). With PreSens Precision Sensing (Regensburg, Germany) technology a high-throughput online multi-parametric analysis method of mammalian cell cellular activity was previously developed (Chapter 4). With this method, it was possible to understand the effects of CO_2 on the CHO-CY01 cell line growth, cellular metabolism, and IgG4 production to find the optimum pH profile for IgG4 optimisation purposes. Therefore, a series if CHO-CY01 cell line cultures at constant, biphasic and multiphasic CO_2 concentrations were performed. Also, two properties of the cell culture system used were determined, buffer capacity (23.29 ± 0.32% (v/v) CO_2 per 1 pH unit) and the gas transfer resistance from the CR1524a ´System Duetz` lids (3.25 ± 0.70% O_2).

At first, CHO-CY01 cell line batch cultures were grown at different constant CO_2 concentrations (0.04%, 1.00%, 2.00%, 5.00%, 10.00%, 15.00% CO_2 and 20.00 % (v/v) CO_2), where 5.00% (v/v) CO_2 was the reference. It was found at atmospheric CO_2 concentration that CHO-CY01 cells were unable to grow and produce IgG4. Also, the cellular survival strategy against the high culture pH was observed with the excessive production of lactate by the cells ($3.5\ g\ L^{-1}$). Whereas below the standard CO_2 concentration, CHO-CY01 cell culture duration decreased, i.e., higher cell death rate. Also, the pH amplitude was almost one pH unit, which means that these cell cultures were not well buffered. Therefore, CHO-CY01 cell line cultures at $CO_2 \leq$ 5.00 % are not considered to be ideal for optimisation purposes. Above standard CO_2 concentration, the pH variation were at most 0.24 pH units. Therefore, CHO-CY01 cell line cultures at these CO_2 concentrations were pH controlled at a cell-self established pH set-point: 7.12 ± 0.24 for 10.00%, 7.05 ± 0.12 for 15.00% and 7.02 ± 0.10 for 20.00% (v/v) CO_2. As a result, a new method for an easy and simple pH control in 24-SRW MTP was found for CHO-CY01 cell line batch cultures. With increasing CO_2 concentration, the *lag* phase duration prolonged, the μ and IVCC decreased which cascaded an increase in q_{Gluc}, q_{Glu}, q_{Lact} and q_{Amm} from a lower glucose consumption rate and maximum lactate concentration due to glycolysis inhibition. The lactate metabolic shift is independent of CO_2 concentration value as it was consistently observed when glucose concentration was below 3.00 – 4.00 $g\ L^{-1}$ and glutamate was below 2.5 $mmol\ L^{-1}$ at all CO_2 concentration values. A similar maximum IgG4 concentration (0.40 ± 0.11 $g\ L^{-1}$) was reached by the CHO-CY01 cells. Nevertheless, the cell growth inhibition at $CO_2 \geq$ 10.00% (v/v) CO_2, CHO-CY01 cells were able to produce the same q_{mAb} between 5.00% and 15.00% (v/v) CO_2 and a 1.81 fold increase at 20.00% (v/v) CO_2.

Therefore, CHO-CYO1 cells utilised the glucose more for IgG4 production than for cell division or lactate production with increasing CO_2 levels.

An apoptotic and cell cycle analysis of CHO-CY01 cell line batch cultures at constant CO_2 concentrations was performed to understand the effect of different CO_2 concentrations on cell death origins and cell cycle population heterogeneity. The CHO-CY01 cell death in 24-SRW MTP was due to apoptosis independently of the CO_2 concentration. For all CO_2 concentrations, CHO-CY01 cell line batch cultures exhibited an asynchronous growth and there was no suggestion that IgG4 production was limited to any specific cell cycle phase. It seems that the regulation of synthesis and secretion of IgG4 is time-dependent, and the productivity increased when cells are arrested and maintained in a 40-50% G1 and S-phases distribution with decreasing cell viabilities and increasing cell diameters (> 15 µm).

From the evaluation of the effects of different CO_2 concentrations in CHO-CY01 cell line fed-batch cultures performed, it was observed the cell survival strategy against high external pH values (pH ≥ 7.5) characterised by a readily lactate production and excessive glucose consumption (more feeding). The viable cell concentration and cell viability profiles were statistically equivalents for CO_2 concentrations between 5.00% and 15.00% (v/v) CO_2. Nonetheless, the lactate and ammonium accumulation levels were similar to batch values at all CO_2 concentration. For a CHO-CY01 cell line fed-batch culture with a pH range of 6.98 ± 0.28 (10.00% (v/v) CO_2), the highest IgG4 production was observed, i.e. 225% increase compared with the batch value.

From the CHO-CY01 cell line culture at biphasic and multiphasic CO_2 concentrations, the first attempt for the pH control through exclusively CO_2 manipulation in 24-SRW MTPs was made and the identification of the pH ranges with different effects on CHO-CY01 cell line growth and IgG4 productivity was possible when interconnecting the kinetic data with the pH values.

Consequently, from the first intuitive attempt at pH control in 24-SRW MTP where a step-by-step shifting of CO_2 concentrations (8.00 - 0.04 % (v/v)) was performed using a decision tree several significant and useful facts were learned. CHO-CY01 cell line culture medium pH between 6.70 - 6.80 caused a cell growth and lactate production arrest. It also increased the cell size, which promoted IgG4 production. However, the lactate consumer advantageous phenotype was lost by the CHO-CY01 cells. Cell culture medium pH below 6.60 promoted apopotosis.

The maximum CO_2 shift amplitude available was from 5.00% to 20.00% (v/v) CO_2. Therefore, two different strategies were used: a step-by-step increase of CO_2 level (2.50% (v/v) CO_2 per step) from the beginning of exponential phase (day 3) up to four steps (multiphasic culture) and; a one step CO_2 shift when the maximum viable cell concentration

(day 7) was reached (biphasic culture). At the first CO_2 shift strategy, the cell survival strategy was worked-around and there was a reduction on lactate production and glucose consumption. Indeed, with this first CO_2 shift (5.00 – 7.50% (v/v) CO_2), the pH reached was between 6.70 - 6.80 (day 3 to 6), which resulted in an almost null net lactate production rate and so, a lower lactate plateau concentration. The other CO_2 shifts were done when the glucose level went below 3.00 $g\ L^{-1}$, e.g. when the fed-batch mode and lactate consumption started. The second CO_2 shift, lowered the pH to values below 6.70, which triggered a boost in ammonium production rate, and stopped the IgG4 production at 0.27 ± 0.03 $g\ L^{-1}$. The third and the final CO_2 shift continued to lower the pH to values below 6.60, which caused the immediate cell numbers decline due to apoptosis. The one step CO_2 shift strategy caused a catastrophic effect on CHO-CY01 cell line growth. This extreme CO_2 shift caused a pH decrease to values below 6.70, which again triggered an increase in ammonium production rate and IgG4 production stagnation at 0.29 ± 0.02 $g\ L^{-1}$. In conclusion, these CO_2 shifts have not fulfilled the aim of increasing CHO-CY01 cell line IgG4 productivity, but from them, it was found the minimum of the optimal pH range to be pH = 6.70, it was considered that CO_2 shifts of 15.00% (v/v) CO_2 difference was too harsh for cells in a non-buffered condition like 5.00% (v/v) CO_2 and, ultimately 5.00% (v/v) CO_2 was no longer considered as a CO_2 concentration reference, being replaced by 10.00% (v/v) CO_2.

In order to understand the CO_2 effects at different phases of cell growth, it was performed CO_2 shifts from 10.00% to 20.00% (v/v) CO_2 were tested at several cell culture time points: beginning of the exponential phase (day 3), mid-exponential point (day 5) and the mid-stationary phase where the viable cell concentration was at maximum (day 9).

The CO_2 shifts during the beginning of the exponential phase had an inhibitory effect on cell growth and subsequently, decreased the glucose consumption, but no effect on IgG4 production. For pH values between 6.60 and 6.80, it was observed a lactate plateau and an increase in ammonium production as soon as the pH went above 6.80, there was lactate consumption and ammonium production arrest. Regarding the overall pH profile, this CO_2 shift slightly lowered the cell culture pH to 6.82 ± 0.24 compared with constant 10.00% (v/v) CO_2. The advantage of such early CO_2 shift resides in a feed volume reduction of 5.6 fold and a 1.8 fold decline in IVCC with similar q_{mAb}. At the CO_2 shift at mid-exponential point (day ?), there was an inhibitory effect on the CHO-CY01 cell growth but to a lesser extent compared with the CO_2 shift on day 3 and IgG4 concentration decline at cell viabilities higher than 71.5% and pH > 7.00 raised concerns in choosing this pH profile for IgG4 productivity optimisation purposes. For the CO_2 shift from 10.00% to 20.00% (v/v) CO_2 at day 9, i.e. mid-stationary phase, there was no impact on cell growth. This CO_2 shift lowered 0.14 pH units, which started the decline phase and shortened the cell cultures by four days. The advantage of doing a CO_2

shift in a mid-stationary phase was to reach the same high IgG4 concentration (1.19 ± 0.05 $g\ L^{-1}$) as the constant CO_2 counterpart (pH 6.8?) with a shorter cell culture time. For all of these CO_2 shift experiments, an increase in ammonium production was observed when pH values were below 6.70 and lactate consumption occurred when pH was above 6.80.

Finally, two semi-empirical mathematical models of CHO-CY01 cell line culture pH using a modified Henderson-Hasselbalch equation were developed. In the pH model 1, it was considered that for every mole of lactate produced, one mole of bicarbonate is utilised. This model could not describe the changing pH of CHO-CY01 cell line batch cultures at CO_2 concentrations below 5.00% (v/v) CO_2. In the pH model 2, it was accounted for the alkalisation effect of ammonium ions as well as the acidification effect of lactate production. The culture pH of CHO-CY01 cell line batch cultures below 2.00% (v/v) CO_2 were incompletely described by pH model 2. For CHO-CY01 cell line fed-batch at constant and biphasic CO_2 cultures, both pH models were able to simulate the pH changes in CHO-CY01 cell line cultures.

Chapter 6 pH Impact on CHO-CY01 Cell Line Kinetics

6.1. Introduction and Aims

Culture pH is one of the key environmental parameters that influence cell metabolism and recombinant protein production. Extracellular pH affects many intracellular properties including intracellular pH, cell metabolism, glucose transport, ATP/ADP ratio, protein synthesis, transport and secretion, and glycosylation of proteins (Borys et al., 1993; Müthing et al., 2003). Yoon et al. (2005) have reported the effect of culture pH in the batch culture of recombinant CHO cells. The q_{Gluc} and q_{Lact} increased with increasing pH, in the pH range of 6.85 to 7.80, whereas the maximum μ was observed at pH 7.2. Kuwae et al. (2005) have addressed the effects of pH on maximizing the recombinant human antithrombin (rAT) in CHO cells. When cells were cultured at pH values of 6.6, 6.8, 7.0, and 7.2, the maximum cell density and maximum lactate concentration decreased with decreasing pH. The highest production level of rAT was obtained at culture pH 6.8 due to the extended culture lifetime. Osman et al. (2001) have studied the effect of pH on growth, metabolism and product secretion of GS-NS0 cells over the range of 6.5 to 9.0. They found that the maximum growth rate and maximum viable cell number occurred at pH 7.3 whereas pH 7.0 was optimum for product formation. The limits of cell growth for this cell line were between pH 7.0 and 8.0 and culturing outside these values resulted in rapid cell death.

At large-scale, mammalian cell culture pH is controlled using the CO_2/HCO_3^- open buffer system. At the beginning of the cell culture pH is controlled by the addition of CO_2 gas. This CO_2 addition maintains the pH dependent equilibrium between CO_2 and bicarbonate. As the culture progresses lactic acid accumulates and alters the equilibrium pH of the culture by reducing the concentration of bicarbonate. This loss of bicarbonate shifts the ratio of CO_2 to bicarbonate and lowers the equilibrium pH. Eventually, there is not enough bicarbonate in the medium to maintain the fermentation set point. At this point batch on–off pulse injection of alkali are made, often to one location on the liquid surface, to maintain the pH set point of the medium (Osman et al., 2002). Thus, the local pH values near the addition point may deviate from the bulk pH, which creates pH gradients. This alkali addition take some time to fully disperse and the extend of such zones may expand with increases in cell culture density and vessel size as culture homogeneity becomes more difficult to achieve (Amanullah et al., 2001; Langheinrich et al., 1999; Nienow et al., 1996; Ozturk, 1996). Therefore, there is the need to consider carefully and control the culture pH to maximise expression of recombinant proteins from a mammalian cell, and to ensure the reproducible glycosylation of the secreted glycoproteins and so product quality.

Chinese hamster ovary (CHO) cells are widely utilised for large-scale pharmaceutical proteins production since they are capable of folding, assembling and post- translationally modifying proteins in a manner that is more compatible with humans (Kildegaard et al., 2013). Proteomic analyses are frequently used in biotechnology as they can provide information on the integrated functions of the whole cell (Dinnis et al., 2006). Proteomic analyses have the advantage that they describe the actual cellular machinery and downstream consequences of alterations in gene expression. 2D-PAGE remains the proteomic workforce to fractionate protein mixtures (Gygi et al., 2000). However, this is a labour intensive technique with technical limitations. Quantitative comparison of protein abundance requires statistical experimental design and analysis to cope with the inherent experimental variation (Molloy et al., 2003). For direct comparisons of protein abundance, comparative proteomics methods such as differential in-gel electrophoresis (DIGE) analysis can be employed using fluorescently stained 2D gels (Rabilloud et al., 2011). The advantages of 2D-DIGE proteomics are: the high sensitivity of the fluorescent dyes, high accuracy on spot resolution, the fewer number of gels as three samples can be compared in the same gel, fast turn-around, and it is cost-effective[9]. Liquid chromatography/mass spectrometry (LC/MS/MS) is a common technique used to identify proteins from 2D gels, their amounts, and their modifications (Baycin-Hizal et al., 2012). The recently sequenced CHO-K1 genome has opened up a new era involving analysis of CHO cells on a systems biology level (Xu et al., 2011). The CHO genomic sequence data have significantly enhanced the capabilities of these proteomics studies. Various CHO-specific databases now provide information on some identified peptides and proteins, thus increasing the confidence of identification (Meleady et al., 2012). In fact, the CHO genomic sequence enabled a large-scale multidimensional proteomic analysis that identified 6164 proteins from both the proteome and glycoproteome of CHO-K1 cell lines (Baycin-Hizal et al., 2012). Thus, the interpretation and analysis of transcriptomic and proteomic data to assess the physiological state of the cells under different growth and production conditions is facilitated (Kildegaard et al., 2013).

The aim in this chapter is to understand the effects of external pH in the CHO-CY01 cell line growth, cellular metabolism, and IgG4 production to find the optimum external pH for IgG4 optimisation purposes. All CHO-CY01 cell line cultures in this chapter were performed in the 5L-STR bioreactor (section 2.1.4). The specific objectives of this chapter are:

- Perform CHO-CY01 cell line batch and fed-batch cultures at different pH set-points
- Execute single and multiple pH shifts in a CHO-CY01 cell line fed-batch cultures

[9] http://www.appliedbiomics.com/support/2d-dige-vs-2d-gel.html

- Generate 2D-DIGE gels for CHO-CY01 cell line fed-batch cultures at different constant pHs and pH shifts
- Identify through mass spectrometry some relevant 2D-DIGE gel protein spots from CHO-CY01 cell line fed-batch culture with pH shift

6.2. CHO-CY01 Cell Line Batch Cultures at Different pH values

In the previous chapter, whereby manipulation of the CO_2 concentration, different pH profiles at 24-SRW MTP scale were obtained. It was found that a culture pH around pH 6.80 would almost stop CHO-CY01 cell growth rate as well as the lactate production rate. At the other end, culture pHs higher that pH 7.40 were associated with high lactate production and low IgG4 productivity. These conclusions were then tested at a fully automated larger scale, 5L-STR. CHO-CY01 cells were inoculated in a 5L-STR bioreactor at three different pH values: the standard pH (pH 7.1); below the standard pH (pH 6.80) and above the standard pH (pH 7.4). Kinetics of CHO-CY01 cell line batch cultures at pH 6.80, 7.10 and 7.40 can be visualised in Figure 6-1 and Figure 6-2, the calculated kinetics are presented in the Table 6-1 and Table C-17. In the Figure 6-4, the determined kinetic parameters from Table 6-1 were plotted against the culture pH and trendlines were fitted to the data. An apoptotic and cell cycle population fractions analysis was also performed and the results are presented in Figure 6-3. The Spearman´s correlation coefficients are shown in Table A-18. The particle size distribution study for all the three culture pHs is presented in Figure B-11 and Table B-11. The online processes parameters, such as pH, $\mathrm{pO_2}$, base addition, temperature and $\mathrm{CO_2}$ profiles are shown in Figure D-1 (pH 7.10), Figure D-2 (pH 6.80) and Figure D-3 (pH 7.40). The overall online processes parameters values are listed in Table 6-4.

At culture pH 6.80, CHO-CY01 cells presented entirely different cell growth, metabolites and IgG4 concentrations profiles. In fact, there was a reduction in the μ (57.9%) and q_{Lact} (93.5%), as predicted from the scale-down studies (Chapter 5). The doubling time ($t_{1/2}$) for CHO-CY01 cells at pH 6.80 had an increase of 138% in comparison with the standard pH ($29.2h$). The result was a substantial increase in the cell culture duration time (8 extra days) and a decrease in the maximum viable cell concentration ($3.5 \times 10^6\ cells\ mL^{-1}$). Also, at this culture pH, CHO-CY01 cells had an extended stationary phase (5 days), uncharacteristic for batch cultures. The glucose and glutamate consumption rates decreased as a direct result of fewer cells present in the bioreactor, however there was no change in q_{Gluc} or q_{Glu} with the culture pH. (Figure 6-2 and Table 6-1). The maximum ammonium concentration reached by the cells was similar at all the culture pHs (~5.9 $mmol\ L^{-1}$). Nevertheless, CHO-CY01 cells at pH 6.80 presented a 1.5-fold increase in q_{Amm}, due to a

20.5% decrease in IVCC. Also, it can be said that CHO-CY01 cells in this culture pH were not lactate producers ($q_{Lact} = 0.02g\ 10^{-9}cells^{-1}day^{-1}$), which means that these cells are more metabolic efficient. Regarding IgG4 productivity, although CHO-CY01 cells produced the monoclonal antibody at a slower race (VP = 26.2 $mg\ L^{-1}\ day^{-1}$), the CHO-CY01 cells ended up producing 8.3% more IgG4 than in the cell culture at standard pH even with significant reduction in the cell numbers. Therefore, there was a 47.9% increase in q_{mAb} (14.72 $mg\ 10^{-9}\ cells^{-1}\ day^{-1}$). This astonishing increase in IgG4 productivity may be related to the fact that the CHO-CY01 cells were quite large (cell diameter > 16 μm), presented a long stationary phase (where the IgG4 bulk production occurred) with $46.3 \pm 8.3\%$ of cells in G1-phase, $31.9 \pm 9.6\%$ cells in S-phase and, $21.8 \pm 2.9\%$ in G2/M-phase. From the cell cycle population (Figure 6-3), there was the characteristic start of the cell culture with more than 60% of cells in G1-phase, followed by a slow decrease of G1 cell population (~40%) with an increase of S-phase cells (~40%) throughout the exponential phase and part of stationary phase. At day 13, there was a shift in G1 and S cell population fractions, which in combination with the increase in the ´no viable´ population reflected on a cease in IgG4 production. At the decline phase, there was again a shift from G1-phase to S-phase. This type of cell cycle population fraction shift has been already observed for CHO-CY01 cell line batch culture in 24-SRW MTP at 20.00% (v/v) CO_2 (pH = 7.02 ± 0.10), but opposite to the cell cycle behaviour at pH 7.10. The cell death causes continued to be due to apoptosis, as the late apoptotic population fraction increased throughout the cell culture (Figure 6-3).

CHO-CY01 cells at culture pH 7.40 showed a similar cell growth rate (μ = 0.025 h^{-1}) and metabolite (glucose, glutamate, lactate and, ammonia) profiles, a longer stationary phase (one extra day) and, a higher specific cell death (2.9-fold) compared with the cells at the standard culture condition. The difference between CHO-CY01 cell line batch cultures at pH 7.10 and pH 7.40 was the speed at which cells produced the IgG4 (VP = 59.4 $mg\ L^{-1}\ day^{-1}$) and the 37.5% increase in the maximum IgG4 concentration (0.66 ± 0.21 $g\ L^{-1}$). For CHO-CY01 cell line batch culture at pH 7.40, the IgG4 production started (day 4) when the G1-Phase fraction was higher than 50% and S-phase fraction was lower than 40% (Figure 6-3). In this pH condition, there was a continuous increase of CHO-CY01 cells in G1-phase (overall 60.1 ± 7.6%) alongside the decrease in S-phase cells, similarly to the. CHO-CY01 cell line batch culture in 24-SRW MTP at 1.00% (v/v) CO_2. Also, it was observed that these cells were slightly larger than the cells at the standard culture conditions but smaller than CHO-CY01 cells at pH 6.80 (Table B-11). This is an indication that the 59.3% increase in VP can be explained by a high G1-phase cell fraction (>50%) early in the cell culture.

At all culture pHs, there was a connection between the lactate and ammonium concentrations profiles. When the lactate concentration was lower than 1.0 $g\ L^{-1}$, there was a

significant increase in ammonium production by the cells (Figure 6-1 D, E). This can be observed by the linear ammonium production at pH 6.80 and the doubling on ammonium concentration at pH 7.10 and 7.40 cultures, when lactate concentration went below 1.0 $g\ L^{-1}$. Also, at these later cultures CHO-CY01 cells consumed lactate and ammonium at the same time (day 5 to 8). There was ammonium production stagnation when there was no more lactate and glucose available for the cells.

The cell culture parameters that were unaffected by the culture pH were the osmolality and, q_{K^+}. The later was excepted as the maximum ammonium concentration reached was similar at all pH values. At CHO-CY01 cell line batch cultures of pH 7.10 and pH 7.40, there was base addition by the pH controller, which slightly increased the osmolality. At the culture pH 6.80, there was no need for base addition and so the pH perturbations due to alkali addition were non-existent. However, the high CO_2 level (36.58 ± 3.60% (v/v)) inside the 5L-STR CHO-CY01 cell line batch culture at pH 6.80, can raise CO_2 stripping concerns. There was a decrease of q_{Na^+} with the increase on the cell culture pH set-point, which was expected. In this case, the lower the external pH, the more CHO-CY01 cells used the sodium as an acid extruder (Figure 5-1) to increase the internal pH.

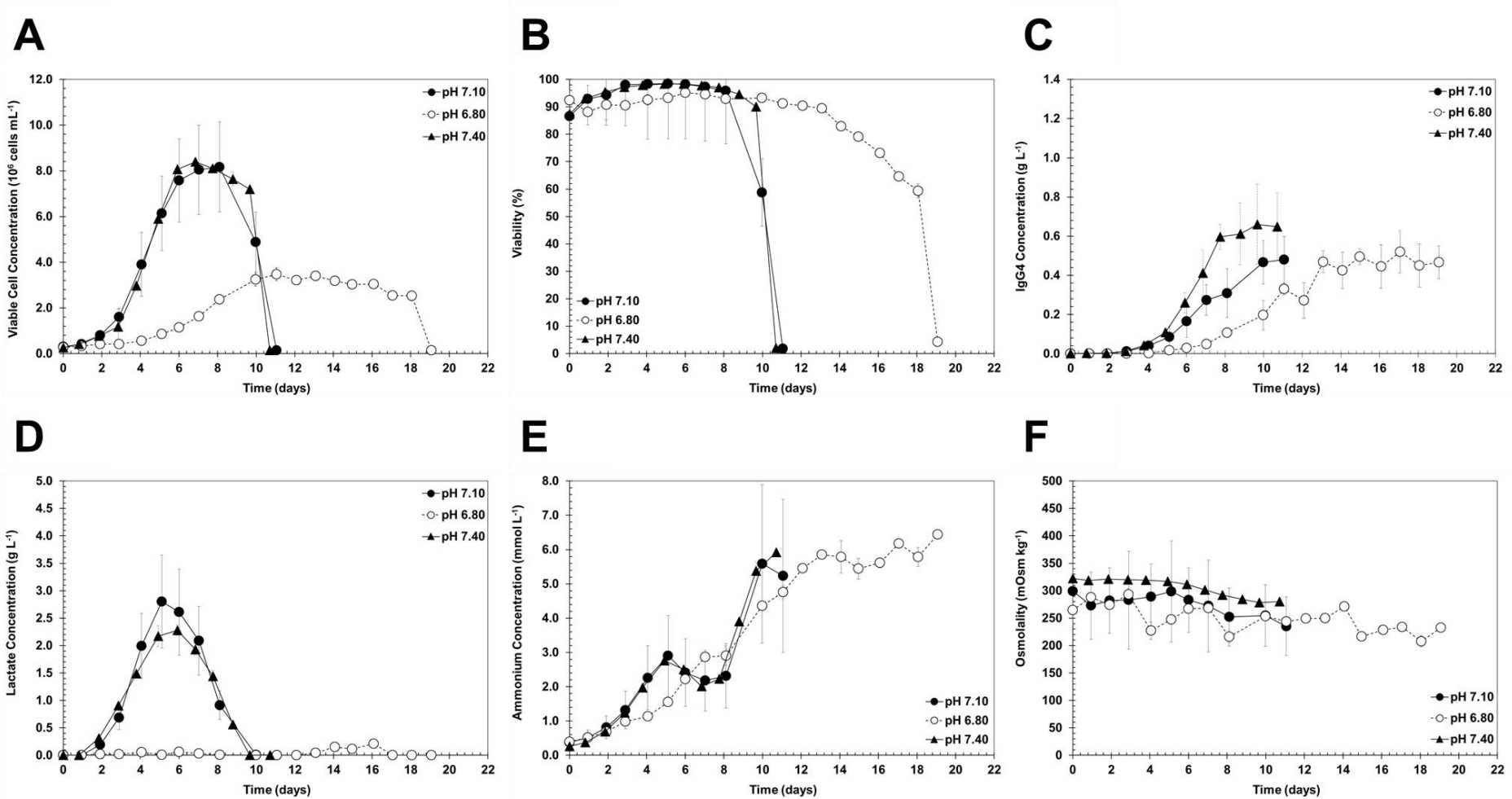

Figure 6-1: Viable cell concentration (A), cell viability (B), IgG4 concentration (C), lactate concentration (D), ammonium concentration (E) and osmolality (F) profiles for 5L-STR CHO-CY01 cell line batch cultures at pH 6.80 (1 replicate), pH 7.10 (1 replicate with historical data ($p > 0.05$)) and pH 7.40 (1 replicate). Error bars represent one standard deviation about the mean.

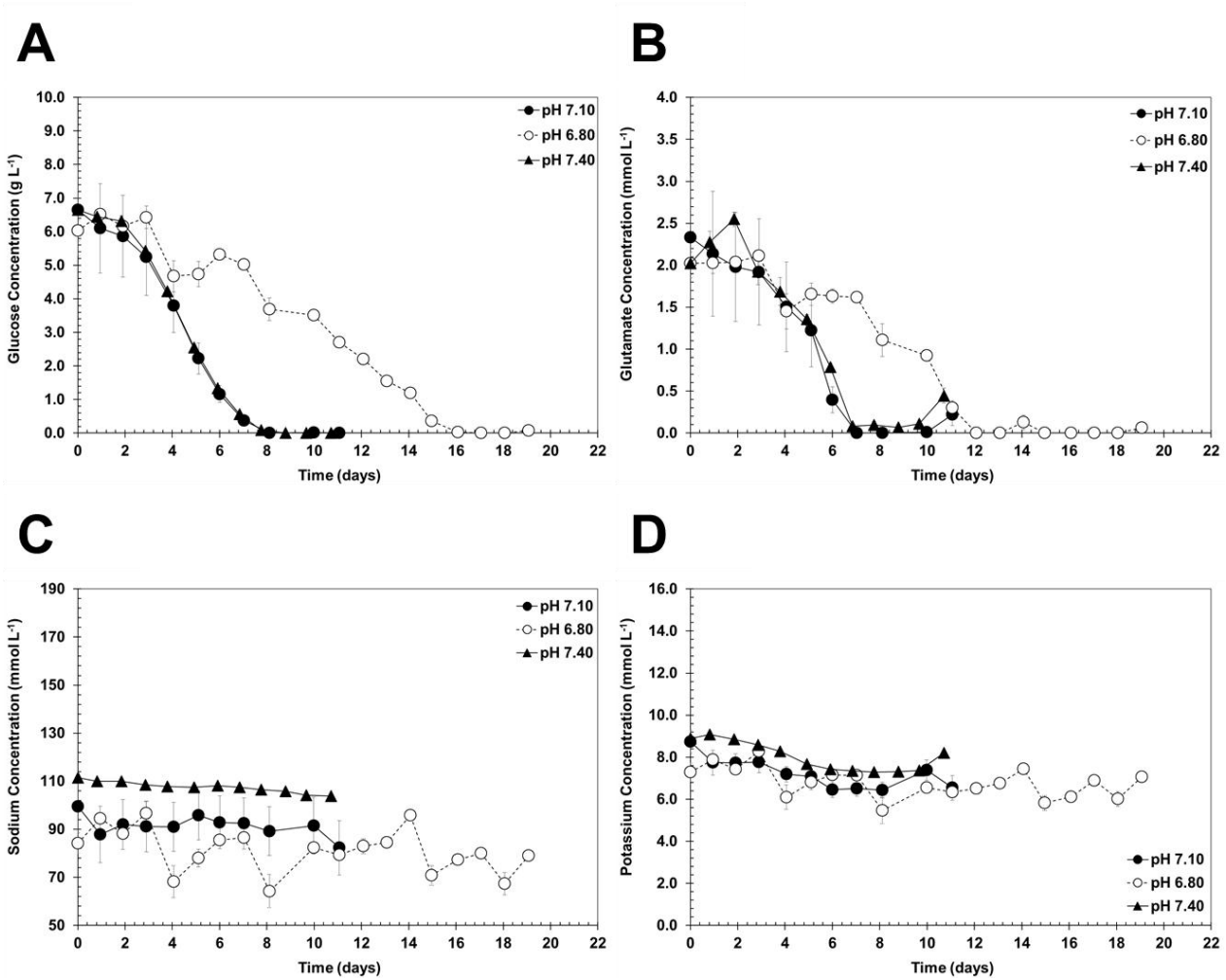

Figure 6-2: Glucose (A), glutamate (B), sodium (C) and potassium (D) concentrations profiles for 5L-STR CHO-CY01 cell line batch cultures at pH 6.80 (1 replicate), pH 7.10 (1 replicate with historical data ($p > 0.05$)) and pH 7.40 (1 replicate). Error bars represent one standard deviation about the mean.

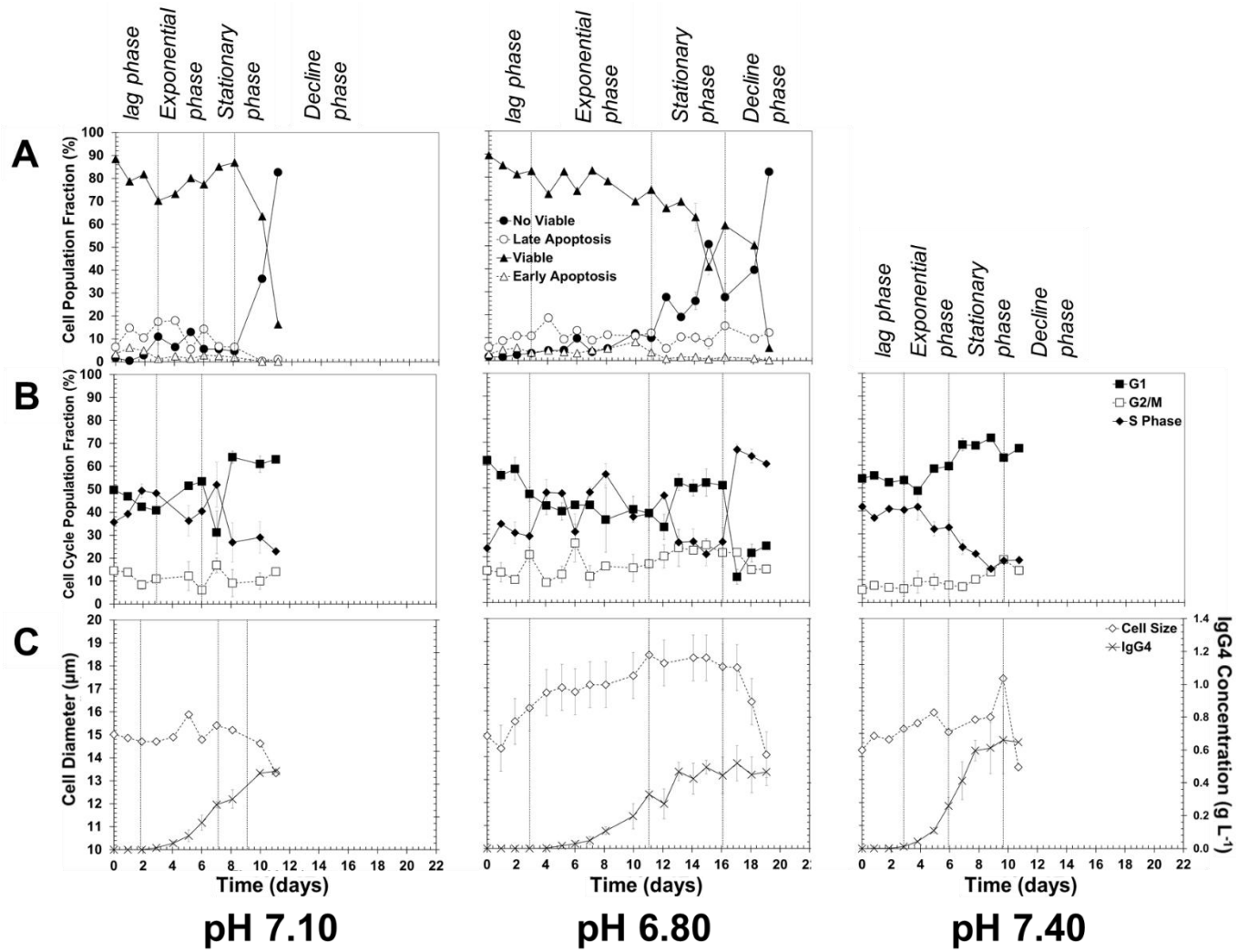

Figure 6-3: Apoptotic (A) and cell cycle (B) population fractions, and viable cell diameter and IgG4 titer (C) profiles for 5L-STR CHO-CY01 cell line batch cultures at different pHs (6.80, 7.10 and 7.40) accordingly to phases of cell growth (lag, exponential, stationary and decline or death phase). The error bars are the standard deviation about the mean.

Table 6-1: Kinetic parameters determined for 5L-STR CHO-CY01 cell line batch cultures at different pH values (6.80, 7.10 and 7.40).

5L-STR pH set-point	**6.80**	**7.10**	**7.40**
VP ($mg\ L^{-1}day^{-1}$)	26.0	37.3 ± 3.3	59.4
IVCC ($10^9\ cells\ day\ L^{-1}$)	38.48	48.39 ± 9.1	49.43
$\mu\ (h^{-1})$	0.010	0.024 ± 0.002	0.025
$t_{1/2}\ (h)$	69.2	29.1 ± 2.3	27.6
$q_{mAb}\ (mg\ 10^{-9}\ cells^{-1}\ day^{-1})$	14.72	9.96 ± 2.16	15.10
$q_{Gluc}\ (g\ 10^{-9}\ cells^{-1}\ day^{-1})$	-0.20	-0.17 ± 0.03	-0.17
$q_{Glu}\ (mmol\ 10^{-9}\ cells\ day^{-1})$	-0.07	-0.06 ± 0.02	-0.05
$q_{Na^+}\ (mmol\ 10^{-9}\ cells^{-1}\ day^{-1})$	-0.56	-0.29	-0.16
$q_{K^+}\ (mmol\ 10^{-9}\ cells^{-1}\ day^{-1})$	-0.05	-0.06	-0.04
$q_{Lact}\ (g\ 10^{-9}\ cells^{-1}\ day^{-1})$	0.02	0.29 ± 0.11	0.28
$q_{Amm}\ (mmol\ 10^{-9}\ cells^{-1}\ day^{-1})$	0.18	0.10 ± 0.016	0.10
Lactate produced / glucose consumed(g/g)	0.03	0.65 ± 0.15	0.44
$\mu_d\ (h^{-1})$	-0.04	-0.05 ± 0.03	-0.15

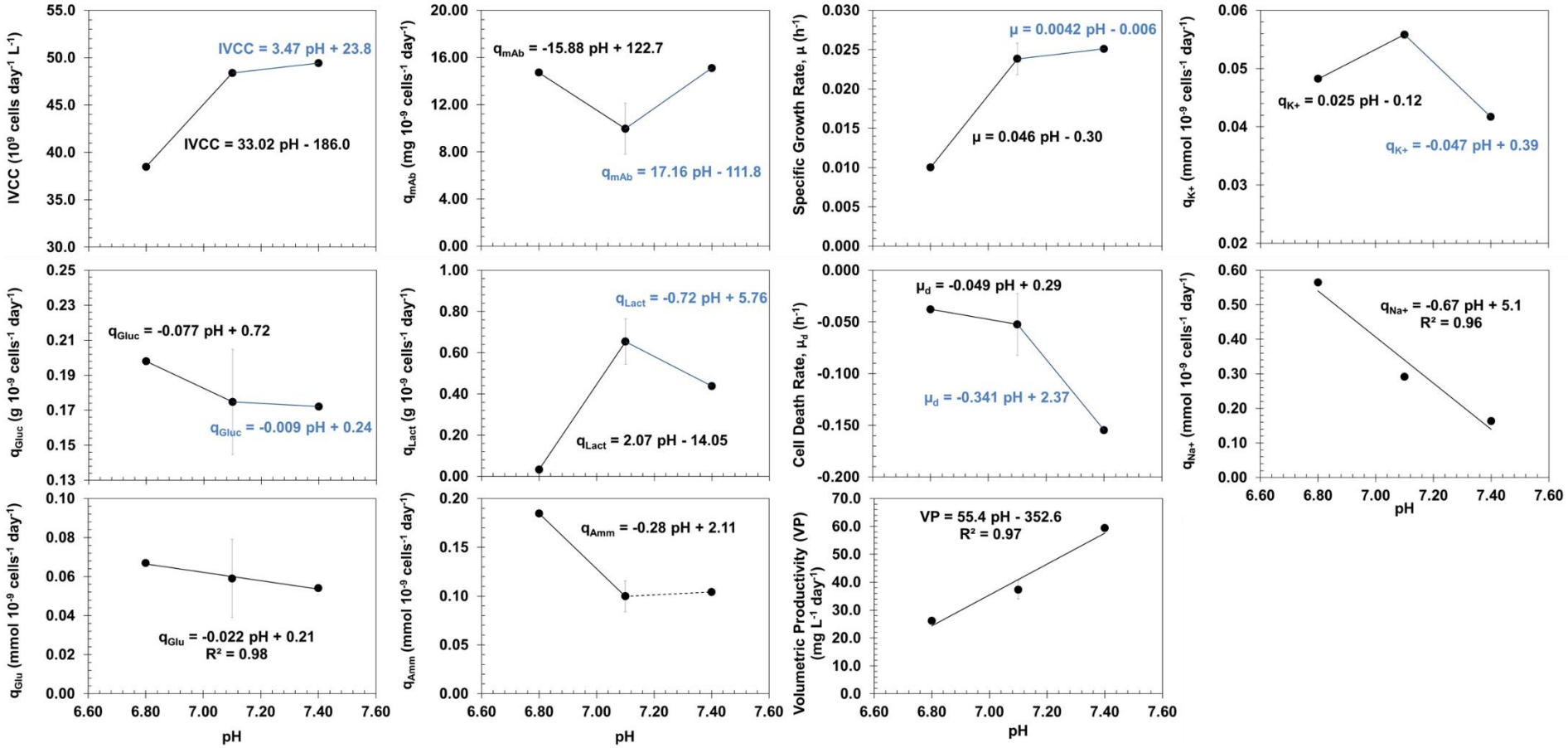

Figure 6-4: Graphical representation of the 5L-STR CHO-CY01 cell line batch cultures at different pHs (6.80, 7.10 and 7.40) kinetic parameters (Table 6-1) and observed trendlines. Error bars represent one standard deviation about the mean

6.3. CHO-CY01 Cell Line Fed-Batch Cultures at Different pH values

From the previous section, it was found that the best culture pH to grow CHO-CY01 cells for IgG4 productivity optimisation purposes was pH 6.80. In this section, the impact of culture pH have on CHO-CY01 cell line growth, metabolism and IgG4 production was further explored. CHO-CY01 cells were inoculated in a 5L-STR bioreactor at different culture pHs: the standard pH (pH 7.10), the current optimum culture pH for IgG4 production (pH 6.80) and an extremely high pH was tested (pH 7.80). The fed-batch cell culture at pH 7.80 was performed to find the upper pH range at which CHO-CY01 cells can grow and produce the monoclonal antibody IgG4 since CHO-CY01 cells at pH 7.10 and pH 7.40 had similar behaviour.

CHO-CY01 cell line fed-batch culture kinetics at pH 6.80, 7.10 and 7.80 are shown in Figure 6-5 and Figure 6-6, the calculated kinetic parameters are presented in Table 6-2 and Table C-18. In Figure 6-7, the determined kinetic parameters from Table 6-2 are plotted against the culture pH and trendlines were fitted to the data. The Spearman´s correlation coefficients are in the Table A-19. The particle size distribution study for all the three culture pHs is presented in Figure B-12 and Table B-12. The online process parameters, such as pH, pO_2, base addition, temperature and CO_2 profiles are in the Figure D-5 (pH 7.10), Figure D-6 (pH 6.80) and Figure D-7 (pH 7.80). The overall online process parameters values are listed in Table 6-4.

The first thing to notice, from this fed-batch study at different culture pH values, was the difficulty shown by CHO-CY01 cells to grow and to produce IgG4 at pH 7.80. At this culture pH, there was the continuous need for the 5L-STR pH controller to add a base to raise the culture pH to the pH set-point. A total of 949.5 mL of sodium carbonate buffer (section 2.1.4) was added, which caused a change in the fluid hydrodynamic conditions (t_m, k_La, P/V). Also, it lead to a sodium accumulation in the cell culture medium (Figure 6-6 C) and so an increase in osmolality (Figure 6-5 F). By contrast, the smallest amount of CO_2 was added to the bioreactor (0.19 ± 0.08%) (Figure D-7: E). From the particle size distribution, it is noticed that cells are in a pH homeostasis and under osmotic stress as the cell diameter is larger than 18µm (Table B-12) and there was a big debris peak throughout the cell culture (Figure B-12). As previously observed, in the CHO-CY01 cell line batch culture in 24-SRW MTP at 0.04% (v/v) CO_2 (and pH > 7.50), cells presented a survival strategy of producing lactate as a way of dealing with high external pH. The CHO-CY01 cells adopted this same strategy when cultured at pH 7.80. There was a 208% increase in the q_{Lact} compared with the reference (pH 7.10) (Figure 6-6). Therefore, the q_{Gluc} increased considerably (2.1-fold), which led to an early start in the feeding process (day 4) and a daily glucose requirement during the fed-batch mode of 2.03 ± 1.32 $g\,L^{-1}\,day^{-1}$. Glutamate was not utilised by the cells and so, there was

accumulation of this amino acid in the cell culture medium (Figure 6-6 B). Once again, the q_{Amm} was constant for pH > 7.10 and the lowest value measured (0.05 $mmol\ 10^{-9}\ cells^{-1}\ day^{-1}$). Regarding cell numbers, there was a decrease in specific cell growth, which resulted in a 65.9% reduction in the IVCC. Since the fewer CHO-CY01 cells at pH 7.80 were in constant struggle for survival, the IgG4 production was not a priority and so, the IgG4 peak concentration obtained was much lower than the reference (pH 7.10) batch mode value. This caused a 37.3% reduction in the q_{mAb}.

The CHO-CY01 cell line fed-batch culture at pH 6.80 exhibited a higher μ compared to the batch value (105% increase) and a 1.4-fold rise in the maximum viable cell concentration ($7.37 \times 10^6\ cells\ L^{-1}$). It can be claimed that the μ was similar (within the error) to the reference value (0.023 h^{-1}). However, the stationary phase was longer (nine days vs. three days (pH 7.10)) and the maximum viable cell concentration was smaller at pH 6.80. The end result was an increase in IVCC of 9.3%. Again, the lactate production was suppressed at pH 6.80 (< 0.99 $g\ L^{-1}$) and as soon as, the fed-batch mode started cells stopped producing lactate (day 8) (Figure 6-5 D). Therefore, the q_{Gluc} and daily feeding requirements by CHO-CY01 cells were minimal at this pH (Figure 6-7). Similarly to 5L-STR CHO-CY01 cell line batch culture, there was a substantial increase (133%) in the q_{Amm} at pH 6.80 compared with the reference, but the ammonium concentration was always lower than $K_{i,Amm}$ (18.1 mM) and $K_{Di,Amm}$ (9.66 mM). Nonetheless, from day 13 onwards the ammonium concentration in the pH 6.80 CHO-CY01 cell culture was higher than $K_{P,Amm}$ (7.1 mM), which caused the IgG4 production slowdown between day 12 and 13. Nevertheless, the VP at pH 6.80 was just 4.8% smaller than at pH 7.10 and there was even an 10.5% increase in q_{mAb}. The IgG4 production stopped when CHO-CY01 cells numbers started to decline, the cell viability was less than 70.0% and the ammonium concentration was higher than 9.17 mM (day 17). However, it is worthwhile mention that for all the pH values tested there was a reduction of q_{Amm} in fed-batch mode (42.2% for pH 6.80 and 54.2% for pH 7.10).

In summary, two important points were taken in this section. The first one was the upper limit of CHO-CY01 cell culture pH is below pH 7.80. The second point being, CHO-CY01 cell line fed-batch culture at pH 6.80 is still considered as the optimum pH for IgG4 production and now the optimum for cell growth as well.

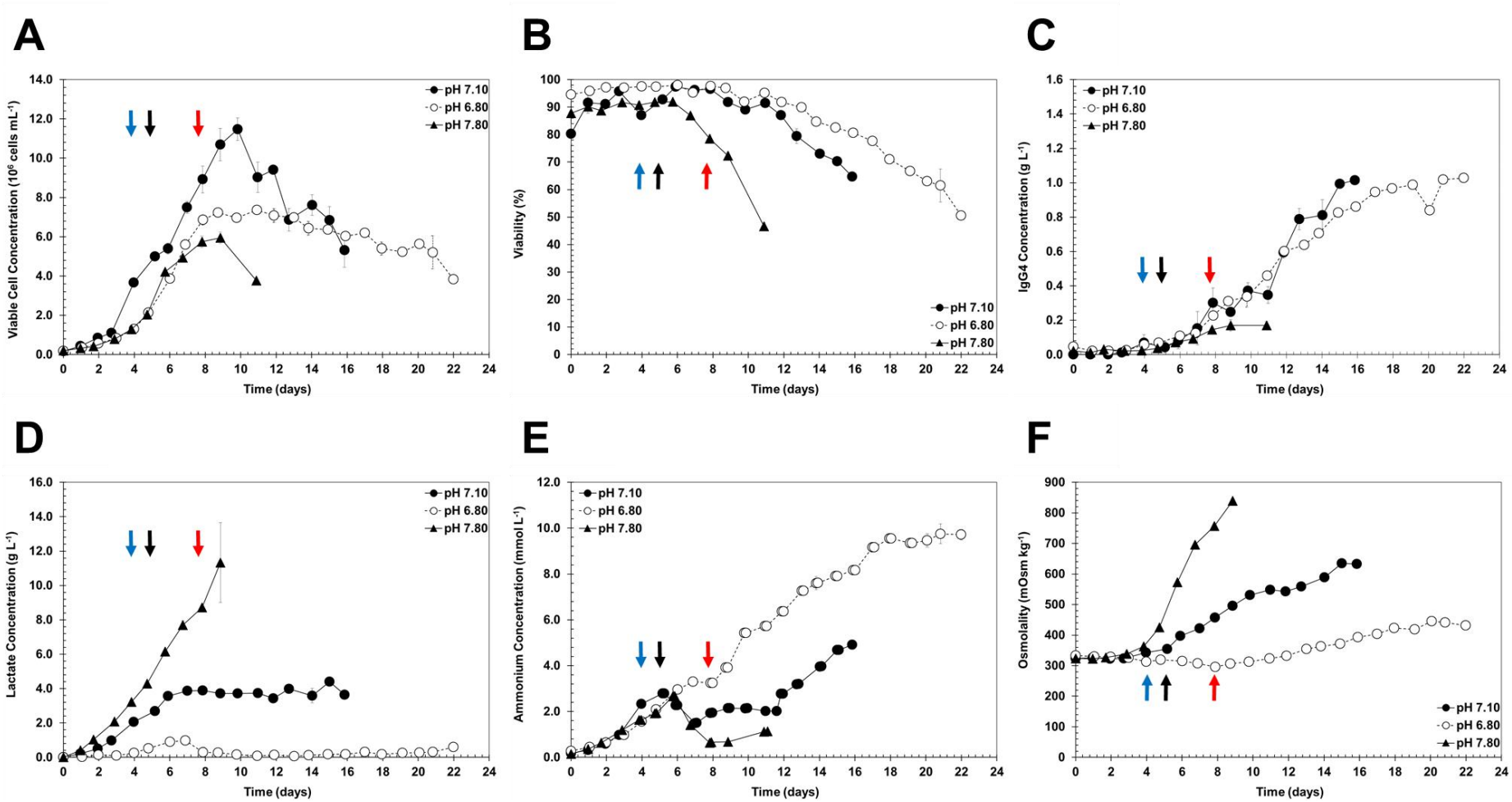

Figure 6-5: Viable cell concentration (A), cell viability (B), IgG4 concentration (C), lactate concentration (D), ammonium concentration (E) and osmolality (F) profiles for 5L-STR CHO-CY01 cell line fed-batch strategy 5 (FB3) cultures at pH 6.80, pH 7.10 and pH 7.80 (1 replicate per condition). The arrow indicates when the feeding started (pH 7.80 – blue; pH 7.10– black; pH 6.80 – red). Error bars represent one standard deviation about the mean.

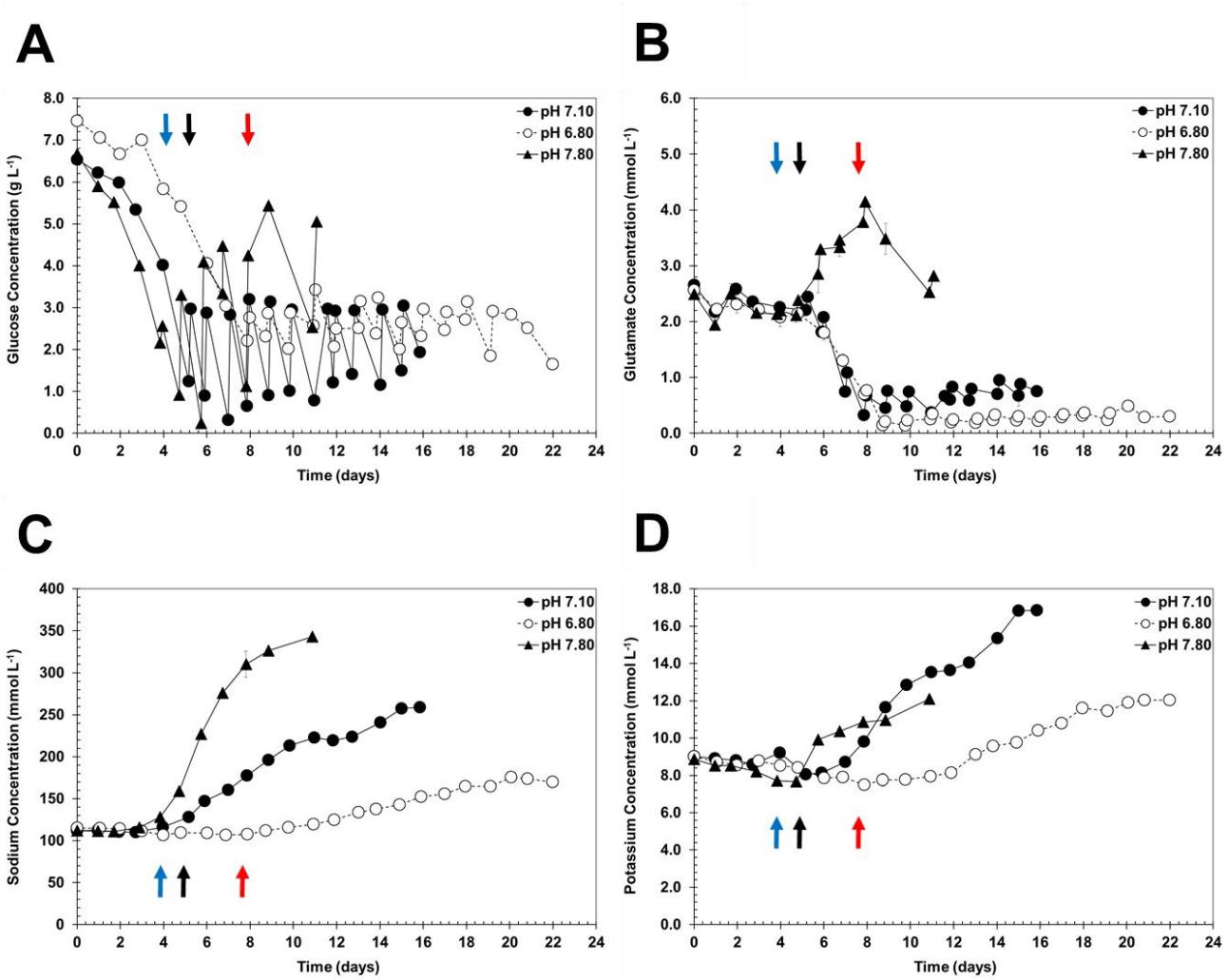

Figure 6-6: Glucose (A), glutamate (B), sodium (C) and potassium (D) concentrations profiles for 5L-STR CHO-CY01 cell line fed-batch strategy 5 (FB3) cultures at pH 6.80, pH 7.10 and pH 7.80 (1 replicate per condition). The arrow indicates when the feeding started (pH 7.80 – blue; pH 7.10– black; pH 6.80 – red). Error bars represent one standard deviation about the mean.

Table 6-2: Kinetic parameters determined for 5L-STR CHO-CY01 cell line fed-batch strategy 5 (FB3) cultures at pH 6.80, pH 7.10 and pH 7.80.

5L-STR pH set-point	**6.80**	**7.10**	**7.80**
VP ($mg\ L^{-1}day^{-1}$)	47.6	50.0	15.3
IVCC ($10^9\ cells\ day\ L^{-1}$)	105.88	96.90	33.05
$\mu\ (h^{-1})$	0.021	0.023	0.019
$t_{1/2}\ (h)$	33.8	29.9	35.7
$q_{mAb}\ (mg\ 10^{-9}\ cells^{-1}\ day^{-1})$	10.50	9.50	5.96
$q_{Gluc}\ (g\ 10^{-9}\ cells^{-1}\ day^{-1})$	-0.15	-0.32	-0.66
$q_{Glu}\ (mmol\ 10^{-9}\ cells^{-1}\ day^{-1})$	-0.04	-0.06	-0.03
$q_{Lact}\ (g\ 10^{-9}\ cells\ day^{-1})$	0.06	0.49	2.02
$q_{Amm}\ (mmol\ 10^{-9}\ cells^{-1}\ day^{-1})$	0.11	0.05	0.05
Lactate produced / Glucose consumed(g/g)	0.22	0.16	0.93
$\mu_d\ (h^{-1})$	-0.002	-0.004	-0.009
Feed volume (% of reactor volume)	5.1	14.9	6.4

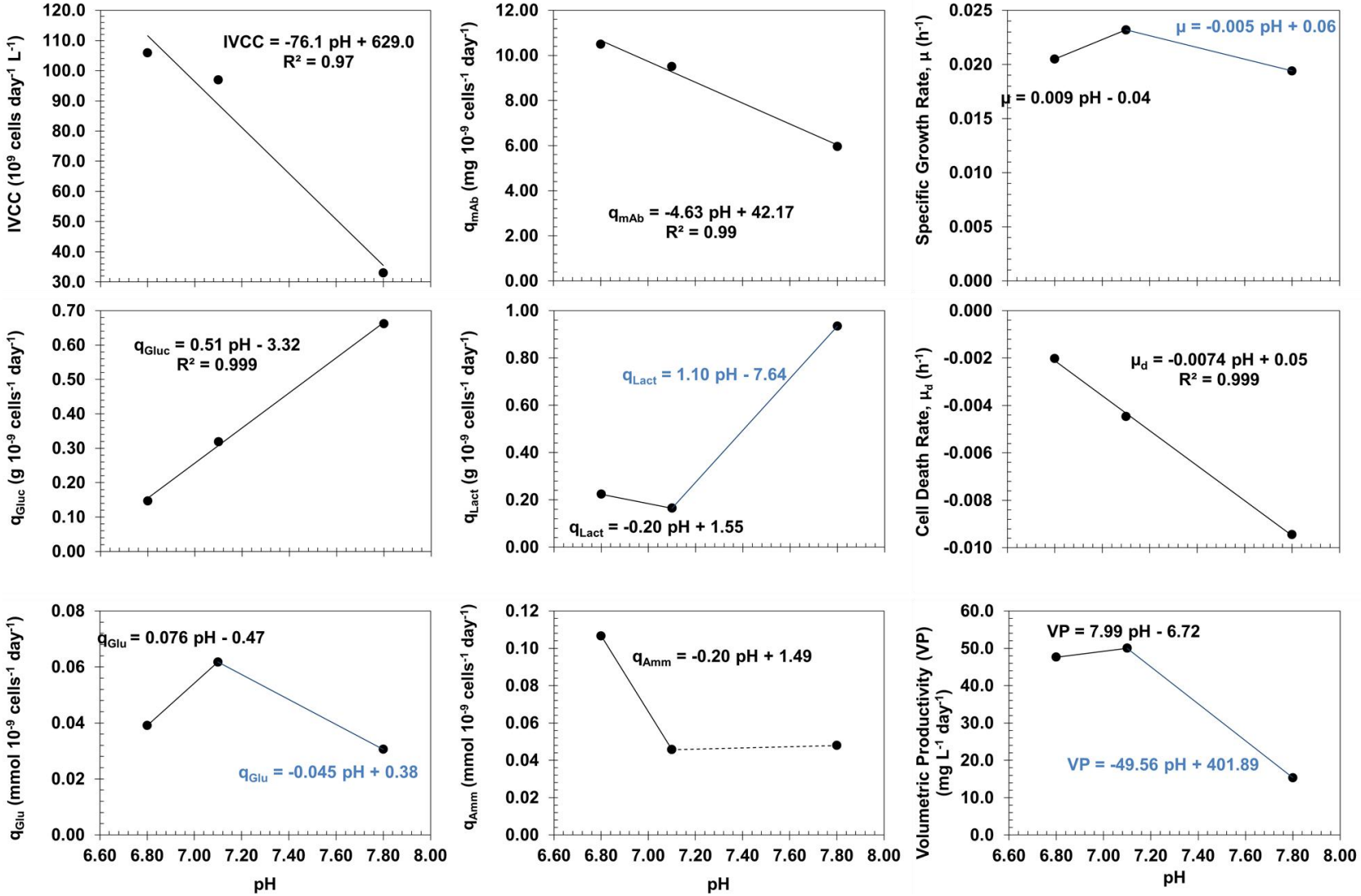

Figure 6-7: Graphical representation of the kinetic parameters determined for 5L-STR CHO-CY01 cell line fed-batch cultures at different pHs (6.80, 7.10 and 7.80) (Table 6-2) and observed trendlines.

6.4. pH shifts in CHO-CY01 Cell Line Fed-Batch Cultures

The next step was to perform different pH shifts, to find the optimum pH profile for IgG4 production by the CHO-CY01 cell line. The different pH shifts cell cultures were compared with CHO-CY01 cell line fed-batch cultures at standard conditions (pH 7.10) and optimal constant pH (pH 6.80). The pH shift evaluation study was divided into two stages. Firstly, it was necessary to test across the pH range. Secondly, once the optimal pH range for CHO-CY01 cell line growth and IgG4 production is found, single and, multiple pH shifts were executed at different cell culture times.

Two pH shifts strategies were designed to determine the CHO-CY01 cell line pH range. CHO-CY01 cells were cultured at the expected minimum (pH 6.60) and maximum (pH 7.60) of the pH range line and so, it was possible to observe the effects on cell viability of those culture pHs readily. When the cell viability dropped below 90% with no cell growth associated during the first days of culture, a pH shift was made to a higher minimum (pH 6.80) or lower maximum (pH 7.10) to maintain the CHO-CY01 cell line fed-batch cultures.

CHO-CY01 cell line fed-batch cultures with the pH shift from pH 6.60 to pH 6.80 (day 2) and pH shift from pH 7.60 to pH 7.10 (day 4) kinetics are visualised in Figure 6-8 and Figure 6-9, the calculated kinetic parameters are presented in Table 6-3 and Table C-19. The Spearman´s correlation coefficients are shown in Table A-20. The particle size distribution study is presented in Figure B-13 and Table B-13. The online process parameters, such as pH, pO_2, base addition, temperature and CO_2 profiles are shown in Figure D-5 (pH 7.10), Figure D-6 (pH 6.80), Figure D-8 (pH shift from pH 6.60 to pH 6.80 (day 2)) and Figure D-9 (pH shift from pH 7.60 to pH 7.10 (day 4)). The overall online process parameters values are listed in Table 6-4.

It has been proven before that CHO-CY01 cell line cultures at pH values below 6.60 (Chapter 5) had an immediate cell death due to apoptosis. However, in a process controlled bioreactor system (5L-STR), this pH value was untested. Although, no apoptotic population fraction analysis was made in CHO-CY01 cell line fed-batch culture with the pH shift from pH 6.60 to pH 6.80 (day 2), a fall in viable cell numbers and cell viability (< 80%) during the first two days of culture at pH 6.60 was observed. Therefore, it can be conclueded that CHO-CY01 cells can not grow at culture pHs lower than pH 6.60. With the pH shift to pH 6.80, CHO-CY01 cells were able to grow and return to high cell viabilities (>90%) four days after the pH shift. It was only after six days in the culture that CHO-CY01 cells started to grow exponentially. By comparing this pH shift with the CHO-CY01 cell line fed-batch culture at pH 6.80, it was noted that a higher viable cell concentration was reached, which caused an increase of 22.4% on IVCC. Also, there was a 238.5% increase in q_{Lact}, with similar q_{Gluc} and the daily glucose consumption rate during feeding. However, the lactate accumulation was smaller than the one

observed in standard cell culture conditions (pH 7.10). These lactate formation was triggered due to the high volume of base added when the pH shift occurred (683.9 mL) and/or by the decrease of CO_2 concentration with time (Figure D-8 E), which is the opposite of the CO_2 profile at constant pH 6.80 (Figure D-6 E). Nevertheless, this initial pH stress caused a considerable reduction of ammonia production (q_{Amm}) (46.0% compared with pH 6.80 and 39.1% compared with pH 7.10). Regarding IgG4 productivity, the initial two days at pH 6.60, slowed the IgG4 production and so, there was a reduction in the VP (Table 6-3). Also, there were more CHO-CY01 cells at the pH shift from pH 6.60 to pH 6.80 for the same IgG4 peak concentration, which reflected in q_{mAb} reduction (13.8% in relation to pH 7.10 and 22.0% in relation to pH 6.80).

It was found that CHO-CY01 cell line batch culture at pH 7.40 behaved similarly to the standard pH and cells at pH 7.80 were under osmotic stress (Section 6.2 and 6.3). Therefore, the mid-point of these pH values (pH 7.60) was tested. Once again, CHO-CY01 cells in culture pHs higher than pH 7.50 presented the survival strategy of producing high amounts of lactate from glucose ($4.46\ g\ L^{-1}$ at day 4, which is already higher than $K_{i,Lact}$). The result was that at the start of the fed-batch mode on day 3 with only $1.32 \pm 0.08\ \times 10^6\ cells\ mL^{-1}$ the cell viability was below 90%. Therefore, it was noticed that pH 7.60 was still too high for the CHO-CY01 cells to grow and the pH shift to pH 7.10 was performed at day 4. As soon as, the CHO-CY01 cells were cultured at pH 7.10, the exponential growth began and the highest viable cell concentration ($14.7\ \times\ 10^6\ cells\ mL^{-1}$) was reached after this pH shift. Also, the highest daily glucose consumption rate ($2.25 \pm 0.63\ g\ L^{-1}day^{-1}$) was observed as a result of a 39.7% increase in q_{Lact} when compared with constant pH 7.10. The highest initial pH also dictated a 39.1% decrease in q_{Amm}. Regarding the IgG4 productivity, there was no change in the q_{mAb} (Table 6-2 and Table 6-3), but there was an increase of 28% in the IgG4 production rate (64.1 $mg\ L^{-1}day^{-1}$). However, the maximum lactate concentration reached (6.51$g\ L^{-1}$) was beyond any kinetic inhibition parameter (Table 4-5).

In summary, the optimal pH range for this CHO-CY01 cell line is between pH > 6.60 and pH ≤ 7.40. The cell culture pH values between pH 7.10 and 7.40 are optimal for CHO-CY01 cell growth and culture pHs: $6.60 < pH \leq 6.80$ are optimal for IgG4 production. Thus, a single pH shifts from pH 7.10 (reference) to pH 6.80 were tried at different CHO-CY01 cell line fed-batch culture times, mid-exponential point (day 5) and the end of exponential phase (day 8), as described in section 5.4.2.2 with the CO_2 shifts. A multiple step pH shift (2-steps), pH shift from pH 7.10 to pH 7.00 on day 4 and then from pH 7.00 to pH 6.80 on day 5 was also tested. This latter strategy can be regarded as a smoother equivalent to the single pH shift from pH 7.10 to pH 6.80 on day 5. The aim was to firstly promote cell growth and then take advantage of such high cell density to promote the IgG4 production.

CHO-CY01 cell line fed-batch culture kinetics with pH shift from pH 7.10 to pH 6.80 (day 5 or 8) and pH shift from pH 7.10 to pH 7.00 on day 4 and then from pH 7.00 to pH 6.80 on day 5 are visualised in Figure 6-10 and Figure 6-11, the calculated kinetic parameters are presented in the Table 6-3 and Table C-19. The Spearman´s correlation coefficients are shown in Table A-21. The particle size distribution study is presented in the Figure B-14 and Table B-14. The online process parameters, such as pH, pO_2, base addition, temperature and CO_2 profiles are in Figure D-5 (pH 7.10), Figure D-6 (pH 6.80), Figure D-10 (pH shift from pH 7.10 to pH 6.80 (day 5)), Figure D-11 (pH shift from pH 7.10 to pH 6.80 (day 8)), and Figure D-12 (pH shift from pH 7.10 to pH 7.00 on day 4 and then from pH 7.00 to pH 6.80 on day 5). The overall online process parameters values are summarised in Table 6-4.

For the single pH shifts, a parallel behaviour can be traced with the CO_2 shift experiements presented in section 5.4.2.2. The CHO-CY01 cells behaved identically at both scales. The pH shift to pH 6.80 during the exponential phase caused an inhibition in the cell growth (13.4% decline in μ and maximum viable cell concentration reached i.e. $5.92 \pm 0.33 \times 10^6 cells\ mL^{-1}$). The pH shift at the beginning of the stationary phase (maximum viable cell concentration), initiated the decline phase. Therefore, in both pH shifts cultures, there was a decrease in the overall cell numbers (~30%). Regarding the IgG4 productivity, there was a decline in the VP (~30%) for both pH shifts, but there was no change in q_{mAb} for the pH shift during exponential phase and a slight decrease for the pH shift culture at the stationary phase when comparing with constant pH culture. The pH shift from pH 7.10 to pH 6.80 at the mid-exponential point increased the q_{mAb} by 24.2% in relation to the same pH shift at the beginning of the stationary phase. The novelty presented at these pH shifts CHO-CY01 cell line fed-batch cultures was the fact that CHO-CY01 cells became lactate consumers whenever the pH was shifted from pH 7.10 to pH 6.80. An ammonium production increase was also observed whenever the pH set-point was changed to pH 6.80, but independently on the day of the pH shift the maximum ammonium concentration reached was similar to the one found at constant pH 6.80. The pH shifts were beneficial to CHO-CY01 cell line process optimisation. There was a reduction of q_{Gluc} (32.6% in the pH shift on day 5 and 42.6% when the pH shift was done on day 8); q_{Glu} (Table 6-3); and q_{Lact} (~60%) when compared with the constant reference pH (pH 7.10). However, there was an increase in q_{Amm} (3.2-fold for the pH shift on day 5 and 2.4-fold for the pH shift on day 8). Nevertheless, these pH shifts were unable to improve the CHO-CY01 cell line fed-batch culture performance at constant pH 6.80, which continues to be the optimal pH value, as there was an increase in q_{Gluc}, q_{Glu}, q_{Lact} and q_{Amm} for the same q_{mAb}.

For the multiple steps pH shifts, the CHO-CY01 cell line growth profile was similar to the one found at constant pH 7.10 and the peak IgG4 concentration ($1.03 g\ L^{-1}$) reached and VP ($47.8\ mg\ L^{-1}\ day^{-1}$) were the same as the ones found at pH 6.80. Also, this peak IgG4

concentration was reached after 16 days, 7 days earlier than at pH 6.80. At this condition, CHO-CY01 cells produced less lactate (2.76$g\ L^{-1}$) during exponential phase in comparison with the standard condition (pH 7.10) and were lactate consumers when culture pH was at pH 6.80. However, the lactate accumulation was higher than using the previous 1-step pH shifts and at constant pH 6.80 but lower than the reference. The IVCC and μ values obtained for these 2-step pH shift culture were similar to the ones reached at constant pH 7.10. However, the glucose consumption rate and lactate production rate had a significant decrease, while the ammonium accumulation was similar to the one found at pH 6.80 (high q_{Amm}). In relation to the current optimal, constant pH 6.80, there was a higher glucose requirement by the cells and so, a 2-fold increase in the feed volume was observed (Table 6-3 and Table 6-4). Also, there was a significant increase in q_{Lact} (0.35 $g\ 10^{-9}\ cells^{-1}\ day^{-1}$) with similar ammonium accumulation ($q_{Amm} = 0.11\ mmol\ 10^{-9}\ cells^{-1}\ day^{-1}$). The fact that there was a six day reduction in the cell culture duration with this two-step pH shift strategy suggests that it could be a possible optimal condition for IgG4 production by CHO-CY01 cells.

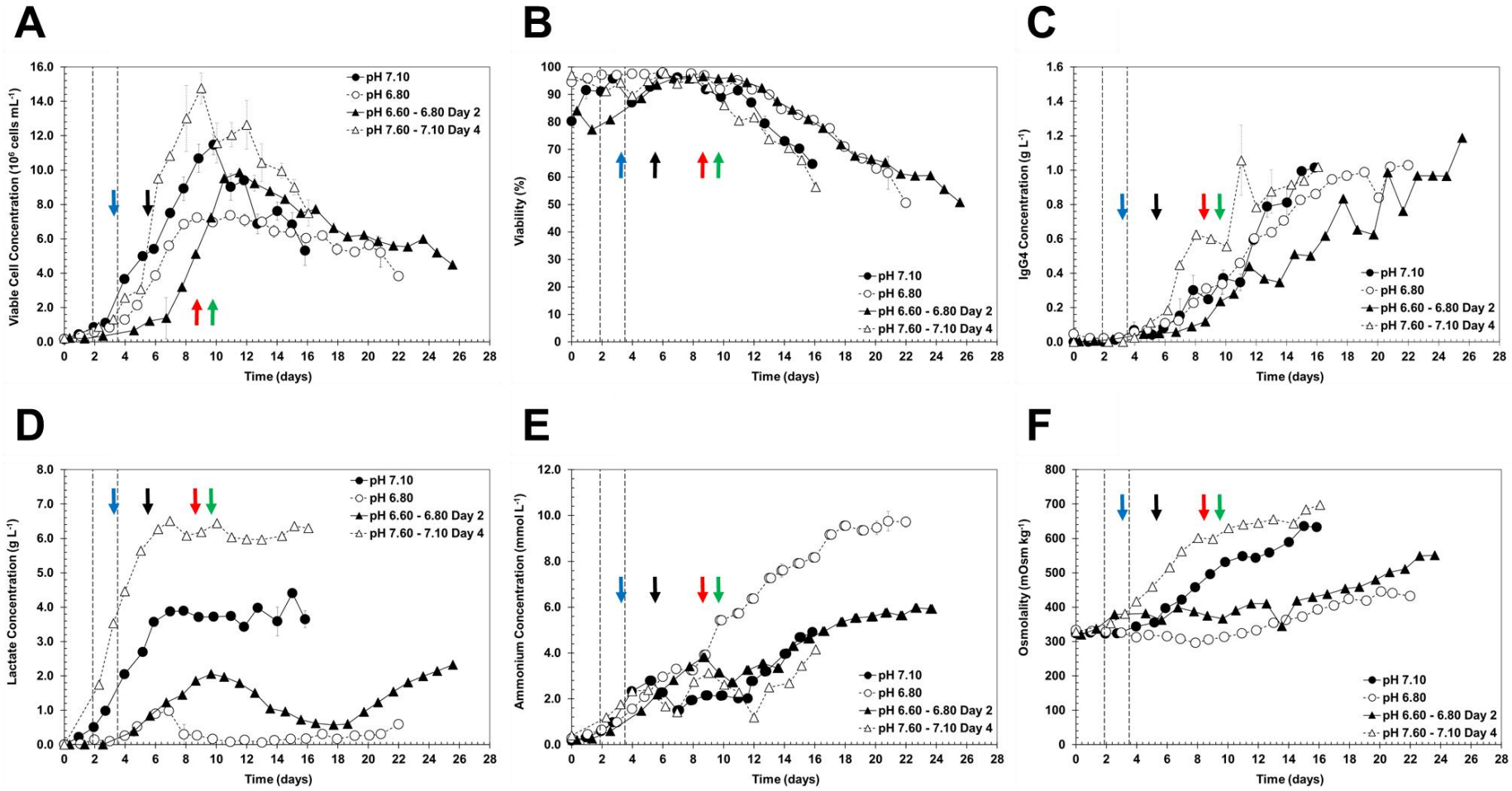

Figure 6-8: Viable cell concentration (A), cell viability (B), IgG4 concentration (C), lactate concentration (D), ammonium concentration (E) and osmolality (F) profiles for 5L-STR CHO-CY01 cell line fed-batch strategy 5 (FB3) cultures with constant pH 6.80 and pH 7.10, pH shift from pH 6.60 to pH 6.80 on day 2 (pH 6.60 – 6.80 Day 2), and pH shift from pH 7.60 to pH 7.10 on day 4 (pH 7.60 – 7.10 Day 4) (1 replicate per condition). The arrow indicates when the feeding started (pH 7.60 – 7.10 Day 4 – blue; pH 7.10– black; pH 6.80 – red; pH 6.60 – 6.80 Day 2– green). Error bars represent one standard deviation about the mean.

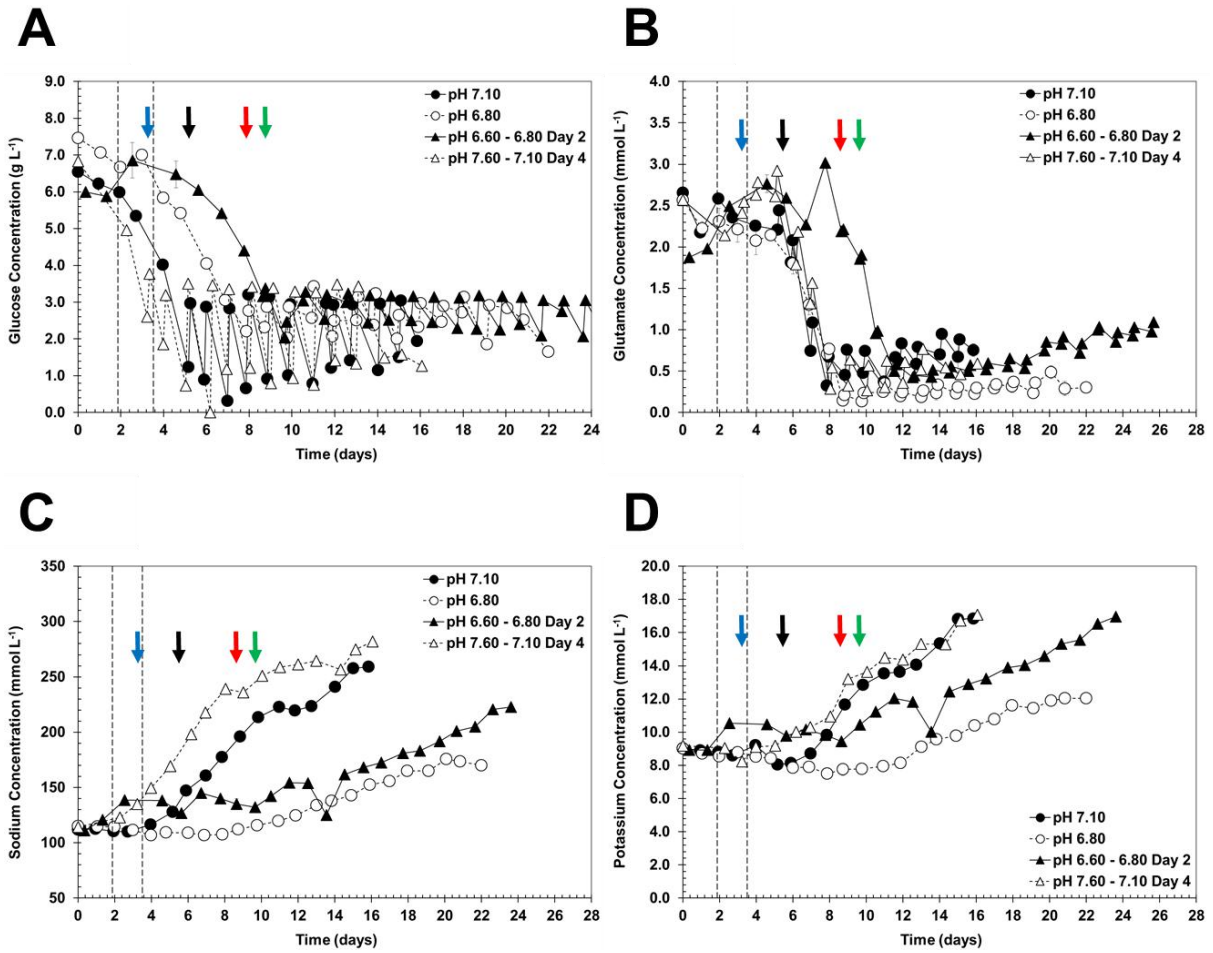

Figure 6-9: Glucose (A), glutamate (B), sodium (C) and potassium (D) concentrations profiles for Viable cell concentration (A), cell viability (B), IgG4 concentration (C), lactate concentration (D), ammonium concentration (E) and osmolality (F) profiles for 5L-STR CHO-CY01 cell line fed-batch strategy 5 (FB3) cultures with constant pH 6.80 and pH 7.10, pH shift from pH 6.60 to pH 6.80 on day 2 (pH 6.60 – 6.80 Day 2), and pH shift from pH 7.60 to pH 7.10 on day 4 (pH 7.60 – 7.10 Day 4) (1 replicate per condition). The arrow indicates when the feeding started (pH 7.60 – 7.10 Day 4 – blue; pH 7.10– black; pH 6.80 – red; pH 6.60 – 6.80 Day 2– green). Error bars represent one standard deviation about the mean.

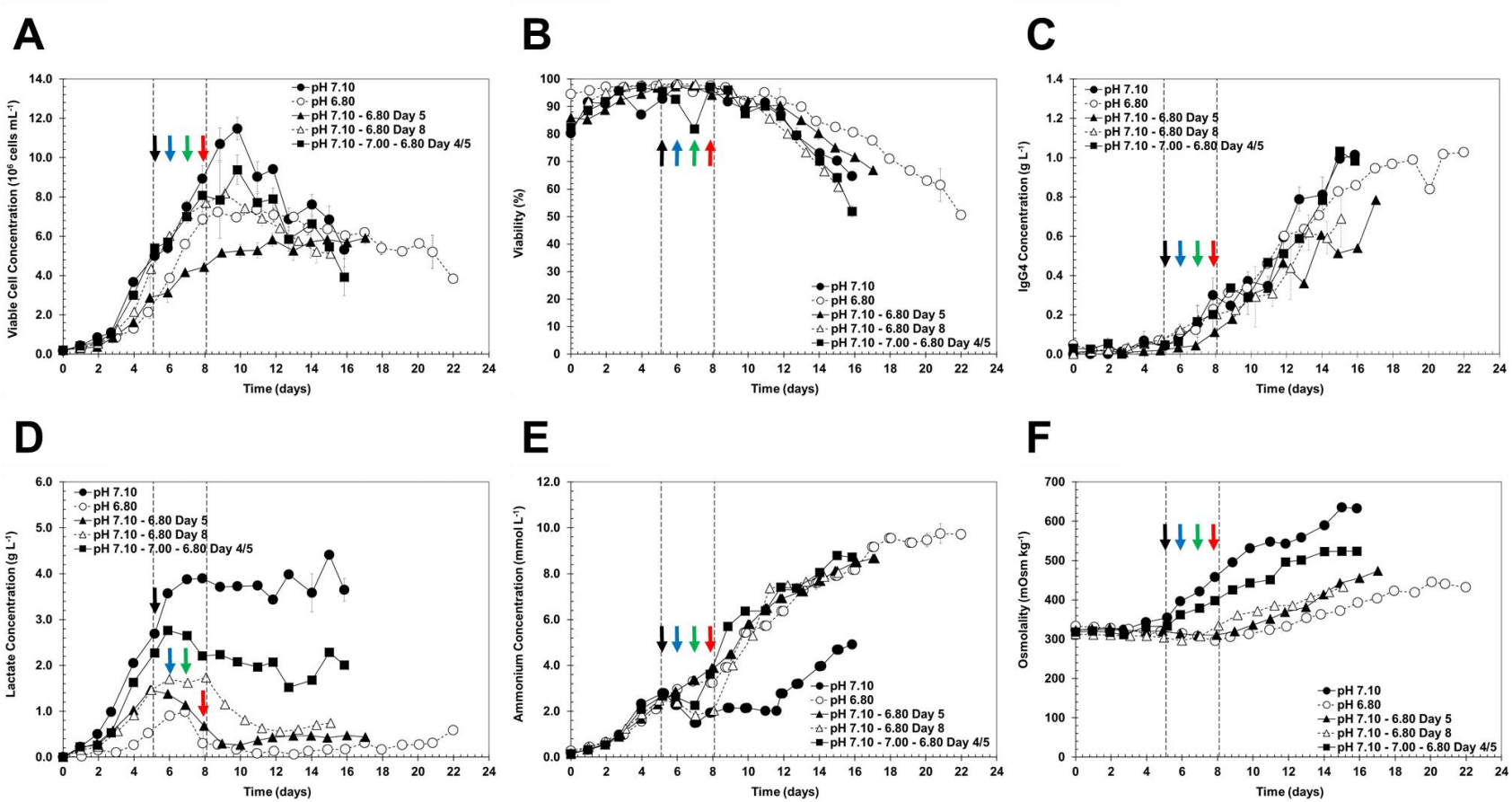

Figure 6-10: Viable cell concentration (A), cell viability (B), IgG4 concentration (C), lactate concentration (D), ammonium concentration (E) and osmolality (F) profiles for 5L-STR CHO-CY01 cell line fed-batch strategy 5 (FB3) cultures with constant pH 6.80 and pH 7.10, pH shifts from pH 7.10 to pH 6.80 on day 5 (pH 7.10 – 6.80 Day 5) or 8 (pH 7.10 – 6.80 Day 8), and pH shift from pH 7.10 to pH 7.00 on day 4, then to pH 6.80 on day 5 (pH 7.10-7.00-6.80 Day 4/5) (1 replicate per condition). The arrow indicates when the feeding started (pH 7.10 and pH 7.10-7.00-6.80 Day 4/5– black; pH 7.10 – 6.80 Day 8 – blue; pH 7.10 – 6.80 Day 5– green; pH 6.80 - red). Error bars represent one standard deviation about the mean.

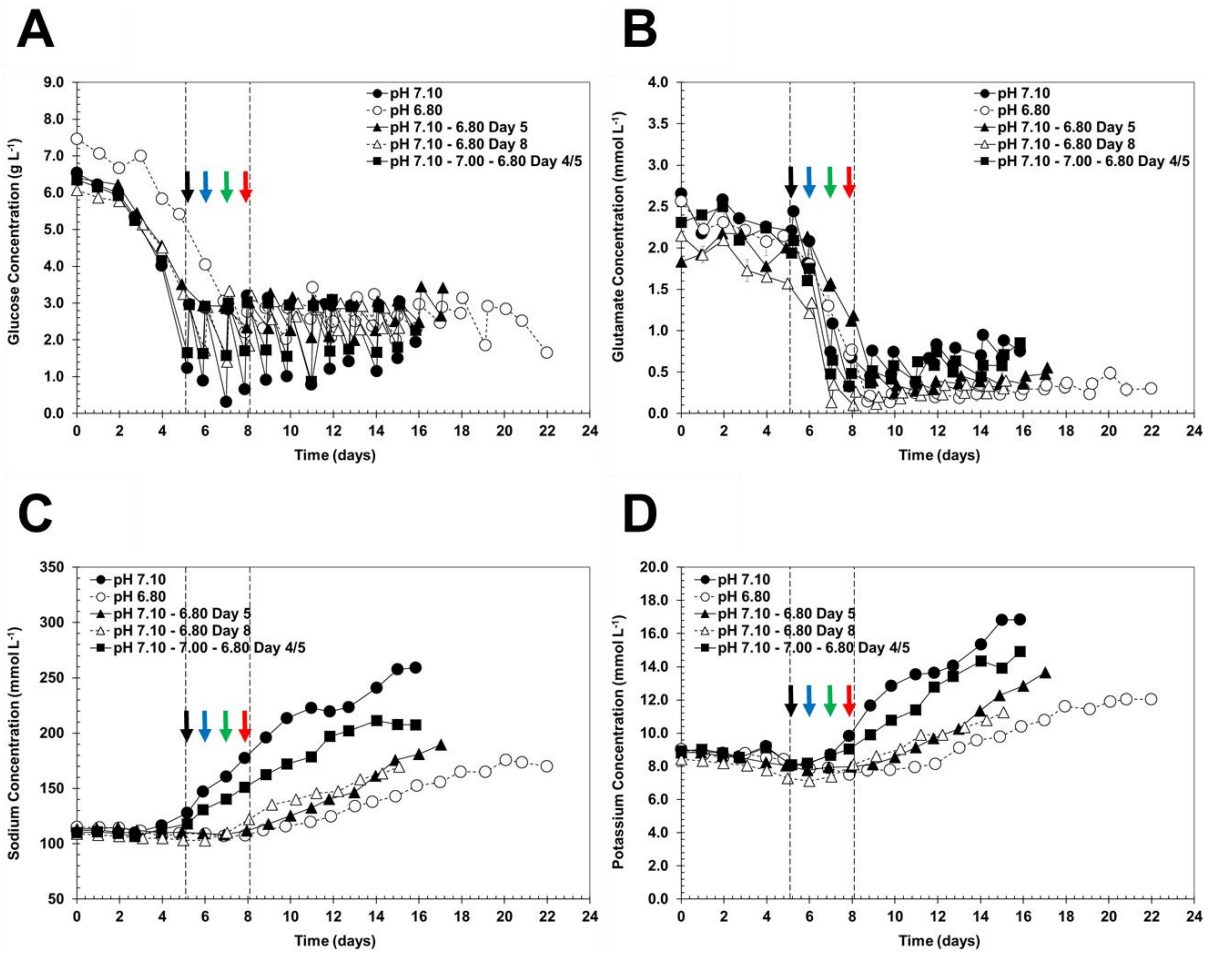

Figure 6-11: Glucose (A), glutamate (B), sodium (C) and potassium (D) concentrations profiles for 5L-STR CHO-CY01 cell line fed-batch strategy 5 (FB3) cultures with constant pH 6.80 and pH 7.10, pH shifts from pH 7.10 to pH 6.80 on day 5 (pH 7.10 – 6.80 Day 5) or 8 (pH 7.10 – 6.80 Day 8), and pH shift from pH 7.10 to pH 7.00 on day 4, then to pH 6.80 on day 5 (pH 7.10-7.00-6.80 Day 4/5) (1 replicate per condition). The arrow indicates when the feeding started (pH 7.10 and pH 7.10-7.00-6.80 Day 4/5– black; pH 7.10 – 6.80 Day 8 – blue; pH 7.10 – 6.80 Day 5– green; pH 6.80 - red). Error bars represent one standard deviation about the mean.

Table 6-3: Kinetic parameters determined for the 5L-STR CHO-CY01 cell line fed-batch cultures with pH shift from pH 6.60 to pH 6.80 on day 2, pH shift from pH 7.60 to pH 7.10 on day 4, pH shift pH 7.10 to pH 6.80 on day 5 or 8, and pH shift from pH 7.10 to pH 7.00 on day 4, then to pH 6.80 on day 5.

5L-STR pH set-point	**6.60 – 6.80**	**7.60 – 7.10**	**7.10 – 6.80**	**7.10 – 7.00 - 6.80**	**7.10 – 6.80**
Day of the pH shift	**Day 2**	**Day 4**	**Day 5**	**Day 4/5**	**Day 8**
VP ($mg\ L^{-1}day^{-1}$)	37.6	64.1	32.9	47.8	35.5
IVCC ($10^9\ cells\ day\ L^{-1}$)	129.59	125.81	65.4	83.45	72.97
$\mu\ (h^{-1})$	0.014	0.023	0.0201	0.024	0.023
$t_{1/2}\ (h)$	51.0	30.8	34.48	28.8	30.8
$q_{mAb}\ (mg\ 10^{-9}\ cells^{-1}\ day^{-1})$	8.19	9.27	10.40	9.95	8.37
$q_{Gluc}\ (g\ 10^{-9}\ cells^{-1}\ day^{-1})$	-0.12	-0.30	-0.22	-0.27	-0.18
$q_{Glu}\ (mmol\ 10^{-9}\ cells^{-1}\ day^{-1})$	-0.02	-0.05	-0.04	-0.05	-0.05
$q_{Lact}\ (g\ 10^{-9}\ cells^{-1}\ day^{-1})$	0.22	0.69	0.20	0.35	0.21
$q_{Amm}\ (mmol\ 10^{-9}\ cells^{-1}\ day^{-1})$	0.06	0.03	0.16	0.11	0.12
Lactate produced / glucose consumed (g/g)	0.15	0.39	0.51	0.38	0.20
$\mu_d\ (h^{-1})$	-0.002	-0.001	n/a	-0.006	-0.003
Feed volume (% of reactor volume)	8.0	18.7	5.5	10.4	7.7

Table 6-4: Values for the process parameters (pH, pO_2, temperature, CO_2, base), and daily glucose and glutamate consumption rates on fed-batch mode for all 5L-STR CHO-CY01 cell line cultures at different pHs.

	5L-STR pH set-point	pH	pO_2 (% (air saturation)	Temperature (°C)	CO_2 (% (v/v))	Base (mL)	Daily Glucose Consumption rate ($g\ L^{-1}day^{-1}$)	Daily Glutamate consumption rate ($mmol\ L^{-1}day^{-1}$)
Batch	**6.80**	6.87 ± 0.01	29.89 ± 0.17	37.00 ± 0.01	36.58 ± 3.60	0.0		
	7.10	7.14 ± 0.04	29.96 ± 0.14	37.00 ± 0.01	17.06 ± 4.91	40.1		
	7.40	7.44 ± 0.04	29.96 ± 0.17	37.00 ± 0.01	10.71 ± 2.02	24.3		
Fed--batch	**6.80**	6.85 ± 0.02	29.96 ± 0.21	37.00 ± 0.01	36.12 ± 2.45	0.0	0.66 ± 0.20	0.08 ± 0.02
	7.10	7.13 ± 0.04	30.00 ± 0.07	37.00 ± 0.01	7.19 ± 2.28	337.0	1.97 ± 0.36	0.27 ± 0.05
	7.80	7.76 ± 0.34	29.92 ± 1.39	36.93 ± 1.61	0.19 ± 0.08	949.5	2.03 ± 1.32	0.24 ± 0.15
pH shifts	**6.60 -6.80 (day 2)**	6.85 ± 0.07	30.55 ± 1.15	37.00 ± 0.01	29.05 ± 7.85	683.9	0.66 ± 0.27	0.08 ± 0.03
	7.60 -7.10 (day 4)	7.21 ± 0.21	29.99 ± 0.09	37.00 ± 0.02	0.86 ± 0.19	806.0	2.25 ± 0.63	0.27 ± 0.08
	Before pH shift						1.25 ± 0.12	0.14 ± 0.01
	After pH shift						2.47 ± 0.29	0.44 ± 0.05
	7.10 - 6-80 (day 5)	6.97 ± 0.13	29.96 ± 0.27	37.00 ± 0.01	25.20 ± 1.10	0.0	0.86 ± 0.15	0.08 ± 0.02
	7.10 - 6-80 (day 8)	7.03 ± 0.14	29.59 ± 2.07	37.00 ± 0.01	20.00 ± 4.91	0.0	0.80 ± 0.55	0.11 ± 0.04
	7.10 - 7.00 - 6.80 (day 4, 5)	6.97 ± 0.12	29.44 ± 1.81	37.00 ± 0.01	15.81 ± 5.05	178.3	1.36 ± 0.25	0.16 ± 0.03

6.5. Proteomic Analysis of CHO-CY01 Cell Line Varying Culture pH

6.5.1 2D-DIGE Proteomics

Two-dimensional (2-D) fluorescence difference gel electrophoresis (DIGE) was performed with supernantants from 5L-STR CHO-CY01 cell line fed-batch cultures at constant pH 6.8 and pH 7.1, and supernantants from cultures with the pH shift from pH 7.10 to pH 6.80 at day 5 or 8. This way it was possible to understand the proteomic impact of external pH on the CHO-CY01 cell line. The Cambridge Centre Proteomics kindly did this experimental work [10].

The decision of which culture time points should be picked to be analysed by the 2D-DIGE proteomic technique was dictated by the aim of unveiling the cellular response when a pH shift from pH 7.10 to pH 6.80 occurred. Since the same 2D-DIGE gel can be loaded with multiple samples, it was decided to choose two-time points per 5L-STR CHO-CY01 cell line fed-batch culture. The pH shifts were done at day 5 or day 8 thus, the culture time point before (day 4 or 7) and after (day 6 or 9) the pH shift was selected. The culture time points from day 4 to 9 of CHO-CY01 cell line fed-batch cultures at constant pHs (pH 6.80 and pH 7.10), were chosen as a comparison. Therefore, it was decided for CHO-CY01 cell line fed-batch culture at pH 6.80 to use the day 6 and 8 samples, and for the standard cell culture conditions, the day 4 and 6 samples. From the SDS-PAGE gel of the supernatant of CHO-CY01 cell line fed-batch culture at pH 7.10 (Figure 6-12), the molecular weight (MW) of a whole IgG4 antibody (~160kDa), IgG4 heavy chain (HC) (~75kDa) and IgG4 light chain (~20kDa)was estimated. From the IgG4 identification HPLC protocol (section 2.2.3), the pI range (6.5 – 7.5) of the monoclonal antibody IgG4 was known.

In Figure 6-13, the 2D-DIGE gels for the four 5L-STR CHO-CY01 cell line fed-batch cultures are visualised where each sample (time point) was marked with a different fluorescence dye (Cy3 or Cy5). In these gels, the IgG4 heavy and light chain spots can be easy visualised, as they are the predominant proteins present. From a qualitative comparison of the gels, it was proven that the choice of time points was correct as a large number of spots in all CHO-CY01 cell line fed-batch cultures was detected. Nevertheless, a quantitative analysis of the 2D-DIGE gels was using the 2D-gel analysis software, Melanie.[11].

In Figure 6-14 the quantitative analysis done to the 2D-DIGE gels is presented, where all the spots with a protein difference ratio of 1.5 were identified (Grzeskowiak et al., 2009) and their variation was colour coded (increase (blue), decrease (red) and similar (green)). In Figure 6-16, the similar spots were excluded. By statistical analysis included in the software, it was possible to determine the percentage of change per gel (Table 6-5). In this quantitative analysis, it was shown that the CHO-CY01 cell line fed-batch culture with the highest degree

[10] http://proteomics.bio.cam.ac.uk/
[11] http://world-2dpage.expasy.org/melanie/

of proteomic variation between time points was the cell culture with pH shift on day 5, followed by the cell culture with pH shift on day 8 and the least proteomic variation between samples was observed in the 5L-STR cell culture at pH 7.10. Therefore, the 2D-DIGE gel for the CHO-CY01 cell line fed-batch culture with the pH shift on day 5 was chosen for further analysis, i.e. protein identification by mass spectrometry. The issue was which spots were relevant enough to be identified. An online available image processing software (Victor Image Processing Library[12]) was used to help in the decision (Figure F-2). The objective was to pick the spots with high volume ratio variation that were also present in the other 2D-DIGE gels. The annotated 2D-DIGE gels are shown in Figure F-1 and the list of Figure F-2 overlapped protein spots are in the Table F-1. In the end, only seven spots were selected (Figure 6-17). In Table 6-6 is the characterisation of those spots through the spot volume ratio, protein mass, pI and gel quadrant summarised.

[12] http://www.catenarysystems.com/demos/compare/comparator.aspx

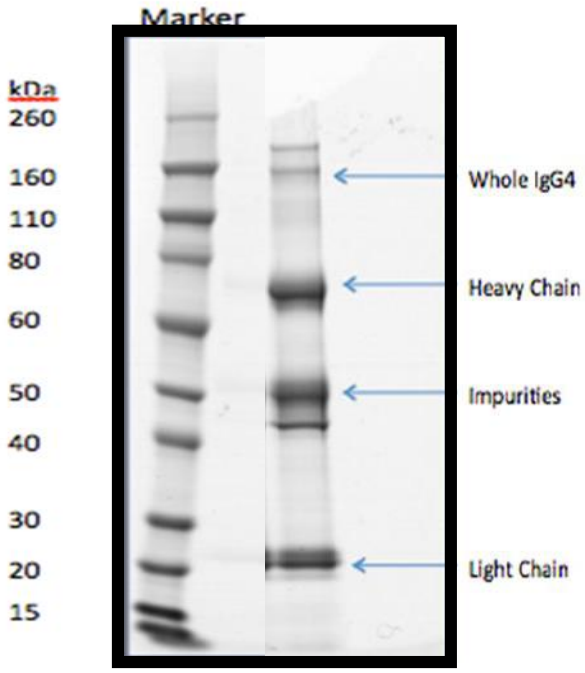

Figure 6-12: SDS-PAGE gel of the supernatant of CHO-CY01 cell line fed-batch culture at pH 7.10. Whole IgG4 antibody (~160 kDa), heavy Chain (~75 kDa), light Chain (~20 kDa) and impurities (~50 kDa).

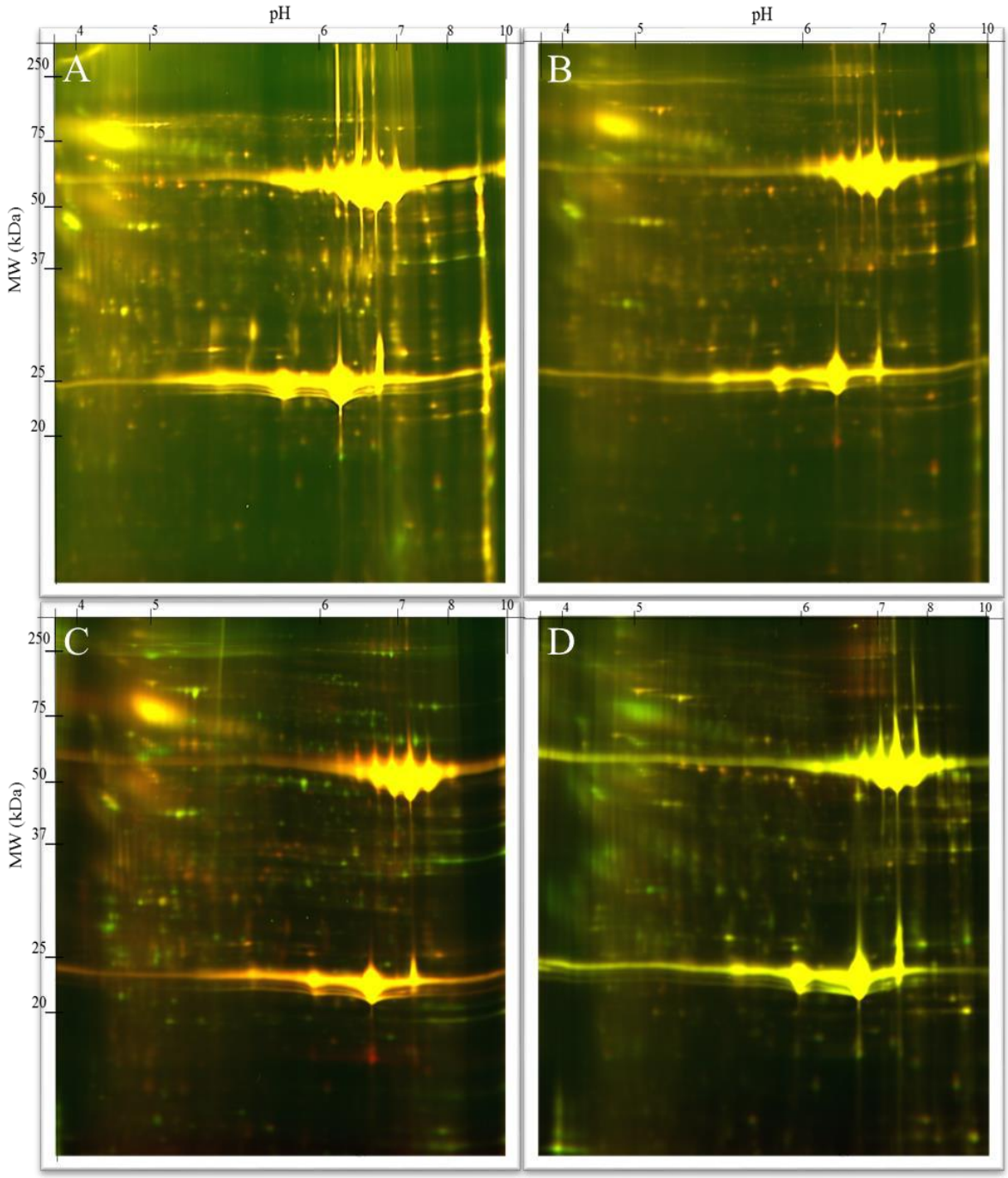

Figure 6-13: Two-dimensional (2-D) fluorescence difference gel electrophoresis (DIGE) of the supernatants from 5L-STR CHO-CY01 cell line fed-batch cultures at different external pHs: pH 6.8 (day 6 (green (Cy3)) and day 8 (red (Cy5))) (A); pH 7.1 (day 4 (green (Cy3)) and day 6 (red (Cy5))) (B); pH shift from pH 7.1 to pH 6.8 on day 5 (day 4 (green (Cy3)) and day 6 (red (Cy5))) (C); and pH shift from pH 7.1 to pH 6.8 day 8 (day 7 (green (Cy3))) and day 9 (red (Cy5))) (D).

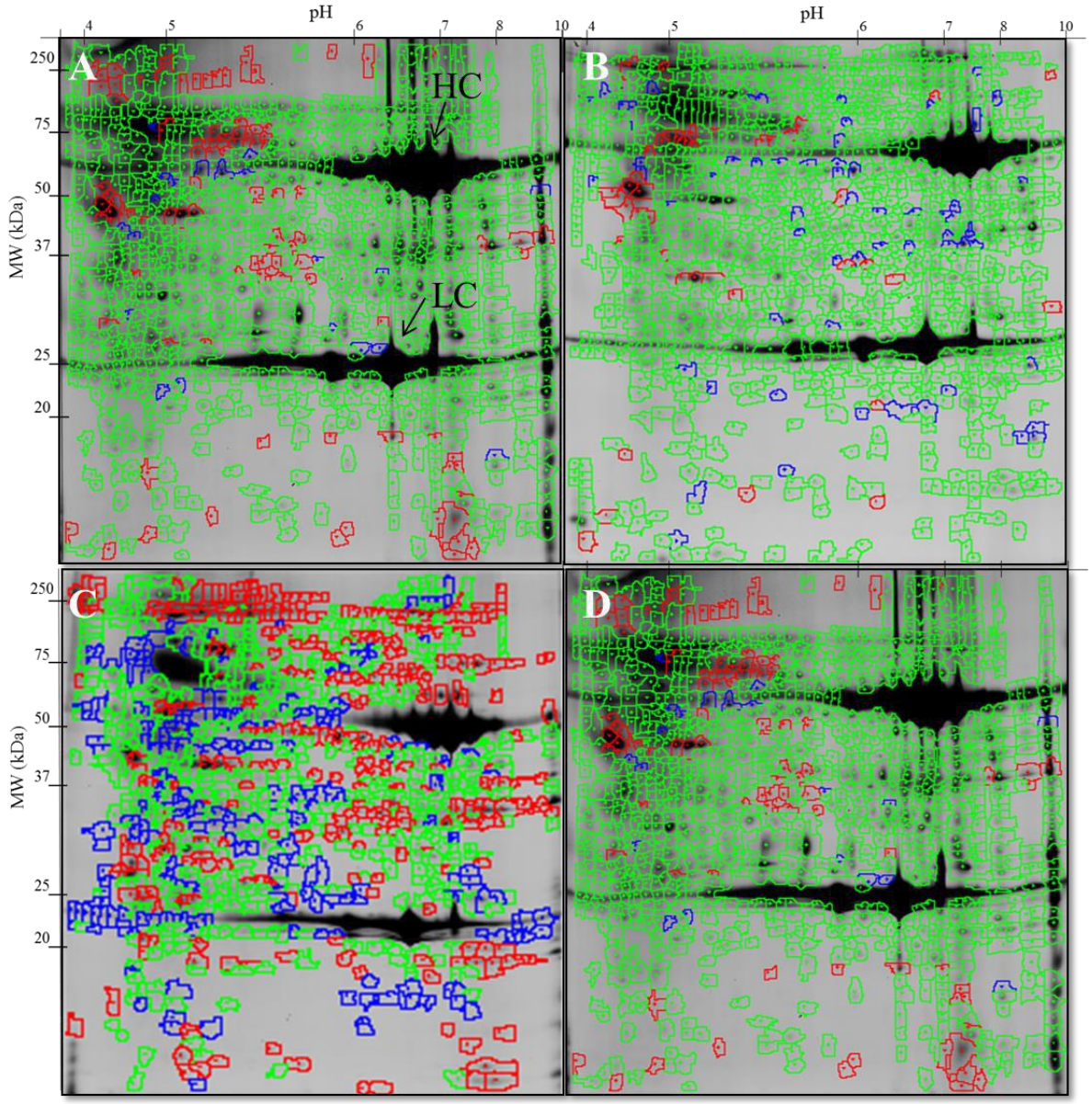

Figure 6-14: Quantitative analysis of protein content in the supernatants of 5L-STR CHO-CY01 cell line fed-batch cultures at different external pHs: pH 6.8 (day 6 and 8) (A); pH 7.1 (day 4 and 6) (B); pH shift from pH 7.1 to pH 6.8 on day 5 (day 4 and 6) (C); and pH shift from pH 7.1 to pH 6.8 on day 8 (day 7 and 9) (D). The spots indicate a protein difference ratio of 1.5. The protein spots that increased in intensity are represented in blue; the protein spots that did not change are in green; and the protein spots that decreased are in red. LC and HC labels represent light chain and heavy chain, respectively.

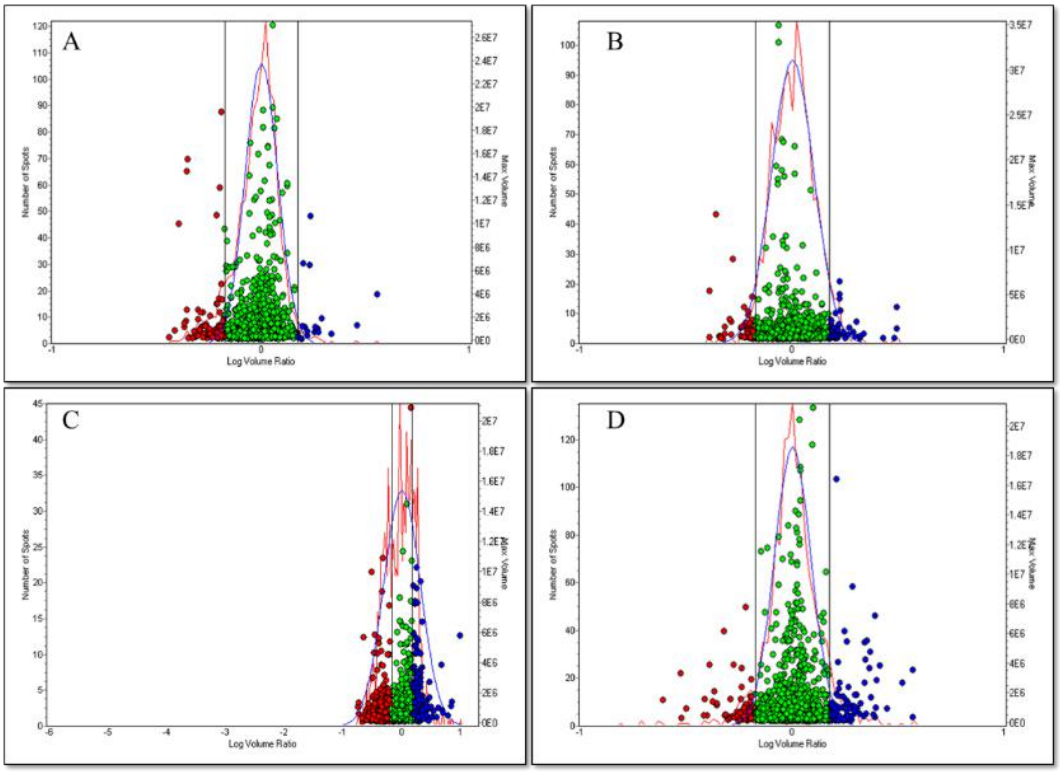

Figure 6-15: Histograms of spot frequency versus log volume ratio of the supernatants from 5L-STR CHO-CY01 cell line fed-batch cultures at different external pHs: pH 6.8 (day 6 and 8) (A); pH 7.1 (day 4 and 6) (B); pH shift from pH 7.1 to pH 6.8 on day 5 (day 4 and 6) (C); and pH shift from pH 7.1 to pH 6.8 on day 8 (day 7 and 9) (D). The differences between spot volumes were determined using 1.5-fold threshold mode. Blue Spots (increased spots), green spots (similar spots), red spots (decreased spots).

Table 6-5: Quantitative analysis of two-dimensional (2-D) fluorescence difference gel electrophoresis (DIGE) of the supernatants from 5L-STR CHO-CY01 cell line fed-batch cultures at different external pHs: pH 6.8 (day 6 and 8); pH 7.1 (day 4 and 6); pH shift from pH 7.1 to pH 6.8 on day 5 (day 4 and 6); and pH shift from pH 7.1 to pH 6.8 on day 8 (day 7 and 9). The differences between spot volumes were determined using 1.5-fold threshold mode.

Spot Statistics	Decreased	Similar	Increased
5L-STR pH 6.8 run(day 8 / day 6)	8.8%	89.4%	1.8%
5L-STR pH 7.1 run(day 6 / day 4)	3.5%	91.5%	5.0%
5L-STR day 5 pH shift from pH 7.1 to pH 6.8 run(day 6 / day 4)	31.1%	47.5%	21.4%
5L-STR day 8 pH shift from pH 7.1 to pH 6.8 run(day 7 / day 9)	5.4%	87.6%	7.0%

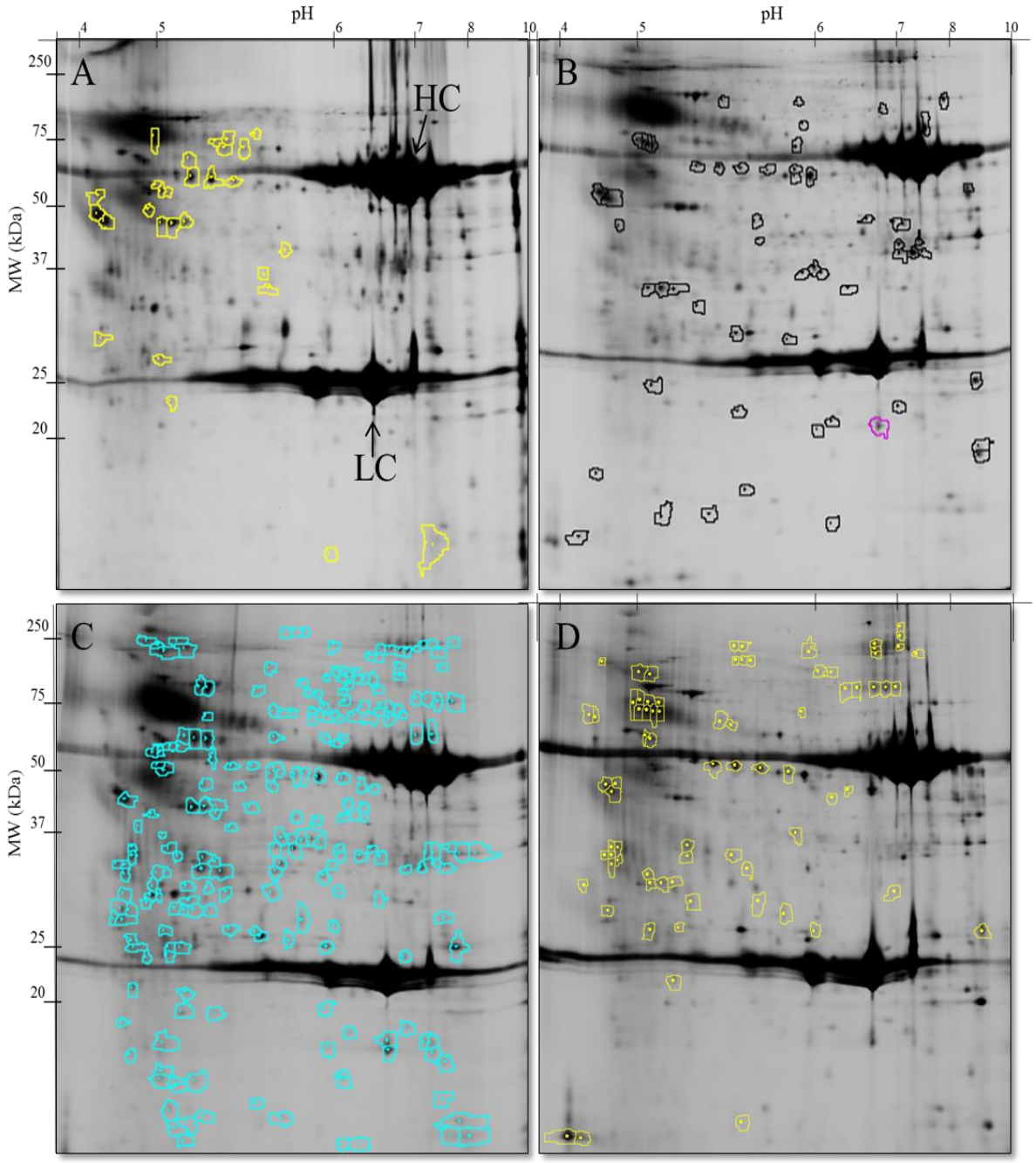

Figure 6-16: 2-D DIGE PAGE CHO-CY01 expression maps of 5L-STR CHO-CY01 cell line fed-batch cultures at different external pHs: pH 6.8 (day 6 and 8) (A); pH 7.1 (day 4 and 6) (B); pH shift from pH 7.1 to pH 6.8 on day 5 (day 4 and 6) (C); and pH shift from pH 7.1 to pH 6.8 on day 8 (day 7 and 9) (D). The spots indicate a protein difference ratio of 1.5 between sample points. LC and HC labels represent light chain and heavy chain, respectively.

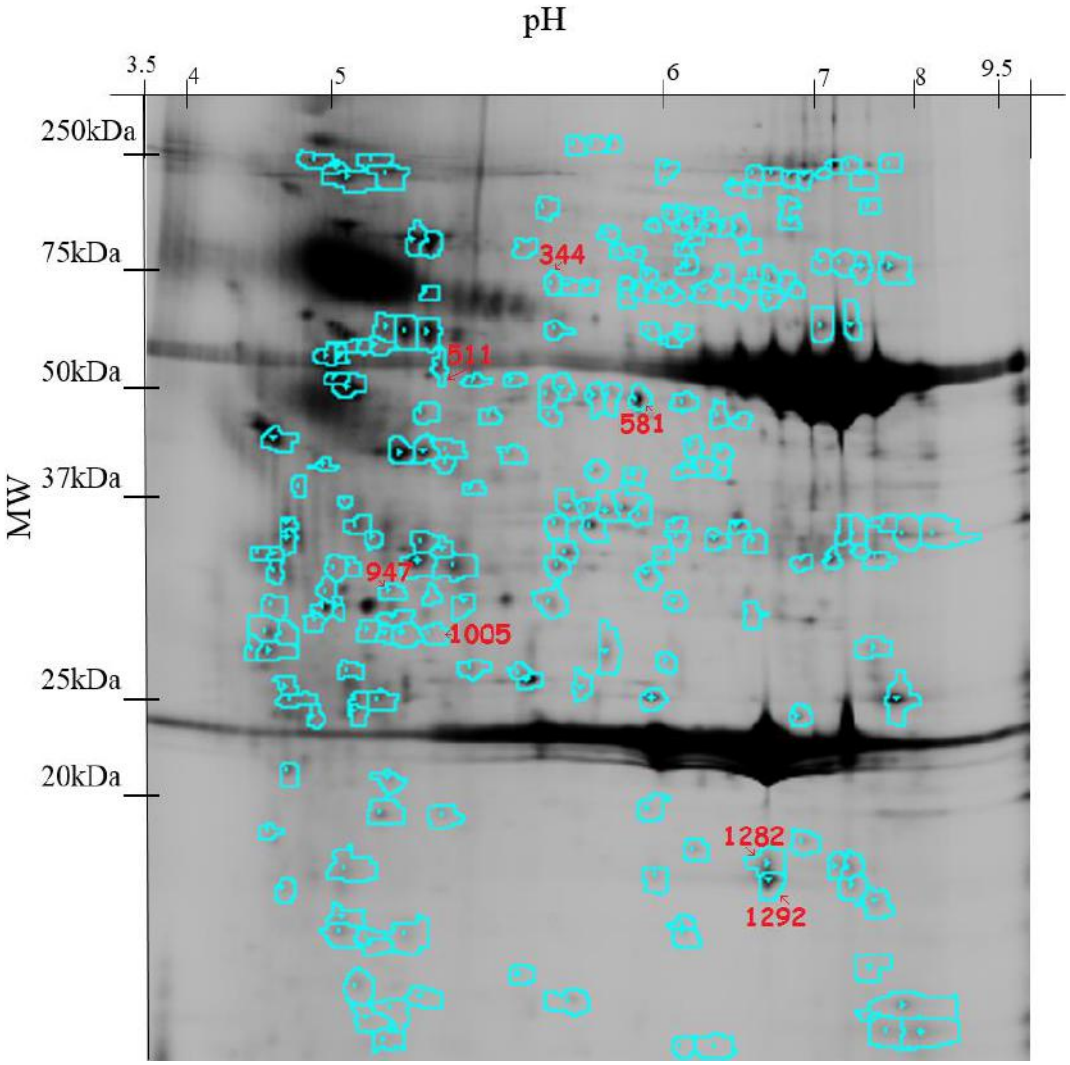

Figure 6-17: 2-D DIGE PAGE CHO-CY01 expression map from 5L-STR CHO-CY01 cell line fed-batch culture with the pH shift from pH 7.10 to pH 6.80 on day 5. The annotated spots were selected for protein identification by mass spectrometry.

Table 6-6: Characterisation of the selected 2D-DIGE gel spots from day 4 and day 6 of 5L-STR pH shift from pH 7.1 to pH 6.8 on day 5.

Spot Number	Volume Ratio	Protein mass (kDa)	pI	Quadrant
344	-3.93	~75	5.5	2
511	2.11	57	5.2	2
581	-2.85	48	5.8	1
947	-2.42	31	5.1	2/3
1005	-1.54	26	5.3	3
1282	4.79	16	6.7	4
1292	9.76	14	6.7	4

6.5.2 Protein Identification by Mass Spectrometry

Since the 2D-DIGE gel of 5L-STR pH Shift from 7.1 to 6.8 of day 4 and day 6 showed the largerest number of alterations, i.e. a higher spot variation it was chosen to be further analysed. Protein identification was performed by mass spectrometry (section 2.2.6.1) and then compared with Uniprot database[13]. From the protein identification method chosen, MS/MS Ions Search (MIS), resulted in a list of protein ´hits´ for each spot, i.e. a list of hypothetical proteins. It was necessary to create statistically reasonable selection criteria for the correct protein identification of each spot. Through the protein score, which is the probability that an observed match is a random event, it was defined that a protein scores greater than 70 is significant ($p < 0.05$). However, the biological significance was accounted for as well. For each protein candidate, the MASCOT 2.3.02 software calculated protein mass and pI. Therefore, it was only considered as candidates, the protein ´hits` that had a maximum 10% variation in these parameters Table 6-6. With the use of Uniprot database, it was possible to know from which organism the protein ´hit` came, its molecular function, cellular location and in what biological process is the protein is involved. From the use of this selection criteria, the protein identification of the seven spots was made (Figure 6-17). In Appendix G, there is the information on the parameters and conditions of the mass spectrometry and database search. The complete protein ´hits` list as well as the protein ´hits` short-list for each spot is also presented in Appendix G. The final protein identification is on the Table 6-7.

It was not possible to identify the annotated protein spots 1282 and 1292 (Figure 6-17), due to their low molecular weight. From the protein identification of the other five protein spots, it was possible to draw some conclusions about their role in the cellular metabolism involved with the pH shift. The reduction of the μ at the CHO-CY01 cell line fed-batch pH shift from pH 7.10 to pH 6.80 on day 5 culture was possibly due to a decrease in the expression of ATP binding (chaperones) proteins (spot 344) and inorganic pyrophosphatase (spot 947), as there was an inhibition of the energy supply to the cells and the protein folding was also compromised. The lower glucose consumption rate may be due the under-expression of alpha-enolase (581), which means that the glycolysis pathway was inhibited when the culture pH shifted to pH 6.80. It was also found that the glutathione synthetase activity (spot 581) increased after the pH shift. This is a clear demonstration that CHO-CY01 cells were under stress when cultured at pH 6.80, which was already suspected by the presence of larger cells (cell diameter > 16 μm).

[13] www.uniprot.org

Table 6-7: Hit number, protein name, organism, gene name, score, coverage (%), calculated mass, calculated pI, molecular function and biological process of the seven annotated protein spots chosen to be identified (www.uniprot.org/). In brackets is the volume ratio.

Spot	**344** (-3.93)	**511** (2.11)	**581** (-2.85)	**947** (-2.42)	**1005** (-1.54)	**1282**	**1292**
Hit number	1	9	1	3	6	14	11
Protein Name	T-complex protein 1 subunit alpha (TCP1)[14]	Glutathione synthetase[15]	Alpha-enolase[16]	Inorganic pyrophosphatase[17]	Glyoxalase domain-containing protein 4 [18]	Putative uncharacterised protein	
Organism	Cricetulus griseus (Chinese hamster) (Cricetulus barabensis griseus)						
Gene Name	I79_009786	I79_007504	I79_020676	I79_006047	I79_014194	I79_024561	
Score	2102	352	2291	863	405	71	89
Coverage (%)	70.1	22.8	73.4	62	34.9	10.6	10.6
Calculated Mass	60814	52441	47011	37373	33479	13623	
Calculated pI	5.71	5.42	5.84	5.19	5.28	6.23	
Molecular function	ATP binding (Chaperone)	ATP binding; Glutathione synthase activity; Metal ion binding (Ligase)	Magnesium ion binding; Phosphopyruvate Hydratase Activity	GTP binding; Inorganic diphosphatase activity; Magnesium ion binding			
Biological process	Protein Folding	Glutathione biosynthesis	Glycolytic process	Intracellular Protein Transport; Phosphate-containing compound metabolic process			

[14] TCP1 is a molecular chaperone. It assists the folding of proteins upon ATP hydrolysis.

[15] Glutathione synthetase is the second enzyme in the glutathione biosynthesis pathway from L-cysteine and L-glutamate. Glutathione protects cells from oxidative stress and contributes to a favourable redox environment both inside and outside the cell (redox buffer) (Njålsson et al., 2005).

[16] Alpha-enolase (ENO) is a glycolytic enzyme the catalyzes the conversion of 2-phosphoglycerate (P2G) to phosphoenolpyruvate (PEP) (step 9).

[17] Inorganic pyrophosphatase (Pyrophosphatase) is an enzyme that catalyzes the conversion of one molecule of pyrophosphate (PPi) to two phosphate ions. It provides the driving force for the activation of fatty acids destined for oxidation.

[18] It belongs to glyoxalase I family and it have not been functionally annotated.

6.6. Conclusion

Culture pH is one of the key environmental parameters that influence cell metabolism and recombinant protein production (Hanson et al., 2007; Osman et al., 2001). Extracellular pH affects many intracellular properties including intracellular pH, cell metabolism, glucose transport, ATP/ADP ratio, protein synthesis, transport and secretion, and glycosylation of proteins (Borys et al., 1993; Müthing et al., 2003). Therefore, it is crucial for the CHO-CY01 cell line (GS-CHO cell line secreting IgG4) process optimisation to understand the impact of pH on the cell growth, mAb productivity and cellular metabolism. Besides, from the previous chapter, whereby through CO_2 concentration manipulation, different pH profiles at 24-SRW MTP scale were generated it was found that a culture pH around pH 6.80 would slow down the CHO-CY01 cell growth rate as well as the lactate production rate with improved q_{mAb}. At the other end, culture pH values higher that pH 7.40 were associated with high glucose consumption leading to high lactate production and low IgG4 productivity. These conclusions from the scale-down approach needed to be tested at a fully automated and controlled larger scale, 5L-STR.

The first approach to study the impact of pH on CHO-CY01 cell line was to culture the cells in batch mode at different external pH values: the standard pH (pH 7.1); below the standard pH (pH 6.80) and above the standard pH (pH 7.4). Secondly, CHO-CY01 cells were inoculated in fed-batch mode at the standard pH (pH 7.10), the optimal culture pH for IgG4 production (pH 6.80) and an extremely high pH (pH 7.80). Thirdly, different single and multiple pH shifts were carried out at different culture times. In this way, the optimal pH range for optimal cell growth, IgG4 productivity, and cellular processes was determined. Also, pH shifts in a GS-CHO cell line performed for IgG4 production optimisation purposes were novel. Finally, 2D-DIGE studies followed by a limited protein identification analysis were carried out to CHO-CY01 cell line fed-batch cultures at constant pHs and with single pH shifts. In this manner, it was possible to understand the impact of external pH on the CHO-CY01 cell line proteome.

It was found that CHO-CY01 cell line batch cultures at pH 7.40 presented a similar cell growth rate (μ = 0.025 h^{-1}) and metabolite (glucose, glutamate, lactate and, ammonia) profiles, but with a higher IgG4 titer and specific cell death (2.9-fold) compared with the cells at the standard culture condition (pH 7.10). Therefore, there was an increase in VP and a culture time reduction. At the same design space, CHO-CY01 cell line batch culture at pH 6.80 exhibited a cell growth inhibition with a 57.9% reduction in μ with an uncharacteristic 5 days stationary phase (5 days), but there was a 47.9% increase in q_{mAb} (14.72 $mg\ 10^{-9}\ cells^{-1}\ day^{-1}$) and CHO-CY01 cells did not produce any lactate. Throughout the pH range tested ($6.80 \leq pH \leq 7.40$), there was no change in q_{Gluc} or q_{Glu} with culture pH.

Although the maximum ammonium concentration reached was similar, a 1.8-fold increase in q_{Amm} was observed. Therefore, few main conclusions can be reached. First, pH 7.10 it is not the optimal pH for IgG4 production in CHO-CY01 cell line. Second, the pH range between 7.10 and 7.40 was found to be the optimal pH range for the cell growth. Third, opposite to what was found by Sellick et al. 2009, the CHO-CY01 cells had higher antibody titers at lower pH (pH 6.80). Forth, the negative effect of lactate common to the mAb bioprocess was eliminated with pH 6.80, without for instance any cell line engineering like the one presented by Chen et al., 2001. Finally, the ammonium production is promoted by the cells at lower pH values (pH 6.80).

Out of the fed-batch study at different pH values: pH 6.80, 7.10 and 7.80, it was clear that CHO-CY01 cells were incapable of growing and secreting IgG4 at pH 7.80. At that external pH, cell diameter was larger than 18 μm and there was a high level of debris (> 13%) throughout the cell culture. This is the indication that cells were in a pH homeostasis and osmotic stress due to constant base addition (949.5 mL). The survival strategy observed in the scale-down approach for pH > 7.50 was also observed at 5L-STR scale, which validates the scale-down model created in this work. There was a 208% increase in the q_{Lact} compared with the reference (pH 7.10), which also represented a higher glucose demand (2.03 ± 1.32 $g\ L^{-1}\ day^{-1}$). With the fed-batch strategy with glucose topping-up to 3.00 $g\ L^{-1}$, it was possible to counteract the cell growth inhibition exbihited by CHO-CY01 cells in batch mode at pH 6.80. Indeed, the μ reached was similar to the reference value (0.023 h^{-1}). Again at this lower pH, there was an uncharacteristic longer stationary phase, higher q_{mAb} and ammonium production, but this was always below the ammonium half-maximum-rate concentrations determined in the previous chapter. Regarding lactate accumulation, although the lactate formation was not stopped, it was considerably reduced at pH 6.80 (< 0.99 $g\ L^{-1}$), which resulted in a minimal q_{Gluc} and daily feeding requirements by CHO-CY01 cells. Consequently, the optimal pH range for IgG4 productivity and CHO-CY01 cell growth was found to be 6.85 ± 0.02 (36.12 ± 2.45% (v/v) CO_2). It is important to note that this range is included in the scale-down approach IgG4 productivity pH range (6.98 ± 0.28 (10.00% (v/v) CO_2)), which once more validates the 24-SRW MTP scale-down model. It is also worthwhile to mention that for all the pH values, there was a reduction of q_{Amm} in fed-batch mode.

Two pH shifts strategies were designed to determine the CHO-CY01 cell line pH range. CHO-CY01 cells were cultured at the expected minimum (pH 6.60) and maximum (pH 7.60) of that pH range. Since cell viability dropped below 90% with no cell growth associated during the first days of culture, a pH shift was made to a higher minimum (pH 6.80) or lower maximum (pH 7.10) value to maintain the CHO-CY01 cell line fed-batch cultures. Therefore, the suitable pH range for CHO-CY01 cell line is $6.60 < pH < 7.60$. From theses pH shifts, it was found that

base addition prompted the lactate production (pH shift from pH 6.60 to 6.80), pH values higher than 7.60 triggered the survival strategy (anaerobic metabolism) to lactate concentrations (6.51$g\ L^{-1}$) beyond any kinetic inhibition parameters and fail to increase the optimal q_{mAb} (10.50 $mg\ 10^{-9} cells^{-1} day^{-1}$).

Single pH shifts from pH 7.10 (reference) to pH 6.80 (optimal) were performed at different culture times, mid-exponential point (day 5) and at the end of the exponential phase (day 8), as done with the CO_2 shifts. The same conclusions drawn from the CO_2 shifts were reached with the pH shifts. The pH shift during the exponential phase caused an inhibition of the cell growth (13.4% decline in μ) and the pH shift at the beginning of the stationary phase, initiated the decline phase. From the 2D-DIGE proteomic analysis and the limited protein identification of the pH shift (day 5) supernatant, It can be suggested that the reduction in the μ was due to a decrease in the expression of ATP binding (chaperones) proteins and inorganic pyrophosphatase, as there was an inhibition of the energy supply to the cells and the protein folding was also compromised. The drop in glucose consumption with the pH shift may be due to under-expression of alpha-enolase when the culture pH shifted to pH 6.80. Therefore, in both pH shifts cultures, there was a decrease in the IVCC (~30%). The earlier the pH shift was done, the higher the q_{mAb} reached, but this value was still below the optimal value (constant pH 6.80). The novelty found in these pH shifts CHO-CY01 cell line fed-batch cultures was the fact that CHO-CY01 cells became lactate consumers and serious ammonium producers whenever the pH shift from pH 7.10 to pH 6.80 occurred. However, the ammonium concentration profile was similar to the one found at constant pH 6.80. The pH shifts were beneficial to CHO-CY01 cell line process optimisation, since they were an improvement from the reference pH. Nevertheless, these pH shifts were unable to surpass the CHO-CY01 cell line fed-batch culture performance at constant pH 6.80, which continues to be the optimal pH value, as the cells exhibited greater q_{Gluc}, q_{Glu}, q_{Lact} and q_{Amm} for the same (pH shift at day 5) or lower (pH shift at day 8) q_{mAb}. Also, from the proteomic analysis it can be concluded that CHO-CY01 cells were under stress (cell diameter > 16 μm) when cultured at pH 6.80, as there was an over-expression of glutathione synthetase (redox buffer).

To further evaluate the response of CHO-CY01 cell line to pH perturbations, the amplitude of the pH shift from pH 7.10 to 6.80 at day 5 was divided into two steps: the pH shift from pH 7.10 to pH 7.00 on day 4 and then from pH 7.00 to pH 6.80 on day 5 was also tested. For this multiple steps pH shifts, the CHO-CY01 cell line growth profile was similar to the one found at constant pH 7.10 (reference) and the peak IgG4 concentration (1.03$g\ L^{-1}$) reached and volumetric productivity (47.8 $mg\ L^{-1}\ day^{-1}$) were the same as the ones found at constant pH 6.80 (optimal). However, there was a higher glucose requirement by the cells and so, a 2-fold increase in the feed volume was observed. Also, there was a significant increase in q_{Lact}

with the same ammonium accumulation. The possible advantage of this pH shift strategy is due to the fact that the peak IgG4 concentration was reached 7 days earlier than in the culture with constant pH 6.80, which suggests that it a possible optimal condition for IgG4 production by CHO-CY01 cells due to the considerable reduction of culture time.

In conclusion, there was a clear validation of the pH perturbations performed at the scale-down model with the high-throughput online multi-parametric analysis method.

Chapter 7 Final Conclusion and Future Work

This section aims to review the thesis objectives, summarise the key research findings and provide future recommendations for this work.

7.1. Final Conclusion

Currently, the production of recombinant therapeutic proteins in mammalian cells plays a significant part in the biopharmaceutical industry ($125 billion by 2020 (Ecker et al., 2015)). Consequently, the increased market has led to a need for increased production volumes and a drive to improve process efficiency. One of the key parameters that have a significant impact on the cell growth and metabolism, mAb productivity and quality (glycosylation) is the pH. Mammalian cell culture medium is prepared with a buffer system to control pH variations, and it usually consists of the CO_2/HCO_3^- system, where CO_2 is the acid and the HCO_3^- is the base. High CO_2 concentrations are known to cause detrimental effects on cell growth, nutrient utilisation, product formation and quality. Therefore, these damaging effects must be carefully considered to achieve higher productivities and better product quality. The maintenance of the pH stability in culture is affected by different factors, including buffer capacity, type of bioreactor, and glucose concentration. This latter is metabolised by the cells at a greater rate than it is needed, which results in the accumulation of toxic by-products (lactate) that lowers the pH. Consequently, a suitable fed-batch strategy that accommodates the by-products reduction is desirable. Small-scale models can be developed and used to support process development studies. By definition, a scale-down model is an incomplete representation of a more complicated, expensive and/or physically larger (commercial) system. They must be used because of the limitations to conducting experimental studies with the at-scale equipment. The performance of the scale down model should match the large scale product and process: the same *change* in inputs results in a substantially similar *change* in outputs. Microwell plates (MTP) are currently used as upstream ultra-scale-down models, where a large design space data sets can be generated (high-throughput). They are multiparallel bioreactors that can be individually controlled. However, the high evaporation rate, the risk of cross-contamination and the low oxygen transfer are some of the disadvantages of these bioreactors. Nevertheless, with the current PreSens Precision Sensing technology allows the online monitoring of some process parameters like temperature, pH and dissolved oxygen of each well and a combination of better MTP lid designs (´system Duetz`), mitigates those issues.

The primary goal of this study was to evaluate the response of mammalian cells to pH perturbations using a parallel microwell approach. To accomplish that purpose, a scale-down

model of the pH effects on an industrial GS-CHO cell line (CHO-CY01) growth and product (IgG4) production was developed. Therefore, a high-throughput approach to CHO-CY01 cell culture process development (Chapter 3) was created and its inter-scalability validated (Chapter 4). Before the CO_2 or pH effects on CHO-CY01 cell line kinetics, it was necessary to known the inhibition kinetics of lactate and ammonium, the two main toxic substances produced by the cell (Chapter 4). The CO_2 study (Chapter 5) was performed in the scale-down model created and validated in this work. Finally, the pH impact on CHO-CY01 cell line kinetics (Chapter 6) was performe to validate the CO_2 study conclusions and to find the optimal external pH range for IgG4 productivity, CHO-CY01 cell line growth and cellular processes.

To design a scale-down model an engineering characterisation (mixing time, Reynolds, Froude, and Phase numbers; $k_L a$) of 24-SRW MTPs under conditions suitable for mammalian cell culture was done. Also, an appropriate engineering basis for scale translation criteria needs to be created. The combination of two common scale translation parameters, mixing time ($< 5\ s$) and energy dissipation rate (P/V = 10 $W\ m^{-3}$), were more capable of defining the operating conditions at which 24-SRW MTP, 5-L STR and SF with a total volume of 125 mL (SF 125 mL) and 250 mL (SF 250 mL) should be run. Through the engineering model of a 5-L STR bioreactor, an engineering characterisation, it was possible to establish the ideal operating conditions for scale translation (shaking speed, fill volume, sterile closure and, selective pressure). The 24-SRW MTP ideal operating conditions are a shaking speed of 220 rpm with an orbital diameter of 25 mm, with a fill volume of 0.85 mL. In this condition, the liquid-phase is “in-phase”, $k_L a$ value is $2.65\ h^{-1}$, the mixing time is $4.7 \pm 0.7\ s$ and, energy dissipation rate (P/V) is $10\ W\ m^{-3}$. The selective pressure that yielded the highest productivity was at 25 µM of MSX. However, for exclusively economic reasons, this selective marker was only added to CHO-CY01 cell line cultures in SFs and 24-SRW MTPs. With the ´system Duetz` lid CR1524a, which has a silicone layer and a metal foil layer with tiny holes for air exchange, the evaporation rate was no more than 34% of the total volume after seventeen days. It was considered adequate lid for both the CHO-CY01 cell batch and the fed-batch cultures. The 24-SRW MTP sacrificial sampling strategy adopted to maintain the same liquid-phase hydrodynamics and minimise the evaporation of the well´s contents and its osmotic effects was to sample firstly the ´corner` wells followed by the ´edge` wells and, at last, the ´internal` wells. Nonetheless, there is well-to-well reproducibility with a 95% confidence. The online monitoring of the process parameters was done using the Presens technology (SDR® system). It did not affect the CHO-CY01 cell line kinetics. Therefore, a 24-SRW MTP sampling strategy was employed for a semi-process controlled system. The standard 24-SRW MTPs were used for the sacrificial sampling method to determine the CHO-CY01 cell line kinetic parameters (viable cell concentration, viability, and metabolite and electrolyte concentrations).

The Presens 24-SRW MTPs (HydroDish®HD24 and OxoDish®OD24 plates) were exclusively used in parallel for the online process parameter measurement. Therefore, a high-throughput online multi-parametric analysis method of mammalian cell cellular activity at 24-SRW MTP was developed.

Fed-batch culture can substantially increase the final antibody concentration and culture VP, as compared with batch culture, while retaining the relative simplicity and reliability of batch cell culture. As a result, a new fed-batch methodology for small-scale systems, i.e. microwell plates and SFs, was developed in this work. This was accomplished by daily feeding (variable volumes) with water-diluted concentrated CD-CHO medium supplemented with glucose ($150.00\ g\ L^{-1}$). At small-scale (24-SRW MTP, 125 mL SF, and 250 mL SF), it was found that a constant glucose concentration top-up of 2.00 $g\ L^{-1}$ (FB2) or 3.00 $g\ L^{-1}$ (FB3) maximised the IgG4 production by CHO-CY01 cells. Subsequently, when the CHO-CY01 cell line was grown in different bioreactor scales, all with similar mixing times and energy dissipation rates (scale translation criteria), it was found that CHO-CY01 cell performance at both fed-batch strategies (FB2 and FB3) were statistically equivalent ($p > 0.05$) for all cell culture parameters, except for lactate (FB2 and FB3) and ammonium (FB2) profiles, which presented higher concentrations at 5-L STR scale. Therefore, it was established the best fed-batch strategy for CHO-CY01 cells was the constant glucose concentration top-up of 3.00 $g\ L^{-1}$ (FB3).

It was noted that CHO-CY01 cell batch cultures in 24-SRW MTP, 125 mL SF, and 250 mL SF accurately describe the cell growth, IgG4 productivity, and cell metabolism encountered at a larger scale (5-L STR). However, in fed-batch cultures, the waste by-products, lactate and ammonium and so, osmolality were under-estimated by these small-scale bioreactors. The reason for this is the lack of control at small-scale. Therefore, it became important to identify the lactate and ammonium inhibitory concentrations and inhibition kinetics in CHO-CY01 cell line culture. Moreover, there was no information available on their influence on the cell growth and mAb productivity of a GS-CHO cell line.

From the apoptotic population analysis of CHO-CY01 cell line cultures in 24-SRW MTP and 5L-STR, it is apparent that the cell death in 24-SRW MTP was exclusively due to apoptosis while the pilot-plant scale bioreactor showed a combined effect of apoptosis until the stationary phase which caused the necrosis at the decline phase. Likewise, on the cell cycle population analysis, the CHO-CY01 cell population dynamics strongly agreed across the bioreactor scales. For 5L-STR and 24-SRW MTP, the CHO-CY01 cell line exhibited an asynchronous growth and there was no suggestion that IgG4 formation was limited to any particular cell cycle phase. It appears that the regulation of synthesis and secretion of IgG4 is time-dependent and that the productivity is increased when the majority of the cells are equally arrested and

maintained in a 40-50% G1 and S-phases with decreasing cell viabilities and increasing cell diameters ($\geq 16\ \mu m$).

In this work, to investigate the inhibitory effects of lactate and ammonium, several initial lactate and ammonium concentrations were added to the CHO-CY01 cell line batch cultures. It was assumed that the lactate and ammonium inhibition of cell growth and IgG4 productivity were mathematically described by a non-competitive type of inhibition model similar to the kinetic model. Half-maximum-rate concentrations of lactate and ammonium for cell growth, cell death, and mAb productivity were determined by a non-linear curve fitting method. In Table 7-1 and Table 7-2, it is summarised the impact of different initial lactate and ammonium concentrations on CHO-CY01 cell line kinetics, respectively. It was hypothesised that at high lactate concentrations, the lactate dehydrogenase (LDH) was inhibited as the glucose consumption rate decreased, and the cells were utilising the lactate as a fuel through intracellular lactate shuttle. This metabolic "switch" is presumed to be driven by a decreased dependence on glycolysis and an enhanced engagement in oxidative pathways for energy production. Two possible mechanisms can explain Ammonia/ammonium CHO-CY01 cell growth inhibition. The first mechanism involves the uptake of the weak base NH_3 into intracellular organelles such as lysosomes, mitochondria, and Golgi apparatus, causing alkalinisation, as Doyle et al. (1990) have proposed. The second mechanism involves the uptake of the weak acid NH_4^+ into the cytoplasm, causing acidification, as proposed by Martinelle et al. (1998). These two mechanisms are correlated with the external pH of the medium. The second mechanism of growth inhibition by NH_4^+ is important at all CHO-CY01 cell culture medium pH values while the growth inhibition by NH_3 is only important at higher pH values (*lag* phase). It was proven that the toxic effect of ammonium on the CHO-CY01 cell line was greater than that of lactate, i.e. the cell growth, metabolism, and productivity were inhibited first by ammonia, then by ammonium and then by ammonium and lactate.

From the high-throughput online multi-parametric analysis method developed and the validation of the 24-SRW MTP as a scale-down model of CHO-CY01 cell line kinetics, it was possible to understand the effects of CO_2 on the CHO-CY01 cell line growth, cellular metabolism, and IgG4 production to find the optimum pH profile for IgG4 optimisation purposes. Therefore, a series of CHO-CY01 cell line cultures at constant, biphasic and multiphasic CO_2 concentrations were done. Also, two properties of the cell culture system used were determined, buffer capacity (23.29 ± 0.32% (v/v) CO_2 per 1 pH unit) and the gas transfer resistance from the CR1524a ´System Duetz` lid (3.25 ± 0.70% O_2). By interconnecting CHO-CY01 cell kinetic data with the pH profiles for CHO-CY01 cell line cultures at constant, biphasic and multiphasic CO_2, it was possible to define culture pH ranges with different effects on CHO-CY01 cell line growth and IgG4 productivity (Table 7-3).

Table 7-1: Impact of different initial lactate concentrations on CHO-CY01 cell line kinetics.

Initial Lactate Concentration ($g\ L^{-1}$)	
0.0 – 1.9	No change in μ, IgG4 productivity or cell metabolism
1.74 ($K_{P,Lact}$)	VP_{max} reduced to half
> 1.9	CHO-CY01 cells became strictly lactate consumers
1.9 – 3.6	Inhibitory effect: reduction of μ, IgG4 productivity and cell metabolism
2.23 ($K_{Di,Lact}$)	k_d doubled
≥ 3.6	Cell growth severely compromised
4.08 ($K_{i,Lact}$)	μ_{max} reduced to half

Table 7-2: Impact of different ammonium concentrations on CHO-CY01 cell line kinetics.

Initial Ammonium Concentration ($mmol\ L^{-1}$)	
0.2 – 4.8	Cell growth was not affected, but the q_{mAb} diminished by 23%.
4.8 – 7.1	Longer *lag*-phase and IVCC declined by 37% with no further reduction in q_{mAb}
7.17 ($K_{P,Amm}$)	VP_{max} reduced to half
9.66 ($K_{Di,Amm}$)	k_d doubled
≥ 9.7	Inhibitory effect: Cell growth and mAb productivity were negatively affected
18.10 ($K_{i,Amm}$)	μ_{max} reduced to half

Two semi-empirical mathematical models of CHO-CY01 cell line culture pH using a modified Henderson-Hasselbalch equation were developed. The model that considered for every mole of lactate produced, one mole of bicarbonate is utilised (pH model 1) can only describe the pH profile of CHO-CY01 cell line batch cultures at CO_2 concentrations above 5.00% (v/v) CO_2. While the pH model 2 that accounts for the alkalisation effect of ammonium ions describe well the CHO-CY01 cell line batch cultures above 2.00% (v/v) CO_2. For CHO-CY01 cell line fed-batch at constant and biphasic CO_2 cultures, both pH models were able to simulate the pH changes in CHO-CY01 cell line cultures.

Table 7-3: Impact of different pH values on CHO-CY01 cell line growth, metabolism and IgG4 productivity obtained from the CO_2 study in 24-SRW MTPs.

pH	
> 7.50	Increased lactate production rate and so, increased glucose consumption rate (Survival Strategy)
> 7.00	No IgG4 production
6.80– 7.00	Constant ammonium ion production rate and increased lactate consumption
6.70 - 6.80	Constant μ and lactate production rate; Increased cell diameter; CHO-CY01 cells lost the lactate consumer phenotype
6.60 -6.70	Increased ammonium ion production rate as well as glutamate consumption rate
< 6.60	Cell death by apoptosis

From the CHO-CY01 cell line batch cultures were grown at different constant CO_2 concentrations, it was found that at atmospheric CO_2 concentration that CHO-CY01 cells exhibited an extreme cellular survival strategy against the high culture pH with the excessive production of lactate and so, they were unable to grow and produce IgG4. Also, below the standard CO_2 concentration (5.00% (v/v)), CHO-CY01 cell cultures were not well buffered therefore CHO-CY01 cell line cultures at $CO_2 \leq$ 5.00 % are not considered to be ideal for optimisation purposes. Above standard CO_2 concentration (buffered cultures), CHO-CY01 cell line batch cultures were pH controlled at a cell-self established pH set-point: 7.12 ± 0.24 for 10.00%, 7.05 ± 0.12 for 15.00% and 7.02 ± 0.10 for 20.00% (v/v) CO_2. As a result, a new method for an easy and simple pH control in 24-SRW MTP was found for CHO-CY01 cell line batch cultures. Also, with increasing CO_2 concentration, the *lag*-phase duration prolonged, the μ and IVCC decreased which cascaded an increase in q_{Gluc}, q_{Glu}, q_{Lact} and q_{Amm} from a lower glucose consumption rate and maximum lactate concentration due to glycolysis inhibition. The lactate metabolic shift is independent of CO_2 concentration value as it was consistently observed when glucose concentration was below 3.00 – 4.00 $g\ L^{-1}$ and glutamate was below 2.5 $mmol\ L^{-1}$ at all CO_2 concentration values. A similar maximum IgG4 concentration (0.40 ± 0.11 $g\ L^{-1}$) was reached by the CHO-CY01 cells independently of the CO_2 concentration. Although there is cell growth inhibition at $CO_2 \geq$ 10.00% (v/v) CO_2, CHO-CY01 cells were able to produce the same q_{mAb} between 5.00% and 15.00% (v/v) CO_2 and a 1.81 fold increase at

20.00% (v/v) CO_2. Therefore, CHO-CYO1 cells utilised the glucose more for IgG4 production than for cell division or lactate production with increasing CO_2 levels.

From the evaluation of the effects of different CO_2 concentrations in CHO-CY01 cell line fed-batch cultures performed, it was observed a similar lactate and ammonium accumulation levels to batch values for all the CO_2 concentrations. It was found the highest IgG4 production (225% increase compared with the batch) for a CHO-CY01 cell line fed-batch culture with a pH range of 6.98 ± 0.28 (10.00% (v/v) CO_2).

In this study through the CHO-CY01 cell line cultures at biphasic and multiphasic CO_2 concentrations (CO_2 shifts), it was possible to manipulate the pH profiles in 24-SRW MTPs. This is novel work contributed to the identification of the pH ranges with different impact on CHO-CY01 cell line growth, IgG4 productivity and cellular processes presented in Table 7-3. It was developed a decision tree for the pH control in 24-SRW MTP with exclusively manipulation of the CO_2 level. I was also study the effects of CO_2 effects at different phases of cell growth. CO_2 shifts from 10.00% to 20.00% (v/v) CO_2 during the beginning of the exponential phase exponential phase had an inhibitory effect on cell growth and subsequently, decreased the glucose consumption, but no effect on IgG4 production. The advantage of such early CO_2 shift resides in a feed volume reduction of 5.6 fold and a 1.8 fold decline in IVCC with similar q_{mAb}. At the CO_2 shift at mid-exponential point, there was an inhibitory effect on the CHO-CY01 cell growth but to a lesser extent compared with the CO_2 shift on day 3 and IgG4 concentration decline at cell viabilities higher than 71.5% and pH > 7.00 raised concerns in choosing this pH profile for IgG4 productivity optimisation purposes. For the CO_2 shift at mid-stationary phase, there was no impact on cell growth. This CO_2 shift lowered 0.14 pH units, which started the decline phase and shortened the cell cultures by four days. The advantage of doing a CO_2 shift in a mid-stationary phase was to reach the same high IgG4 concentration (1.19 ± 0.05 $g\ L^{-1}$) as the constant CO_2 counterpart with a shorter cell culture time.

With CO_2 shifts different pH profiles at 24-SRW MTP scale were generated. It was found that a culture pH around pH 6.80 would slow down the CHO-CY01 cell growth rate as well as the lactate production rate with improved q_{mAb}. At the other end, culture pH values higher that pH 7.40 were associated with high glucose consumption leading to high lactate production and low IgG4 productivity. These conclusions from the scale-down approach needed to be tested at a fully automated and controlled larger scale, 5L-STR. Therefore, the first approach was to grow CHO-CY01 cells in batch mode at three different pHs: the standard pH (pH 7.1); below the standard pH (pH 6.80) and above the standard pH (pH 7.4). Secondly, CHO-CY01 cells were inoculated in fed-batch mode at the standard pH (pH 7.10), the optimal culture pH for IgG4 production (pH 6.80) and an extremely high pH (pH 7.80). Thirdly, different

pH shifts were done to found the optimum pH profile for IgG4 production by the CHO-CY01 cell line. Finally, 2-D DIGE was performed on 5L-STR CHO-CY01 cell line fed-batch cultures at constant pHs, and with the pH shifts, followed by protein identification by mass spectrometry and Uniprot database search. In this way, it was possible to understand the proteomic impact of the external pH on the CHO-CY01 cell line.

It was found that CHO-CY01 cell line batch cultures at pH 7.40 were similar to pH 7.10 on cell growth rate and metabolite profiles, but with a higher IgG4 titer and specific cell death. Therefore, there was an increase in VP and a culture time reduction. CHO-CY01 cell line batch culture at pH 6.80 exhibited a cell growth inhibition with a 57.9% reduction in μ with an uncharacteristic 5 days stationary phase (5 days), but there was a 47.9% increase in q_{mAb} and CHO-CY01 cells did not produce any lactate. Therefore, pH 7.10 it is not the optimal pH for IgG4 production in CHO-CY01 cell line, pH range between 7.10 and 7.40 was found to be the optimal pH range for the cell growth, opposite to what was found by Sellick et al. 2009, the CHO-CY01 cells had higher antibody titers at lower pH (pH 6.80), the negative effect of lactate common to the mAb bioprocess was eliminated with pH 6.80, and the ammonium production is promoted by the cells at lower pH values (pH 6.80).

From the fed-batch study at different pH values, it was clear that CHO-CY01 cells were incapable of growing and secreting IgG4 at pH 7.80. At this pH, the survival strategy observed in the scale-down approach for pH > 7.50 was also noted at 5L-STR scale, which validates the scale-down model created in this work. There was a 208% increase in the q_{Lact} compared with the standard, which also represented a higher glucose demand (2.03 ± 1.32 $g\ L^{-1}\ day^{-1}$). It is also worthwhile to mention that for all the pH values, there was a reduction of q_{Amm} at fed-batch mode. With the fed-batch strategy with glucose topping-up to 3.00 $g\ L^{-1}$ (FB3), it was possible to counteract the cell growth inhibition exbihited by CHO-CY01 cells in batch mode at pH 6.80. Indeed, the μ reached was similar to the standard value. Again at this lower pH, there was an uncharacteristic longer stationary phase, higher q_{mAb} and ammonium production, but this was always below the ammonium half-maximum-rate concentrations. Although the lactate formation was not null, it was considerably supressed at pH 6.80 (< 0.99 $g\ L^{-1}$), which reflected in a minimal q_{Gluc} and daily feeding requirements by CHO-CY01 cells. Consequently, the optimal pH range for IgG4 productivity and CHO-CY01 cell growth is 6.85 ± 0.02 (36.12 ± 2.45% (v/v) CO_2). It is important to note that this range is included in the scale-down approach IgG4 productivity pH range (6.98 ± 0.28 (10.00% (v/v) CO_2)), which once more validates the 24-SRW MTP scale-down model.

Tracing a parallel with the CO_2 shifts, pH shifts were also performed, which consists in a novel work. From the first two pH shifts strategies designed (pH 6.60 to 6.80 and pH 7.60 to 7.10), it was found that the pH range for CHO-CY01 cell line is $6.60 < pH < 7.60$, base addition

prompted the lactate production and again pH values higher than 7.60 triggered the survival strategy (anaerobic metabolism). Also, single pH shifts from pH 7.10 (reference) to pH 6.80 (optimal) were performed at different culture times, mid-exponential point (day 5) and at the end of the exponential phase (day 8), as done with the CO_2 shifts. The same conclusions grasped with the CO_2 shifts were reached with the pH shifts. The pH shift during the exponential phase caused an inhibition of the cell growth with a μ decline and the pH shift at the beginning of the stationary phase, initiated the decline phase. From the 2D-DIGE proteomic analysis and the limited protein identification of the pH shift at day 5 supernatant, It can be assumed that the reduction in the μ was due to a decrease in the expression of ATP binding (chaperones) proteins and inorganic pyrophosphatase, as there was an inhibition of the energy supply to the cells and the protein folding was also compromised. The drop in glucose consumption with the pH shift was due to under-expression of alpha-enolase when the culture pH shifted to pH 6.80. Therefore, at the both pH shifts cultures, there was a decrease in the IVCC, which can benefit the downstream process. The early the pH shift was done, the higher the q_{mAb} reached, but still below the optimal value (constant pH 6.80). A important conclusion taken from these pH shifts CHO-CY01 cell line fed-batch cultures was the fact that CHO-CY01 cells became lactate consumers and serious ammonium producers whenever the pH was shifted from pH 7.10 to pH 6.80 occurred. However, the ammonium concentration profile was similar to the one found at constant pH 6.80. The pH shifts were beneficial to CHO-CY01 cell line process optimisation, since they were an improvement from the reference pH. Nevertheless, these pH shifts were unable to surpass the CHO-CY01 cell line fed-batch culture at constant pH 6.80 process, which continues to be the optimal pH range, as they exhibited greater q_{Gluc}, q_{Glu}, q_{Lact} and q_{Amm} for the same (pH shift at day 5) or lower (pH shift at day 8) q_{mAb}. Also, from the proteomic analysis it was concluded that CHO-CY01 cells were under stress (cell diameter > 16 μm) when cultured at pH 6.80, as there was an over-expression of glutathione synthetase (redox buffer).

To further evaluate the response of CHO-CY01 cell line to pH perturbations, the amplitude of the pH shift from pH 7.10 to 6.80 at day 5 was divided into two steps. For this multiple steps pH shifts, the CHO-CY01 cell line growth profile was similar to the one found at constant pH 7.10 and the peak IgG4 concentration (1.03$g\ L^{-1}$) reached and volumetric productivity (47.8 $mg\ L^{-1}\ day^{-1}$) were the same as the ones found at constant pH 6.80 (optimal). However, there was a higher glucose requirement by the cells and so, a 2-fold increase in the feed volume was observed. Also, there was a significant increase in q_{Lact} with the same ammonium accumulation. The possible advantage of this pH shift is reliable on the fact that the peak IgG4 concentration was reached 7 days earlier than pH 6.80, which turns it

as a possible optimal condition for IgG4 production by CHO-CY01 cells due to the considerable reduction of culture time.

7.2. Future Work

Considering future work and recommendations, an experimental study to determine the experimental $k_L a$ values in 24-SRW MTP and the gas transfer resistance of ´system Duetz` lids is most needed. Using an CO_2 incubator with oxygen control, it would be possible to set for all the bioreactor scales the same initial dissolved oxygen concentration and thus, further improving the scale-down model. The only process parameter that was not evaluated in the search of the optimal CHO-CY01 cell line culture condition was the temperature, which is a critical parameter in mammalian cell cultures. Therefore, a design of experiment (DoE) approach at 24-SRW MTPs with shaking speed, fill volume, CO_2 concentration, pH, DOT and temperature as inputs would provide a more comprehensive process optimisation of CHO-CY01 cell line culture. Several other different fed-batch strategies may have been explored, i.e., different glucose concentrations feeding profiles, the use of different commercially available fed-batch media and, the addition of selected amino acids. With an extracellular amino acid quantification of the CHO-CY01 cell line culture medium, it would be possible to generate a metabolic flux map of the CHO-CY01 cell metabolism and so, a better feed could have been designed and further understanding of the pH effect could be reached. Also, it could explain the metabolic pathways involved in the lactate consumption, at different CO_2 concentrations and/or external pH. The measurement of the internal pH could also shine a light on the cellular metabolism, mainly on the lactate and ammonium metabolism, at different CO_2 concentrations and/or external pH profiles. With the online pH monitoring at 24-SRW MTP, a PID controller could have been created to have the pH control by exclusively manipulating the CO_2 level inside the CO_2 incubator at a first approach. Ultimately, more constant CO_2 concentrations and/or external pH values should have been tested. Also, different CO_2/pH shifts should have to be done, by varying the CO_2/pH amplitude, number of CO_2/pH shifts, short term vs long term CO_2/pH shifts and the time point of the CO_2/pH shift. At last, a proteomic analysis by 2D-DIGE PAGE in combination with protein spot identification techniques to CHO-CY01 cell line cultures at different CO_2/pH profiles would allow a better understanding of cellular metabolism and so, giving space to its optimisation. An IgG4 product quality test should be done all across the bioreactor scales and conditions not only to understand the impact of the CO_2/pH on IgG4 glycosylation patterns but also to implement a quality-by-design approach. From all the data collected in this work, a mathematical model (kinetic or structured) to describe the CHO-CY01 cell line behaviour at different culture CO_2/pH could be formulated.

Chapter 8 References

Abu-Reesh, I., & Kargi, F. (1989). Biological Responses of Hybridoma Cells to Defined Hydrodynamic Shear Stress. *Journal of Biotechnology*, *9*(3), 167–178.

Adams, G. P., & Weiner, L. M. (2005). Monoclonal Antibody Therapy of Cancer. *Nature Biotechnology*, *23*(9), 1147–57.

Agrawal, V., & Bal, M. (2012). Strategies for Rapid Production of Therapeutic Proteins in Mammalian Cells. *Bioprocess International*, 32 – 40.

Al-Rubeai, M., & Emery, A N. (1990). Mechanisms and Kinetics of Monoclonal Antibody Synthesis and Secretion in Synchronous and Asynchronous Hybridoma Cell Cultures. *Journal of Biotechnology*, *16*(1-2), 67–85.

Al-Rubeai, M., Singh, R. P., AI-Rubeai, M., & Singht, R. P. (1998). Apoptosis in Cell Culture. *Current Opinion in Biotec*, *9*(2), 152–156.

Altamirano, C., Cairó, J. J., & Gòdia, F. (2001). Decoupling Cell Growth and Product Formation in Chinese Hamster Ovary Cells Through Metabolic Control. *Biotechnology and Bioengineering*, *76*(4), 351–360.

Altamirano, C., Paredes, C., Illanes, A., Cairó, J. J., & Gòdia, F. (2004). Strategies for Fed-Batch Cultivation of t-PA Producing CHO cells: Substitution of Glucose and Glutamine and Rational Design of Culture Medium. *Journal of Biotechnology*, *110*(2), 171–179.

Altamirano, C., Berrios, J., Vergara, M., & Becerra, S. (2013). Advances in Improving Mammalian Cells Metabolism for Recombinant Protein Production. *Electronic Journal of Biotechnology*, *16*(3).

Amanullah, A., McFarlane, C. M., Emery, A. N., & Nienow, a. W. (2001). Scale-Down Model to Simulate Spatial pH Variations in Large-Scale Bioreactors. *Biotechnology and Bioengineering*, *73*(5), 390–399.

Amanullah, A., Buckland, B. C., & Nienow, A. W. (2004). Mixing in the Fermentation and Cell Culture Industries. In E. L. Paul, V. A. Atiemo-Obeng, & S. M. Kresta (Eds.), *Handbook of Industrial Mixing* (pp. 1071–1170). John Wiley & Sons, Inc.

Andersen, D. C., & Goochee, C. F. (1995). The Effect of Ammonia on the O-linked Glycosylation of Granulocyte-colony-stimulating Factor Produced by Chinese-Hamster Ovary Cells. *Biotechnology and Bioengineering*, *47*(1), 96–105.

Andersen, D. C., Bridges, T., Gawlitzek, M., & Hoy, C. (2000). Multiple Cell Culture Factors Can Affect the Glycosylation of Asn-184 in Plasminogen Activator. *Biotechnology and Bioengineering*, *70*, 25–31.

Andersen, D. C., & Reilly, D. E. (2004). Production Technologies for Monoclonal Antibodies and Their Fragments. *Current Opinion in Biotechnology*, *15*(5), 456–62.

Arden, N., & Betenbaugh, M. J. (2004). Life and Death in Mammalian Cell Culture: Strategies for Apoptosis Inhibition. *Trends in Biotechnology*, *22*(4), 174–80.

Baez, A., & Shiloach, J. (2014). Effect of Elevated Oxygen Concentration on Bacteria, Yeasts, and Cells Propagated for Production of Biological Compounds. *Microbial Cell Factories*, *13*(1), 1–7.

Bahia, D., Cheung, R., Buchs, M., Geisse, S., & Hunt, I. (2005). Optimisation of Insect Cell Growth in Deep-Well Blocks: Development of a High-Throughput Insect Cell Expression Screen. *Protein*

Expression and Purification, *39*(1), 61–70.

Balcarcel, R. R., & Clark, L. M. (2003). Metabolic Screening of Mammalian Cell Cultures Using Well-plates. *Biotechnology Progress*, *19*(1), 98–108.

Bareither, R., & Pollard, D. (2011). A Review of Advanced Small-Scale Parallel Bioreactor Technology for Accelerated Process Development: Current State and Future Need. *Biotechnology Progress*, *27*(1), 2–14.

Barrett, T. A., Wu, A., Zhang, H., Levy, M. S., & Lye, G. J. (2010). Microwell Engineering Characterization for Mammalian Cell Culture Process Development. *Biotechnology and Bioengineering*, *105*(2), 260–75.

Berson, R. E., & Friederichs, G. (2008). A Self-feeding Roller Bottle for Continuous Cell Culture. *Biotechnology Progress*, *24*(1), 154–157.

Betts, J. I., & Baganz, F. (2006). Miniature Bioreactors: Current Practices and Future Opportunities. *Microbial Cell Factories*, *5*(21), 1–14.

Bi, J.-X., & Zeng, A.-P. (2005). Cell Culture Kinetics and Modeling. In *Cell Culture Technology for Pharmaceutical and Cell-Based* (pp. 299–348). CRC Press.

Bibila, T. A., Ranucci, C. S., Glazomitsky, K., Buckland, B. C., & Aunins, J. G. (1994). Monoclonal Antibody Process Development Using Medium Concentrates. *Biotecchonoly Progress*, *10*, 87–96.

Bibila, T. A., Robinson, D. K., & Obinson, D. K. (1995). In Pursuit of the Optimal Fed-Batch Process for Monoclonal Antibody Production. *Biotechnology Progress*, *11*(1), 1–13.

Birch, J. R., & Racher, A. J. (2006). Antibody Production. *Advanced Drug Delivery Reviews*, *58*(5-6), 671–85.

Bloemkolk, J. W., Gray, M. R., Merchant, F., & Mosmann, T. R. (1992). Effect of Temperature on Hybridoma Cell Cycle and MAb Production. *Biotechnology and Bioengineering*, *40*(3), 427–31.

Blombach, B., & Takors, R. (2015). CO_2 – Intrinsic Product, Essential Substrate, and Regulatory Trigger of Microbial and Mammalian Production Processes. *Frontiers in Bioengineering and Biotechnology*, *3*(August), 1–11.

Bollati-Fogolín, M., Forno, G., Nimtz, M., Conradt, H. S., Etcheverrigaray, M., & Kratje, R. (2005). Temperature Reduction in Cultures of hGM-CSF-Expressing CHO Cells: Effect on Productivity and Product Quality. *Biotechnology Progress*, *21*(1), 17–21.

Boron, W. F. (2004). Regulation of Intracellular pH. *Advances in Physiology Education*, *28*(1-4), 160–79.

Borys, M. C., Linzer, D. I. H., & Papoutsakis, E. T. (1993). Culture pH Affects Expression Rates and Glycosylation of Recombinant Mouse Placental Lactogen Proteins by Chinese Hamster Ovary (CHO) Cells. *Nature Biotechnology*, *11*(6), 720–724.

Borys, M. C., Linzer, D. I., & Papoutsakis, E. T. (1994). Ammonia Affects the Glycosylation Patterns of Recombinant Mouse Placental Lactogen-I by Chinese Hamster Ovary Cells in a pH-Dependent Manner. *Biotechnology and Bioengineering*, *43*(6), 505–514.

Brandt, B., Hidalgo, A., & Bornscheuer, U. T. (2006). Immobilization of Enzymes in Microtiter Plate Scale. *Biotechnology Journal*, *1*(5), 582–7.

Bree, M. A, Dhurjati, P., Geoghegan, R. F., & Robnett, B. (1988). Kinetic Modelling of Hybridoma Cell

Growth and Immunoglobulin Production in a Large-Scale Suspension Culture. *Biotechnology and Bioengineering*, *32*(8), 1067–72.

Brooks, G. A, Dubouchaud, H., Brown, M., Sicurello, J. P., & Butz, C. E. (1999). Role of Mitochondrial Lactate Dehydrogenase and Lactate Oxidation in the Intracellular Lactate Shuttle. *Proceedings of the National Academy of Sciences of the United States of America*, *96*(3), 1129–1134.

Brown, M. E., Renner, G., Field, R. P., & Hassell, T. (1992). Process Development for the Production of Recombinant Antibodies Using the Glutamine Synthetase (GS) System. *Cytotechnology*, *9*(1-3), 231–236.

Büchs, J., Maier, U., Milbradt, C., & Zoels, B. (2000a). Power Consumption in Shaking Flasks on Rotary Shaking Machines: I. Power Consumption Measurement in Unbaffled Flasks at Low Liquid Viscosity. *Biotechnology and Bioengineering*, *68*(6), 589–93.

Büchs, J., Maier, U., Milbradt, C., & Zoels, B. (2000b). Power Consumption in Shaking Flasks on Rotary Shaking Machines: II. Nondimensional Description of Specific Power Consumption and Flow Regimes in Unbaffled Flasks at Elevated Liquid Viscosity. *Biotechnology and Bioengineering*, *68*(6), 594–601.

Büchs, J. (2001). Introduction to Advantages and Problems of Shaken Cultures. *Biochemical Engineering Journal*, *7*(2), 91–98.

Bujalski, W., Takenaka, K., Paolini, S., Jahoda, M., Paglianti, A., Takahashi, K., & Etchells, A. W. (1999). Suspension and Liquid Homogenization in High Solids Concentration Stirred Chemical Reactors. *Chemical Engineering Research and Design*, *77*(3), 241–247.

Bursch, W., Karwan, A., Mayer, M., Dornetshuber, J., Fröhwein, U., Schulte-Hermann, R., Gerner, C. (2008). Cell Death and Autophagy: Cytokines, Drugs, and Nutritional factors. *Toxicology*, *254*(3), 147–57.

Burton, Z. F., Sutherland, T., & Eisenberg, D. (1981). Refinements in the Rapid Isolation of Glutamine Synthetase from Escherichia coli. *Arch Biochem Biophys*, *211*(1), 507–509.

Burton, D. R. (1987). Structure and Function of Antibodies. In F. Calabi & M. S. Neuberger (Eds.), *Molecular Genetics of Immunglobulin.pdf* (pp. 1–50). New York: Elsevier Science Publishers B. V.

Butler, M. (2005). Animal Cell Cultures: Recent Achievements and Perspectives in the Production of Biopharmaceuticals. *Applied Microbiology and Biotechnology*, *68*(3), 283–91.

Butler, M. (2006). Optimisation of the Cellular Metabolism of Glycosylation for Recombinant Proteins Produced by Mammalian Cell Systems. *Cytotechnology*, *50*(1-3), 57–76.

Carson, K. L. (2005). Flexibility - The Guiding Principle for Antibody Manufacturing. *Nature Biotechnology*, *23*(9), 1054–8.

Chadd, H. E., & Chamow, S. M. (2001). Therapeutic Antibody Expression Technology. *Current Opinion in Biotechnology*, *12*(2), 188–94.

Chen, K., Liu, Q., Xie, L., Sharp, P. A., & Wang, D. I. C. (2001). Engineering of a Mammalian Cell Line for Reduction of Lactate Formation and High Monoclonal Antibody Production. *Biotechnology and Bioengineering*, *72*(1), 55–61.

Chen, P., & Harcum, S. W. (2005). Effects of Amino Acid Additions on Ammonium Stressed CHO Cells. *Journal of Biotechnology*, *117*(3), 277–86.

Cheng, A. T. Y., Zhou, Y., Gupta, A., Hunek, B., & Grinter, N. (2012). Method for Controlling pH,

Osmolality and Dissolved Carbon Dioxide Levels in a Mammalian Cell Culture Process to Enhance Cell Viability and Biologic Product Yield. United States Patent (US 8,178,318 B2).

Chisti, Y. (1993). Animal Cell Culture in Stirred Bioreactors : Observations on Scale-Up. *Bioprocess Engineering*, *9*, 191–196.

Chisti, Y. (2001). Hydrodynamic Damage to Animal Cells*. Critical Reviews in Biotechnology.* 21(2), 67–110.

Chu, L., & Robinson, D. K. (2001). Industrial Choices for Protein Production by Large-Scale Cell Culture. *Current Opinion in Biotechnology*, *12*(2), 180–7.

Chuppa, S., Tsai, Y. S., Yoon, S., Shackleford, S., Rozales, C., Bhat, R., Naveh, D. (1997). Fermentor Temperature as a Tool for Control of High-Density Perfusion Cultures of Mammalian Cells. *Biotechnology and Bioengineering*, *55*(2), 328–338.

Clark, K. J. R., Griffiths, J., Bailey, K. M., & Harcum, S. W. (2005). Gene-Expression Profiles for Five Key Glycosylation Genes for Galactose-Fed CHO Cells Expressing Recombinant IL-4/13 Cytokine Trap. *Biotechnology and Bioengineering*, *90*, 568–577.

Cohen, J., & Wilson, A. (2009). New Challenges to Medicare Beneficiary Access to mAbs. *mAbs*, *1*(1), 56–66.

Connon, S. A, & Giovannoni, S. J. (2002). High-Throughput Methods for Culturing Microorganisms in Very-Low-Nutrient Media Yield Diverse New Marine Isolates High-Throughput Methods for Culturing Microorganisms in Very-Low-Nutrient Media Yield Diverse New Marine Isolates. *Applied and Environmental Microbiology*, *68*(8), 3878–3885.

Cowger, N., O'Connor, K., Hammond, T., Lacks, D., & Navar, G. (1999). Characterization of Bimodal Cell Death of Insect Cells in a Rotating-Wall Vessel and Shaker flask. *Biotechnology and Bioengineering*, *64*(1), 14–26.

Cruz, H. J. H. J., Freitas, C. M. C., Alves, P. M. P., Moreira, J. L. J., & Carrondo, M. J. T. (2000). Effects of Ammonia and Lactate on Growth, Metabolism, and Productivity of BHK Cells. *Enzyme and Microbial Technology*, *27*(1-2), 43–52.

Curling, E. M., Hayter, P. M., Baines, a J., Bull, a T., Gull, K., Strange, P. G., & Jenkins, N. (1990). Recombinant Human Interferon-Gamma. Differences in Glycosylation and Proteolytic Processing Lead to Heterogeneity in Batch Culture. *The Biochemical Journal*, *272*(2), 333–337.

Del Val, I. J., Kontoravdi, C., & Nagy, J. M. (2010). Towards the Implementation of Quality by Design to the Production of Therapeutic Monoclonal Antibodies with Desired Glycosylation Patterns. *Biotechnology Progress*, *26*(6),

Deshpande, R. R., & Heinzle, E. (2004). On-line Oxygen Uptake Rate and Culture Viability Measurement of Animal Cell Culture Using Microplates with Integrated Oxygen Sensors. *Biotechnology Letters*, *26*(9), 763–767.

DeZengotita, V. M., Kimura, R., & Miller, W. M. (1998). Effects of CO_2 and Osmolality on Hybridoma Cells: Growth, Metabolism and Monoclonal antibody production. *Cytotechnology*, *28*(1-3), 213–227.

DeZengotita, V. M., Schmelzer, A. E., & Miller, W. M. (2002). Characterization of Hybridoma Cell Responses to Elevated pCO_2 and osmolality: Intracellular pH, Cell Size, Apoptosis, and Metabolism. *Biotechnology and Bioengineering*, *77*(4), 369–380.

Dijk, M. A., & Van De Winkel, J. G. J. (2001). Human Antibodies as Next Generation Therapeutics. *Current Opinion in Chemical Biology*, *5*, 368–374.

Dinnis, D. M., & James, D. C. (2005). Engineering Mammalian Cell Factories For Improved Recombinant Monoclonal Antibody Production: Lessons from Nature? *Biotechnology and Bioengineering*, *91*, 180–189.

Doig, S. D., Pickering, S. C. R., Lye, G. J., & Woodley, J. M. (2002). The Use of Microscale Processing Technologies for Quantification of Biocatalytic Baeyer-Villiger Oxidation Kinetics. *Biotechnology and Bioengineering*, *80*(1), 42–9.

Doig, S. D., Pickering, S. C. R., Lye, G. J., & Baganz, F. (2005). Modelling Surface Aeration Rates in Shaken Microtitre Plates Using Dimensionless Groups. *Chemical Engineering Science*, *60*(10), 2741–2750.

Doig, S. D., Baganz, F., & Lye, G. J. (2006). High-Throughput Screening and Process Optimisation. In C. Ratledge & B. Kristiansen (Eds.), *Basic Biotechnology* (3rd ed., pp. 289–305). Cambridge: Cambridge University Press.

Dove, A. (2002). Uncorking the Biomanufacturing Bottleneck. *Nature Biotechnology*, *20*, 777–779.

Doyle, C., & Butler, M. (1990). The Effect of pH on the Toxicity of Ammonia to a Murine Hybridoma. *Journal of Biotechnology*, *15*(1-2), 91–100.

Duetz, W. A., Rüedi, L., Hermann, R., O'Connor, K., Büchs, J., & Witholt, B. (2000). Methods for Intense Aeration, Growth, Storage, and Replication of Bacterial Strains in Microtiter Plates. *Applied and Environmental Microbiology*, *66*(6), 2641–2646.

Duetz, W. A., & Witholt, B. (2001). Effectiveness of Orbital Shaking for the Aeration of Suspended Bacterial Cultures in Square-Deepwell Microtiter Plates. *Biochemical Engineering Journal*, *7*(2), 113–115.

Ecker, D. M., Jones, S. D., & Levine, H. L. (2015). The Therapeutic Monoclonal Antibody Market. *mAbs*, *7*(1), 9–14.

Elmahdi, I., Baganz, F., Dixon, K., Harrop, T., Sugden, D., & Lye, G. J. (2003). pH Control in Microwell Fermentations of S. erythraea CA340: Influence on Biomass Growth Kinetics and Erythromycin Biosynthesis. *Biochemical Engineering Journal*, *16*(3), 299–310.

Europa, A. F., Gambhir, A., Fu, P. C., & Hu, W. S. (2000). Multiple Steady States with Distinct Cellular Metabolism in Continuous Culture of Mammalian Cells. *Biotechnology and Bioengineering*, *67*(1), 25–34.

Fenge, C., Klein, C., Heuer, C., Siegel, U., & Fraune, E. (1993). Agitation, Aeration and Perfusion Modules for Cell Culture Bioreactors. *Cytotechnology*, *11*, 233–244.

Fenge, C., & Lüllau, E. (2006). Cell Culture Bioreactors. In S. S. Ozturk & W.-S. Hu (Eds.), *Cell culture technology for pharmaceutical and cell-based therapies.* (pp. 155–224). CRC Press.

Fernandes, P., Fernandes, P., Cabral, J., & Cabral, J. (2006). Microlitre/Millilitre Shaken Bioreactors in Fermentative and Biotransformation Processes - A Review. *Biocatalysis and Biotransformationand Biotransformation*, *24*(4), 237–252.

Ferreira-Torres, C., Micheletti, M., & Lye, G. J. (2005). Microscale Process Evaluation of Recombinant Biocatalyst Libraries: Application to Baeyer-Villiger Monooxygenase Catalysed Lactone Synthesis.

Bioprocess and Biosystems Engineering, *28*(2), 83–93.

Fitzpatrick, L., Jenkins, H. a, & Butler, M. (1993). Glucose and Glutamine Metabolism of a Murine B-lymphocyte Hybridoma Grown in Batch Culture. *Applied Biochemistry and Biotechnology*, *43*, 93–116.

Fogolín, M. B., Wagner, R., Etcheverrigaray, M., & Kratje, R. (2004). Impact of Temperature Reduction and Expression of Yeast Pyruvate Carboxylase on hGM-CSF-producing CHO Cells. *Journal of Biotechnology*, *109*(1-2), 179–191.

Fox, S. R., Patel, U. A, Yap, M. G. S., & Wang, D. I. C. (2004). Maximizing Interferon-Gamma Production by Chinese Hamster Ovary Cells Through Temperature Shift optimization: Experimental and Modeling. *Biotechnology and Bioengineering*, *85*(2), 177–184.

Franek, F. (1995). Starvation-Induced Programmed Death of Hybridoma Cells: Prevention by Amino Acid Mixtures. *Biotechnology and Bioengineering*, *45*, 86–90.

Frenzel, A., Hust, M., & Schirrmann, T. (2013). Expression of Recombinant Antibodies. *Frontiers in Immunology*, *4*(July), 1–20.

Freyer, S. A., König, M., & Künkel, A. (2004). Validating Shaking Flasks as Representative Screening Systems. *Biochemical Engineering Journal*, *17*(3), 169–173.

Furukawa, K., & Ohsuye, K. (1998). Effect of Culture Temperature on a Recombinant CHO Cell Line Producing a C-terminal α-amidating Enzyme. *Cytotechnology*, *26*(2), 153–64.

Fussenegger, M., & Bailey, J. E. (1998). Molecular Regulation of Cell-Cycle Progression and Apoptosis in Mammalian Cells: Implications for Biotechnology. *Biotechnology Progress*, *14*(6), 807–33.

Gadgil, M. (2014). Development of a Mathematical Model for Animal Cell Culture Without pH Control and its Application for Evaluation of Clone Screening Outcomes in Shake Flask Culture. *Journal of Chemical Technology and Biotechnology*, *90*(October 2013), 166 – 175.

Ge, X., Hanson, M., Shen, H., Kostov, Y., Brorson, K. a., Frey, D. D., Rao, G. (2006). Validation of an Optical Sensor-Based High-Throughput Bioreactor System for Mammalian Cell Culture. *Journal of Biotechnology*, *122*(3), 293–306.

Giaever, G., Chu, A. M., Ni, L., Connelly, C., Riles, L., Véronneau, S., Johnston, M. (2002). Functional Profiling of the Saccharomyces Cerevisiae Genome. *Nature*, *418*(6896), 387–391.

Gill, N. K., Appleton, M., Baganz, F., & Lye, G. J. (2008). Design and Characterisation of a Miniature Stirred Bioreactor System for Parallel Microbial Fermentations. *Biochemical Engineering Journal*, *39*(1), 164–176.

Girard, P., Jordan, M., Tsao, M., & Wurm, F. M. (2001). Small-Scale Bioreactor System for Process Development and Optimization. *Biochemical Engineering Journal*, *7*(2), 117–119.

Glacken, M. W., Fleischaker, R. J., & Sinskey, A. J. (1986). Serum in Cultures of Mammalian Cells. *Biotechnology*, *XXVIII*, 1376–1389

Glacken, M. W. (1988a). Catabolic Control of Mammalian Cell Culture. *Nature Biotechnology*, *6*(9), 1041–1050.

Glacken, M. W., Adema, E., & Sinskey, A J. (1988b). Mathematical Descriptions of Hybridoma Culture Kinetics: I. Initial Metabolic Rates. *Biotechnology and Bioengineering*, *32*(4), 491–506.

Gladden, L. B. (2004). Lactate Metabolism: a New Paradigm for the Third Millennium. *The Journal of Physiology*, *558*(Pt 1), 5–30.

Gódia, F., Cairó, J. J., & Cairo, J. (2006). Cell Metabolism. In S. S. Ozturk & W.-S. Hu (Eds.), *Cell culture technology for pharmaceutical and cell-based therapies* (pp. 1–10). CRC Press.

Goochee, C. F., & Monica, T. (1990). Environmental Effects on Protein Glycosylation. *Nature Biotechnology*, *8*(14), 421.

Goudar, C. T., Joeris, K., Konstantinov, K. B., & Piret, J. M. (2005). Logistic Equations Effectively Model Mammalian Cell Batch and Fed-Batch Kinetics by Logically Constraining the Fit. *Biotechnology Progress*, *21*(4), 1109–18.

Gramer, M. J., & Ogorzalek, T. (2007). A Semi-Empirical Mathematical Model Useful for Describing the Relationship Between Carbon Dioxide, pH, Lactate and Base in a Bicarbonate-Buffered Cell-Culture Process. *Biotechnology and Applied Biochemistry*, *47*(Pt 4), 197–204.

Gray, D. R., Chen, S., Howarth, W., Inlow, D., & Maiorella, B. L. (1996). CO_2 in Large-Scale and High-Density CHO Cell Perfusion Culture. *Cytotechnology*, *22*(1-3), 65–78.

Griffiths, B. (2000). Scaling-up of Animal Cell Cultures. In John R. W. Masters (Ed.), *Animal cell culture : a practical approach* (pp. 19–67). Oxford University Press.

Gronemeyer, P., Ditz, R., & Strube, J. (2014). Trends in Upstream and Downstream Process Development for Antibody Manufacturing. *Bioengineering*, *1*(4), 188–212.

Grzeskowiak, J. K., Tscheliessnig, A., Toh, P. C., Chusainow, J., Lee, Y. Y., Wong, N., & Jungbauer, A. (2009). 2-D DIGE to Expedite Downstream Process Development for Human Monoclonal Antibody Purification. *Protein Expression and Purification*, *66*(1), 58–65.

Guarino, R. D., Dike, L. E., Haq, T. A., Rowley, J. A., Pitner, J. B., & Timmins, M. R. (2004). Method for Determining Oxygen Consumption Rates of Static Cultures from Microplate Measurements of Pericellular Dissolved Oxygen Concentration. *Biotechnology and Bioengineering*, *86*(7), 775–787.

Guilmanov, V., Ballistreri, A., Impallomeni, G., & Gross, R. A. (2002). Oxygen Transfer Rate and Sophorose Lipid Production by Candida bombicola. *Biotechnology and Bioengineering*, *77*(5), 489–494.

Gupta, A., & Rao, G. (2003). A Study of Oxygen Transfer in Shake Flasks Using a Non-Invasive Oxygen Sensor. *Biotechnology and Bioengineering*, *84*(3), 351–358.

Haggstrom, L. (2000). Cell Metabolism, Animal. In R. E. Spier (Ed.), *The Encyclopedia of Cell Technology* (pp. 392–411). Hoboken, NJ, USA: John Wiley & Sons, Inc.

Hale, G. (2006). Therapeutic Antibodies - Delivering the Promise? *Advanced Drug Delivery Reviews*, *58*(5-6), 633–9.

Hansen, H. A., & Emborg, C. (1994). Influence of Ammonium on Growth, Metabolism, and Productivity of a Continuous Suspension Chinese Hamster Ovary Cell Culture. *Biotechnology Progress*, *10*(1), 121–4.

Hanson, M. A., Ge, X., Kostov, Y., Brorson, K. A., Moreira, A. R., & Rao, G. (2007). Comparisons of Optical pH and Dissolved Oxygen Sensors with Traditional Electrochemical Probes during Mammalian Cell Culture. *Biotechnology and Bioengineering*, *97*(4), 833–841.

Harms, P., Kostov, Y., & Rao, G. (2002). Bioprocess Monitoring. *Current Opinion in Biotechnology*, *13*(2), 124–127.

Hassell, T., Gleave, S., & Butler, M. (1991). Growth Inhibition in Animal Cell Culture. *Applied*

Biochemistry and Biotechnology, *30*(1), 29–41.

Heath, C., & Kiss, R. (2007). Cell Culture Process Development: Advances in Process Engineering. *Biotechnology Progress*, *23*(1), 46–51.

Henzler, H., & Schedel, M. (1991). Bioprocess Engineering Suitability of the Shaking Flask for Oxygen Supply to Microbiological Cultures. *Bioprocess Engineering*, *7*, 123–131.

Hermann, R., Lehmann, M., & Büchs, J. (2003). Characterization of Gas-Liquid Mass Transfer Phenomena in Microtiter Plates. *Biotechnology and Bioengineering*, *81*(2), 178–186.

Hevehan, D. L., & Miller, W. M. (1999). Hypoxia, Effect on Animal Cells. In M. C. Flickinger & S. W. Drew (Eds.), *Encyclopedia of Bioprocess Technology: Fermentation, Biocatalysis, and Bioseparation* (pp. 1418–1433). Hoboken, NJ, USA: John Wiley & Sons, Inc.

Ho, S. N. (2006). Intracellular Water Homeostasis and the Mammalian Cellular Osmotic Stress Response. *Journal of Cellular Physiology*, *206*(1), 9–15.

Hsu, W. T., Aulakh, R. P. S., Traul, D. L., & Yuk, I. H. (2012). Advanced Microscale Bioreactor System: A Representative Scale-Down Model for Bench-Top Bioreactors. *Cytotechnology*, *64*(6), 667–678.

Hu, W.-S., & Aunins, J. G. (1997). Large-Scale Mammalian Cell Culture. *Current Opinion in Biotechnology*, *8*, 148–153.

Hu, W., Berdugo, C., & Chalmers, J. J. (2011). The Potential of Hydrodynamic Damage to Animal Cells of Industrial Relevance: Current Understanding. *Cytotechnology*, *63*(5), 445–460.

Hwang, S. O., & Lee, G. M. (2008). Nutrient Deprivation Induces Autophagy As Well As Apoptosis in Chinese Hamster Ovary Cell Culture. *Biotechnology and Bioengineering*, *99*(3), 678–685.

Iammarino, M., Nti-gyabaah, J., Chandler, M., Roush, D., & Göklen, K. (2007). Impact of Cell Density and Viability on Primary Clarification of Mammalian Cell Broth. *Bioprocess International*, (November), 38–50.

Jacob, N. M., Hu, W., & Yap, M. (2009). Using Genomic Tools to Improve the Production of Biologics. *Chemical Engineering Progress*, *105*(11), 35–42.

Jain, E., & Kumar, A. (2008). Upstream Processes in Antibody Production: Evaluation of Critical Parameters. *Biotechnology Advances*, *26*(1), 46–72.

Jansen, M., Veurink, J. H., Euverink, G. J. W., & Dijkhuizen, L. (2003). Growth of the Salt-Tolerant Yeast Zygosaccharomyces rouxii in Microtiter Plates: Effects of NaCl, pH and Temperature on Growth and Fusel Alcohol Production from Branched-Chain Amino Acids. *FEMS Yeast Research*, *3*, 313–318.

Jardon, M., & Garnier, A. (2003). pH, $\mathrm{pCO_2}$, and Temperature Effect on R-adenovirus Production. *Biotechnol. Prog.*, *19*(1), 202–208.

Jefferis, R. (2002). Glycosylation of Recombinant IgG4 Antibodies and its Relevence for Therapeutic Applications (A Soupcon of Sugar Helps thE Medicine Work). In M. Al-Rubeai (Ed.), *Cell engineering volume 3: Glycosylation* (Vol. 3, pp. 93–107). Dordrecht: Kluwer Academic Publishers.

John, G. T., & Heinzle, E. (2001). Quantitative Screening Method for Hydrolases in Microplates using pH Indicators: Determination of Kinetic Parameters by Dynamic pH Monitoring. *Biotechnology and Bioengineering*, *72*(6), 620–7.

John, G. T., Klimant, I., Wittmann, C., & Heinzle, E. (2003). Integrated Optical Sensing of Dissolved

Oxygen in Microtiter Plates: A Novel Tool for Microbial Cultivation. *Biotechnology and Bioengineering*, *81*(7), 829–836.

Jorjani, P., & Ozturk, S. S. (1999). Effects of Cell Density and Temperature on Oxygen Consumption Rate for Different Mammalian Cell Lines. *Biotechnology and Bioengineering*, *64*(3), 349–356.

Jun, S. C., Kim, M. S., Hong, H. J., & Lee, G. M. (2006). Limitations to the Development of Humanized Antibody Producing Chinese Hamster Ovary Cells Using Glutamine Synthetase-Mediated Gene Amplification. *Biotechnology Progress*, *22*(3), 770–80.

Jung, Y. K., & Hur, W. (2000). A New Method of On-Line Measurement of Buffer Capacity and Alkali Consumption Rate of a Fermentation Process. *Journal of Bioscience and Bioengineering*, *90*(5), 580–582.

Karra, S., Sager, B., & Karim, M. N. (2010). Multi-Scale Modeling of Heterogeneities in Mammalian Cell Culture Processes. *Industrial & Engineering Chemistry Research*, *49*(17), 7990–8006.

Kato, I., & Tanaka, H. (1998). Development of a Novel Box-Shaped Shake Flask with Efficient Gas Exchange Capacity. *Journal of Fermentation and Bioengineering*, *85*(4), 404–409.

Kato, Y., Peter, C. P., Akgun, A., & Büchs, J. (2004). Power Consumption and Heat Transfer Resistance in Large Rotary Shaking Vessels. *Biochemical Engineering Journal*, *21*(1), 83–91.

Kaufmann, H., Mazur, X., Fussenegger, M., & Bailey, J. E. (1999). Influence of Low Temperature on Productivity, Proteome and Protein Phosphorylation of CHO Cells. *Biotechnology and Bioengineering*, *63*(5), 573–82.

Kelley, B. (2009). Industrialization of mAb Production Technology: the Bioprocessing Industry at a Crossroads. *mAbs*, *1*(5), 443–52.

Kensy, F., John, G. T., Hofmann, B., & Büchs, J. (2005a). Characterisation of Operation Conditions and Online Monitoring of Physiological Culture Parameters in Shaken 24-Well Microtiter Plates. *Bioprocess and Biosystems Engineering*, *28*(2), 75–81.

Kensy, F., Zimmermann, H. F., Knabben, I., Anderlei, T., Trauthwein, H., Dingerdissen, U., & Büchs, J. (2005b). Oxygen Transfer Phenomena in 48-Well Microtiter Plates: Determination by Optical Monitoring of Sulfite Oxidation and Verification by Real-Time Measurement during Microbial Growth. *Biotechnology and Bioengineering*, *89*(6), 698–708.

Kim, M. S., Kim, N. S., Sung, Y. H., & Lee, G. M. (2002). Biphasic Culture Strategy Based on Hyperosmotic Pressure for Improved Humanized Antibody Production in Chinese Hamster Ovary Cell Culture. *In Vitro Cellular & Developmental Biology. Animal*, *38*(6), 314–319.

Kim, S. H., Lee, G. M., Kim, H. S., Lee, G. M., Kim, S. H., & Lee, G. M. (2007). Differences in Optimal pH and Temperature for Cell Growth and Antibody Production between two Chinese Hamster Ovary Clones Derived from the Same Parental Clone. *Journal of Microbiology and Biotechnology*, *17*(5), 712–720.

Kimura, R., & Miller, W. M. (1996). Effects of Elevated $\mathrm{pCO_2}$ and/or Osmolality on the Growth and Recombinant tPA Production of CHO Cells. *Biotechnology and Bioengineering*, *52*, 152–160.

Kimura, R., & Miller, W. M. (1997). Glycosylation of CHO-derived Recombinant tPA Produced under Elevated $\mathrm{pCO_2}$. *Biotechnology Progress*, *13*(3), 311–317.

Kohler, G., & Milstein, C. (1975). Continuous Cultures of Fused Cells Secreting Antibody of Predefined

Specificity. *Nature*, *256*, 495–497.

Kohn, R. A., & Dunlap, T. F. (1998). Calculation of the Buffering Capacity of Bicarbonate in the Rumen and In Vitro. *Journal of Animal Science*, *76*(6), 1702–1709.

Kostov, Y., Harms, P., Randers-Eichhorn, L., & Rao, G. (2001). Low-Cost Microbioreactor for High-Throughput Bioprocessing. *Biotechnology and Bioengineering*, *72*(3), 346–52.

Kumar, S., Wittmann, C., & Heinzle, E. (2004). Minibioreactors. *Biotechnology Letters*, *26*(1), 1–10.

Kumar, N., Gammell, P., & Clynes, M. (2007). Proliferation Control Strategies to Improve Productivity and Survival during CHO Based Production Culture: A Summary of Recent Methods Employed and the Effects of Proliferation Control in Product Secreting CHO Cell Lines. *Cytotechnology*, *53*(1-3), 33–46.

Kunkel, J. P., Jan, D. C. H., Jamieson, J. C., & Butler, M. (1998). Dissolved Oxygen Concentration in Serum-Free Continuous Culture Affects N-Linked Glycosylation of a Monoclonal Antibody. *Journal of Biotechnology*, *62*(1), 55–71.

Kunkel, J. P., Jan, D. C., Butler, M., & Jamieson, J. C. (2000). Comparisons of the Glycosylation of a Monoclonal Antibody Produced under Nominally Identical Cell Culture Conditions in Two Different Bioreactors. *Biotechnology Progress*, *16*(3), 462–70.

Kurano, N., Leist, C., Messi, F., Kurano, S., & Fiechter, A. (1990a). Growth Behavior of Chinese Hamster Ovary Cells in a Compact Loop Bioreactor: 1. Effects of Physical and Chemical Environments. *Journal of Biotechnology*, *15*(1-2), 101–112.

Kurano, N., Leist, C., Messi, F., Kurano, S., & Fiechter, A. (1990b). Growth Behavior of Chinese Hamster Ovary Cells in a Compact Loop Bioreactor. 2. Effects of Medium Components and Waste Products. *Journal of Biotechnology*, *15*(1-2), 113–128.

Kuwae, S., Ohda, T., Tamashima, H., Miki, H., & Kobayashi, K. (2005). Development of a Fed-Batch Culture Process for Enhanced Production of Recombinant Human Antithrombin by Chinese Hamster Ovary Cells. *Journal of Bioscience and Bioengineering*, *100*(5), 502–510.

Lamping, S., Zhang, H., Allen, B., & Ayazi Shamlou, P. (2003). Design of a Prototype Miniature Bioreactor for High Throughput Automated Bioprocessing. *Chemical Engineering Science*, *58*(3-6), 747–758.

Langheinrich, C., & Nienow, A. W. (1999). Control of pH in Large-Scale, Free Suspension Animal Cell Bioreactors: Alkali Addition and pH Excursions. *Biotechnology and Bioengineering*, *66*(3), 171–9.

Lao, M. S., & Toth, D. (1997). Effects of Ammonium and Lactate on Growth and Metabolism of a Recombinant Chinese Hamster Ovary Cell Culture. *Biotechnology Progress*, *13*(5), 688–91.

Lara, A. R., Galindo, E., Ramírez, O. T., & Palomares, L. a. (2006). Living with Heterogeneities in Bioreactors: Understanding the Effects of Environmental Gradients on Cells. *Molecular Biotechnology*, *34*(3), 355–381.

Lee, G. M., & Koo, J. (2009). Osmolarity Effects, Chinese Hamster Ovary Cell Culture. In Michael C. Flickinge (Ed.), *Encyclopedia of Industrial Biotechnology: Bioprocess, Bioseparation, and Cell Technology 7*. Hoboken, NJ, USA: John Wiley & Sons, Inc.

Leelavatcharamas, V., Emery, a N., & Al-Rubeai, M. (1999). Use of Cell Cycle Analysis to Characterise Growth and Interferon-Gamma Production in Perfusion Culture of CHO Cells. *Cytotechnology*, *30*(1-

3), 59–69.

Lewis, G., Lugg, R., Lee, K., & Wales, R. (2010). Novel Automated Micro-Scale Bioreactor Technology: A Qualitative and Quantitative Mimic for Early Process Development. *Bioprocessing Journal*, *9*(1).

Li, F., Hashimura, Y., Pendleton, R., Harms, J., Collins, E., & Lee, B. (2006). A Systematic Approach for Scale-Down Model Development and Characterization of Commercial Cell Culture Processes. *Biotechnology Progress*, *22*(3), 696–703.

Li, F., Vijayasankaran, N., Shen, A., Kiss, R., & Amanullah, A. (2010). Cell Culture Processes for Monoclonal Antibody Production. *mAbs*, *2*(5), 466–479.

Lilley, K. S., & Friedman, D. B. (2004). All about DIGE: Quantification Technology for Differential-Display 2D-Gel Proteomics. *Expert Review of Proteomics*, *1*(4), 401–409.

Liu, C. M., & Hong, L. N. (2001). Development of a Shaking Bioreactor System for Animal Cell Cultures. *Biochemical Engineering Journal*, *7*(2), 121–125.

Lloyd, D. R., Holmes, P., Jackson, L. P., Emery, A N., & Al-Rubeai, M. (2000). Relationship Between Cell Size, Cell Cycle and Specific Recombinant Protein Productivity. *Cytotechnology*, *34*(1-2), 59–70.

Lotter, S., & Büchs, J. (2004). Utilization of Specific Power Input Measurements for Optimization of Culture Conditions in Shaking Flasks. *Biochemical Engineering Journal*, *17*(3), 195–203.

Lueking, A., Horn, M., Eickhoff, H., Bu, K., Lehrach, H., & Walter, G. (1999). Protein Microarrays for Gene Expression and Antibody Screening. *Analytical Biochemistry*, *270*, 103–111.

Luo, J., Vijayasankaran, N., Autsen, J., Santuray, R., Hudson, T., Amanullah, A., & Li, F. (2012). Comparative Metabolite Analysis to Understand Lactate Metabolism Shift in Chinese Hamster Ovary Cell Culture Process. *Biotechnology and Bioengineering*, *109*(1), 146–156.

Lye, G. J., Ayazi-Shamlou, P., Baganz, F., Dalby, P. a, & Woodley, J. M. (2003). Accelerated Design of Bioconversion Processes using Automated Microscale Processing Techniques. *Trends in Biotechnology*, *21*(1), 29–37.

MacKenzie, C. G., MacKenzie, J. B., & Beck, P. (1961). The Effect of pH on Growth, Protein Synthesis, and Lipid-Rich Particles of Cultured Mammalian Cells. *The Journal of Biophysical and Biochemical Cytology*, *9*, 141–156.

Maier, U., & Büchs, J. (2001). Characterisation of the Gas – Liquid Mass Transfer in Shaking Bioreactors. *Biochemical Engineering Journal*, *7*(2), 99–106.

Marks, D. M. (2003). Equipment Design Considerations for Large Scale Cell Culture. *Cytotechnology*, *42*(1), 21–33.

Marques, M. P. C., Cabral, J. M. S., & Fernandes, P. (2009). High Throughput in Biotechnology: from Shake-Flasks to Fully Instrumented Microfermentors. *Recent Patents on Biotechnology*, *3*(2), 124–40.

Martinelle, K., Westlund, A., & Häggström, L. (1998). Saturable Ammonium Ion Transport in Myeloma and Hybridoma Cells is Mediated by the Na+K+2Cl- Cotransporter. *Biotechnology Letters*, *20*(1), 81–86.

McDermott, R. H., & Butler, M. (1993). Uptake of Glutamate, not Glutamine Synthetase, Regulates Adaptation of Mammalian Cells to Glutamine-Free Medium. *Journal of Cell Science*, *104*, 51–58.

McDowell, C. L., Papoutsakis, E. T., & Borys, M. C. (2003). Animal Cell Culture, Physiochemical Effects

of pH. In *Encyclopedia of Cell Technology* (pp. 212–220). Hoboken, NJ, USA: John Wiley & Sons, Inc.

McKenna, M. C. (2013). Glutamate Pays its Own Way in Astrocytes. *Frontiers in Endocrinology*, *4*(DEC), 1–6.

McLimas, W. F. (1972). The Gaseous Environment of the Mammalian Cell Culture. In G. Rothblat & Vincent J. Cristofalo (Eds.), *Growth, Nutrition and Metabolism of Cells in Culture* (pp. 137–169). London: Academic Press.

McQueen, A., & Bailey, J. E. (1990a). Effect of Ammonium Ion and Extracellular pH on Hybridoma Cell Metabolism and Antibody Production. *Biotechnology and Bioengineering*, *35*(11), 1067–77.

McQueen, A., & Bailey, J. E. (1990b). Mathematical Modeling of the Effects of Ammonium Ion on the Intracellular pH of Hybridoma Cells. *Biotechnology and Bioengineering*, *35*(3), 897–906.

McQueen, A., & Bailey, J. E. (1991). Bioprocess Engineering Growth Inhibition of Hybridoma Cells by Ammonium Ion : correlation with effects on intracellular pH, *6*, 49–61.

Merten, O.-W. (2006). Introduction to Animal Cell Culture Technology-Past, Present and Future. *Cytotechnology*, *50*(1-3), 1–7.

Micheletti, M., Barrett, T., Doig, S. D., Baganz, F., Levy, M. S., Woodley, J. M., & Lye, G. J. (2006a). Fluid Mixing in Shaken Bioreactors: Implications for Scale-up Predictions from Microlitre-Scale Microbial and Mammalian Cell Cultures. *Chemical Engineering Science*, *61*(9), 2939–2949.

Micheletti, M., & Lye, G. J. (2006b). Microscale Bioprocess Optimisation. *Current Opinion in Biotechnology*, *17*(6), 611–8.

Miller, W. M., Blanch, H. W., & Wilke, C. R. (1988). A Kinetic Analysis of Hybridoma Growth and Metabolism in Batch and Continuous Suspension Culture: Effect of Nutrient Concentration, Dilution Rate, and pH. *Biotechnology and Bioengineering*, *32*(8), 947–965.

Minas, W., Bailey, J. E., & Duetz, W. (2000). Streptomycetes in Micro-Cultures: Growth, Production of Secondary Metabolites, and Storage and Retrieval in the 96-Well Format. *Antonie van Leeuwenhoek*, *78*(3-4), 297–305.

Mirabet, M., Navarro, A., Lopez, A., Canela, E. I., Mallol, J., Lluis, C., & Franco, R. (1997). Ammonium Toxicity in Different Cell Lines. *Biotechnology and Bioengineering*, *56*(5), 530–7.

Mohan, C., Kim, Y.-G., Koo, J., & Lee, G. M. (2008). Assessment of Cell Engineering Strategies for Improved Therapeutic Protein Production in CHO Cells. *Biotechnology Journal*, *3*(5), 624–630.

Moore, A., Mercer, J., Dutina, G., Donahue, C. J., Bauer, K. D., Mather, J. P., Ryll, T. (1997). Effects of Temperature Shift on Cell Cycle, Apoptosis and Nucleotide Pools in CHO Cell Batch Cultues. *Cytotechnology*, *23*(1-3), 47–54.

Moses, S., & Manahan, M. (2012). Assessment of AMBR™ as a Model for High-Throughput Cell Culture Process Development Strategy. *Advances in Bioscience*, *2012*(November), 918–927.

Mostafa, S. S., & Gu, X. (2003). Strategies for Improved dCO_2 Removal in Large-Scale Fed-Batch Cultures. *Biotechnology Progress*, *19*(1), 45–51.

Mrotzek, C., Anderlei, T., Henzler, H. J., & Büchs, J. (2001). Mass Transfer Resistance of Sterile Plugs in Shaking Bioreactors. *Biochemical Engineering Journal*, *7*(2), 107–112.

Mulukutla, B. C., Khan, S., Lange, A., & Hu, W.-S. (2010). Glucose Metabolism in Mammalian Cell

Culture: New Insights for Tweaking Vintage Pathways. *Trends in Biotechnology*, *28*(9), 476–84.

Mulukutla, B. C., Gramer, M., & Hu, W.-S. S. (2012). On Metabolic Shift to Lactate Consumption in Fed-Batch Culture of Mammalian Cells. *Metabolic Engineering*, *14*(2), 138–149.

Müthing, J., Kemminer, S. E., Conradt, H. S., Šagi, D., Nimtz, M., Kärst, U., Peter-Katalinić, J. (2003). Effects of Buffering Conditions and Culture pH on Production Rates and Glycosylation of Clinical Phase I Anti-Melanoma Mouse IgG3 Monoclonal Antibody R24. *Biotechnology and Bioengineering*, *83*(3), 321–34.

Naciri, M., Kuystermans, D., & Al-Rubeai, M. (2008). Monitoring pH and Dissolved Oxygen in Mammalian Cell Culture using Optical Sensors. *Cytotechnology*, *57*(3), 245–50.

Nealon, A. J., O'Kennedy, R. D., Titchener-Hooker, N. J., & Lye, G. J. (2006). Quantification and Prediction of Jet Macro-Mixing Times in Static Microwell Plates. *Chemical Engineering Science*, *61*(15), 4860–4870.

Nienow, A. W. (2006). Reactor Engineering in Large Scale Animal Cell Culture. *Cytotechnology*, *50*(1-3), 9–33.

Nienow, A. W., Langheinrich, C., Stevenson, N. C., Emery, A. N., Clayton, T. M., & Slater, N. K. H. (1996). Homogenisation and Oxygen Transfer Rates in Large Agitated and Sparged Animal Cell Bioreactors: Some Implications for Growth and Production. *Cytotechnology*, *22*(1-3), 87–94.

Nienow, A. W., Rielly, C. D., Brosnan, K., Bargh, N., Lee, K., Coopman, K., & Hewitt, C. J. (2013). The Physical Characterisation of a Microscale Parallel Bioreactor Platform with an Industrial CHO Cell Line Expressing an IgG4. *Biochemical Engineering Journal*, *76*, 25–36.

Nilsang, S., Nandakumar, K. S., Galaev, I. Y., Rakshit, S. K., Holmdahl, R., Mattiasson, B., & Kumar, A. (2007). Monoclonal Antibody Production using a New Supermacroporous Cryogel Bioreactor. *Biotechnology Progress*, *23*(4), 932–9.

Njålsson, R., & Norgren, S. (2005). Physiological and Pathological Aspects of GSH Metabolism. *Acta Paediatrica*, *94*(2), 132–137.

Nyberg, G. B., Balcarcel, R. R., Follstad, B. D., Stephanopoulos, G., & Wang, D. I. (1999). Metabolic Effects on Recombinant Interferon-Gamma Glycosylation in Continuous Culture of Chinese Hamster Ovary Cells. *Biotechnology and Bioengineering*, *62*(3), 336–47.

O'Callaghan, P. M., & James, D. C. (2008). Systems Biotechnology of Mammalian Cell Factories. *Briefings in Functional Genomics and Proteomics*, *7*(2), 95–110.

Oguchi, S., Saito, H., Tsukahara, M., & Tsumura, H. (2006). pH Condition in Temperature Shift Cultivation Enhances Cell Longevity and Specific hMab Productivity in CHO Culture. *Cytotechnology*, *52*(3), 199–207.

Olds, E. G. (1938). Distributions of Sums of Squares of Rank Differences for Small Numbers of Individuals. *The Annals of Mathematical Statistics*, *9*(2), 133–148.

Oliveira, J. E., Damiani, R., Vorauer-Uhl, K., Bartolini, P., & Ribela, M. T. C. P. (2008). Influence of a Reduced CO_2 Environment on the Secretion Yield, Potency and N-Glycan Structures of Recombinant Thyrotropin from CHO Cells. *Molecular Biotechnology*, *39*(2), 159–166.

Omasa, T., Higashiyama, K., Shioya, S., & Suga, K. (1992). Effects of Lactate Concentration on Hybridoma Culture in Lactate-Controlled Fed-Batch Operation. *Biotechnology and Bioengineering*,

39(5), 556–564.

Onyeaka, H., Nienow, A. W., & Hewitt, C. J. (2003). Further Studies Related to the Scale-Up of High Cell Density *Escherichia coli* Fed-Batch Fermentations: *Biotechnology and Bioengineering*, *84*(4), 474–484.

Oosterhuis, N. M. G. (1984). Scale-Up of Bioreactors, a Scale-Down Approach. Delft University of Technology.

Osman, J. J., Birch, J., & Varley, J. (2001). The Response of GS-NS0 Myeloma Cells to pH Shifts and pH Perturbations. *Biotechnology and Bioengineering*, *75*(1), 63–73.

Osman, J. J., Birch, J., & Varley, J. (2002). The Response of GS-NS0 Myeloma Cells to Single and Multiple pH Perturbations. *Biotechnology and Bioengineering*, *79*(4), 398–407.

Ozturk, S. S., & Palsson, B. O. (1990). Effects of Dissolved Oxygen on Hybridoma Cell Growth, Metabolism, and Antibody Production Kinetics in Continuous Culture. *Biotechnology Progress*, *6*(6), 437–46.

Ozturk, S. S., & Palsson, B. O. (1991a). Effect of Medium Osmolarity on Hybridoma Growth, Metabolism, and Antibody Production. *Biotechnology and Bioengineering*, *37*, 989–993.

Ozturk, S. S., & Palsson, B. O. (1991b). Growth, Metabolic, and Antibody Production Kinetics of Hybridoma Cell Culture: 2. Effects of Serum Concentration, Dissolved Oxygen Concentration, and Medium pH in a Batch Reactor. *Biotechnology Progress*, *7*(6), 481–494.

Ozturk, S. S., Riley, M. R., & Palsson, B. O. (1992). Effects of Ammonia and Lactate on Hybridoma Growth, Metabolism, and Antibody Production. *Biotechnology and Bioengineering*, *39*(4), 418–431.

Ozturk, S. S. (1996). Engineering Challenges in High Density Cell Culture Systems. *Cytotechnology*, *22*(1-3), 3–16.

Palomares, L. a, & Ramirez, O. T. (1996). The Effect of Dissolved Oxygen Tension and the Utility of Oxygen Uptake Rate in Insect Cell Culture. *Cytotechnology*, *22*(1-3), 225–37.

Pattison, R. N., Swamy, J., Mendenhall, B., Hwang, C., & Frohlich, B. T. (2000). Measurement and Control of Dissolved Carbon Dioxide in Mammalian Cell Culture Processes using an *in-situ* Fiber Optic Chemical Sensor. *Biotechnology Progress*, *16*(5), 769–774.

Perani, A., Singh, R. P., Chauhan, R., & Al-Rubeai, M. (1998). Variable Functions of bcl-2 in Mediating Bioreactor Stress-Induced Apoptosis in Hybridoma Cells. *Cytotechnology*, *28*(1-3), 177–188.

Petch, D., & Butler, M. (1994). Profile of Energy Metabolism in a Murine Hybridoma: Glucose and Glutamine Utilization. *Journal of Cellular Physiology*, *161*(1), 71–6.

Peter, C. P., Suzuki, Y., & Büchs, J. (2006). Hydromechanical Stress in Shake Flasks: Correlation for the Maximum Local Energy Dissipation Rate. *Biotechnology and Bioengineering*, *93*(6), 1164–1176.

Philp, A., Macdonald, A. L., & Watt, P. W. (2005). Lactate - A Signal Coordinating Cell and Systemic Function. *The Journal of Experimental Biology*, *208*(Pt 24), 4561–4575.

Poole, R. C., & Halestrap, A. P. (1993). Transport of Lactate and other Monocarboxylates Across Mammalian Plasma Membranes. *The American Journal of Physiology*, *264*(4 Pt 1), C761–C782.

Pörtner, R., & Schäfer, T. (1996). Modelling Hybridoma Cell Growth and Metabolism - A Comparison of Selected Models and Data. *Journal of Biotechnology*, *49*(1-3), 119–35.

Quan, C., Alcala, E., Petkovska, I., Matthews, D., Canova-Davis, E., Taticek, R., & Ma, S. (2008). A

Study in Glycation of a Therapeutic Recombinant Humanized Monoclonal Antibody: Where it is, how it got there, and how it affects charge-based behavior. *Anal Biochem*, *373*(2), 179–191.

Raval, K., Kato, Y., & Büchs, J. (2007). Comparison of Torque Method and Temperature Method for Determination of Power Consumption in Disposable Shaken Bioreactors. *Biochemical Engineering Journal*, *34*(3), 224–227.

Renner, W. a., Jordan, M., Eppenberger, H. M., & Leist, C. (1993). Cell-Cell Adhesion and Aggregation: Influence on the Growth Behavior of CHO Cells. *Biotechnology and Bioengineering*, *41*(2), 188–193.

Restelli, V.; Butler, M. (2002). The Effect of Cell Culture Parameters on Protein Glycosylation. *Cell Engineering*, *3*, 61–92.

Rieseberg, M., Kasper, C., Reardon, K. F., & Scheper, T. (2001). Flow Cytometry in Biotechnology. *Applied Microbiology and Biotechnology*, *56*(3-4), 350–360.

Roche Innovatis AG. (2002). Cell Counter + Analyser System Model TT Operator Manual. *Casy Operator Manual*.

Rodrigues, M. E., Costa, A. R., Henriques, M., Azeredo, J., & Oliveira, R. (2010). Technological Progresses in Monoclonal Antibody Production Systems. *Biotechnology Progress*, *26*(2), 332–351.

Rodriguez, J., Spearman, M., Huzel, N., & Butler, M. (2005). Enhanced Production of Monomeric Interferon-Beta by CHO Cells Through the Control of Culture Conditions. *Biotechnology Progress*, *21*(1), 22–30.

Roos, A., & Boron, W. F. (1981). Intracellular pH. *Physiological Reviews*, *61*(2), 296–434.

Roque, A. C. A., Lowe, C. R., & Taipa, M. A. (2004). Antibodies and Genetically Engineered Related Molecules: Production and Purification. *Biotechnology Progress*, *20*(3), 639–54.

Rössler, B., Lübben, H., & Kretzmer, G. (1996). Temperature : A Simple Parameter for Process Optimization in Fed-Batch Cultures of Recombinant Chinese Hamster Ovary Cells. *Enzyme and Microbial Technology*, *18*, 423–427.

Ruitenberg, E. J., Brosi, B. J., & Steerenberg, P. a. (1976). Direct Measurement of Microplates and its Application to Enzyme-Linked Immunosorbent Assay. *Journal of Clinical Microbiology*, *3*(5), 541–542.

Sandadi, S., Ensari, S., & Kearns, B. (2005). Heuristic Optimization of Antibody Production by Chinese Hamster Ovary Cells. *Biotechnology Progress*, *21*(5), 1537–1542.

Schatz, S. M., Kerschbaumer, R. J., Gerstenbauer, G., Kral, M., Dorner, F., & Scheiflinger, F. (2003). Higher Expression of Fab Antibody Fragments in a CHU Cell Line at Reduced Temperature. *Biotechnology and Bioengineering*, *84*(4), 433–438.

Schmelzer, A. E., & Miller, W. M. (2002). Hyperosmotic Stress and Elevated $\mathrm{pCO_2}$ Alter monoclonal Antibody Charge Distribution and Monosaccharide Content. *Biotechnology Progress*, *18*(2), 346–353.

Schmid, G., Blanch, H. W., & Wilke, C. R. (1990). Hybridoma Growth, Metabolism, And Product Formation In HEPES-Buffered Medium: II. Effect of pH. *Biotechnology Letters*, *12*(9), 633–638.

Schneider, M., Marison, I. W., & Von Stockar, U. (1996). The Importance of Ammonia in Mammalian Cell Culture. *Journal of Biotechnology*, *46*(3), 161–85.

Scolnik, P. A. (2009). mAbs: a Business Perspective. *mAbs*, *1*(2), 179–84.

Sellick, C., Maqsood, A., Croxford, A., Dickson, A., Goodacre, R., & Stephens, G. (2009). Optimizing CHO Cell Culture Conditions. *Genetic Engineering and Biotechnology News*, *29*(17), 29–31.

Senger, R. S., & Karim, M. N. (2003). Effect of Shear Stress on Intrinsic CHO Culture State and Glycosylation of Recombinant Tissue-Type Plasminogen Activator Protein. *Biotechnology Progress*, *19*(4), 1199–1209.

Severns, M. L., Schoeppner, S. L., Cozart, M. J., Friedman, L. I., & Schanfield, M. S. (1984). Automated Determination of ABO/Rh in Microplates. *Vox Sanguinis*, *47*(4), 293–303.

Shi, M., Xie, Z., Yu, M., Shen, B., & Guo, N. (2005). Controlled Growth of Chinese Hamster Ovary Cells and High Expression of Antibody-IL-2 Fusion Proteins by Temperature Manipulation. *Biotechnology Letters*, *27*(23-24), 1879–1884.

Shukla, A. A, & Thömmes, J. (2010). Recent Advances in Large-Scale Production of Monoclonal Antibodies and Related Proteins. *Trends in Biotechnology*, *28*(5), 253–61.

Sidoli, F. R., Mantalaris, A., & Asprey, S. P. (2004). Modelling of Mammalian Cells and Cell Culture Processes. *Cytotechnology*, *44*(1-2), 27–46.

Silk, N. J., Denby, S., Lewis, G., Kuiper, M., Hatton, D., Field, R., Lye, G. J. (2009). Fed-Batch Operation of an Industrial Cell Culture Process in Shaken Microwells. *Biotechnology Letters*, *32*(1), 73–78.

Silk, N. J. (2014). *High Throughput Approaches to Mammalian Cell Culture Process Development*. University College London EngD thesis.

Simpson, N. H., Milner, A. E., & Al-Rubeai, M. (1997). Prevention of Hybridoma Cell Death by bcl-2 During Suboptimal Culture Conditions. *Biotechnology and Bioengineering*, *54*(1), 1–16.

Smales, C. M., Dinnis, D. M., Stansfield, S. H., Alete, D., Sage, E. a, Birch, J. R., James, D. C. (2004). Comparative Proteomic Analysis of GS-NS0 Murine Myeloma Cell Lines with Varying Recombinant Monoclonal Antibody Production Rate. *Biotechnology and Bioengineering*, *88*(4), 474–88.

Smith, J.A, & Martin, L. (1973). Do Cells Cycle? *Proceedings of the National Academy of Sciences of the United States of America*, *70*(4), 1263–1267.

Storring, P. L. (1992). Assaying Glycoprotein Hormones - The Influence of Glycosylation on Immunoreactivity. *Trends in Biotechnology*, *10*(12), 427–32.

Suberbie, M. D. L. V. (2013). *Characterisation of the Bioreactor Environment and its Effect on Mammalian Cell Performance in Suspension Culture during Antibody Production*. University College London PhD thesis.

Sung, K. Y., Jong, K. H., & Gyun, M. L. (2004). Effect of Simultaneous Application of Stressful Culture Conditions on Specific Productivity and Heterogeneity of Erythropoietin in Chinese Hamster Ovary Cells. *Biotechnology Progress*, *20*(4), 1293–1296.

Suresh, S., Srivastava, V. C., & Mishra, I. M. (2009). Critical Analysis of Engineering Aspects of Shaken Flask Bioreactors. *Critical Reviews in Biotechnology*, *29*(4), 255–278.

Sureshkumar, G. K., & Mutharasan, R. (1991). The Influence of Temperature on a Monoclonal Antibody Production. *Biotechnology and Bioengineering*, *37*, 292–295.

Tait, A. S. S., Hogwood, C. E. M. E. M., Smales, C. M. M., & Bracewell, D. G. G. (2012). Host Cell Protein Dynamics in the Supernatant of a mAb Producing CHO Cell Line. *Biotechnology and Bioengineering*, *109*(4), 971–82.

Takuma, S., Hirashima, C., & Piret, J. M. (2007). Dependence on Glucose Limitation of the $\mathrm{pCO_2}$ Influences on CHO Cell Growth, Metabolism and IgG Production. *Biotechnology and Bioengineering*,

97(6), 1479–1488.

Tan, R.-K., Eberhard, W., & Büchs, J. (2011). Measurement and Characterization of Mixing Time in Shake Flasks. *Chemical Engineering Science*, *66*(3), 440–447.

Thomas, R. C. (1995). Bicarbonate Briefly CO_2-Free. *Nature*, *374*, 597–598.

Tolosa, L., Kostov, Y., Harms, P., & Rao, G. (2002). Noninvasive Measurement of Dissolved Oxygen in Shake Flasks. *Biotechnology and Bioengineering*, *80*(5), 594–597.

Trummer, E., Fauland, K., Seidinger, S., Schriebl, K., Lattenmayer, C., Kunert, R., Müller, D. (2006a). Process Parameter Shifting: Part I. Effect of DOT, pH, and Temperature on the Performance of Epo-Fc Expressing CHO Cells Cultivated in Controlled Batch Bioreactors. *Biotechnology and Bioengineering*, *94*(6), 1033–1044.

Trummer, E., Fauland, K., Seidinger, S., Schriebl, K., Lattenmayer, C., Kunert, R., Muller, D. (2006b). Process Parameter Shifting: Part II. Biphasic Cultivation - A Tool for Enhancing the Volumetric Productivity of Batch Processes Using Epo-Fc Expressing CHO Cells. *Biotechnology and Bioengineering*, *94*(6), 1045–1052.

Tsao, Y.-S. S., Cardoso, A. G., Condon, R. G. G., Voloch, M., Lio, P., Lagos, J. C., Liu, Z. (2005). Monitoring Chinese Hamster Ovary Cell Culture by the Analysis of Glucose and Lactate Metabolism. *Journal of Biotechnology*, *118*(3), 316–327.

Tsotsou, G. E., Cass, A. E. G., & Gilardi, G. (2002). High Throughput Assay for Cytochrome P450 BM3 for Screening Libraries of Substrates and Combinatorial Mutants. *Biosensors and Bioelectronics*, *17*(1-2), 119–131.

Vallejos, J. R., Kostov, Y., Ram, A., French, J. A., Marten, M. R., & Rao, G. (2006). Optical Analysis of Liquid Mixing in a Minibioreactor. *Biotechnology and Bioengineering*, *93*(5), 906–911.

Van Cruchten, S., & Van den Broeck, W. (2002). Morphological and Biochemical Aspects of Apoptosis, Oncosis and Necrosis. *Anatomia, Histologia, Embryologia*, *31*(4), 214–223.

Van Engeland, M., Nieland, L. J. W., Ramaekers, F. C. S., Schutte, B., & Reutelingsperger, C. P. M. (1998). A Review on an Apoptosis Detection System Based on Phosphatidyserine Exposure. *Cytometry*, *31*, 1–9.

Varley, J., & Birch, J. (1999). Reactor Design for Large Scale Suspension Animal Cell Culture. *Cytotechnology*, *29*(3), 177–205.

Verma, R., Boleti, E., & George, A J. (1998). Antibody Engineering: Comparison of Bacterial, Yeast, Insect and Mammalian Expression Systems. *Journal of Immunological Methods*, *216*(1-2), 165–81.

Walsh, G. (2014). Biopharmaceutical Benchmarks 2014. *Nature Biotechnology*, *32*(7), 992–1000.

Weiss, S., John, G. T., Klimant, I., & Heinzle, E. (2002). Modeling of Mixing in 96-Well Microplates Observed with Fluorescence Indicators. *Biotechnology Progress*, *18*(4), 821–30.

Weuster-Botz, D., Altenbach-Rehm, J., & Arnold, M. (2001). Parallel Substrate Feeding and pH-Control in Shaking-Flasks. *Biochemical Engineering Journal*, *7*(2), 163–170.

Whitford, W. G. (2006). Fed-Batch Mammalian Cell Culture in Bioproduction. *BioProcess International*, *4*, 30–40.

Wittmann, C., Kim, H. M., John, G., & Heinzle, E. (2003). Characterization and Application of an Optical Sensor for Quantification of Dissolved O_2 in Shake-Flasks. *Biotechnology Letters*, *25*, 377–380.

Wu, P., Ray, N. G., & Shuler, M. L. (1993). A Computer Model for Intracellular pH Regulation in Chinese Hamster Ovary Cells. *Biotechnology Progress*, *9*(4), 374–384.

Wurm, F. M. (2004). Production of Recombinant Protein Therapeutics in Cultivated Mammalian Cells. *Nature Biotechnology*, *22*(11), 1393–8.

Xie, L., Zhou, W., & Robinson, D. (2003). Protein Production by Large-Scale Mammalian Cell Culture. In *Gene Transfer and Expression in Mammalian Cells (New Comprehensive Biochemistry)* (Vol. 38, pp. 605–623).

Xie, J., Wu, H., Dai, C., Pan, Q., Ding, Z., Hu, D., Hu, X. (2014). Beyond Warburg Effect - Dual Metabolic Nature of Cancer Cells. *Scientific Reports*, *4*, 4927.

Xing, Z., Li, Z., Chow, V., & Lee, S. S. (2008). Identifying Inhibitory Threshold Values of Repressing Metabolites in CHO Cell Culture using Multivariate Analysis Methods. *Biotechnology Progress*, *24*(3), 675–683.

Xing, Z., Bishop, N., Leister, K., & Li, Z. J. (2010). Modeling Kinetics of a Large-Scale Fed-Batch CHO Cell Culture by Markov Chain Monte Carlo Method. *Biotechnology Progress*, *26*(1), 208–19.

Yang, J.-D., Lu, C., Stasny, B., Henley, J., Guinto, W., Gonzalez, C., Ille, E. (2007). Fed-Batch Bioreactor Process Scale-Up from 3-L to 2,500-L Scale for Monoclonal Antibody Production from Cell Culture. *Biotechnology and Bioengineering*, *98*(1), 141–154.

Yavorsky, D., Blanck, R., Lambalot, C., & Brunkow, R. (2003). The Clarification of Bioreactor Cell Cultures for Biopharmaceuticals. *Pharmaceutical Technology*, (March), 62–76.

Yoon, S. K., Ahn, Y., & Han, K. (2002). Enhancement of Recombinant Erythropoietin Production in CHO Cells in an Incubator without CO_2 Addition. *Cytotechnology*, *37*, 119–132.

Yoon, S. K., Kim, S. H., & Lee, G. M. (2003). Effect of Low Culture Temperature on Specific Productivity and Transcription Level of Anti-4-1BB Antibody in Recombinant Chinese Hamster Ovary Cells. *Biotechnology Progress*, *19*(4), 1383–1386.

Yoon, S. K., Choi, S. L., Song, J. Y., & Lee, G. M. (2005). Effect of Culture pH on Erythropoietin Production by Chinese Hamster Ovary Cells Grown in Suspension at 32.5 and 37.0° C. *Biotechnology and Bioengineering*, *89*(3), 345–356.

Yoon, S. K., Hong, J. K., Choo, S. H., Song, J. Y., Park, H. W., & Lee, G. M. (2006a). Adaptation of Chinese Hamster Ovary Cells to Low Culture Temperature: Cell Growth and Recombinant Protein Production. *Journal of Biotechnology*, *122*(4), 463–472.

Yoon, S. K., Kim, S. H., Song, J. Y., & Lee, G. M. (2006b). Biphasic Culture Strategy for Enhancing Volumetric Erythropoietin Productivity of Chinese Hamster Ovary Cells. *Enzyme and Microbial Technology*, *39*(3), 362–365.

Yuk, I. H., Zhang, B., Yang, Y., Dutina, G., Leach, K. D., Vijayasankaran, N., Joly, J. C. (2011). Controlling Glycation of Recombinant Antibody in Fed-Batch Cell Cultures. *Biotechnology and Bioengineering*, *108*(11), 2600–2610.

Yun, H. S., & Gyun, M. L. (2005). Enhanced Human Thrombopoietin Production by Sodium Butyrate Addition to Serum-Free Suspension Culture of Bcl-2-Overexpressing CHO Cells. *Biotechnology Progress*, *21*(1), 50–57.

Zagari, F., Jordan, M., Stettler, M., Broly, H., & Wurm, F. M. (2013). Lactate Metabolism Shift in CHO

Cell Culture: the Role of Mitochondrial Oxidative Activity. *New Biotechnology*, *30*(2), 238–45.

Zanghi, J. a., Schmelzer, A. E., Mendoza, T. P., Knop, R. H., & Miller, W. M. (1999). Bicarbonate Concentration and Osmolality are Key Determinants in the Inhibition of CHO Cell Polysialylation under Elevated pCO_2 or pH. *Biotechnology and Bioengineering*, *65*(2), 182–191.

Zeng, A P. (1996). Mathematical Modeling and Analysis of Monoclonal Antibody Production by Hybridoma Cells. *Biotechnology and Bioengineering*, *50*(3), 238–247.

Zhang, H., Williams-Dalson, W., Keshavarz-Moore, E., & Shamlou, P. A. (2005). Computational-Fluid-Dynamics (CFD) Analysis of Mixing and Gas-Liquid Mass Transfer in Shake Flasks. *Biotechnology and Applied Biochemistry*, *41*, 1–8.

Zhang, H., Lamping, S. R., Pickering, S. C. R., Lye, G. J., & Shamlou, P. A. (2008). Engineering Characterisation of a Single Well from 24-Well and 96-Well Microtitre Plates. *Biochemical Engineering Journal*, *40*(1), 138–149.

Zheng, J. Y., & Janis, L. J. (2006). Influence of pH, Buffer Species, and Storage Temperature on Physicochemical Stability of a Humanized Monoclonal Antibody LA298. *International Journal of Pharmaceutics*, *308*(1-2), 46–51.

Zhou, W., Rehm, J., Europa, A., & Hu, W. S. (1997). Alteration of Mammalian Cell Metabolism by Dynamic Nutrient Feeding. *Cytotechnology*, *24*(2), 99–108.

Zhou, M., Crawford, Y., Ng, D., Tung, J., Pynn, A. F. J., Meier, A., Shen, A. (2011). Decreasing Lactate Level and Increasing Antibody Production in Chinese Hamster Ovary cells (CHO) by Reducing the Expression of Lactate Dehydrogenase and Pyruvate Dehydrogenase Kinases. *Journal of Biotechnology*, *153*(1-2), 27–34.

Zhu, M. M., Goyal, A., Rank, D. L., Gupta, S. K., Vanden Boom, T., & Lee, S. S. (2005). Effects of Elevated pCO_2 and Osmolality on Growth of CHO Cells and Production of Antibody-Fusion Protein B1: A Case Study. *Biotechnology Progress*, *21*(1), 70–77.

Zielke, H. R., Ozand, P. T., Tildon, J. T., Sevdalian, D. A., & Cornblath, M. (1978). Reciprocal Regulation of Glucose and Glutamine Utilization by Cultured Human Diploid Fibroblasts. *Journal of Cellular Physiology*, *95*(1), 41–8.

Zielke, H. R., Sumbilla, C. M., Zielke, C. L., Tildon, J. T., & Ozand, P. T. (1984). Glutamine Metabolism by Cultured Mammalian Cells. In D. Häussinger & H. Sies (Eds.), *Glutamine Metabolism in Mammalian Tissues* (pp. 247–254). Berlin, Heidelberg: Springer Berlin Heidelberg.

Zimmermann, H. F., John, G. T., Trauthwein, H., Dingerdissen, U., & Huthmacher, K. (2003). Rapid Evaluation of Oxygen and Water Permeation Through Microplate Sealing Tapes. *Biotechnology Progress*, *19*(3), 1061–1063.

Appendix A: Spearman´s Rank Correlation Coefficient

Spearman´s rank correlation coefficients (r) is a nonparametric measure of statistical dependence between two variables. The assignment of ranks to experimental values of *n* ranked variables is the first step in nonparametric statistical assays. Where rank 1 corresponds to the highest value, rank 2 to the second-highest value, etc., until rank *n*, which marks the lowest value. Next, the rank differences d_i of the two series and the sums from rank square differences $\sum d_i^2$ have to be calculated. The formula for the rank correlation coefficient, *r*, is given by,

$$r = 1 - \frac{6 \sum d_i^2}{n^3 - n}$$

Equation A.1

according to Spearman (Olds, 1938). The theoretical rank correlation coefficients *r* range from –1 to +1 and the values can be interpreted as follow, for values of $|r|$ of 0.9 to 1, the correlation is very strong; for values between 0.7 and 0.9, the correlation is strong; for values between 0.5 and 0.7 the correlation is moderate; for values lower than 0.5 the correlation is low and for r values smaller than 0.2 the correlation is negligible.

In this work, the variables of interest were, viable cell number (VCN); cell viability (Viab), IgG4 concentration (IgG4); glutamate concentration (Glu); glucose concentration (Gluc); lactate concentration (Lact), ammonium concentration (Amm), osmolality (Osm), pH, temperature (T), CO_2 concentration and volume of base added to 5L-STR.

The end result of Spearman´s rank correlation coefficients (*r*) determination for *n* variables is a lower triangular $n \times n$ matrix. For each CHO-CY01 cell line culture a Spearman´s rank correlation coefficients $n \times n$ matrix was generated and presented in a table. The very strong and strong correlations are indicated in bold.

Table A-1: Spearman´s rank correlation coefficients (*r*) determined for 24-SRW MTP CHO-CY01 cell batch cultures with different fill volumes (0.50, 0.85, 1.00 and 1.50 mL).

0.50 mL	VCN	Viab	IgG4	Glu	Gluc	Lact	Amm	Osm
VCN	1.00							
Viab	0.40	1.00						
IgG4	0.42	-0.10	1.00					
Glu	-0.63	-0.54	-0.33	1.00				
Gluc	**-0.78**	-0.35	**-0.72**	**0.81**	1.00			
Lact	0.51	-0.17	**0.72**	-0.18	-0.69	1.00		
Amm	0.37	-0.22	**0.73**	-0.09	-0.61	**0.95**	1.00	
Osm	-0.17	-0.56	-0.01	**0.76**	0.41	0.21	0.15	1.00

0.85 mL	VCN	Viab	IgG4	Glu	Gluc	Lact	Amm	Osm
	1.00							
	-0.20	1.00						
	0.73	**-0.73**	1.00					
	-0.88	0.53	**-0.90**	1.00				
	-0.91	0.43	**-0.88**	**0.96**	1.00			
	0.35	0.50	-0.11	0.09	-0.03	1.00		
	0.90	-0.38	**0.82**	**-0.86**	**-0.93**	0.15	1.00	
	0.39	-0.29	0.33	-0.41	-0.47	-0.27	0.60	1.00

1.00 mL								
VCN	1.00							
Viab	0.29	1.00						
IgG4	0.47	-0.66	1.00					
Glu	-0.69	0.39	**-0.87**	1.00				
Gluc	**-0.70**	0.46	**-0.91**	**0.94**	1.00			
Lact	0.46	0.30	0.04	-0.17	-0.23	1.00		
Amm	0.36	**-0.74**	**0.88**	**-0.72**	**-0.87**	0.14	1.00	
Osm	-0.02	0.31	-0.15	0.14	0.26	-0.03	-0.35	1.00

1.50 mL								
	1.00							
	0.56	1.00						
	0.74	0.24	1.00					
	-0.82	-0.32	**-0.95**	1.00				
	-0.95	-0.46	**-0.89**	**0.94**	1.00			
	0.47	0.44	-0.11	0.00	-0.29	1.00		
	0.90	0.46	0.70	-0.69	**-0.88**	0.56	1.00	
	-0.34	-0.13	-0.58	0.61	0.45	0.51	-0.08	1.00

Table A-2: Spearman´s rank correlation coefficients (*r*) determined for 24-SRW MTP CHO-CY01 cell batch cultures at different shaking speeds (100, 150, 180, 220, 250 and 300 rpm).

100 rpm	*VCN*	*Viab*	*IgG4*	*Glu*	*Gluc*	*Lact*	*Amm*	*Osm*	*pH*
VCN	1.00								
Viab	0.44	1.00							
IgG4	0.61	-0.39	1.00						
Glu	-0.29	0.10	-0.55	1.00					
Gluc	-0.44	0.53	**-0.88**	0.65	1.00				
Lact	0.44	-0.56	**0.86**	-0.39	**-0.93**	1.00			
Amm	0.32	-0.67	**0.90**	-0.53	**-0.95**	**0.96**	1.00		
Osm	0.26	-0.39	0.55	0.22	-0.39	0.69	0.60	1.00	
pH	-0.03	**0.80**	-0.60	0.36	**0.81**	**-0.89**	**-0.89**	**-0.76**	1.00

150 rpm	*VCN*	*Viab*	*IgG4*	*Glu*	*Gluc*	*Lact*	*Amm*	*Osm*	*pH*
	1.00								
	0.28	1.00							
	0.50	-0.63	1.00						
	-0.60	0.55	**-0.99**	1.00					
	-0.72	0.44	**-0.94**	**0.97**	1.00				
	0.41	0.44	-0.29	0.21	-0.01	1.00			
	0.56	-0.57	**0.91**	**-0.91**	**-0.94**	-0.04	1.00		
	-0.08	0.62	**-0.77**	**0.74**	0.57	**0.77**	-0.53	1.00	
	-0.53	-0.43	0.17	-0.09	0.15	**-0.96**	-0.08	-0.67	1.00

180 rpm									
VCN	1.00								
Viab	0.36	1.00							
IgG4	0.51	-0.57	1.00						
Glu	-0.51	0.57	**-0.99**	1.00					
Gluc	-0.67	0.44	**-0.96**	**0.95**	1.00				
Lact	0.55	0.43	-0.10	0.09	-0.16	1.00			
Amm	0.53	-0.51	**0.80**	**-0.81**	**-0.90**	0.37	1.00		
Osm	-0.06	0.42	-0.62	0.60	0.43	**0.75**	-0.12	1.00	
pH	-0.58	0.11	-0.39	0.40	0.61	**-0.77**	**-0.84**	-0.38	1.00

220 rpm									
	1.00								
	0.22	1.00							
	0.60	-0.56	1.00						
	-0.65	0.55	**-0.96**	1.00					
	-0.77	0.42	**-0.93**	**0.95**	1.00				
	0.39	0.46	-0.27	0.18	-0.07	1.00			
	0.58	-0.54	**0.80**	**-0.82**	**-0.88**	0.10	1.00		
	-0.37	0.47	**-0.79**	**0.79**	0.66	0.61	-0.50	1.00	

250 rpm									
VCN	1.00								
Viab	0.25	1.00							
IgG4	0.61	-0.59	1.00						
Glu	-0.59	0.61	**-0.96**	1.00					
Gluc	**-0.72**	0.49	**-0.95**	**0.96**	1.00				
Lact	0.48	0.45	-0.12	0.02	-0.17	1.00			
Amm	0.57	-0.56	**0.86**	**-0.87**	**-0.94**	0.17	1.00		
Osm	0.06	**0.85**	**-0.71**	0.66	0.52	0.66	-0.49	1.00	
pH	-0.45	-0.27	0.00	0.11	0.28	**-0.94**	-0.30	-0.52	1.00

300 rpm									
	1.00								
	0.43	1.00							
	0.39	-0.60	1.00						
	-0.34	0.55	**-0.97**	1.00					
	-0.63	0.42	**-0.94**	**0.87**	1.00				
	0.40	0.54	-0.38	0.48	0.13	1.00			
	0.39	-0.50	**0.80**	-0.67	**-0.84**	0.12	1.00		
	0.17	0.53	-0.49	0.53	0.33	**0.92**	0.00	1.00	
	-0.51	-0.52	0.33	-0.47	-0.02	**-0.91**	-0.11	-0.69	1

Table A-3: Spearman´s rank correlation coefficients (*r*) determined for 24-SRW MTP CHO-CY01 cell batch cultures sealed with CR1524 and CR1524a ´system Duetz` lids at 2.00% (v/v) CO_2.

CR1524	*VCN*	*Viab*	*IgG4*	*Glu*	*Gluc*	*Lact*	*Amm*	*Osm*	*pH*
VCN	1.00								
Viab	0.36	1.00							
IgG4	0.50	-0.55	1.00						
Glu	-0.51	0.50	**-0.98**	1.00					
Gluc	-0.56	0.50	**-0.87**	**0.88**	1.00				
Lact	0.62	-0.04	0.41	-0.47	**-0.71**	1.00			
Amm	**0.73**	-0.14	0.65	-0.63	**-0.84**	**0.90**	1.00		
Osm	-0.02	**0.70**	-0.58	0.61	**0.80**	-0.41	-0.48	1.00	
pH									

CR1524a	*VCN*	*Viab*	*IgG4*	*Glu*	*Gluc*	*Lact*	*Amm*	*Osm*	*pH*
	1.00								
	-0.17	1.00							
	0.98	-0.53	1.00						
	-0.88	0.58	**-0.96**	1.00					
	-0.99	0.17	**-0.92**	**0.87**	1.00				
	0.57	0.60	0.20	-0.03	-0.51	1.00			
	0.46	**0.76**	-0.05	0.21	-0.28	**0.91**	1.00		
	-0.88	0.11	**-0.81**	**0.77**	**0.92**	-0.59	-0.32	1.00	

Table A-4: Spearman´s rank correlation coefficients (*r*) determined for CHO-CY01 cell batch in a standard 24-SRW MTP and in HydroDish®HD24 at 5.00% (v/v) CO_2.

24-SRW MTP	*VCN*	*Viab*	*IgG4*	*Glu*	*Gluc*	*Lact*	*Amm*	*Osm*	*pH*
VCN	1.00								
Viab	0.03	1.00							
IgG4	**0.94**	0.12	1.00						
Glu	**-0.90**	0.16	**-0.85**	1.00	0.00				
Gluc	**-0.93**	0.00	**-0.93**	**0.95**	1.00				
Lact	0.28	**0.83**	0.19	0.00	-0.13	1.00			
Amm	0.52	0.62	0.58	-0.32	-0.56	**0.70**	1.00		
Osm	-0.67	0.13	-0.68	**0.77**	**0.81**	0.17	-0.32	1.00	
pH									

HydroDish® HD24	*VCN*	*Viab*	*IgG4*	*Glu*	*Gluc*	*Lact*	*Amm*	*Osm*	*pH*
	1.00								
	-0.30	1.00							
	0.86	-0.60	1.00						
	-0.93	0.50	**-0.85**	**0.88**	1.00				
	-0.48	0.43	-0.35	0.64	0.26	1.00			
	0.62	-0.67	**0.77**	-0.29	-0.64	0.24	1.00		
	-0.75	**0.79**	-0.67	**0.75**	0.51	**0.75**	-0.23	1.00	
	-0.04	-0.29	-0.15	0.27	0.48	-0.34	-0.23	-0.32	1.00
	0.53	-0.21	0.70	-0.49	**-0.77**	0.19	**0.70**	-0.05	**-0.76**

Table A-5: Spearman´s rank correlation coefficients (*r*) determined for CHO-CY01 cell batch in a standard 24-SRW MTP and in HydroDish®HD24 at 2.00% (v/v) CO_2.

24-SRW MTP	*VCN*	*Viab*	*IgG4*	*Glu*	*Gluc*	*Lact*	*Amm*	*Osm*	*pH*
VCN	1.00								
Viab	-0.17	1.00							
IgG4	**0.98**	-0.53	1.00						
Glu	**-0.88**	0.58	**-0.96**	1.00					
Gluc	**-0.99**	0.17	**-0.92**	**0.87**	1.00				
Lact	0.57	0.60	0.20	-0.03	-0.51	1.00			
Amm	0.46	**0.76**	-0.05	0.21	-0.28	**0.91**	1.00		
Osm	**-0.88**	0.11	**-0.81**	**0.77**	**0.92**	-0.59	-0.32	1.00	
pH									
T									

HydroDish® HD24	*VCN*	*Viab*	*IgG4*	*Glu*	*Gluc*	*Lact*	*Amm*	*Osm*	*pH*	*T*
	1.00									
	0.45	1.00								
	0.93	0.26	1.00							
	-0.83	-0.39	**-0.93**	1.00						
	-0.97	-0.26	**-0.90**	**0.85**	1.00					
	0.62	-0.21	0.24	-0.05	-0.56	1.00				
	0.65	0.08	0.13	0.05	-0.46	**0.91**	1.00			
	-0.79	0.02	-0.56	0.34	**0.76**	**-0.89**	**-0.81**	1.00		
	-0.45	-0.49	0.17	-0.24	0.11	-0.51	**-0.80**	0.40	1.00	
	0.61	-0.23	0.28	-0.11	-0.58	**0.97**	**0.81**	**-0.90**	-0.37	1.00

Table A-6: Spearman´s rank correlation coefficients (*r*) determined of 24-SRW MTP CHO-CY01 cell batch cultures with different MSX concentrations (0, 25, 50 and 75 µM).

***0* µM**	*VCN*	*Viab*	*IgG4*	*Glu*	*Gluc*	*Lact*	*Amm*	*Osm*	*pH*
VCN	1.00								
Viab	0.52	1.00							
IgG4	0.34	-0.49	1.00						
Glu	-0.41	0.45	**-0.97**	1.00					
Gluc	-0.40	0.53	**-0.96**	**0.95**	1.00				
Lact	0.56	-0.38	**0.85**	**-0.85**	**-0.96**	1.00			
Amm	0.56	-0.38	**0.91**	**-0.91**	**-0.98**	**0.99**	1.00		
Osm	**0.86**	0.32	0.40	-0.35	-0.47	0.64	0.63	1.00	
pH									

***25* µM**	*VCN*	*Viab*	*IgG4*	*Glu*	*Gluc*	*Lact*	*Amm*	*Osm*	*pH*
	1.00								
	0.08	*1.00*							
	0.43	*-0.81*	*1.00*						
	-0.68	0.62	**-0.92**	1.00					
	-0.71	0.63	**-0.93**	**0.96**	1.00				
	0.88	0.34	0.07	-0.34	-0.42	1.00			
	0.83	-0.42	**0.73**	**-0.85**	**-0.92**	0.69	1.00		
	0.27	**0.87**	-0.65	0.39	0.41	0.59	-0.12	1.00	
	-0.65	0.68	**-0.92**	**0.95**	**0.97**	-0.34	**-0.88**	0.51	1.00

***50* µM**	*VCN*	*Viab*	*IgG4*	*Glu*	*Gluc*	*Lact*	*Amm*	*Osm*	*pH*
VCN	1.00								
Viab	0.36	1.00							
IgG4	**0.71**	-0.33	1.00						
Glu	**-0.72**	0.24	**-0.98**	1.00					
Gluc	**-0.76**	0.32	**-0.97**	**0.91**	1.00				
Lact	**0.80**	-0.21	**0.89**	**-0.81**	**-0.97**	1.00			
Amm	**0.80**	-0.21	**0.91**	**-0.83**	**-0.97**	**0.99**	1.00		
Osm	0.22	0.15	0.21	-0.21	-0.25	0.30	0.27	1.00	
pH									

***75* µM**	*VCN*	*Viab*	*IgG4*	*Glu*	*Gluc*	*Lact*	*Amm*	*Osm*	*pH*
	1.00								
	0.32	1.00							
	0.91	0.24	1.00						
	-0.86	-0.02	**-0.94**	1.00					
	-0.99	-0.21	**-0.93**	**0.88**	1.00				
	0.70	0.52	0.56	-0.27	-0.67	1.00			
	0.60	0.65	0.45	-0.15	-0.56	**0.97**	1.00		
	-0.60	0.21	-0.43	**0.83**	0.62	0.08	0.20	1.00	

Table A-7: Spearman´s rank correlation coefficients (*r*) determined for CHO-CY01 cell batch culture at different bioreactor scales, 5L-STR; 24-SRW MTP; SF 125 mL and SF 250 mL.

5L-STR	*VCN*	*Viab*	*IgG4*	*Glu*	*Gluc*	*Lact*	*Amm*	*Osm*	*pH*	*T*	CO_2	*Base*
VCN	1.00											
Viab	0.38	1.00										
IgG4	0.33	**-0.71**	1.00									
Glu	**-0.70**	0.36	**-0.89**	1.00								
Gluc	-0.69	0.40	**-0.89**	**0.99**	1.00							
Lact	**0.73**	0.48	-0.13	-0.27	-0.32	1.00						
Amm	0.24	**-0.72**	**0.89**	**-0.75**	**-0.81**	0.00	1.00					
Osm	-0.03	**0.73**	**-0.85**	0.67	0.64	0.43	-0.66	1.00				
pH	-0.48	-0.27	0.12	0.11	0.23	**-0.80**	-0.15	-0.44	1.00			
T	-0.27	-0.30	0.09	0.13	0.13	-0.35	0.03	0.10	0.12	1.00		
CO_2	-0.55	0.41	**-0.89**	**0.93**	**0.89**	-0.01	-0.63	**0.80**	-0.13	0.09	1.00	
Base	0.39	0.23	-0.14	-0.06	-0.17	**0.70**	0.10	0.43	**-0.97**	-0.05	0.12	1.00

24-SRW MTP	*VCN*	*Viab*	*IgG4*	*Glu*	*Gluc*	*Lact*	*Amm*	*Osm*	*pH*	*T*
VCN	1.00									
Viab	0.25	1.00								
IgG4	0.60	-0.56	1.00							
Glu	-0.63	0.56	**-0.97**	1.00						
Gluc	-0.64	0.58	**-0.95**	**0.97**	1.00					
Lact	0.62	0.55	-0.13	0.04	-0.06	1.00				
Amm	0.57	-0.60	**0.81**	**-0.85**	**-0.94**	0.21	1.00			
Osm	-0.10	0.59	**-0.74**	0.68	0.57	0.68	-0.37	1.00		
pH	**-0.72**	-0.47	-0.04	0.12	0.23	**-0.94**	-0.35	-0.48	1.00	
T	0.41	-0.17	0.43	-0.41	-0.48	0.34	0.53	0.12	-0.29	1.00

SF 125 mL	*VCN*	*Viab*	*IgG4*	*Glu*	*Gluc*	*Lact*	*Amm*	*Osm*
VCN	1.00							
Viab	0.35	1.00						
IgG4	0.61	-0.46	1.00					
Glu	-0.63	0.43	**-0.98**	1.00				
Gluc	-0.60	0.52	**-0.97**	**0.95**	1.00			
Lact	0.47	0.56	-0.13	0.20	0.04	1.00		
Amm	0.00	**-0.84**	0.59	-0.51	**-0.71**	-0.05	1.00	
Osm	-0.51	0.30	**-0.76**	0.70	**0.71**	0.15	-0.35	1.00

SF 250 mL	*VCN*	*Viab*	*IgG4*	*Glu*	*Gluc*	*Lact*	*Amm*	*Osm*
VCN	1.00							
Viab	0.06	1.00						
IgG4	**0.71**	-0.64	1.00					
Glu	**-0.83**	0.48	**-0.96**	1.00				
Gluc	**-0.78**	0.55	**-0.95**	**0.98**	1.00			
Lact	0.61	0.47	0.06	-0.19	-0.20	1.00		
Amm	0.45	**-0.82**	**0.86**	**-0.81**	**-0.87**	0.06	1.00	
Osm	-0.56	0.13	-0.54	0.61	0.60	-0.10	-0.31	1.00

Table A-8: Spearman´s rank correlation coefficients (*r*) determined for CHO-CY01 cell batch culture at different initial lactate concentrations (0.0, 0.7, 1.9, 2.7, 3.6 and 4.7 $g\ L^{-1}$).

0.0 g/L	*VCN*	*Viab*	*IgG4*	*Glu*	*Gluc*	*Lact*	*Amm*	*Osm*
VCN	1.00							
Viab	0.35	1.00						
IgG4	0.61	-0.46	1.00					
Glu	-0.63	0.43	**-0.98**	1.00				
Gluc	-0.60	0.52	**-0.97**	**0.95**	1.00			
Lact	0.47	0.56	-0.13	0.20	0.04	1.00		
Amm	0.00	**-0.84**	0.59	-0.51	**-0.71**	-0.05	1.00	
Osm	-0.51	0.30	**-0.76**	0.70	**0.71**	0.15	-0.35	1.00

0.7 g/L	*VCN*	*Viab*	*IgG4*	*Glu*	*Gluc*	*Lact*	*Amm*	*Osm*
VCN	1.00							
Viab	0.30	1.00						
IgG4	0.29	**-0.82**	1.00					
Glu	**-0.70**	0.44	**-0.84**	1.00				
Gluc	-0.60	0.54	**-0.90**	**0.97**	1.00			
Lact	0.07	**0.76**	**-0.73**	0.47	0.48	1.00		
Amm	0.18	**-0.74**	**0.86**	**-0.73**	**-0.83**	-0.38	1.00	
Osm	-0.47	0.68	**-0.96**	**0.93**	**0.96**	0.69	**-0.80**	1.00

1.9 g/L	*VCN*	*Viab*	*IgG4*	*Glu*	*Gluc*	*Lact*	*Amm*	*Osm*
VCN	1.00							
Viab	0.41	1.00						
IgG4	0.17	**-0.79**	1.00					
Glu	-0.65	0.39	**-0.82**	1.00				
Gluc	-0.36	0.68	**-0.95**	**0.91**	1.00			
Lact	0.08	**0.86**	**-0.89**	0.65	**0.85**	1.00		
Amm	-0.04	**-0.91**	**0.92**	-0.67	**-0.88**	**-0.88**	1.00	
Osm	-0.40	0.63	**-0.93**	**0.93**	**0.96**	**0.84**	**-0.84**	1.00

2.7 g/L	*VCN*	*Viab*	*IgG4*	*Glu*	*Gluc*	*Lact*	*Amm*	*Osm*
VCN	1.00							
Viab	0.41	1.00						
IgG4	0.17	**-0.79**	1.00					
Glu	-0.65	0.39	**-0.82**	1.00				
Gluc	-0.36	0.68	**-0.95**	**0.91**	1.00			
Lact	0.08	**0.86**	**-0.89**	0.65	**0.85**	1.00		
Amm	-0.04	**-0.91**	**0.92**	-0.67	**-0.88**	**-0.88**	1.00	
Osm	-0.40	0.63	**-0.93**	**0.93**	**0.96**	**0.84**	**-0.84**	1.00

3.6 g/L	*VCN*	*Viab*	*IgG4*	*Glu*	*Gluc*	*Lact*	*Amm*	*Osm*
VCN	1.00							
Viab	-0.18	1.00						
IgG4	**0.82**	-0.63	1.00					
Glu	**-0.84**	0.45	**-0.89**	1.00				
Gluc	-0.48	**0.81**	**-0.80**	0.62	1.00			
Lact	**-0.83**	**0.91**	**-0.93**	**0.92**	**0.74**	1.00		
Amm	0.58	**-0.85**	**0.84**	**-0.82**	**-0.83**	**-0.97**	1.00	
Osm	**-0.75**	0.43	**-0.77**	**0.92**	0.53	**0.80**	**-0.77**	1.00

4.7 g/L	*VCN*	*Viab*	*IgG4*	*Glu*	*Gluc*	*Lact*	*Amm*	*Osm*
VCN	1.00							
Viab	**0.70**	1.00						
IgG4	-0.63	**-0.89**	1.00					
Glu	0.64	**0.76**	**-0.72**	1.00				
Gluc	0.51	**0.93**	**-0.94**	**0.72**	1.00			
Lact	0.47	**0.91**	**-0.93**	**0.71**	**0.99**	1.00		
Amm	-0.51	**-0.92**	**0.95**	**-0.74**	**-0.99**	**-0.99**	1.00	
Osm	0.58	**0.96**	**-0.93**	**0.75**	**0.99**	**0.99**	**-0.99**	1.00

Table A-9: Spearman´s rank correlation coefficients (r) determined for CHO-CY01 cell batch culture at different initial ammonium concentrations (0.2, 4.8, 7.1, 9.7 and 11.2 $mmol\ L^{-1}$).

0.2 mM	*VCN*	*Viab*	*IgG4*	*Glu*	*Gluc*	*Lact*	*Amm*	*Osm*
VCN	1.00							
Viab	0.35	1.00						
IgG4	0.61	-0.46	1.00					
Glu	-0.63	0.43	**-0.98**	1.00				
Gluc	-0.60	0.52	**-0.97**	**0.95**	1.00			
Lact	0.47	0.56	-0.13	0.20	0.04	1.00		
Amm	0.00	**-0.84**	0.59	-0.51	**-0.71**	-0.05	1.00	
Osm	-0.51	0.30	**-0.76**	0.70	**0.71**	0.15	-0.35	1.00

4.8 mM	*VCN*	*Viab*	*IgG4*	*Glu*	*Gluc*	*Lact*	*Amm*	*Osm*
	1.00							
	0.26	1.00						
	0.55	-0.55	1.00					
	-0.62	0.50	**-0.97**	1.00				
	-0.72	0.44	**-0.95**	**0.98**	1.00			
	-0.06	0.48	-0.67	0.55	0.46	1.00		
	-0.48	-0.39	-0.15	0.06	0.14	0.14	1.00	
	-0.61	0.51	**-0.99**	**0.97**	**0.97**	0.67	0.17	1.00

7.1 mM								
VCN	1.00							
Viab	-0.07	1.00						
IgG4	**0.79**	-0.44	1.00					
Glu	**-0.78**	0.62	**-0.89**	1.00				
Gluc	**-0.90**	0.44	**-0.96**	**0.94**	1.00			
Lact	-0.20	0.51	-0.62	0.45	0.44	1.00		
Amm	-0.62	-0.43	-0.58	0.26	0.49	0.27	1.00	
Osm	**-0.83**	0.49	**-0.97**	**0.93**	**0.97**	0.63	0.50	1.00

9.7 mM								
	1.00							
	0.11	1.00						
	0.68	-0.58	1.00					
	-0.79	0.43	**-0.90**	1.00				
	-0.78	0.52	**-0.95**	**0.96**	1.00			
	-0.27	0.49	-0.67	0.47	0.50	1.00		
	-0.89	0.22	**-0.88**	**0.88**	**0.90**	0.54	1.00	
	-0.78	0.51	**-0.97**	**0.95**	**0.98**	0.65	**0.92**	1.00

11.2 mM								
VCN	1.00							
Viab	-0.09	1.00						
IgG4	**0.77**	-0.59	1.00					
Glu	**-0.79**	0.34	**-0.71**	1.00				
Gluc	**-0.80**	0.65	**-0.94**	0.78	1.00			
Lact	-0.19	0.63	-0.61	0.09	0.53	1.00		
Amm	**-0.80**	0.47	**-0.89**	**0.73**	**0.92**	0.51	1.00	
Osm	**-0.76**	0.67	**-0.94**	**0.73**	**0.99**	0.63	**0.94**	1.00

Table A-10: Spearman´s rank correlation coefficients (*r*) determined for CHO-CY01 cell batch culture at different initial sodium concentrations (95, 99, 103, 108 and 118 $mmol\ L^{-1}$).

118 mM	*VCN*	*Viab*	*IgG4*	*Glu*	*Gluc*	*Lact*	*Amm*	*Osm*	*pH*
VCN	1.00								
Viab	0.35	1.00							
IgG4	0.61	-0.46	1.00						
Glu	-0.63	0.43	**-0.98**	1.00					
Gluc	-0.60	0.52	**-0.97**	**0.95**	1.00				
Lact	0.47	0.56	-0.13	0.20	0.04	1.00			
Amm	0.00	**-0.84**	0.59	-0.51	**-0.71**	-0.05	1.00		
Osm	-0.51	0.30	**-0.76**	0.70	**0.71**	0.15	-0.35	1.00	
pH									

108 mM	*VCN*	*Viab*	*IgG4*	*Glu*	*Gluc*	*Lact*	*Amm*	*Osm*	*pH*
	1.00								
	0.27	1.00							
	0.49	-0.66	1.00						
	-0.73	0.42	**-0.93**	1.00					
	-0.69	0.49	**-0.95**	**0.98**	1.00				
	0.16	0.48	-0.46	0.26	0.23	1.00			
	0.46	-0.62	**0.87**	**-0.79**	**-0.88**	-0.14	1.00		
	-0.56	0.59	**-0.99**	**0.94**	**0.96**	0.49	**-0.82**	1.00	
	-0.45	-0.38	0.14	0.08	0.12	**-0.93**	-0.15	-0.16	1.00

103 mM									
VCN	1.00								
Viab	0.22	1.00							
IgG4	0.60	-0.61	1.00						
Glu	**-0.73**	0.47	**-0.97**	1.00					
Gluc	**-0.71**	0.51	**-0.97**	**0.99**	1.00				
Lact	0.06	0.53	-0.50	0.31	0.27	1.00			
Amm	0.50	-0.59	**0.81**	**-0.86**	**-0.89**	-0.05	1.00		
Osm	-0.64	0.58	**-1.00**	**0.98**	**0.97**	0.48	**-0.83**	1.00	
pH	-0.34	-0.31	0.11	0.09	0.13	**-0.91**	-0.33	-0.09	1.00

99 mM									
	1.00								
	0.19	1.00							
	0.70	-0.56	1.00						
	-0.78	0.46	**-0.97**	1.00					
	-0.74	0.52	**-0.97**	**0.99**	1.00				
	-0.01	0.57	-0.50	0.34	0.33	1.00			
	0.52	-0.61	**0.84**	**-0.86**	**-0.91**	-0.21	1.00		
	-0.65	0.62	**-0.99**	**0.96**	**0.97**	0.53	**-0.87**	1.00	
	-0.29	-0.34	0.10	0.08	0.10	**-0.90**	-0.19	-0.13	1.00

95 mM									
VCN	1.00								
Viab	0.22	1.00							
IgG4	0.62	-0.60	1.00						
Glu	-0.70	0.50	**-0.97**	1.00					
Gluc	-0.68	0.54	**-0.98**	**0.99**	1.00				
Lact	-0.08	0.62	-0.67	0.50	0.50	1.00			
Amm	0.44	-0.65	**0.86**	**-0.88**	**-0.91**	-0.35	1.00		
Osm	-0.63	0.60	**-0.99**	**0.98**	**0.99**	0.63	**-0.88**	1.00	
pH	-0.41	-0.28	0.01	0.18	0.18	**-0.72**	-0.28	0.03	1.00

Table A-11: Spearman´s rank correlation coefficients (*r*) determined for different CHO-CY01 cell fed-batch cultures in SF 125 mL and SF 250 mL.

SF 125 mL FB Strategy 2

	VCN	*Viab*	*IgG4*	*Glu*	*Gluc*	*Lact*	*Amm*	*Osm*
VCN	1.00							
Viab	0.08	1.00						
IgG4	0.47	**-0.74**	1.00					
Glu	-0.61	0.68	**-0.95**	1.00				
Gluc	-0.67	0.54	**-0.83**	**0.87**	1.00			
Lact	0.22	0.68	-0.53	0.44	0.09	1.00		
Amm	0.56	0.28	-0.03	-0.07	-0.48	**0.80**	1.00	
Osm	0.05	**0.90**	-0.68	0.64	0.46	**0.74**	0.34	1.00

SF 250 mL FB Strategy 2

	VCN	*Viab*	*IgG4*	*Glu*	*Gluc*	*Lact*	*Amm*	*Osm*
VCN	1.00							
Viab	-0.28	1.00						
IgG4	0.61	**-0.83**	1.00					
Glu	**-0.89**	0.64	**-0.85**	1.00				
Gluc	**-0.81**	0.40	-0.65	**0.83**	1.00			
Lact	-0.19	0.70	-0.58	0.43	-0.01	1.00		
Amm	0.48	-0.34	0.43	-0.51	**-0.81**	0.30	1.00	
Osm	0.33	**-0.81**	**0.82**	-0.59	-0.40	-0.54	0.33	1.00

SF 125 mL FB Strategy 3

	VCN	*Viab*	*IgG4*	*Glu*	*Gluc*	*Lact*	*Amm*	*Osm*
VCN	1.00							
Viab	-0.22	1.00						
IgG4	0.34	**-0.86**	1.00					
Glu	**-0.85**	0.66	**-0.73**	1.00				
Gluc	-0.62	0.19	-0.24	0.52	1.00			
Lact	0.06	0.68	-0.51	0.35	-0.40	1.00		
Amm	0.65	-0.15	0.25	-0.50	**-0.92**	0.51	1.00	
Osm	**0.84**	-0.43	0.47	**-0.86**	-0.40	-0.25	0.43	1.00

SF 250 mL FB Strategy 3

	VCN	*Viab*	*IgG4*	*Glu*	*Gluc*	*Lact*	*Amm*	*Osm*
VCN	1.00	0.00						
Viab	-0.43	1.00						
IgG4	0.62	**-0.89**	1.00					
Glu	**-0.95**	0.66	**-0.79**	1.00				
Gluc	-0.56	0.11	-0.32	0.53	1.00			
Lact	-0.27	**0.71**	-0.60	0.44	-0.40	1.00		
Amm	0.56	-0.44	0.52	-0.59	**-0.84**	0.21	1.00	
Osm	0.67	**-0.82**	**0.89**	**-0.79**	-0.33	-0.52	0.57	1.00

SF 125 mL FB Strategy 4

	VCN	*Viab*	*IgG4*	*Glu*	*Gluc*	*Lact*	*Amm*	*Osm*
VCN	1.00							
Viab	-0.16	1.00						
IgG4	0.52	**-0.87**	1.00					
Glu	**-0.85**	0.60	**-0.86**	1.00				
Gluc	**-0.85**	0.58	**-0.82**	**0.96**	1.00			
Lact	0.04	0.58	-0.53	0.34	0.16	1.00		
Amm	0.45	-0.35	0.41	-0.50	-0.67	0.40	1.00	
Osm	**-0.91**	0.52	**-0.96**	**0.96**	**0.89**	0.17	-0.42	1.00

SF 250 mL FB Strategy 4

	VCN	*Viab*	*IgG4*	*Glu*	*Gluc*	*Lact*	*Amm*	*Osm*
VCN	1.00							
Viab	-0.13	1.00						
IgG4	0.55	**-0.83**	1.00					
Glu	**-0.84**	0.53	**-0.86**	1.00				
Gluc	**-0.90**	0.46	**-0.79**	**0.95**	1.00			
Lact	0.05	0.35	-0.46	0.31	0.08	1.00		
Amm	**0.77**	-0.50	**0.74**	**-0.81**	**-0.91**	0.05	1.00	
Osm	**-0.77**	-0.24	-0.31	0.64	**0.71**	-0.32	-0.51	1.00

SF 125 mL FB Strategy 5

	VCN	*Viab*	*IgG4*	*Glu*	*Gluc*	*Lact*	*Amm*	*Osm*
VCN	1.00							
Viab	-0.17	1.00						
IgG4	0.62	**-0.81**	1.00					
Glu	**-0.90**	0.49	**-0.85**	1.00				
Gluc	**-0.89**	0.37	**-0.72**	**0.92**	1.00			
Lact	0.02	0.19	-0.25	0.11	-0.24	1.00		
Amm	0.60	-0.69	**0.79**	**-0.73**	**-0.84**	0.29	1.00	
Osm	0.22	-0.09	0.21	-0.10	-0.02	-0.34	0.02	1.00

SF 250 mL FB Strategy 5

	VCN	*Viab*	*IgG4*	*Glu*	*Gluc*	*Lact*	*Amm*	*Osm*
VCN	1.00							
Viab	-0.24	1.00						
IgG4	0.52	**-0.92**	1.00					
Glu	**-0.95**	0.41	-0.68	1.00				
Gluc	**-0.91**	0.42	-0.65	**0.94**	1.00			
Lact	-0.08	0.55	-0.57	0.22	0.02	1.00		
Amm	0.53	-0.64	**0.72**	-0.63	**-0.79**	0.10	1.00	
Osm	0.30	**-0.93**	**0.86**	-0.35	-0.30	-0.54	0.30	1.00

Table A-12: Spearman´s rank correlation coefficients (*r*) determined for CHO-CY01 cell line fed-batch strategy 4 (FB2) and fed-batch strategy 5 (FB3) cultures at different bioreactor scales, 5L-STR; 24-SRW MTP; SF 125 mL and SF 250 mL.

	VCN	Viab	IgG4	Glu	Gluc	Lact	Amm	Osm	pH	T	CO_2	Base
5L-STR FB2												
VCN	1.00											
Viab	-0.09	1.00										
IgG4	0.52	**-0.81**	1.00									
Glu	**-0.92**	0.33	**-0.72**	1.00								
Gluc	**-0.93**	0.39	**-0.72**	**0.91**	1.00							
Lact	**0.70**	**-0.76**	**0.93**	**-0.82**	**-0.87**	1.00						
Amm	0.52	**-0.85**	**0.93**	-0.66	**-0.74**	**0.95**	1.00					
Osm	0.29	**-0.88**	**0.79**	-0.50	-0.51	**0.81**	**0.87**	1.00				
pH	-0.63	0.11	-0.33	0.52	0.66	-0.47	-0.44	-0.13	1.00			
T	-0.36	0.08	-0.23	0.26	0.37	-0.34	-0.30	-0.17	0.34	1.00		
CO_2	**-0.83**	0.60	**-0.87**	**0.91**	**0.95**	**-0.97**	**-0.89**	-0.69	0.58	0.36	1.00	
Base	0.41	-0.61	0.57	-0.40	-0.64	**0.70**	**0.72**	0.60	-0.42	-0.15	-0.67	1.00

	VCN	Viab	IgG4	Glu	Gluc	Lact	Amm	Osm	pH	T	CO_2	Base
5L-STR FB3												
	0.00											
	0.00	0.00										
	VCN/ml	**%Viab**	igg4 g/l									
	1.00	0.00	0.00	0.00								
	0.00	1.00	0.00	**0.00**	0.00							
	0.47	-0.81	1.00	**0.00**	**0.00**	0.00						
	-0.90	0.23	**-0.69**	1.00	0.00	**0.00**	0.00					
	-0.90	0.01	**-0.49**	**0.82**	1.00	**0.00**	**0.00**	0.00				
	0.88	-0.20	0.66	-0.88	-0.96	1.00	0.00	0.00	0.00			
	0.48	-0.70	0.88	-0.57	-0.62	0.74	1.00	0.00	0.00	0.00		
	0.70	-0.65	0.94	**-0.86**	**-0.67**	**0.80**	0.83	**1.00**	0.00	0.00	0.00	
	-0.01	-0.40	0.38	-0.26	0.26	-0.14	-0.04	0.36	**1.00**	0.00	0.00	0.00

	VCN	Viab	IgG4	Glu	Gluc	Lact	Amm	Osm	pH	T	CO_2	Base
24-SRW MTP FB2												
VCN	1.00											
Viab	-0.32	1.00										
IgG4	0.65	**-0.91**	1.00									
Glu	**-0.89**	0.52	**-0.81**	1.00								
Gluc	**-0.95**	0.44	**-0.75**	**0.96**	1.00							
Lact	0.15	0.53	-0.45	0.19	0.05	1.00						
Amm	**0.82**	-0.60	**0.78**	**-0.75**	**-0.84**	0.11	1.00					
Osm	0.33	**-0.92**	**0.81**	-0.43	-0.39	-0.30	0.62	1.00				
pH	-0.54	0.00	-0.17	0.26	0.40	-0.60	-0.60	-0.19	1.00			
T	-0.06	-0.32	0.24	-0.08	-0.08	-0.18	0.17	0.44	-0.03	1.00		

	VCN	Viab	IgG4	Glu	Gluc	Lact	Amm	Osm	pH	T	CO_2	Base
24-SRW MTP FB3												
	1.00											
	-0.03	1.00										
	0.33	**-0.92**	1.00									
	-0.77	0.33	-0.56	1.00								
	-0.79	0.23	-0.45	**0.89**	1.00							
	-0.14	0.71	**-0.75**	0.42	0.11	1.00						
	0.34	**-0.72**	**0.72**	-0.41	-0.55	-0.19	1.00					
	0.13	**-0.70**	**0.65**	-0.05	0.01	-0.44	0.65	1.00				
	-0.03	0.05	0.02	-0.06	0.30	-0.60	-0.55	-0.13	1.00			
	0.57	-0.47	0.58	-0.48	-0.69	0.00	**0.84**	0.52	-0.68	1.00		

	VCN	Viab	IgG4	Glu	Gluc	Lact	Amm	Osm	pH	T	CO_2	Base
SF 125 mL FB2												
VCN	1.00											
Viab	-0.16	1.00										
IgG4	0.52	**-0.87**	1.00									
Glu	**-0.85**	0.60	**-0.86**	1.00								
Gluc	**-0.85**	0.58	**-0.82**	**0.96**	1.00							
Lact	0.04	0.58	-0.53	0.34	0.16	1.00						
Amm	0.45	-0.35	0.41	-0.50	-0.67	0.40	1.00					
Osm	**-0.91**	0.52	**-0.96**	**0.96**	**0.89**	0.17	-0.42	1.00				

	VCN	Viab	IgG4	Glu	Gluc	Lact	Amm	Osm	pH	T	CO_2	Base
SF 125 mL FB3												
	1.00											
	-0.17	1.00										
	0.62	**-0.81**	1.00									
	-0.90	0.49	**-0.85**	1.00								
	-0.89	0.37	**-0.72**	**0.92**	1.00							
	0.02	0.19	-0.25	0.11	-0.24	1.00						
	0.60	-0.69	**0.79**	**-0.73**	**-0.84**	0.29	1.00					
	0.22	-0.09	0.21	-0.10	-0.02	-0.34	0.02	1.00				

	VCN	Viab	IgG4	Glu	Gluc	Lact	Amm	Osm	pH	T	CO_2	Base
SF 250 mL FB2												
VCN	1.00											
Viab	-0.13	1.00										
IgG4	0.55	**-0.83**	1.00									
Glu	**-0.84**	0.53	**-0.86**	1.00								
Gluc	**-0.90**	0.46	**-0.79**	**0.95**	1.00							
Lact	0.05	0.35	-0.46	0.31	0.08	1.00						
Amm	**0.77**	-0.50	**0.74**	**-0.81**	**-0.91**	0.05	1.00					
Osm	**-0.77**	-0.24	-0.31	0.64	**0.71**	-0.32	-0.51	1.00				

	VCN	Viab	IgG4	Glu	Gluc	Lact	Amm	Osm	pH	T	CO_2	Base
SF 250 mL FB3												
	1.00											
	-0.24	1.00										
	0.52	**-0.92**	1.00									
	-0.95	0.41	-0.68	1.00								
	-0.91	0.42	-0.65	**0.94**	1.00							
	-0.08	0.55	-0.57	0.22	0.02	1.00						
	0.53	-0.64	**0.72**	-0.63	**-0.79**	0.10	1.00					
	0.30	**-0.93**	**0.86**	-0.35	-0.30	-0.54	0.30	1.00				

Table A-13: Spearman´s rank correlation coefficients (*r*) determined for profiles for CHO-CY01 cell line batch cultures in 24-SRW-MTP at different CO_2 (0.04%; 1.00%; 2.00%; 10.00%; 15.00%; and 20.00% (v/v) CO_2).

0.04%	VCN	Viab	IgG4	Glu	Gluc	Lact	Amm	Osm	pH	T	pO_2
VCN	1.00										
Viab	**0.98**	1.00									
IgG4	-0.39	-0.42	1.00								
Glu	-0.31	-0.32	-0.21	1.00							
Gluc	0.61	0.57	**-0.82**	0.35	1.00						
Lact	**-0.71**	-0.69	0.44	0.60	-0.50	1.00					
Amm	**-0.76**	**-0.77**	**0.85**	0.14	**-0.77**	0.67	1.00				
Osm	-0.12	-0.14	-0.33	**0.90**	0.56	0.26	-0.02	1.00			
pH	0.50	0.46	**-0.71**	0.36	**0.72**	-0.11	**-0.73**	0.27	1.00		
T	-0.68	-0.67	0.48	0.49	-0.57	**0.98**	0.64	0.11	-0.08	1.00	
pO_2											

1.00%	VCN	Viab	IgG4	Glu	Gluc	Lact	Amm	Osm	pH	T	pO_2
	1.00										
	-0.12	1.00									
	0.65	**-0.75**	1.00								
	-0.82	0.47	**-0.93**	1.00							
	-0.86	0.55	**-0.90**	**0.92**	1.00						
	0.37	0.50	-0.30	0.09	-0.09	1.00					
	0.76	-0.39	0.51	-0.51	**-0.75**	0.47	1.00				
	-0.40	0.54	-0.62	0.52	0.68	0.01	-0.46	1.00			
	-0.36	-0.59	0.36	-0.13	-0.02	**-0.88**	-0.41	-0.15	1.00		
	0.28	-0.38	0.31	-0.23	-0.45	0.24	0.46	-0.38	0.16	1.00	
	0.41	-0.28	0.32	-0.31	-0.55	0.42	0.54	-0.52	-0.01	**0.90**	1.00

2.00%											
VCN	1.00										
Viab	0.03	1.00									
IgG4	**0.76**	-0.32	1.00								
Glu	-0.69	0.53	**-0.94**	1.00							
Gluc	**-0.79**	0.50	**-0.90**	**0.93**	1.00						
Lact	**0.73**	0.33	0.25	-0.14	-0.41	1.00					
Amm	**0.72**	-0.47	0.52	-0.63	**-0.81**	0.60	1.00				
Osm	-0.06	-0.10	0.04	0.08	0.07	-0.06	-0.02	1.00			
pH	**-0.78**	-0.51	-0.34	0.20	0.36	**-0.87**	-0.43	-0.04	1.00		
T	0.04	0.02	0.00	0.06	-0.11	0.27	0.12	-0.52	0.14	1.00	
pO_2											

10.00%											
	1.00										
	0.38	1.00									
	0.32	**-0.73**	1.00								
	-0.72	0.34	**-0.84**	1.00							
	-0.56	0.54	**-0.93**	**0.95**	1.00						
	0.33	0.59	-0.52	0.11	0.21	1.00					
	0.64	-0.38	**0.81**	**-0.88**	**-0.93**	-0.04	1.00				
	-0.23	0.63	**-0.75**	**0.76**	**0.77**	0.26	-0.66	1.00			
	-0.47	-0.66	0.46	-0.01	-0.15	**-0.98**	-0.03	-0.26	1.00		
	0.30	0.00	0.16	-0.26	-0.28	0.39	0.42	0.02	-0.45	1.00	
	-0.04	-0.46	0.37	-0.24	-0.39	0.11	0.46	-0.19	-0.10	0.86	1.00

15.00%											
VCN	1.00										
Viab	0.30	1.00									
IgG4	0.56	-0.54	1.00								
Glu	**-0.76**	0.34	**-0.95**	1.00							
Gluc	-0.60	0.54	**-0.97**	**0.94**	1.00						
Lact	**0.87**	0.41	0.26	-0.48	-0.39	1.00					
Amm	0.52	-0.64	**0.96**	**-0.91**	**-0.98**	0.30	1.00				
Osm	0.18	-0.64	0.68	-0.60	-0.64	-0.01	**0.73**	1.00			
pH	**-0.72**	0.17	-0.62	**0.74**	**0.72**	-0.67	-0.69	-0.24	1.00		
T	0.03	0.29	-0.33	0.21	0.23	0.25	-0.27	-0.56	-0.31	1.00	
pO_2	**-0.87**	0.04	-0.64	**0.83**	0.70	**-0.75**	-0.66	-0.29	**0.86**	-0.08	1.00

20.00%											
	1.00										
	-0.33	1.00									
	0.94	-0.59	1.00								
	-0.85	0.65	**-0.96**	1.00							
	-0.87	0.69	**-0.96**	**0.98**	1.00						
	0.70	-0.52	**0.71**	**-0.74**	**-0.80**	1.00					
	0.91	-0.43	**0.84**	**-0.79**	**-0.86**	**0.89**	1.00				
	0.05	0.68	-0.27	0.40	0.35	0.04	0.14	1.00			
	0.73	-0.68	**0.88**	**-0.89**	**-0.89**	0.52	0.65	-0.53	1.00		
	-0.43	0.21	-0.46	0.44	0.47	-0.31	-0.42	0.24	-0.50	1.00	

Table A-14: Spearman´s rank correlation coefficients (r) determined for CHO-CY01 cell *line f*ed batch strategy 5 (FB3) cultures in 24-SRW-MTPs at 5.00%, 10.00%, and 15.00% (v/v) CO_2.

5.00%

	VCN	Viab	IgG4	Glu	Gluc	Lact	Amm	Osm	pH	T
VCN	1.00									
Viab	-0.03	1.00								
IgG4	0.33	**-0.92**	1.00							
Glu	**-0.77**	0.33	-0.56	1.00						
Gluc	**-0.79**	0.23	-0.45	**0.89**	1.00					
Lact	-0.14	**0.71**	**-0.75**	0.42	0.11	1.00				
Amm	0.34	**-0.72**	**0.72**	-0.41	-0.55	-0.19	1.00			
Osm	0.13	**-0.70**	0.65	-0.05	0.01	-0.44	0.65	1.00		
pH	-0.03	0.05	0.02	-0.06	0.30	-0.60	-0.55	-0.13	1.00	
T	0.57	-0.47	0.58	-0.48	-0.69	0.00	**0.84**	0.52	-0.68	1.00

10.00%

VCN	1.00									
Viab	-0.03	1.00								
IgG4	0.36	**-0.91**	1.00							
Glu	**-0.80**	0.54	**-0.79**	1.00						
Gluc	**-0.86**	0.38	-0.66	**0.94**	1.00					
Lact	0.03	0.45	-0.51	0.26	0.14	1.00				
Amm	0.60	**-0.72**	**0.90**	**-0.90**	**-0.82**	-0.29	1.00			
Osm	0.12	**-0.86**	**0.82**	-0.52	-0.39	-0.45	0.68	1.00		
pH	-0.32	0.18	-0.19	0.34	0.37	-0.49	-0.40	-0.17	1.00	
T	0.08	0.31	-0.20	-0.03	-0.03	0.25	-0.10	-0.42	-0.21	1.00

15.00%

VCN	1.00									
Viab	-0.02	1.00								
IgG4	0.54	**-0.77**	1.00							
Glu	**-0.76**	0.55	**-0.89**	1.00						
Gluc	**-0.88**	0.43	**-0.82**	**0.95**	1.00					
Lact	0.17	0.44	-0.45	0.25	0.04	1.00				
Amm	**0.92**	-0.35	**0.83**	**-0.89**	**-0.97**	0.05	1.00			
Osm	0.12	-0.18	0.21	-0.02	-0.12	0.04	0.26	1.00		
pH	-0.62	-0.12	-0.08	0.21	0.44	**-0.73**	-0.52	-0.22	1.00	
T	0.21	0.08	-0.01	0.10	-0.08	0.44	0.20	0.34	**-0.73**	1.00

Table A-15: Spearman´s rank correlation coefficients (*r*) determined for CHO-CY01 cell line batch culture at constant 5.00% (v/v) CO_2 and the first CO_2 multiphasic CHO-CY01 cell line batch cultivation in 24-SRW-MTPs (pH shift 1).

5.00%	VCN	Viab	IgG4	Glu	Gluc	Lact	Amm	Osm	pH	T	CO_2
VCN	VCN/ml										
Viab	0.00	0.00									
IgG4	1.00	0.00	0.00								
Glu	0.42	0.00	**0.40**	0.00							
Gluc	0.06	0.36	**-0.42**	**0.00**	0.00						
Lact	-0.63	0.56	-0.97	1.00	0.00	0.00					
Amm	-0.64	0.58	**-0.95**	**0.97**	**1.00**	0.00	0.00				
Osm	0.62	0.55	**-0.13**	0.04	-0.06	1.00	0.00	0.00			
pH	**0.57**	-0.60	0.81	-0.85	-0.94	**0.21**	1.00	0.00	0.00		
T	-0.10	0.59	-0.74	0.68	0.57	0.68	-0.37	1.00	0.00	0.00	
CO_2											

pH Shift 1

VCN	1.00										
Viab	-0.25	1.00									
IgG4	**0.83**	-0.57	1.00								
Glu	**-0.75**	0.60	**-0.98**	1.00							
Gluc	**-0.89**	0.53	**-0.97**	**0.94**	1.00						
Lact	**0.95**	-0.33	**0.75**	-0.66	**-0.86**	1.00					
Amm	**0.95**	-0.39	**0.89**	**-0.84**	**-0.95**	**0.94**	1.00				
Osm	-0.13	-0.19	-0.25	0.30	0.23	-0.07	-0.17	1.00			
pH	**-0.78**	-0.17	-0.38	0.26	0.51	**-0.83**	**-0.70**	0.22	1.00		
T	0.20	-0.57	0.28	-0.23	-0.23	0.33	0.30	0.08	-0.21	1.00	
CO_2	**-0.97**	0.41	**-0.85**	**0.77**	**0.93**	**-0.97**	**-0.96**	0.05	**0.73**	-0.28	1.00

Table A-16: Spearman´s rank correlation coefficients (*r*) determined for CHO-CY01 cell line fed batch strategy 5 (FB3) cultures in 24-SRW-MTPs with constant 5.00% (v/v) CO_2, CO_2 shift from 5.00% to 20.00% (v/v) CO_2 on day 7 (1 step) and CO_2 shift from 5.00% to 7.50% on day 2, then to 10.00% on day 7, then to 12.50% on day 8, and then to 15.0% (v/v) CO_2 on day 10 (4 steps).

CO_2 (% (v/v))

	VCN	Viab	IgG4	Glu	Gluc	Lact	Amm	Osm	pH	T	CO_2
5.00											
VCN	1.00										
Viab	-0.03	1.00									
IgG4	0.33	**-0.92**	1.00								
Glu	**-0.77**	0.33	-0.56	1.00							
Gluc	**-0.79**	0.23	-0.45	**0.89**	1.00						
Lact	-0.14	**0.71**	**-0.75**	0.42	0.11	1.00					
Amm	0.34	**-0.72**	**0.72**	-0.41	-0.55	-0.19	1.00				
Osm	0.13	**-0.70**	0.65	-0.05	0.01	-0.44	0.65	1.00			
pH	-0.03	0.05	0.02	-0.06	0.30	-0.60	-0.55	-0.13	1.00		
T	0.57	-0.47	0.58	-0.48	-0.69	0.00	**0.84**	0.52	-0.68	1.00	
CO_2											
5.00 - 20.00 (day 7)											
VCN	1.00										
Viab	-0.16	1.00									
IgG4	**0.84**	-0.61	1.00								
Glu	**-0.94**	0.41	**-0.93**	1.00							
Gluc	**-0.94**	0.28	**-0.83**	**0.91**	1.00						
Lact	**0.72**	-0.62	**0.83**	**-0.78**	**-0.88**	1.00					
Amm	**0.77**	-0.65	**0.89**	**-0.84**	**-0.80**	**0.89**	1.00				
Osm	0.49	**-0.83**	**0.81**	-0.64	-0.48	0.69	**0.87**	1.00			
pH	**-0.87**	0.42	**-0.86**	**0.90**	**0.87**	**-0.86**	**-0.95**	-0.70	1.00		
T	0.48	-0.10	0.37	-0.34	-0.62	0.57	0.44	0.26	-0.38	1.00	
CO_2	0.61	-0.63	**0.78**	-0.67	-0.53	0.65	**0.90**	**0.89**	**-0.80**	0.26	1.00
5.00 - 7.50 - 10.00 -12.50 - 15.00 (day 2, 7, 8, 10)											
VCN	1.00										
Viab	0.05	1.00									
IgG4	**0.70**	-0.37	1.00								
Glu	**-0.89**	0.32	**-0.89**	1.00							
Gluc	**-0.95**	0.15	**-0.78**	**0.94**	1.00						
Lact	0.56	-0.57	0.59	-0.67	**-0.74**	1.00					
Amm	**0.71**	-0.63	**0.85**	**-0.90**	**-0.84**	**0.84**	1.00				
Osm	-0.06	**-0.73**	0.56	-0.31	-0.07	0.38	0.52	1.00			
pH	**-0.72**	0.22	-0.60	**0.70**	**0.85**	**-0.89**	**-0.72**	-0.07	1.00		
T	0.29	-0.03	0.19	-0.22	-0.40	0.62	0.24	0.02	**-0.71**	1.00	
CO_2	0.60	-0.69	**0.81**	**-0.86**	**-0.76**	**0.81**	**0.98**	0.60	-0.65	0.20	1.00

Table A-17: Spearman´s rank correlation coefficients (r) determined CHO-CY01 cell line fed batch strategy 5 (FB3) cultures in 24-SRW-MTPs with constant 10.00% (v/v) CO_2 and CO_2 shifts from 10.00% to 20.00% (v/v) CO_2 at day 3, 5 and 9.

CO_2 (% (v/v))

	VCN	Viab	IgG4	Glu	Gluc	Lact	Amm	Osm	pH	T	CO_2
10.00											
VCN	1.00										
Viab	-0.03	1.00									
IgG4	0.36	**-0.91**	1.00								
Glu	**-0.80**	0.54	**-0.79**	1.00							
Gluc	**-0.86**	0.38	-0.66	**0.94**	1.00						
Lact	0.03	0.45	-0.51	0.26	0.14	1.00					
Amm	0.60	**-0.72**	**0.90**	**-0.90**	**-0.82**	-0.29	1.00				
Osm	0.12	**-0.86**	**0.82**	-0.52	-0.39	-0.45	0.68	1.00			
pH	-0.32	0.18	-0.19	0.34	0.37	-0.49	-0.40	-0.17	1.00		
T	0.08	0.31	-0.20	-0.03	-0.03	0.25	-0.10	-0.42	-0.21	1.00	
CO_2											
10.00 - 20.00 (day 3)											
VCN	1.00										
Viab	-0.47	1.00									
IgG4	**0.83**	-0.63	1.00								
Glu	**-0.95**	0.47	**-0.82**	1.00							
Gluc	**-0.91**	0.48	**-0.80**	**0.97**	1.00						
Lact	0.14	-0.24	-0.21	-0.16	-0.22	1.00					
Amm	**0.96**	-0.64	**0.82**	**-0.95**	**-0.94**	0.28	1.00				
Osm	0.51	**-0.86**	**0.71**	-0.45	-0.39	0.02	0.60	1.00			
pH	-0.60	0.07	-0.31	0.57	0.57	-0.50	-0.59	-0.23	1.00		
T	0.63	-0.22	0.46	-0.60	-0.55	0.36	0.62	0.48	**-0.89**	1.00	
CO_2	**0.80**	-0.29	0.51	**-0.73**	**-0.71**	0.35	**0.80**	0.34	**-0.82**	0.65	1.00
10.00 - 20.00 (day 5)											
VCN	1.00										
Viab	-0.64	1.00									
IgG4	**0.82**	**-0.82**	1.00								
Glu	**-0.95**	0.58	**-0.75**	1.00							
Gluc	**-0.91**	0.44	-0.65	**0.96**	1.00						
Lact	0.03	0.38	-0.27	-0.19	-0.32	1.00					
Amm	**0.95**	**-0.77**	**0.82**	**-0.95**	**-0.89**	0.04	1.00				
Osm	**0.72**	**-0.97**	**0.86**	-0.61	-0.47	-0.44	**0.80**	1.00			
pH	-0.51	0.23	-0.33	0.53	0.54	-0.37	-0.51	-0.29	1.00		
T	0.38	-0.35	0.37	-0.37	-0.32	0.00	0.40	0.40	**-0.89**	1.00	
CO_2	**0.91**	-0.52	0.68	**-0.92**	**-0.89**	0.19	**0.90**	0.56	-0.51	0.37	1.00
10.00 - 20.00 (day 9)											
VCN	1.00										
Viab	-0.19	1.00									
IgG4	0.59	**-0.89**	1.00								
Glu	**-0.86**	0.53	**-0.84**	1.00							
Gluc	**-0.92**	0.33	-0.67	**0.85**	1.00						
Lact	-0.06	0.52	-0.53	0.41	-0.07	1.00					
Amm	**0.72**	**-0.75**	**0.93**	**-0.84**	**-0.81**	-0.28	1.00				
Osm	0.37	**-0.89**	**0.87**	-0.57	-0.41	-0.46	**0.82**	1.00			
pH	**-0.77**	0.25	-0.54	0.69	**0.74**	-0.02	**-0.72**	-0.39	1.00		
T	0.47	-0.16	0.31	-0.37	-0.58	0.24	0.41	0.27	-0.12	1.00	
CO_2	0.49	**-0.76**	**0.89**	**-0.75**	-0.47	-0.66	**0.84**	**0.84**	-0.55	0.18	1.00

Table A-18: Spearman´s rank correlation coefficients (*r*) determined for 5L-STR CHO-CY01 cell line batch cultures at different pHs (pH 6.80, 7.10 and 7.40).

	VCN	Viab	IgG4	Glu	Gluc	Lact	Amm	Osm	pH	T	CO_2	Base
5L-STR pH 7.10												
VCN	1.00											
Viab	0.38	1.00										
IgG4	0.33	-0.71	1.00									
Glu	**-0.70**	0.36	**-0.89**	1.00								
Gluc	-0.69	0.40	**-0.89**	**0.99**	1.00							
Lact	**0.73**	0.48	-0.13	-0.27	-0.32	1.00						
Amm	0.24	**-0.72**	**0.89**	**-0.75**	**-0.81**	0.00	1.00					
Osm	-0.03	**0.73**	**-0.85**	0.67	0.64	0.43	-0.66	1.00				
pH	-0.48	-0.27	0.12	0.11	0.23	**-0.80**	-0.15	-0.44	1.00			
T	-0.27	-0.30	0.09	0.13	0.13	-0.35	0.03	0.10	0.12	1.00		
CO_2	-0.55	0.41	**-0.89**	**0.93**	**0.89**	-0.01	-0.63	**0.80**	-0.13	0.09	1.00	
Base	0.39	0.23	-0.14	-0.06	-0.17	**0.70**	0.10	0.43	**-0.97**	-0.05	0.12	1.00
5L-STR pH 6.80												
VCN	1.00											
Viab	0.13	1.00										
IgG4	0.68	-0.58	1.00									
Glu	**-0.76**	0.49	**-0.96**	1.00								
Gluc	-0.65	0.61	**-0.97**	**0.97**	1.00							
Lact	0.32	0.03	0.33	-0.31	-0.35	1.00						
Amm	**0.74**	-0.54	**0.95**	**-0.97**	**-0.95**	0.27	1.00					
Osm	-0.41	0.38	-0.56	0.64	**0.71**	-0.11	-0.55	1.00				
pH	-0.34	0.41	-0.56	0.48	0.57	-0.27	-0.56	0.42	1.00			
T	0.35	0.23	-0.03	-0.12	-0.07	0.13	0.15	-0.04	-0.10	1.00		
CO_2	0.49	-0.13	0.36	-0.45	-0.42	0.16	0.51	-0.34	-0.64	0.57	1.00	
Base												
5L-STR pH 7.40												
VCN	1.00											
Viab	0.40	1.00										
IgG4	0.52	-0.47	1.00									
Glu	**-0.75**	0.25	**-0.92**	1.00								
Gluc	**-0.73**	0.32	**-0.92**	**0.97**	1.00							
Lact	0.70	0.44	-0.03	-0.30	-0.35	1.00						
Amm	0.29	-0.64	**0.82**	**-0.72**	**-0.81**	-0.07	1.00					
Osm	-0.39	0.55	**-0.98**	**0.85**	**0.85**	0.19	**-0.87**	1.00				
pH	-0.50	-0.13	-0.19	0.28	0.44	-0.61	-0.31	0.14	1.00			
T	0.19	-0.21	0.27	-0.31	-0.38	0.18	0.49	-0.30	-0.52	1.00		
CO_2	-0.23	0.39	**-0.71**	0.63	0.52	0.31	-0.46	0.70	-0.51	0.20	1.00	
Base	0.44	0.20	-0.08	-0.11	-0.21	0.65	0.08	0.17	-0.53	0.31	0.25	1.00

Table A-19: Spearman´s rank correlation coefficients (*r*) determined for 5L-STR CHO-CY01 cell line fed-batch strategy 5 (FB3) cultures at pH 6.80, 7.10 and 7.80.

5L-STR pH 7.10 FB3

	VCN	Viab	IgG4	Glu	Gluc	Lact	Amm	Osm	pH	T	CO_2	Base
VCN	1.00											
Viab	0.00	1.00										
IgG4	0.47	**-0.81**	1.00									
Glu	**-0.90**	0.23	-0.69	1.00								
Gluc	**-0.90**	0.01	-0.49	**0.82**	1.00							
Lact	**0.88**	-0.20	0.66	**-0.88**	**-0.96**	1.00						
Amm	0.48	-0.70	**0.88**	-0.57	-0.62	**0.74**	1.00					
Osm	**0.70**	-0.65	**0.94**	**-0.86**	-0.67	**0.80**	**0.83**	1.00				
pH	-0.01	-0.40	0.38	-0.26	0.26	-0.14	-0.04	0.36	1.00			
T	-0.38	0.11	-0.21	0.26	0.38	-0.37	-0.28	-0.30	-0.08	1.00		
CO_2	**-0.84**	0.35	-0.68	**0.87**	**0.74**	**-0.78**	-0.54	**-0.83**	-0.25	0.37	1.00	
Base	-0.08	0.29	-0.32	0.32	-0.21	0.03	0.07	-0.32	**-0.74**	-0.24	0.25	1.00

5L-STR pH 6.80 FB3

VCN	1.00											
Viab	-0.23	1.00										
IgG4	0.58	**-0.87**	1.00									
Glu	**-0.92**	0.53	**-0.81**	1.00								
Gluc	**-0.93**	0.51	**-0.75**	**0.95**	1.00							
Lact	0.05	-0.06	-0.09	0.09	-0.18	1.00						
Amm	0.67	**-0.84**	**0.98**	**-0.86**	**-0.82**	-0.01	1.00					
Osm	0.18	**-0.95**	**0.88**	-0.48	-0.40	-0.07	**0.83**	1.00				
pH	-0.60	0.37	-0.52	0.66	0.58	0.17	-0.56	-0.33	1.00			
T	0.30	0.38	-0.13	-0.15	-0.11	-0.13	-0.08	-0.27	-0.12	1.00		
CO_2	0.50	-0.35	0.35	-0.47	-0.62	0.62	0.47	0.23	-0.42	0.23	1.00	
Base												

5L-STR pH 7.80 FB3

VCN	1.00											
Viab	**-0.70**	1.00										
IgG4	**0.94**	**-0.89**	1.00									
Glu	**0.90**	**-0.79**	**0.93**	1.00								
Gluc	-0.44	-0.19	-0.20	-0.19	1.00							
Lact	**0.98**	**-0.74**	**0.95**	**0.84**	-0.41	1.00						
Amm	0.24	0.44	-0.04	-0.08	-0.81	0.24	1.00					
Osm	**0.99**	**-0.80**	**0.97**	**0.92**	-0.30	**0.98**	0.10	1.00				
pH	-0.54	0.20	-0.42	-0.36	0.58	-0.59	-0.50	-0.49	1.00			
T	-0.24	-0.21	-0.05	-0.04	0.58	-0.23	-0.57	-0.15	-0.08	1.00		
CO_2	-0.20	0.22	-0.18	-0.17	-0.02	-0.16	0.10	-0.22	0.44	-0.52	1.00	
Base	0.19	0.36	-0.03	-0.13	**-0.87**	0.20	**0.89**	0.06	-0.51	-0.47	-0.08	1.00

Table A-20: Spearman´s rank correlation coefficients (*r*) determined for 5L-STR CHO-CY01 cell line fed-batch strategy 5 (FB3) cultures with pH shift from pH 6.60 to 6.80 on day 2, and pH shift from pH 7.60 to 7.10 on day 4.

pH 6.60 - 6.80 Day 2

	VCN	Viab	IgG4	Glu	Gluc	Lact	Amm	Osm	pH	T	CO_2	Base
VCN	1.00											
Viab	0.01	1.00										
IgG4	0.45	**-0.84**	1.00									
Glu	**-0.80**	0.44	-0.69	1.00								
Gluc	**-0.86**	0.34	**-0.72**	**0.78**	1.00							
Lact	0.49	-0.15	0.48	-0.23	-0.63	1.00						
Amm	0.60	-0.60	**0.90**	-0.65	**-0.83**	0.48	1.00					
Osm	0.31	**-0.80**	**0.90**	-0.49	-0.51	0.36	**0.85**	1.00				
pH	0.44	-0.01	0.32	-0.19	-0.44	0.40	0.56	0.41	1.00			
T	-0.36	-0.14	-0.12	0.23	0.22	-0.10	-0.12	0.06	-0.39	1.00		
CO_2	-0.59	**0.74**	**-0.94**	**0.81**	**0.79**	-0.40	**-0.92**	**-0.82**	-0.46	0.20	1.00	
Base	-0.33	0.02	-0.25	0.29	0.46	-0.35	-0.37	-0.12	0.12	0.24	0.28	1.00

pH 7.60 - 7.10 Day 4

VCN	1.00											
Viab	-0.23	1.00										
IgG4	**0.74**	**-0.78**	1.00									
Glu	**-0.89**	0.54	**-0.90**	1.00								
Gluc	-0.69	0.21	-0.49	0.50	1.00							
Lact	**0.80**	-0.38	0.67	-0.68	**-0.96**	1.00						
Amm	0.40	-0.66	0.61	-0.53	-0.58	0.65	1.00					
Osm	**0.84**	-0.70	**0.95**	**-0.92**	-0.68	**0.84**	0.68	1.00				
pH	-0.51	0.23	-0.46	0.37	0.46	-0.55	-0.35	-0.56	1.00			
T	-0.40	0.26	-0.32	0.32	**0.76**	**-0.73**	-0.50	-0.47	-0.01	1.00		
CO_2	0.62	-0.05	0.33	-0.39	**-0.82**	**0.79**	0.48	0.52	-0.59	-0.58	1.00	
Base	-0.59	0.22	-0.56	0.63	0.04	-0.23	-0.09	-0.51	0.56	-0.17	-0.30	1.00

Table A-21: Spearman´s rank correlation coefficients (r) determined for 5L-STR CHO-CY01 cell line fed-batch strategy 5 (FB3) cultures with pH shifts from pH 7.10 to 6.80 on day 5 or 8, and pH shift from pH 7.10 to 7.00 on day 4, then to pH 6.80 on day 5.

pH 7.10 - 6.80 Day 5

	VCN	Viab	IgG4	Glu	Gluc	Lact	Amm	Osm	pH	T	CO_2	Base
VCN	1.00											
Viab	-0.37	1.00										
IgG4	**0.81**	**-0.79**	1.00									
Glu	**-0.91**	0.47	**-0.83**	1.00								
Gluc	**-0.95**	0.11	-0.63	**0.79**	1.00							
Lact	-0.07	0.48	-0.32	0.42	-0.18	1.00						
Amm	**0.95**	-0.61	**0.93**	**-0.91**	**-0.84**	-0.16	1.00					
Osm	0.61	**-0.93**	**0.92**	-0.63	-0.40	-0.29	**0.81**	1.00				
pH	**-0.93**	0.21	-0.64	**0.77**	**0.91**	0.00	**-0.81**	-0.43	1.00			
T	0.10	0.14	0.05	0.03	-0.16	0.27	0.11	0.02	-0.08	1.00		
CO_2	0.59	**-0.73**	**0.77**	-0.47	-0.49	0.05	**0.72**	**0.83**	-0.52	-0.14	1.00	
Base												

pH 7.10 - 7.00 - 6.80 Day 4/5

VCN	1.00											
Viab	-0.08	1.00										
IgG4	0.44	**-0.84**	1.00									
Glu	**-0.93**	0.33	-0.65	1.00								
Gluc	**-0.90**	0.18	-0.52	**0.85**	1.00							
Lact	**0.79**	-0.10	0.36	-0.69	**-0.92**	1.00						
Amm	0.69	-0.62	**0.92**	**-0.80**	**-0.73**	0.55	1.00					
Osm	0.66	-0.69	**0.94**	**-0.81**	-0.68	0.49	**0.98**	1.00				
pH	**-0.92**	0.27	-0.57	**0.90**	**0.93**	**-0.88**	**-0.75**	**-0.74**	1.00			
T	-0.61	-0.38	0.06	0.42	0.47	-0.50	-0.15	-0.12	0.44	1.00		
CO_2	0.27	**-0.86**	**0.97**	-0.49	-0.36	0.19	**0.87**	**0.89**	-0.40	0.22	1.00	
Base	-0.14	0.23	-0.23	0.25	-0.15	0.19	-0.15	-0.26	0.16	-0.03	-0.23	1.00

pH 7.10 - 6.80 Day 8

VCN	1.00											
Viab	-0.14	1.00										
IgG4	0.53	**-0.93**	1.00									
Glu	**-0.92**	0.46	**-0.74**	1.00								
Gluc	**-0.93**	0.28	-0.62	**0.88**	1.00							
Lact	0.66	0.39	0.00	-0.42	**-0.73**	1.00						
Amm	0.58	**-0.85**	**0.93**	**-0.74**	-0.61	-0.04	1.00					
Osm	0.46	**-0.92**	**0.95**	**-0.70**	-0.46	-0.20	**0.94**	1.00				
pH	-0.61	**0.73**	**-0.84**	**0.76**	0.52	0.12	**-0.92**	**-0.92**	1.00			
T	0.13	0.53	-0.18	-0.02	-0.16	0.37	-0.11	-0.28	0.21	1.00		
CO_2	**-0.75**	-0.03	-0.21	0.70	0.57	-0.35	-0.23	-0.25	0.41	0.15	1.00	
Base												

Appendix B: CASY Cell Counter Particle Size Distribution

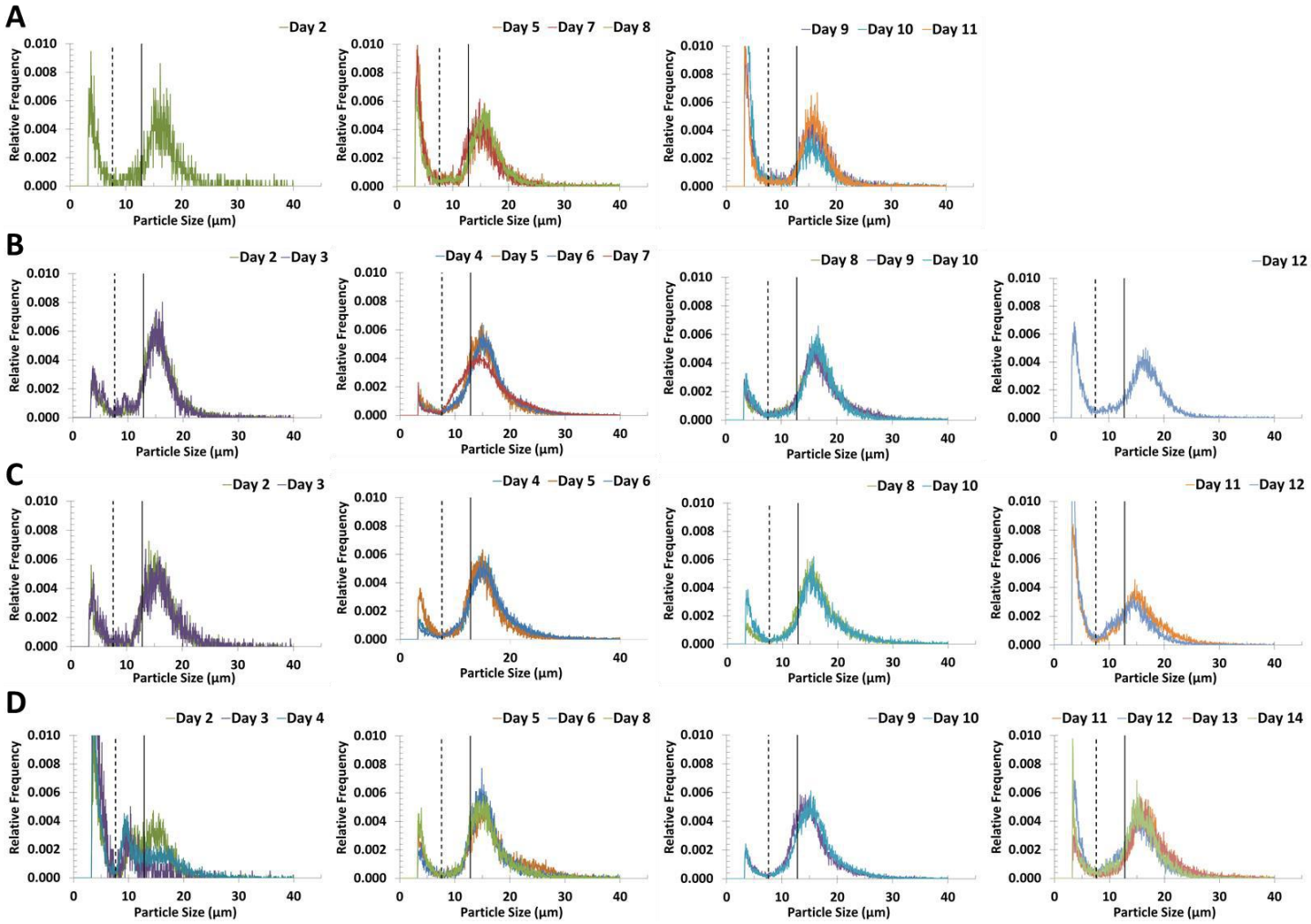

Figure B-1: CASY cell counter particle size distribution for 24-SRW MTP CHO-CY01 cell batch cultures with different fill volumes: 0.50 (A); 0.85 (B); 1.00 (C) and 1.50 mL (D).

Table B-1: Viable cell number (VCN); cell diameter, viability, larger particles (> 40 µm), dead cells (7.6 – 12.8 µm), debris (< 7.6 µm) and total impurities in each stage of 24-SRW MTP CHO-CY01 cell batch cultures with different fill volumes (0.50, 0.85, 1.00 and 1.50 $\boldsymbol{mL}$).

	Time (days)	VCN (10^6 cells mL^{-1})	Cell Diameter (µm)	Viability (%)	Larger Particles (%)	Dead Cells (%)	Debris (%)	Total Impurities (%)
0.50 mL								
Adaptation period	0 - 4	0.2	17.2	95.4	26.4	5.5	19.3	51.3
Exponential period	5 - 8	0.4 ± 0.2	16.5 ± 0.5	94.1 ± 1.0	17.8 ± 10.7	8.5 ± 2.2	23.5 ± 7.5	49.8 ± 3.6
Beginning of decline period	9 - 11	0.3 ± 0.1	16.8 ± 0.1	93.7 ± 1.9	12.1 ± 0.4	6.0 ± 1.1	32.4 ± 11.4	50.6 ± 11.3
Decline period								
0.85 mL								
Adaptation period	0 - 3	0.5 ± 0.0	16.1 ± 0.1	94.2 ± 2.8	10.0 ± 3.5	10.3 ± 1.3	12.1 ± 2.1	32.4 ± 6.9
Exponential period	4 - 7	3.5 ± 2.4	16.4 ± 0.3	94.0 ± 2.5	18.2 ± 10.5	14.8 ± 4.9	4.5 ± 0.9	37.6 ± 9.1
Beginning of decline period	8 - 10	4.6 ± 1.5	17.6 ± 0.1	95.4 ± 0.6	49.5 ± 3.5	4.3 ± 0.5	5.8 ± 1.4	59.6 ± 2.6
Decline period	12	3.7	17.1	93.2	26.9	6.7	19.9	53.6
1.00 mL								
Adaptation period	0 - 3	0.3 ± 0.0	16.4 ± 0.2	96.4 ± 2.0	14.0 ± 8.6	8.9 ± 0.0	13.2 ± 0.2	36.1 ± 8.9
Exponential period	4 - 7	2.2 ± 1.7	16.7 ± 0.0	95.6 ± 0.5	22.2 ± 5.7	10.6 ± 0.6	4.7 ± 1.8	37.5 ± 4.5
Beginning of decline period	8 - 10	3.6 ± 0.8	17.2 ± 0.4	96.1 ± 0.3	42.1 ± 1.1	6.3 ± 1.2	5.8 ± 3.1	54.2 ± 3.0
Decline period	11 - 12	5.1 ± 1.2	16.1 ± 0.8	89.5 ± 4.8	29.3 ± 7.8	10.6 ± 0.9	25.8 ± 4.1	65.7 ± 12.8
1.50 mL								
Adaptation period	0 - 4	0.1 ± 0.1	15.2 ± 1.1	68.8 ± 16.0	9.8 ± 4.3	20.3 ± 3.4	45.4 ± 14.6	75.5 ± 15.5
Exponential period	5 - 8	0.9 ± 0.2	16.9 ± 0.8	96.6 ± 0.4	34.2 ± 1.3	7.4 ± 0.6	7.9 ± 2.2	49.5 ± 2.7
Beginning of decline period	9 - 10	2.4 ± 0.0	16.2 ± 0.4	95.5 ± 0.7	23.3 ± 5.8	13.3 ± 4.3	5.9 ± 0.6	42.5 ± 0.9
Decline period	11 - 14	4.8 ± 1.4	17.0 ± 0.7	94.6 ± 2.3	48.6 ± 10.7	5.6 ± 2.5	9.3 ± 4.2	63.4 ± 6.1

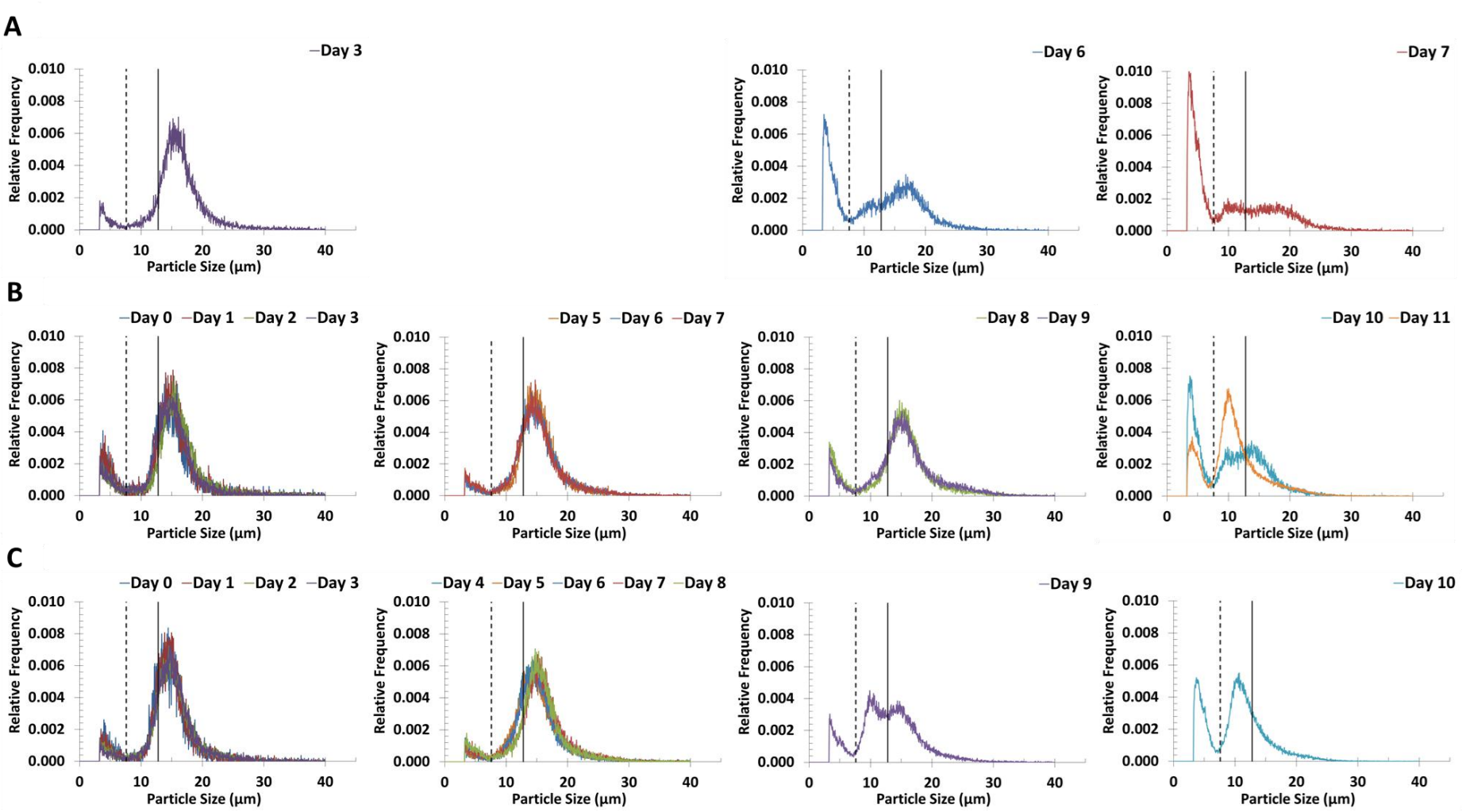

Figure B-2: CASY cell counter particle size distribution for 24-SRW MTP CHO-CY01 cell batch cultures at different shaking speeds: 100 (A); 150 (B); 180 (C); 220 (D); 250 (E) and 300 $\boldsymbol{rpm}$ (F).

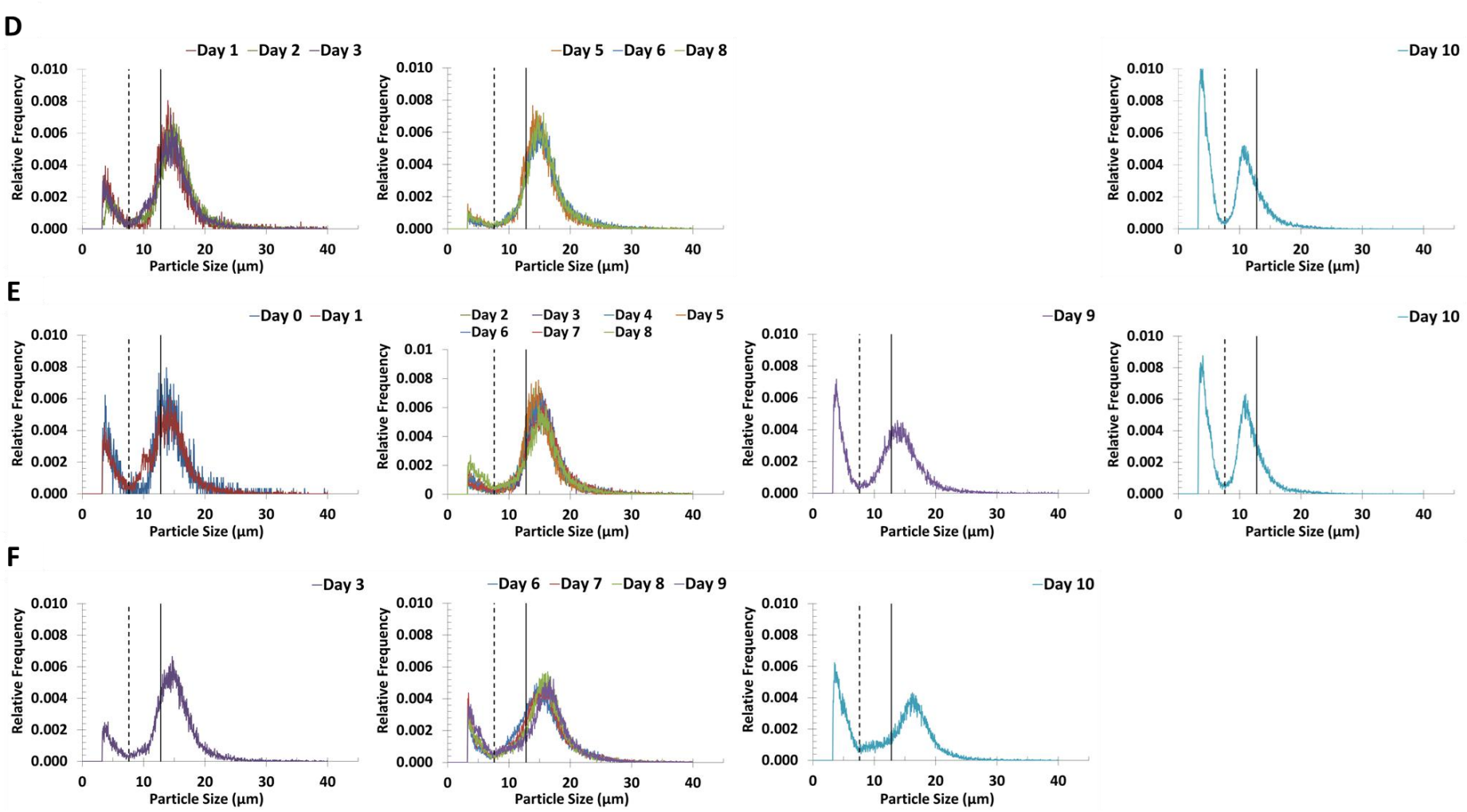

Figure B-2: (Continued)

Table B-2: VCN; cell diameter, viability, larger particles, dead cells, debris and total impurities in each stage of 24-SRW MTP CHO-CY01 cell batch cultures in 24-SRW MTP at different shaking speeds (100, 150, 180, 220, 250 and 300 $\boldsymbol{rpm}$).

	Time (days)	VCN (10^6 cells mL^{-1})	Cell Diameter (µm)	Viability (%)	Larger Particles (%)	Dead Cells (%)	Debris (%)	Total Impurities (%)
100 rpm								
Adaptation period	3	0.9	16.8	96.9	10.2	8.2	5.5	23.9
Exponential period	4							
Beginning of decline period	6	1.0	16.9	87.6	8.6	14.7	30.6	54.0
Decline period	7	0.7	17.3	81.0	9.2	14.9	44.7	68.8
150 rpm								
Adaptation period	0 - 3	0.6 ± 0.4	16.0 ± 0.4	96.7 ± 0.3	15.9 ± 4.3	7.1 ± 5.1	10.1 ± 2.6	33.2 ± 4.2
Exponential period	4 - 7	4.8 ± 1.6	15.5 ± 0.5	92.5 ± 6.9	20.6 ± 5.0	13.9 ± 1.4	4.3 ± 0.9	38.8 ± 6.1
Beginning of decline period	8 - 9	6.9 ± 1.7	16.8 ± 0.2	94.6 ± 1.1	40.5 ± 1.9	8.0 ± 1.2	7.3 ± 1.8	55.9 ± 1.2
Decline period	10 - 11	4.2 ± 1.4	14.6 ± 0.4	68.2 ± 12.3	4.1 ± 5.4	40.2 ± 19.8	26.5 ± 9.0	70.8 ± 5.4
180 rpm								
Adaptation period	0 - 3	0.9 ± 0.7	15.6 ± 0.3	97.0 ± 0.6	10.4 ± 3.4	10.3 ± 6.9	6.0 ± 1.7	26.7 ± 6.4
Exponential period	4 - 8	5.1 ± 1.2	16.0 ± 0.4	94.8 ± 1.1	22.9 ± 11.2	14.4 ± 5.8	3.9 ± 0.9	41.3 ± 6.9
Beginning of decline period	9	3.6	15.5	77.6	8.7	33.8	12.1	54.6
Decline period	10	5.2	14.0	68.3	1.0	45.6	27.5	74.1
220 rpm								
Adaptation period	0 - 3	0.6 ± 0.5	15.3 ± 0.4	95.1 ± 1.8	11.4 ± 2.1	15.3 ± 2.0	11.3 ± 2.4	38.0 ± 5.9
Exponential period	4 - 8	6.0 ± 1.3	16.0 ± 0.3	96.1 ± 0.5	21.4 ± 3.5	11.6 ± 1.3	3.8 ± 0.7	36.7 ± 1.9
Beginning of decline period	9							
Decline period	10	5.3	13.3	70.9	1.5	36.8	45.2	83.4
250 rpm								
Adaptation period	0 - 1	0.2 ± 0.2	15.0 ± 0.0	92.2 ± 5.9	1.8 ± 2.5	12.3 ± 17.5	19.6 ± 2.7	23.0 ± 32.3
Exponential period	2 - 8	3.9 ± 2.5	16.0 ± 0.4	95.6 ± 1.2	19.5 ± 9.4	11.2 ± 2.4	5.8 ± 2.1	36.5 ± 8.6
Beginning of decline period	9	5.2	15.1	91.2	14.3	17.2	26.3	57.7
Decline period	10	5.6	13.0	72.5	2.6	41.2	38.9	82.8
300 rpm								
Adaptation period	0 - 3	1.0	15.6	94.6	4.8	16.5	11.0	32.3
Exponential period	4 - 9	4.3 ± 1.4	16.5 ± 0.3	92.5 ± 0.9	20.2 ± 9.5	12.6 ± 4.6	11.5 ± 1.8	44.3 ± 5.8
Beginning of decline period	10	5.3	16.6	88.7	25.6	9.7	24.1	59.4
Decline period								

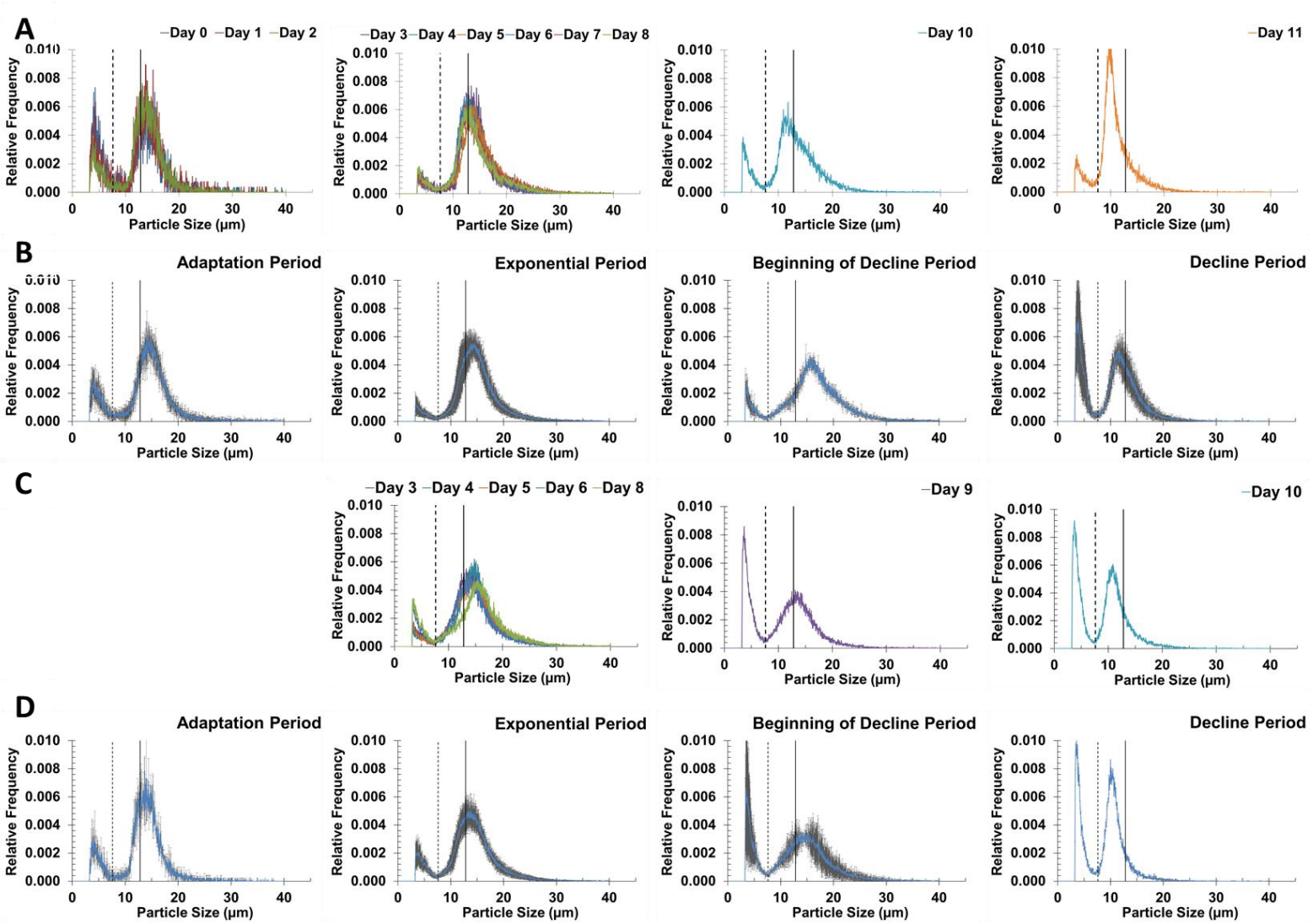

Figure B-3: CASY cell counter particle size distribution for standard CHO-CY01 cell batch culture at different bioreactor scales, 5L-STR (A); 24-SRW MTP (B); SF 125 mL (C) and SF 250 mL (D).

Table B-3: VCN; cell diameter, viability, larger particles, dead cells, debris and total impurities for standard CHO-CY01 cell batch culture at different bioreactor scales, 5L-STR; 24-SRW MTP; SF 125 mL and SF 250 mL.

	Time (days)	VCN (10^6 cells mL^{-1})	Cell Diameter (μm)	Viability (%)	Larger Particles (%)	Dead Cells (%)	Debris (%)	Total Impurities (%)
5L-STR								
Adaptation period	0 - 2	0.3 ± 0.2	14.9 ± 0.2	94.2 ± 1.8	10.3 ± 11.8	14.1 ± 12.3	18.6 ± 3.8	43.0 ± 2.9
Exponential period	3 - 8	4.2 ± 1.8	15.2 ± 0.4	94.0 ± 1.5	21.3 ± 16.0	23.5 ± 6.7	5.2 ± 1.1	50.0 ± 10.9
Beginning of decline period	10	5.1	14.6	86.5	29.7	26.8	10.5	67.0
Decline period	11	3.6	13.3	50.1	4.1	65.7	11.1	80.9
24-SRW MTP								
Adaptation period	0 - 3	0.6 ± 0.4	15.6 ± 0.3	94.6 ± 1.2	17.8 ± 9.1	12.6 ± 3.6	13.4 ± 4.3	43.8 ± 7.4
Exponential period	4 - 8	4.8 ± 2.0	15.5 ± 0.9	94.5 ± 2.2	22.0 ± 14.7	19.1 ± 10.9	4.5 ± 1.1	45.6 ± 8.1
Beginning of decline period	9 - 10	12.2 ± 7.1	17.5 ± 0.2	94.1 ± 0.1	55.3 ± 25.9	5.7 ± 2.6	4.7 ± 3.9	65.7 ± 19.5
Decline period	10 - 11	5.4 ± 1.8	13.7 ± 0.5	79.6 ± 9.1	7.6 ± 5.7	34.8 ± 2.3	29.9 ± 16.8	72.4 ± 11.7
SF 125 mL								
Adaptation period	0 - 2							
Exponential period	3 - 8	4.4 ± 2.5	16.0 ± 0.5	92.4 ± 1.2	17.4 ± 11.9	18.6 ± 5.9	7.7 ± 2.7	43.7 ± 7.0
Beginning of decline period	9	6.9	14.9	85.4	13.8	22.1	28.7	64.5
Decline period	10	5.8	13.2	67.3	7.8	41.5	34.4	83.7
SF 250 mL								
Adaptation period	0 - 2	0.7 ± 0.3	14.7 ± 0.2	96.0 ± 0.4	10.0 ± 1.8	20.4 ± 3.9	13.2 ± 3.3	43.7 ± 1.3
Exponential period	3 - 8	3.3 ± 1.4	15.3 ± 0.7	91.9 ± 3.0	11.7 ± 8.4	24.0 ± 6.9	10.1 ± 3.1	45.8 ± 7.9
Beginning of decline period	9	6.0 ± 0.3	16.0 ± 1.6	88.2 ± 3.6	15.1 ± 15.1	18.1 ± 7.6	22.8 ± 16.2	56.0 ± 8.7
Decline period	10	3.7	12.7	52.1	4.2	52.4	33.0	89.6

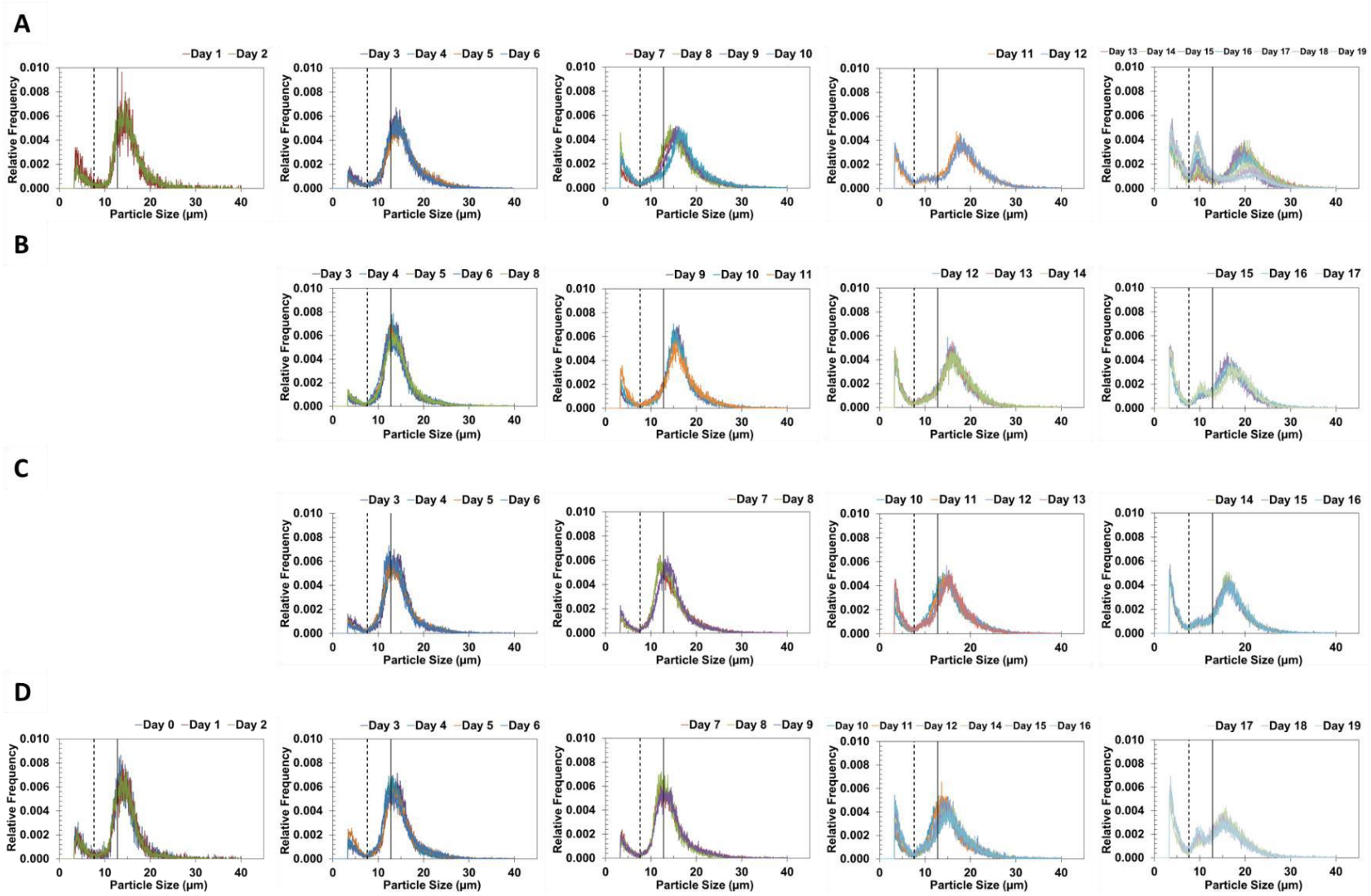

Figure B-4: CASY cell counter particle size distribution for CHO-CY01 cell line fed-batch strategy 4 (FB2) cultures at different bioreactor scales, 5L-STR (A); 24-SRW MTP (B); SF 125 mL (C) and SF 250 mL (D).

Table B-4: VCN; cell diameter, viability, larger particles, dead cells, debris and total impurities for CHO-CY01 cell line fed-batch strategy 4 (FB2) cultures at different bioreactor scales, 5L-STR; 24-SRW MTP; SF 125 mL and SF 250 mL.

	Time (days)	VCN (10^6 cells mL^{-1})	Cell Diameter (μm)	Viability (%)	Larger Particles (%)	Dead Cells (%)	Debris (%)	Total Impurities (%)
5L-STR FB2								
Adaptation period	1 - 2	0.6 ± 0.3	15.5 ± 0.1	96.9 ± 0.5	9.1 ± 3.0	14.8 ± 0.2	10.6 ± 3.5	17.2 ± 23.8
Exponential period	3 - 6	3.5 ± 1.8	15.9 ± 0.3	94.8 ± 1.0	16.9 ± 7.1	17.1 ± 0.6	5.1 ± 1.4	39.0 ± 6.8
Stationary period	7 - 10	4.9 ± 0.5	17.1 ± 0.7	94.7 ± 0.4	26.7 ± 4.6	9.7 ± 2.3	8.3 ± 2.0	44.7 ± 2.5
Beginning of decline period	11 - 12	4.8 ± 0.1	19.2 ± 0.2	92.9 ± 1.0	46.1 ± 4.0	5.2 ± 0.7	9.1 ± 1.8	60.4 ± 1.5
Decline period	13 - 19	7.2 ± 9.4	19.1 ± 0.9	76.2 ± 10.3	41.8 ± 15.0	13.8 ± 6.3	15.8 ± 5.3	71.4 ± 9.1
24-SRW MTP FB2								
Adaptation period								
Exponential period	3 - 8	3.8 ± 2.5	14.8 ± 0.2	93.2 ± 2.2	9.9 ± 5.6	28.9 ± 4.9	3.9 ± 0.7	42.6 ± 3.9
Stationary period	9 - 11	5.5 ± 1.2	16.8 ± 0.3	96.0 ± 0.5	35.8 ± 2.1	6.6 ± 0.7	5.8 ± 2.0	48.2 ± 3.9
Beginning of decline period	12 - 14	4.6 ± 1.1	17.2 ± 0.3	94.4 ± 0.4	37.2 ± 2.9	6.7 ± 0.6	10.3 ± 0.5	54.3 ± 2.7
Decline period	15 - 17	4.8 ± 0.8	17.8 ± 0.4	91.5 ± 1.7	42.2 ± 5.6	7.8 ± 0.9	11.3 ± 2.3	61.3 ± 3.6
SF 125 mL FB2								
Adaptation period								
Exponential period	3 - 6	3.1 ± 1.9	15.0 ± 0.3	93.5 ± 1.4	11.9 ± 11.4	26.1 ± 2.4	4.9 ± 1.5	42.8 ± 9.9
Stationary period	7 - 9	8.0 ± 0.5	15.1 ± 0.2	92.0 ± 0.9	27.3 ± 9.8	23.9 ± 6.4	4.8 ± 0.4	56.0 ± 4.2
Beginning of decline period	10 - 13	7.0 ± 1.8	16.5 ± 0.3	93.2 ± 0.6	30.4 ± 5.2	11.8 ± 2.9	9.2 ± 2.9	51.4 ± 2.9
Decline period	14 - 16	5.4 ± 0.8	17.4 ± 0.1	92.0 ± 0.8	38.7 ± 6.5	7.4 ± 0.6	11.9 ± 0.6	58.0 ± 5.6
SF 250 mL FB2								
Adaptation period	0 - 2	0.6 ± 0.4	15.0 ± 0.1	96.1 ± 0.7	8.3 ± 4.8	15.3 ± 10.6	8.8 ± 1.0	32.4 ± 5.8
Exponential period	3 - 6	2.5 ± 0.6	15.1 ± 0.4	93.8 ± 1.0	11.4 ± 4.7	25.6 ± 4.6	8.2 ± 1.7	45.2 ± 1.9
Stationary period	7 - 9	5.1 ± 0.7	14.8 ± 0.4	92.9 ± 0.2	26.1 ± 6.9	25.1 ± 4.4	6.0 ± 0.0	57.2 ± 3.9
Beginning of decline period	10 - 16	4.9 ± 1.1	16.3 ± 0.4	92.6 ± 1.1	33.6 ± 3.0	12.5 ± 3.0	9.9 ± 2.6	56.0 ± 1.4
Decline period	17 - 19	4.3 ± 1.1	16.8 ± 0.1	85.6 ± 3.6	37.6 ± 2.2	12.2 ± 0.9	14.7 ± 2.1	64.5 ± 5.1

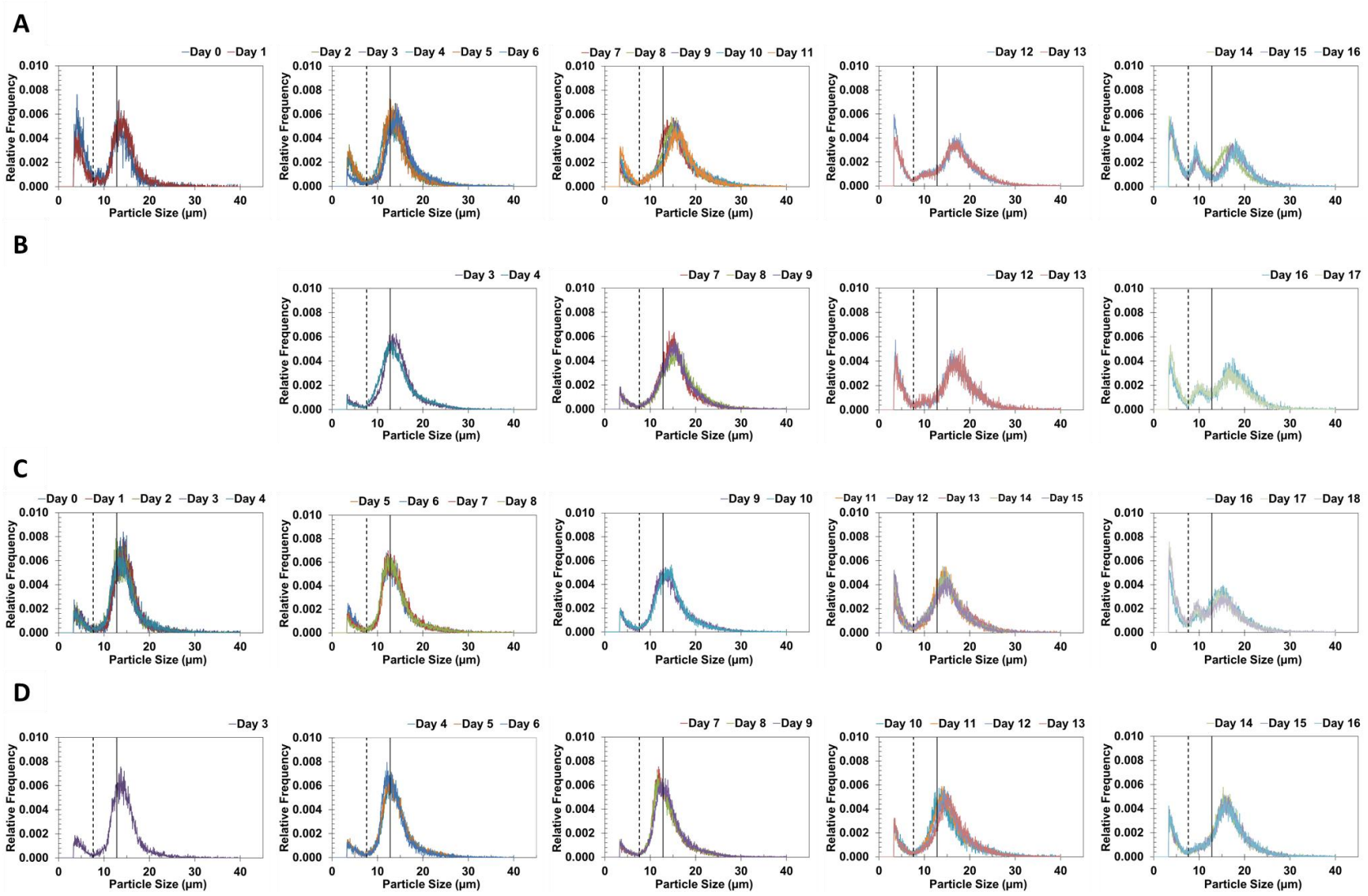

Figure B-5: CASY cell counter particle size distribution for CHO-CY01 cell line fed-batch strategy 5 (FB3) cultures at different bioreactor scales, 5L-STR (A); 24-SRW MTP (B); SF 125 mL (C) and SF 250 mL (D).

Table B-5: VCN; cell diameter, viability, larger particles, dead cells, debris and total impurities for CHO-CY01 cell line fed-batch strategy 5 (FB3) cultures at different bioreactor scales, 5L-STR; 24-SRW MTP; SF 125 mL and SF 250 mL.

	Time (days)	VCN (10^6 cells mL^{-1})	Cell Diameter (μm)	Viability (%)	Larger Particles (%)	Dead Cells (%)	Debris (%)	Total Impurities (%)
5L-STR FB3								
Adaptation period	0 - 1	0.3 ± 0.1	14.8 ± 0.2	91.4 ± 3.2	9.2 ± 3.2	9.5 ± 13.4	25.4 ± 6.8	44.1 ± 3.4
Exponential period	2 - 6	2.7 ± 2.0	15.1 ± 0.4	94.2 ± 1.6	17.5 ± 12.8	20.3 ± 6.0	9.7 ± 3.6	47.4 ± 8.6
Stationary period	7 - 11	7.4 ± 1.5	16.9 ± 0.6	94.4 ± 0.4	35.6 ± 9.5	9.5 ± 2.9	5.9 ± 0.9	51.1 ± 7.8
Beginning of decline period	12 - 13	6.3 ± 0.7	18.0 ± 0.2	91.4 ± 0.6	40.0 ± 4.2	7.5 ± 1.1	12.9 ± 1.8	60.4 ± 1.3
Decline period	14 - 16	6.3 ± 0.4	17.8 ± 0.8	78.9 ± 2.9	43.0 ± 13.6	11.8 ± 3.2	15.9 ± 3.0	70.7 ± 7.5
24-SRW MTP FB3								
Adaptation period								
Exponential period	3 - 6	2.4 ± 0.9	15.2 ± 0.0	91.1 ± 3.2	4.4 ± 0.7	30.2 ± 5.0	4.2 ± 0.6	38.8 ± 3.7
Stationary period	7 - 9	6.3 ± 0.9	16.4 ± 0.4	95.3 ± 0.2	30.8 ± 0.3	11.5 ± 0.8	4.4 ± 0.1	46.7 ± 1.1
Beginning of decline period	10 - 15	3.2 ± 0.3	18.1 ± 0.1	94.1 ± 0.8	54.9 ± 11.8	3.8 ± 0.5	9.2 ± 3.2	68.0 ± 8.2
Decline period	16 - 17	3.1 ± 0.0	17.8 ± 0.2	87.3 ± 2.0	43.6 ± 0.0	9.6 ± 0.8	12.1 ± 2.4	65.3 ± 3.1
SF 125 mL FB3								
Adaptation period	0 - 4	0.9 ± 0.6	15.0 ± 0.2	95.6 ± 0.9	10.0 ± 2.5	17.4 ± 10.2	8.9 ± 0.5	36.3 ± 8.3
Exponential period	5 - 8	4.4 ± 1.7	14.8 ± 0.0	93.1 ± 0.9	23.0 ± 8.8	26.3 ± 2.2	6.1 ± 2.0	55.4 ± 5.6
Stationary period	9 - 10	6.8 ± 0.5	15.5 ± 0.1	91.9 ± 0.2	28.4 ± 4.2	20.5 ± 3.0	5.9 ± 0.2	54.7 ± 1.5
Beginning of decline period	11 - 16	5.5 ± 1.4	16.3 ± 0.3	92.4 ± 1.4	38.2 ± 8.6	11.3 ± 1.7	9.4 ± 2.6	59.0 ± 6.0
Decline period	17 - 19	4.9 ± 0.9	16.6 ± 0.0	83.7 ± 3.9	38.2 ± 4.6	12.7 ± 1.1	16.7 ± 2.2	67.6 ± 5.8
SF 250 mL FB3								
Adaptation period	0 - 3	0.9 ± 0.0	14.9 ± 0.0	95.2 ± 0.0	5.7 ± 0.0	23.5 ± 0.0	8.6 ± 0.0	37.7 ± 0.0
Exponential period	4 - 6	3.0 ± 1.4	14.6 ± 0.3	92.5 ± 0.5	12.3 ± 10.4	30.9 ± 1.0	5.9 ± 1.0	49.1 ± 8.6
Stationary period	7 - 9	7.1 ± 0.2	14.7 ± 0.2	91.1 ± 1.2	26.6 ± 9.5	28.8 ± 6.2	4.0 ± 0.4	59.3 ± 3.0
Beginning of decline period	10 - 13	5.2 ± 1.3	16.4 ± 0.4	94.1 ± 0.5	41.1 ± 8.9	10.7 ± 2.5	6.3 ± 0.8	58.0 ± 7.7
Decline period	14 - 16	5.0 ± 0.6	17.3 ± 0.1	93.8 ± 0.6	48.9 ± 6.0	5.8 ± 0.7	7.7 ± 1.6	62.5 ± 3.8

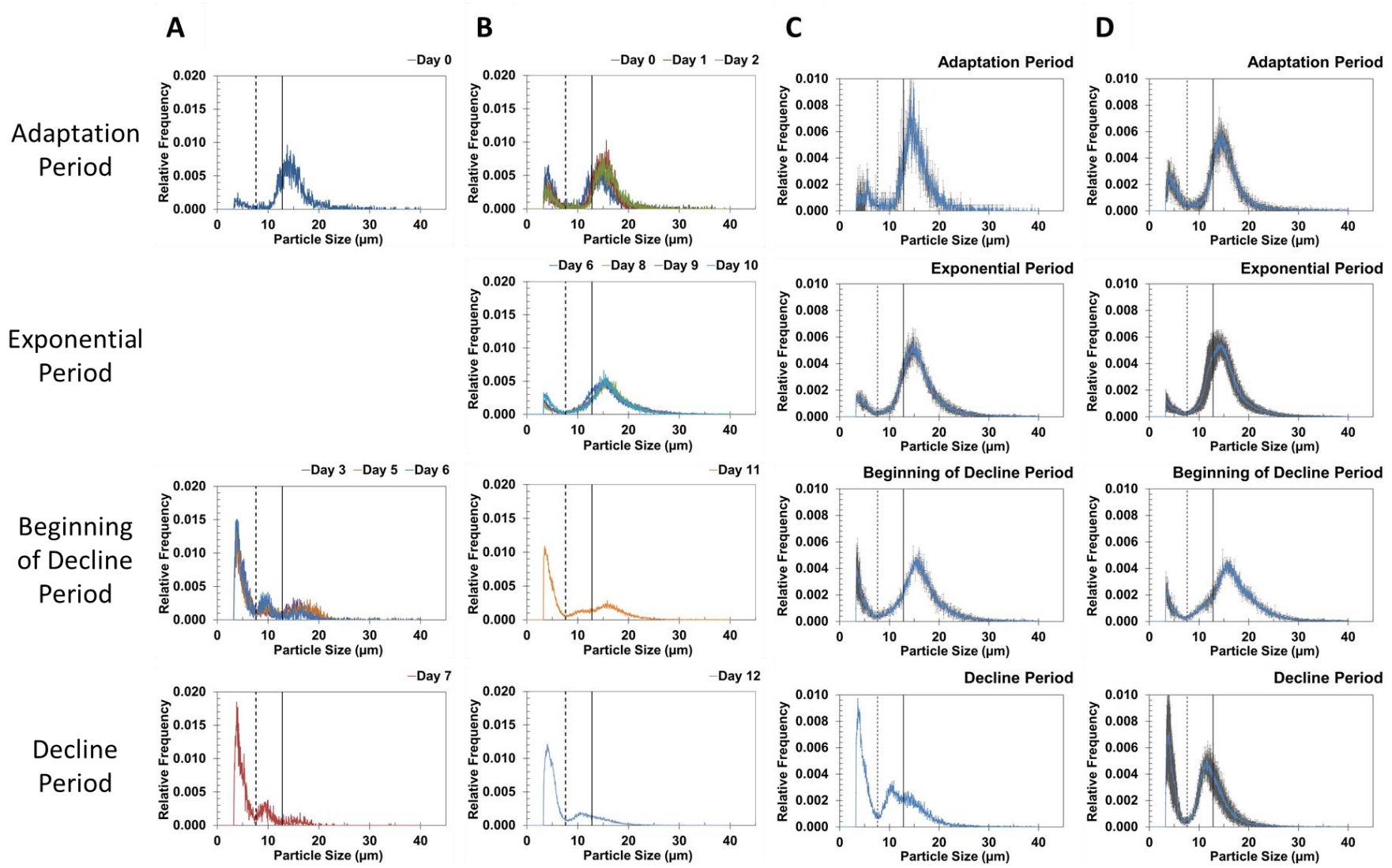

Figure B-6: CASY cell counter particle size distribution for CHO-CY01 cell line batch cultures in 24-SRW-MTP at different CO_2 (0.04% (A); 1.00% (B); 2.00% (C); 5.00% (D); 10.00% (E); 15.00% (F); and 20.00% (v/v) CO_2 (G)).

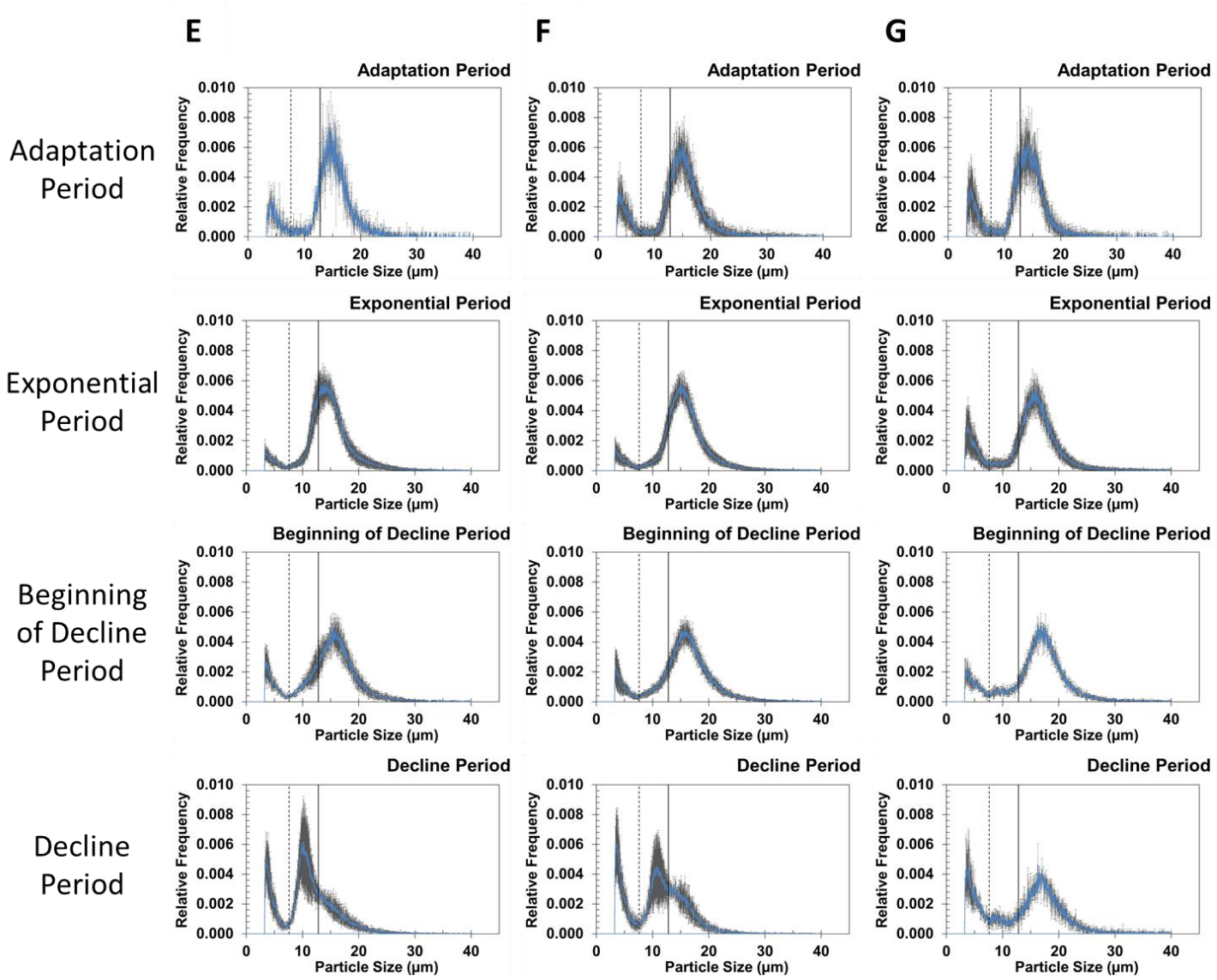

Figure B-6 (Continued)

Table B-6: VCN; cell diameter, viability, larger particles, dead cells, debris and total impurities for CHO-CY01 cell line batch cultures in 24-SRW-MTP at different CO_2 (0.04%; 1.00%; 2.00%; 5.00%; 10.00%; 15.00%; and 20.00% (v/v) CO_2).

CO_2 (% (v/v))	Time (days)	VCN (10^6 cells mL^{-1})	Cell Diameter (µm)	Viability (%)	Larger Particles (%)	Dead Cells (%)	Debris (%)	Total Impurities (%)
0.04								
Adaptation period	0	0.9	15.3	97.0	41.8	0.0	4.1	45.9
Exponential period								
Beginning of decline period	3 - 6	0.1 ± 0.0	15.8 ± 0.7	63.4 ± 11.5	9.5 ± 6.5	15.8 ± 2.7	55.3 ± 0.7	80.6 ± 7.694
Decline period	7	0.05	14.4	39.8	5.3	19.1	68.3	92.7
1.00								
Adaptation period	0 - 2	0.3 ± 0.1	15.6 ± 0.6	95.9 ± 1.6	8.0 ± 4.9	4.7 ± 4.3	17.6 ± 7.1	10.6 ± 17.92
Exponential period	6 - 10	4.7 ± 1.3	16.9 ± 0.4	94.8 ± 0.6	34.8 ± 15.1	9.3 ± 3.6	6.2 ± 3.1	50.3 ± 10.15
Beginning of decline period	11	4.8	16.4	84.8	15.3	12.0	42.3	69.6
Decline period	12	3.9	14.4	69.6	2.5	16.9	66.6	86.0
2.00								
Adaptation period	0 - 2	0.3 ± 0.1	15.7 ± 0.5	95.5 ± 0.8	18.5 ± 16.7	10.2 ± 2.3	8.6 ± 5.2	37.3 ± 13.8
Exponential period	3 - 8	4.3 ± 2.7	16.3 ± 0.5	95.8 ± 0.5	34.3 ± 15.6	9.8 ± 2.7	6.2 ± 2.6	50.4 ± 11.2
Beginning of decline period	8 - 9	7.0 ± 2.3	16.9 ± 0.3	93.7 ± 1.7	38.3 ± 24.9	8.1 ± 3.4	11.1 ± 7.4	57.5 ± 14.1
Decline period	10 - 11	7.0 ± 0.0	14.9 ± 0.0	73.8 ± 0.0	37.6 ± 0.0	17.0 ± 0.0	27.6 ± 0.0	82.2 ± 0.0
5.00								
Adaptation period	0 - 3	0.6 ± 0.4	15.6 ± 0.3	94.6 ± 1.2	17.8 ± 9.1	12.6 ± 3.6	13.4 ± 4.3	43.8 ± 7.4
Exponential period	4 - 8	4.8 ± 2.0	15.5 ± 0.9	94.5 ± 2.2	22.0 ± 14.7	19.1 ± 10.9	4.5 ± 1.1	45.6 ± 8.1
Beginning of decline period	9 - 10	12.2 ± 7.1	17.5 ± 0.2	94.1 ± 0.1	55.3 ± 25.9	5.7 ± 2.6	4.7 ± 3.9	65.7 ± 19.5
Decline period	10 - 11	5.4 ± 1.8	13.7 ± 0.5	79.6 ± 9.1	7.6 ± 5.7	34.8 ± 2.3	29.9 ± 16.8	72.4 ± 11.7
10.00								
Adaptation period	0 - 2	0.4 ± 0.1	15.8 ± 0.1	96.4 ± 0.8	13.0 ± 4.6	10.4 ± 0.2	10.4 ± 2.3	33.7 ± 6.8
Exponential period	3 - 9	3.1 ± 2.3	15.4 ± 0.7	95.2 ± 1.2	12.9 ± 9.7	19.3 ± 5.5	5.5 ± 1.6	37.8 ± 6.8
Beginning of decline period	9 - 10	5.9 ± 1.2	16.4 ± 0.7	92.9 ± 1.0	20.9 ± 5.1	13.3 ± 4.4	9.9 ± 3.5	44.2 ± 3.1
Decline period	10- 12	3.9 ± 1.2	14.1 ± 1.1	61.6 ± 12.5	5.5 ± 2.4	51.0 ± 16.8	18.0 ± 7.0	74.5 ± 9.4
15.00								
Adaptation period	0 - 3	0.3 ± 0.1	15.8 ± 0.5	96.5 ± 1.1	19.3 ± 8.6	7.7 ± 5.0	12.3 ± 4.5	39.2 ± 9.2
Exponential period	3 - 10	3.4 ± 1.9	16.3 ± 0.4	96.0 ± 0.8	24.0 ± 9.7	10.1 ± 2.9	5.4 ± 2.5	39.5 ± 8.1
Beginning of decline period	11 - 12	6.1 ± 1.2	16.9 ± 0.4	94.3 ± 1.1	28.2 ± 5.7	9.4 ± 1.4	7.3 ± 2.7	44.9 ± 7.0
Decline period	12- 14	5.6 ± 1.6	14.4 ± 0.8	77.4 ± 7.1	5.0 ± 4.4	35.5 ± 15.1	25.2 ± 9.3	65.7 ± 7.7
20.00								
Adaptation period	0 - 2	0.2 ± 0.1	14.9 ± 0.3	95.8 ± 1.0	16.6 ± 8.7	14.4 ± 7.6	13.9 ± 8.0	45.0 ± 5.5
Exponential period	3 - 9	1.2 ± 0.9	16.7 ± 0.4	95.0 ± 1.4	24.0 ± 9.1	7.4 ± 1.9	12.2 ± 6.1	43.6 ± 7.1
Beginning of decline period	9 - 10	3.6 ± 1.4	17.8 ± 0.1	93.6 ± 0.6	37.2 ± 13.4	6.1 ± 1.6	7.6 ± 0.3	50.9 ± 11.6
Decline period	10- 12	3.3 ± 2.0	17.7 ± 0.2	88.5 ± 1.9	51.6 ± 14.9	6.1 ± 2.7	12.0 ± 1.1	69.7 ± 11.3

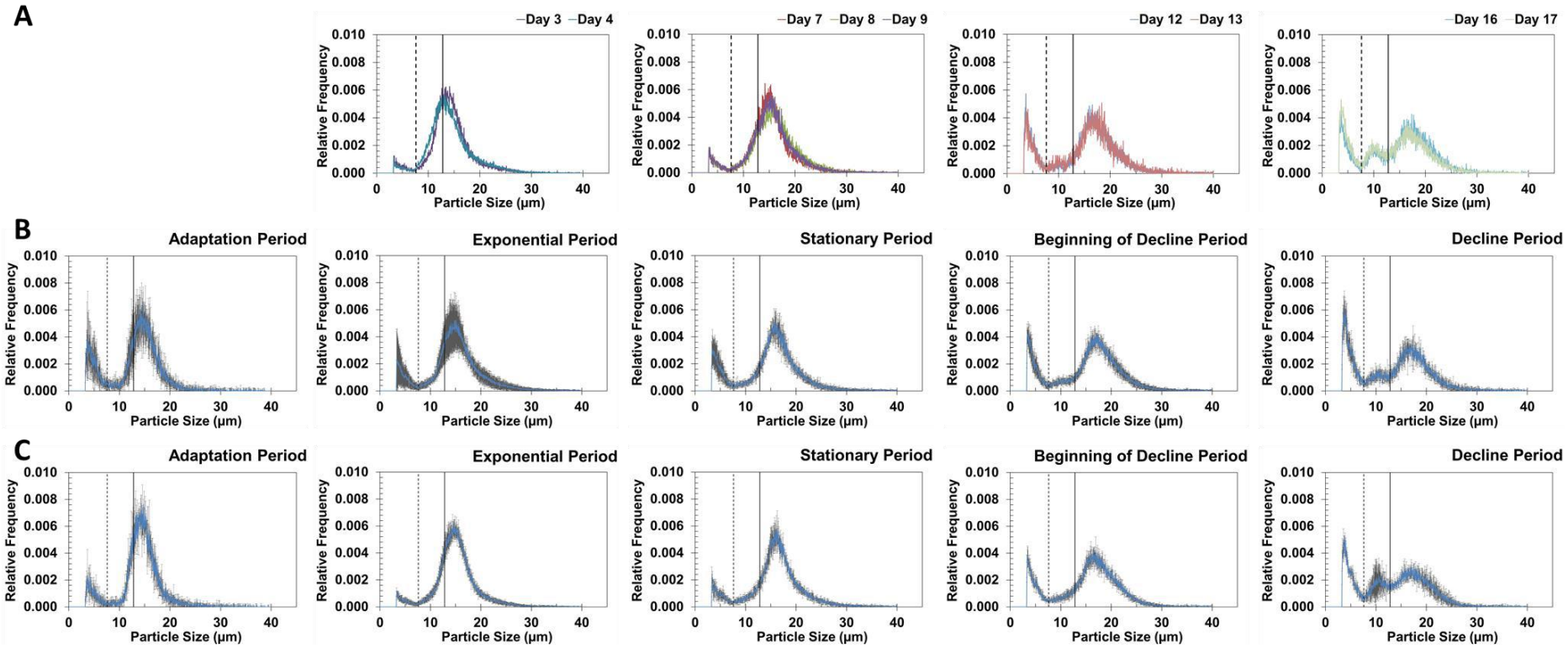

Figure B-7: CASY cell counter particle size distribution for CHO-CY01 cell line *f*ed batch strategy 5 (FB3) cultures in 24-SRW-MTPs at 5.00% (A), 10.00% (B), and 15.00% (v/v) CO_2 (C).

Table B-7: VCN, cell diameter, viability, larger particles, dead cells, debris and total impurities for CHO-CY01 cell line *f*ed batch strategy 5 (FB3) cultures in 24-SRW-MTPs at 5.00%, 10.00%, and 15.00% (v/v) CO_2.

CO_2 (% (v/v))	Time (days)	VCN (10^6 cells mL^{-1})	Cell Diameter (µm)	Viability (%)	Larger Particles (%)	Dead Cells (%)	Debris (%)	Total Impurities (%)
5.00								
Adaptation period								
Exponential period	3 - 6	2.4 ± 0.9	15.2 ± 0.0	91.1 ± 3.2	4.4 ± 0.7	30.2 ± 5.0	4.2 ± 0.6	38.8 ± 3.7
Stationary period	7 - 9	6.3 ± 0.9	16.4 ± 0.4	95.3 ± 0.2	30.8 ± 0.3	11.5 ± 0.8	4.4 ± 0.1	46.7 ± 1.1
Beginning of decline period	10 - 15	3.2 ± 0.3	18.1 ± 0.1	94.1 ± 0.8	54.9 ± 11.8	3.8 ± 0.5	9.2 ± 3.2	68.0 ± 8.2
Decline period	16 - 17	3.1 ± 0.0	17.8 ± 0.2	87.3 ± 2.0	43.6 ± 0.0	9.6 ± 0.8	12.1 ± 2.4	65.3 ± 3.1
10.00								
Adaptation period	0 - 2	0.2 ± 0.1	15.5 ± 0.7	94.5 ± 2.2	9.3 ± 4.4	13.9 ± 6.0	17.6 ± 7.6	40.8 ± 7.4
Exponential period	3 - 7	3.1 ± 2.1	16.5 ± 1.4	94.6 ± 2.3	30.3 ± 18.3	11.6 ± 4.8	7.0 ± 4.2	48.9 ± 15.7
Stationary period	7 - 11	4.3 ± 0.8	17.2 ± 0.2	94.7 ± 1.4	42.4 ± 7.1	5.8 ± 0.5	9.5 ± 4.5	57.6 ± 6.3
Beginning of decline period	12 - 16	4.1 ± 2.0	18.3 ± 0.3	93.7 ± 1.2	48.5 ± 6.3	4.6 ± 0.6	10.1 ± 2.7	63.2 ± 4.4
Decline period	17 - 19	2.0 ± 0.2	17.7 ± 0.3	88.6 ± 1.6	46.3 ± 4.8	7.1 ± 0.6	15.7 ± 3.6	69.1 ± 3.2
15.00								
Adaptation period	0 - 2	0.3 ± 0.2	15.2 ± 0.3	97.2 ± 0.1	7.8 ± 4.6	9.2 ± 8.0	9.0 ± 2.9	26.0 ± 9.7
Exponential period	3 - 7	5.1 ± 3.0	15.8 ± 0.2	95.0 ± 1.0	18.1 ± 10.8	15.0 ± 3.5	3.9 ± 0.5	37.0 ± 7.8
Stationary period	7 - 11	6.3 ± 1.8	17.3 ± 0.2	95.1 ± 0.7	39.1 ± 6.5	6.5 ± 1.5	5.7 ± 1.7	51.3 ± 4.2
Beginning of decline period	12 - 16	5.2 ± 0.3	18.0 ± 0.1	93.8 ± 0.6	42.6 ± 2.0	5.7 ± 0.7	10.2 ± 0.4	58.5 ± 2.2
Decline period	17 - 19	4.0 ± 0.2	17.3 ± 0.9	85.4 ± 7.2	37.2 ± 17.4	13.1 ± 8.6	16.1 ± 4.8	66.4 ± 4.0

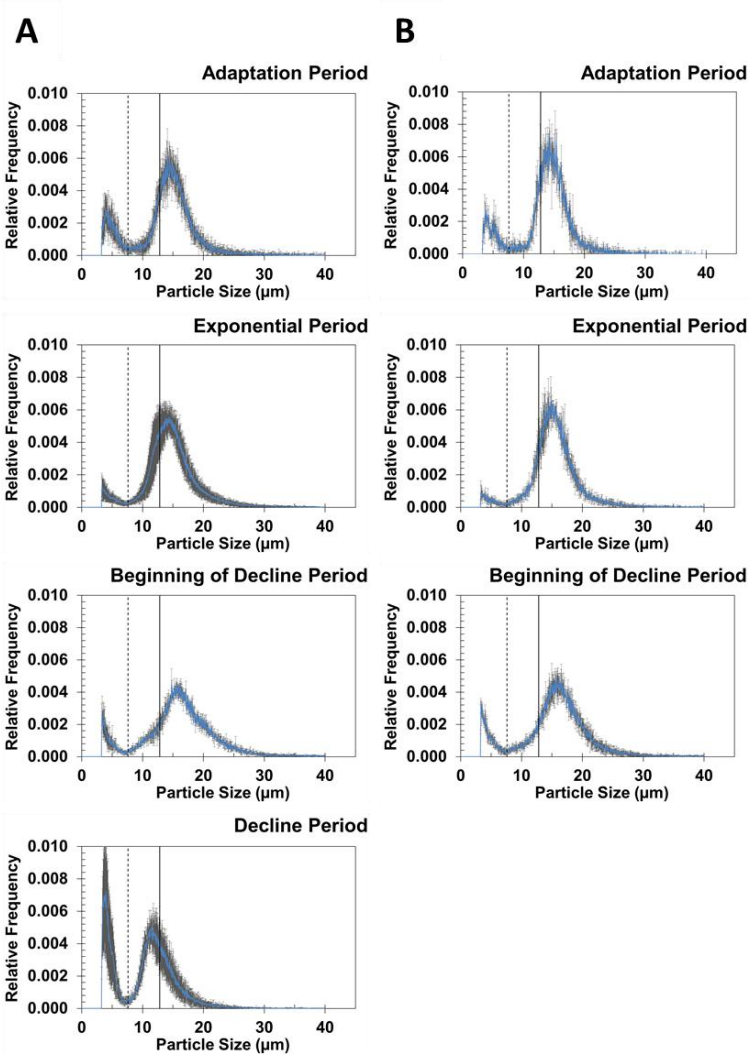

Figure B-8: CASY cell counter particle size distribution for CHO-CY01 cell line batch cultures in 24-SRW-MTPs at constant 5.00% (v/v) CO_2 (A) and the first CO_2 multiphasic culture (pH shift 1) (B).

Table B-8: VCN, cell diameter, viability, larger particles, dead cells, debris and total impurities for CHO-CY01 cell line batch cultures in 24-SRW-MTPs at constant 5.00% (v/v) $\boldsymbol{CO_2}$ and pH shift 1.

	Time (days)	VCN (10^6 cells mL^{-1})	Cell Diameter (µm)	Viability (%)	Larger Particles (%)	Dead Cells (%)	Debris (%)	Total Impurities (%)
5.00 % (v/v) CO_2								
Adaptation period	0 - 3	0.6 ± 0.4	15.6 ± 0.3	94.6 ± 1.2	17.8 ± 9.1	12.6 ± 3.6	13.4 ± 4.3	43.8 ± 7.4
Exponential period	4 - 8	4.8 ± 2.0	15.5 ± 0.9	94.5 ± 2.2	22.0 ± 14.7	19.1 ± 10.9	4.5 ± 1.1	45.6 ± 8.1
Beginning of decline period	9 - 10	12.2 ± 7.1	17.5 ± 0.2	94.1 ± 0.1	55.3 ± 25.9	5.7 ± 2.6	4.7 ± 3.9	65.7 ± 19.5
Decline period	10 - 11	5.4 ± 1.8	13.7 ± 0.5	79.6 ± 9.1	7.6 ± 5.7	34.8 ± 2.3	29.9 ± 16.8	72.4 ± 11.7
pH Shift 1								
Adaptation period	0 - 3	0.7 ± 0.3	15.2 ± 0.2	96.1 ± 0.6	9.2 ± 1.1	14.8 ± 2.2	11.9 ± 0.5	35.9 ± 3.9
Exponential period	4 - 5	2.5 ± 0.2	16.0 ± 0.4	96.0 ± 0.3	6.8 ± 1.7	13.2 ± 2.2	4.1 ± 0.9	24.1 ± 0.5
Beginning of decline period	6 - 9	3.7 ± 1.5	17.1 ± 0.5	94.7 ± 0.4	25.6 ± 9.8	8.5 ± 0.9	9.5 ± 2.3	43.6 ± 6.8
Decline period								

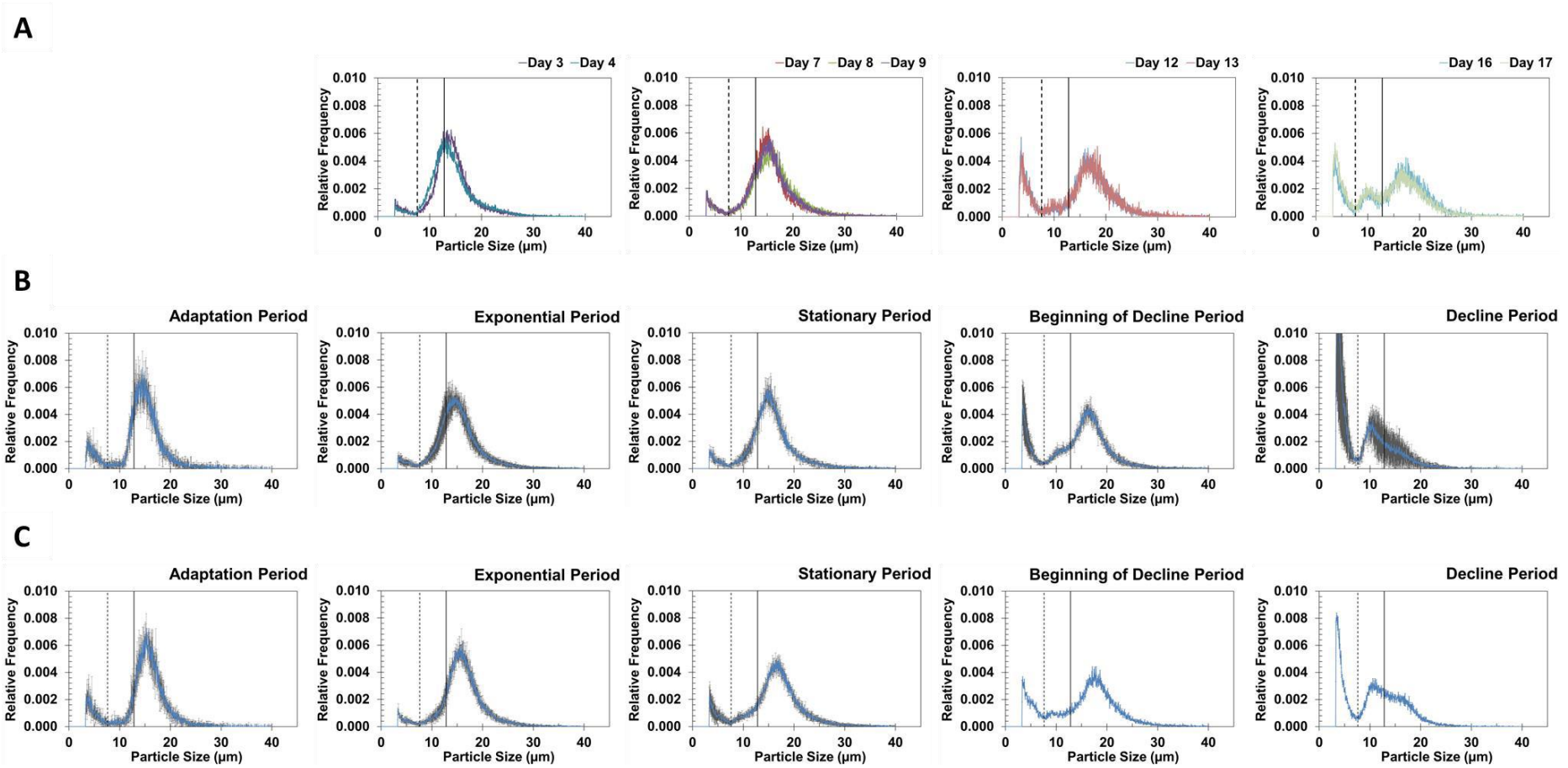

Figure B-9: CASY cell counter particle size distribution for CHO-CY01 cell line fed batch strategy 5 (FB3) cultures in 24-SRW-MTPs with constant 5.00% (v/v) CO_2 (A), CO_2 shift from 5.00% to 20.00% (v/v) CO_2 on day 7 (1 step) (B) and CO_2 shift from 5.00% to 7.50% on day 2, then to 10.00% on day 7, then to 12.50% on day 8, and then to 15.0% (v/v) CO_2 on day 10 (4 steps) (C).

Table B-9: VCN, cell diameter, viability, larger particles, dead cells (µm), debris and total impurities for CHO-CY01 cell line fed batch strategy 5 (FB3) cultures in 24-SRW-MTPs with constant 5.00% (v/v) CO_2, CO_2 shift from 5.00% to 20.00% (v/v) CO_2 on day 7 (1 step) and CO_2 shift from 5.00% to 7.50% on day 2, then to 10.00% on day 7, then to 12.50% on day 8, and then to 15.0% (v/v) CO_2 on day 10 (4 steps).

CO_2 (% (v/v))	Time (days)	VCN (10^6 cells mL^{-1})	Cell Diameter (µm)	Viability (%)	Larger Particles (%)	Dead Cells (%)	Debris (%)	Total Impurities (%)
5.00								
Adaptation period								
Exponential period	3 - 6	2.4 ± 0.9	15.2 ± 0.0	91.1 ± 3.2	4.4 ± 0.7	30.2 ± 5.0	4.2 ± 0.6	38.8 ± 3.7
Stationary period	7 - 9	6.3 ± 0.9	16.4 ± 0.4	95.3 ± 0.2	30.8 ± 0.3	11.5 ± 0.8	4.4 ± 0.1	46.7 ± 1.1
Beginning of decline period	10 - 15	3.2 ± 0.3	18.1 ± 0.1	94.1 ± 0.8	54.9 ± 11.8	3.8 ± 0.5	9.2 ± 3.2	68.0 ± 8.2
Decline period	16 - 17	3.1 ± 0.0	17.8 ± 0.2	87.3 ± 2.0	43.6 ± 0.0	9.6 ± 0.8	12.1 ± 2.4	65.3 ± 3.1
5.00 - 20.00 (day 7)								
Adaptation period	0 - 2	0.3	15.6	97.0	7.8	8.4	9.3	25.4
Exponential period	3 - 6	3.6 ± 2.1	15.9 ± 0.7	93.8 ± 2.0	11.0 ± 1.6	19.2 ± 6.3	4.1 ± 1.4	34.2 ± 5.3
Stationary Period	7 - 8	5.7 ± 1.3	16.3 ± 0.1	94.8 ± 1.9	38.4 ± 21.0	10.6 ± 5.9	3.5 ± 0.4	52.5 ± 14.7
Beginning of decline period	9 - 12	7.4 ± 0.5	17.0 ± 0.3	91.9 ± 1.7	36.6 ± 6.3	9.2 ± 1.8	11.5 ± 5.3	57.3 ± 2.6
Decline period	13 - 14	4.2 ± 4.8	14.6 ± 0.3	65.5 ± 12.8	11.6 ± 2.1	25.8 ± 11.1	42.5 ± 25.3	79.9 ± 16.3
5.00 - 7.50 - 10.00 - 12.50 - 15.00 (day 2, 7, 8, 9, 10)								
Adaptation period	0 - 2	0.4 ± 0.2	16.2 ± 0.3	96.9 ± 0.2	9.3 ± 3.1	4.6 ± 3.9	10.1 ± 2.7	24.0 ± 2.6
Exponential period	3 - 5	2.2 ± 1.0	16.7 ± 0.3	96 ± 1	7.0 ± 3.4	10.7 ± 3.4	4.5 ± 0.6	22.2 ± 2.6
Stationary Period	6 - 8	5.1 ± 1.4	17.6 ± 0.3	94.4 ± 1.4	32.4 ± 13.1	7.5 ± 0.9	5.9 ± 1.5	45.8 ± 13.8
Beginning of decline period	10	4.0	18.4	90.6	40.5	7.3	11.1	58.9
Decline period	11	6.0	15.2	78.7	22.6	23.0	25.3	70.9

13.

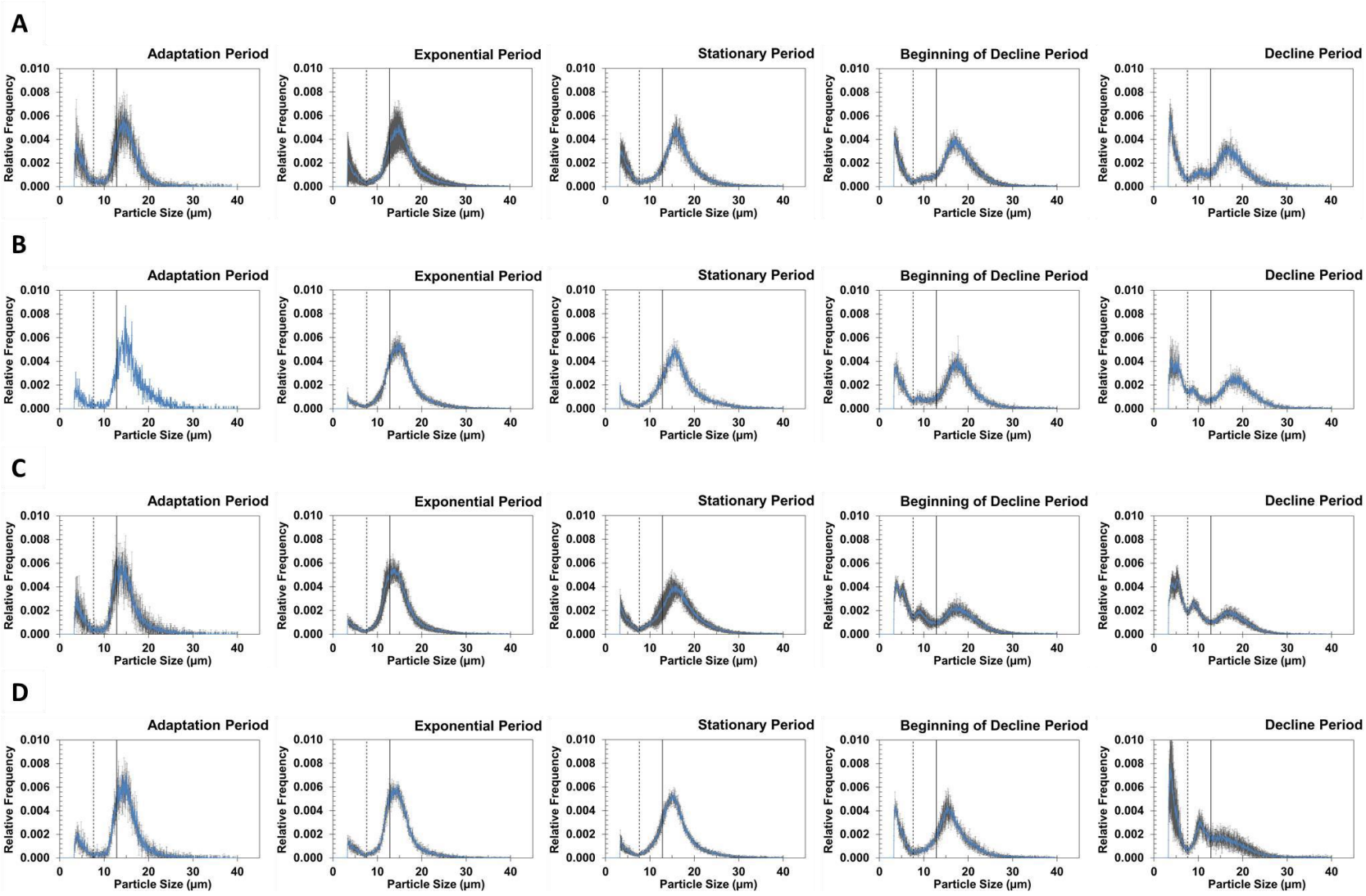

Figure B-10: CASY cell counter particle size distribution for CHO-CY01 cell line fed batch strategy 5 (FB3) cultures in 24-SRW-MTPs with constant 10.00% (v/v) CO_2 (A) and CO_2 shifts from 10.00% to 20.00% (v/v) CO_2 at day 3 (B), 5 (C) and 9 (D).

Table B-10: VCN, cell diameter, viability, larger particles, dead cells (µm), debris and total impurities for CHO-CY01 cell line fed batch strategy 5 (FB3) cultures in 24-SRW-MTPs with constant 10.00% (v/v) CO_2 and CO_2 shifts from 10.00% to 20.00% (v/v) CO_2 at day 3, 5 and 9.

CO_2 (% (v/v))	Time (days)	VCN (10^6 cells mL^{-1})	Cell Diameter (µm)	Viability (%)	Larger Particles (%)	Dead Cells (%)	Debris (%)	Total Impurities (%)
10.00								
Adaptation period	0 - 2	0.2 ± 0.1	15.5 ± 0.7	94.5 ± 2.2	9.3 ± 4.4	13.9 ± 6.0	17.6 ± 7.6	40.8 ± 7.4
Exponential period	3 - 7	3.1 ± 2.1	16.5 ± 1.4	94.6 ± 2.3	30.3 ± 18.3	11.6 ± 4.8	7.0 ± 4.2	48.9 ± 15.7
Stationary period	7 - 11	4.3 ± 0.8	17.2 ± 0.2	94.7 ± 1.4	42.4 ± 7.1	5.8 ± 0.5	9.5 ± 4.5	57.6 ± 6.3
Beginning of decline period	12 - 16	4.1 ± 2.0	18.3 ± 0.3	93.7 ± 1.2	48.5 ± 6.3	4.6 ± 0.6	10.1 ± 2.7	63.2 ± 4.4
Decline period	17 - 19	2.0 ± 0.2	17.7 ± 0.3	88.6 ± 1.6	46.3 ± 4.8	7.1 ± 0.6	15.7 ± 3.6	69.1 ± 3.2
10.00 - 20.00 (day 3)								
Adaptation period	0	0.2	16.4	97.4	10.0	0.0	7.7	17.7
Exponential period	3 - 7	2.4 ± 1.3	16.0 ± 0.3	94.8 ± 1.1	14.2 ± 11.1	16.5 ± 2.3	4.1 ± 0.8	34.8 ± 9.1
Stationary Period	8 - 9	7.2 ± 0.4	17.2 ± 0.3	95.2 ± 0.2	42.7 ± 2.4	8.4 ± 0.6	3.3 ± 0.5	54.4 ± 2.5
Beginning of decline period	10 - 12	4.4 ± 0.4	18.4 ± 0.3	91.3 ± 1.0	46.4 ± 11.9	5.6 ± 1.3	11.2 ± 2.5	63.2 ± 8.4
Decline period	13 - 14	7.0 ± 3.1	18.9 ± 0.1	81.9 ± 0.8	66.3 ± 5.3	4.8 ± 0.4	11.0 ± 3.6	82.1 ± 1.4
10.00 - 20.00 (day 5)								
Adaptation period	0 - 2	0.2 ± 0.0	15.4 ± 0.9	95.6 ± 2.0	11.4 ± 3.0	13.9 ± 12.1	13.2 ± 6.7	38.5 ± 19.8
Exponential period	3 - 7	2.5 ± 1.4	15.3 ± 0.6	93.6 ± 1.5	12.2 ± 6.1	23.2 ± 5.3	5.6 ± 1.1	41.0 ± 8.3
Stationary Period	8 - 12	6.0 ± 1.7	17.4 ± 0.8	93.3 ± 1.4	46.7 ± 9.4	8.1 ± 4.3	6.4 ± 1.9	61.1 ± 6.1
Beginning of decline period	12 - 16	5.0 ± 1.3	18.2 ± 0.7	78.2 ± 4.4	54.9 ± 11.6	8.0 ± 1.7	15.3 ± 4.7	78.2 ± 6.5
Decline period	17 - 21	5.6 ± 0.3	17.2 ± 0.4	68.7 ± 5.3	29.1 ± 6.4	17.3 ± 3.0	27.2 ± 5.8	73.5 ± 3.9
10.00 - 20.00 (day 9)								
Adaptation period	0 - 2	0.3 ± 0.1	15.5 ± 0.1	96.8 ± 0.4	7.9 ± 1.7	9.9 ± 8.6	9.8 ± 1.3	27.6 ± 8.9
Exponential period	3 - 5	1.9 ± 1.0	15.3 ± 0.2	95.1 ± 0.4	5.9 ± 2.1	21.0 ± 1.9	7.2 ± 2.0	34.1 ± 3.1
Stationary Period	6 - 9	5.1 ± 1.4	16.4 ± 0.3	94.5 ± 0.6	30.4 ± 18.9	11.8 ± 4.6	4.4 ± 0.8	46.5 ± 14.2
Beginning of decline period	10 - 12	4.7 ± 1.4	17.1 ± 0.6	93.2 ± 1.6	43.2 ± 16.5	6.7 ± 2.0	12.1 ± 2.7	62.0 ± 12.9
Decline period	13 - 15	3.3 ± 2.0	16.7 ± 0.6	77.1 ± 7.8	52.7 ± 28.2	12.7 ± 9.2	14.2 ± 4.8	79.7 ± 14.8

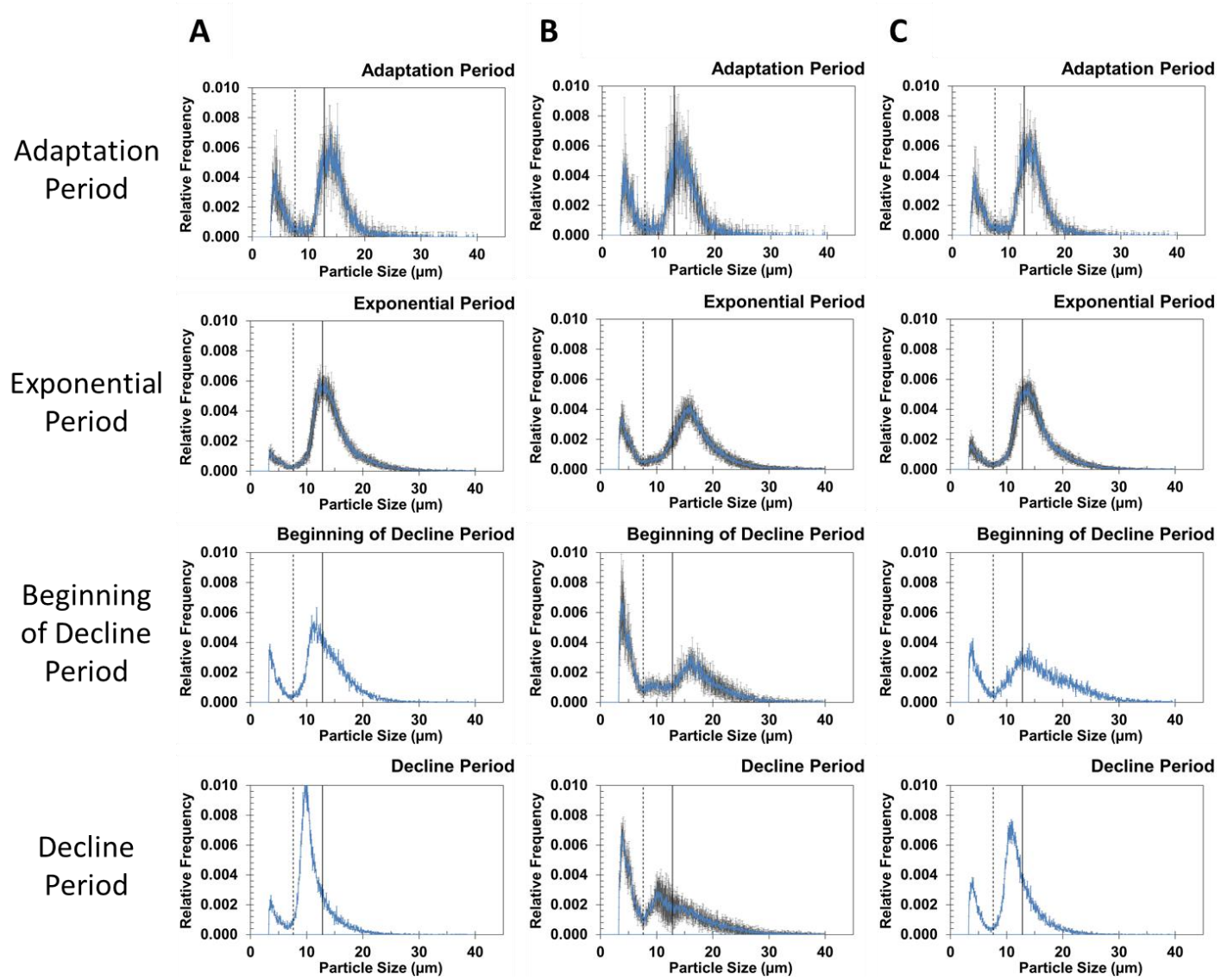

Figure B-11: CASY cell counter particle size distribution for 5L-STR CHO-CY01 cell line batch cultures at pH 6.80 (B), 7.10 (A) and 7.40 (C).

Table B-11: VCN, cell diameter, viability, larger particles, dead cells (µm), debris and total impurities for 5L-STR CHO-CY01 cell line batch cultures at different pHs (pH 6.80, 7.10 and 7.40).

	Time (days)	VCN (10^6 cells mL^{-1})	Cell Diameter (µm)	Viability (%)	Larger Particles (%)	Dead Cells (%)	Debris (%)	Total Impurities (%)
5L-STR pH 7.10 Batch								
Adaptation period	0 - 2	0.3 ± 0.2	14.9 ± 0.2	94.2 ± 1.8	10.3 ± 11.8	14.1 ± 12.3	18.6 ± 3.8	43.0 ± 2.9
Exponential period	3 - 8	4.2 ± 1.8	15.2 ± 0.4	94.0 ± 1.5	21.3 ± 16.0	23.5 ± 6.7	5.2 ± 1.1	50.0 ± 10.9
Beginning of decline period	10	5.1	14.6	86.5	29.7	26.8	10.5	67.0
Decline period	11	3.6	13.3	50.1	4.1	65.7	11.1	80.9
5L-STR pH 6.80 Batch								
Adaptation period	0 - 3	0.3 ± 0.1	14.9 ± 0.6	93.8 ± 1.3	10.8 ± 4.7	12.2 ± 10.8	19.0 ± 0.9	42.0 ± 13.3
Exponential period	3 - 12	1.5 ± 1.0	17.2 ± 0.7	93.4 ± 0.7	31.2 ± 17.9	8.5 ± 2.7	12.7 ± 3.8	52.4 ± 12.5
Beginning of decline period	13 - 15	2.8 ± 1.8	17.7 ± 1.0	85.4 ± 3.6	54.7 ± 12.5	6.3 ± 2.2	17.1 ± 9.1	78.1 ± 1.3
Decline period	16- 19	2.7 ± 0.7	16.6 ± 1.8	74.4 ± 4.5	37.6 ± 29.3	17.8 ± 12.4	23.5 ± 10.5	78.9 ± 8.2
5L-STR pH 7.40 Batch								
Adaptation period	0 - 3	0.5 ± 0.4	14.6 ± 0.3	94.4 ± 1.9	7.4 ± 1.7	12.6 ± 11.1	17.3 ± 3.8	37.3 ± 5.8
Exponential period	3 - 9	5.1 ± 2.4	15.5 ± 0.3	94.3 ± 0.8	24.8 ± 17.0	18.2 ± 2.9	6.6 ± 1.9	49.6 ± 14.6
Beginning of decline period	10	3.4	17.4	89.5	32.8	14.5	12.6	59.9
Decline period	11	5.0	13.5	75.0	7.9	49.4	15.4	72.7

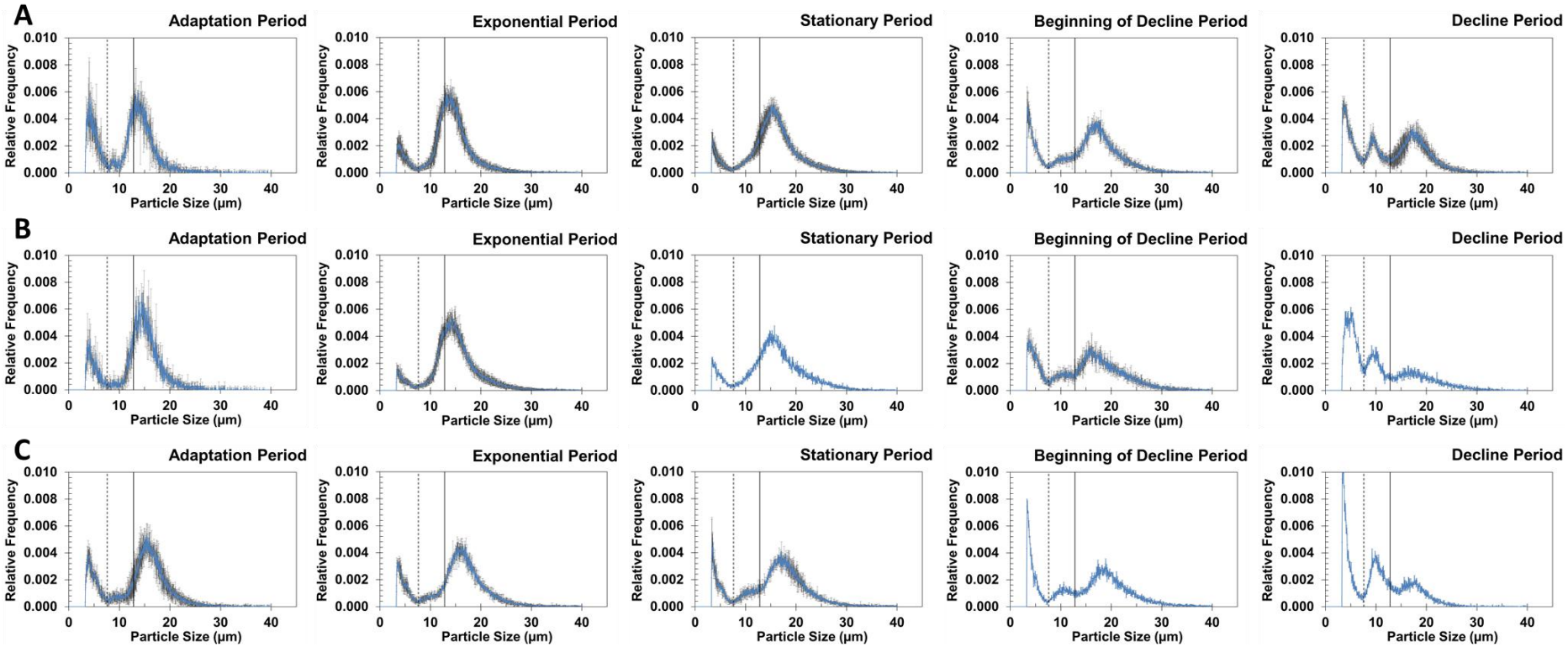

Figure B-12: CASY cell counter particle size distribution for 5L-STR CHO-CY01 cell line fed-batch strategy 5 (FB3) cultures at pH 6.80 (B), 7.10 (A) and 7.80 (C).

Table B-12: VCN, cell diameter, viability, larger particles, dead cells (µm), debris and total impurities for 5L-STR CHO-CY01 cell line fed-batch strategy 5 (FB3) cultures at pH 6.80, 7.10 and 7.80.

	Time (days)	VCN (10^6 cells mL^{-1})	Cell Diameter (µm)	Viability (%)	Larger Particles (%)	Dead Cells (%)	Debris (%)	Total Impurities (%)
5L-STR pH 7.10 FB3								
Adaptation period	0 - 1	0.3 ± 0.1	14.8 ± 0.2	91.4 ± 3.2	9.2 ± 3.2	9.5 ± 13.4	25.4 ± 6.8	44.1 ± 3.4
Exponential period	2 - 6	2.7 ± 2.0	15.1 ± 0.4	94.2 ± 1.6	17.5 ± 12.8	20.3 ± 6.0	9.7 ± 3.6	47.4 ± 8.6
Stationary Period	7 - 11	7.4 ± 1.5	16.9 ± 0.6	94.4 ± 0.4	35.6 ± 9.5	9.5 ± 2.9	5.9 ± 0.9	51.1 ± 7.8
Beginning of decline period	12 - 13	6.3 ± 0.7	18.0 ± 0.2	91.4 ± 0.6	40.0 ± 4.2	7.5 ± 1.1	12.9 ± 1.8	60.4 ± 1.3
Decline period	14 - 16	6.3 ± 0.4	17.8 ± 0.8	78.9 ± 2.9	43.0 ± 13.6	11.8 ± 3.2	15.9 ± 3.0	70.7 ± 7.5
5L-STR pH 6.80 FB3								
Adaptation period	0 - 1	0.2 ± 0.1	15.5 ± 0.1	95.6 ± 0.2	5.5 ± 2.1	7.8 ± 11.1	16.1 ± 1.6	29.5 ± 7.3
Exponential period	2 - 9	2.4 ± 1.7	15.9 ± 0.4	94.6 ± 1.0	16.3 ± 12.9	17.7 ± 1.3	6.2 ± 1.9	40.2 ± 11.0
Stationary Period	11	5.3	17.4	93.9	33.6	9.9	7.2	50.7
Beginning of decline period	14 - 16	4.3 ± 1.3	18.6 ± 0.3	89.3 ± 1.7	42.0 ± 7.5	8.0 ± 1.3	13.4 ± 3.3	63.4 ± 2.9
Decline period	18	2.9	17.8	66.7	26.8	18.0	31.5	76.3
5L-STR pH 7.80 FB3								
Adaptation period	0 - 3	0.4 ± 0.2	16.6 ± 0.7	92.8 ± 0.9	7.0 ± 2.7	6.8 ± 4.6	19.7 ± 1.8	33.5 ± 3.1
Exponential period	4 - 6	1.9 ± 0.6	17.4 ± 0.1	93.7 ± 1.3	23.0 ± 11.8	8.4 ± 2.0	12.7 ± 3.5	44.1 ± 7.5
Stationary Period	7 - 8	3.7 ± 0.6	18.2 ± 0.3	92.6 ± 2.1	35.9 ± 4.4	7.8 ± 0.9	10.5 ± 1.7	54.3 ± 7.0
Beginning of decline period	9	3.4	19.4	90.2	48.5	6.9	12.8	68.2
Decline period	12	3.3	16.0	69.9	31.8	21.3	24.6	77.6

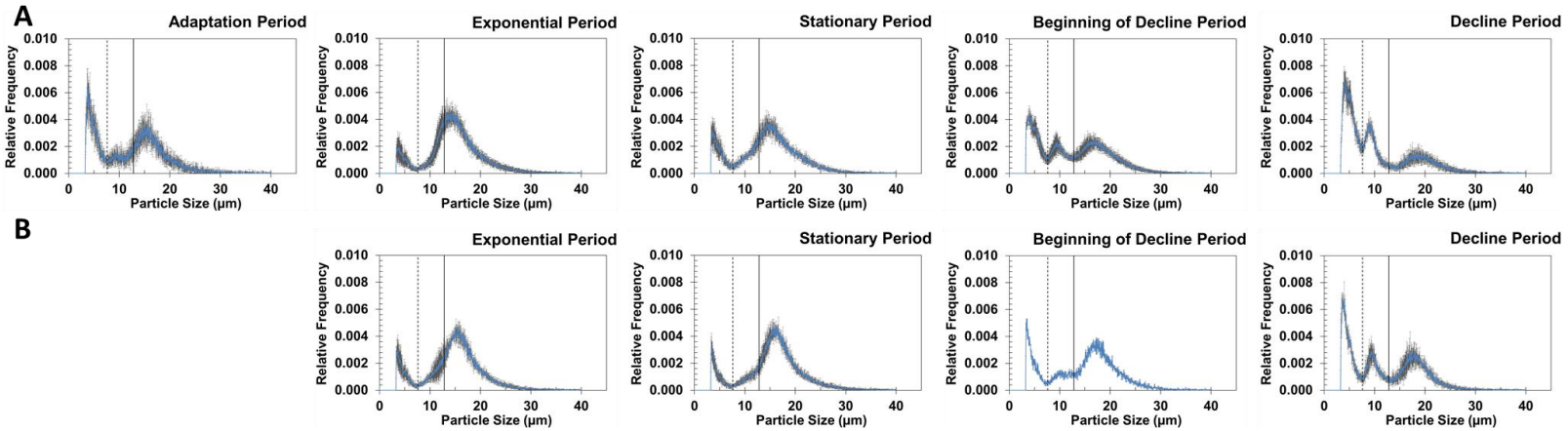

Figure B-13: CASY cell counter particle size distribution for 5L-STR CHO-CY01 cell line fed-batch strategy 5 (FB3) cultures with pH shift from pH 6.60 to 6.80 on day 2 (A), and pH shift from pH 7.60 to 7.10 on day 4 (B).

Table B-13: VCN, cell diameter, viability, larger particles, dead cells (µm), debris and total impurities for 5L-STR CHO-CY01 cell line fed-batch strategy 5 (FB3) cultures with pH shift from pH 6.60 to 6.80 on day 2, and pH shift from pH 7.60 to 7.10 on day 4.

	Time (days)	VCN (10^6 cells mL^{-1})	Cell Diameter (µm)	Viability (%)	Larger Particles (%)	Dead Cells (%)	Debris (%)	Total Impurities (%)
5L-STR FB3 pH Shift: pH 6.60 - 6.80 Day 2								
Adaptation period	0 - 4	0.3 ± 0.1	16.8 ± 0.8	85.2 ± 4.3	12.9 ± 6.3	14.2 ± 4.0	28.4 ± 5.0	55.4 ± 5.6
Exponential period	5 - 12	3.3 ± 2.3	16.3 ± 0.5	93.9 ± 1.2	18.9 ± 7.0	16.5 ± 4.1	8.6 ± 4.3	44.0 ± 4.3
Stationary Period	13 - 15	5.1 ± 0.6	17.0 ± 0.4	90.8 ± 1.8	29.6 ± 2.8	12.3 ± 1.2	12.1 ± 3.4	53.9 ± 4.3
Beginning of decline period	16 - 21	4.6 ± 0.4	17.7 ± 0.2	78.7 ± 6.6	31.8 ± 3.8	14.2 ± 2.5	20.5 ± 3.4	66.5 ± 5.1
Decline period	22 - 26	3.0 ± 0.4	18.5 ± 0.4	58.2 ± 4.5	50.0 ± 5.7	12.6 ± 1.5	23.4 ± 3.2	86.0 ± 2.9
5L-STR FB3 pH Shift: pH 7.60 - 7.10 Day 4								
Adaptation period								
Exponential period	3 - 6	2.0 ± 1.0	16.8 ± 0.3	93.2 ± 0.5	11.4 ± 4.6	13.7 ± 3.8	12.2 ± 4.3	37.3 ± 4.5
Stationary Period	7 - 10	8.0 ± 1.7	17.5 ± 0.4	94.2 ± 1.1	40.2 ± 5.3	7.2 ± 1.8	6.9 ± 1.1	54.3 ± 4.7
Beginning of decline period	12	7.1	18.2	89.9	44.8	7.7	11.9	64.4
Decline period	13 - 16	5.0 ± 1.4	17.8 ± 0.4	75.3 ± 6.3	45.1 ± 9.1	11.7 ± 2.4	19.3 ± 4.1	76.1 ± 5.1

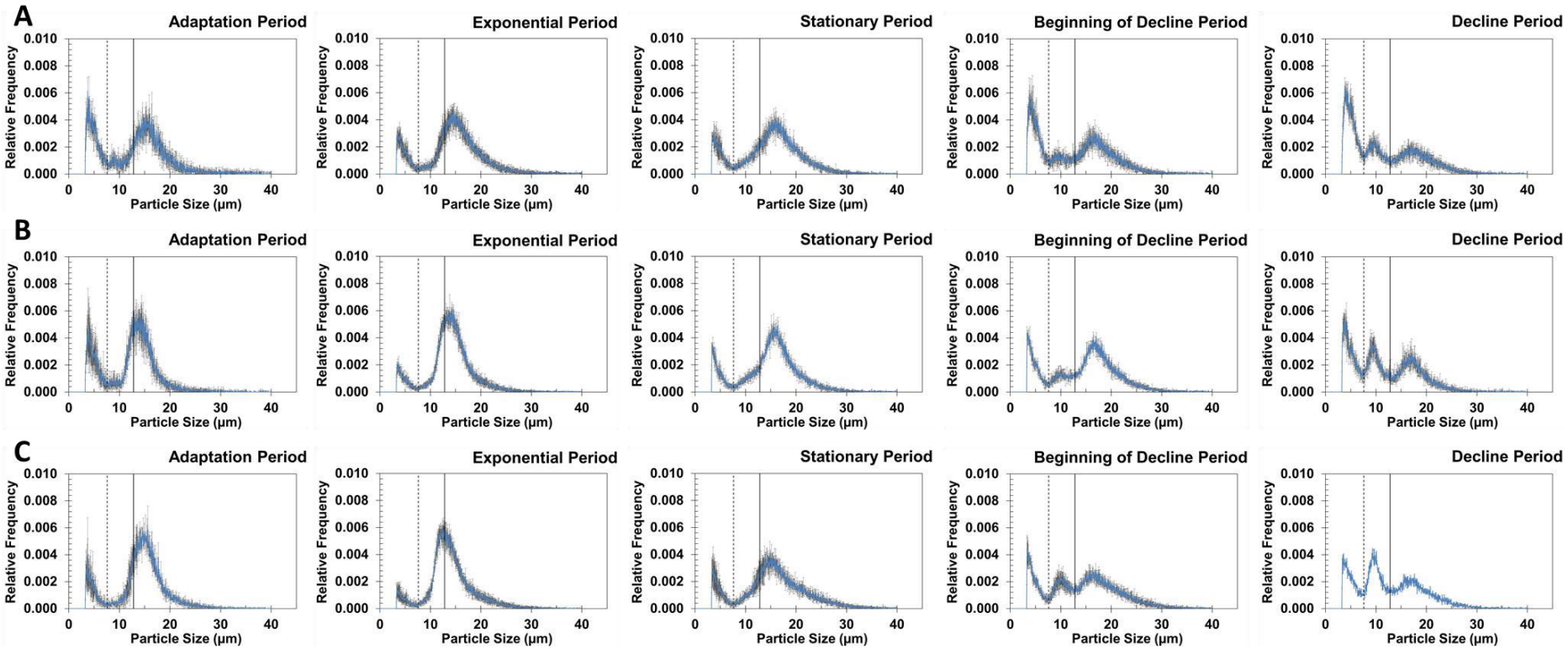

Figure B-14: CASY cell counter particle size distribution for 5L-STR CHO-CY01 cell line fed-batch strategy 5 (FB3) cultures with pH shifts from pH 7.10 to 6.80 on day 5 (A) or 8 (C), and pH shift from pH 7.10 to 7.00 on day 4, then to pH 6.80 on day 5 (B).

Table B-14: VCN, cell diameter, viability, larger particles, dead cells (µm), debris and total impurities for 5L-STR CHO-CY01 cell line fed-batch strategy 5 (FB3) cultures with pH shifts from pH 7.10 to 6.80 on day 5 or 8, and pH shift from pH 7.10 to 7.00 on day 4, then to pH 6.80 on day 5.

	Time (days)	VCN (106 cells mL-1)	Cell Diameter (µm)	Viability (%)	Larger Particles (%)	Dead Cells (%)	Debris (%)	Total Impurities (%)
5L-STR FB3 pH Shift: pH 7.10 - 6.80 Day 5								
Adaptation period	0 - 2	0.3 ± 0.1	16.8 ± 0.2	89.2 ± 2.0	22.7 ± 9.2	6.4 ± 5.8	22.6 ± 4.0	51.8 ± 11.5
Exponential period	3 - 7	1.8 ± 1.0	16.6 ± 0.3	94.3 ± 0.9	37.1 ± 11.6	9.7 ± 2.2	10.0 ± 3.2	56.8 ± 8.4
Stationary Period	8 - 10	5.4 ± 0.6	17.3 ± 0.2	92.4 ± 0.8	45.7 ± 8.4	8.1 ± 1.9	8.6 ± 0.9	62.4 ± 7.1
Beginning of decline period	11 - 14	4.0 ± 1.7	17.8 ± 0.3	84.9 ± 2.7	61.0 ± 4.6	5.8 ± 1.5	13.2 ± 1.5	80.0 ± 2.4
Decline period	15 - 17	4.1 ± 1.5	17.7 ± 0.1	73.3 ± 4.4	48.8 ± 5.5	11.0 ± 1.8	20.7 ± 3.3	80.5 ± 2.3
5L-STR FB3 pH Shift: pH 7.10 - 7.00 - 6.80 Day 4/5								
Adaptation period	0 - 2	0.4 ± 0.2	14.9 ± 0.1	91.8 ± 3.3	7.3 ± 4.1	12.9 ± 11.2	22.7 ± 8.9	43.0 ± 7.3
Exponential period	3 - 8	3.4 ± 2.4	15.2 ± 0.3	94.8 ± 0.2	14.4 ± 13.2	20.2 ± 3.2	8.2 ± 2.1	42.9 ± 8.7
Stationary Period	10 - 11	6.3 ± 2.1	17.0 ± 0.1	93.1 ± 0.1	27.8 ± 5.7	9.8 ± 1.6	10.4 ± 0.8	48.0 ± 5.0
Beginning of decline period	12 - 13	6.2 ± 0.3	17.9 ± 0.1	88.8 ± 2.3	34.1 ± 0.2	9.7 ± 1.6	13.8 ± 0.1	57.6 ± 1.5
Decline period	14 - 16	6.2 ± 1.0	16.9 ± 0.4	69.5 ± 6.3	49.3 ± 17.3	14.3 ± 5.7	16.3 ± 6.5	79.9 ± 6.0
5L-STR FB3 pH Shift: pH 7.10 - 6.80 Day 8								
Adaptation period	0 - 3	0.8 ± 0.4	15.9 ± 0.3	95.7 ± 0.3	6.2 ± 0.5	13.1 ± 4.8	13.5 ± 5.6	32.8 ± 0.2
Exponential period	4 - 7	3.1 ± 1.5	15.0 ± 0.4	92.5 ± 1.1	12.1 ± 6.1	29.8 ± 3.8	6.1 ± 2.2	48.0 ± 3.6
Stationary Period	8 - 10	4.6 ± 1.4	17.7 ± 0.4	93.4 ± 1.2	38.0 ± 4.0	9.3 ± 1.0	8.5 ± 3.1	55.8 ± 4.2
Beginning of decline period	12 - 14	4.7 ± 0.9	18.1 ± 0.5	83.1 ± 4.0	38.0 ± 5.0	13.5 ± 3.6	13.3 ± 1.1	64.8 ± 0.7

Appendix C: Observed Metabolic Yield Coefficients

The determination of the observed metabolic yield coefficients ($Y'_{P/S}$) were essential to understand the complex metabolism of CHO-CY01 cell kinetics. The observed yields were estimated as described in the Section 2.3.13.

Table C-1: $Y'_{P/S}$ for different 24-SRW MTP CHO-CY01 cell batch cultures fill volumes (0.50, 0.85, 1.00 and 1.50 mL).

$\boldsymbol{V_L\ (mL)}$	**0.50**	**0.85**	**1.00**	**1.50**
$Y'_{X/Gluc}\ (10^9\ cells/g)$	-0.168	-1.001	-1.090	-1.023
$Y'_{X/Glu}\ (10^9\ cells/mmol)$	-0.362	-3.128	-3.388	-4.540
$Y'_{IgG4/Gluc}\ (g/g)$	-0.004	-0.051	-0.046	-0.006
$Y'_{IgG4/Glu}\ (g/mmol)$	-0.007	-0.133	-0.145	-0.052
$Y'_{IgG4/X}\ (g/10^9\ cells)$	0.038	0.044	0.038	0.011
$Y'_{Lact/Gluc}\ (g/g)$	-0.231	-0.690	-0.774	-0.940
$Y'_{Lact/Glu}\ (g/mmol)$	-0.317	-2.505	-0.010	-2.765
$Y'_{Lact/X}\ (g/10^9\ cells)$	1.930	0.775	1.033	1.215
$Y'_{Amm/Gluc}\ (mmol/g)$	-0.146	-0.731	-0.569	-0.985
$Y'_{Amm/Glu}\ (mmol/mmol)$	-0.010	-2.569	-1.389	-3.172
$Y'_{Amm/X}\ (mmol/10^9\ cells)$	1.540	0.782	0.488	1.267

Table C-2: $Y'_{P/S}$ for different 24-SRW MTP CHO-CY01 cell batch cultures at different shaking speeds (100, 150, 180, 220, 250 and 300 rpm).

$N\ (rpm)$	**100**	**150**	**180**	**220**	**250**	**300**
$Y'_{X/Gluc}\ (10^9\ cells/g)$	-0.38	-1.15	-1.49	-1.46	-1.15	-0.91
$Y'_{X/Glu}\ (10^9\ cells/mmol)$	-0.35	-2.41	-4.20	-3.01	-2.43	-1.92
$Y'_{IgG4/Gluc}\ (g/g)$	-0.02	-0.05	-0.03	-0.03	-0.05	-0.06
$Y'_{IgG4/Glu}\ (g/mmol)$	-0.06	-0.11	-0.10	-0.07	-0.10	-0.15
$Y'_{IgG4/X}\ (g/10^9\ cells)$	0.04	0.04	0.02	0.02	0.04	0.06
$Y'_{Lact/Gluc}\ (g/g)$	-0.61	-0.44	-0.39	-0.33	-0.58	-0.82
$Y'_{Lact/Glu}\ (g/mmol)$	-0.93	-0.94	-0.92	-0.56	-1.93	-0.97
$Y'_{Lact/X}\ (g/10^9\ cells)$	1.26	0.34	0.24	0.19	0.60	0.93
$Y'_{Amm/Gluc}\ (mmol/g)$	-0.90	-0.74	-0.76	-0.81	-0.81	-0.96
$Y'_{Amm/Glu}\ (mmol/mmol)$	-2.01	-2.76	-2.27	-2.27	-2.94	2.55
$Y'_{Amm/X}\ (mmol/10^9\ cells)$	1.74	0.73	0.54	0.70	0.86	1.11

Table C-3: $Y'_{P/S}$ for 24-SRW MTP CHO-CY01 cell batch cultures sealed with CR1524 and CR1524a ´system Duetz` lids at 2.00% (v/v) CO_2.

´System Duetz` Lid	CR1524	CR1524a
$Y'_{X/Gluc}$ $(10^9\ cells/g)$	-1.01	-1.42
$Y'_{X/Glu}$ $(10^9\ cells/mmol)$	-1.97	-2.60
$Y'_{IgG4/Gluc}$ (g/g)	-0.04	-0.06
$Y'_{IgG4/Glu}$ $(g/mmol)$	-0.11	-142.00
$Y'_{IgG4/X}$ $(g/10^9\ cells)$	0.03	0.03
$Y'_{Lact/Gluc}$ (g/g)	-0.41	-0.94
$Y'_{Lact/Glu}$ $(g/mmol)$	-0.66	4.67
$Y'_{Lact/X}$ $(g/10^9\ cells)$	0.33	0.47
$Y'_{Amm/Gluc}$ $(mmol/g)$	-0.51	-0.71
$Y'_{Amm/Glu}$ $(mmol/mmol)$	-0.76	1.82
$Y'_{Amm/X}$ $(mmol/10^9\ cells)$	0.43	0.40

Table C-4: $Y'_{P/S}$ for CHO-CY01 cell batch in a standard 24-SRW MTP and in HydroDish®HD24 at 5.00% (v/v) CO_2.

	24-SRW MTP	HydroDish®HD24
$Y'_{X/Gluc}$ $(10^9\ cells/g)$	-1.59	-0.74
$Y'_{X/Glu}$ $(10^9\ cells/mmol)$	-3.47	-1.54
$Y'_{IgG4/Gluc}$ (g/g)	-0.04	-0.03
$Y'_{IgG4/Glu}$ $(g/mmol)$	-0.07	-0.05
$Y'_{IgG4/X}$ $(g/10^9\ cells)$	0.03	0.03
$Y'_{Lact/Gluc}$ (g/g)	-0.46	-0.90
$Y'_{Lact/Glu}$ $(g/mmol)$	-0.97	3.95
$Y'_{Lact/X}$ $(g/10^9\ cells)$	0.27	1.46
$Y'_{Amm/Gluc}$ $(mmol/g)$	-0.57	-0.65
$Y'_{Amm/Glu}$ $(mmol/mmol)$	-1.32	1.92
$Y'_{Amm/X}$ $(mmol/10^9\ cells)$	0.34	0.95

Table C-5: $Y'_{P/S}$ for CHO-CY01 cell batch in a 24-SRW MTP and in HydroDish®HD24 at 2.00% (v/v) CO_2.

	24-SRW MTP	HydroDish®HD24
Exponential Phase $(days)$	8.77	7.94
$Y'_{X/Gluc}$ $(10^9\ cells/g)$	-1.42	-1.10
$Y'_{X/Glu}$ $(10^9\ cells/mmol)$	-2.60	-2.21
$Y'_{IgG4/Gluc}$ (g/g)	-0.06	-0.09
$Y'_{IgG4/Glu}$ $(g/mmol)$	-0.14	-0.23
$Y'_{IgG4/X}$ $(g/10^9\ cells)$	0.03	0.06
$Y'_{Lact/Gluc}$ (g/g)	-0.94	-0.98
$Y'_{Lact/Glu}$ $(g/mmol)$	4.67	4.08
$Y'_{Lact/X}$ $(g/10^9\ cells)$	0.47	0.52
$Y'_{Amm/Gluc}$ $(mmol/g)$	-0.71	-0.56
$Y'_{Amm/Glu}$ $(mmol/mmol)$	1.82	-0.43
$Y'_{Amm/X}$ $(mmol/10^9\ cells)$	0.40	0.38

Table C-6**:** $Y'_{P/S}$ for 24-SRW MTP CHO-CY01 cell batch cultures with different MSX concentrations (0, 25, 50 and 75 µM).

MSX Concentration (µM)	**0**	**25**	**50**	**75**
Exponential Phase ($days$)	5.99	7.94	6.95	7.98
$Y'_{X/Gluc}$ $(10^9\ cells/g)$	-2.00	-1.17	-1.26	-0.82
$Y'_{X/Glu}$ $(10^9\ cells/mmol)$	-7.07	-2.99	-7.28	-2.88
$Y'_{IgG4/Gluc}$ (g/g)	-0.04	-0.03	-0.04	-0.05
$Y'_{IgG4/Glu}$ $(g/mmol)$	-0.14	-0.10	-0.21	-0.21
$Y'_{IgG4/X}$ $(g/10^9\ cells)$	0.02	0.03	0.03	0.06
$Y'_{Lact/Gluc}$ (g/g)	-0.59	-0.51	-0.62	-0.60
$Y'_{Lact/Glu}$ $(g/mmol)$	-1.93	-1.17	-3.39	-0.19
$Y'_{Lact/X}$ $(g/10^9\ cells)$	0.28	0.44	0.49	0.75
$Y'_{Amm/Gluc}$ $(mmol/g)$	-0.94	-0.89	-0.98	-1.03
$Y'_{Amm/Glu}$ $(mmol/mmol)$	-3.13	-2.17	-5.13	0.29
$Y'_{Amm/X}$ $(mmol/10^9\ cells)$	0.46	0.76	0.77	1.31

Table C-7**:** $Y'_{P/S}$ for standard CHO-CY01 cell batch culture at different bioreactor scales, 5L-STR; 24-SRW MTP; SF 125 mL and SF 250 mL.

	5L-STR	**24-SRW MTP**	**SF 125 mL**	**SF 250 mL**
$Y'_{X/Gluc}$ $(10^9\ cells/g)$	-1.46	-1.35 ± 0.14	-1.19 ± 0.11	-1.34 ± 0.20
$Y'_{X/Glu}$ $(10^9\ cells/mmol)$	-3.84	-2.51 ± 0.24	-2.84 ± 0.41	-2.82 ± 0.48
$Y'_{IgG4/Gluc}$ (g/g)	-0.04	-0.04 ± 0.01	-0.08 ± 0.03	-0.10 ± 0.01
$Y'_{IgG4/Glu}$ $(g/mmol)$	-0.10	-0.10 ± 0.04	-0.20 ± 0.04	-0.21 ± 0.03
$Y'_{IgG4/X}$ $(g/10^9\ cells)$	0.02	0.03 ± 0.00	0.05 ± 0.01	0.06 ± 0.01
$Y'_{Lact/Gluc}$ (g/g)	-0.70	-0.36 ± 0.13	-0.85 ± 0.36	-1.30 ± 1.48
$Y'_{Lact/Glu}$ $(g/mmol)$	-3.04	-1.07 ± 0.63	-2.36 ± 1.08	-1.01 ± 0.04
$Y'_{Lact/X}$ $(g/10^9\ cells)$	0.47	0.27 ± 0.12	0.78 ± 0.35	0.67 ± 0.55
$Y'_{Amm/Gluc}$ $(mmol/g)$	-0.52	-0.77 ± 0.08	-0.56 ± 0.18	-2.10 ± 2.89
$Y'_{Amm/Glu}$ $(mmol/mmol)$	-2.27	-1.66 ± 0.56	-1.50 ± 0.52	-0.87 ± 0.16
$Y'_{Amm/X}$ $(mmol/10^9\ cells)$	0.45	0.65 ± 0.08	0.66 ± 0.05	1.02 ± 1.17

Table C-8: $Y'_{P/S}$ for CHO-CY01 cell batch culture at different initial lactate concentrations (0.*0*, *0.7*, *1.9*, *2.7*, *3.6 and 4.7* g L^{-1}).

Lactate Concentration (g L^{-1})	**0.0**	**0.7**	**1.9**	**2.7**	**3.6**	**4.7**
$Y'_{X/Gluc}$ (10^9 $cells/g$)	-1.19 ± 0.11	-1.35	-1.27 ± 0.28	-0.95 ± 0.44	-0.38 ± 0.10	-0.29 ± 0.12
$Y'_{X/Glu}$ (10^9 $cells/mmol$)	-2.84 ± 0.41	-1.77	-2.02 ± 0.05	-1.38 ± 0.18	-0.50 ± 0.30	-0.04 ± 0.06
$Y'_{IgG4/Gluc}$ (g/g)	-0.08 ± 0.03	-0.08	-0.04 ± 0.01	-0.08 ± 0.01	-0.04 ± 0.02	-0.03 ± 0.01
$Y'_{IgG4/Glu}$ ($g/mmol$)	-0.20 ± 0.04	-0.10	-0.07 ± 0.00	-0.12 ± 0.03	-0.06 ± 0.04	0.00 ± 0.00
$Y'_{IgG4/X}$ ($g/10^9$ $cells$)	0.05 ± 0.01	0.06	0.04 ± 0.01	0.07 ± 0.01	0.06 ± 0.01	0.02 ± 0.01
$Y'_{Lact/Gluc}$ (g/g)	-0.85 ± 0.36	-0.15	-0.18			
$Y'_{Lact/Glu}$ ($g/mmol$)	-2.36 ± 1.08	-0.13	-0.12			
$Y'_{Lact/X}$ ($g/10^9$ $cells$)	0.78 ± 0.35	0.09	0.16			
$Y'_{Amm/Gluc}$ ($mmol/g$)	-0.56 ± 0.18	-0.44	-0.39 ± 0.09	-0.30 ± 0.12	-0.32 ± 0.15	-0.91 ± 0.01
$Y'_{Amm/Glu}$ ($mmol/mmol$)	-1.50 ± 0.52	-0.53	-0.67 ± 0.32	-0.36 ± 0.09	-0.38 ± 0.06	-0.05 ± 0.11
$Y'_{Amm/X}$ ($mmol/10^9$ $cells$)	0.66 ± 0.05	0.50	0.27 ± 0.13	0.27 ± 0.07	0.89 ± 0.78	3.36 ± 1.42

Table C-9: $Y'_{P/S}$ for CHO-CY01 cell batch culture at different initial ammonium concentrations (0.2, 4.8, 7.1, 9.7 and 11.2 $mmol\ L^{-1}$).

Ammonium Concentration ($mmol\ L^{-1}$)	**0.2**	**4.8**	**7.1**	**9.7**	**11.2**
$Y'_{X/Gluc}$ $(10^9\ cells/g)$	-1.19 ± 0.11	-1.49	-1.17	-0.97	-0.77
$Y'_{X/Glu}$ $(10^9\ cells/mmol)$	-2.84 ± 0.41	-3.22	-2.47	-3.25	-2.08
$Y'_{IgG4/Gluc}$ (g/g)	-0.08 ± 0.03	-0.07	-0.06	-0.07	-0.07
$Y'_{IgG4/Glu}$ $(g/mmol)$	-0.20 ± 0.04	-0.15	-0.12	-0.23	-0.14
$Y'_{IgG4/X}$ $(g/10^9\ cells)$	0.05 ± 0.01	0.04	0.04	0.06	0.06
$Y'_{Lact/Gluc}$ (g/g)	-0.85 ± 0.36	-0.20	-0.17	-0.11	-0.18
$Y'_{Lact/Glu}$ $(g/mmol)$	-2.36 ± 1.08		-0.10		
$Y'_{Lact/X}$ $(g/10^9\ cells)$	0.78 ± 0.35	0.22	0.15	0.14	0.15
$Y'_{Amm/Gluc}$ $(mmol/g)$	-0.56 ± 0.18	-0.66	-1.19		
$Y'_{Amm/Glu}$ $(mmol/mmol)$	-1.50 ± 0.52				
$Y'_{Amm/X}$ $(mmol/10^9\ cells)$	0.66 ± 0.05	0.63	1.29		

Table C-10: $Y'_{P/S}$ for CHO-CY01 cell batch culture at different initial sodium concentrations (95, 99, 103, 108 and 118 $mmol\ L^{-1}$).

Sodium Concentration ($mmol\ L^{-1}$)	**95**	**99**	**103**	**108**	**118**
$Y'_{X/Gluc}$ $(10^9\ cells/g)$	-0.94	-0.95	-1.07 ± 0.08	-1.32	-1.19 ± 0.11
$Y'_{X/Glu}$ $(10^9\ cells/mmol)$	-1.50	-1.47	-1.62 ± 0.27	-1.80	-2.84 ± 0.41
$Y'_{IgG4/Gluc}$ (g/g)	-0.09	-0.09	-0.08 ± 0.00	-0.06	-0.08 ± 0.03
$Y'_{IgG4/Glu}$ $(g/mmol)$	-0.15	-0.15	-0.12 ± 0.01	-0.08	-0.20 ± 0.04
$Y'_{IgG4/X}$ $(g/10^9\ cells)$	0.07	0.08	0.06 ± 0.00	0.04	0.05 ± 0.01
$Y'_{Lact/Gluc}$ (g/g)	-0.12	-0.15	-0.24 ± 0.07	-0.32	-0.85 ± 0.36
$Y'_{Lact/Glu}$ $(g/mmol)$	-0.15	-0.21	-0.27 ± 0.11	-0.50	-2.36 ± 1.08
$Y'_{Lact/X}$ $(g/10^9\ cells)$	0.36	0.17	0.32 ± 0.15	0.22	0.78 ± 0.35
$Y'_{Amm/Gluc}$ $(mmol/g)$	-1.02	-0.93	-0.95 ± 0.07	-0.86	-0.56 ± 0.18
$Y'_{Amm/Glu}$ $(mmol/mmol)$	-1.37	-1.48	-1.39 ± 0.17	-1.23	-1.50 ± 0.52
$Y'_{Amm/X}$ $(mmol/10^9\ cells)$	2.83	1.21	1.24 ± 0.16	-1.32	0.66 ± 0.05

Table C-11: $Y'_{P/S}$ for CHO-CY01 cell line fed-batch strategy 4 (FB2) and fed-batch strategy 5 (FB3) cultures at different bioreactor scales, 5L-STR; 24-SRW MTP; SF 125 mL and SF 250 mL.

	Fed-Batch Strategy 4 (FB2)				Fed-Batch Strategy 5 (FB3)			
	5L-STR	**24-SRW MTP**	**SF 125 mL**	**SF 250 mL**	**5L-STR**	**24-SRW MTP**	**SF 125 mL**	**SF 250 mL**
Exponential Phase (days)	1 - 7	1 - 7	0 - 7	2 - 7	3 - 9	3 - 8	2 - 7	0 - 7
$Y'_{X/Gluc}$ $(10^9\ cells/g)$	-0.88	-1.73	-1.77	-1.74	-1.37	-1.02	-1.72	-1.79
$Y'_{X/Glu}$ $(10^9\ cells/mmol)$	-3.31	-4.73	-3.79	-4.10	-3.31	-1.64	-3.74	-3.90
$Y'_{IgG4/Gluc}$ (g/g)	-0.02	-0.05	-0.04	-0.05	-0.03	-0.09	-0.05	-0.03
$Y'_{IgG4/Glu}$ $(g/mmol)$	-0.06	-0.17	-0.08	-0.10	-0.11	-0.15	-0.09	-0.06
$Y'_{IgG4/X}$ $(g/10^9\ cells)$	0.015	0.022	0.020	0.022	0.023	0.051	0.028	0.016
$Y'_{Lact/Gluc}$ (g/g)	-0.39	-0.53	-0.42	-0.87	-0.55	-0.15	-0.49	-0.67
$Y'_{Lact/Glu}$ $(g/mmol)$	-1.33	-3.68	-0.71	-4.85	-1.00	-0.35	n/a	-2.31
$Y'_{Lact/X}$ $(g/10^9\ cells)$	0.44	0.32	0.34	0.57	0.40	0.16	0.52	0.75
$Y'_{Amm/Gluc}$ $(mmol/g)$	-0.32	-0.79	-0.72	-0.75	-0.40	-0.62	-0.50	-0.86
$Y'_{Amm/Glu}$ $(mmol/mmol)$	-1.98	-5.11	-1.63	-3.31	-12.76	-1.36	-0.83	-1.84
$Y'_{Amm/X}$ $(mmol/10^9\ cells)$	0.41	0.43	0.58	0.62	0.48	0.61	0.36	0.68

Table C-12: $Y'_{P/S}$ for CHO-CY01 cell line batch cultures in 24-SRW-MTP at different CO_2 (0.04%; 1.00%; 2.00%; 5.00%, 10.00%; 15.00%; and 20.00% (v/v) CO_2).

CO_2 (% (v/v))	1.00	2.00	5.00	10.00	15.00	20.00
Exponential Phase (days)	2 ± 8	3 ± 7	2 ± 7	2 ± 7	3 ± 8	5 ± 12
$Y'_{X/Gluc}$ $(10^9\ cells/g)$	-0.86 ± 0.24	-1.39 ± 0.06	-1.35 ± 0.14	-1.13	-2.14 ± 2.27	-1.49 ± 1.19
$Y'_{X/Glu}$ $(10^9\ cells/mmol)$	-1.99 ± 1.00	-3.33 ± 0.05	-2.51 ± 0.24	-2.73	-4.16 ± 4.62	-3.70 ± 3.79
$Y'_{IgG4/Gluc}$ (g/g)	-0.08 ± 0.04	-0.06 ± 0.00	-0.04 ± 0.01	-0.05	-0.06 ± 0.03	-0.13 ± 0.06
$Y'_{IgG4/Glu}$ $(g/mmol)$	-0.15 ± 0.04	-0.17 ± 0.01	-0.10 ± 0.04	-0.12	-0.11 ± 0.06	-0.30 ± 0.22
$Y'_{IgG4/X}$ $(g/10^9\ cells)$	0.06 ± 0.03	0.04 ± 0.00	0.03 ± 0.00	0.04	0.03 ± 0.01	0.07 ± 0.01
$Y'_{Lact/Gluc}$ (g/g)	-0.88 ± 0.31	-0.58 ± 0.08	-0.36 ± 0.13	-0.23	-0.89 ± 0.75	-0.60 ± 0.45
$Y'_{Lact/Glu}$ $(g/mmol)$	-0.12 ± 5.50	-0.72 ± 0.07	-1.07 ± 0.63	-0.65	-1.64 ± 1.24	-1.28 ± 1.50
$Y'_{Lact/X}$ $(g/10^9\ cells)$	1.13 ± 0.61	0.55 ± 0.04	0.27 ± 0.12	0.22	0.82 ± 0.79	0.36 ± 0.02
$Y'_{Amm/Gluc}$ $(mmol/g)$	-0.85 ± 0.36	-0.72 ± 0.12	-0.77 ± 0.08	-0.37	-1.77 ± 1.42	-2.16 ± 1.58
$Y'_{Amm/Glu}$ $(mmol/mmol)$	-2.63 ± 1.92	-1.67 ± 0.60	-1.66 ± 0.56	-0.88	-3.38 ± 2.89	-2.50 ± 7.00
$Y'_{Amm/X}$ $(mmol/10^9\ cells)$	1.12 ± 0.09	0.59 ± 0.25	0.65 ± 0.08	0.32	0.96 ± 0.19	1.17 ± 0.39

Table C-13**:** $Y'_{P/S}$ for CHO-CY01 cell *line f*ed batch strategy 5 (FB3) cultures in 24-SRW-MTPs at 5.00%, 10.00%, and 15.00% (v/v) CO_2.

CO_2 (% (v/v))	**5.00**	**10.00**	**15.00**
Exponential Phase (days)	3 ± 8	2 ± 7	2 ± 6
$Y'_{X/Gluc}$ $(10^9\ cells/g)$	-1.02	-2.16 ± 0.35	-2.39
$Y'_{X/Glu}$ $(10^9\ cells/mmol)$	-1.64	-4.03 ± 1.40	-7.04
$Y'_{IgG4/Gluc}$ (g/g)	-0.09	-0.06 ± 0.01	-0.04
$Y'_{IgG4/Glu}$ $(g/mmol)$	-0.15	-0.12 ± 0.01	-0.15
$Y'_{IgG4/X}$ $(g/10^9\ cells)$	0.05	0.03 ± 0.00	0.02
$Y'_{Lact/Gluc}$ (g/g)	-0.15	-0.56 ± 0.34	-0.45
$Y'_{Lact/Glu}$ $(g/mmol)$	-0.35	-1.28 ± 0.99	-1.22
$Y'_{Lact/X}$ $(g/10^9\ cells)$	0.16	0.26 ± 0.19	0.19
$Y'_{Amm/Gluc}$ $(mmol/g)$	-0.62	-0.71 ± 0.10	-1.08
$Y'_{Amm/Glu}$ $(mmol/mmol)$	-1.36	-1.26 ± 0.41	-3.10
$Y'_{Amm/X}$ $(mmol/10^9\ cells)$	0.61	0.33 ± 0.02	0.45

Table C-14**:** $Y'_{P/S}$ for CHO-CY01 cell line batch culture at constant 5.00% (v/v) CO_2 and the first CO_2 multiphasic CHO-CY01 cell line batch cultivation in 24-SRW-MTPs (pH shift 1).

CO_2 (% (v/v))	**5.00**	**pH Shift 1**
Exponential Phase (days)	2 - 7	2 - 4
$Y'_{X/Gluc}$ $(10^9\ cells/g)$	-1.35 ± 0.14	-1.15
$Y'_{X/Glu}$ $(10^9\ cells/mmol)$	-2.51 ± 0.24	
$Y'_{IgG4/Gluc}$ (g/g)	-0.04 ± 0.01	-0.02
$Y'_{IgG4/Glu}$ $(g/mmol)$	-0.10 ± 0.04	-0.01
$Y'_{IgG4/X}$ $(g/10^9\ cells)$	0.03 ± 0.00	0.02
$Y'_{Lact/Gluc}$ (g/g)	-0.36 ± 0.13	-0.88
$Y'_{Lact/Glu}$ $(g/mmol)$	-1.07 ± 0.63	
$Y'_{Lact/X}$ $(g/10^9\ cells)$	0.27 ± 0.12	0.72
$Y'_{Amm/Gluc}$ $(mmol/g)$	-0.77 ± 0.08	-0.83
$Y'_{Amm/Glu}$ $(mmol/mmol)$	-1.66 ± 0.56	
$Y'_{Amm/X}$ $(mmol/10^9\ cells)$	0.65 ± 0.08	0.70

Table C-15: $Y'_{P/S}$ for CHO-CY01 cell line fed batch strategy 5 (FB3) cultures in 24-SRW-MTPs with constant 5.00% (v/v) CO_2, CO_2 shift from 5.00% to 20.00% (v/v) CO_2 on day 7 (1 step) and CO_2 shift from 5.00% to 15.0% (v/v) CO_2 10 (4 steps).

CO_2 (% (v/v))	5.00	5.00 -20.00 (day 7)	5.00 -7.50 -- 10.00 – 12.50 -- 15.00 (day 2, 7, 8, 10)
Exponential Phase (days)	3 ± 8	2 ± 7	2 ± 5
$Y'_{X/Gluc}$ $(10^9\ cells/g)$	-1.02	-1.44	-1.24
$Y'_{X/Glu}$ $(10^9\ cells/mmol)$	-1.64	-2.43	-3.75
$Y'_{IgG4/Gluc}$ (g/g)	-0.09	-0.05	-0.02
$Y'_{IgG4/Glu}$ $(g/mmol)$	-0.15	-0.09	-0.05
$Y'_{IgG4/X}$ $(g/10^9\ cells)$	0.051	0.033	0.019
$Y'_{Lact/Gluc}$ (g/g)	-0.15	-0.25	-0.07
$Y'_{Lact/Glu}$ $(g/mmol)$	-0.35	-0.38	-0.20
$Y'_{Lact/X}$ $(g/10^9\ cells)$	0.16	0.17	
$Y'_{Amm/Gluc}$ $(mmol/g)$	-0.62	-0.80	0.04
$Y'_{Amm/Glu}$ $(mmol/mmol)$	-1.36	-1.50	-0.53
$Y'_{Amm/X}$ $(mmol/10^9\ cells)$	0.61	0.79	-1.83

Table C-16: $Y'_{P/S}$ for CHO-CY01 cell line fed batch strategy 5 (FB3) cultures in 24-SRW-MTPs with constant 10.00% (v/v) CO_2 and CO_2 shifts from 10.00% to 20.00% (v/v) CO_2 at day 3, 5 and 9.

CO_2 (% (v/v))	10.00	10.00 – 20.00 Day 3	10.00 – 20.00 Day 5	10.00 – 20.00 Day 9
Exponential Phase (days)	2 ± 7	3 ± 8	2 ± 9	2 ± 7
$Y'_{X/Gluc}$ $(10^9\ cells/g)$	-2.16 ± 0.35	-1.09	-1.40 ± 0.23	-1.36
$Y'_{X/Glu}$ $(10^9\ cells/mmol)$	-4.03 ± 1.40	-2.42	-3.65 ± 0.58	-2.56
$Y'_{IgG4/Gluc}$ (g/g)	-0.06 ± 0.01	-0.05	-0.05 ± 0.02	-0.06
$Y'_{IgG4/Glu}$ $(g/mmol)$	-0.12 ± 0.01	-0.13	-0.13 ± 0.04	-0.12
$Y'_{IgG4/X}$ $(g/10^9\ cells)$	0.028 ± 0.005	0.041	0.04 ± 0.01	0.05
$Y'_{Lact/Gluc}$ (g/g)	-0.56 ± 0.34	-0.11	-0.19 ± 0.03	-0.33
$Y'_{Lact/Glu}$ $(g/mmol)$	-1.28 ± 0.99	-0.34	-0.48 ± 0.18	-0.40
$Y'_{Lact/X}$ $(g/10^9\ cells)$	0.26 ± 0.19	0.09	0.13 ± 0.04	-0.21
$Y'_{Amm/Gluc}$ $(mmol/g)$	-0.71 ± 0.10	-1.28	-1.23 ± 0.10	-1.14
$Y'_{Amm/Glu}$ $(mmol/mmol)$	-1.26 ± 0.41	-2.80	-3.25 ± 0.50	-1.16
$Y'_{Amm/X}$ $(mmol/10^9\ cells)$	0.33 ± 0.02	1.19	0.90 ± 0.11	0.79

Table C-17**:** $Y'_{P/S}$ for 5L-STR CHO-CY01 cell line batch cultures at different pHs (pH 6.80, 7.10 and 7.40)**.**

5L-STR Batch	**pH 7.10**	**pH 6.80**	**pH 7.40**
Exponential Phase (days)	3 ± 6	3 ± 11	3 ± 6
$Y'_{X/Gluc}$ $(10^9\ cells/g)$	-1.46	-0.85	-1.69
$Y'_{X/Glu}$ $(10^9\ cells/mmol)$	-3.84	-1.96	-6.08
$Y'_{IgG4/Gluc}$ (g/g)	-0.04	-0.07	-0.06
$Y'_{IgG4/Glu}$ $(g/mmol)$	-0.10	-0.18	-0.22
$Y'_{IgG4/X}$ $(g/10^9\ cells)$	0.02	0.06	0.03
$Y'_{Lact/Gluc}$ (g/g)	-0.70	-0.02	-0.35
$Y'_{Lact/Glu}$ $(g/mmol)$	-3.04	-0.07	-1.17
$Y'_{Lact/X}$ $(g/10^9\ cells)$	0.47	0.05	0.20
$Y'_{Amm/Gluc}$ $(mmol/g)$	-0.52	-1.07	-0.53
$Y'_{Amm/Glu}$ $(mmol/mmol)$	-2.27	-2.47	-2.67
$Y'_{Amm/X}$ $(mmol/10^9\ cells)$	0.45	1.26	0.32

Table C-18**:** $Y'_{P/S}$ for 5L-STR CHO-CY01 cell line fed-batch strategy 5 (FB3) cultures at pH 6.80, 7.10 and 7.80.

5L-STR FB3	**pH 7.10**	**pH 6.80**	**pH 7.80**
Exponential Phase (days)	3 ± 9	0 ± 8	3 ± 8
$Y'_{X/Gluc}$ $(10^9\ cells/g)$	-1.37	-1.28	-0.80
$Y'_{X/Glu}$ $(10^9\ cells/mmol)$	-3.31	-4.10	5.45
$Y'_{IgG4/Gluc}$ (g/g)	-0.03	-0.03	-0.02
$Y'_{IgG4/Glu}$ $(g/mmol)$	-0.11	-0.11	0.15
$Y'_{IgG4/X}$ $(g/10^9\ cells)$	0.02	0.03	0.02
$Y'_{Lact/Gluc}$ (g/g)	-0.55	-0.25	-1.01
$Y'_{Lact/Glu}$ $(g/mmol)$	-1.00	-0.92	6.91
$Y'_{Lact/X}$ $(g/10^9\ cells)$	0.40	0.20	1.24
$Y'_{Amm/Gluc}$ $(mmol/g)$	-0.40	-0.62	-0.33
$Y'_{Amm/Glu}$ $(mmol/mmol)$	-12.76	-1.81	-2.00
$Y'_{Amm/X}$ $(mmol/10^9\ cells)$	0.48	0.47	0.40

Table C-19**:** $Y'_{P/S}$ for 5L-STR CHO-CY01 cell line fed-batch strategy 5 (FB3) cultures with pH shift from pH 6.60 to 6.80 on day 2, pH shift from pH 7.60 to 7.10 on day 4, with pH shifts from pH 7.10 to 6.80 on day 5 or 8, and pH shift from pH 7.10 to 7.00 on day 4, then to pH 6.80 on day 5.

pH	**6.60 - 6.80**	**7.60 - 7.10**	**7.10 - 6.80**	**7.10 - 7.00 - 6.80**	**7.10 - 6.80**
5L-STR FB3	**Day 2**	**Day 4**	**Day 5**	**Day 4/5**	**Day 8**
Exponential Phase (days)	3 ± 12	3 ± 9	2 ± 7	2 ± 7	2 ± 7
$Y'_{X/Gluc}$ $(10^9\ cells/g)$	-1.90	-2.30	-1.01	-1.29	-1.43
$Y'_{X/Glu}$ $(10^9\ cells/mmol)$	-4.56	-5.42	-3.64	-3.01	-3.28
$Y'_{IgG4/Gluc}$ (g/g)	-0.06	-0.09	-0.01	-0.02	-0.03
$Y'_{IgG4/Glu}$ $(g/mmol)$	-0.18	-0.27	-0.03	-0.06	-0.08
$Y'_{IgG4/X}$ $(g/10^9\ cells)$	0.03	0.04	0.01	0.02	0.02
$Y'_{Lact/Gluc}$ (g/g)	-0.41	-1.04	-0.44	-0.52	-0.36
$Y'_{Lact/Glu}$ $(g/mmol)$	-0.97	-0.94	-1.70	-2.73	-1.83
$Y'_{Lact/X}$ $(g/10^9\ cells)$	0.26	0.24	0.65	0.45	0.27
$Y'_{Amm/Gluc}$ $(mmol/g)$	-0.80	-0.30	-0.77	-0.51	-0.71
$Y'_{Amm/Glu}$ $(mmol/mmol)$	0.02	2.49	-2.60	-2.94	-3.20
$Y'_{Amm/X}$ $(mmol/10^9\ cells)$	0.59	0.53	0.72	0.45	0.45

Appendix D: 5L-STR BIOSTAT Online Data

D.1. 5L-STR Online process parameters of CHO-CY01 cell line batch cultures

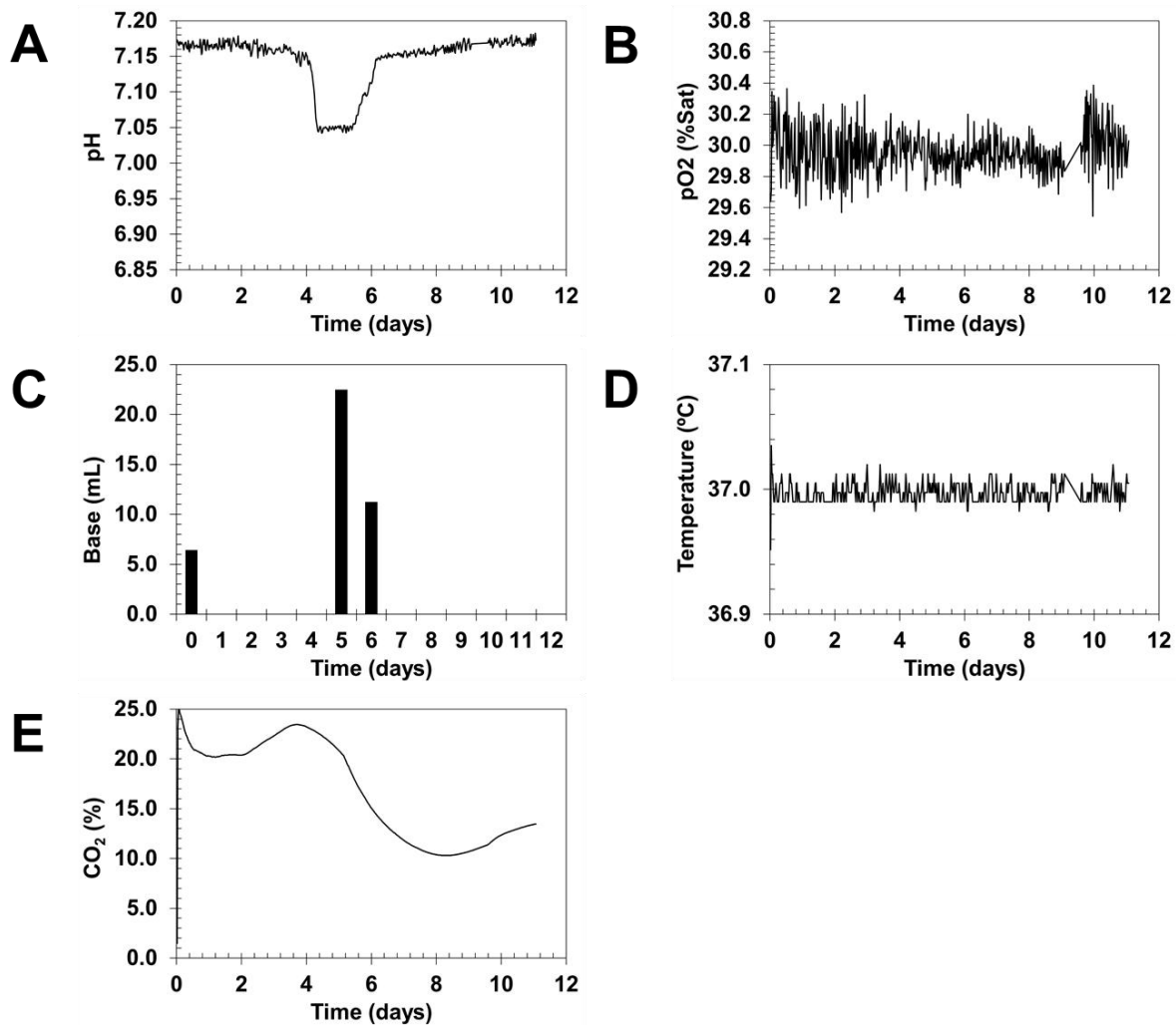

Figure D-1: CHO-CY01 cell line batch culture at pH 7.10 online process parameters, pH (A), pO_2 (% air saturation (% sat)) (B), volume of base added (C), temperature (D), and calculated CO_2 volume percentage (E).

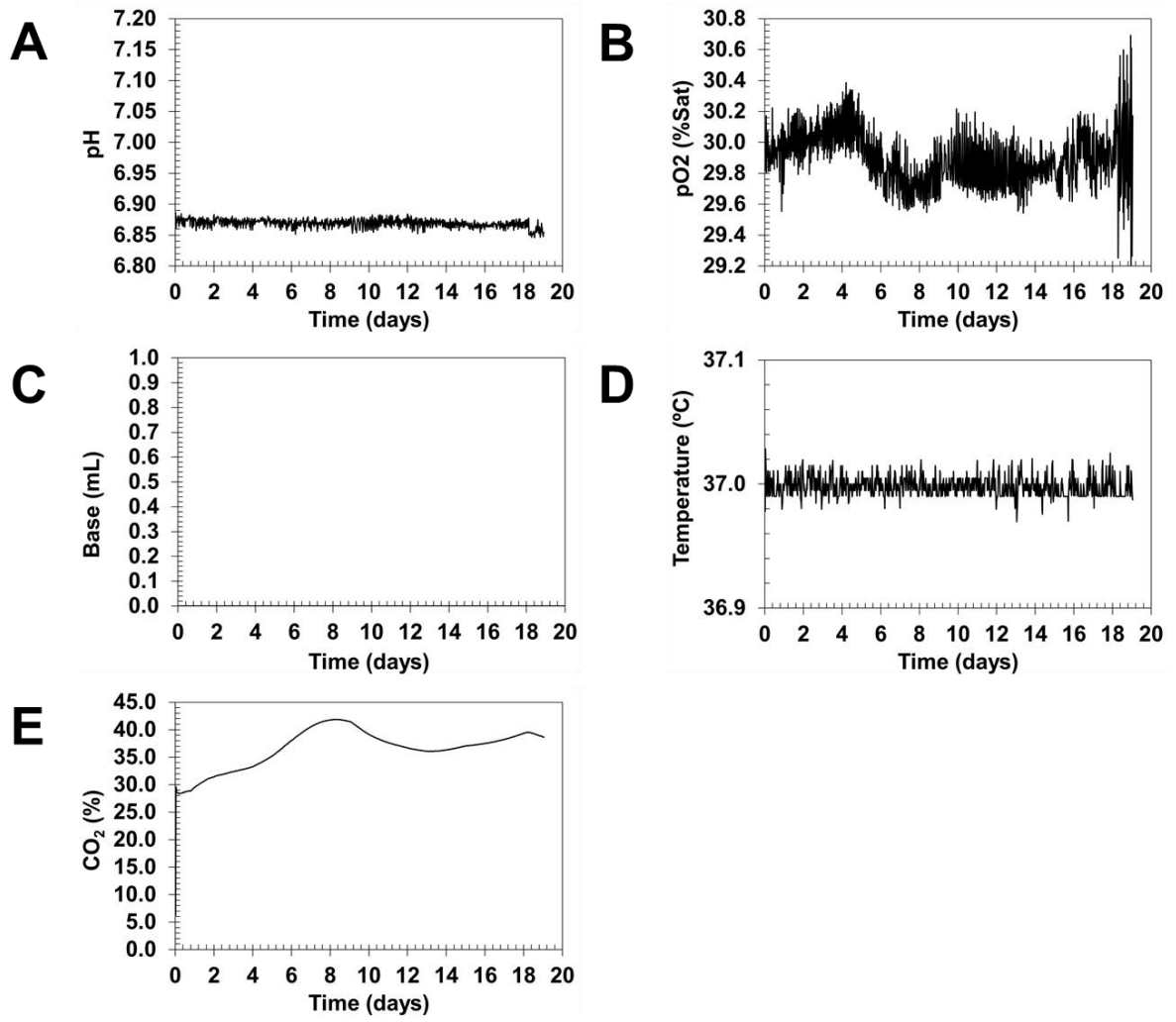

Figure D-2: CHO-CY01 cell line batch culture at pH 6.80 online process parameters, pH (A), pO_2 (% air saturation (% sat)) (B), volume of base added (C), temperature (D), and calculated CO_2 volume percentage (E).

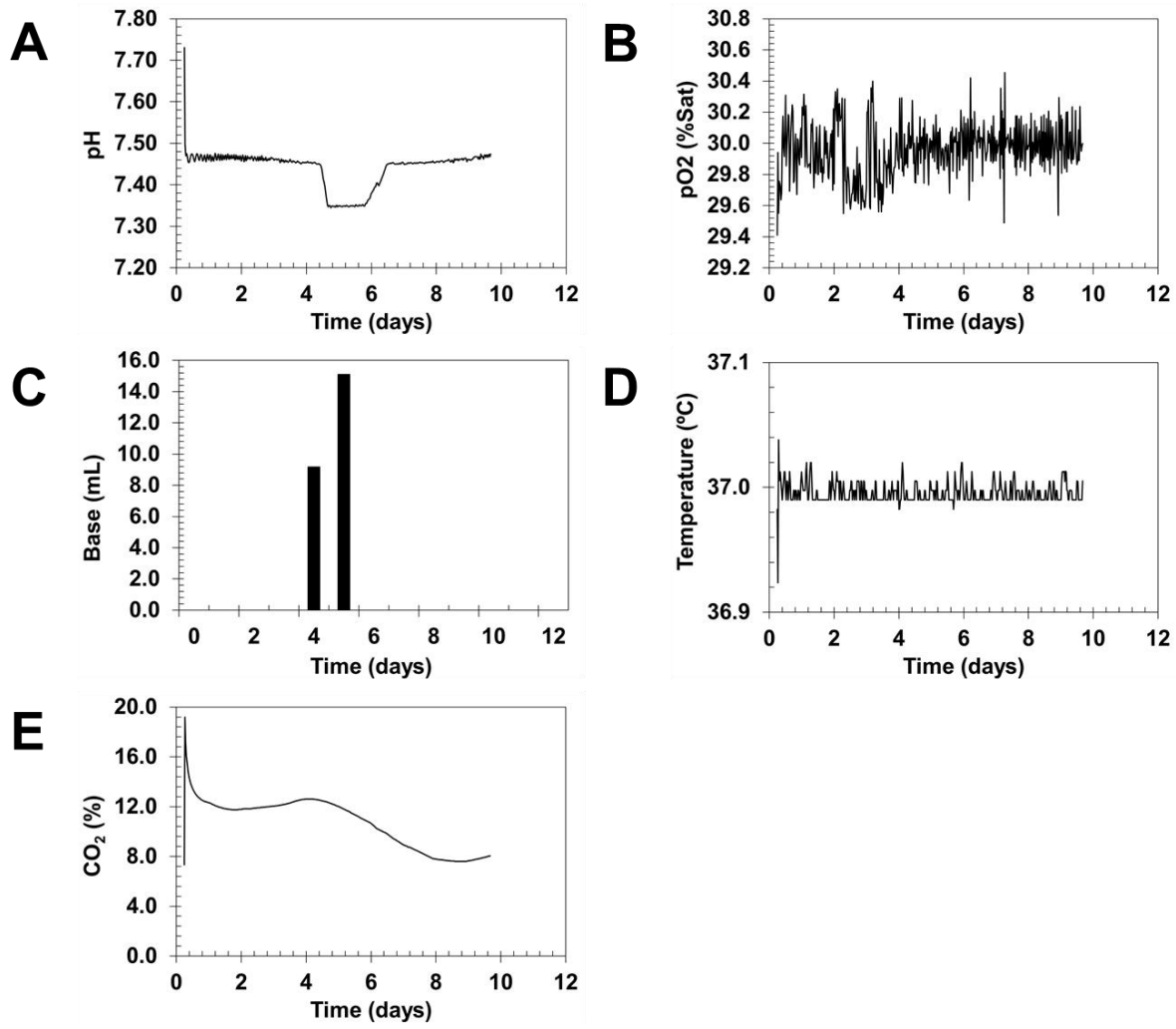

Figure D-3. CHO-CY01 cell line batch culture at pH 7.40 online process parameters, pH (A), pO_2 (% air saturation (% sat)) (B), volume of base added (C), temperature (D), and calculated CO_2 volume percentage (E).

D.2. 5L-STR Online process parameters of CHO-CY01 cell line fed-batch cultures

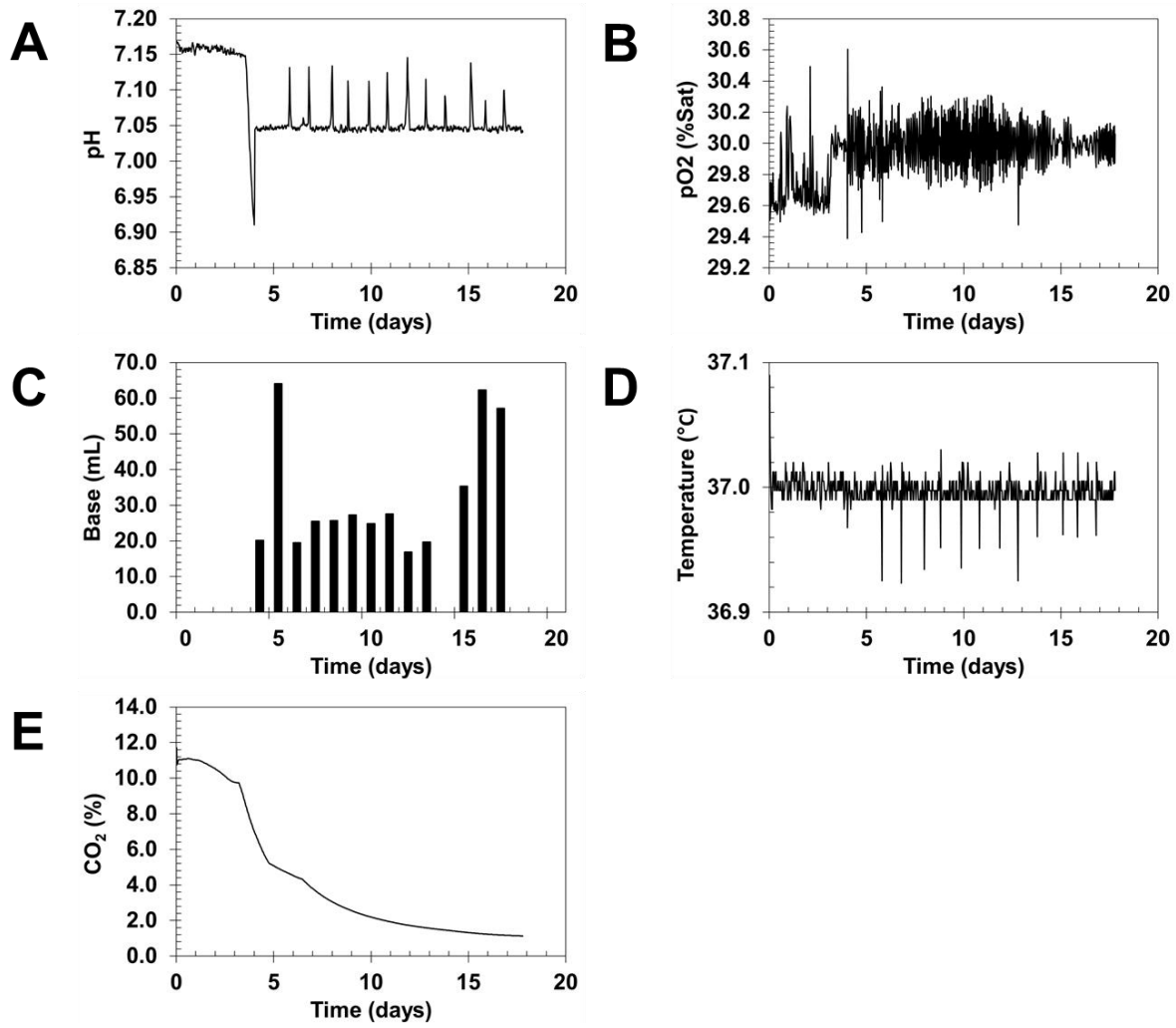

Figure D-4: CHO-CY01 cell line fed-batch strategy 4 (FB2) culture at pH 7.10 online process parameters, pH (A), pO_2 (% air saturation (% sat)) (B), volume of base added (C), temperature (D), and calculated CO_2 volume percentage (E).

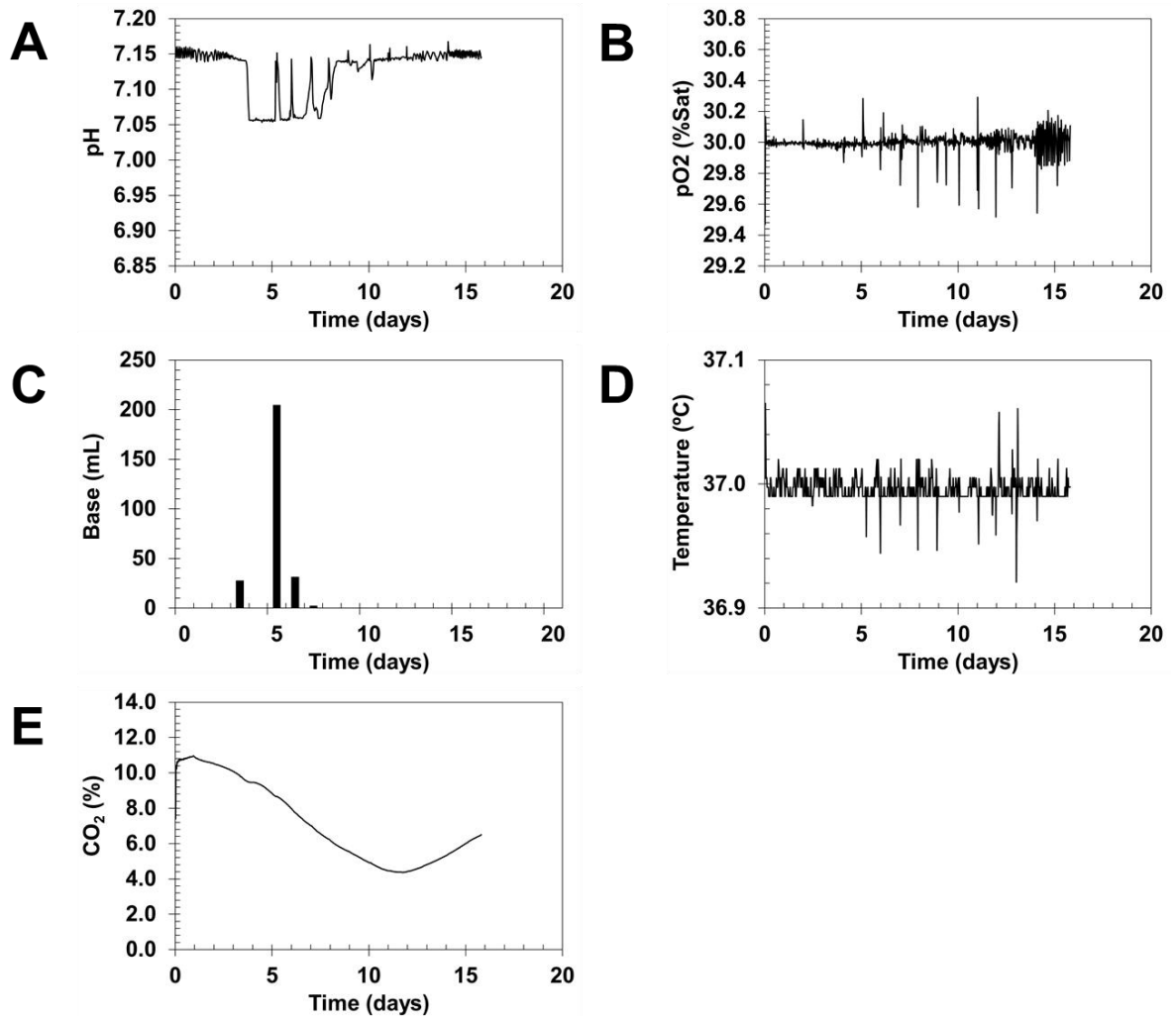

Figure D-5: CHO-CY01 cell line fed-batch strategy 5 (FB3) culture at pH 7.10 online process parameters, pH (A), pO_2 (% air saturation (% sat)) (B), volume of base added (C), temperature (D), and calculated CO_2 volume percentage (E).

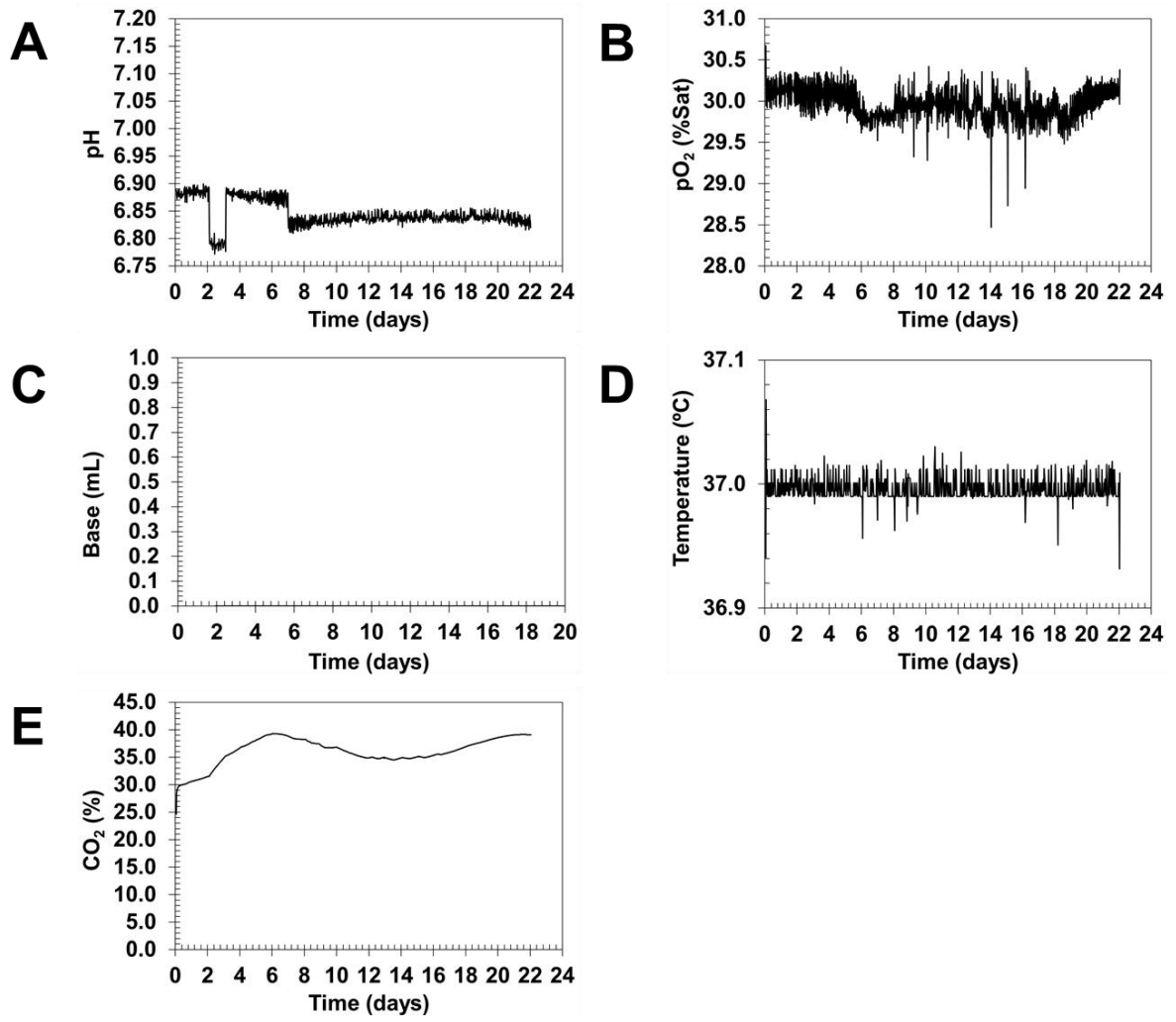

Figure D-6: CHO-CY01 cell line fed-batch strategy 5 (FB3) culture at pH 6.80 online process parameters, pH (A), pO_2 (% air saturation (% sat)) (B), volume of base added (C), temperature (D), and calculated CO_2 volume percentage (E).

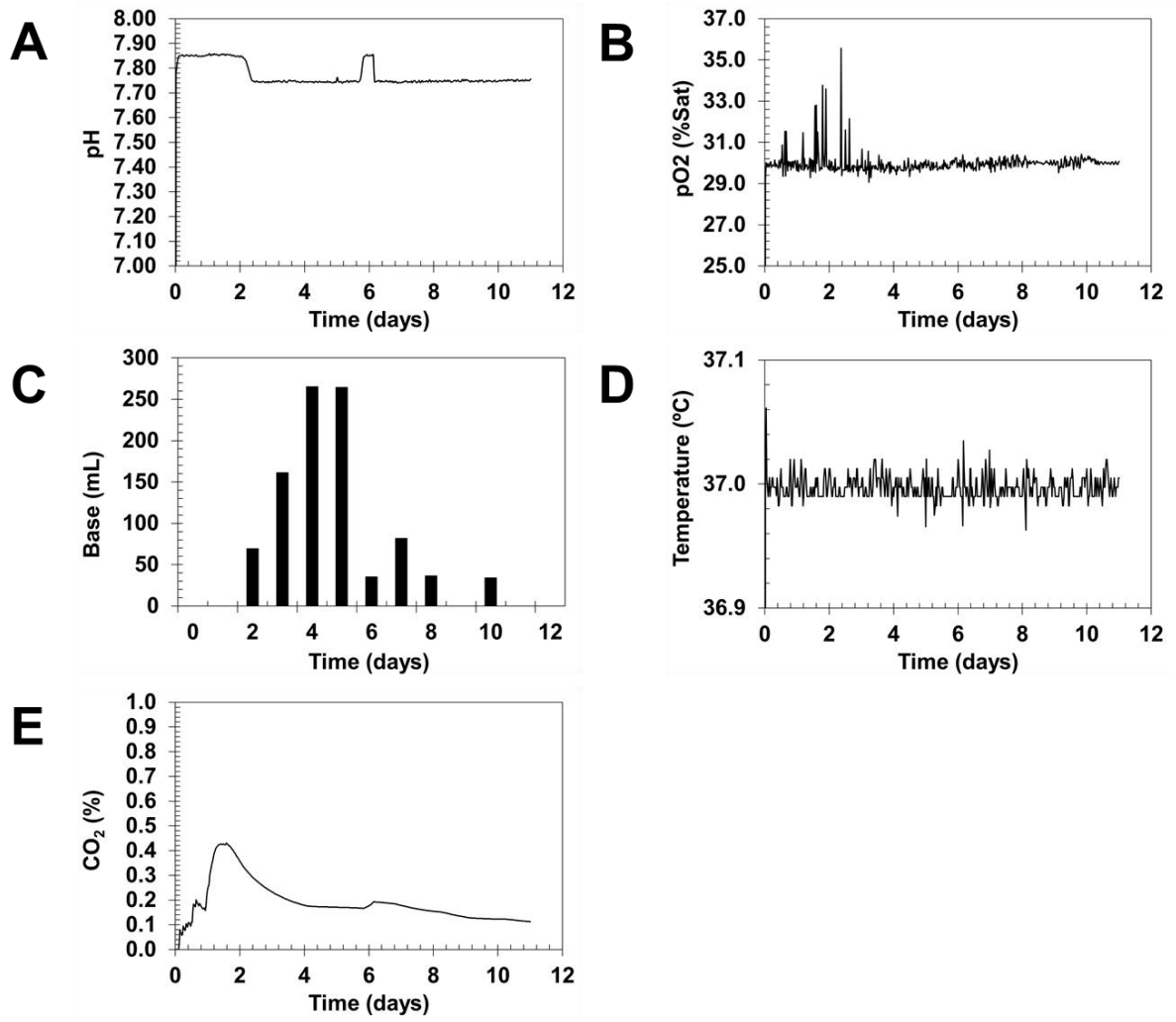

Figure D-7: CHO-CY01 cell line fed-batch strategy 5 (FB3) culture at pH 7.80 online process parameters, pH (A), pO_2 (% air saturation (% sat)) (B), volume of base added (C), temperature (D), and calculated CO_2 volume percentage (E).

D.2. 5L-STR Online process parameters of CHO-CY01 cell line fed-batch cultures with pH shift

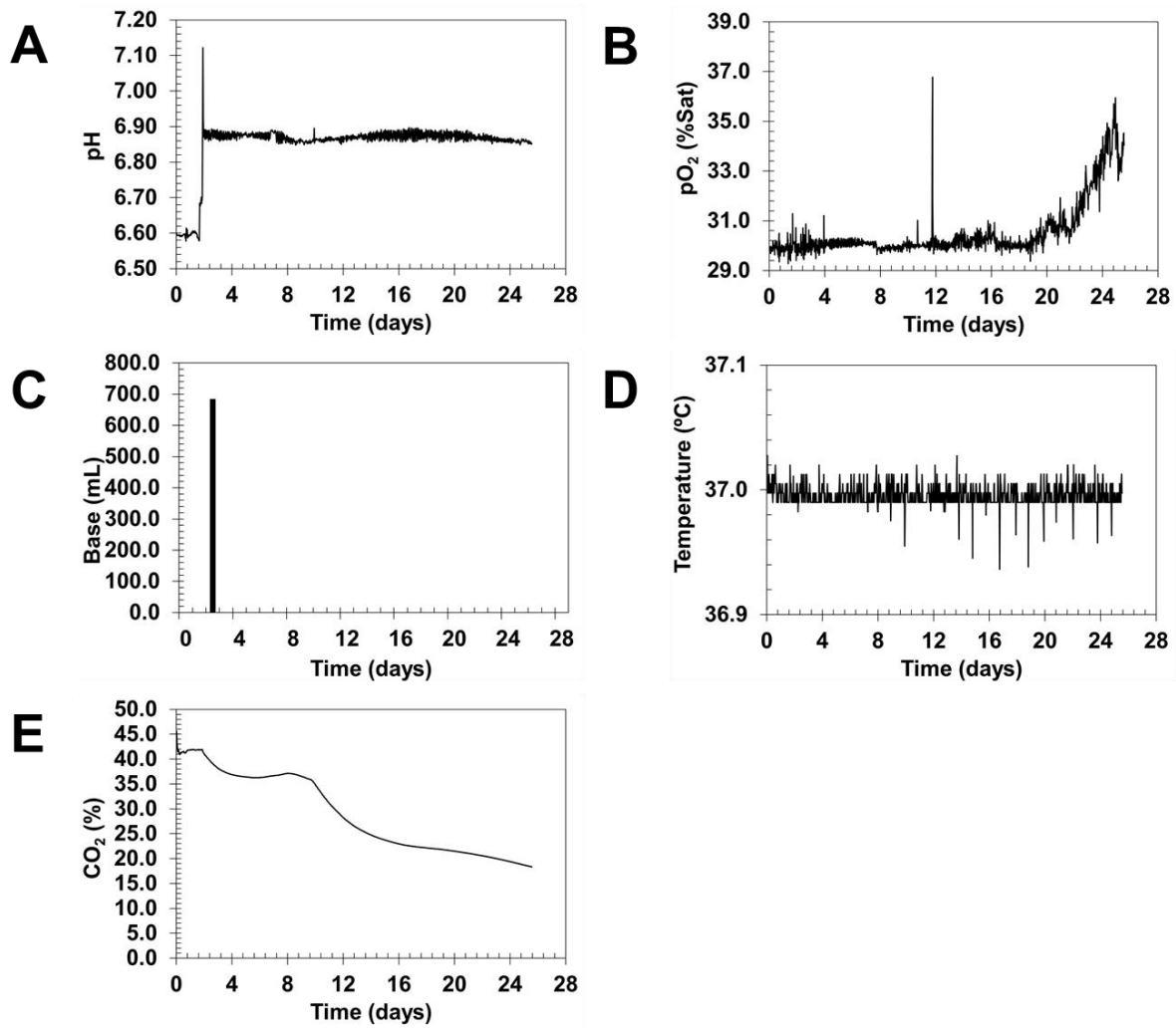

Figure D-8: CHO-CY01 cell line fed-batch strategy 5 (FB3) culture with pH shift from pH 6.60 to pH 6.80 on day 2 online process parameters, pH (A), pO_2 (% air saturation (% sat)) (B), volume of base added (C), temperature (D), and calculated CO_2 volume percentage (E).

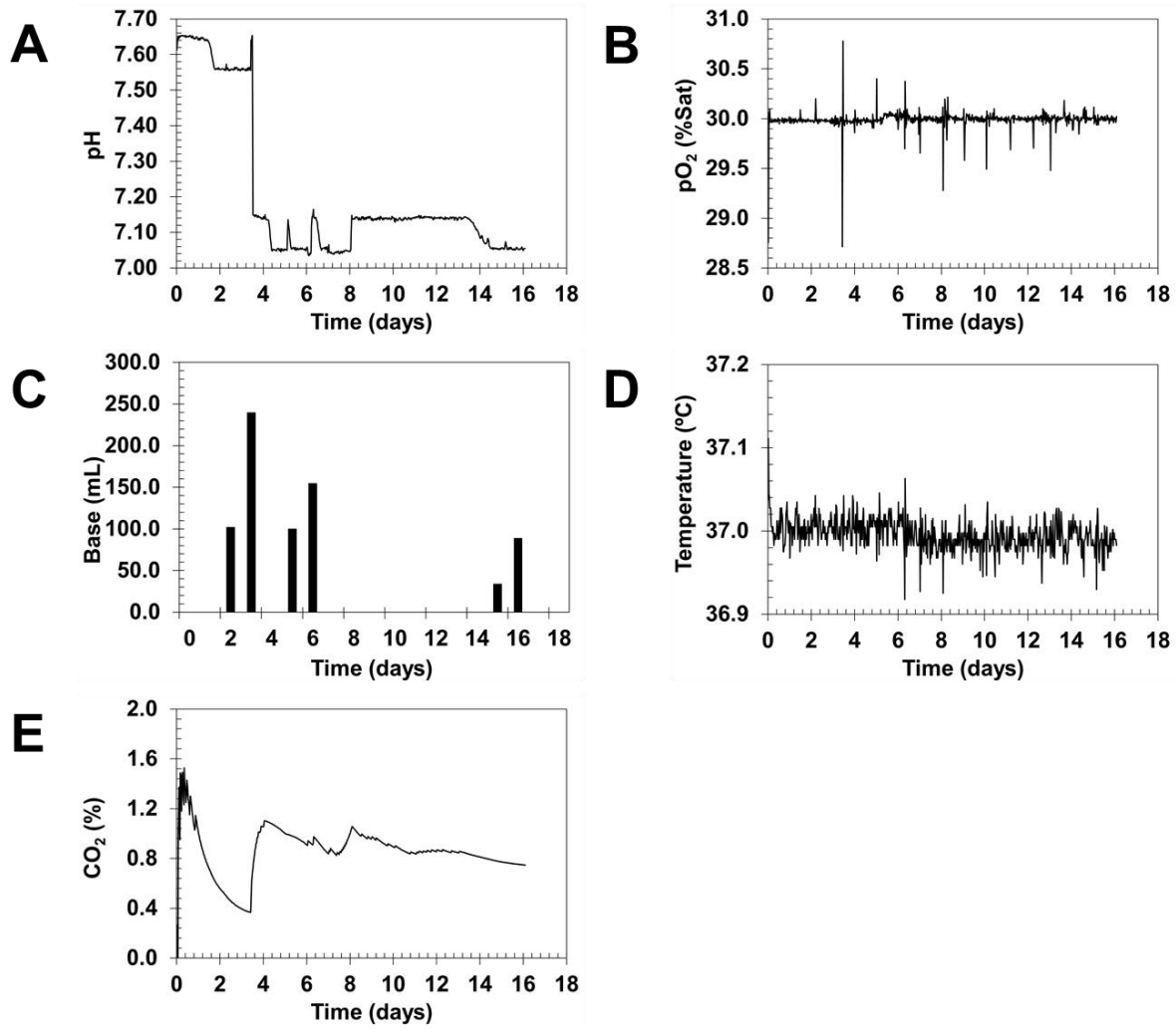

Figure D-9: CHO-CY01 cell line fed-batch strategy 5 (FB3) culture with pH shift from pH 7.60 to pH 7.10 on day 4 online process parameters, pH (A), pO_2 (% air saturation (% sat)) (B), volume of base added (C), temperature (D), and calculated CO_2 volume percentage (E).

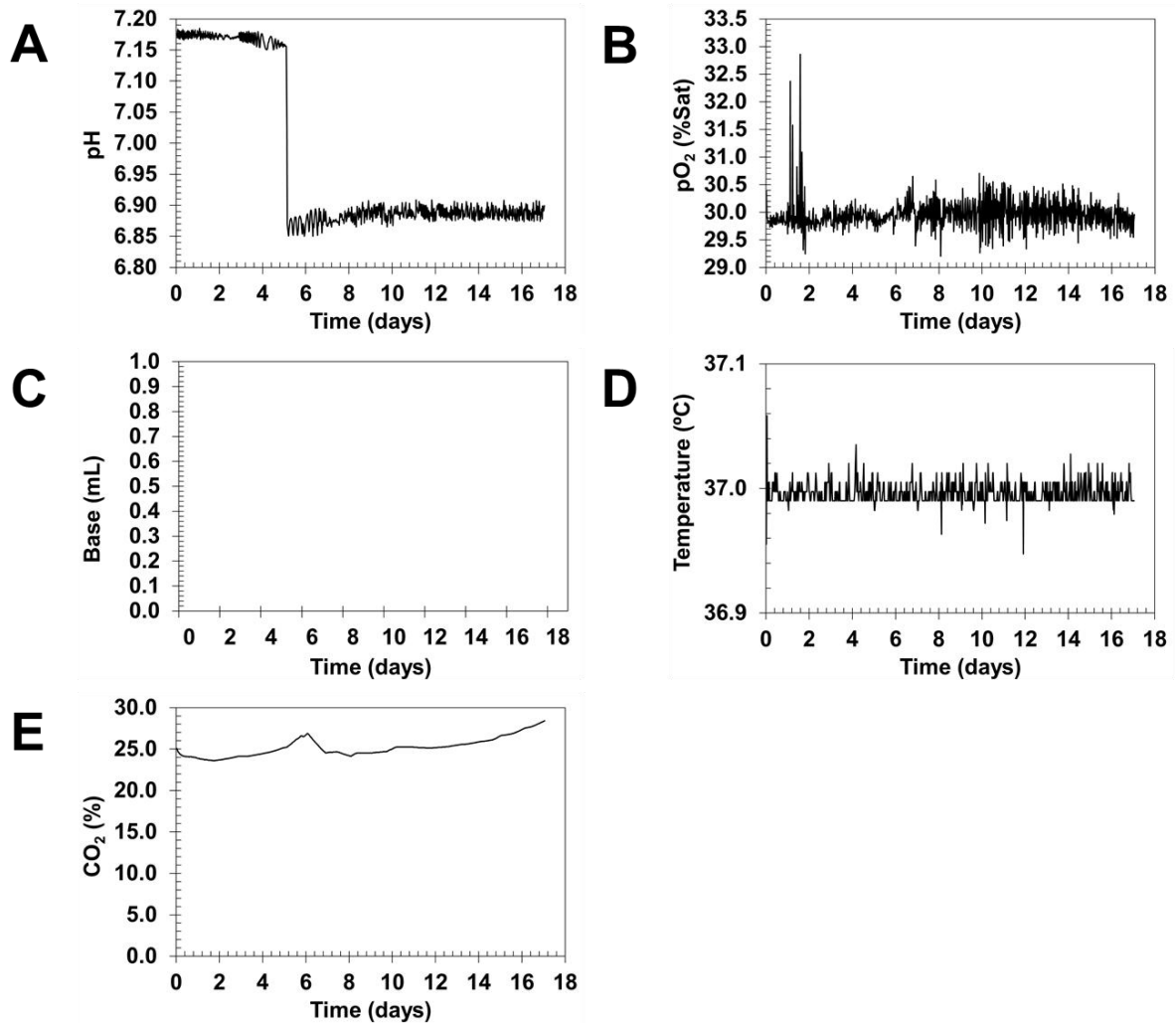

Figure D-10: CHO-CY01 cell line fed-batch strategy 5 (FB3) culture with pH shift from pH 7.10 to pH 6.80 on day 5 online process parameters, pH (A), pO_2 (% air saturation (% sat)) (B), volume of base added (C), temperature (D), and calculated CO_2 volume percentage (E).

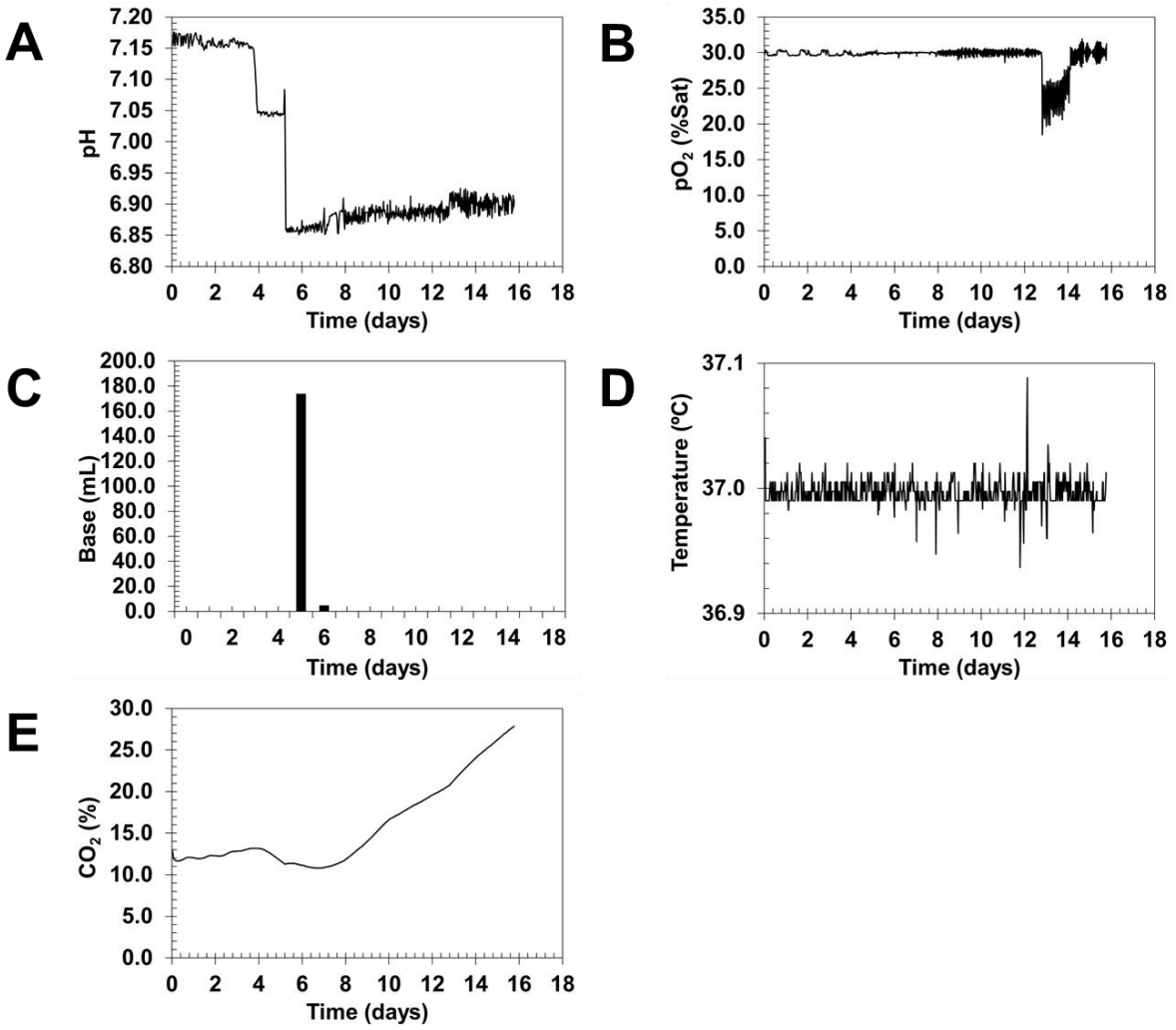

Figure D-11: CHO-CY01 cell line fed-batch strategy 5 (FB3) culture with pH shift from pH 7.10 to pH 7.00 on day 4, then to pH 6.80 on day 5 online process parameters, pH (A), pO_2 (% air saturation (% sat)) (B), volume of base added (C), temperature (D), and calculated CO_2 volume percentage (E).

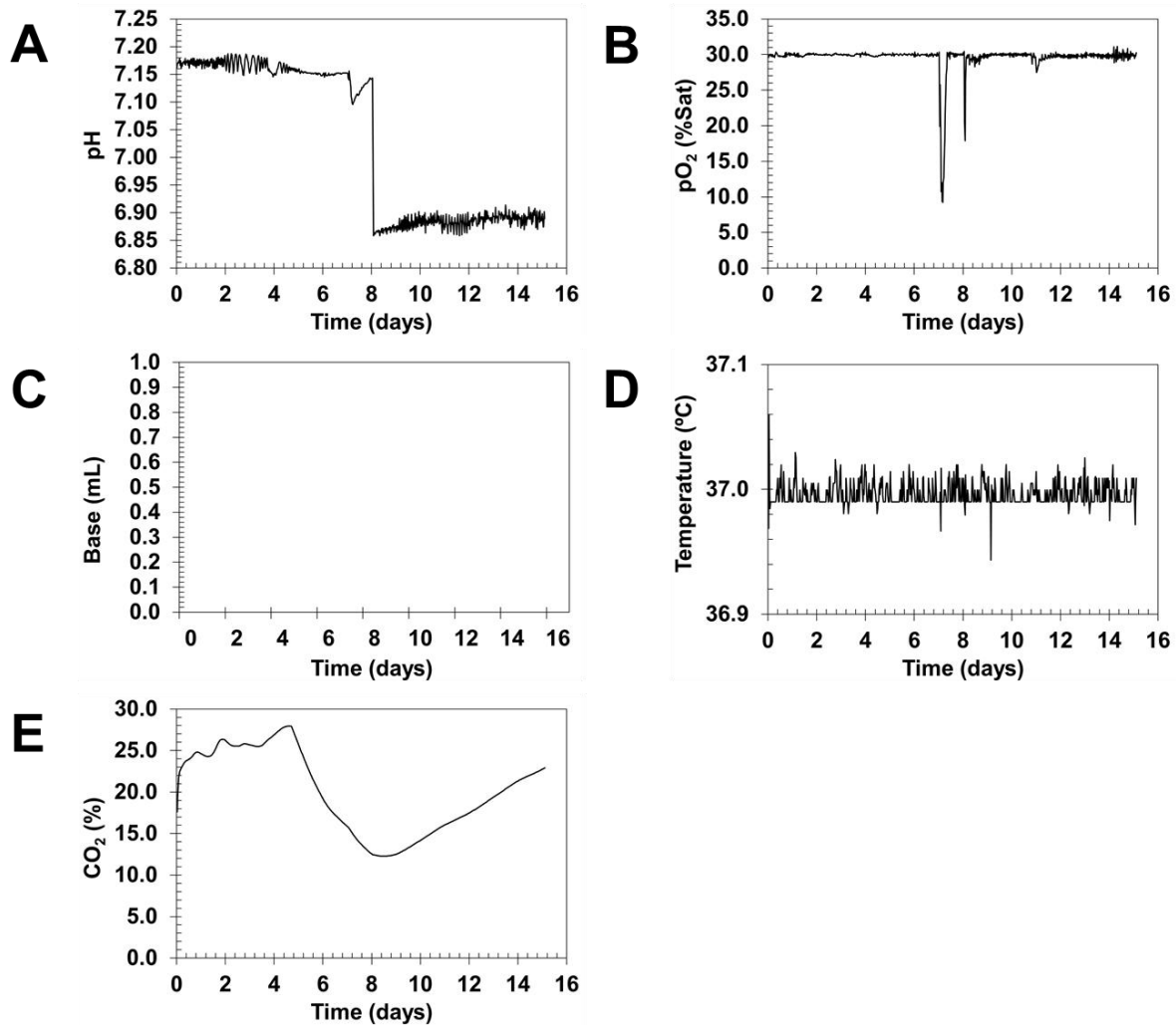

Figure D-12: CHO-CY01 cell line fed-batch strategy 5 (FB3) culture with pH shift from pH 7.10 to pH 6.80 at day 8 online process parameters, pH (A), pO_2 (% air saturation (% sat)) (B), volume of base added (C), temperature (D), and calculated CO_2 volume percentage (E).

Appendix E: 24-SRW MTP Well-to-Well Reproducibility

It was assumed throughout this work that each well in a 24-SRW MTP was equivalent to the other 23 wells. In fed-batch mode, cell cultures in the microwell plates present a higher variability in the cell culture parameters in the parameters than in batch mode, due to feeding volume variability. In order to test such assumption, a variability test was performed. CHO-CY01 cell line was cultured in fed-batch mode (strategy 5 (FB3) in a 24-SRW MTPS and at the harvest point (day 17), all cell culture parameters, such as, viable cell concentration (VCC), cell viability, osmolality, pH, IgG4, glutamate, glucose, lactate, and ammonium concentrations were experimentally measured for each one of the 24 wells. These data were normalized or standardized to bring all of the variables into proportion with one another and so comparable.

Standardized data will reflect how many standard deviations from the average that that data lies, with the following normal distribution curve representing the probability of each standard deviation for a normal distribution. The z-score was calculated to standardize the data, and it reflects how many standard deviations from the average that the data point falls (Equation E.1). Therefore, it provided an assessment on how off-target is the data. A negative z-score means the raw value is below the mean and, a positive score means that the raw value is above the mean. Normalized data will reduce the data to the same range (canonical form) (Equation E.2).

$$\frac{x - \bar{x}}{\sigma}$$

Equation E.1

$$\frac{x - x_{min}}{x_{max} - x_{min}}$$

Equation E.2

where, x is the cell culture parameter (variables), $\bar{x}$ is the average, σ is the standard deviation, x_{min} is the minimum variable value and x_{max} is the maximum variable value.

In a first approach, 24 wells will be looked upon by the standardization of the data (Figure E-2). Afterwards, the normalized cell culture parameters data were divided into the three wells configurations (Figure 3.11), ´Corner`, ´Edge` and ´Internal` wells previously defined in Section 3.3.

For a 95 % confidence level, the z-scores range from -1.96 and 1.96. Therefore, if the z-score computed is between -1.96 and 1.96 the null hypothesis can not be rejected, but if the z-score falls outside that range, it is possible to reject the null hypothesis, the pattern exhibited is probably too unusual. From Figure E-2, it can be said, apart from well A2 and B6, that the well are representative of each other and do not vary from the mean no more than absolute 1.96. The data for well A1 was not presented as the well content was lost due to evaporation.

The reason behind the VCC, osmolality, pH, lactate and IgG4 concentration irreproducibility of A2 well may be interconnected with the well location in the plate, ´edge` well. Excessive evaporation caused an excessive fill volume reduction and consequently a different hydrodynamic environment to the cells. In terms of well A6, the z-score of 2.99 may be associated with experimental error measurement as all the other parameter are within the confidence level.

After normalizing all the cell culture variables into 24-SRWMTP and the three well configuration, it can be understood, which wells are causing the overall variability in the cell culture parameters. From **Figure E-1**, the ´edge` and ´corner` wells are the ones which mean differs significantly from the overall mean while the ´internal` wells present a similar mean for all cell culture parameters. Generally speaking, it is the ´corner` wells that cause the highest variability as already notice in the evaporation studies.

In conclusion, it can be said, as expected, that each well in the 24-SRW MTP are representative of each other. However, the ´Corner` wells are the principal contributors for the variability present in the CHO-CY01 cell culture parameters.

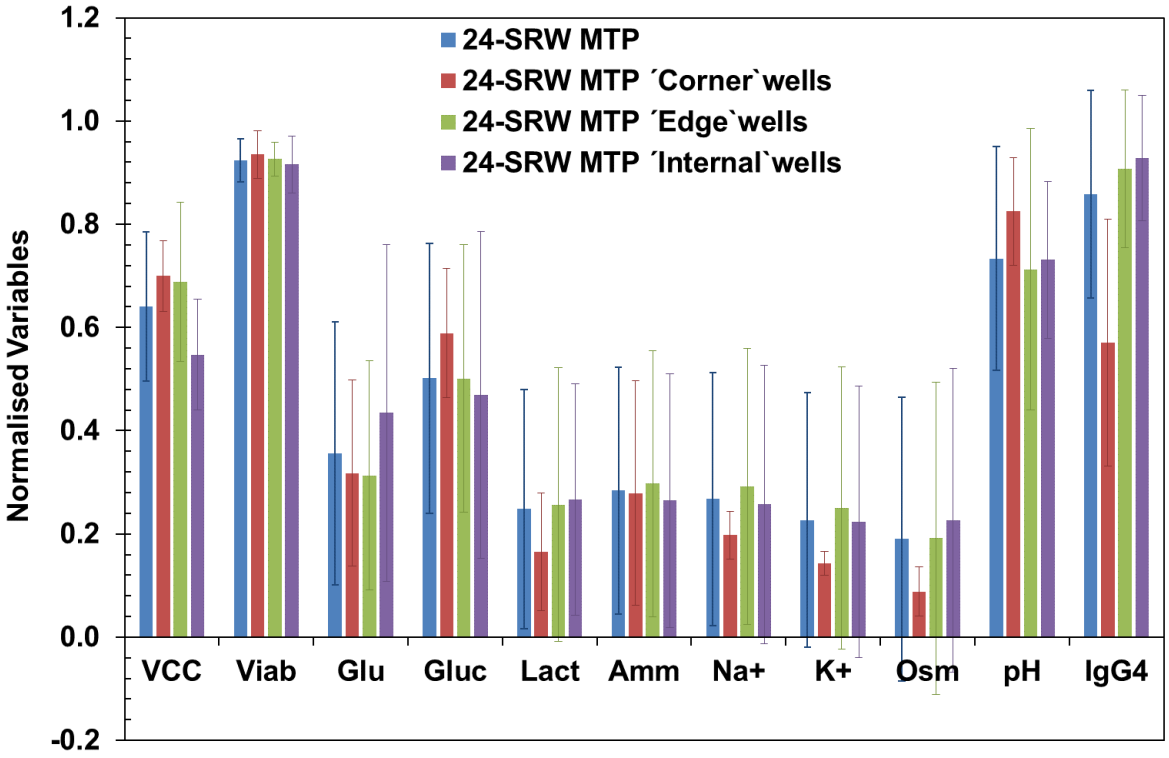

Figure E-1: Normalisation of CHO-CY01 cell line fed-batch culture parameters at the harvest point (day 17), Viable cell concentration (VCC), viability (Viab), osmolality (Osm), pH, IgG4, glutamate (Glu), glucose (Gluc), lactate (Lact), ammonium (Amm), sodium (Na^+), and potassium (K^+) concentrations. The error bars are the standard deviation around the mean.

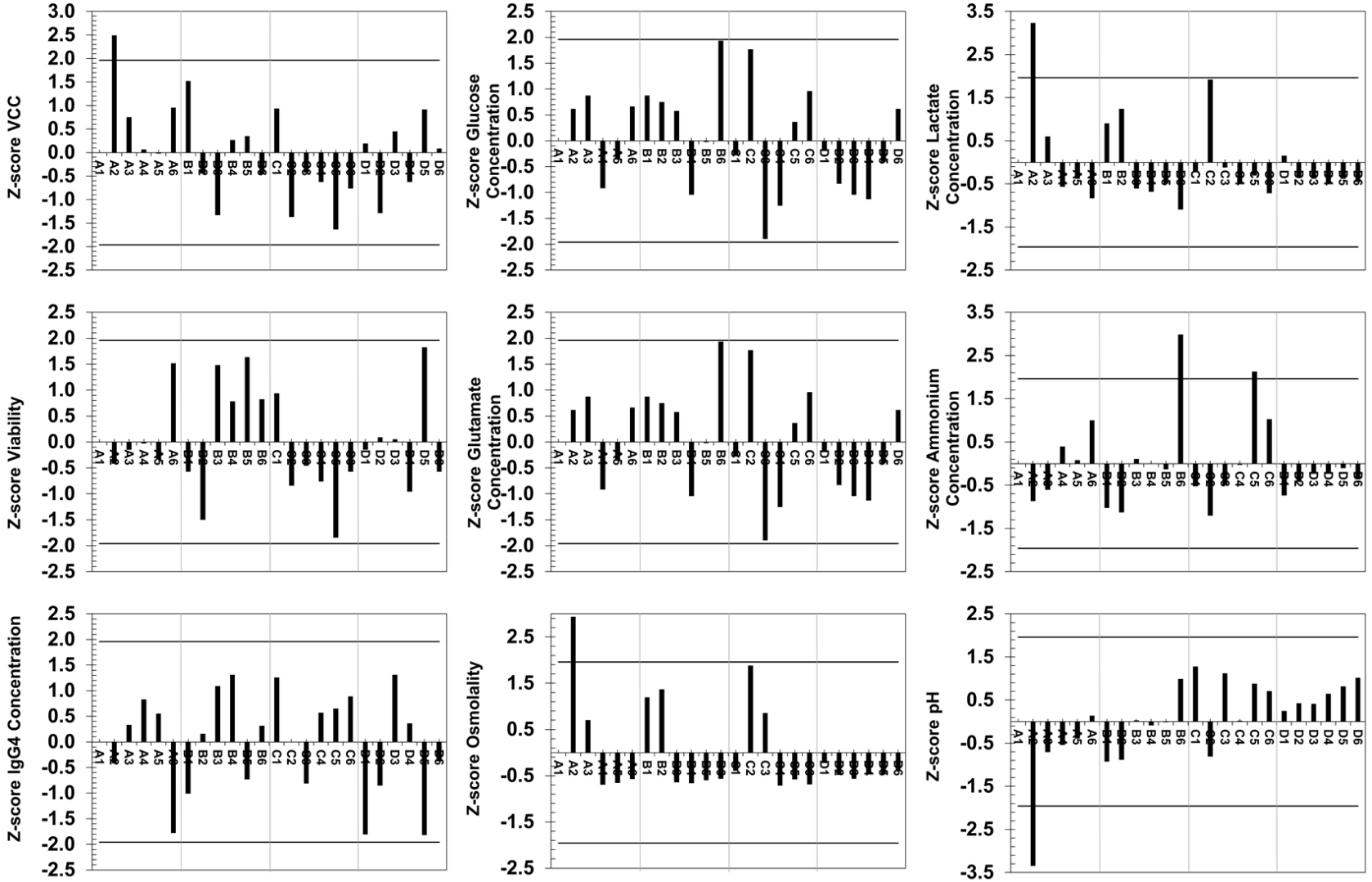

Figure E-2, z-scores of day 17 CHO-CY01 cell line fed-batch culture parameters, Viable cell concentration (VCC), viability, osmolality, pH, IgG4, glutamate, glucose, lactate and ammonium concentrations. For a 95% confidence level, the z-scores are -1.96 and 1.96 (straight solid lines).

Appendix F: Annotated 2D-DIGE Gels and Overlapped 2D-DIGE Gels

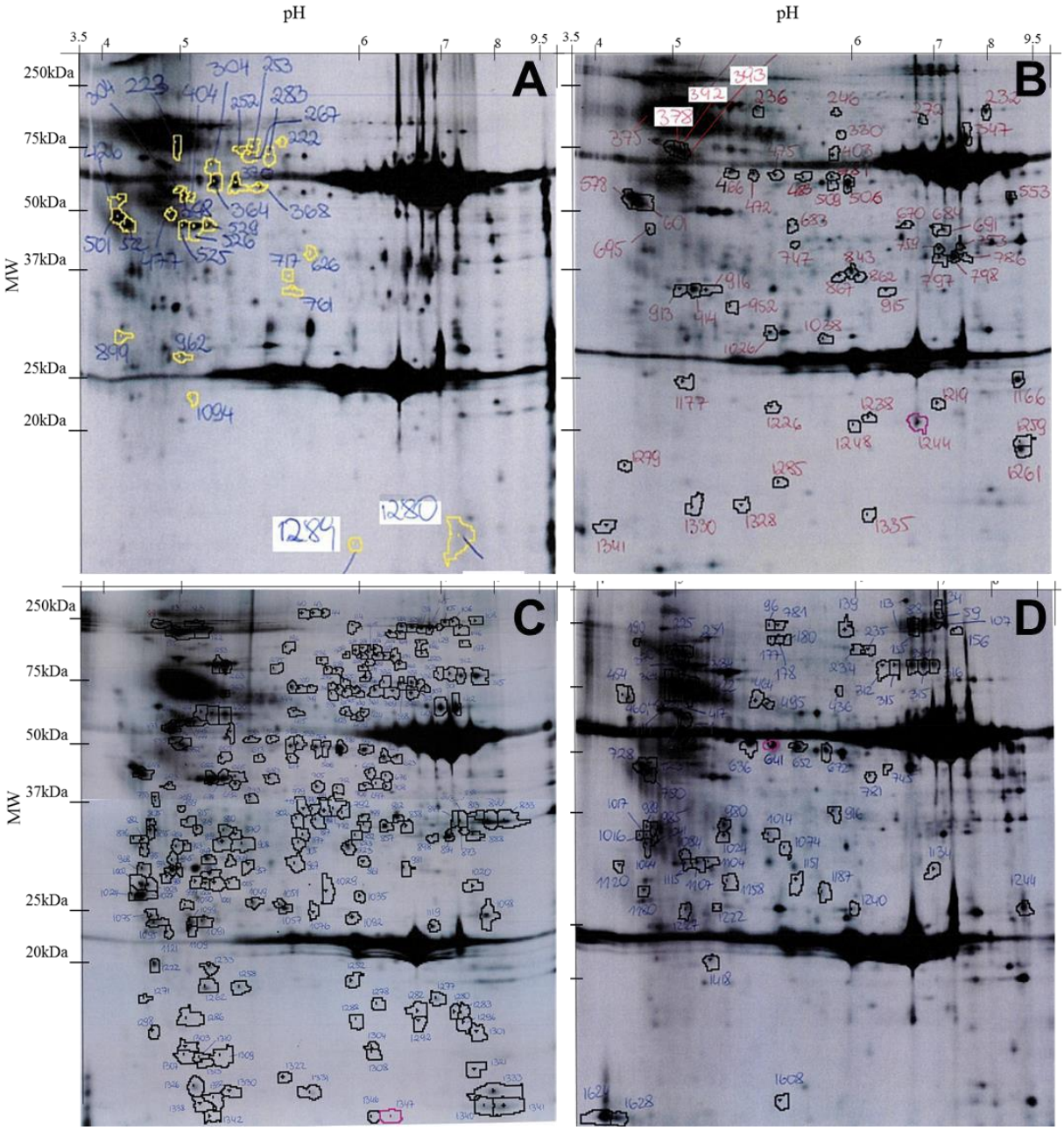

Figure F-1: Annotated 2-D DIGE PAGE CHO-CY01 expression maps of 5L-STR runs at different external pHs. pH 6.8 (A); pH 7.1 (B); day 5 pH shift from pH 7.1 to pH 6.8 (C); day 8 pH shift from pH 7.1 to pH 6.8 (D). The spots indicate a protein difference ratio of 1.5 between sample points.

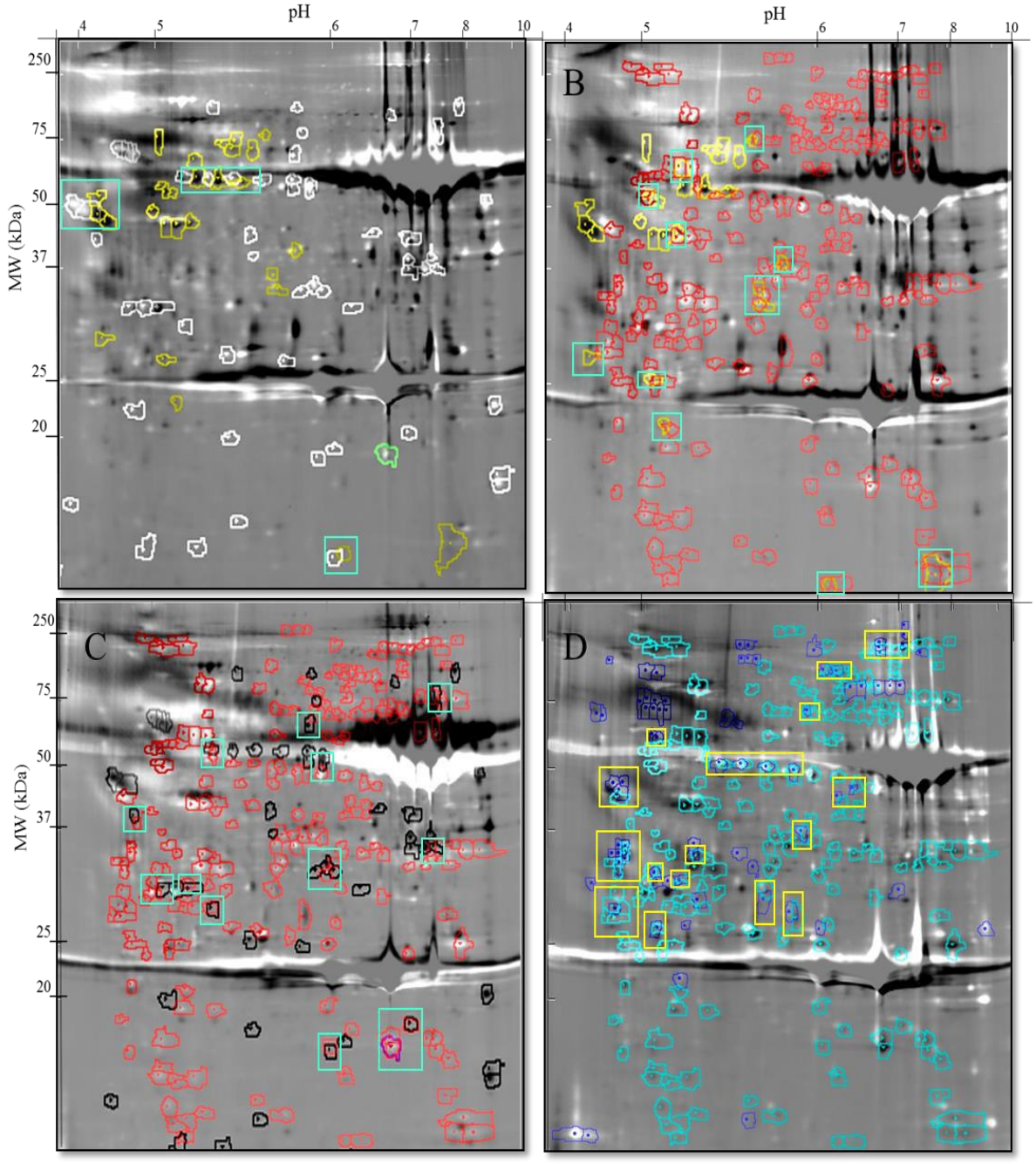

Figure F-2: Image overlapping of the 2-D DIGE PAGE CHO-CY01 expression maps of 5L-STR CHO-CY01 cell line fed-batch cultures at different external pHs: pH 6.8 and pH 7.10 (A); pH 6.80 and pH shift from pH 7.1 to pH 6.8 on day 5 (B); pH 7.10 and pH shift from pH 7.1 to pH 6.8 on day 5 (C); pH shift from pH 7.1 to pH 6.8 on day 5 and pH shift from pH 7.1 to pH 6.8 on day 8 (D). The boxes are a visual indication of the overlapped spots.

Table F-1: Annotation number of overlapped spots from Figure F-2 with volume ratio in brackets. The highlight spots indicate the spots chosen for protein identification.

	pH 6.8 vs pH 7.1 (Figure 6-17 (A))		**day 5 pH shift vs. pH 6.8 (Figure 6-17 (B))**		**day 5 pH shift vs. pH 7.1 (Figure 6-17 (C))**		**day 5 pH shift vs. day 8 pH shift (Figure 6-17 (D))**	
	pH 6.8	**pH 7.1**	**day 5 pH shift**	**pH 6.8**	**day 5 pH shift**	**pH 7.1**	**day 5 pH shift**	**day 8 pH shift**
Quadrant 1 (pH > 5.6; MW > 32 kDa)					376 (-2.61) 581 (-2.85) 923 (-2.56) 883 (-2.31) 847 (-1.57) 838 (-2.09)	403 (1.60) 506 (1.68) 867 (-2.17) 843 (2.01) 862 (-2.21) 798 (1.67) 753 (1.74) 786 (1.52)	145 (-3.06) 124 (-1.67) 128 (-1.95) 220 (-2.36) 214 (-1.73) 204 (-1.93) 340 (1.81) 568 (-2.23); 566 (-2.65) 625 (-3.68) 665 (-3.05) 772 (1.52); 784 (1.71)	107 (-1.68) 88 (-4.07) 113 (1.97) 155 (-1.74) 234 (-1.75) 235 (-1.64) 436 (1.60) 672 (-1.56) 745 (-3.35) 781 (-1.56) 916 (1.77)
Quadrant 2 (pH< 5.6; MW > 32 kDa)	501 (-2.25) 364 (1.59) 370 (1.7) 368 (1.95)	601 (-2.29) 466 (1.57) 472 (1.65) 475 (1.66)	905 (2.36) 802 (1.63); 877 (2.25) 770 (1.56); 784 (1.71) 344 (-3.93) 415 (1.75) 533 (1.69); 552 (2.1) 682 (-2.15)	761 (-1.51)) 717 (-2.01) 626 (-2.11) 222 (-1.52) 304 (-1.76) 398 (289); 404 (1.81) 529 (-1.65)	511 (2.11) 420 (1.57) 805 (1.62) 974 (-2.00) 947 (-2.42)	466 (1.57) 695 (-1.64) 913 (-2.09) 916 (-1.98)	444 (-5.64); 451 (-5.42) 538 (2.06) 540 (2.46) 562 (-2.09); 553 (-1.77) 648 (-1.62) 882 (1.65); 915 (1.57); 835 (1.5); 805 (1.62) 903 (-3.65); 904 (-1.77) 850 (2.1)	506; 566 636 (-1.66) 641 (-2.11) 652 (-1.90) 750 (1.81) 1044 (1.99); 1041 (1.91); 985 (2.10) 1084 (2.23) 1024 (1.54)
Quadrant 3 (pH < 5.6; MW < 32kDa)			1233 (-1.94) 1099 (-2.44); 1109 (-2.04); 1091 (-1.7) 1024 (-2.46)	1094 (2.18) 962 (-1.55) 899 (-1.56)	1005 (-1.54)	952 (-1.94)	967 (1.53) 947 (-2.42) 1050 (1.58) 1000 (-1.88)	1151 (1.58) 1104 (1.84) 1227 (1.74) 1180 (1.52)
Quadrant 4 (pH > 5.6; MW < 32 kDa)	1289 (-2.77)	1335 (-2.46)	1333 (-1.63); 1340 (-2.66); 1341 (-1.73) 1346 (-4.8); 1347 (-3.17)	1280 (-2.49) 1289 (-2.77)	1277 (-1.68) 1282 (4.79); 1292 (9.76) 1288 (4.94)	1219(1.53) 1244 (3.12) 1248 (2.07)	1029 (1.89)	1187 64)

Appendix G: Protein Identification by Mass Spectrometry, Raw Data

Table G-1, Detailed description of the mass spectrometry conditions performed at each 2D-DIGE gel spot analysed.

Spot Number	**344**	**511**	**581**	**947**	**1005**	**1282**	**1292**
Peak list format	Mascot generic						
Search type	MIS (MS/MS Ions Search)						
Mascot version	2.3.02						
Database	1,,cRAP 2,,CHO_UniProt_Jul15						
Fasta file	1,,cRAP_FullIdentifiers.fasta 2,,uniprot_chinese_hamster.fasta						
Total sequences	35353						
Total residues	14777203						
Sequences after taxonomy filter	35353						
Number of queries	3771	3563	4497	3047	3096	3012	3049
Decoy							
Number of matches above identity threshold in search of real database	582	412	661	311	270	270	237
Number of matches above identity threshold in search of decoy database	0	0	0	0	0	0	0
Number of matches above homology threshold in search of real database	665	474	747	368	307	311	279
Number of matches above homology threshold in search of decoy database	0	0	0	0	0	0	0
Fixed modifications							
Identifier	Carbamidomethyl (C)						
Variable modifications							
Identifier 1	Deamidated (NQ)						
Identifier 2	Oxidation (M)						
Search Parameters							
Taxonomy filter	All entries						
Enzyme	Trypsin						
Maximum Missed Cleavages	2						
Fixed modifications	Carbamidomethyl (C)						
Variable modifications	Deamidated (NQ),Oxidation (M)						
Peptide Mass Tolerance	25						
Peptide Mass Tolerance Units	ppm						
Fragment Mass Tolerance	0.8						
Fragment Mass Tolerance Units	Da						
Mass values	Monoisotopic						
Instrument type	ESI-TRAP						
Format parameters							
Significance threshold	0.05						
Max. number of hits	0						
Use MudPIT protein scoring	0						
Ions score cut-off	20						
Include same-set proteins							
Include sub-set proteins	0						
Include unassigned	0						
Require bold red	1						
Use homology threshold	0						
Group protein families	0						
Protein ´hits`	**49**	54	40	33	37	29	22

Table G-2, Spot 344 protein ´hits` list with protein description (prot_desc), score, threshold (prot_thresh), mass, coverage (prot_cov) and pI.

prot_hit_num	prot_acc	prot_desc	prot_score	prot_thresh	prot_mass	prot_matches	prot_cover	prot_pi
1	2,,tr|G3HGP6|G3HGP6_CRIGR	T-complex protein 1 subunit alpha OS=Cricetulus griseus GN=I79_009786 PE=3 SV=1	2102	58	60814	255	70.1	5.71
2	1,,sp|cRAP054|P04264|K2C1_HUMAN	Keratin, type II cytoskeletal 1 OS=Homo sapiens GN=KRT1 PE=1 SV=6	1317	58	66170	72	35.6	8.15
3	1,,sp|cRAP041|P35527|K1C9_HUMAN	Keratin, type I cytoskeletal 9 OS=Homo sapiens GN=KRT9 PE=1 SV=3	1164	58	62255	69	41.4	5.14
4	1,,sp|cRAP039|P13645|K1C10_HUMAN	Keratin, type I cytoskeletal 10 OS=Homo sapiens GN=KRT10 PE=1 SV=6	798	58	59020	37	30.0	5.13
5	1,,sp|cRAP053|P35908|K22E_HUMAN	Keratin, type II cytoskeletal 2 epidermal OS=Homo sapiens GN=KRT2 PE=1 SV=2	609	58	65678	25	23.6	8.07
6	2,,tr|G3IBN9|G3IBN9_CRIGR	Keratin, type II cytoskeletal 71 OS=Cricetulus griseus GN=I79_021070 PE=3 SV=1	592	58	134008	32	10.5	6.18
7	2,,tr|G3I8F9|G3I8F9_CRIGR	Keratin, type I cytoskeletal 14 OS=Cricetulus griseus GN=I79_019828 PE=3 SV=1	522	58	52954	30	22.2	5.09
8	1,,sp|cRAP002|P02768|ALBU_HUMAN	Serum albumin OS=Homo sapiens GN=ALB PE=1 SV=2	444	58	71317	21	15.8	5.92
9	2,,tr|G3IBN8|G3IBN8_CRIGR	Keratin, type II cytoskeletal 6A OS=Cricetulus griseus GN=I79_021069 PE=3 SV=1	364	58	48841	18	18.6	8.11
10	2,,tr|G3H6I5|G3H6I5_CRIGR	Interleukin-1 receptor-like 1 OS=Cricetulus griseus GN=I79_005946 PE=4 SV=1	304	58	38221	13	24.5	9.18
11	2,,tr|G3I8G0|G3I8G0_CRIGR	Keratin, type I cytoskeletal 17 OS=Cricetulus griseus GN=I79_019831 PE=3 SV=1	290	58	48303	15	15.0	5.00
12	1,,sp|cRAP112|P00761|TRYP_PIG	Trypsin OS=Sus scrofa PE=1 SV=1	248	58	25078	81	32.9	7.00
13	1,,sp|cRAP015|P02666|CASB_BOVIN	Beta-casein OS=Bos taurus GN=CSN2 PE=1 SV=2	244	58	25148	12	17.9	5.26
14	1,,sp|cRAP040|O77727|K1C15_SHEEP	Keratin, type I cytoskeletal 15 OS=Ovis aries GN=KRT15 PE=2 SV=1	211	58	48740	12	8.8	4.73
15	2,,tr|G3I8G1|G3I8G1_CRIGR	Keratin, type I cytoskeletal 42 OS=Cricetulus griseus GN=I79_019833 PE=3 SV=1	196	58	51118	11	9.6	5.12
16	2,,tr|A0A061IMX3|A0A061IMX3_CRIGR	Inositol-3-phosphate synthase 1-like protein OS=Cricetulus griseus GN=H671_1g1140 PE=4 SV=1	192	58	61463	8	9.1	5.84
17	2,,tr|A0A061I523|A0A061I523_CRIGR	Procollagen C-endopeptidase enhancer 1 OS=Cricetulus griseus GN=H671_4g12064 PE=4 SV=1	183	58	51099	7	11.5	8.16
18	2,,tr|G3I9L7|G3I9L7_CRIGR	EGF-containing fibulin-like extracellular matrix protein 1 OS=Cricetulus griseus GN=I79_020269 PE=4 SV=1	172	58	50780	6	9.8	4.95
19	2,,tr|G3HQK5|G3HQK5_CRIGR	UDP-N-acetylhexosamine pyrophosphorylase OS=Cricetulus griseus GN=I79_013109 PE=4 SV=1	156	58	59079	7	8.2	6.04
20	1,,sp|cRAP013|P02662|CASA1_BOVIN	Alpha-S1-casein OS=Bos taurus GN=CSN1S1 PE=1 SV=2	149	58	24570	6	14.0	4.98
21	2,,tr|G3HXN7|G3HXN7_CRIGR	Beta-hexosaminidase OS=Cricetulus griseus GN=I79_015800 PE=3 SV=1	137	58	60463	4	6.8	6.92
22	2,,tr|G3IK05|G3IK05_CRIGR	Lactadherin (Fragment) OS=Cricetulus griseus GN=I79_024197 PE=4 SV=1	124	58	22841	6	14.1	6.88
23	2,,tr|G3ICD3|G3ICD3_CRIGR	Lactadherin OS=Cricetulus griseus GN=I79_021326 PE=4 SV=1	96	58	16256	3	15.7	9.45
24	2,,tr|A0A061IJI9|A0A061IJI9_CRIGR	Valyl-tRNA synthetase-like protein OS=Cricetulus griseus GN=H671_1g2778 PE=3 SV=1	81	58	262941	4	1.0	6.39

Table G-2 (Continued)

prot_hit_num	prot_acc	prot_desc	prot_score	prot_thresh	prot_mass	prot_matches	prot_cover	prot_pi
25	2,,tr|G3I1H5|G3I1H5_CRIGR	Legumain OS=Cricetulus griseus GN=I79_017232 PE=4 SV=1	78	58	50060	4	5.9	6.07
26	2,,tr|A0A061I6C1|A0A061I6C1_CRIGR	Discoidin, CUB and LCCL domain-containing protein 2 (Fragment) OS=Cricetulus griseus GN=H671_4g12593 PE=4 SV=1	72	58	62296	5	3.2	7.68
27	2,,tr|A0A061I1R3|A0A061I1R3_CRIGR	Citron Rho-interacting kinase isoform 1 OS=Cricetulus griseus GN=H671_4g13393 PE=4 SV=1	71	58	233409	4	0.7	6.01
28	2,,tr|G3IL03|G3IL03_CRIGR	Putative uncharacterized protein OS=Cricetulus griseus GN=I79_024561 PE=4 SV=1	64	58	13623	2	10.6	6.23
29	2,,tr|A0A061ILH1|A0A061ILH1_CRIGR	Anionic trypsin-2-like protein OS=Cricetulus griseus GN=H671_1g2974 PE=3 SV=1	62	58	26501	5	8.2	6.85
30	2,,tr|G3HG83|G3HG83_CRIGR	T-complex protein 1 subunit gamma OS=Cricetulus griseus GN=I79_009604 PE=3 SV=1	54	58	61152	2	2.0	6.23
31	2,,tr|G3HR98|G3HR98_CRIGR	EF-hand calcium-binding domain-containing protein 5 OS=Cricetulus griseus GN=I79_013363 PE=4 SV=1	54	58	181264	3	0.9	6.09
32	2,,tr|A0A061HTV8|A0A061HTV8_CRIGR	Echinoderm microtubule-associated protein-like 1-like protein OS=Cricetulus griseus GN=H671_21466 PE=4 SV=1	51	58	81907	2	2.7	6.17
33	2,,tr|G3HD94|G3HD94_CRIGR	Desmoplakin OS=Cricetulus griseus GN=I79_008473 PE=4 SV=1	47	58	330268	2	0.6	6.53
34	1,,sp|cRAP016|P02668|CASK_BOVIN	Kappa-casein OS=Bos taurus GN=CSN3 PE=1 SV=1	43	58	21370	2	5.8	6.30
35	2,,tr|G3IAS8|G3IAS8_CRIGR	Kinesin-like protein OS=Cricetulus griseus GN=I79_020709 PE=3 SV=1	41	58	186563	2	1.2	6.11
36	2,,tr|G3HAC6|G3HAC6_CRIGR	Titin OS=Cricetulus griseus GN=I79_007374 PE=4 SV=1	40	58	4035768	2	0.1	5.75
37	2,,tr|A0A061IKA1|A0A061IKA1_CRIGR	Lipoprotein lipase OS=Cricetulus griseus GN=H671_1g2493 PE=3 SV=1	39	58	55119	2	1.6	7.94
38	2,,tr|G3IFW2|G3IFW2_CRIGR	Dual specificity protein phosphatase CDC14A OS=Cricetulus griseus GN=I79_022636 PE=4 SV=1	38	58	47057	2	1.9	9.25
39	2,,tr|A0A061IJY8|A0A061IJY8_CRIGR	Sal-like protein 2 OS=Cricetulus griseus GN=H671_1g2258 PE=4 SV=1	37	58	158003	2	0.6	6.15
40	2,,tr|G3I3U5|G3I3U5_CRIGR	Nidogen-1 OS=Cricetulus griseus GN=I79_018113 PE=4 SV=1	35	58	30813	2	4.0	8.41
41	2,,tr|A0A061IJ03|A0A061IJ03_CRIGR	WD repeat and FYVE domain-containing protein 3 isoform 1 OS=Cricetulus griseus GN=H671_1g2581 PE=4 SV=1	35	58	417568	2	0.2	6.37
42	2,,tr|G3GSM8|G3GSM8_CRIGR	Uncharacterized protein KIAA0226 OS=Cricetulus griseus GN=I79_000645 PE=4 SV=1	34	58	99896	2	0.7	5.87
43	2,,tr|A0A069C7Y3|A0A069C7Y3_CRIGR	Actin, cytoplasmic 1 OS=Cricetulus griseus GN=H671_4g12234 PE=3 SV=1	34	58	103832	1	1.1	6.02
44	2,,tr|G3GXS9|G3GXS9_CRIGR	Transcription factor 23 OS=Cricetulus griseus GN=I79_002572 PE=4 SV=1	32	58	30928	2	3.2	10.08
45	2,,tr|G3HDI5|G3HDI5_CRIGR	Leukotriene B4 receptor 2 OS=Cricetulus griseus GN=I79_008531 PE=4 SV=1	32	58	34318	1	2.2	10.24
46	2,,tr|G3HT48|G3HT48_CRIGR	Transmembrane protein TTMA OS=Cricetulus griseus GN=I79_014066 PE=4 SV=1	31	58	39524	4	2.2	10.26
47	2,,tr|G3HHZ8|G3HHZ8_CRIGR	DNA polymerase epsilon subunit 3 OS=Cricetulus griseus GN=I79_010260 PE=4 SV=1	31	58	16739	1	16.4	4.60
48	1,,sp|cRAP014|P02663|CASA2_BOVIN	Alpha-S2-casein OS=Bos taurus GN=CSN1S2 PE=1 SV=2	30	58	26173	2	4.5	8.54
49	2,,tr|A0A061I7G5|A0A061I7G5_CRIGR	Olfactory receptor 52Z1-like protein OS=Cricetulus griseus GN=H671_3g10101 PE=3 SV=1	30	58	79207	4	1.1	8.38

Table G-3, Spot 344 protein identification short-list.

prot_hit_num	prot_desc	prot_score	prot_mass	prot_cover	prot_pi	GO - Molecular function
1	T-complex protein 1 subunit alpha OS=Cricetulus griseus GN=I79_009786 PE=3 SV=1	2102	60814	70.1	5.71	ATP binding
3	Keratin, type I cytoskeletal 9 OS=Homo sapiens GN=KRT9 PE=1 SV=3	1164	62255	41.4	5.14	structural constituent of cytoskeleton
4	Keratin, type I cytoskeletal 10 OS=Homo sapiens GN=KRT10 PE=1 SV=6	798	59020	30	5.13	structural constituent of epidermis
7	Keratin, type I cytoskeletal 14 OS=Cricetulus griseus GN=I79_019828 PE=3 SV=1	522	52954	22.2	5.09	structural molecule activity
8	Serum albumin OS=Homo sapiens GN=ALB PE=1 SV=2	444	71317	15.8	5.92	antioxidant activity; chaperone binding; copper ion binding; DNA binding; drug binding; fatty acid binding; pyridoxal phosphate binding; toxic substance binding
16	Inositol-3-phosphate synthase 1-like protein OS=Cricetulus griseus GN=H671_1g1140 PE=4 SV=1	192	61463	9.1	5.84	inositol-3-phosphate synthase activity
19	UDP-N-acetylhexosamine pyrophosphorylase OS=Cricetulus griseus GN=I79_013109 PE=4 SV=1	156	59079	8.2	6.04	uridylyltransferase activity
25	Legumain OS=Cricetulus griseus GN=I79_017232 PE=4 SV=1	78	50060	5.9	6.07	peptidase activity

Table G-4, Spot 511 protein ´hits` list with protein description (prot_desc), score, threshold (prot_thresh), mass, coverage (prot_cov) and pI.

prot_hit_num	prot_acc	prot_desc	prot_score	prot_thresh	prot_mass	prot_matches	prot_cover	prot_pi
1	1,,sp|cRAP054|P04264|K2C1_HUMAN	Keratin, type II cytoskeletal 1 OS=Homo sapiens GN=KRT1 PE=1 SV=6	1131	58	66170	57	32.6	8.15
2	1,,sp|cRAP041|P35527|K1C9_HUMAN	Keratin, type I cytoskeletal 9 OS=Homo sapiens GN=KRT9 PE=1 SV=3	1011	58	62255	63	36.1	5.14
3	1,,sp|cRAP039|P13645|K1C10_HUMAN	Keratin, type I cytoskeletal 10 OS=Homo sapiens GN=KRT10 PE=1 SV=6	1007	58	59020	50	32.5	5.13
4	1,,sp|cRAP053|P35908|K22E_HUMAN	Keratin, type II cytoskeletal 2 epidermal OS=Homo sapiens GN=KRT2 PE=1 SV=2	603	58	65678	26	20.3	8.07
5	2,,tr|G3IBN9|G3IBN9_CRIGR	Keratin, type II cytoskeletal 71 OS=Cricetulus griseus GN=I79_021070 PE=3 SV=1	583	58	134008	29	9.4	6.18
6	2,,tr|G3I8F9|G3I8F9_CRIGR	Keratin, type I cytoskeletal 14 OS=Cricetulus griseus GN=I79_019828 PE=3 SV=1	565	58	52954	37	22.2	5.09
7	1,,sp|cRAP002|P02768|ALBU_HUMAN	Serum albumin OS=Homo sapiens GN=ALB PE=1 SV=2	464	58	71317	22	16.6	5.92
8	2,,tr|G3I8G0|G3I8G0_CRIGR	Keratin, type I cytoskeletal 17 OS=Cricetulus griseus GN=I79_019831 PE=3 SV=1	375	58	48303	18	15.0	5.00
9	2,,tr|G3HAP7|G3HAP7_CRIGR	Glutathione synthetase OS=Cricetulus griseus GN=I79_007504 PE=3 SV=1	352	58	52441	17	22.8	5.42
10	2,,tr|G3IIF5|G3IIF5_CRIGR	Keratin, type II cytoskeletal 5 OS=Cricetulus griseus GN=I79_023623 PE=3 SV=1	300	58	48256	13	13.7	5.58
11	2,,tr|G3IBN8|G3IBN8_CRIGR	Keratin, type II cytoskeletal 6A OS=Cricetulus griseus GN=I79_021069 PE=3 SV=1	283	58	48841	12	12.9	8.11
12	2,,tr|A0A061I456|A0A061I456_CRIGR	RuvB-like 2 OS=Cricetulus griseus GN=H671_6g15973 PE=4 SV=1	266	58	51252	10	15.1	5.49
13	1,,sp|cRAP112|P00761|TRYP_PIG	Trypsin OS=Sus scrofa PE=1 SV=1	258	58	25078	81	32.9	7.00
14	1,,sp|cRAP015|P02666|CASB_BOVIN	Beta-casein OS=Bos taurus GN=CSN2 PE=1 SV=2	243	58	25148	15	17.9	5.26
15	1,,sp|cRAP040|O77727|K1C15_SHEEP	Keratin, type I cytoskeletal 15 OS=Ovis aries GN=KRT15 PE=2 SV=1	240	58	48740	13	10.8	4.73
16	2,,tr|G3HC84|G3HC84_CRIGR	Heat shock protein HSP 90-beta OS=Cricetulus griseus GN=I79_008088 PE=4 SV=1	236	58	48119	14	16.7	5.33
17	2,,tr|G3IKX2|G3IKX2_CRIGR	Pigment epithelium-derived factor OS=Cricetulus griseus GN=I79_024527 PE=3 SV=1	231	58	10566	10	43.6	5.23
18	2,,tr|A0A061I494|A0A061I494_CRIGR	Leucine-rich repeat flightless-interacting protein 2 isoform 2 OS=Cricetulus griseus GN=H671_4g11863 PE=4 SV=1	230	58	52413	8	12.1	5.69
19	2,,tr|G3I692|G3I692_CRIGR	Cytosolic non-specific dipeptidase OS=Cricetulus griseus GN=I79_019004 PE=4 SV=1	206	58	53322	11	19.6	5.63
20	2,,tr|G3HEI6|G3HEI6_CRIGR	Lysyl oxidase-like 1 OS=Cricetulus griseus GN=I79_008970 PE=4 SV=1	192	58	62938	8	13.4	6.14
21	1,,sp|cRAP013|P02662|CASA1_BOVIN	Alpha-S1-casein OS=Bos taurus GN=CSN1S1 PE=1 SV=2	157	58	24570	10	11.2	4.98
22	2,,tr|A0A061IEQ4|A0A061IEQ4_CRIGR	ATP-dependent RNA helicase DDX39A OS=Cricetulus griseus GN=H671_3g9859 PE=4 SV=1	152	58	51261	6	7.5	5.39
23	2,,tr|A0A061I107|A0A061I107_CRIGR	Heat shock protein HSP 90-alpha (Fragment) OS=Cricetulus griseus GN=H671_5g13886 PE=3 SV=1	132	58	79865	6	4.2	5.10
24	2,,tr|A0A061I523|A0A061I523_CRIGR	Procollagen C-endopeptidase enhancer 1 OS=Cricetulus griseus GN=H671_4g12064 PE=4 SV=1	119	58	51099	5	6.8	8.16
25	2,,tr|G3INX6|G3INX6_CRIGR	Spliceosome RNA helicase BAT1 OS=Cricetulus griseus GN=I79_025672 PE=4 SV=1	110	58	18448	5	23.9	5.42

Table G-4 (Continued)

prot_hit_num	prot_acc	prot_desc	prot_score	prot_thresh	prot_mass	prot_matches	prot_cover	prot_pi
26	2,,tr|G3HD94|G3HD94_CRIGR	Desmoplakin OS=Cricetulus griseus GN=I79_008473 PE=4 SV=1	108	58	330268	6	1.3	6.53
27	2,,tr|G3HZH3|G3HZH3_CRIGR	Spliceosome RNA helicase BAT1 OS=Cricetulus griseus GN=I79_016476 PE=4 SV=1	93	58	32893	5	9.4	5.95
28	2,,tr|G3I6I6|G3I6I6_CRIGR	Tubulin alpha-1A chain OS=Cricetulus griseus GN=I79_019110 PE=3 SV=1	90	58	50774	4	7.3	4.94
29	2,,tr|G3IQ06|G3IQ06_CRIGR	Pigment epithelium-derived factor OS=Cricetulus griseus GN=I79_026091 PE=4 SV=1	88	58	6731	6	32.8	5.22
30	2,,tr|G3HMV7|G3HMV7_CRIGR	Tissue alpha-L-fucosidase OS=Cricetulus griseus GN=I79_012074 PE=4 SV=1	83	58	53560	3	4.1	6.02
31	2,,tr|G3HEZ1|G3HEZ1_CRIGR	Eukaryotic peptide chain release factor subunit 1 OS=Cricetulus griseus GN=I79_009142 PE=4 SV=1	76	58	45677	4	7.2	5.33
32	2,,tr|G3HWE4|G3HWE4_CRIGR	Nidogen-1 OS=Cricetulus griseus GN=I79_015301 PE=4 SV=1	71	58	79844	3	2.9	4.75
33	2,,tr|G3I0F7|G3I0F7_CRIGR	Alpha-N-acetylgalactosaminidase OS=Cricetulus griseus GN=I79_016839 PE=3 SV=1	62	58	47705	2	4.6	7.99
34	2,,tr|G3HLU9|G3HLU9_CRIGR	Junction plakoglobin OS=Cricetulus griseus GN=I79_011694 PE=4 SV=1	54	58	128795	3	1.5	5.10
35	2,,tr|G3HG75|G3HG75_CRIGR	Nestin OS=Cricetulus griseus GN=I79_009594 PE=4 SV=1	51	58	200208	3	1.4	4.19
36	2,,tr|A0A061IG65|A0A061IG65_CRIGR	Collagen alpha-2(V) chain (Fragment) OS=Cricetulus griseus GN=H671_2g5665 PE=4 SV=1	51	58	143875	2	1.4	6.01
37	2,,tr|G3HEB6|G3HEB6_CRIGR	TGF-beta receptor type III OS=Cricetulus griseus GN=I79_008897 PE=4 SV=1	50	58	94618	2	2.9	5.65
38	2,,tr|G3IL03|G3IL03_CRIGR	Putative uncharacterized protein OS=Cricetulus griseus GN=I79_024561 PE=4 SV=1	47	58	13623	2	10.6	6.23
39	2,,tr|A0A061IA70|A0A061IA70_CRIGR	Dynein heavy chain domain-containing protein 1 OS=Cricetulus griseus GN=H671_3g9023 PE=4 SV=1	43	58	517928	2	0.9	6.86
40	2,,tr|G3GV17|G3GV17_CRIGR	Mimitin, mitochondrial OS=Cricetulus griseus GN=I79_001543 PE=4 SV=1	41	58	19726	2	3.6	9.12
41	2,,tr|A0A061IJY8|A0A061IJY8_CRIGR	Sal-like protein 2 OS=Cricetulus griseus GN=H671_1g2258 PE=4 SV=1	41	58	158003	2	0.6	6.15
42	2,,tr|G3HDI5|G3HDI5_CRIGR	Leukotriene B4 receptor 2 OS=Cricetulus griseus GN=I79_008531 PE=4 SV=1	37	58	34318	2	2.2	10.24
43	2,,tr|A0A061IIQ3|A0A061IIQ3_CRIGR	Protocadherin alpha-4-like protein (Fragment) OS=Cricetulus griseus GN=H671_2g7210 PE=4 SV=1	36	58	265865	4	0.5	4.83
44	2,,tr|G3I8W2|G3I8W2_CRIGR	Beta-1,4-galactosyltransferase 1 OS=Cricetulus griseus GN=I79_019994 PE=4 SV=1	35	58	30282	2	3.5	9.04
45	2,,tr|G3I3U5|G3I3U5_CRIGR	Nidogen-1 OS=Cricetulus griseus GN=I79_018113 PE=4 SV=1	34	58	30813	1	5.8	8.41
46	2,,tr|A0A061I1R3|A0A061I1R3_CRIGR	Citron Rho-interacting kinase isoform 1 OS=Cricetulus griseus GN=H671_4g13393 PE=4 SV=1	33	58	233409	2	0.4	6.01
47	1,,sp|cRAP014|P02663|CASA2_BOVIN	Alpha-S2-casein OS=Bos taurus GN=CSN1S2 PE=1 SV=2	32	58	26173	1	4.5	8.54
48	2,,tr|A0A061ILH1|A0A061ILH1_CRIGR	Anionic trypsin-2-like protein OS=Cricetulus griseus GN=H671_1g2974 PE=3 SV=1	30	58	26501	4	8.2	6.85
49	2,,tr|A0A061I6R0|A0A061I6R0_CRIGR	Cyclin-dependent kinase 16 OS=Cricetulus griseus GN=H671_4g11456 PE=4 SV=1	30	58	20381	1	6.1	5.07

Table G-4 (Continued)

prot_hit_num	prot_acc	prot_desc	prot_score	prot_thresh	prot_mass	prot_matches	prot_cover	prot_pi
50	2,,tr|A0A061IBG9|A0A061IBG9_CRIGR	Alanine aminotransferase 2-like protein OS=Cricetulus griseus GN=H671_3g10405 PE=4 SV=1	30	58	58601	2	2.3	8.41
51	2,,tr|G3GXS9|G3GXS9_CRIGR	Transcription factor 23 OS=Cricetulus griseus GN=I79_002572 PE=4 SV=1	30	58	30928	2	3.2	10.08
52	2,,tr|G3HT48|G3HT48_CRIGR	Transmembrane protein TTMA OS=Cricetulus griseus GN=I79_014066 PE=4 SV=1	29	58	39524	2	2.2	10.26
53	2,,tr|A0A061HV67|A0A061HV67_CRIGR	Uncharacterized protein OS=Cricetulus griseus GN=H671_xg20438 PE=4 SV=1	29	58	64870	1	1.1	9.62
54	2,,tr|A0A061IB67|A0A061IB67_CRIGR	Glycine N-acyltransferase-like protein Keg1-like protein OS=Cricetulus griseus GN=H671_3g10034 PE=4 SV=1	28	58	29492	2	2.8	5.86

Table G-5, Spot 511 protein identification short-list.

prot_hit_num	prot_desc	prot_score	prot_mass	prot_cover	prot_pi	GO - Molecular function
2	Keratin, type I cytoskeletal 9 OS=Homo sapiens GN=KRT9 PE=1 SV=3	1011	62255	36.1	5.14	structural constituent of cytoskeleton
3	Keratin, type I cytoskeletal 10 OS=Homo sapiens GN=KRT10 PE=1 SV=6	1007	59020	32.5	5.13	structural constituent of epidermis
6	Keratin, type I cytoskeletal 14 OS=Cricetulus griseus GN=I79_019828 PE=3 SV=1	565	52954	22.2	5.09	structural molecule activity
8	Keratin, type I cytoskeletal 17 OS=Cricetulus griseus GN=I79_019831 PE=3 SV=1	375	48303	15	5	structural molecule activity
9	Glutathione synthetase OS=Cricetulus griseus GN=I79_007504 PE=3 SV=1	352	52441	22.8	5.42	ATP binding; glutathione synthase activity; metal ion binding
12	RuvB-like 2 OS=Cricetulus griseus GN=H671_6g15973 PE=4 SV=1	266	51252	15.1	5.49	ATP binding; ATP-dependent 5'-3' DNA helicase activity; damaged DNA binding
16	Heat shock protein HSP 90-beta OS=Cricetulus griseus GN=I79_008088 PE=4 SV=1	236	48119	16.7	5.33	ATP binding
22	ATP-dependent RNA helicase DDX39A OS=Cricetulus griseus GN=H671_3g9859 PE=4 SV=1	152	51261	7.5	5.39	ATP binding; helicase activity; nucleic acid binding
23	Heat shock protein HSP 90-alpha (Fragment) OS=Cricetulus griseus GN=H671_5g13886 PE=3 SV=1	132	79865	4.2	5.1	ATP binding

Table G-6, Spot 581 protein ´hits` list with protein description (prot_desc), score, threshold (prot_thresh), mass, coverage (prot_cov) and pI.

prot_hit_num	prot_acc	prot_desc	prot_score	prot_thresh	prot_mass	prot_matches	prot_cover	prot_pi
1	2,,tr|G3IAQ0|G3IAQ0_CRIGR	Alpha-enolase OS=Cricetulus griseus GN=I79_020676 PE=3 SV=1	2291	58	47011	481	73.4	5.84
2	1,,sp|cRAP054|P04264|K2C1_HUMAN	Keratin, type II cytoskeletal 1 OS=Homo sapiens GN=KRT1 PE=1 SV=6	1145	58	66170	47	32.1	8.15
3	1,,sp|cRAP041|P35527|K1C9_HUMAN	Keratin, type I cytoskeletal 9 OS=Homo sapiens GN=KRT9 PE=1 SV=3	818	58	62255	36	33.5	5.14
4	1,,sp|cRAP039|P13645|K1C10_HUMAN	Keratin, type I cytoskeletal 10 OS=Homo sapiens GN=KRT10 PE=1 SV=6	778	58	59020	30	27.9	5.13
5	1,,sp|cRAP002|P02768|ALBU_HUMAN	Serum albumin OS=Homo sapiens GN=ALB PE=1 SV=2	533	58	71317	28	19.0	5.92
6	1,,sp|cRAP053|P35908|K22E_HUMAN	Keratin, type II cytoskeletal 2 epidermal OS=Homo sapiens GN=KRT2 PE=1 SV=2	510	58	65678	20	20.2	8.07
7	2,,tr|G3GUQ0|G3GUQ0_CRIGR	Gamma-enolase OS=Cricetulus griseus GN=I79_001417 PE=3 SV=1	330	58	47540	50	14.5	4.94
8	2,,tr|G3GWV2|G3GWV2_CRIGR	Enolase OS=Cricetulus griseus GN=I79_002236 PE=3 SV=1	286	58	21077	77	18.8	6.53
9	1,,sp|cRAP112|P00761|TRYP_PIG	Trypsin OS=Sus scrofa PE=1 SV=1	267	58	25078	81	32.9	7.00
10	1,,sp|cRAP015|P02666|CASB_BOVIN	Beta-casein OS=Bos taurus GN=CSN2 PE=1 SV=2	224	58	25148	14	17.9	5.26
11	2,,tr|G3IBN9|G3IBN9_CRIGR	Keratin, type II cytoskeletal 71 OS=Cricetulus griseus GN=I79_021070 PE=3 SV=1	196	58	134008	9	4.2	6.18
12	2,,tr|G3HLZ7|G3HLZ7_CRIGR	Alanyl-tRNA synthetase domain-containing protein 1 OS=Cricetulus griseus GN=I79_011741 PE=4 SV=1	185	58	45290	9	12.6	5.95
13	2,,tr|G3I3U5|G3I3U5_CRIGR	Nidogen-1 OS=Cricetulus griseus GN=I79_018113 PE=4 SV=1	146	58	30813	5	13.7	8.41
14	1,,sp|cRAP013|P02662|CASA1_BOVIN	Alpha-S1-casein OS=Bos taurus GN=CSN1S1 PE=1 SV=2	143	58	24570	9	11.2	4.98
15	2,,tr|G3I0W1|G3I0W1_CRIGR	Alpha-enolase OS=Cricetulus griseus GN=I79_017003 PE=4 SV=1	122	58	15557	38	20.9	5.00
16	2,,tr|A0A061IC58|A0A061IC58_CRIGR	Elongation factor 1-gamma OS=Cricetulus griseus GN=H671_3g9663 PE=4 SV=1	102	58	52185	4	6.0	7.11
17	2,,tr|G3I8F9|G3I8F9_CRIGR	Keratin, type I cytoskeletal 14 OS=Cricetulus griseus GN=I79_019828 PE=3 SV=1	100	58	52954	6	4.6	5.09
18	2,,tr|G3HI49|G3HI49_CRIGR	Alpha-enolase OS=Cricetulus griseus GN=I79_010316 PE=4 SV=1	99	58	17171	27	16.8	8.59
19	2,,tr|G3GR73|G3GR73_CRIGR	Rab GDP dissociation inhibitor beta OS=Cricetulus griseus GN=H671_3g8659 PE=4 SV=1	97	58	51048	4	6.7	5.93
20	2,,tr|G3I2H6|G3I2H6_CRIGR	N-acetyllactosaminide beta-1,3-N-acetylglucosaminyltransferase OS=Cricetulus griseus GN=I79_017583 PE=4 SV=1	84	58	47913	5	6.3	7.16
21	2,,tr|G3IL03|G3IL03_CRIGR	Putative uncharacterized protein OS=Cricetulus griseus GN=I79_024561 PE=4 SV=1	83	58	13623	2	10.6	6.23
22	2,,tr|G3HLL7|G3HLL7_CRIGR	Glial fibrillary acidic protein OS=Cricetulus griseus GN=I79_011607 PE=3 SV=1	79	58	49159	3	4.7	5.39
23	2,,tr|G3HRJ5|G3HRJ5_CRIGR	Calcitonin gene-related peptide type 1 receptor OS=Cricetulus griseus GN=I79_013440 PE=4 SV=1	79	58	50278	4	7.3	6.36
24	1,,sp|cRAP014|P02663|CASA2_BOVIN	Alpha-S2-casein OS=Bos taurus GN=CSN1S2 PE=1 SV=2	54	58	26173	3	9.5	8.54
25	2,,tr|G3HCU8|G3HCU8_CRIGR	26S protease regulatory subunit 8 OS=Cricetulus griseus GN=I79_008315 PE=3 SV=1	47	58	47826	2	1.4	6.21

Table G-6 (Continued)

prot_hit_num	prot_acc	prot_desc	prot_score	prot_thresh	prot_mass	prot_matches	prot_cover	prot_pi
26	2,,tr|G3HMF4|G3HMF4_CRIGR	FERM and PDZ domain-containing protein 1 OS=Cricetulus griseus GN=I79_011914 PE=4 SV=1	47	58	125711	2	1.6	5.47
26	2,,tr|G3HMF4|G3HMF4_CRIGR	FERM and PDZ domain-containing protein 1 OS=Cricetulus griseus GN=I79_011914 PE=4 SV=1	47	58	125711	2	1.6	5.47
27	2,,tr|G3I4W7|G3I4W7_CRIGR	Cathepsin D OS=Cricetulus griseus GN=H671_3g9701 PE=3 SV=1	44	58	44539	1	2.5	6.54
28	2,,tr|A0A061IL88|A0A061IL88_CRIGR	Guanine nucleotide exchange factor DBS isoform 2 OS=Cricetulus griseus GN=H671_1g1757 PE=4 SV=1	44	58	142490	4	1.4	5.83
29	2,,tr|A0A061HV65|A0A061HV65_CRIGR	Protein Shroom4 OS=Cricetulus griseus GN=H671_xg20443 PE=4 SV=1	42	58	169475	5	1.2	6.25
30	2,,tr|A0A061HZW4|A0A061HZW4_CRIGR	Mirror-image polydactyly protein OS=Cricetulus griseus GN=H671_5g13786 PE=4 SV=1	39	58	52092	2	2.0	5.20
31	2,,tr|G3I220|G3I220_CRIGR	Cytoskeleton-associated protein 4 OS=Cricetulus griseus GN=I79_017443 PE=4 SV=1	39	58	36338	3	2.8	4.74
32	2,,tr|G3I2X3|G3I2X3_CRIGR	Casein kinase II subunit alpha~ OS=Cricetulus griseus GN=I79_017768 PE=4 SV=1	39	58	37568	2	4.0	8.70
33	2,,tr|G3GU09|G3GU09_CRIGR	Pleckstrin-likey domain-containing family G member 1 OS=Cricetulus griseus GN=I79_001155 PE=4 SV=1	35	58	159737	6	0.5	5.77
34	2,,tr|G3HDI5|G3HDI5_CRIGR	Leukotriene B4 receptor 2 OS=Cricetulus griseus GN=I79_008531 PE=4 SV=1	35	58	34318	1	2.2	10.24
35	2,,tr|G3GUK8|G3GUK8_CRIGR	Polypeptide N-acetylgalactosaminyltransferase OS=Cricetulus griseus GN=I79_001371 PE=3 SV=1	34	58	58969	5	1.4	7.57
36	2,,tr|G3GTS6|G3GTS6_CRIGR	26S proteasome non-ATPase regulatory subunit 11 OS=Cricetulus griseus GN=I79_001065 PE=4 SV=1	34	58	29771	2	3.0	6.24
37	2,,tr|G3H055|G3H055_CRIGR	Alpha-(1,3)-fucosyltransferase 10 OS=Cricetulus griseus GN=I79_003503 PE=3 SV=1	32	58	41306	2	1.7	6.19
38	2,,tr|G3I5W0|G3I5W0_CRIGR	Zinc finger protein castor-like 1 OS=Cricetulus griseus GN=I79_018869 PE=4 SV=1	31	58	168825	1	1.0	8.69
39	2,,tr|G3HV01|G3HV01_CRIGR	Protein FAM102A (Fragment) OS=Cricetulus griseus GN=I79_014774 PE=4 SV=1	30	58	92009	2	1.7	9.38
40	2,,tr|G3HCB2|G3HCB2_CRIGR	Ribonuclease 3 OS=Cricetulus griseus GN=I79_008119 PE=3 SV=1	29	58	160428	2	0.5	8.00

Table G-7, Spot 581 protein identification short-list.

prot_hit_num	prot_desc	prot_score	prot_mass	prot_cover	prot_pi	GO - Molecular function
1	Alpha-enolase OS=Cricetulus griseus GN=I79_020676 PE=3 SV=1	2291	47011	73.4	5.84	magnesium ion binding; phosphopyruvate hydratase activity
12	Alanyl-tRNA synthetase domain-containing protein 1 OS=Cricetulus griseus GN=I79_011741 PE=4 SV=1	185	45290	12.6	5.95	alanine-tRNA ligase activity; ATP binding; nucleic acid binding
19	Rab GDP dissociation inhibitor beta OS=Cricetulus griseus GN=H671_3g8659 PE=4 SV=1	97	51048	6.7	5.93	Rab GDP-dissociation inhibitor activity
23	Calcitonin gene-related peptide type 1 receptor OS=Cricetulus griseus GN=I79_013440 PE=4 SV=1	79	50278	7.3	6.36	G-protein coupled receptor activity; serine-type endopeptidase inhibitor activity

Table G-8, Spot 947 protein ´hits` list with protein description (prot_desc), score, threshold (prot_thresh), mass, coverage (prot_cov) and pI.

prot_hit_num	prot_acc	prot_desc	prot_score	prot_thresh	prot_mass	prot_matches	prot_cover	prot_pi
1	1,,sp|cRAP054|P04264|K2C1_HUMAN	Keratin, type II cytoskeletal 1 OS=Homo sapiens GN=KRT1 PE=1 SV=6	1019	58	66170	45	28.9	8.15
2	1,,sp|cRAP041|P35527|K1C9_HUMAN	Keratin, type I cytoskeletal 9 OS=Homo sapiens GN=KRT9 PE=1 SV=3	889	58	62255	55	35.2	5.14
3	2,,tr|G3H6S8|G3H6S8_CRIGR	Inorganic pyrophosphatase OS=Cricetulus griseus GN=I79_006047 PE=4 SV=1	863	58	37373	68	62	5.19
4	1,,sp|cRAP002|P02768|ALBU_HUMAN	Serum albumin OS=Homo sapiens GN=ALB PE=1 SV=2	331	58	71317	16	12.8	5.92
5	1,,sp|cRAP039|P13645|K1C10_HUMAN	Keratin, type I cytoskeletal 10 OS=Homo sapiens GN=KRT10 PE=1 SV=6	314	58	59020	14	13	5.13
6	2,,tr|G3IAQ0|G3IAQ0_CRIGR	Alpha-enolase OS=Cricetulus griseus GN=I79_020676 PE=3 SV=1	300	58	47011	13	17.5	5.84
7	1,,sp|cRAP015|P02666|CASB_BOVIN	Beta-casein OS=Bos taurus GN=CSN2 PE=1 SV=2	264	58	25148	12	20.5	5.26
8	2,,tr|G3I8F9|G3I8F9_CRIGR	Keratin, type I cytoskeletal 14 OS=Cricetulus griseus GN=I79_019828 PE=3 SV=1	251	58	52954	12	11.2	5.09
9	1,,sp|cRAP112|P00761|TRYP_PIG	Trypsin OS=Sus scrofa PE=1 SV=1	237	58	25078	82	29.4	7.00
10	2,,tr|A0A061I3S4|A0A061I3S4_CRIGR	Deoxyhypusine hydroxylase-like protein (Fragment) OS=Cricetulus griseus GN=H671_5g14444 PE=4 SV=1	211	58	15387	10	60.4	4.73
11	2,,tr|G3HSJ6|G3HSJ6_CRIGR	Deoxyhypusine hydroxylase OS=Cricetulus griseus GN=Dohh PE=3 SV=1	209	58	50190	10	14.5	5.62
12	2,,tr|G3IBN9|G3IBN9_CRIGR	Keratin, type II cytoskeletal 71 OS=Cricetulus griseus GN=I79_021070 PE=3 SV=1	207	58	134008	9	4.2	6.18
13	2,,tr|A0A061IDI5|A0A061IDI5_CRIGR	Exosome component 10 isoform 1 OS=Cricetulus griseus GN=H671_2g6267 PE=3 SV=1	158	58	133745	7	3.2	6.49
14	2,,tr|G3H177|G3H177_CRIGR	Vesicular integral-membrane protein VIP36 OS=Cricetulus griseus GN=H671_3g8834 PE=4 SV=1	130	58	40544	6	11.5	6.46
15	1,,sp|cRAP013|P02662|CASA1_BOVIN	Alpha-S1-casein OS=Bos taurus GN=CSN1S1 PE=1 SV=2	102	58	24570	4	10.3	4.98
16	2,,tr|G3GUR1|G3GUR1_CRIGR	Complement C1r-A subcomponent OS=Cricetulus griseus GN=I79_001432 PE=3 SV=1	100	58	81529	4	5.4	5.71
17	2,,tr|A0A061IKA1|A0A061IKA1_CRIGR	Lipoprotein lipase OS=Cricetulus griseus GN=H671_1g2493 PE=3 SV=1	89	58	55119	5	5.5	7.94
18	2,,tr|A0A061I3S9|A0A061I3S9_CRIGR	Guanine nucleotide-binding protein G(I)/G(S)/G(T) subunit beta-2-like protein OS=Cricetulus griseus GN=H671_4g12066 PE=4 SV=1	68	58	33072	4	7.4	5.71
19	2,,tr|G3HNJ3|G3HNJ3_CRIGR	Clusterin OS=Cricetulus griseus GN=I79_012331 PE=3 SV=1	68	58	52352	6	4.5	5.52
20	2,,tr|A0A061I1R3|A0A061I1R3_CRIGR	Citron Rho-interacting kinase isoform 1 OS=Cricetulus griseus GN=H671_4g13393 PE=4 SV=1	60	58	233409	3	0.9	6.01
21	2,,tr|G3HCU8|G3HCU8_CRIGR	26S protease regulatory subunit 8 OS=Cricetulus griseus GN=I79_008315 PE=3 SV=1	57	58	47826	3	4.0	6.21
22	2,,tr|G3H8F4|G3H8F4_CRIGR	Dystroglycan OS=Cricetulus griseus GN=I79_006654 PE=4 SV=1	48	58	97304	1	1.6	8.72
23	2,,tr|A0A061IQ31|A0A061IQ31_CRIGR	Ankyrin-2 OS=Cricetulus griseus GN=H671_1g1756 PE=4 SV=1	43	58	467069	3	0.7	5.29
24	2,,tr|G3IL03|G3IL03_CRIGR	Putative uncharacterized protein OS=Cricetulus griseus GN=I79_024561 PE=4 SV=1	41	58	13623	2	10.6	6.23
25	2,,tr|G3I4D4|G3I4D4_CRIGR	Ribonuclease T2 OS=Cricetulus griseus GN=I79_018311 PE=3 SV=1	37	58	30092	2	2.7	6.25

Table G-8 (Continued)

prot_hit_num	prot_acc	prot_desc	prot_score	prot_thresh	prot_mass	prot_matches	prot_cover	prot_pi
26	2,,tr|G3HDI5|G3HDI5_CRIGR	Leukotriene B4 receptor 2 OS=Cricetulus griseus GN=I79_008531 PE=4 SV=1	37	58	34318	1	2.2	10.24
27	2,,tr|G3IF51|G3IF51_CRIGR	Tapasin-related protein OS=Cricetulus griseus GN=I79_022366 PE=4 SV=1	32	58	28960	1	3.6	4.96
28	2,,tr|A0A061IBG9|A0A061IBG9_CRIGR	Alanine aminotransferase 2-like protein OS=Cricetulus griseus GN=H671_3g10405 PE=4 SV=1	31	58	58601	2	2.3	8.41
29	2,,tr|A0A061IQT5|A0A061IQT5_CRIGR	Polypeptide N-acetylgalactosaminyltransferase-like protein 2 OS=Cricetulus griseus GN=H671_1g1912 PE=4 SV=1	30	58	64969	7	1.2	8.15
30	2,,tr|A0A061IIQ3|A0A061IIQ3_CRIGR	Protocadherin alpha-4-like protein (Fragment) OS=Cricetulus griseus GN=H671_2g7210 PE=4 SV=1	30	58	265865	3	0.5	4.83
31	2,,tr|A0A061I6H5|A0A061I6H5_CRIGR	39S ribosomal protein L24 OS=Cricetulus griseus GN=H671_4g11513 PE=3 SV=1	30	58	19732	1	8.8	9.30
32	2,,tr|G3GXS9|G3GXS9_CRIGR	Transcription factor 23 OS=Cricetulus griseus GN=I79_002572 PE=4 SV=1	29	58	30928	2	3.2	10.08
33	2,,tr|G3HXA8|G3HXA8_CRIGR	Zinc finger FYVE domain-containing protein 16 OS=Cricetulus griseus GN=I79_015627 PE=4 SV=1	29	58	168796	1	0.5	4.74

Table G-9, Spot 947 protein identification short-list

prot_hit_num	prot_desc	prot_score	prot_mass	prot_cover	prot_pi	GO - Molecular function
3	Inorganic pyrophosphatase OS=Cricetulus griseus GN=I79_006047 PE=4 SV=1	863	37373	62	5.19	GTP binding; inorganic diphosphatase activity; inorganic diphosphatase activity; magnesium ion binding
7	Beta-casein OS=Bos taurus GN=CSN2 PE=1 SV=2	264	25148	20.5	5.26	
15	Alpha-S1-casein OS=Bos taurus GN=CSN1S1 PE=1 SV=2	102	24570	10.3	4.98	
18	Guanine nucleotide-binding protein G(I)/G(S)/G(T) subunit beta-2-like protein OS=Cricetulus griseus GN=H671_4g12066 PE=4 SV=1	68	33072	7.4	5.71	

Table G-10, Spot 1005 protein ´hits` list with protein description (prot_desc), score, threshold (prot_thresh), mass, coverage (prot_cov) and pI.

prot_hit_num	prot_acc	prot_desc	prot_score	prot_thresh	prot_mass	prot_matches	prot_cover	prot_pi
1	1,,sp|cRAP039|P13645|K1C10_HUMAN	Keratin, type I cytoskeletal 10 OS=Homo sapiens GN=KRT10 PE=1 SV=6	829	58	59020	35	28.8	5.13
2	1,,sp|cRAP054|P04264|K2C1_HUMAN	Keratin, type II cytoskeletal 1 OS=Homo sapiens GN=KRT1 PE=1 SV=6	792	58	66170	37	25.6	8.15
3	2,,tr|G3GUR1|G3GUR1_CRIGR	Complement C1r-A subcomponent OS=Cricetulus griseus GN=I79_001432 PE=3 SV=1	528	58	81529	42	15.6	5.71
4	1,,sp|cRAP002|P02768|ALBU_HUMAN	Serum albumin OS=Homo sapiens GN=ALB PE=1 SV=2	479	58	71317	24	18.9	5.92
5	1,,sp|cRAP053|P35908|K22E_HUMAN	Keratin, type II cytoskeletal 2 epidermal OS=Homo sapiens GN=KRT2 PE=1 SV=2	458	58	65678	18	15.8	8.07
6	2,,tr|G3HTG9|G3HTG9_CRIGR	Glyoxalase domain-containing protein 4 OS=Cricetulus griseus GN=I79_014194 PE=4 SV=1	405	58	33479	18	34.9	5.28
7	1,,sp|cRAP112|P00761|TRYP_PIG	Trypsin OS=Sus scrofa PE=1 SV=1	252	58	25078	83	32.9	7.00
8	1,,sp|cRAP015|P02666|CASB_BOVIN	Beta-casein OS=Bos taurus GN=CSN2 PE=1 SV=2	226	58	25148	13	17.9	5.26
9	1,,sp|cRAP013|P02662|CASA1_BOVIN	Alpha-S1-casein OS=Bos taurus GN=CSN1S1 PE=1 SV=2	149	58	24570	7	11.2	4.98
10	2,,tr|G3IBN9|G3IBN9_CRIGR	Keratin, type II cytoskeletal 71 OS=Cricetulus griseus GN=I79_021070 PE=3 SV=1	139	58	134008	5	2.6	6.18
11	2,,tr|G3HLZ2|G3HLZ2_CRIGR	Proteasome activator complex subunit 3 OS=Cricetulus griseus GN=I79_011736 PE=4 SV=1	131	58	29602	6	10.2	5.69
12	1,,sp|cRAP041|P35527|K1C9_HUMAN	Keratin, type I cytoskeletal 9 OS=Homo sapiens GN=KRT9 PE=1 SV=3	102	58	62255	6	4.7	5.14
13	2,,tr|Q9EPP7|Q9EPP7_CRIGR	Cathepsin Z OS=Cricetulus griseus GN=ctsz PE=2 SV=1	96	58	34691	4	6.2	7.52
14	2,,tr|G3HQX0|G3HQX0_CRIGR	40S ribosomal protein SA OS=Cricetulus griseus GN=I79_013226 PE=3 SV=1	77	58	19836	4	14.0	9.35
15	2,,tr|A0A061I1R3|A0A061I1R3_CRIGR	Citron Rho-interacting kinase isoform 1 OS=Cricetulus griseus GN=H671_4g13393 PE=4 SV=1	74	58	233409	4	0.7	6.01
16	2,,tr|A0A061IH04|A0A061IH04_CRIGR	Nucleobindin-2-like protein OS=Cricetulus griseus GN=H671_3g8966 PE=4 SV=1	68	58	53059	2	5.4	4.94
17	2,,tr|A0A061IKA1|A0A061IKA1_CRIGR	Lipoprotein lipase OS=Cricetulus griseus GN=H671_1g2493 PE=3 SV=1	67	58	55119	4	5.5	7.94
18	2,,tr|G3HNJ3|G3HNJ3_CRIGR	Clusterin OS=Cricetulus griseus GN=I79_012331 PE=3 SV=1	63	58	52352	5	4.5	5.52
19	2,,tr|G3I4D4|G3I4D4_CRIGR	Ribonuclease T2 OS=Cricetulus griseus GN=I79_018311 PE=3 SV=1	58	58	30092	3	6.6	6.25
20	2,,tr|A0A061IJ82|A0A061IJ82_CRIGR	Disintegrin and metalloproteinase domain-containing protein 22 OS=Cricetulus griseus GN=H671_1g2508 PE=4 SV=1	52	58	84373	2	2.0	7.99
21	2,,tr|G3GUR8|G3GUR8_CRIGR	Sarcolemmal membrane-associated protein OS=Cricetulus griseus GN=I79_001441 PE=4 SV=1	51	58	94946	3	1.6	5.14
22	2,,tr|A0A061I2T2|A0A061I2T2_CRIGR	Uncharacterized protein OS=Cricetulus griseus GN=H671_4g13030 PE=4 SV=1	45	58	275575	2	1.0	5.87
23	2,,tr|G3IL03|G3IL03_CRIGR	Putative uncharacterized protein OS=Cricetulus griseus GN=I79_024561 PE=4 SV=1	44	58	13623	2	10.6	6.23
24	2,,tr|G3HXL6|G3HXL6_CRIGR	Annexin OS=Cricetulus griseus GN=I79_015744 PE=3 SV=1	42	58	90556	2	1.4	5.44

Table G-10 (Continued)

prot_hit_num	prot_acc	prot_desc	prot_score	prot_thresh	prot_mass	prot_matches	prot_cover	prot_pi
25	2,,tr|G3I2G0|G3I2G0_CRIGR	UPF0696 protein C11orf68-like OS=Cricetulus griseus GN=I79_017602 PE=4 SV=1	39	58	27633	1	4.4	5.28
26	2,,tr|G3IFW2|G3IFW2_CRIGR	Dual specificity protein phosphatase CDC14A OS=Cricetulus griseus GN=I79_022636 PE=4 SV=1	35	58	47057	2	1.9	9.25
27	2,,tr|A0A061IIQ3|A0A061IIQ3_CRIGR	Protocadherin alpha-4-like protein (Fragment) OS=Cricetulus griseus GN=H671_2g7210 PE=4 SV=1	35	58	265865	4	0.5	4.83
28	2,,tr|A0A061IH36|A0A061IH36_CRIGR	F-actin-capping protein subunit beta-like protein OS=Cricetulus griseus GN=H671_2g6288 PE=4 SV=1	34	58	34189	2	3.3	6.02
29	2,,tr|A0A061IKC1|A0A061IKC1_CRIGR	Pyruvate kinase OS=Cricetulus griseus GN=H671_1g2487 PE=3 SV=1	34	58	31744	1	3.8	5.36
30	2,,tr|A0A061I1S5|A0A061I1S5_CRIGR	Microtubule-associated protein RP/EB family member 1-like protein OS=Cricetulus griseus GN=H671_6g16114 PE=4 SV=1	34	58	29799	2	7.6	6.85
31	2,,tr|G3HT48|G3HT48_CRIGR	Transmembrane protein TTMA OS=Cricetulus griseus GN=I79_014066 PE=4 SV=1	31	58	39524	4	2.2	10.26
32	2,,tr|G3HZV5|G3HZV5_CRIGR	Seprase OS=Cricetulus griseus GN=I79_016619 PE=4 SV=1	30	58	64402	1	2.7	8.57
33	2,,tr|G3GXS9|G3GXS9_CRIGR	Transcription factor 23 OS=Cricetulus griseus GN=I79_002572 PE=4 SV=1	30	58	30928	2	3.2	10.08
34	2,,tr|A0A061IBG9|A0A061IBG9_CRIGR	Alanine aminotransferase 2-like protein OS=Cricetulus griseus GN=H671_3g10405 PE=4 SV=1	30	58	58601	2	2.3	8.41
35	1,,sp|cRAP014|P02663|CASA2_BOVIN	Alpha-S2-casein OS=Bos taurus GN=CSN1S2 PE=1 SV=2	29	58	26173	2	4.5	8.54
36	2,,tr|G3H0J9|G3H0J9_CRIGR	Homeobox-containing protein 1 OS=Cricetulus griseus GN=I79_003659 PE=4 SV=1	29	58	24544	2	3.2	5.58
37	2,,tr|A0A061I6H5|A0A061I6H5_CRIGR	39S ribosomal protein L24 OS=Cricetulus griseus GN=H671_4g11513 PE=3 SV=1	29	58	19732	1	8.8	9.30

Table G-11, Spot 1005 protein identification short-list.

prot_hit_num	prot_desc	prot_score	prot_mass	prot_cover	prot_pi	GO - Molecular function
6	Glyoxalase domain-containing protein 4 OS=Cricetulus griseus GN=I79_014194 PE=4 SV=1	405	33479	34.9	5.28	
8	Beta-casein OS=Bos taurus GN=CSN2 PE=1 SV=2	226	25148	17.9	5.26	antioxidant activity; calcium ion binding; enzyme inhibitor activity; metalloendopeptidase inhibitor activity; potassium channel inhibitor activity; protein homodimerization activity; transporter activity
9	Alpha-S1-casein OS=Bos taurus GN=CSN1S1 PE=1 SV=2	149	24570	11.2	4.98	
11	Proteasome activator complex subunit 3 OS=Cricetulus griseus GN=I79_011736 PE=4 SV=1	131	29602	10.2	5.69	

Table G-12, Spot 1282 protein ´hits` list with protein description (prot_desc), score, threshold (prot_thresh), mass, coverage (prot_cov) and pI.

prot_hit_num	prot_acc	prot_desc	prot_score	prot_thresh	prot_mass	prot_matches	prot_cover	prot_pi
1	1,,sp|cRAP041|P35527|K1C9_HUMAN	Keratin, type I cytoskeletal 9 OS=Homo sapiens GN=KRT9 PE=1 SV=3	1111	58	62255	69	41.4	5.14
2	1,,sp|cRAP054|P04264|K2C1_HUMAN	Keratin, type II cytoskeletal 1 OS=Homo sapiens GN=KRT1 PE=1 SV=6	1103	58	66170	53	29.8	8.15
3	1,,sp|cRAP039|P13645|K1C10_HUMAN	Keratin, type I cytoskeletal 10 OS=Homo sapiens GN=KRT10 PE=1 SV=6	488	58	59020	23	18.0	5.13
4	1,,sp|cRAP002|P02768|ALBU_HUMAN	Serum albumin OS=Homo sapiens GN=ALB PE=1 SV=2	406	58	71317	19	14.4	5.92
5	1,,sp|cRAP053|P35908|K22E_HUMAN	Keratin, type II cytoskeletal 2 epidermal OS=Homo sapiens GN=KRT2 PE=1 SV=2	367	58	65678	19	14.2	8.07
6	1,,sp|cRAP008|P00722|BGAL_ECOLI	Beta-galactosidase OS=Escherichia coli (strain K12) GN=lacZ PE=1 SV=2	292	58	117321	12	7.8	5.28
7	2,,tr|G3IBN9|G3IBN9_CRIGR	Keratin, type II cytoskeletal 71 OS=Cricetulus griseus GN=I79_021070 PE=3 SV=1	288	58	134008	12	4.8	6.18
8	1,,sp|cRAP112|P00761|TRYP_PIG	Trypsin OS=Sus scrofa PE=1 SV=1	260	58	25078	80	32.9	7.00
9	2,,tr|G3I8F9|G3I8F9_CRIGR	Keratin, type I cytoskeletal 14 OS=Cricetulus griseus GN=I79_019828 PE=3 SV=1	233	58	52954	12	9.7	5.09
10	1,,sp|cRAP015|P02666|CASB_BOVIN	Beta-casein OS=Bos taurus GN=CSN2 PE=1 SV=2	193	58	25148	13	20.5	5.26
11	2,,tr|G3IBN8|G3IBN8_CRIGR	Keratin, type II cytoskeletal 6A OS=Cricetulus griseus GN=I79_021069 PE=3 SV=1	165	58	48841	5	6.8	8.11
12	1,,sp|cRAP013|P02662|CASA1_BOVIN	Alpha-S1-casein OS=Bos taurus GN=CSN1S1 PE=1 SV=2	138	58	24570	6	11.2	4.98
13	1,,sp|cRAP040|O77727|K1C15_SHEEP	Keratin, type I cytoskeletal 15 OS=Ovis aries GN=KRT15 PE=2 SV=1	112	58	48740	6	6.2	4.73
14	2,,tr|G3IL03|G3IL03_CRIGR	Putative uncharacterized protein OS=Cricetulus griseus GN=I79_024561 PE=4 SV=1	71	58	13623	4	10.6	6.23
15	2,,tr|G3HG75|G3HG75_CRIGR	Nestin OS=Cricetulus griseus GN=I79_009594 PE=4 SV=1	60	58	200208	3	1.4	4.19
16	2,,tr|G3HV01|G3HV01_CRIGR	Protein FAM102A (Fragment) OS=Cricetulus griseus GN=I79_014774 PE=4 SV=1	47	58	92009	2	2.6	9.38
17	2,,tr|A0A061I9Y7|A0A061I9Y7_CRIGR	Synaptotagmin-like protein 2 isoform 3 OS=Cricetulus griseus GN=H671_3g9103 PE=4 SV=1	46	58	240850	2	1.0	5.69
18	2,,tr|G3HD94|G3HD94_CRIGR	Desmoplakin OS=Cricetulus griseus GN=I79_008473 PE=4 SV=1	45	58	330268	3	0.7	6.53
19	2,,tr|A0A061I7Q5|A0A061I7Q5_CRIGR	Protein FAM55C-like protein OS=Cricetulus griseus GN=H671_4g13229 PE=4 SV=1	44	58	53799	1	1.9	9.06
21	2,,tr|G3GXS9|G3GXS9_CRIGR	Transcription factor 23 OS=Cricetulus griseus GN=I79_002572 PE=4 SV=1	33	58	30928	2	3.2	10.08
22	2,,tr|G3GV17|G3GV17_CRIGR	Mimitin, mitochondrial OS=Cricetulus griseus GN=I79_001543 PE=4 SV=1	32	58	19726	2	3.6	9.12
23	2,,tr|A0A061I7G5|A0A061I7G5_CRIGR	Olfactory receptor 52Z1-like protein OS=Cricetulus griseus GN=H671_3g10101 PE=3 SV=1	32	58	79207	2	1.1	8.38
24	2,,tr|G3HHZ8|G3HHZ8_CRIGR	DNA polymerase epsilon subunit 3 OS=Cricetulus griseus GN=I79_010260 PE=4 SV=1	31	58	16739	1	16.4	4.60
25	2,,tr|A0A061I1R3|A0A061I1R3_CRIGR	Citron Rho-interacting kinase isoform 1 OS=Cricetulus griseus GN=H671_4g13393 PE=4 SV=1	30	58	233409	2	0.4	6.01
26	2,,tr|A0A061HZ50|A0A061HZ50_CRIGR	60S ribosomal protein L10-like protein OS=Cricetulus griseus GN=H671_xg20756 PE=4 SV=1	30	58	14934	1	7.2	9.6

Table G-12 (Continued)

prot_hit_num	prot_acc	prot_desc	prot_score	prot_thresh	prot_mass	prot_matches	prot_cover	prot_pi
27	2,,tr|A0A061I6H5|A0A061I6H5_CRIGR	39S ribosomal protein L24 OS=Cricetulus griseus GN=H671_4g11513 PE=3 SV=1	29	58	19732	2	8.8	9.3
28	2,,tr|G3GZZ5|G3GZZ5_CRIGR	Putative uncharacterized protein OS=Cricetulus griseus GN=I79_003443 PE=4 SV=1	29	58	5291	1	52	10.61
29	2,,tr|A0A061HV65|A0A061HV65_CRIGR	Protein Shroom4 OS=Cricetulus griseus GN=H671_xg20443 PE=4 SV=1	28	58	169475	3	0.5	6.25

Table G-13, Spot 1282 protein identification short-list.

prot_hit_num	prot_desc	prot_score	prot_mass	prot_cover	prot_pi	GO - Molecular function
8	Trypsin OS=Sus scrofa PE=1 SV=1	260	25078	32.9	7	metal ion binding; serine-type endopeptidase activity
10	Beta-casein OS=Bos taurus GN=CSN2 PE=1 SV=2	193	25148	20.5	5.26	antioxidant activity; calcium ion binding; enzyme inhibitor activity; metalloendopeptidase inhibitor activity; potassium channel inhibitor activity; protein homodimerization activity; transporter activity
14	Putative uncharacterized protein OS=Cricetulus griseus GN=I79_024561 PE=4 SV=1	71	13623	10.6	6.23	

Table G-14, Spot 1292 protein ´hits` list with protein description (prot_desc), score, threshold (prot_thresh), mass, coverage (prot_cov) and pI

prot_hit_num	prot_acc	prot_desc	prot_score	prot_thresh	prot_mass	prot_matches	prot_cover	prot_pi
1	1,,sp|cRAP054|P04264|K2C1_HUMAN	Keratin, type II cytoskeletal 1 OS=Homo sapiens GN=KRT1 PE=1 SV=6	946	58	66170	41	24.7	8.15
2	1,,sp|cRAP041|P35527|K1C9_HUMAN	Keratin, type I cytoskeletal 9 OS=Homo sapiens GN=KRT9 PE=1 SV=3	809	58	62255	45	32.3	5.14
3	1,,sp|cRAP039|P13645|K1C10_HUMAN	Keratin, type I cytoskeletal 10 OS=Homo sapiens GN=KRT10 PE=1 SV=6	544	58	59020	25	19.7	5.13
4	1,,sp|cRAP053|P35908|K22E_HUMAN	Keratin, type II cytoskeletal 2 epidermal OS=Homo sapiens GN=KRT2 PE=1 SV=2	497	58	65678	22	20.2	8.07
5	1,,sp|cRAP002|P02768|ALBU_HUMAN	Serum albumin OS=Homo sapiens GN=ALB PE=1 SV=2	380	58	71317	17	12.8	5.92
6	1,,sp|cRAP015|P02666|CASB_BOVIN	Beta-casein OS=Bos taurus GN=CSN2 PE=1 SV=2	266	58	25148	14	20.5	5.26
7	1,,sp|cRAP112|P00761|TRYP_PIG	Trypsin OS=Sus scrofa PE=1 SV=1	236	58	25078	80	32.9	7.00
8	2,,tr|G3IBN9|G3IBN9_CRIGR	Keratin, type II cytoskeletal 71 OS=Cricetulus griseus GN=I79_021070 PE=3 SV=1	201	58	134008	8	3.4	6.18
10	1,,sp|cRAP013|P02662|CASA1_BOVIN	Alpha-S1-casein OS=Bos taurus GN=CSN1S1 PE=1 SV=2	133	58	24570	6	11.2	4.98
11	2,,tr|G3IL03|G3IL03_CRIGR	Putative uncharacterized protein OS=Cricetulus griseus GN=I79_024561 PE=4 SV=1	89	58	13623	30	10.6	6.23
12	2,,tr|G3HG75|G3HG75_CRIGR	Nestin OS=Cricetulus griseus GN=I79_009594 PE=4 SV=1	57	58	200208	2	1.4	4.19
13	2,,tr|G3HCU8|G3HCU8_CRIGR	26S protease regulatory subunit 8 OS=Cricetulus griseus GN=I79_008315 PE=3 SV=1	46	58	47826	2	4.0	6.21
14	2,,tr|A0A061HVU3|A0A061HVU3_CRIGR	WW domain-binding protein 11 OS=Cricetulus griseus GN=H671_8g19454 PE=4 SV=1	40	58	69921	2	0.9	7.75
15	2,,tr|G3GXS9|G3GXS9_CRIGR	Transcription factor 23 OS=Cricetulus griseus GN=I79_002572 PE=4 SV=1	36	58	30928	2	3.2	10.08
16	2,,tr|A0A061I1R3|A0A061I1R3_CRIGR	Citron Rho-interacting kinase isoform 1 OS=Cricetulus griseus GN=H671_4g13393 PE=4 SV=1	35	58	233409	2	0.4	6.01
17	2,,tr|G3HQ07|G3HQ07_CRIGR	Transcription factor AP-2 delta OS=Cricetulus griseus GN=I79_012895 PE=4 SV=1	34	58	39373	2	2.0	6.69
18	2,,tr|A0A061IIQ3|A0A061IIQ3_CRIGR	Protocadherin alpha-4-like protein (Fragment) OS=Cricetulus griseus GN=H671_2g7210 PE=4 SV=1	33	58	265865	3	0.5	4.83
19	2,,tr|G3HT48|G3HT48_CRIGR	Transmembrane protein TTMA OS=Cricetulus griseus GN=I79_014066 PE=4 SV=1	29	58	39524	2	2.2	10.26
20	2,,tr|A0A061IL80|A0A061IL80_CRIGR	Uncharacterized protein OS=Cricetulus griseus GN=H671_2g5916 PE=4 SV=1	29	58	20447	1	6.2	7.82
21	2,,tr|G3HKB0|G3HKB0_CRIGR	Peptidyl-prolyl cis-trans isomerase OS=Cricetulus griseus GN=I79_011130 PE=3 SV=1	28	58	18078	2	9.2	7.82
22	2,,tr|G3IJV3|G3IJV3_CRIGR	E3 ubiquitin-protein ligase RNF216 OS=Cricetulus griseus GN=I79_024141 PE=4 SV=1	28	58	23858	1	4.0	6.97

Table G-15, Spot 1282 protein identification short-list.

prot_hit_num	prot_desc	prot_score	prot_mass	prot_cover	prot_pi	GO - Molecular function
6	Beta-casein OS=Bos taurus GN=CSN2 PE=1 SV=2	266	25148	20.5	5.26	
7	Trypsin OS=Sus scrofa PE=1 SV=1	236	25078	32.9	7	
11	Putative uncharacterized protein OS=Cricetulus griseus GN=I79_024561 PE=4 SV=1	89	13623	10.6	6.23	
22	E3 ubiquitin-protein ligase RNF216 OS=Cricetulus griseus GN=I79_024141 PE=4 SV=1	28	23858	4	6.97	ligase activity